FIRST TOTAL SYNTHESIS OF NAGELAMIDE W AND DEVELOPMENT OF NITROGEN CONTAINING HETEROCYCLIC COMPOUNDS AS 20S PROTEASOME MODULATORS

By

Dare E. George

A DISSERTATION

Submitted to
Michigan State University
in partial fulfillment of the requirements
for the degree of

Chemistry – Doctor of Philosophy

2024

ABSTRACT

Nitrogen-containing heterocyclic compounds are vital in organic chemistry due to their unique properties and reactivity, playing key roles in pharmaceuticals, agrochemicals, and functional materials. Over 75% of FDA-approved drugs include these heterocycles, underscoring their importance in modern medicine. The discovery of novel N-heterocyclic compounds with significant biological activities is rapidly expanding, driven by advances in synthetic methodologies like transition metal-catalysis and biocatalysis.

Looking ahead, the importance of N-heterocyclic compounds is expected to grow. The advent of new technologies and an increasing understanding of disease mechanisms will likely drive the demand for novel pharmaceuticals incorporating nitrogen heterocycles. This trend is anticipated to lead to the discovery of new drugs with improved efficacy and safety profiles, addressing unmet medical needs and enhancing patient outcomes.

This dissertation focuses on developing new methods for synthesizing N-heterocyclic compounds, specifically pyrazoles and pyridines, through reactions of epoxides with hydrazine and ammonia, respectively. Both established and novel methodologies were also utilized to synthesize the nitrogen-containing natural product nagelamide W in 11 linear steps, resulting in an overall yield of 6%. Additionally, N-heterocyclic compounds were evaluated as 20S proteasome modulators and used as chemical probes to elucidate their binding sites on the 20S proteasome. These efforts aim to enhance the understanding and application of N-heterocycles in medicinal and biological sciences.

ACKNOWLEDGEMENTS

First, I would like to thank my advisor, Dr. Jetze Tepe for your unwavering support throughout my PhD journey. Thank you for believing in me, constantly motivating me, pushing me to my full potential, and giving me the space to explore ideas and grow to be the independent scientist that I am today. Your mentorship and support have made my PhD journey a memorable one. I am also grateful for the fellowship and program opportunities you forwarded my way and encouraged me to apply for. Lastly, thank you for assembling such an amazing, brilliant, and supportive group of people with whom I have had the pleasure of working over the past five years. It has been a great honor to be part of your group, and I appreciate the opportunity immensely.

To my lab mates, current and past, thank you for your support and being part of my PhD experience. To Shafaat – thank you for training me when I first joined the lab, even though I have little to no experience, your willingness to train me and answer my questions is one of the foundations of the chemist I am today. To Katarina, Grace, Taylor, Sophie, and Allison – thank you all for your suggestion, guidance, and always checking how things are going with me in the lab. To Charles and Konika, thank you for walking this journey with me every step of the way. From, first committee meeting, to second year oral, and to seminar. Thank you for being such good and supportive friends. To Evan, you became my lab buddy; brainstorming and troubleshooting reactions with you were invaluable experiences that greatly enriched my research and made the lab an enjoyable and collaborative environment. To Allison, Sydney, and Shannon, thank you for your collaboration and being such a wonderful teammate. To Daniel, Kyra, Bahar, Miracle, Ayoob, Christi, and Linh – thank you for supports and for being wonderful lab mates. It's being an honor to have worked alongside every one of you.

To my committee members, Dr. Huang, Dr. Draths, and Dr. Maleczka, thank you for your supports, guidance and invaluable feedback over the years. I have learned a great deal from each of you, whether through our meetings or by taking your class. To Dr. Wulff, it has been a pleasure learning from you during my time at MSU. Taking your classes and working on the natural product database with you have been invaluable sources of knowledge. Thank you for sharing your expertise in chemistry, as well as insights and stories beyond the field. I would also like to thank Dr. Tony Schilmiller for helping me with mass spectrometry over the years, and Dr. Dan Holmes and Dr. Li Xie for their help with my NMR problems.

I would also like to extend my gratitude to the people from my undergraduate university. To my mentors, Dr. Tomide Fadare and Dr. Feyisola Olatunji, thank you for your constant motivation and support. You both gave me the confidence to pursue a PhD, and without your guidance, my journey might have taken a different path. To my OAU friends, Fiyinfoluwa, Felix, Glory, and Raheemat, I appreciate you and thank you for being such great friends. To my childhood friend, Emmanuel, thank you for being such an amazing friend that I could always rely on.

To my parents and siblings, I love you all and hope I have made you proud. Thank you for your endless support, encouragement, and for constantly checking up on me. Mom, I love you so much. I couldn't have done this without you – your prayers and motivation kept me going.

To all my friends within the department and outside, thank you for being such wonderful friends. Bismarck, Ryan, and Konika – we call ourselves the “best four”. Thank you for being there throughout this PhD journey. To the Nigerian community and my close friends – Michael, Chidiogo, Femi, Ebenezer, Daniel, Rofiat, Omolade, Sodiq, Paninga, Kunle, Mark, Emmanuel, John, and many others – you all became my family in the U.S. and have been people I could always

rely on. To Miracle, thank you for being a wonderful friend and partner. Your constant support means the world to me, and I am grateful for your love and for having you in my life.

TABLE OF CONTENTS

LIST OF ABBREVIATIONS

AD	Alzheimer's disease
AFM	Atomic force microscopy
ALS	Amyotrophic lateral sclerosis
AMC	Amino methyl coumarin
ATP	Adenosine Triphosphate
Boc	Tert-butoxycarbonyl
Bn	Benzyl
BTZ	Bortezomib
Calcd	Calculated
C-L	Caspase-Like
CaMKII	Ca 2+ /Calmodulin-dependent protein kinase II
cAMP	Cyclic adenosine monophosphate
CAS	Chemical abstracts service
CDI	Carbonyldiimidazole
CDK	Cyclin-dependent kinase
cGMP	Cyclic guanosine monophosphate
CP	Core particle
CT-L	Chymotrypsin-Like
Da	Dalton
DBDMH	1,3-dibromo-5,5-dimethylhydantoin
DCM	Dichloromethane
DEAD	Diethyl azodicarboxylate

DIBAL-H	di-isobutylaluminum hydride
DIPEA	N,N-diisopropylethylamine
DMAP	4-dimethylaminopyridine
DMF	dimethylformamide
DMF-DMA	N,N-Dimethylformamide dimethylacetal
DMSO	dimethylsulfoxide
dppf	1,1,-bis(diphenylphosphino)ferrocene
DUBs	deubiquitinating enzymes
DYRK2	Dual specificity tyrosine-phosphorylation-regulated kinase 2
EC200	200% Effective Concentration
EDC/EDCI	1-ethyl-3-(3-dimethylaminopropyl)carbodiimide
Equiv	Equivalent
ESI	Electrospray ionization
FDA	U.S. Food and Drug Administration
FTIR	Fourier transform infrared
GST	Glutathione S-transferase
HBTU	Hexafluorophosphate benzotriazole tetramethyl uronium
HD	Huntington's disease
HFIP	Hexafluoro-2-propanol
HOSA	Hydroxylamine-O-sulfonic acid
Htt	Huntingtin
HWE	Horner–Wadsworth–Emmons
IC_{50}	half-maximal inhibitory concentration

IDPs	Intrisically disordered proteins
LUMO	Lowest unoccupied molecular orbital
MAPK	Mitogen-activated protein kinase
MAPT	Microtubule-associated protein tau
MDa	Mega dalton
MeOH	Methanol
MHz	Megahertz
MP	Melting point
MW	Molecular weight
NBA	N-bromoacetamide
NBS	N-bromosuccinimide
ND	Not detected
NDP	No detected product
NFTs	Neurofibrillary tangles
NIH	National Institutes of Health
NMR	Nuclear magnetic resonance
NOE	Nuclear overhauser effect
NR	No reaction
NRF2	Nuclear factor (erythroid-derived 2)-like 2
NSAID	Non-steroidal anti-inflammatory drug
PAL	Photo affirnity labelling
PD	Parkinson’s disease
PDE3	Phosphodiesterase type-3

PDE4	Phosphodiesterase type-4
PDE5	Phosphodiesterase type-5
PEG	Polyethylene glycol
PGPH	peptidylglutamyl-peptide hydrolyzing
PKA	Protein kinase A
PPh3	Triphenylphosphine
PySeSePy	Dipyridyl diselenide
RNA	Ribonucleic acid
ROESY	Rotating frame overhause effect spectroscopy
RP	Regulatory particle
RT	Room temperature
RU	Response unit
SAR	Structure activity relationship
SDS	Sodium dodecyl sulfate
siRNA	Small interfering ribonucleic acid
SNc	Substantia nigra pars compacta
SOCl2	Thionylchloride
SOD1	superoxide dismutase 1
SPR	Surface plasma resonance
t-BHQ	tert-Butylhydroquinone
T-L	Trypsin-like
TEA	Triethylamine
TFA	Trifluoroacetic acid

THF	Tetrahydrofuran
TLC	Thin-layer chromatography
TMS	Trimethylsilane
TOF	Time of flight
Ub	Ubiquitin
UPS	Ubiquitin-proteasome system
UV	Ultraviolet

Chapter 1: Synthesis of 3,4-disubstituted 1H-pyrazole and 3,5-disubstituted pyridines from epoxides*

1.1 Introduction

Pyrazole and pyridine are essential nitrogen-containing heterocycles present in wide varieties of important biological molecules, pharmaceuticals, and other chemical compounds.[1-3] Pyrazole, with its five-membered ring containing two adjacent nitrogen atoms, is a fundamental scaffold in medicinal chemistry. It serves as the core structure for numerous drugs, including FDA-approved nonsteroidal anti-inflammatory drugs (NSAIDs) lonazolac and celecoxib (**Figure 1.1**). Additionally, pyrazole derivatives exhibit a wide range of biological activities such as antitumor, antimicrobial, and antiviral properties, making them valuable targets in drug discovery and development.[4]

Figure 1.1: some FDA-approved drugs with pyrazole or pyridine scaffolds

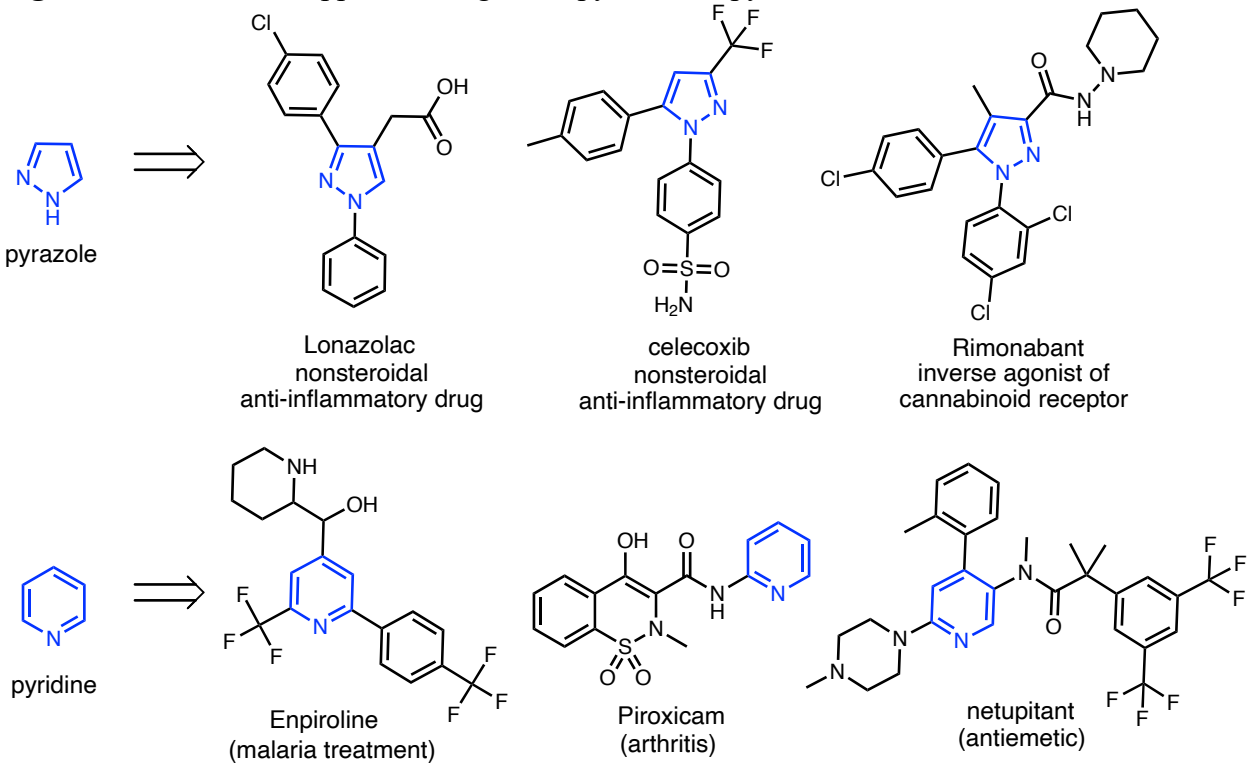

* This chapter is reproduced in part with permission from reference 35. Copyright 2022 American Chemical Society

Pyridine, a six-membered aromatic ring containing one nitrogen atom, is another essential heterocycle in both natural and synthetic chemistry.[5] It is a key component in various biologically active molecules, pharmaceuticals, and agrochemicals. Pyridine derivatives are also extensively used as building blocks in drug synthesis and as solvents in chemical reactions due to their unique properties. The diverse functionalities and reactivities of pyrazole and pyridine derivatives contribute significantly to their widespread presence in biology and chemistry, making them indispensable in various scientific fields.

Several classical approaches to synthesize pyrazoles and pyridines include the Knorr pyrazole synthesis,[6] Boger pyridine synthesis,[7] Chichibabin pyridine synthesis,[8] Kröhnke pyridine synthesis,[9] and the Hantzsch pyridine synthesis,[10] which have been well documented in the literature. Recent literature reviews have properly documented the synthesis of pyrazoles[11-14] and pyridines[15-18] via several approaches. However, some of these existing methods suffer from one or more limitations including low yields, high temperatures, a high proportion of byproducts, harsh reaction conditions, limited availability of substrates, and tedious multistep procedures, which require isolation of intermediates. Several recent modifications have been made to address some of these limitations.[19-20] However, the synthesis of 3,4-disubstituted 1H-pyrazoles[21-26] and 3,5-disubstituted pyridines[27-30] using readily available starting materials such as aldehydes, ketones, alkenes, alkynes, is still limited to a few reports. In this chapter, Shafaat Mehedi and I developed a new approach to access pyrazoles and pyridines through the utilization of the readily available epoxides with hydrazine or ammonia.

In an initial study, Mehedi et al[31] reported the synthesis of 2,3-disubstituted quinolines from the reaction of aliphatic or aromatic epoxides and aromatic amines in the presence of scandium(III) triflate as Lewis acid (**Scheme 1.1a**). Inspired by a reported study where the authors *in-situ*

generated aldehydes from epoxides and other similar reported conversions,[32-34] we report the one-pot synthesis of 3,4-disubstitued 1*H*-pyrazoles from epoxides and hydrazine using scandium(III) triflate as Lewis acid and N-bromosuccinimide (NBS) as oxidant (**Scheme 1.1c**). Similar to a Chichibabin-type pyridine synthesis (**Scheme 1.1b**), we also expanded the reaction scope to one-pot 3,5-disubstituted pyridine synthesis from the reaction of ammonia and epoxides using scandium(III) triflate and iron(III) chloride (**Scheme 1.1d**).

Scheme 1.1: Previous work and our approach to access pyrazoles and pyridines

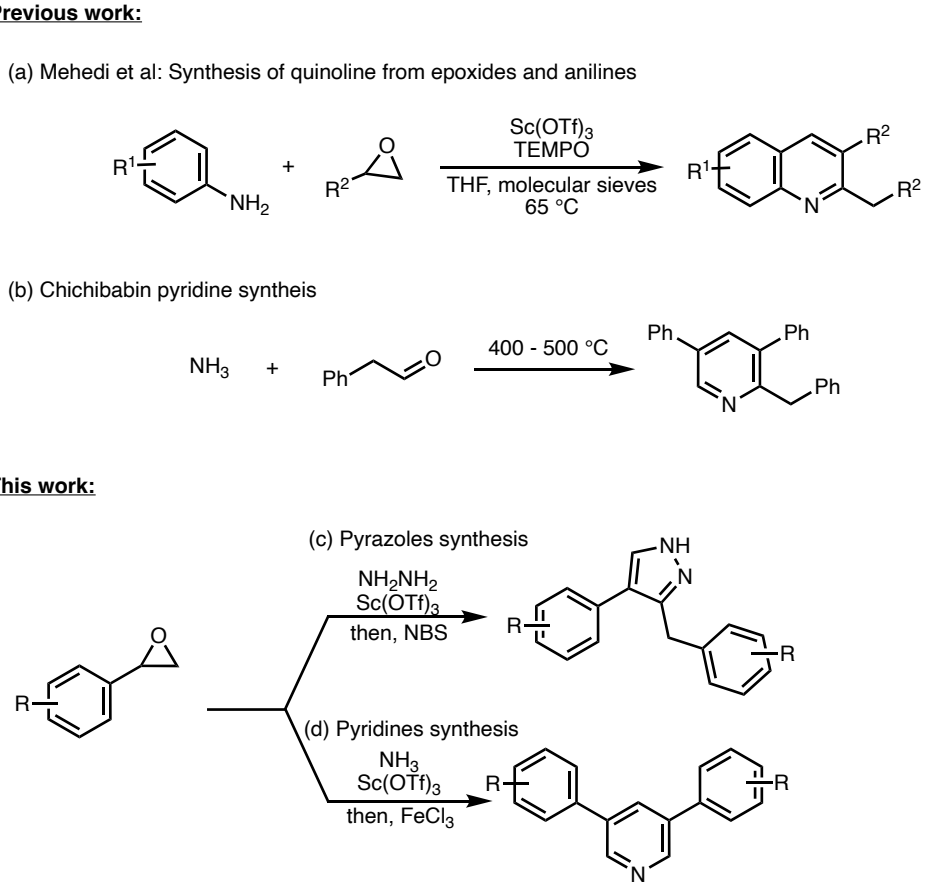

1.2 Results and Discussion

1.2.1 Synthesis of 3,4-disubstituted 1H-pyrazole

We started our study by first investigating the synthesis of pyrazoles by treating 2 equivalents of styrene oxide (**1-1a**) with a single equivalent of hydrazine in the presence of 0.25

equivalent of $Sc(OTf)_3$ as Lewis acid in tetrahydrofuran (THF) at 65 °C (**Table 1.1**, **entry 1**).[35] This reaction resulted in mixtures of *cis* and *trans* pyrazoline (**1-2**) in 1:4 cis/trans ratio in 69% yield after 15 hours. Increasing the reaction time to 24 hours led to no significant change in reaction yield (**Table 1.1**, **entry 2**). When $Sc(OTf)_3$ was increased to 0.5 equivalent, the formation of product reduced to 62% (**Table 1.1**, **entry 3**). Increasing the equivalent of styrene epoxide from 2 to 3 equivalents also led to a decrease in the desired product yield to 57% (**Table 1.1**, **entry 4**). Running the reaction in dichloromethane at 37 °C or room temperature also led to decrease in reaction yield to 31% and 23% respectively (**Table 1.1**, **entry 5 & 6**). In addition to screening of temperature and equivalent, we tried substituting $Sc(OTf)_3$ with iron(III) chloride ($FeCl_3$) or triflic acid (TfOH), $FeCl_3$ gave lower yield relative to $Sc(OTf)_3$ and only trace amount of product was observed when TfOH was used (**Table 1.1**, **entry 7&8**). It is critical to mention that no product was isolated in the absence of the acid nor under basic conditions (**Table 1.1**, **entry 9&10**).

Table 1.1: Optimization of pyrazoline synthesis

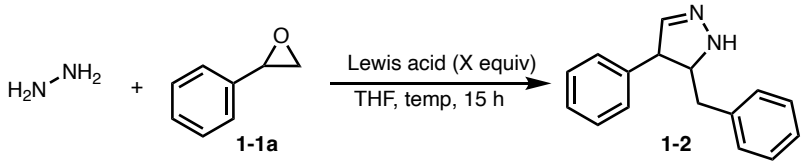

entry	equiv of 1-1a	acid	X equiv	temp (°C)	Yield of 1-2 (%)[a]
1	2	$Sc(OTf)_3$	0.25	65	69
2[b]	2	$Sc(OTf)_3$	0.25	65	68
3	2	$Sc(OTf)_3$	0.5	65	62
4	3	$Sc(OTf)_3$	0.25	65	57
5[c]	2	$Sc(OTf)_3$	0.25	37	31
6[d]	2	$Sc(OTf)_3$	0.25	rt	23
7	2	$FeCl_3$	0.25	65	33
8	2	TfOH	0.25	65	trace
9	2	-	-	65	N/A
10[e]	2	-	-	65	N/A

[a]mixture of cis and trans (**1-2**). [b]reaction ran for 24 h. [c]reaction was ran in dichloromethane. [d]rt = roomtemperature. [e]reaction ran with 1 equivalent of triethylamine.

Following the optimization of reaction condition, we evaluated various oxidants for the conversion of the pyrazoline to the pyrazole final product. Among the various oxidants we evaluated, diacetoxyiodobenzene ($PhI(OAc)_2$, potassium peroxymonosulfate (oxone), ferric oxide (Fe_2O_3), manganese dioxide (MnO_2), iodine (I_2), bromine (Br_2), *N*-bromosuccinimide (NBS), 1,3-dibromo-5,5-dimethylhydantoin (DBDMH), *N*-bromoacetamide (NBA), and *N*-bromosaccharin, only DBDMH and NBS showed significant conversion of the pyrazoline to the desired 1*H*-pyrazole (**1-3a**) product, with NBS (2 equivalents) offering the best yield of 64% (**Table 1.2, Entry 8**). When the amount of NBS was increased to 2.5 equivalent, there was no significant improvement in isolated product yield. Also, decreasing the amount of NBS to 1 equivalent resulted in reduction of the product yield to 37%. Given that over 90% of the intermediate pyrazoline converted to pyrazole, the 69% of pyrazoline formed in the first step led to 64% of pyrazole in the second step using N-bromosuccinimide (NBS). From this screen and optimization, we moved to explore the substrate scope of this methodology using various epoxides.

Table 1.2: Optimization of pyrazole synthesis

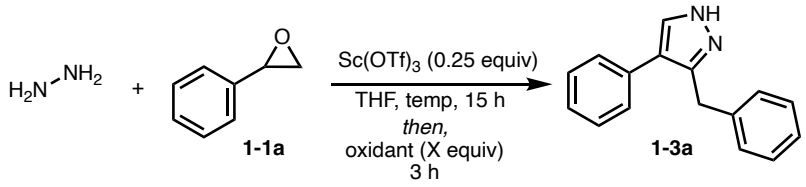

Entry	Oxidant	X equiv oxidant	temp (°C)	Yield of 1-3a (%)
1	$PhI(OAc)_2$	1	65	NDP
2	$PhI(OAc)_2$	2	65	NDP

Table 1.2 (cont'd)

3	Oxone	1	65	NDP
4	Fe_2O_3	1	65	NDP
5	MnO_2	1	65	NDP
6[a]	I_2	1	110	NDP
7	NBS	1	65	37
8	**NBS**	**2**	**65**	**64**
9	NBS	2.5	65	63
10	DBDMH	2	65	48
11	*N*-bromoacetamide	2	65	trace
12	*N*-bromosaccharine	2	65	13
13	Br_2	2	65	trace

NDP: No desired product. [a]reaction was ran in DMSO

Using different substituted styrene epoxides (**1-1**) as shown in **Scheme 1.2**, both electron withdrawing and electron donating groups are well tolerated and leading to the corresponding pyrazoles in 45-67% yields (**1-3b – 1-3g**). Epoxides with electron donation group such as 4-methoxy styrene oxide and 4-ethyl styrene oxide gave good yields, 62% and 67% respectively (**1-3b** – **1-3c**). This is possibly due to the increased in rate of the in-situ formed aldehydes from the epoxides. Epoxide with poor electron withdrawing groups gave lower yields (**1-3d** – **1-3g**) and when strong electron withdrawing groups like 4-NO_2 (**1-3h**) and 4-CF_3 (**1-3i**) were used, the reaction did not provide any desired product. It is also important to note that alkyl epoxides did not provide any desired product as well.

Scheme 1.2: Substrate scope for pyrazole synthesis

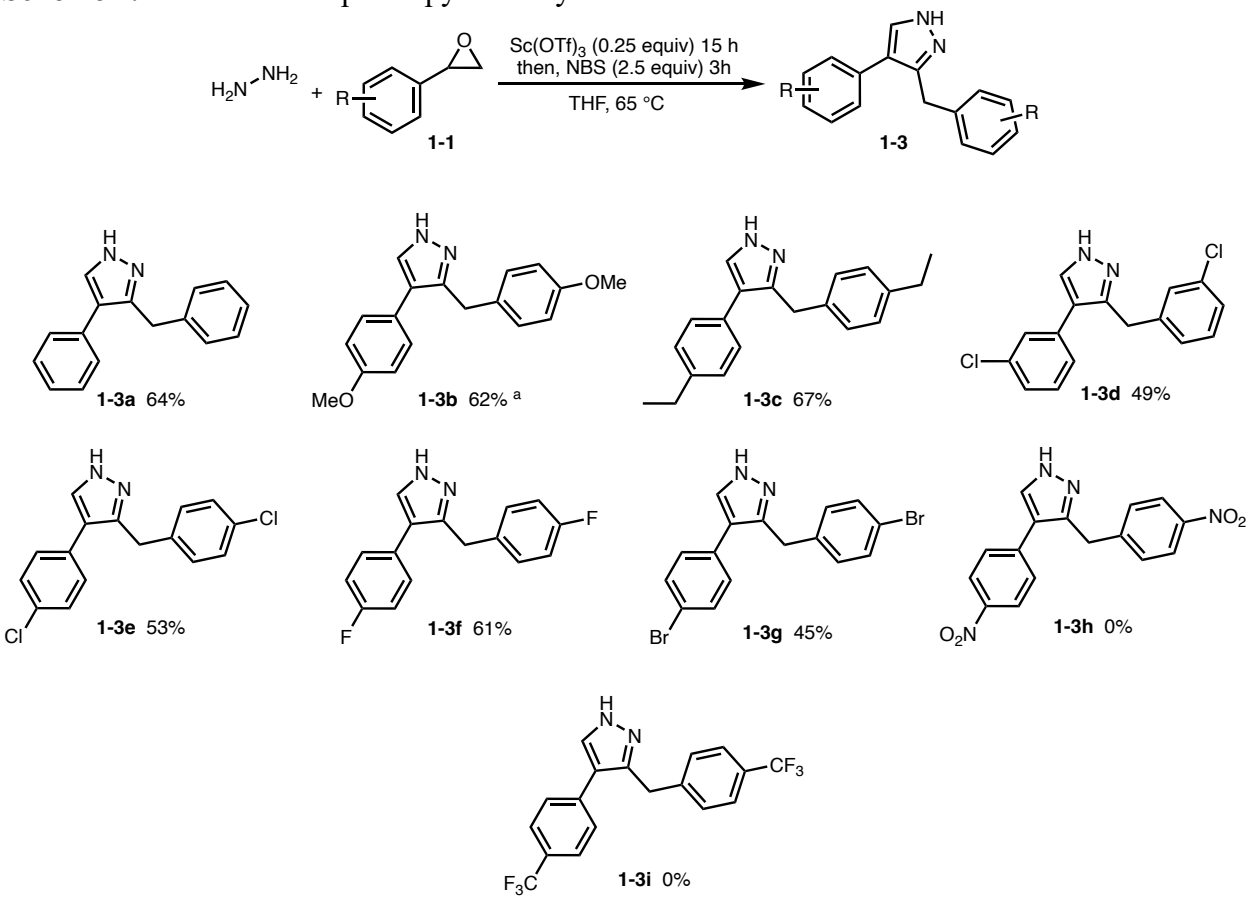

[a]1.2 equiv of NBS was used.

While earlier study[31] suggests that the reaction begins with the transformation of epoxides into aldehydes, the complete mechanism remains unclear. In the attempt to determine the plausible mechanism of the reaction, we have found that when phenylhydrazine (**1-4**) was treated with **1-1a**, the reaction provided the Fischer indole[36] product **1-5** (**Scheme 1.3**) in excellent yield (83%).[37] This result indicates the possible formation of hydrazone, as a key intermediate in the reaction mechanism. To further explore this, we found that treatment of cinnamaldehyde **1-6** with hydrazine under the optimized reaction condition afforded 97% of the pyrazoline product **1-7**.

Scheme 1.3: Synthesis of indole and pyrazoline

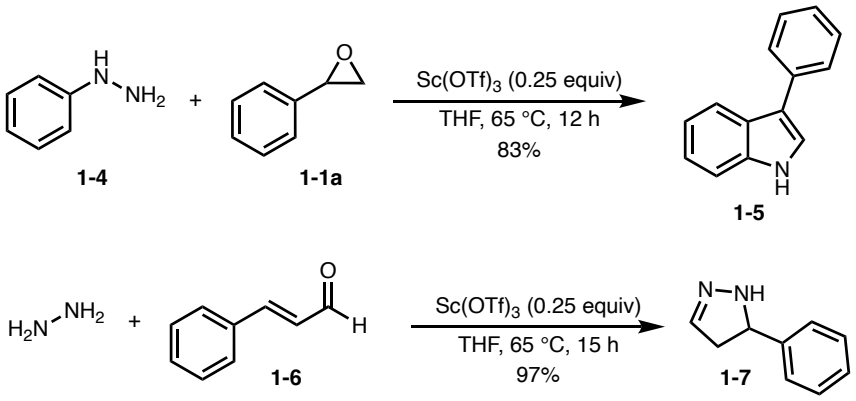

Therefore, based on the observed results (See mechanistic experiment 1 – 4 in experimental section), as well as from previous report (See reference 31: supplemental, mechanistic experiment 3) two plausible mechanisms are proposed in **Scheme 1.4**. The reaction is initiated following the rapid *in situ* generations of aldehyde **I**, which further converts to hydrazone **II** in the proposed **pathway 1**.[38] The intermediate **II** and its tautomer or enol **III** could then undergo a Mannich-type reaction to generate intermediate **IV**. Further cyclization (a 5-exo-trig cyclization) and dehydration or elimination of hydrazine in **IV** produced the intermediate pyrazoline. Due to the pyrazole formation being observed only with the *N*-Br reagents, the reaction may form the intermediate **VI** upon treatment with NBS. Finally, deprotonation and isomerization of **VI** generate the pyrazole. Alternatively, **pathway 2**, the hydrazine could undergo double condensation with two molecules of aldehyde **I** to generate intermediate **VIII**. This intermediate could undergo cyclization to give the pyrazoline intermediate. However, such cyclization would invoke an unfavored 5-endo-trig cyclization. However, if the cyclization of intermediate **VIII** proceeds through carbocation formation, then **pathway 2** could be another possible mechanism to access the pyrazole (**Scheme 1.3** eq 2, see also mechanistic experiment 1 and 2 in experimental).

Scheme 1.4: Proposed mechanisms for pyrazole synthesis

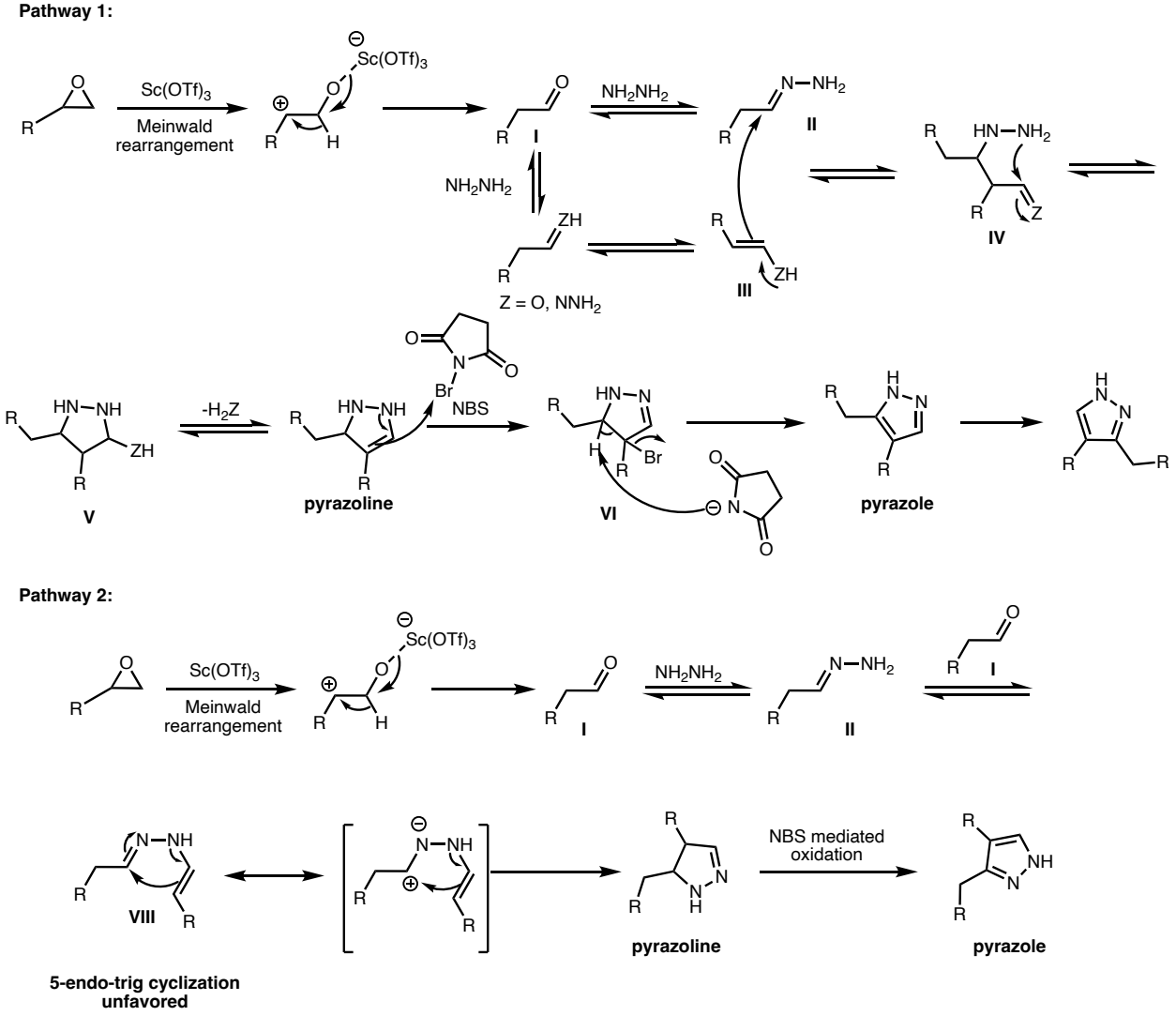

1.2.2 Synthesis of 3,5-disubstituted pyridines

To further extend the scope of this reaction, we expanded the methodology to a Chichibabin-type pyridine synthesis (**Scheme 1.1d**) using epoxides and ammonia instead of hydrazine. We started by treating three equivalents of epoxides with ammonia using the optimized condition as in the pyrazoline synthesis. This reaction provided 52% of the desired pyridine **1-4a** (**Table 1.3**, **entry 3**). Further optimization gave 83% of desired product when two equivalent of ammonia solution was used with 0.125 equiv of $Sc(OTf)_3$ at 110 °C (**Table 1.3**, **entry 8**). Previous study reported $FeCl_3$ to facilitate debenzylation at the C-2 position of the quinolines[31-32], based on

these reports, addition of 0.5 equivalent of $FeCl_3$ was used to increase the *in situ* dealkylation at the C-2 position of the pyridine leading to increased reaction yield, up to 94% (**Table 1.3**, **entry 10**).

Table 1.3: Optimization of pyridine synthesis

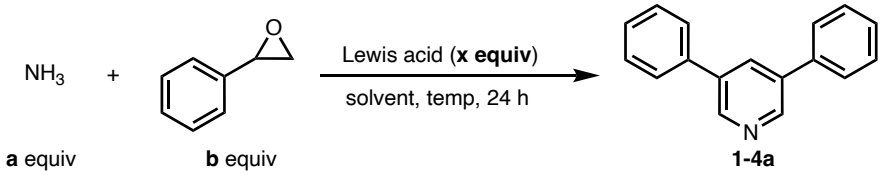

entry	a	b	solvent	Lewis Acid	x	temp (°C)	yield %
1	1	3	THF	$Sc(OTf)_3$	0.5	65	43
2	1	4	THF	$Sc(OTf)_3$	0.5	65	50
3	1	4	THF	$Sc(OTf)_3$	0.25	65	52
4	1	4	1,4-Dioxane + THF	$Sc(OTf)_3$	0.25	110	39
5	1	1	1,4-Dioxane + THF	$Sc(OTf)_3$	0.25	110	53
6	2	1	THF	$Sc(OTf)_3$	0.25	65	54
7	2	1	1,4-Dioxane + THF	$Sc(OTf)_3$	0.25	110	70
8	2	1	1,4-Dioxane + THF	$Sc(OTf)_3$	0.125	110	83
9	2	1	1,4-Dioxane + THF	$Sc(OTf)_3$ + $FeCl_3$	0.125 + 0.25	110	91

Table 1.3 (cont'd)

10	2	1	1,4-Dioxane + THF	$Sc(OTf)_3$ + $FeCl_3$	0.125 + 0.5	110	94
11	2	1	1,4-Dioxane + THF	$FeCl_3$	0.5	110	57
12	2	1	1,4-Dioxane + THF	$FeCl_3$	1	110	45

After the optimization of the reaction condition, we explored the reaction scope (**Scheme 1.5**) by treating various epoxides **1-1** with ammonia solution under the optimized condition. Similar to the result obtained from the pyrazole reaction scope, electron-donating group on phenyl ring gave good yields (**1-4b**) while electron withdrawing group gave lower yields (**1-4c-g**). It is important to mention that a moderate yield of 55% of the pyridine was isolated with 2-chlorostyrene oxide was used, likely due to the steric effect of chlorine at the *ortho* position.

Scheme 1.5: Substrate scope of the pyridine synthesis

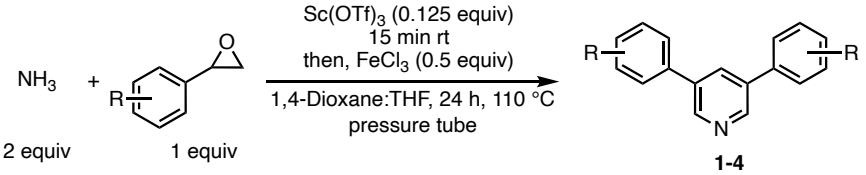

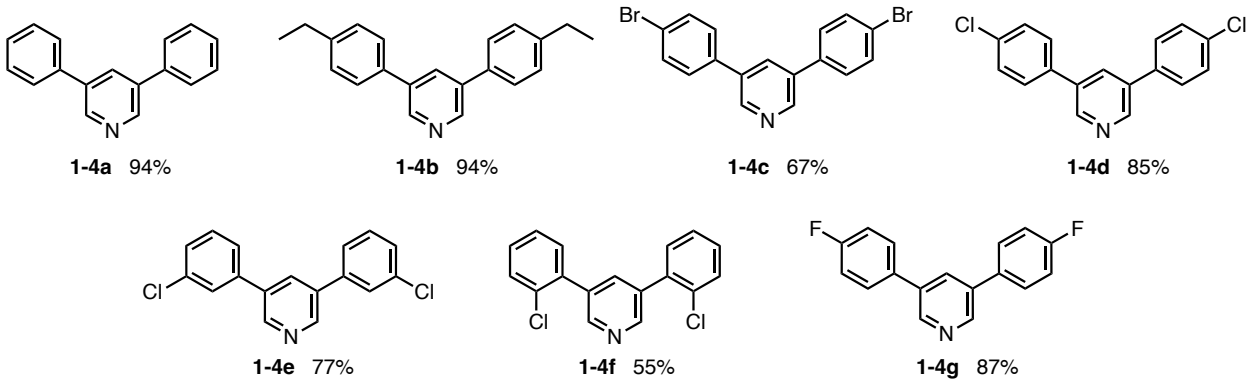

Based on the observed results (See mechanistic experiment 5 in experimental) we proposed a plausible mechanism in **Scheme 1.6**. Similar to the pyrazole synthesis, at first, the reaction initiated by rapid formation of aldehyde **I**, which undergoes condensation with ammonia to give imine **II**. A Mannich-type reaction between the generated imine **II** and the enol tautomer or enamine **III** could generate intermediate **IV**. After that, the condensation of another aldehyde **I** to the intermediate **IV**, followed by tautomerism and cyclization generates the intermediate **VI**. Elimination of ammonia or dehydration of **VI** forms the intermediate **VII**. Finally, debenzylation[27,32,39] at the C-2 position provides the final pyridine product.

Scheme 1.6: Proposed mechanism for the synthesis of pyridine

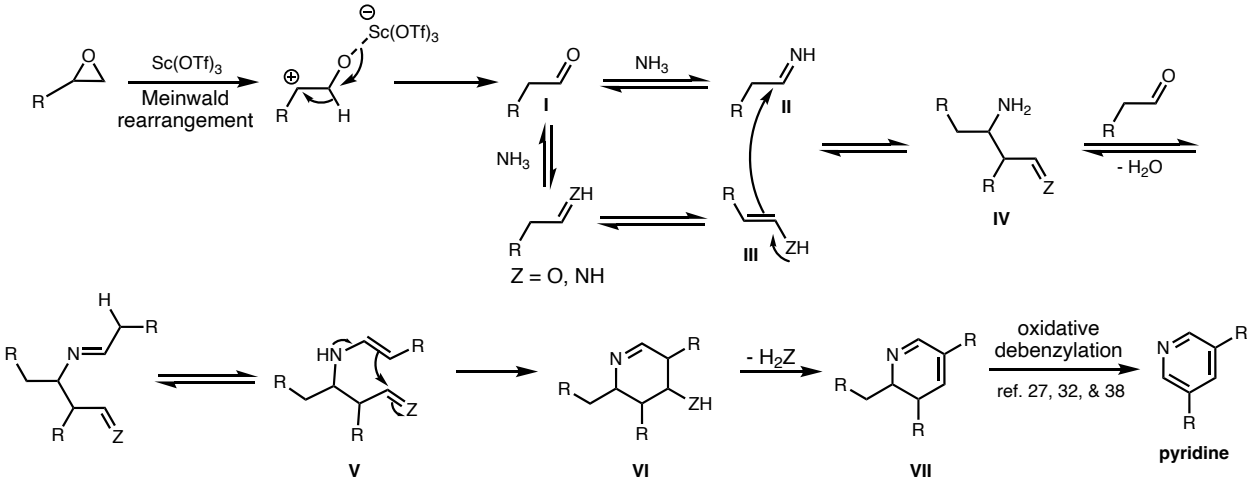

1.3 Conclusions

In conclusion, we have established a new approach to synthesis 3,4-disubstituted 1H-pyrazoles and 3,5-disubstituted pyridines using easily accessible epoxides as the starting material. These reactions accommodate a range of aromatic epoxides, producing the corresponding pyrazole and pyridine product with moderate to excellent yields.

1.4 Experimental section

General information

Commercially available reagents were used without additional purification. All reactions were performed under an argon atmosphere with commercial-grade reagents. All chemicals and solvents were purchased from commercial sources and used without further purification. Styrene oxide (1a) (CAS no. 96-09-3), phenylhydrazine (5) (CAS no. 100-63-0), and *trans*-cinnamaldehyde (7) (CAS no. 14371-10-9) were purchased from Sigma Aldrich. Scandium(III) triflate (CAS no. 144026-79-9), *N*-bromosuccinimide (CAS no. 128-08-5), and iron(III) chloride anhydrous (CAS no. 7705-08-0) were purchased from Oakwood Chemicals. Other epoxides were purchased from Enamine. N-bromosuccinimide was recrystallized before use and stored in the dark. THF was dried under 3Å molecular sieve and checked for any water content before using it in the reaction. All flasks were

oven-dried overnight and cooled under argon. Hydrazine monohydrate (N_2H_4 64-65 %, reagent grade, 98%) was purchased from Sigma Aldrich and used in all pyrazole reactions. A 0.4 M solution of ammonia in THF was purchased from Sigma Aldrich and used in all pyridine reactions. All NMR spectra were recorded on a 500 MHz spectrometer. Signal multiplicities are given as s (singlet), bs (broad singlet), d (doublet), t (triplet), dd (doublet of doublet), and m (multiplet). The mass spectrometer ionization method was ESI with a Quadrupole detector and infrared spectra were recorded on a Jasco Series 6600 FTIR spectrometer.

General method for the synthesize of 1H-pyrazoles (1-3)

To a solution of dry tetrahydrofuran (THF) (5 mL) in a 50 mL dry round bottom flask, different substituted epoxides (2 equiv, 1 mmol) were added, followed by $Sc(OTf)_3$ (0.25 equiv, 0.125 mmol) at room temperature. After 15 minutes, hydrazine monohydrate (1 equiv, 0.5 mmol) was added at room temperature. The reaction was placed under argon gas and was refluxed for 15 hours at 65 °C in oil bath. Then, *N*-bromosuccinimide (NBS) (2.5 equiv, 1.25 mmol) was added and stirred for 3 hours at 65 °C. After that, the reaction mixture was cooled to room temperature and the solvent was evaporated under reduced pressure. Then 10 mL of dichloromethane and 10 mL saturated $NaHCO_3$ solution was added, and the solution was extracted with 3×10 mL of dichloromethane. The combined organic layer was collected and evaporated under reduced pressure and crude products were purified by column chromatography.

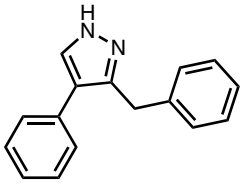

3-benzyl-4-phenyl-1H-pyrazole (**1-3a**): Purified with automated CombiFlash chromatography (silica gel, 20-40 microns, gradient 25% ethyl acetate in hexane) to give yellow solid (75 mg,

64%). mp = 135 – 137 °C. ^{1}H NMR (500 MHz, CD_2Cl_2) δ 7.56 (s, 1H), 7.30 – 7.26 (m, 4H), 7.23 – 7.08 (m, 6H), 4.09 (s, 2H). $^{13}C\{^{1}H\}$ NMR (125 MHz, CD_2Cl_2) δ 141.2, 137.8, 133.8, 132.5, 127.91, 127.85, 127.8, 126.9, 125.8, 125.6, 119.5, 31.0. IR (neat, cm^{-1}): 3125, 2964, 1606, 1521, 1259. HRMS (ESI-TOF) m/z: $[M+H]^+$ calcd for ($C_{16}H_{15}N_2^+$) 235.1230; Found 235.1239.

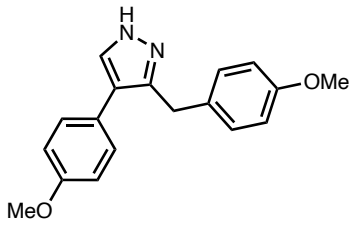

3-(4-methoxybenzyl)-4-(4-methoxyphenyl)-1H-pyrazole (**1-3b**): Purified with automated CombiFlash chromatography (silica gel, 20-40 microns, gradient 40% ethyl acetate in hexane) to give yellow oil (91 mg, 62%). ^{1}H NMR (500 MHz, CD_2Cl_2) δ 7.60 (s, 1H), 7.31 (d, *J* = 8.7 Hz, 2H), 7.10 (d, *J* = 8.7 Hz, 2H), 6.92 (d, *J* = 8.7 Hz, 2H), 6.83 (d, *J* = 8.7 Hz, 2H), 4.09 (s, 2H), 3.82 (s, 3H), 3.77 (s, 3H). $^{13}C\{^{1}H\}$ NMR (125 MHz, CD_2Cl_2) δ 158.3, 142.0, 134.3, 130.6, 129.5, 128.8, 126.7, 125.7, 119.7, 113.98, 113.96, 55.20, 55.15, 30.8. IR (neat, cm^{-1}): 3143, 2907, 1610, 1509, 1241. HRMS (ESI-TOF) m/z: $[M+H]^+$ calcd for ($C_{18}H_{19}N_2O_2^+$) 295.1441; found 295.1449.

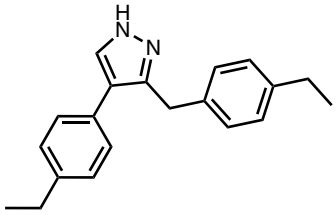

3-(4-ethylbenzyl)-4-(4-ethylphenyl)-1H-pyrazole (**1-3c**): Purified with automated CombiFlash chromatography (silica gel, 20-40 microns, gradient 35% ethyl acetate in hexane) to give a clear oil (97 mg, 67%). ^{1}H NMR (500 MHz, CD_2Cl_2) δ 7.45 (s, 1H), 7.19 (d, *J* = 8.1 Hz, 2H), 7.10 (d, *J* = 8.1 Hz, 2H), 7.02 (d, *J* = 8.1 Hz, 2H), 6.98 (d, *J* = 8.1 Hz, 2H), 4.02 (s, 2H), 2.55 (q, *J* = 7.6 Hz, 2H), 2.50 (q, *J* = 7.6 Hz, 2H), 1.14 (t, *J* = 7.6 Hz, 3H), 1.09 (t, *J* = 7.6 Hz, 3H). $^{13}C\{^{1}H\}$ NMR (125 MHz, CD_2Cl_2) δ 141.8, 141.7, 141.0, 135.1, 133.8, 129.8, 127.7, 127.32, 127.31, 126.8,

119.3, 30.4, 27.7, 27.6, 14.68, 14.66. IR (neat, cm^{-1}): 3019, 2922, 1614, 1513. HRMS (ESI-TOF) m/z: $[M+H]^+$ calcd for ($C_{20}H_{23}N_2^+$) 291.1856; Found 291.1863.

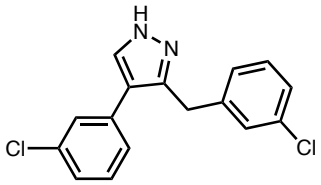

3-(3-chlorobenzyl)-4-(3-chlorophenyl)-1H-pyrazole (**1-3d**): Purified with automated CombiFlash chromatography (silica gel, 20-40 microns, gradient 30% ethyl acetate in hexane) to give a clear oil (74 mg, 49%). ^1H NMR (500 MHz, CD_2Cl_2) δ 7.57 (s, 1H), 7.25 – 7.19 (m, 2H), 7.18 – 7.10 (m, 4H), 7.08 (s, 1H), 6.98 (d, J = 6.5 Hz, 1H), 4.04 (s, 2H). $^{13}C\{^1H\}$ NMR (125 MHz, CD_2Cl_2) δ 142.2, 139.9, 134.2, 133.5, 132.3, 129.19, 129.17, 127.8, 126.9, 126.1, 125.9, 125.7, 125.6, 125.2, 118.6, 30.9. IR (neat, cm^{-1}): 3153, 2961, 1599, 1260. HRMS (ESI-TOF) m/z: $[M+H]^+$ calcd for ($C_{16}H_{13}Cl_2N_2^+$) 303.0451, 305.0521; Found 303.0459, 305.0432.

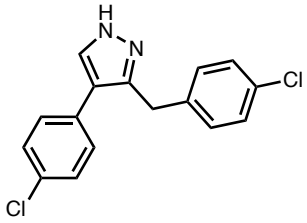

3-(4-chlorobenzyl)-4-(4-chlorophenyl)-1H-pyrazole (**1-3e**): Purified with automated CombiFlash chromatography (silica gel, 20-40 microns, gradient 30% ethyl acetate in hexane) to give a light yellow oil (80 mg, 53%). ^1H NMR (500 MHz, CD_2Cl_2) δ 7.48 (s, 1H), 7.24 – 7.21 (m, 2H), 7.17 – 7.10 (m, 4H), 6.98 – 6.95 (m, 2H), 3.99 (s, 2H). $^{13}C\{^1H\}$ NMR (125 MHz, CD_2Cl_2) δ 141.9, 136.5, 132.4, 131.4, 130.9, 129.0, 128.2, 128.04, 127.96, 127.9, 118.7, 30.4. IR (neat, cm^{-1}): 3133, 2920, 1601, 1489. HRMS (ESI-TOF) m/z: $[M+H]^+$ calcd for ($C_{16}H_{13}Cl_2N_2^+$) 303.0451, 305.0521; Found 303.0458, 305.0431.

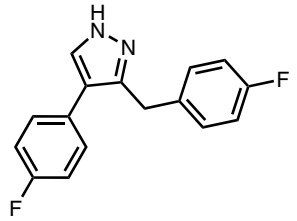

3-(4-fluorobenzyl)-4-(4-fluorophenyl)-1H-pyrazole (**1-3f**): Purified with automated CombiFlash chromatography (silica gel, 20-40 microns, gradient 30% ethyl acetate in hexane) to give a white solid (82 mg, 61%). mp = 88 – 90 °C. ^{1}H NMR (500 MHz, CD_2Cl_2) δ 7.50 (s, 1H), 7.21 – 7.17 (m, 2H), 7.04 – 6.92 (m, 4H), 6.90 – 6.82 (m, 2H), 4.00 (s, 2H). $^{13}C\{^{1}H\}$ NMR (125 MHz, CD_2Cl_2) δ161.9 (d, *J* = 244.0 Hz), 161.8 (d, *J* = 243.0 Hz), 133.7, 132.7, 129.2 (d, *J* = 8.0 Hz), 128.7 (d, *J* = 8.0 Hz), 128.49, 128.46, 118.8, 114.7 (d, *J* = 21.0 Hz), 114.6 (d, *J* = 21.0 Hz), 30.2. IR (neat, cm^{-1}): 3036, 2916, 1607, 1506, 1220. HRMS (ESI-TOF) m/z: $[M+H]^+$ calcd for ($C_{16}H_{13}F_2N_2^+$) 271.1041; Found 271.1049.

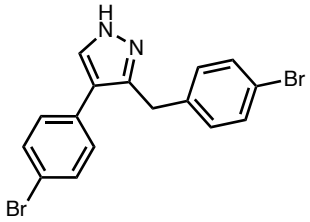

3-(4-bromobenzyl)-4-(4-bromophenyl)-1H-pyrazole (**1-3g**): Purified with automated CombiFlash chromatography (silica gel, 20-40 microns, gradient 30% ethyl acetate in hexane) to give a white solid (88 mg, 45%). mp: 152 – 154 °C. ^{1}H NMR (500 MHz, CD_2Cl_2) δ 7.51 (s, 1H), 7.40 (d, *J* = 8.5 Hz, 2H), 7.30 (d, *J* = 8.4 Hz, 2H), 7.12 (d, *J* = 8.5 Hz, 2H), 6.94 (d, *J* = 8.4 Hz, 2H), 3.99 (s, 2H). $^{13}C\{^{1}H\}$ NMR (125 MHz, CD_2Cl_2) δ 142.1, 137.0, 132.4, 131.3, 131.0, 130.9, 129.5, 128.6, 119.5, 118.8, 30.6. IR (neat, cm^{-1}): 3127, 2922, 1517, 1486, 1259. HRMS (ESI-TOF) m/z: $[M+H]^+$ calcd for ($C_{16}H_{13}Br_2N_2^+$) 390.9440, 392.9420; Found 390.9450, 392.9427.

Mechanistic experiments for pyrazole

Experiment 1

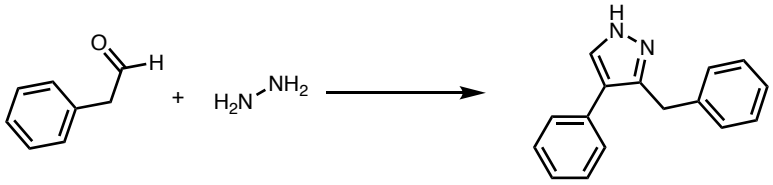

3-benzyl-4-phenyl-1*H*-pyrazole (**1-3a**): To a solution of dry tetrahydrofuran (THF) (5 mL) in a 50 mL dry round bottom flask, phenylacetaldehyde (2 equiv, 2 mmol) was added, followed by $Sc(OTf)_3$ (0.25 equiv, 0.25 mmol) at room temperature. After 15 minutes, hydrazine monohydrate (1 equiv, 1 mmol) was added at room temperature. The reaction was placed under argon gas and was refluxed for 15 hours at 65 °C in oil bath. Then, *N*-bromosuccinimide (NBS) (2.5 equiv, 2.5 mmol) was added and stirred for 3 hours at 65 °C. After that, the reaction mixture was cooled to room temperature and the solvent was evaporated under reduced pressure. Then 15 mL of dichloromethane and 15 mL saturated $NaHCO_3$ solution was added, and the solution was extracted with 3×15 mL of dichloromethane. The combined organic layer was collected and evaporated under reduced pressure and the crude product was purified using automated CombiFlash chromatography (silica gel, 20-40 microns, gradient 25% ethyl acetate in hexane) to yield the desired product (117 mg, 50%).

Experiment 2

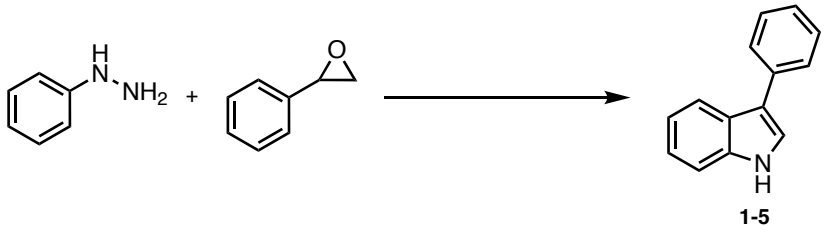

3-phenyl-1H-indole (**1-5**): To a solution of dry tetrahydrofuran (THF) (5 mL) in a 50 mL dry round bottom flask, styrene oxide **1-1a** (2 equiv, 1 mmol) was added, followed by $Sc(OTf)_3$ (0.25

equiv, 0.125 mmol) at room temperature. After 15 minutes, phenylhydrazine **1-4** (1 equiv, 0.5 mmol) was added at room temperature. The reaction was placed under argon gas and was refluxed for 12 hours at 65 °C under air in the oil bath. After that, the reaction mixture was cooled to room temperature and the solvent was evaporated under reduced pressure. Then 10 mL of dichloromethane and 10 mL saturated $NaHCO_3$ solution was added, and the solution was extracted with 3×10 mL of dichloromethane. The combined organic layer was collected and evaporated under reduced pressure and the crude product 3-phenylindole (**1-5**) was purified using automated CombiFlash chromatography (silica gel, 20-40 microns, gradient 10% ethyl acetate in hexane) to give a light brown solid (80 mg, 83%). mp = 85 – 86 °C. ^{1}H NMR (500 MHz, CD_2Cl_2) δ 8.13 (bs, 1H), 7.82 (d, *J* = 8.0 Hz, 1H), 7.60 – 7.52 (m, 2H), 7.35 – 7.30 (m, 2H), 7.28 (d, *J* = 8.0 Hz, 1H), 7.22 (d, *J* = 2.6 Hz, 1H), 7.18 – 7.14 (m, 1H), 7.14 – 7.10 (m, 1H), 7.08 – 7.05 (m, 1H). ^{13}C{^{1}H} NMR (125 MHz, CD_2Cl_2) δ 135.9, 134.8, 128.0, 126.5, 125.1, 124.7, 121.5, 121.2, 119.4, 118.8, 117.0, 110.7. IR (neat, cm^{-1}): 3398, 3051, 1594, 1453, 1260. HRMS (ESI-TOF) m/z: $[M+H]^+$ calcd for ($C_{14}H_{12}N^+$) 194.0964; Found 194.0966. The spectroscopic data are consistence with previous literature reports.[40]

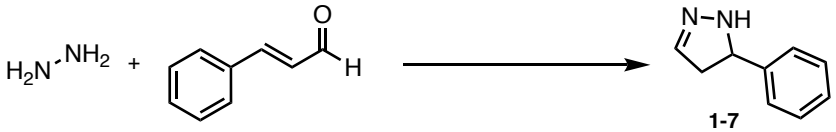

1-7

5-phenyl-4,5-dihydro-1H-pyrazole (**1-7**): To a solution of dry tetrahydrofuran (THF) (5 mL) in a 50 mL dry round bottom flask, cinnamaldehyde (**1-6**) (2 equiv, 1 mmol) was added, followed by $Sc(OTf)_3$ (0.25 equiv, 0.125 mmol) at room temperature. After 15 minutes, hydrazine monohydrate (1 equiv, 0.5 mmol) was added at room temperature. The reaction was placed under argon gas and was refluxed for 15 hours at 65 °C in oil bath. After that, the reaction mixture was cooled to room temperature and the solvent was evaporated under reduced pressure. Then 10 mL of

dichloromethane and 10 mL saturated $NaHCO_3$ solution was added, and the solution was extracted with 3×10 mL of dichloromethane. The combined organic layer was evaporated under reduced pressure and the crude product was purified using automated CombiFlash chromatography (silica gel, 20-40 microns, gradient 35% ethyl acetate in hexane) to give a yellow oil (71 mg, 97%). ^{1}H NMR (500 MHz, CD_2Cl_2) δ 7.23 – 7.18 (m, 4H), 7.17 – 7.15 (m, 1H), 6.65 (t, *J* = 1.6 Hz, 1H), 5.70 (s, 1H), 4.59 (dd, *J* = 10.5, 9.5 Hz, 1H), 2.99 (ddd, *J* = 17.1, 10.5, 1.6 Hz, 1H), 2.54 (ddd, *J* = 17.1, 9.5, 1.6 Hz, 1H). ^{13}C{^{1}H} NMR (125 MHz, CD_2Cl_2) δ 142.3, 141.7, 127.8, 126.6, 125.5, 61.6, 41.9. IR (neat, cm^{-1}): 3032, 2961, 1645, 1586. HRMS (ESI-TOF) m/z: $[M+H]^+$ calcd for ($C_9H_{11}N_2^+$) 147.0917; Found 147.0923.

Experiment 3

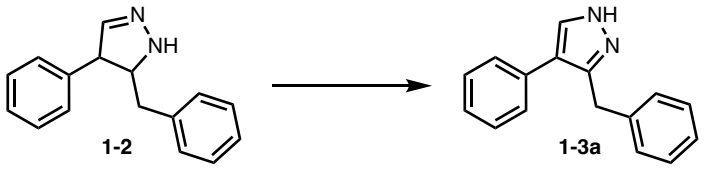

3-benzyl-4-phenyl-1*H*-pyrazole (**1-3a**): To a solution of dry tetrahydrofuran (THF) (5 mL) in a 50 mL dry round bottom flask, a mixture of *cis* and *trans 3-benzyl-4-phenyl-4,5-dihydro-1H-pyrazole* (**1-2**) (1 equiv, 0.5 mmol) was added. Then, *N*-bromosuccinimide (NBS) (2 equiv, 1 mmol) was added and stirred for 3 hours at 65 °C. After that, the reaction mixture was cooled to room temperature and the solvent was evaporated under reduced pressure. Then 15 mL of dichloromethane and 15 mL water was added, and the solution was extracted with 3×15 mL of dichloromethane. The combined organic layer was collected and evaporated under reduced pressure and the crude product (**1-3a**) was purified using automated CombiFlash chromatography (silica gel, 20-40 microns, gradient 25% ethyl acetate in hexane) to yield the desired product (109 mg, 93%).

Experiment 4

To a solution of dry tetrahydrofuran (THF) (1 mL) in a 4 mL vial, styrene oxide (2 equiv, 0.1 mmol) were added, followed by $Sc(OTf)_3$ (0.25 equiv, 0.0125 mmol) at room temperature. After that, hydrazine monohydrate (1 equiv, 0.05 mmol) was added at room temperature. The reaction was placed under argon gas and was refluxed for 2 hours at 65 °C in oil bath. Then, a crude mass was checked using a mass spectrometer by ESI (+) method with a Quadrupole detector (**Figure 1.2**) Then, *N*-bromosuccinimide (NBS) (2.5 equiv, 0.125 mmol) was added and another crude mass spec was checked after 15 mins (**Figure 1.3**).

Figure 1.2: Mass spec after 2h of addition of hydrazine

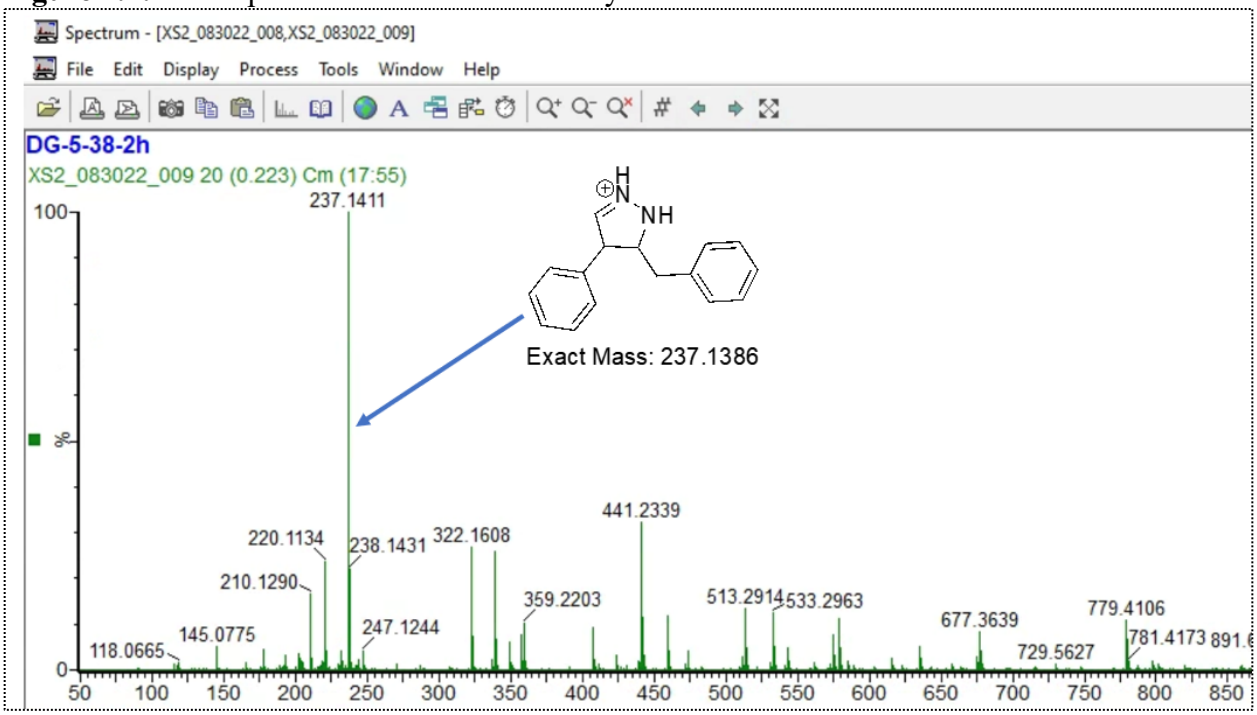

Figure 1.3: Mass spec after addition of NBS

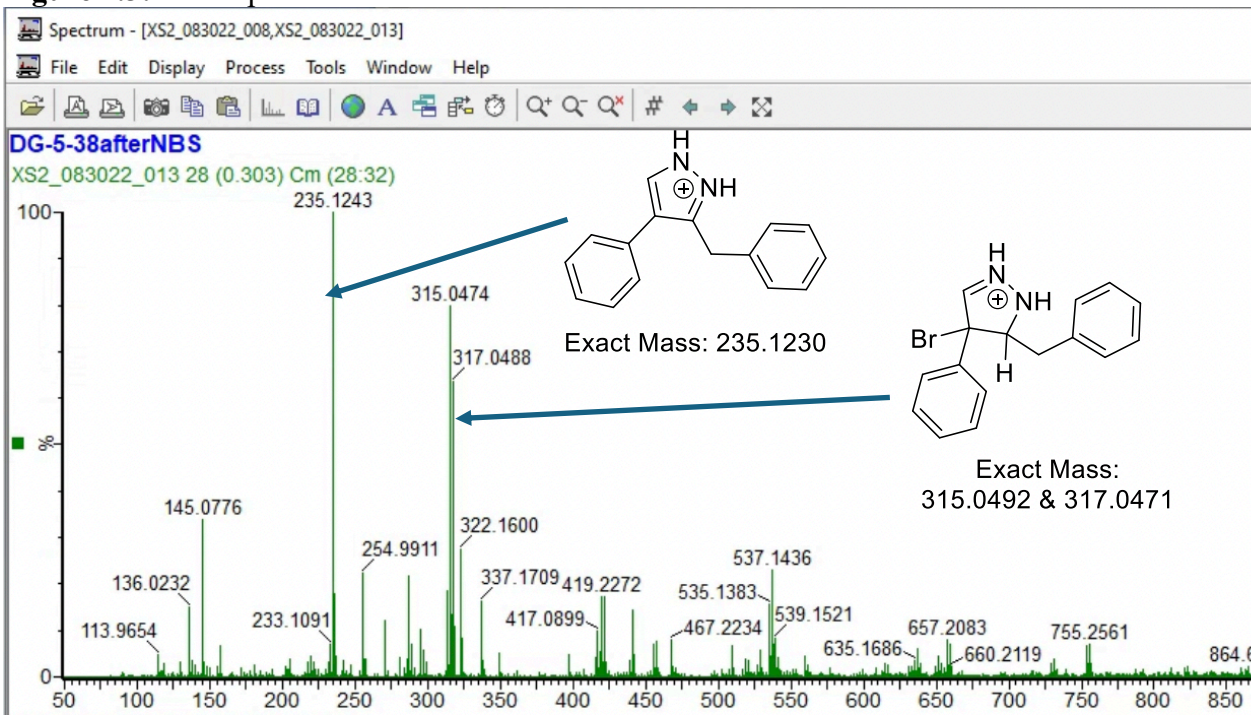

General method for the synthesize of pyridines (1-4)

To a solution of dry 1,4-dioxane (2 mL) in a 50 mL dry pressure tube, different substituted epoxides (1 equiv, 1 mmol) were added, followed by $Sc(OTf)_3$ (0.125 equiv, 0.125 mmol) at room temperature. After 15 minutes, 0.4 M ammonia in tetrahydrofuran (THF) solution (2 equiv, 2 mmol, 5 mL) was added dropwise, followed by $FeCl_3$ (0.5 equiv, 0.5 mmol) was added at room temperature. The pressure tube was then sealed and placed in an oil bath. Then, the temperature of the oil bath was slowly (in 30 minutes) raised to 110 °C and the reaction was run for 24 hours at 110 °C. After that, the reaction mixture was cooled to room temperature and the solvent was evaporated under reduced pressure. Then 10 mL of dichloromethane and 10 mL saturated $NaHCO_3$ solution was added, and the solution was extracted with 3×10 mL of dichloromethane. The combined organic layer was collected and evaporated under reduced pressure and crude products

were purified using automated CombiFlash chromatography (silica gel, 20-40 microns, gradient 7.5-12.5% ethyl acetate in hexane).

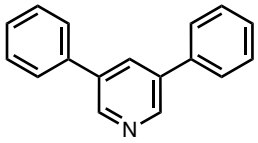

3,5-diphenylpyridine (**1-4a**)[26]: Purified with automated CombiFlash chromatography (silica gel, 20-40 microns, gradient 7.5% ethyl acetate in hexane) to give a light yellow solid (72 mg, 94%). mp = 132 – 135 °C. ^{1}H NMR (500 MHz, $CDCl_3$) δ 8.84 (d, *J* = 1.8 Hz, 2H), 8.06 (t, *J* = 1.8 Hz, 1H), 7.65 (d, *J* = 7.5 Hz, 4H), 7.51 (t, *J* = 7.5 Hz, 4H), 7.44 (t, *J* = 7.5 Hz, 2H). ^{13}C{^{1}H} NMR (125 MHz, $CDCl_3$) δ 146.9, 137.6, 136.5, 132.8, 129.0, 128.1, 127.1. IR (neat, cm^{-1}): 3056, 3034, 2957, 1576. HRMS (ESI-TOF) m/z: $[M+H]^+$ calcd for ($C_{17}H_{14}N^+$) 232.1121; Found 232.1129.

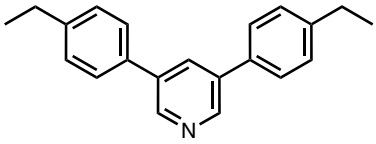

3,5-bis(4-ethylphenyl)pyridine (**1-4b**): Purified with automated CombiFlash chromatography (silica gel, 20-40 microns, gradient 12.5% ethyl acetate in hexane) to give a white solid (90 mg, 94%). mp = 130 – 132 °C. ^{1}H NMR (500 MHz, CD_2Cl_2) δ 8.69 (s, 2H), 7.99 – 7.95 (m, 1H), 7.51 (d, *J* = 7.7 Hz, 4H), 7.26 (d, *J* = 7.7 Hz, 4H), 2.63 (q, *J* = 7.6 Hz, 4H), 1.19 (t, *J* = 7.6 Hz, 6H). ^{13}C{^{1}H} NMR (125 MHz, CD_2Cl_2) δ 145.8, 143.8, 135.6, 134.4, 131.4, 127.8, 126.3, 27.8, 14.7. IR (neat, cm^{-1}): 3027, 2961, 1513, 1259. HRMS (ESI-TOF) m/z: $[M+H]^+$ calcd for ($C_{21}H_{22}N^+$) 288.1747; Found 288.1763.

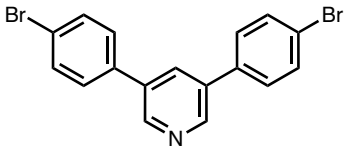

3,5-bis(4-bromophenyl)pyridine (**1-4c**): Purified with automated CombiFlash chromatography (silica gel, 20-40 microns, gradient 10% ethyl acetate in hexane) to give a white solid (87 mg, 67%). mp = 165 – 168 °C. ^{1}H NMR (500 MHz, CD_2Cl_2) δ 8.72 (d, *J* = 2.2 Hz, 2H), 7.93 (t, *J* = 2.2 Hz, 1H), 7.59 – 7.55 (m, 4H), 7.48 – 7.45 (m, 4H). ^{13}C{^{1}H} NMR (125 MHz, CD_2Cl_2) δ 146.3, 135.9, 134.7, 131.52, 131.47, 128.1, 121.8. IR (neat, cm^{-1}): 3069, 2962, 1590, 1486, 1258. HRMS (ESI-TOF) m/z: $[M+H]^+$ calcd for ($C_{17}H_{12}Br_2N^+$) 387.9331, 389.9311; Found 387.9341, 389.9326.

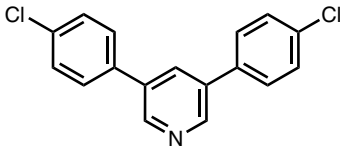

3,5-bis(4-chlorophenyl)pyridine (**1-4d**): Purified with automated CombiFlash chromatography (silica gel, 20-40 microns, gradient 10% ethyl acetate in hexane) to give a white solid (85 mg, 85%). mp = 170 – 172 °C. ^{1}H NMR (500 MHz, CD_2Cl_2) δ 8.71 (d, *J* = 2.2 Hz, 2H), 7.93 (t, *J* = 2.2 Hz, 1H), 7.55 – 7.51 (m, 4H), 7.46 – 7.37 (m, 4H). ^{13}C{^{1}H} NMR (125 MHz, CD_2Cl_2) δ 146.4, 135.5, 134.6, 133.6, 131.6, 128.5, 127.8. IR (neat, cm^{-1}): 3027, 2964, 1595, 1494, 1386. HRMS (ESI-TOF) m/z: $[M+H]^+$ calcd for ($C_{17}H_{12}Cl_2N^+$) 300.0341, 302.0312; Found 300.0350, 302.0323.

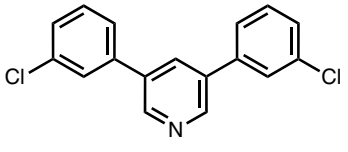

3,5-bis(3-chlorophenyl)pyridine (**1-4e**): Purified with automated CombiFlash chromatography (silica gel, 20-40 microns, gradient 10% ethyl acetate in hexane) to give a light yellow solid (77 mg, 77%). mp = 153 – 155 °C. ^{1}H NMR (500 MHz, CD_2Cl_2) δ 8.73 (t, *J* = 2.5 Hz, 2H), 7.95 – 7.94 (m, 1H), 7.63 – 7.54 (m, 2H), 7.50 – 7.46 (m, 2H), 7.42 – 7.30 (m, 4H). ^{13}C{^{1}H} NMR (125

MHz, CD_2Cl_2) δ 146.7, 138.7, 134.5, 134.1, 131.9, 129.7, 127.5, 126.5, 124.7. IR (neat, cm^{-1}): 3052, 2959, 1565, 1259. HRMS (ESI-TOF) m/z: $[M+H]^+$ calcd for ($C_{17}H_{12}Cl_2N^+$) 300.0352, 302.0326; Found 300.0350, 302.0323.

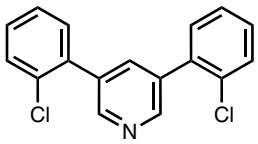

3,5-bis(2-chlorophenyl)pyridine (**1-4f**): Purified with automated CombiFlash chromatography (silica gel, 20-40 microns, gradient 10% ethyl acetate in hexane) to give a pale yellow solid (55 mg, 55%). mp = 132 – 134 °C. ^1H NMR (500 MHz, CD_2Cl_2) δ 8.60 (d, J = 2.1 Hz, 2H), 7.84 (t, J = 2.1 Hz, 1H), 7.49 – 7.41 (m, 2H), 7.36 – 7.34 (m, 2H), 7.33 – 7.30 (m, 3H), 7.29 – 7.27 (m, 1H). $^{13}C\{^1H\}$ NMR (125 MHz, CD_2Cl_2) δ 148.2, 136.8, 135.9, 133.5, 131.9, 130.7, 129.3, 128.8, 126.5. IR (neat, cm^{-1}): 3007, 2962, 1563, 1258. HRMS (ESI-TOF) m/z: $[M+H]^+$ calcd for ($C_{17}H_{12}Cl_2N^+$) 300.0341, 302.0312; Found 300.0349, 302.0322.

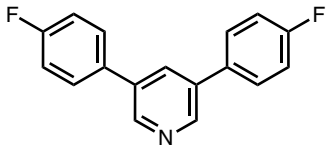

3,5-bis(4-fluorophenyl)pyridine (**1-4g**): Purified with automated CombiFlash chromatography (silica gel, 20-40 microns, gradient 10% ethyl acetate in hexane) to give a white solid (77 mg, 87%). mp = 170 – 171 °C. ^1H NMR (500 MHz, CD_2Cl_2)) δ 8.68 (d, J = 2.2 Hz, 2H), 7.91 (t, J = 2.2 Hz, 1H), 7.57 – 7.54 (m, 4H), 7.15 – 7.11 (m, 4H). $^{13}C\{^1H\}$ NMR (125 MHz, CD_2Cl_2) δ 163.2 (d, J = 246.0 Hz), 146.1, 135.0, 133.2, 131.6, 128.3 (d, J = 8.5 Hz), 115.3 (d, J = 21.5 Hz). IR (neat, cm^{-1}): 3087, 1603, 1512, 1223. HRMS (ESI-TOF) m/z: $[M+H]^+$ calcd for ($C_{17}H_{12}F_2N^+$) 268.0932; Found 268.0939.

Mechanistic experiments for pyridines

Experiment-5

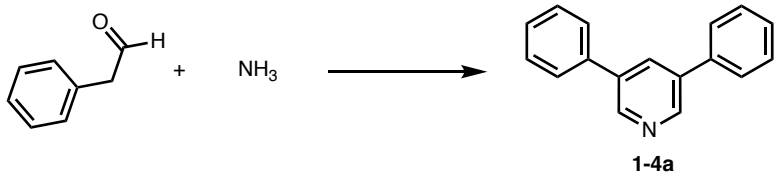

1-4a

3,5-diphenylpyridine (**1-4a**): To a solution of dry 1,4-dioxane (2 mL) in a 50 mL dry pressure tube, phenylacetaldehyde (1 equiv, 1 mmol) was added, followed by $Sc(OTf)_3$ (0.125 equiv, 0.125 mmol) at room temperature After 15 minutes, 0.4 M ammonia in THF solution (2 equiv, 2 mmol, 5 mL) was added dropwise, followed by $FeCl_3$ (0.5 equiv, 0.5 mmol) was added at room temperature. The pressure tube was then sealed and placed in an oil bath. Then, the temperature of the oil bath was slowly (in 30 minutes) raised to 110 °C and the reaction was run for 24 hours at 110 °C. After that, the reaction mixture was cooled to room temperature and the solvent was evaporated under reduced pressure. Then 10 mL of dichloromethane and 10 mL saturated $NaHCO_3$ solution was added, and the solution was extracted with 3×10 mL of dichloromethane. The combined organic layer was collected and evaporated under reduced pressure and the crude product (**1-4a**) was purified using automated CombiFlash chromatography (silica gel, 20-40 microns, gradient 7.5% ethyl acetate in hexane) to give the desired product (55 mg, 72%).

Experiment 6

To a solution of dry 1,4-dioxane (2.0 mL) in a 15 mL pressure tube, styrene oxide (1 equiv, 1.0 mmol) were added, followed by $Sc(OTf)_3$ (0.125 equiv, 0.125 mmol) at room temperature After 15 minutes, 0.4 M ammonia in tetrahydrofuran (THF) solution (2 equiv, 2 mmol, 5 mL) was added dropwise, followed by $FeCl_3$ (0.5 equiv, 0.5 mmol) was added at room temperature. The pressure tube was then sealed and placed in an oil bath. Then, the temperature of the oil bath was slowly

(in 30 minutes) raised to 110 °C and the reaction was run for 1 hours at 110 °C. After that, a crude mass was checked using a mass spectrometer by ESI (+) method with a Quadrupole detector (**Figure 1.4)**.

Figure 1.4: Mass spec after 1h of the pyridine synthesis reaction

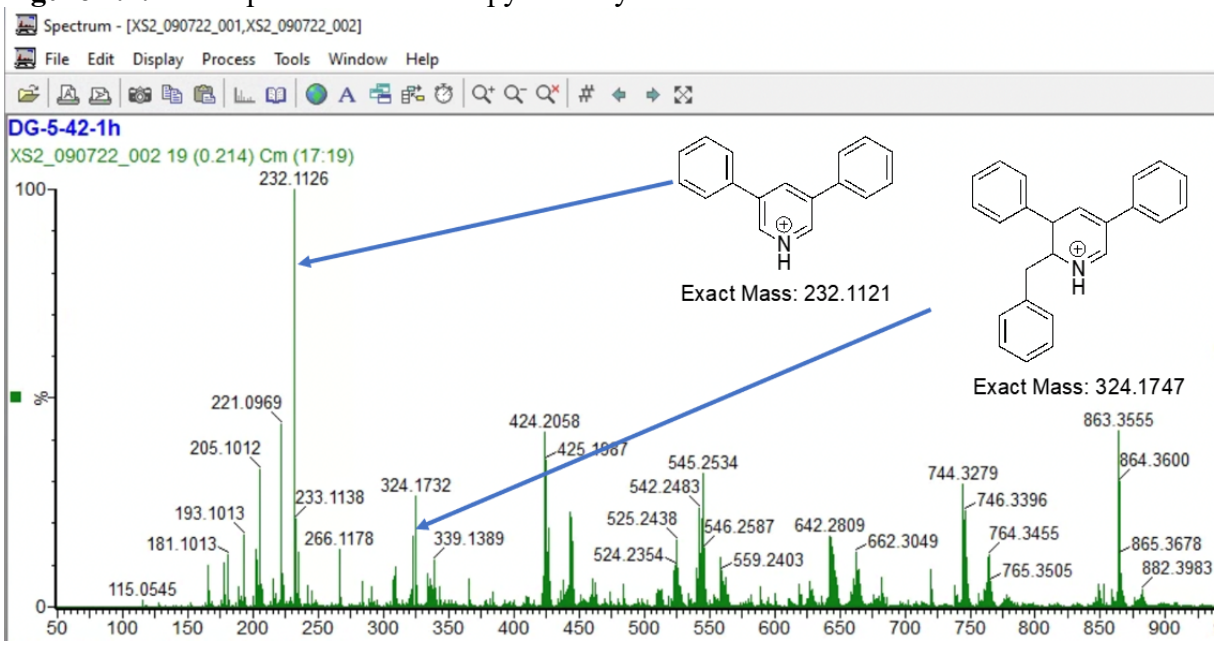

REFERENCES

1. Kajita, Y.; Ikeda, S.; Yoshikawa, M.; Fukuda, H.; Watanabe, E.; Yano, J.; Lane, W.; Miyamoto, M.; Ishii, T.; Nishi, T.; et al., *J. Med. Chem.* **2022**, *65*, 3343-3358.

2. Di Fruscia, P.; Carbone, A.; Bottegoni, G.; Berti, F.; Giacomina, F.; Ponzano, S.; Pagliuca, C.; Fiasella, A.; Pizzirani, D.; Ortega, J. A.; et al., *J. Med. Chem.* **2021**, *64*, 13327-13355.

3. Barreiro, E. J. Privileged Scaffolds in Medicinal Chemistry: An Introduction. In *Privileged Scaffolds in Medicinal Chemistry: Design, Synthesis, Evaluation*, Bräse, S. Ed.; The Royal Society of Chemistry, 2015; pp 1-15.

4. Naim, M. J.; Alam, O.; Nawaz, F.; Alam, M. J.; Alam, P., *J Pharm Bioallied Sci* **2016**, *8*, 2-17.

5. Altaf, A. A.; Shahzad, A.; Gul, Z.; Rasool, N.; Badshah, A.; Lal, B.; Khan, E., *J. Drug Des. Med. Chem.* **2015**, *1*, 1-11.

6. Li, J. J. Knorr Pyrazole Synthesis. In *Name Reactions*, Springer, 2021; pp 298-300.

7. Boger, D. L.; Panek, J. S., *J. Org. Chem.* **1981**, *46*, 2179-2182.

8. Li, J. J. Chichibabin Pyridine Synthesis. In *Name Reactions*, Springer, 2021; pp 83-85.

9. Li, J. J. Kröhnke Pyridine Synthesis. In *Name Reactions*, Springer, 2021; pp 307-309.

10. Li, J. J. Hantzsch dihydropyridine synthesis. In *Name Reactions*, 2021; p 241.

11. Ameziane El Hassani, I.; Rouzi, K.; Assila, H.; Karrouchi, K.; Ansar, M. h., *Reactions* **2023**, *4*, 478-504.

12. Fustero, S.; Sánchez-Roselló, M.; Barrio, P.; Simón-Fuentes, A., *Chem. Rev.* **2011**, *111*, 6984-7034.

13. Ebenezer, O.; Shapi, M.; Tuszynski, J. A., *Biomedicines* **2022**, *10*, 1124.

14. Ríos, M.-C.; Portilla, J., *Chemistry* **2022**, *4*, 940-968.

15. Cen, K.; Usman, M.; Shen, W.; Liu, M.; Yang, R.; Cai, J., *Org. Biomol. Chem.* **2022**, *20*, 7391-7404.

16. Islam, M. B.; Islam, M. I.; Nath, N.; Emran, T. B.; Rahman, M. R.; Sharma, R.; Matin, M. M., *Biomed Res. Int.* **2023**, *2023*, 9967591.

17. Kumar S, L.; Tabassum, S.; K S, S.; Govindaraju, S., *ChemistrySelect* **2022**, *7*, e202203668.

18. Gulevich, A. V.; Dudnik, A. S.; Chernyak, N.; Gevorgyan, V., *Chem. Rev.* **2013**, *113*, 3084-3213.

19. Fustero, S.; Simon-Fuentes, A.; Sanz-Cervera, J. F., *Org. Prep. Proced. Int.* **2009**, *41*, 253-290.

20. Hill, M. D., *Chem. Eur. J.* **2010**, *16*, 12052-12062.

21. Guo, Y. H.; Wang, G. D.; Wei, L.; Wan, J. P., *J. Org. Chem.* **2019**, *84*, 2984-2990.

22. Qu, Z. H.; Zhang, F.; Deng, G. J.; Huang, H. W., *Org. Lett.* **2019**, *21*, 8239-8243.

23. Flood, D. T.; Hintzen, J. C. J.; Bird, M. J.; Cistrone, P. A.; Chen, J. S.; Dawson, P. E., *Angew. Chem. Int. Ed.* **2018**, *57*, 11634-11639.

24. Deng, X. H.; Mani, N. S., *Org. Lett.* **2006**, *8*, 3505-3508.

25. Armstrong, A.; Jones, L. H.; Knight, J. D.; Kelsey, R. D., *Org. Lett.* **2005**, *7*, 713-716.

26. Yang, G.; Xie, X.; Cheng, M.; Gao, X.; Lin, X.; Li, K.; Cheng, Y.; Liu, Y., *Chin. Chem. Lett.* **2021**.

27. Xiang, J. C.; Wang, M.; Cheng, Y.; Wu, A. X., *Org. Lett.* **2016**, *18*, 24-27.

28. Yan, R. L.; Zhou, X. Q.; Li, M.; Li, X. N.; Kang, X.; Liu, X. X.; Huo, X.; Huang, G. S., *RSC Adv.* **2014**, *4*, 50369-50372.

29. Yu, L. B.; Chen, D. P.; Li, J.; Ramirez, J.; Wang, P. G.; Bott, S. G., *J. Org. Chem.* **1997**, *62*, 208-211.

30. Liu, J.; Wang, C. X.; Wu, L. S.; Liang, F.; Huang, G. S., *Synthesis* **2010**, 4228-4234.

31. Al Mehedi, M. S.; Tepe, J. J., *J. Org. Chem.* **2020**, *85*, 6741-6746.

32. Zhang, Y.; Wang, M.; Li, P.; Wang, L., *Org. Lett.* **2012**, *14*, 2206-2209.

33. Sharghi, H.; Aberi, M.; Khataminejad, M.; Shiri, P., *Beilstein J. Org. Chem.* **2017**, *13*, 1977-1981.

34. Ali, S.; Khan, A. T., *Org. Biomol. Chem.* **2021**, *19*, 3255-3262.

35. Mehedi, M. S. A.; George, D. E.; Tepe, J. J., *J. Org. Chem.* **2022**, *87*, 16820-16828.

36. Li, J. J. Fischer Indole Synthesis. In *Name Reactions*, Springer, 2021; pp 197-199.

37. Donald, J. R.; Taylor, R. J. K., *Synlett* **2009**, *2009*, 59-62.

38. Zhang, X.; Kang, J.; Niu, P.; Wu, J.; Yu, W.; Chang, J., *J. Org. Chem.* **2014**, *79*, 10170-10178.

39. Hu, L.; Liu, Y. A.; Liao, X., *Sci. Adv.* **2017**, *3*, e1700826.

40. Shen, M.; Leslie, B. E.; Driver, T. G., *Angew. Chem. Int. Ed.* **2008**, *47*, 5056-5059.

APPENDIX

Figure 1.5: ^{1}H and $^{13}C\{1H\}$ NMR spectra of **1-3a**

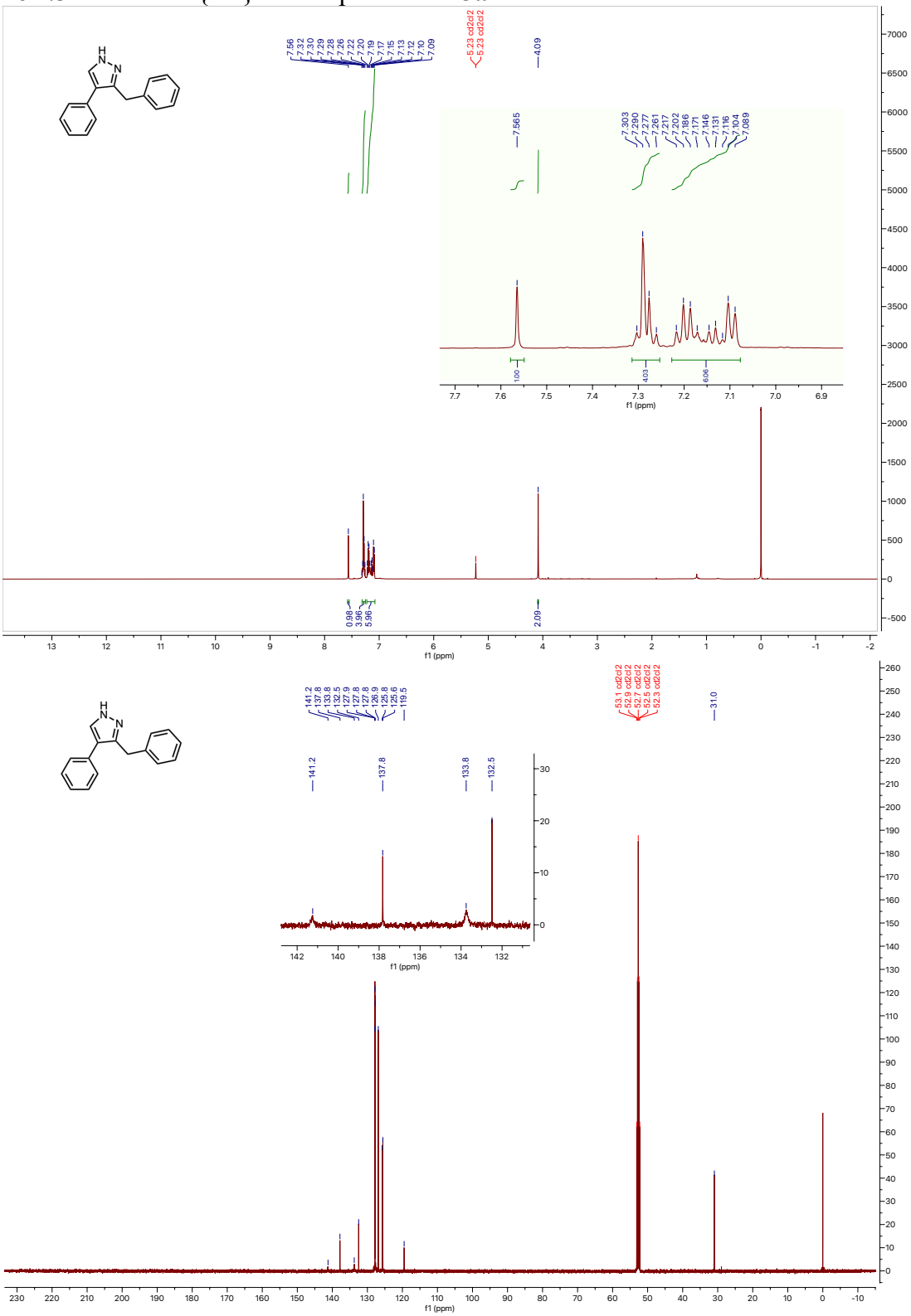

Figure 1.6: ^{1}H and $^{13}C\{1H\}$ NMR spectra of **1-3b**

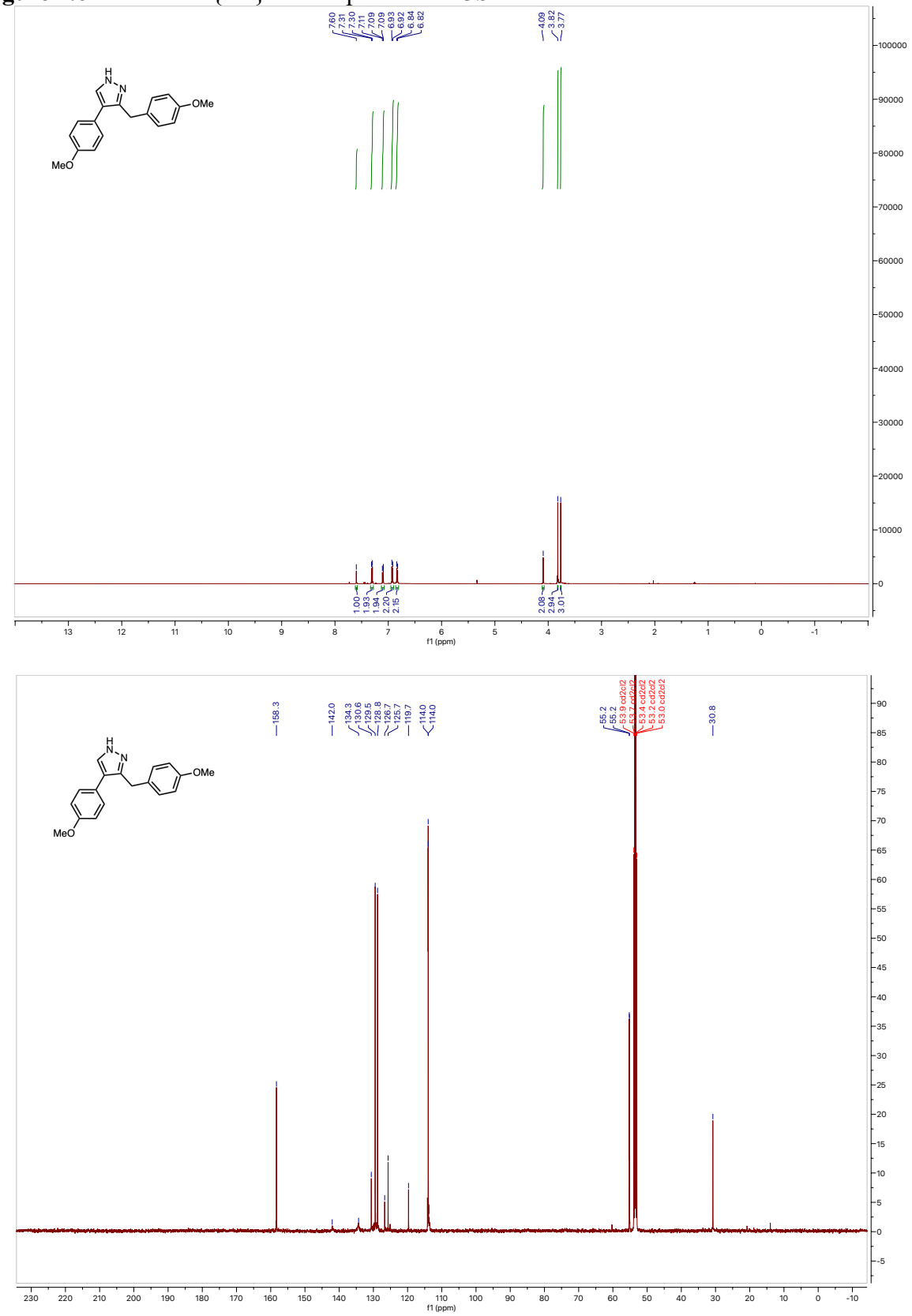

Figure 1.7: ^{1}H and $^{13}C\{1H\}$ NMR spectra of **1-3c**

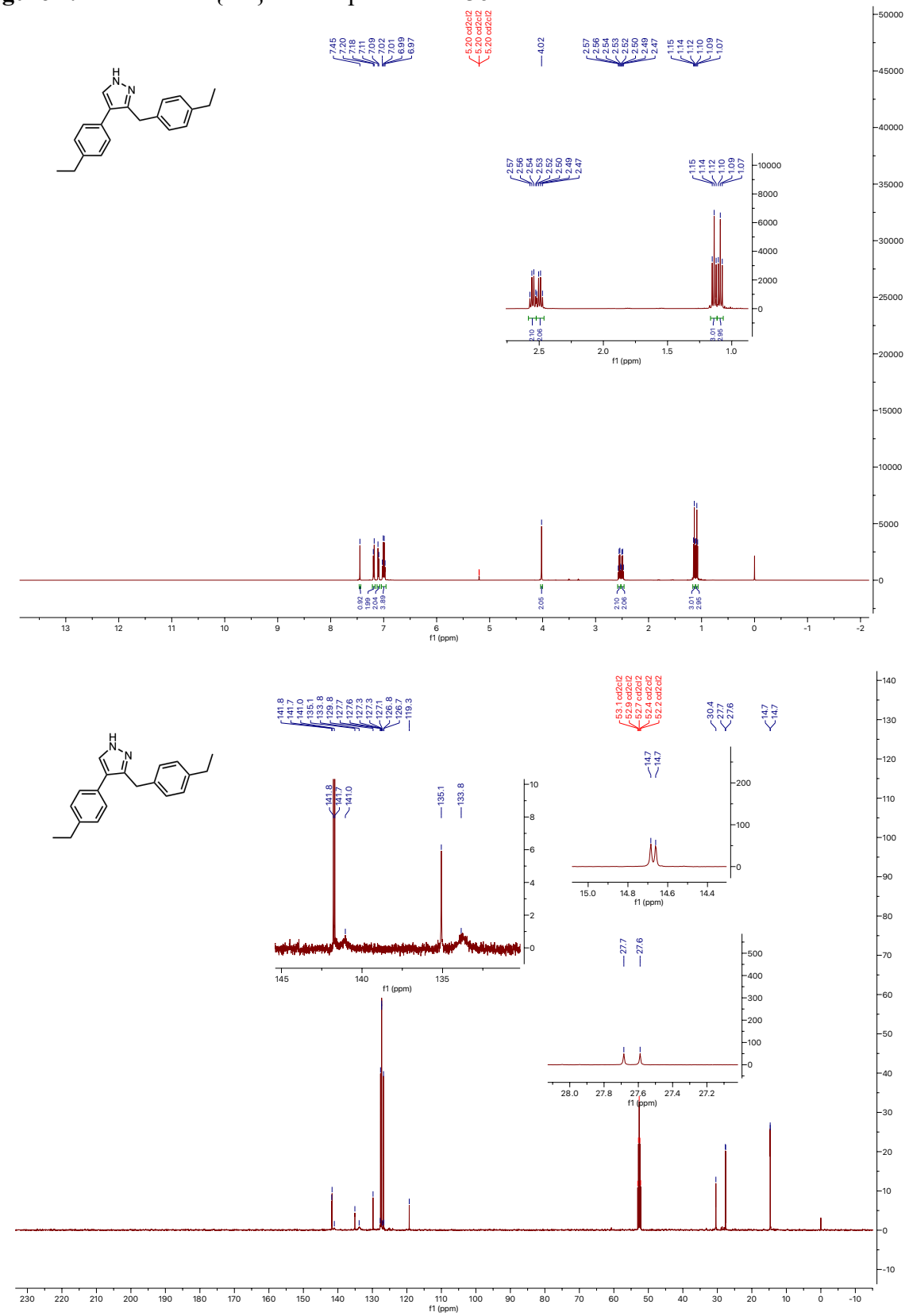

Figure 1.8: ^{1}H and $^{13}C\{1H\}$ NMR spectra of **1-3d**

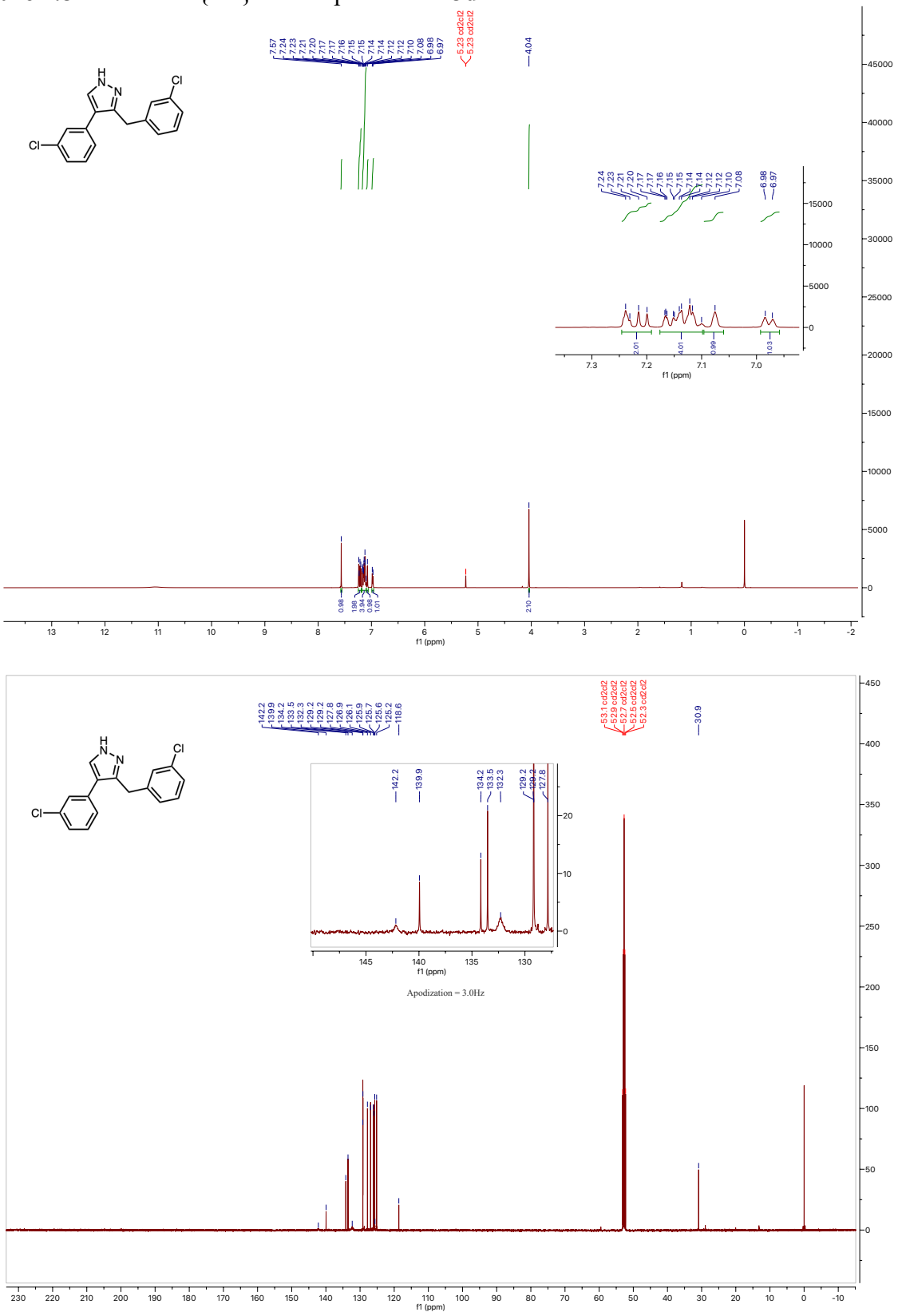

Figure 1.9: ^{1}H and $^{13}C\{1H\}$ NMR spectra of **1-3e**

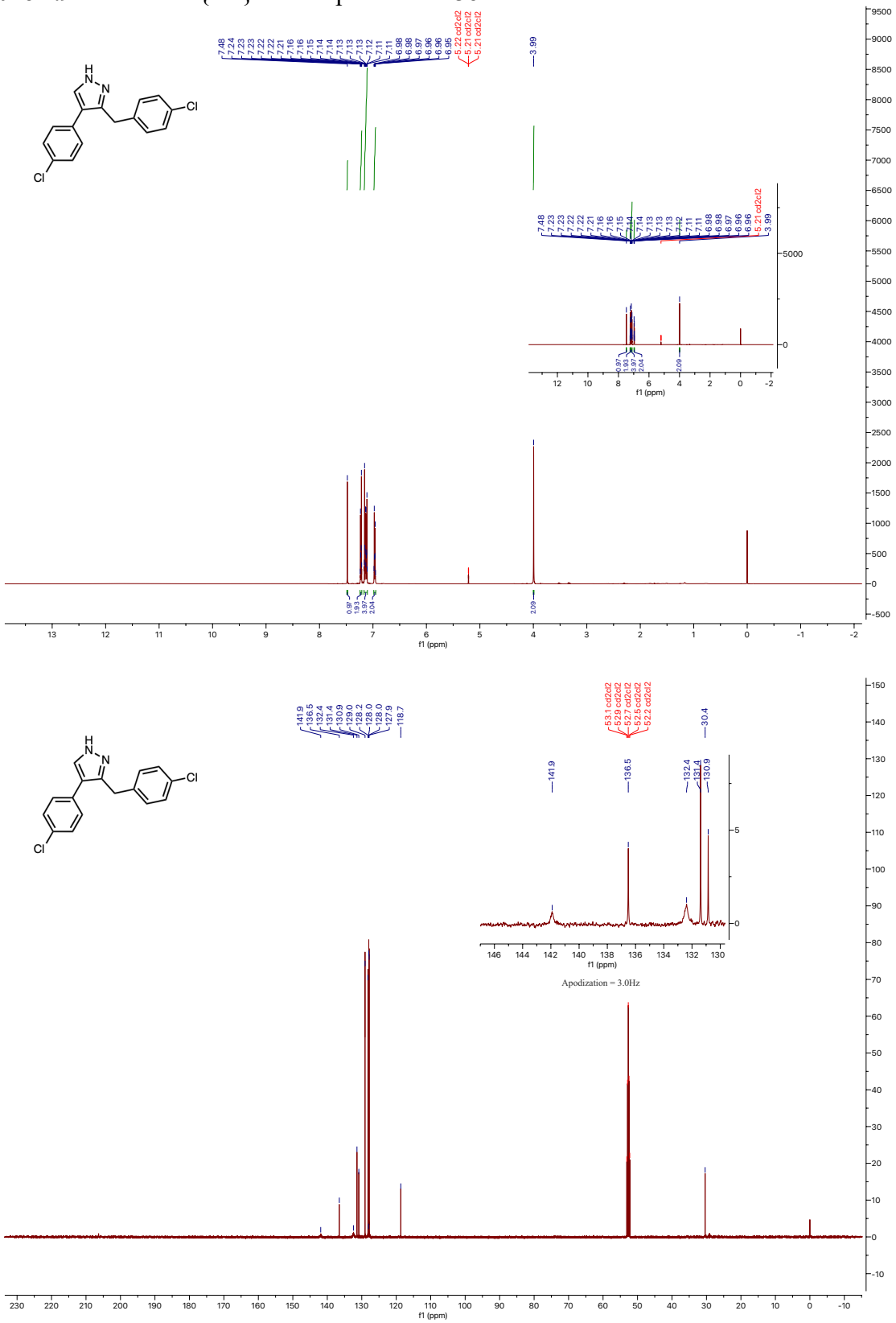

Figure 1.10: ^{1}H and $^{13}C\{1H\}$ NMR spectra of **1-3f**

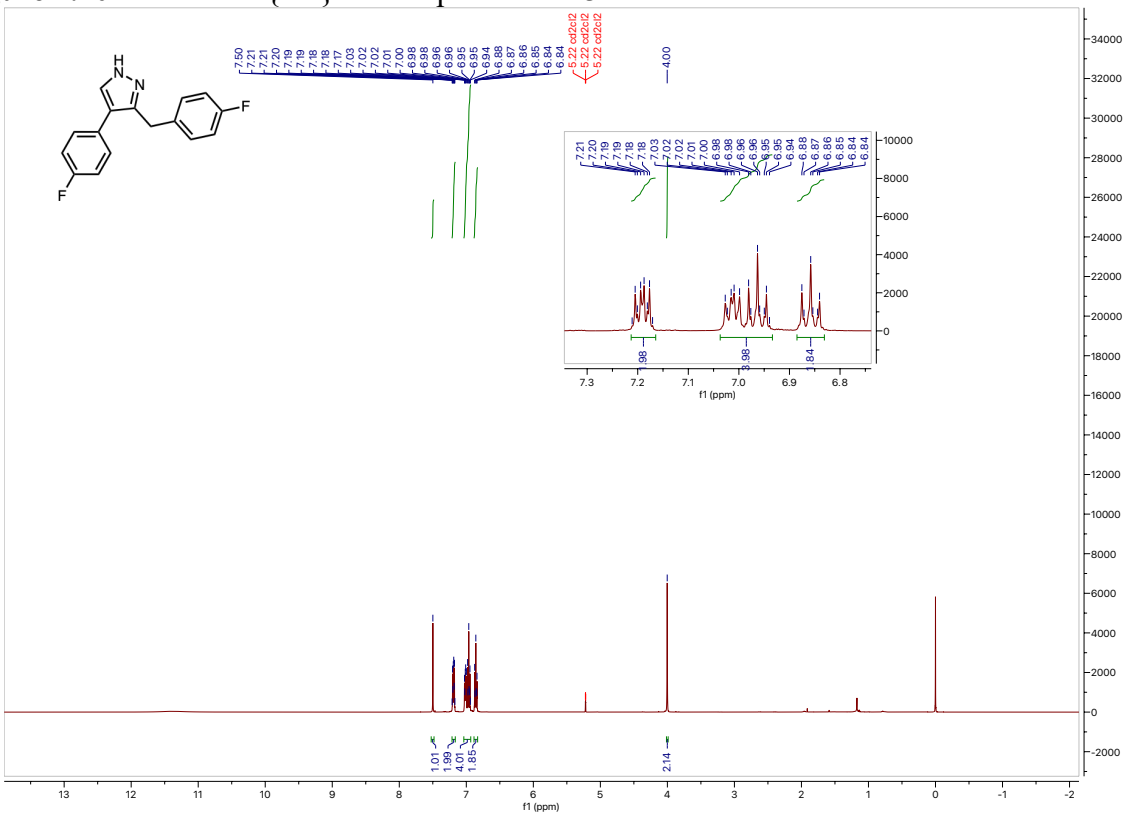

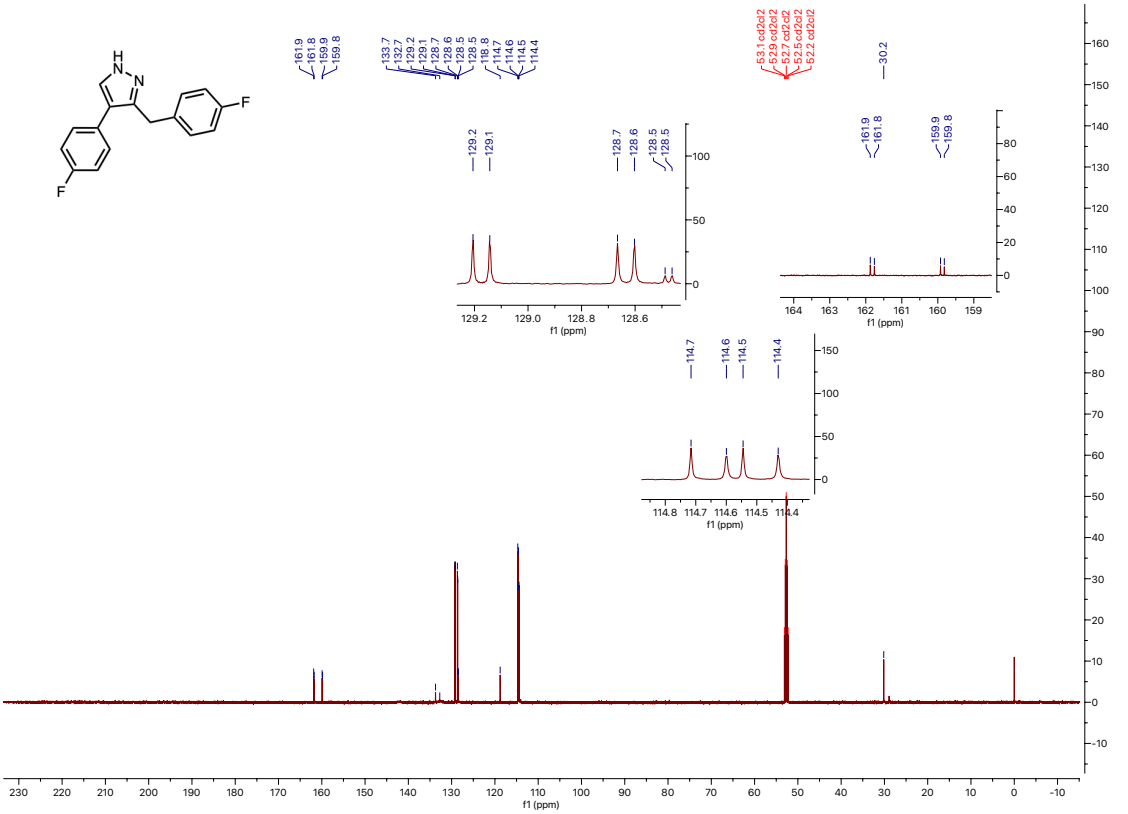

Figure 1.11: ^{1}H and $^{13}C\{1H\}$ NMR spectra of **1-3g**

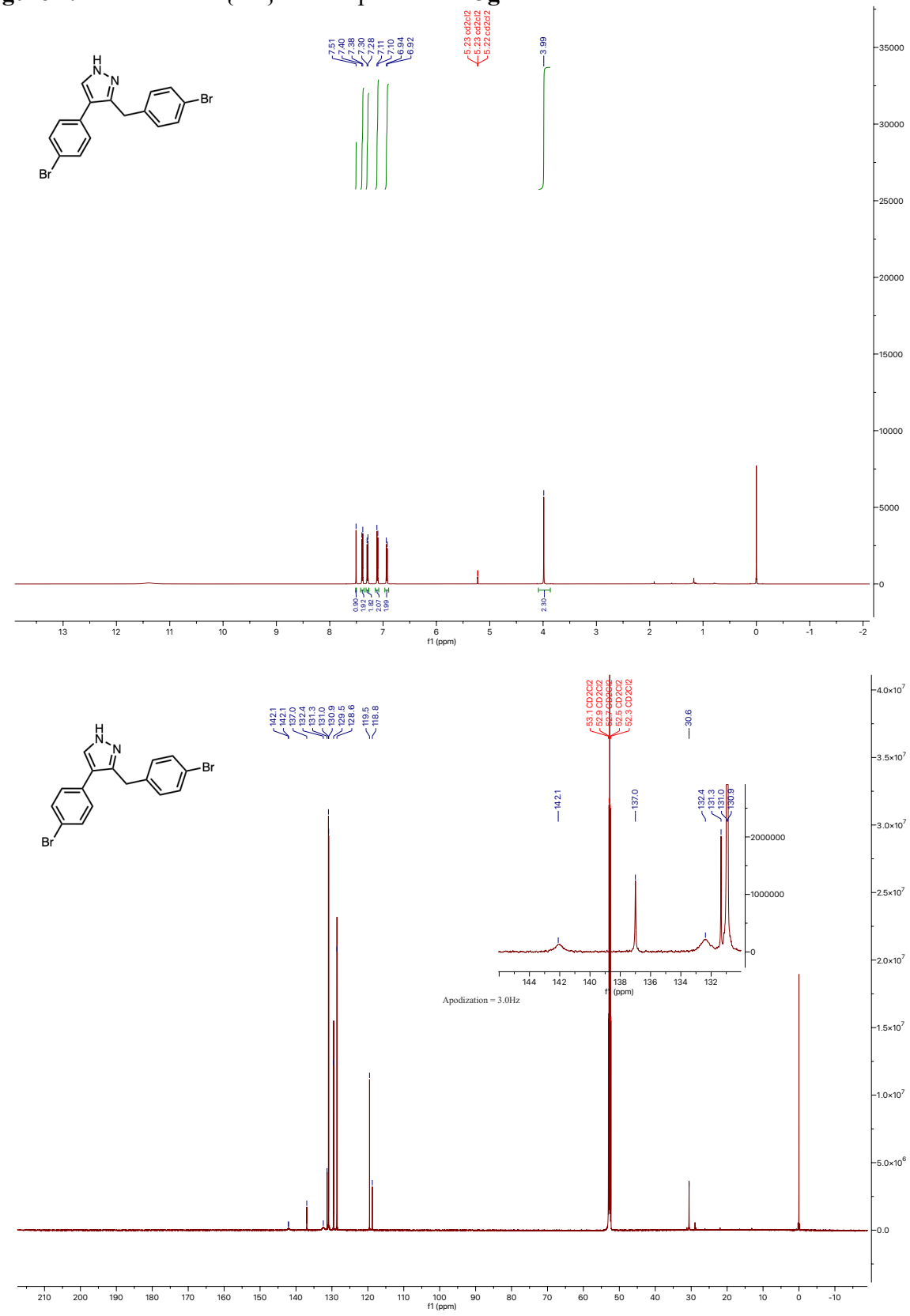

Figure 1.12: ^{1}H and $^{13}C\{1H\}$ NMR spectra of **1-2**

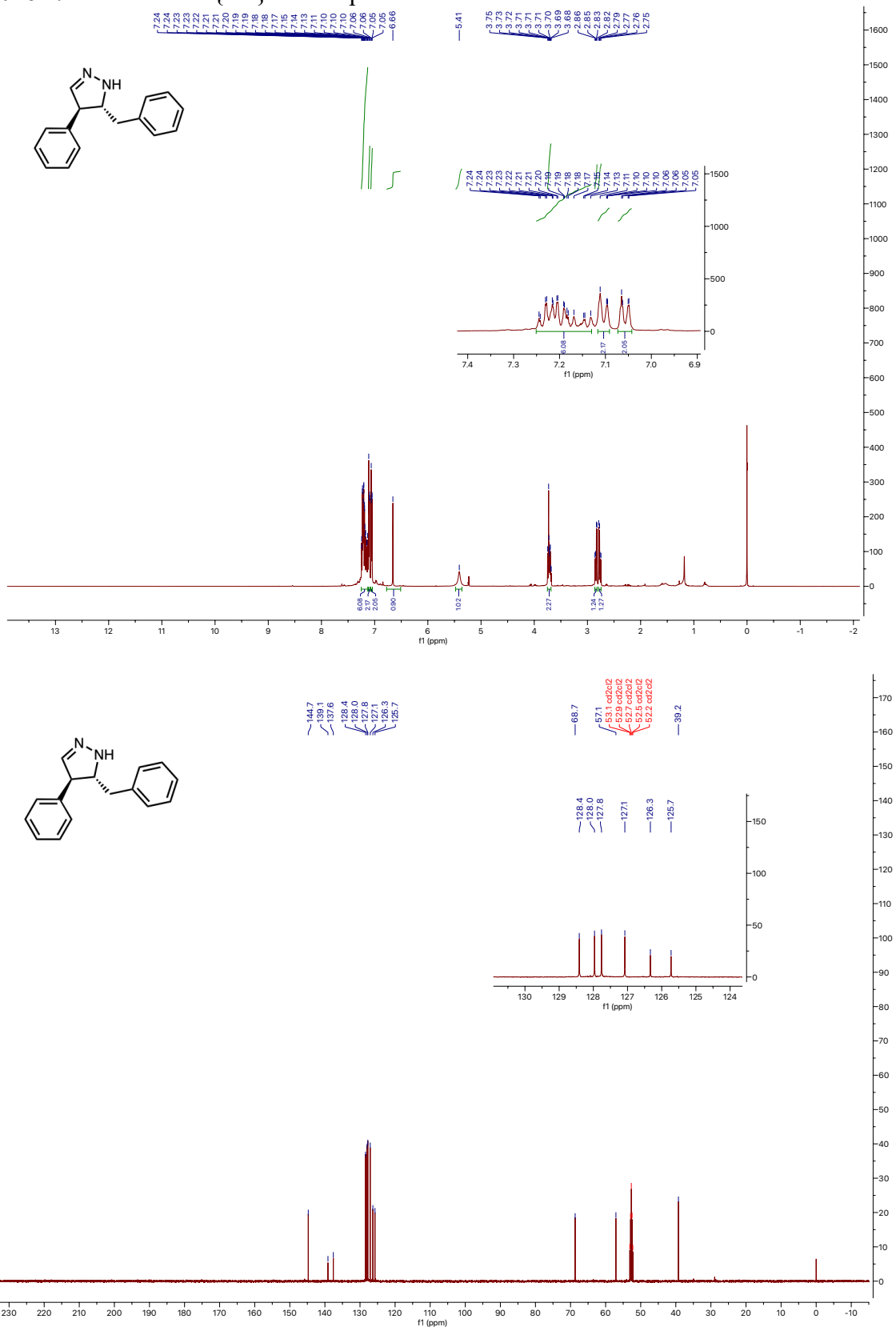

Figure 1.13: ^{1}H and $^{13}C\{1H\}$ NMR spectra of **1-5**

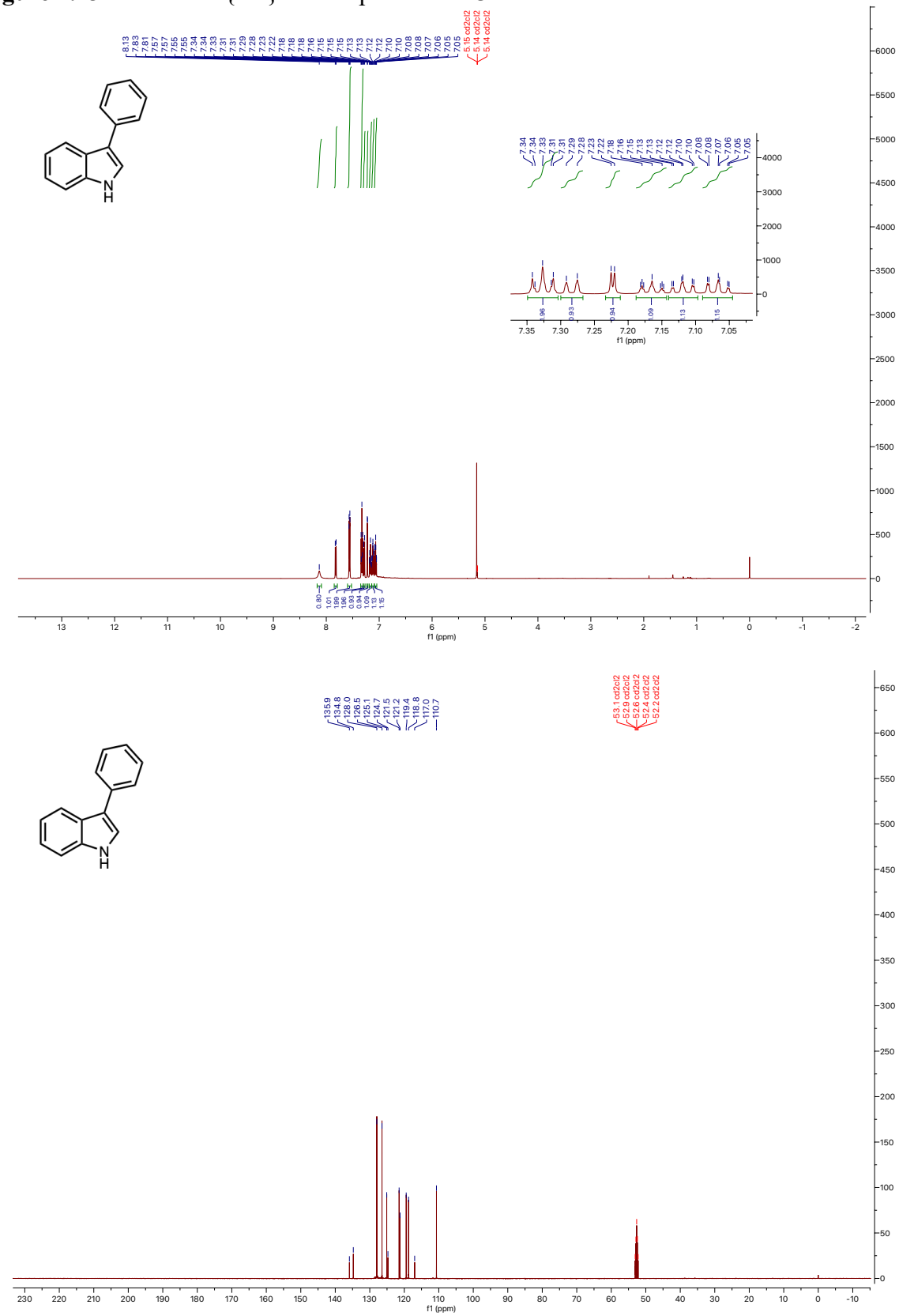

Figure 1.14: ^{1}H and $^{13}C\{1H\}$ NMR spectra of **1-7**

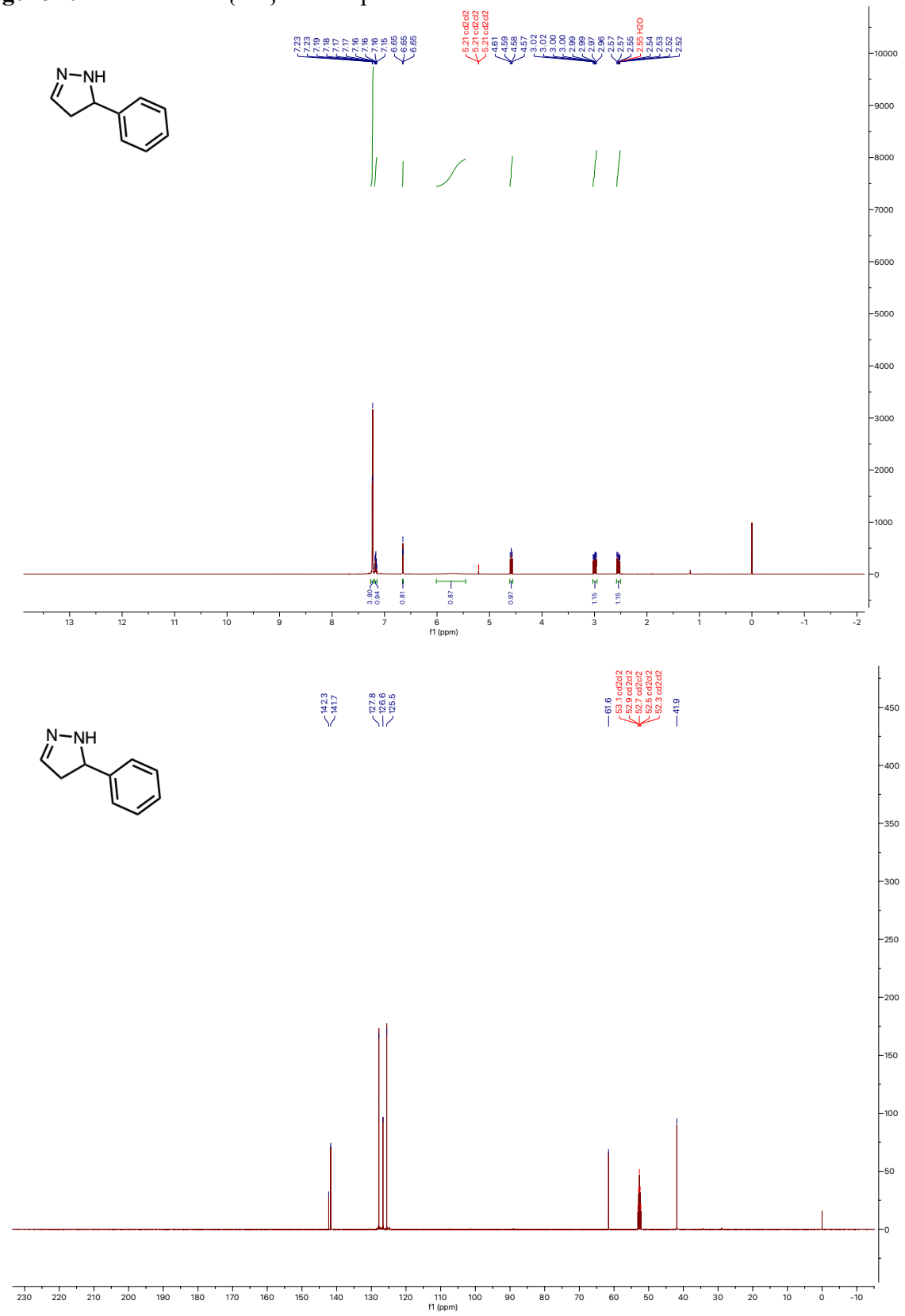

Figure 1.15: ^{1}H and $^{13}C\{1H\}$ NMR spectra of **1-4a**

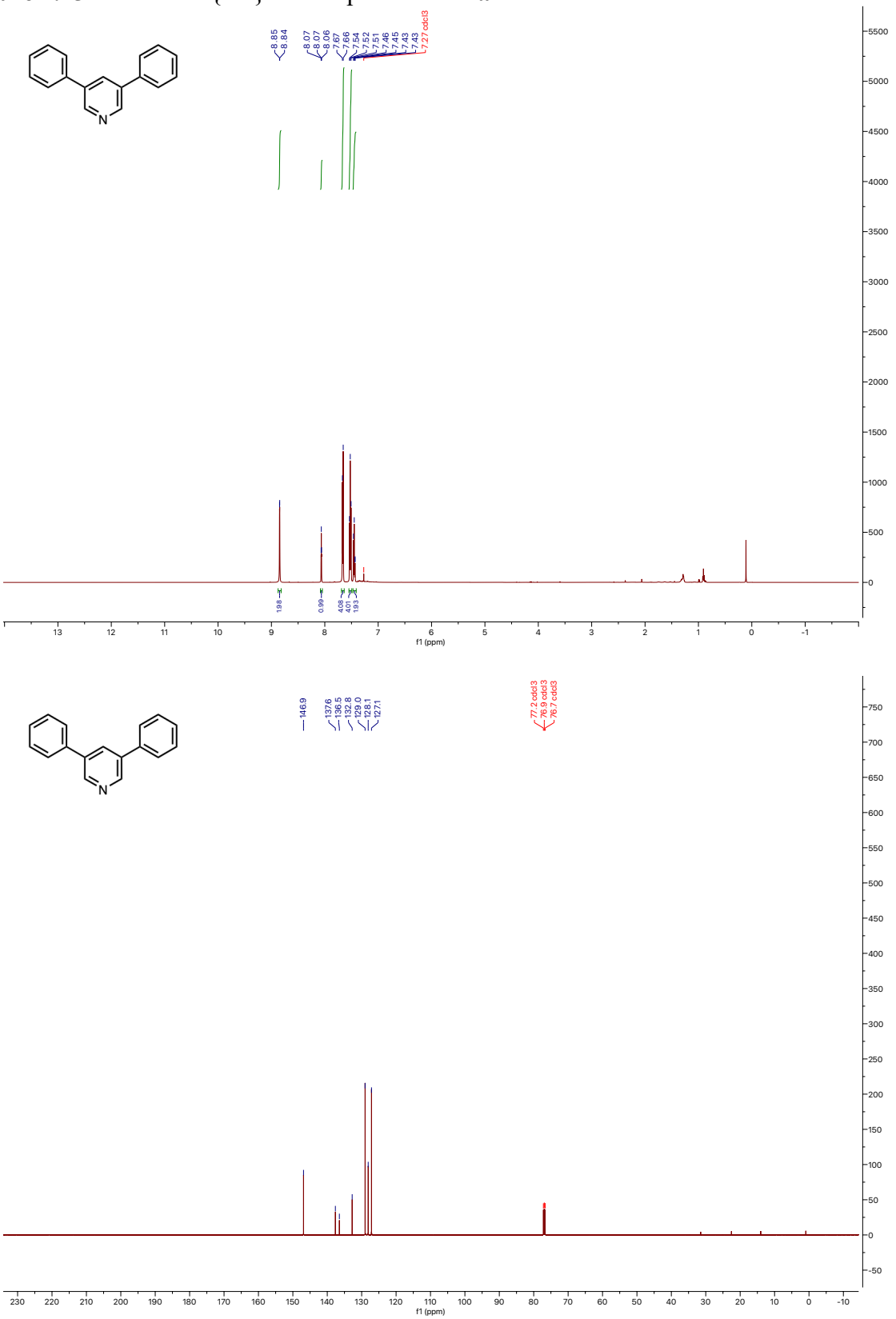

Figure 1.16: ^{1}H and $^{13}C\{1H\}$ NMR spectra of **1-4b**

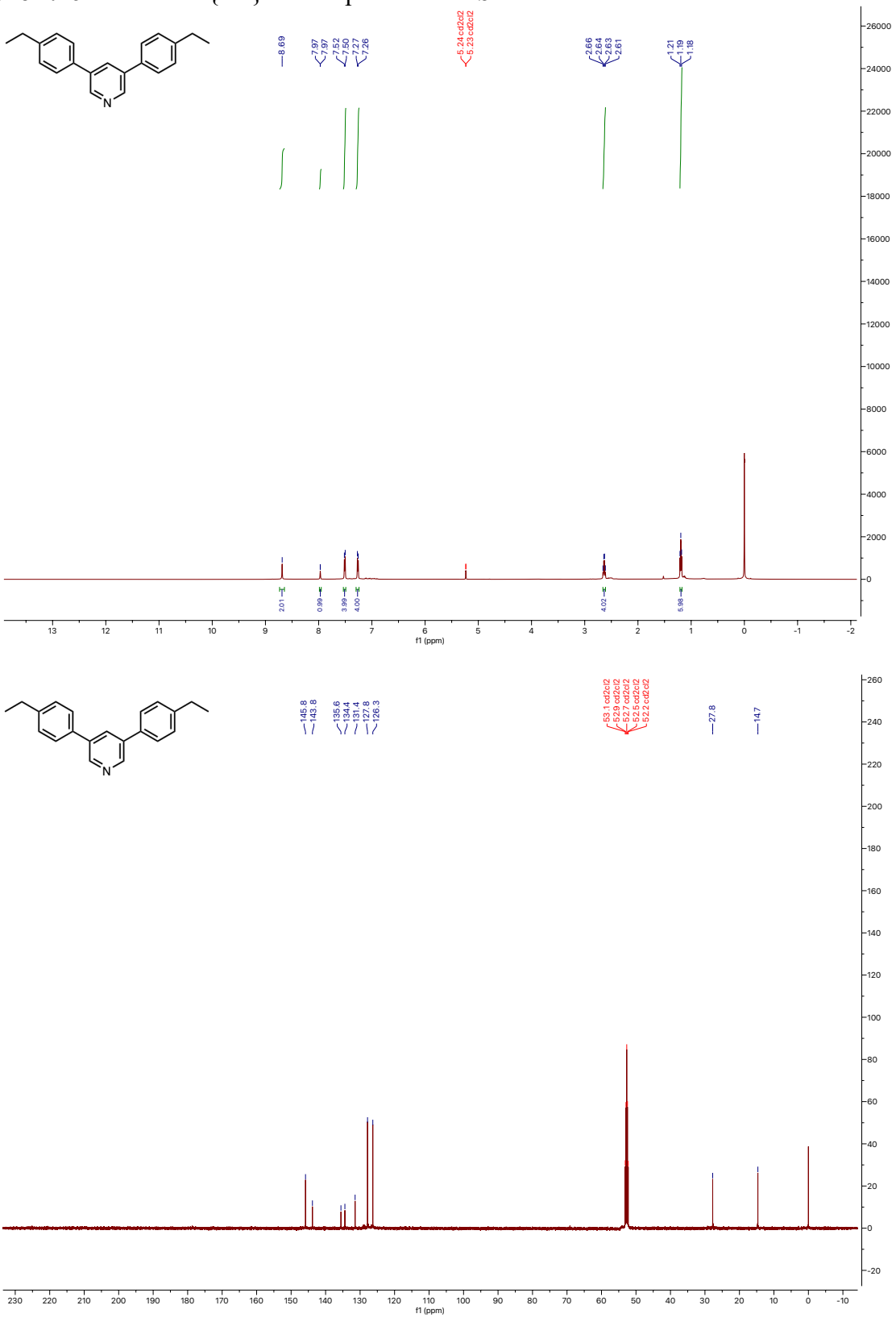

Figure 1.17: ^{1}H and $^{13}C\{1H\}$ NMR spectra of **1-4c**

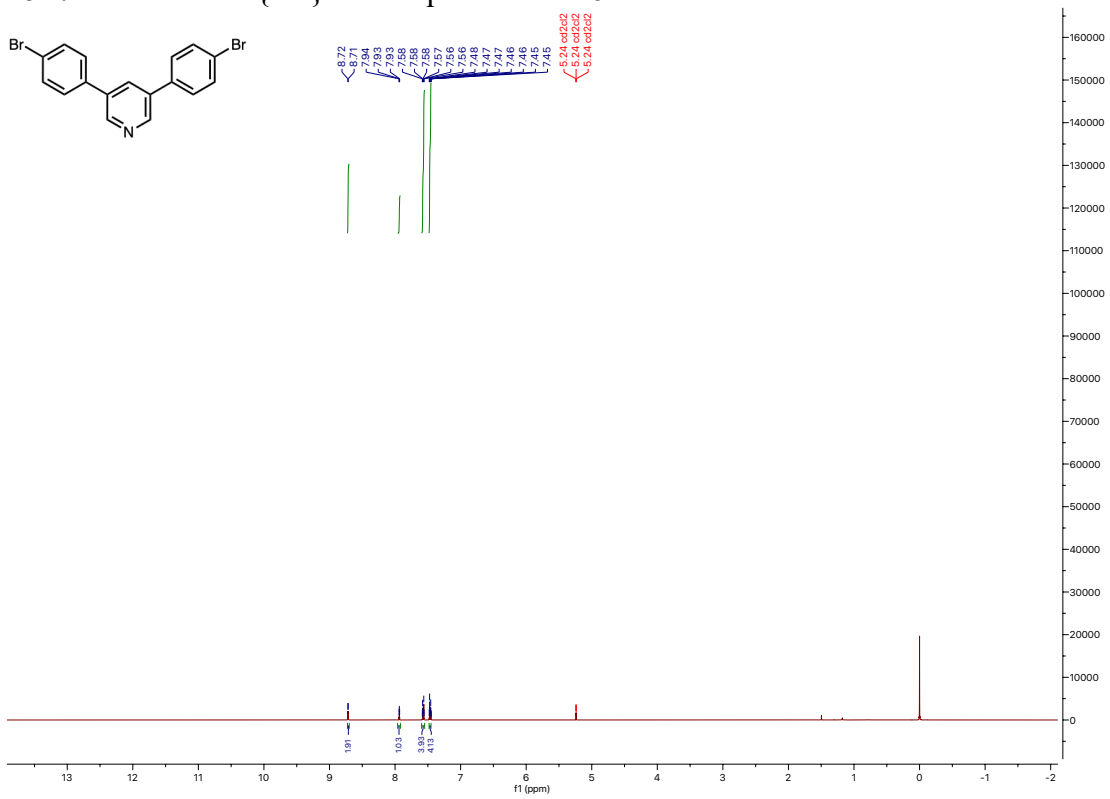

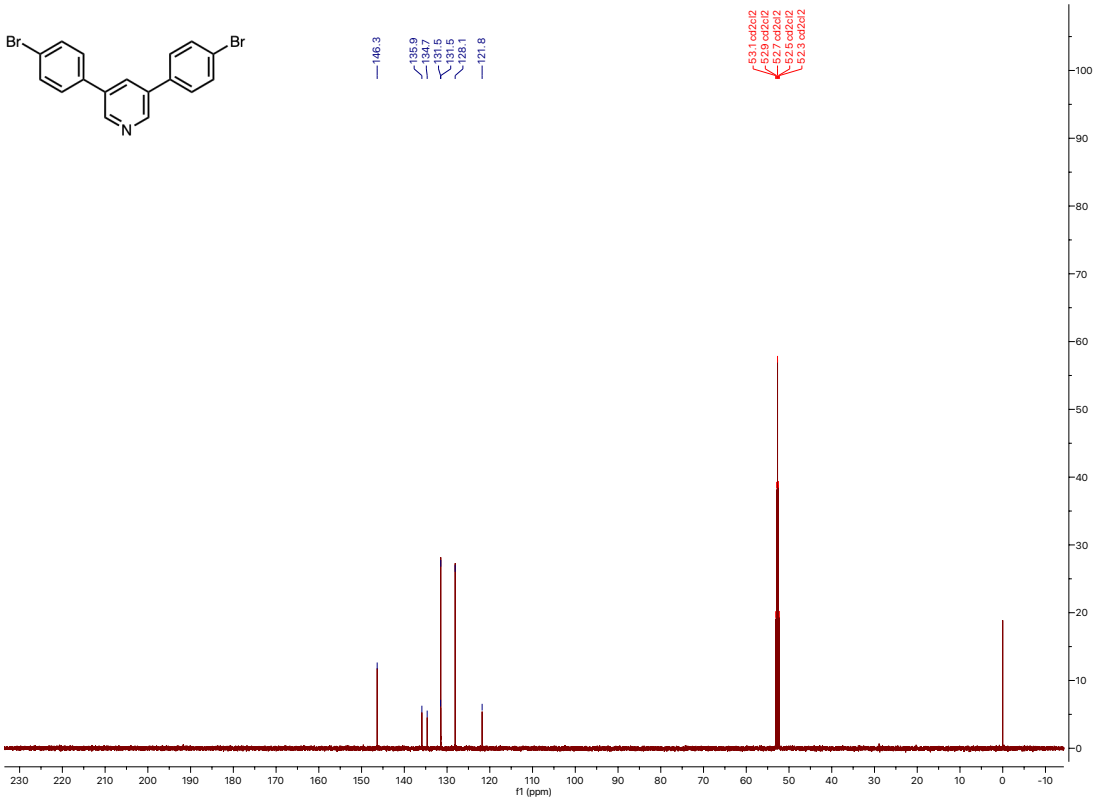

Figure 1.18: ^{1}H and $^{13}C\{1H\}$ NMR spectra of **1-4d**

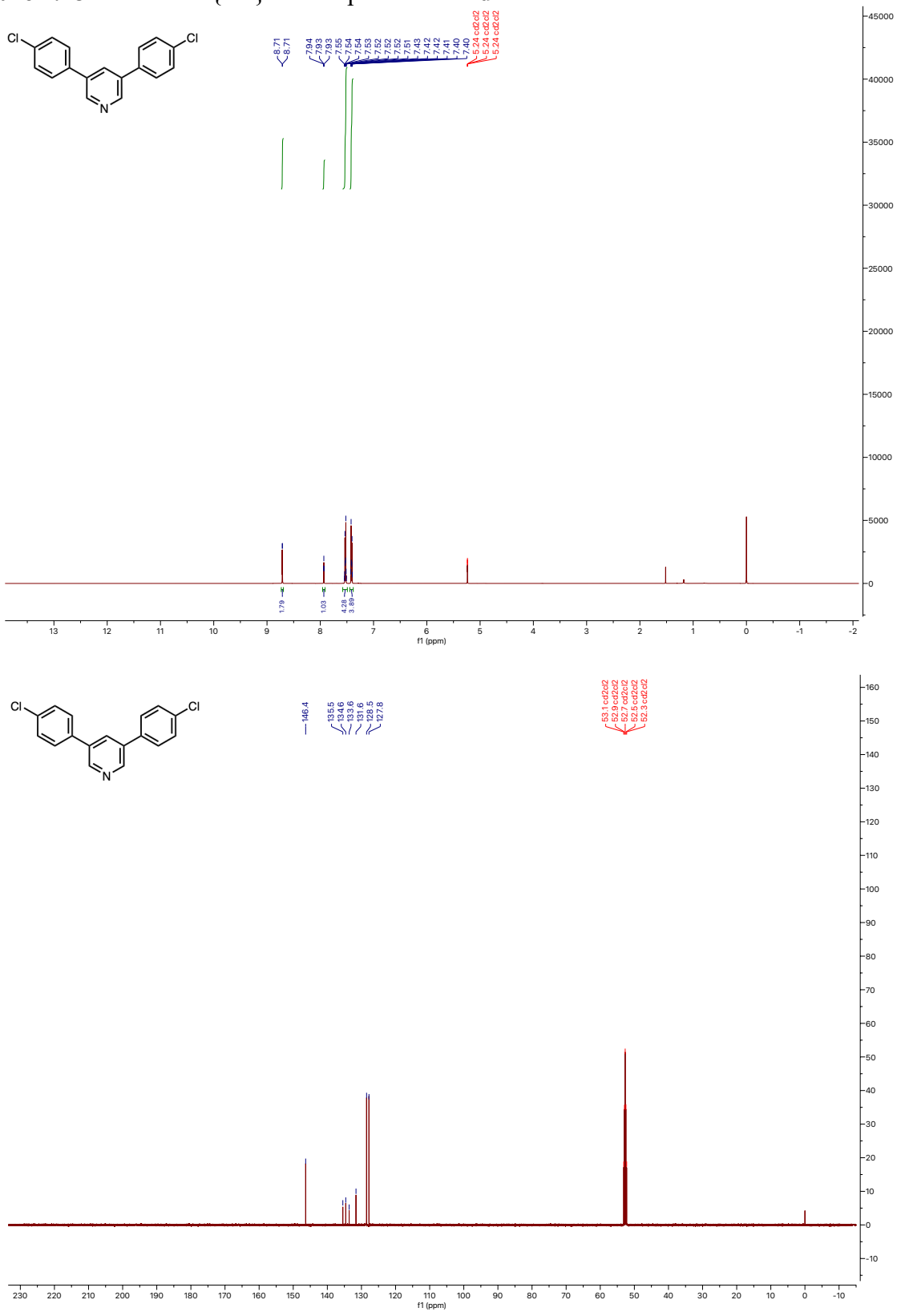

Figure 1.19: ^{1}H and $^{13}C\{1H\}$ NMR spectra of **1-4e**

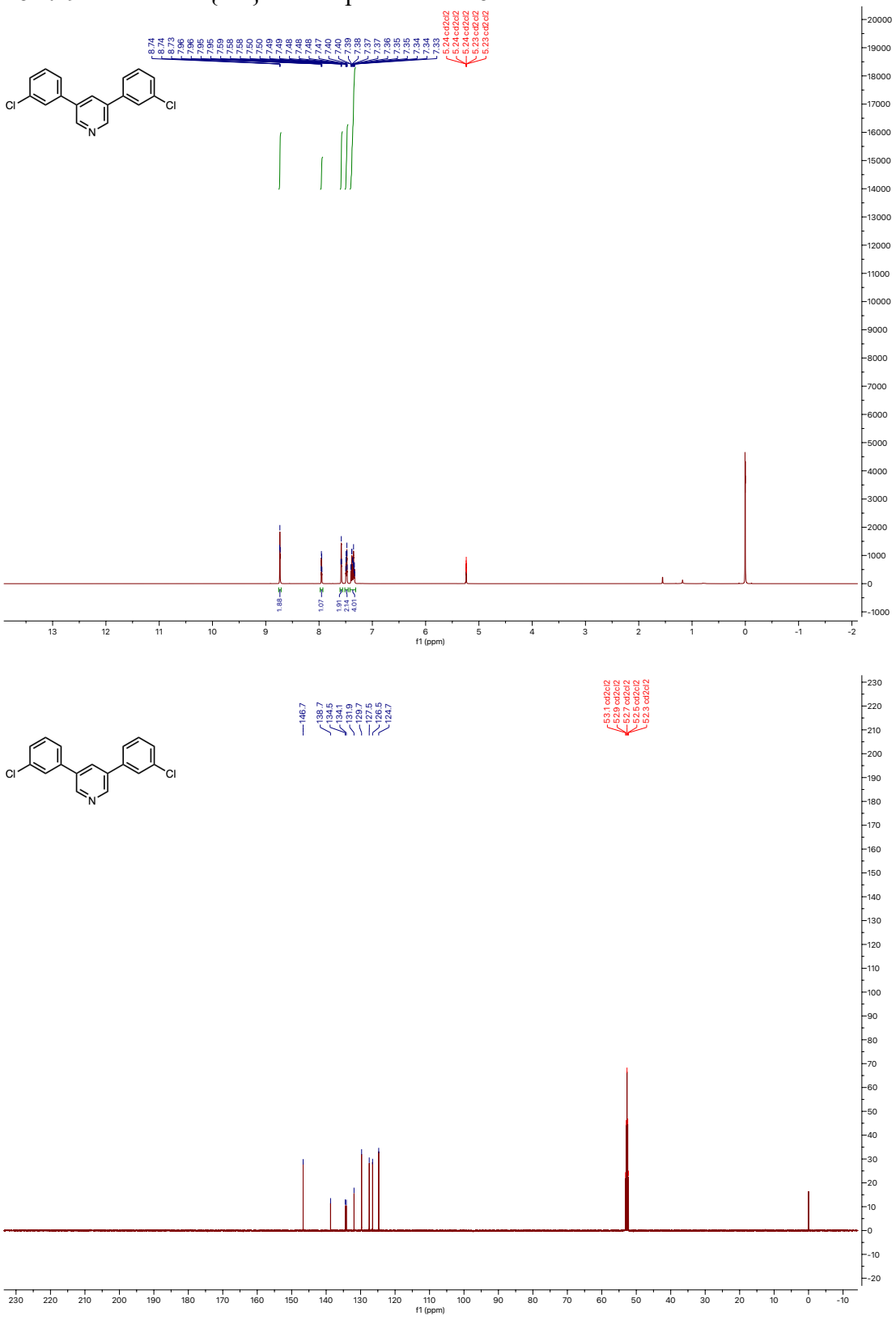

Figure 1.20: ^{1}H and $^{13}C\{1H\}$ NMR spectra of **1-4f**

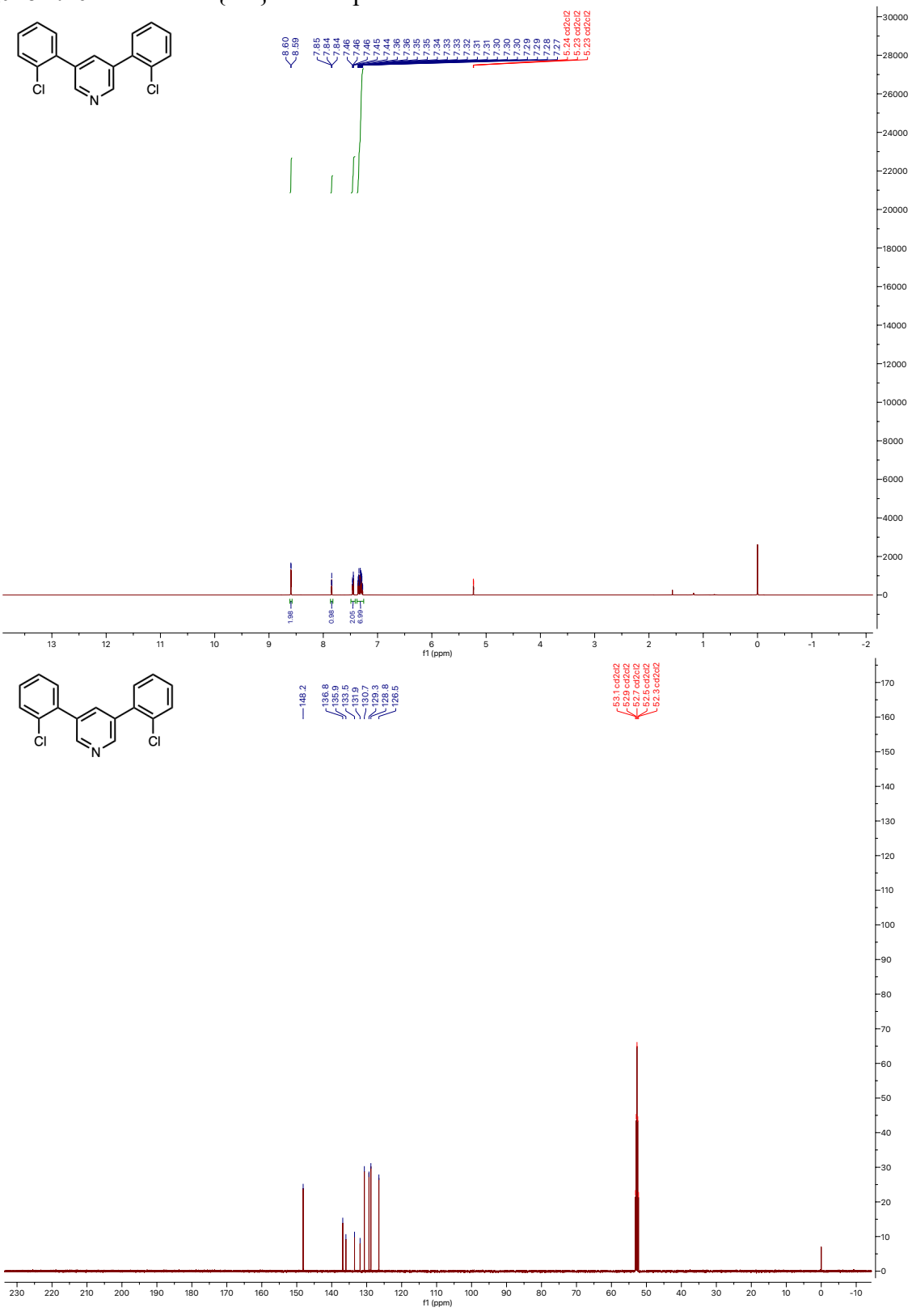

Figure 1.21: ^{1}H and $^{13}C\{1H\}$ NMR spectra of **1-4g**

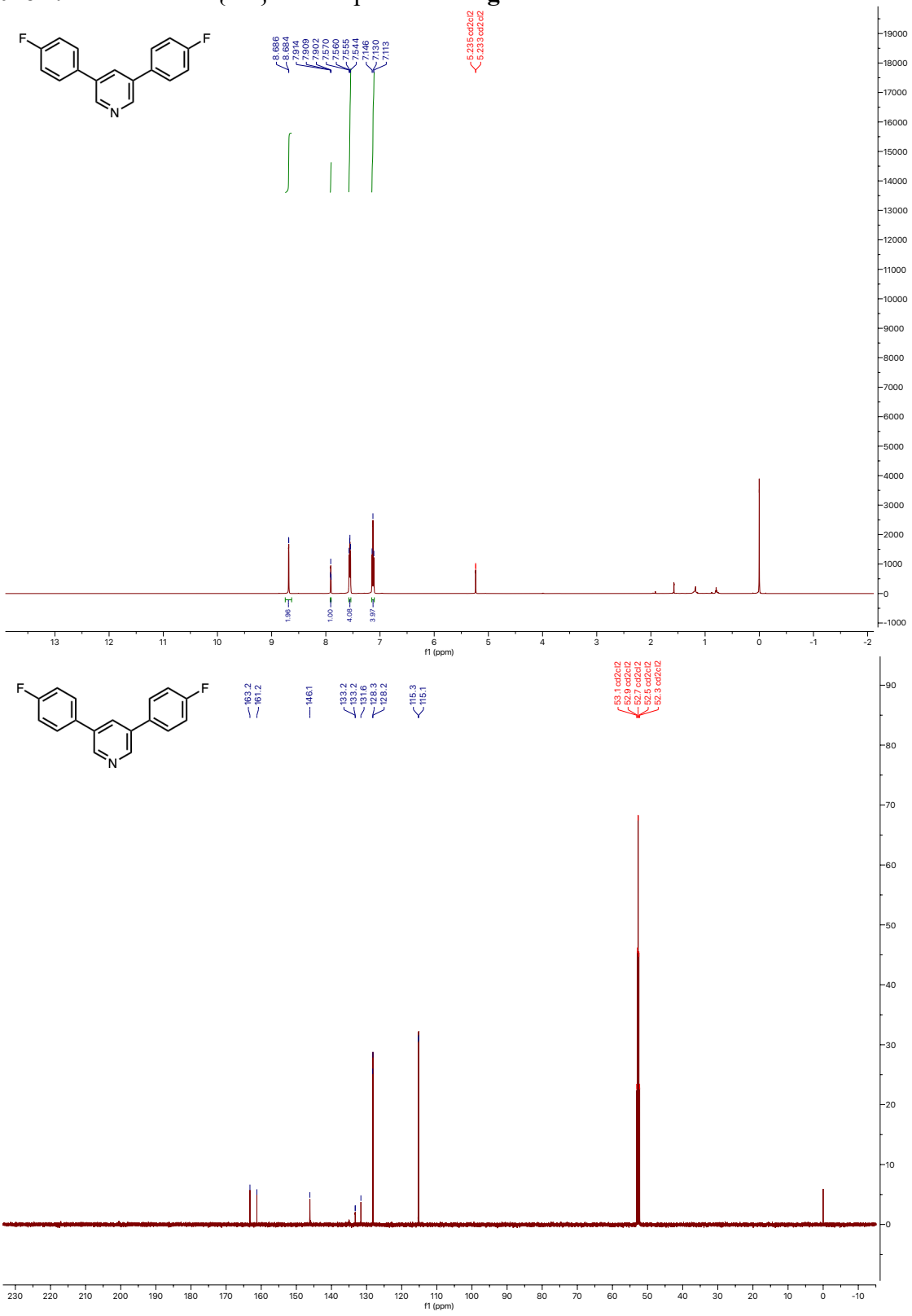

Chapter 2: First total synthesis of nagelamide W*

2.1 Introduction

Pyrrole imidazole alkaloids are marine metabolites with highly diverse structures ranging from the simplest member of the family, oroidin, to the most complex members - stylissadines A and B isolated till date.[1] These alkaloids have a high N to C ratios (~ 1:2) and show a diverse range of pharmacological properties including antibacterial, antifungal and anticancer activities.[2-5] The intriguing biological properties and unique structural features of these compounds have attracted several chemists to target them for total synthesis, aiming to further investigate their biological properties. The pyrrole imidazole alkaloids are often classified as cyclic or acyclic as either monomeric, dimeric, or tetrameric pyrrole imidazole alkaloids based on the number of oroidin units in the alkaloid structure (**Figure 2.1**) .[4,6] The biosynthesis of pyrrole imidazole alkaloids, also known as oroidin alkaloids are hypothesized to be from oroidin and its congeners: hymenidin and clathrodin (**Figure 2.1**).[7-8] This biosynthesis is believed to occur through a variety of oxidation, cyclization, or dimerization, but only a few specifics are known.[9-11]

***** This chapter is reproduced in part with permission from reference 40. Copyright 2024 American Chemical Society

Figure 2.1: Structure of oroidin, its congeners, and selected examples of different classes of oroidin alkaloids

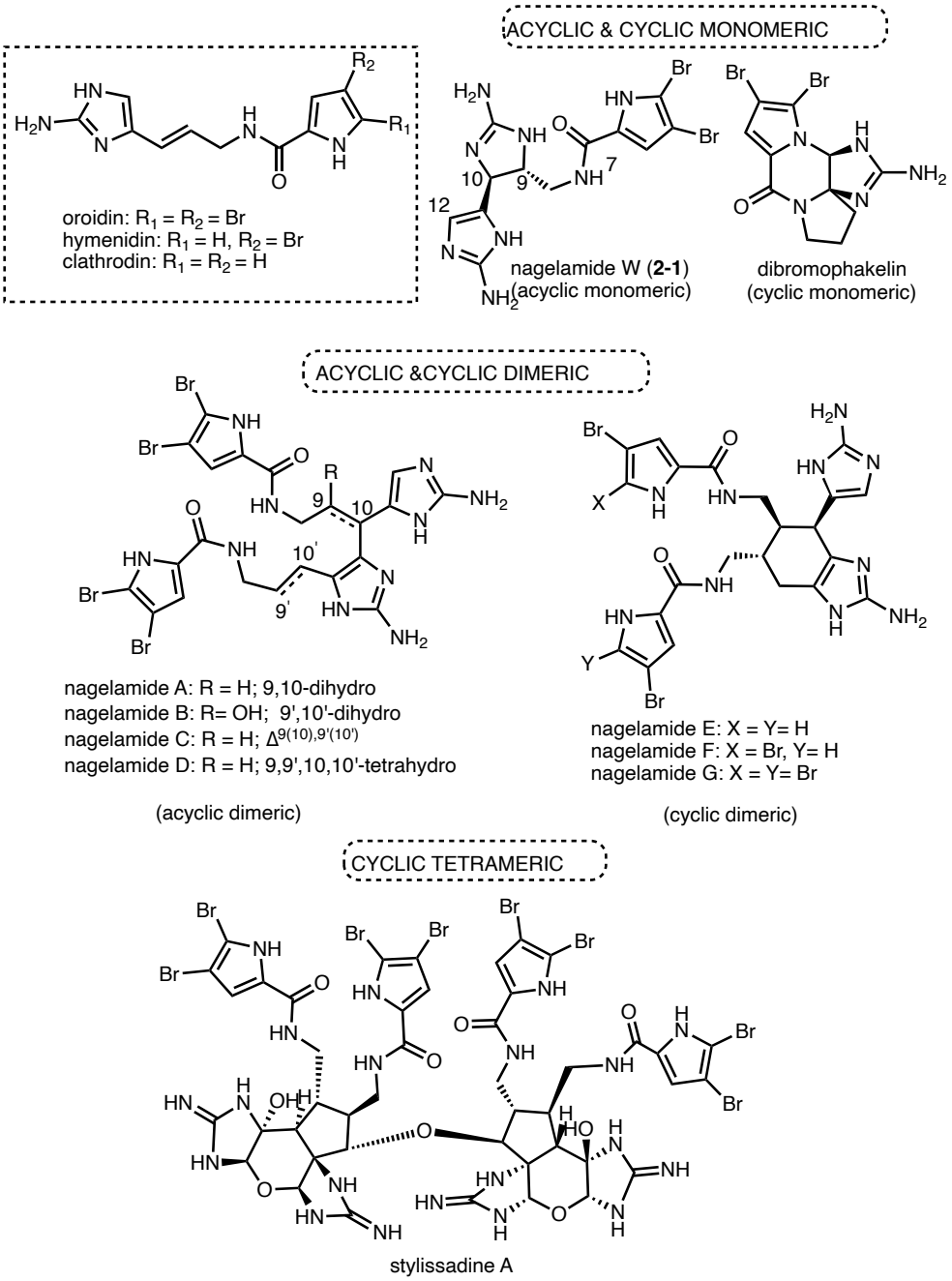

The nagelamides are a class of over 30 pyrrole imidazole alkaloids with remarkable structural diversity. These alkaloids were isolated predominantly by the Kobayashi lab from marine sponges found mostly from Pacific and Caribbean variants of sponges.[12] The nagelamides first appeared in the literature in 2004 when nagelamides A-H were reported by the Kobayashi lab

(**Figure 2.1**).[13] Since then, additional members of this family of natural products have been isolated and reported. Over the decades, several groups have developed different strategies to access these natural products but only nagelamides D[14-15] and E[16] have succumbed to total synthesis and no other total synthesis has appeared in the literature till date.[17] Additionally, de novo synthesis of nagelamide H and didebromonagelamide A has been reported.[18]

Nagelamide W (**2-1**) (**Figure 2.1**) was isolated from marine sponges *Agelas sp.* collected from Kerama Island, Okinawa in 2013.[19] The natural product was isolated alongside nagelamide U and V. During isolation, the relative stereochemistry of nagelamide W at the imidazoline core was assigned based on the ROESY correlation of H-9/H-12 and 7-NH/H-10, which suggests an *anti*-relationship for H-9 and H-10, and a *trans* configuration was assigned but the absolute stereochemistry was not determined. Nagelamide W was isolated as a colorless solid and was found to be optically active $[\alpha]_D^{20}$ = – 1.2 (*c* 0.25, MeOH). Nagelamide W is hypothesized to be biologically made by guanidination of the olefine in oroidin as depicted in **Scheme 2.1**. The biological properties of nagelamide W is underexplored and it is only known to have moderate antimicrobial activity against *Candida albicans* (IC_{50} 4μg/mL).[19] This furthers strengthen why nagelamide W should be synthesized to further explore its biological activity**.**

Scheme 2.1: Proposed biological pathway for the synthesis of Nagelamide W

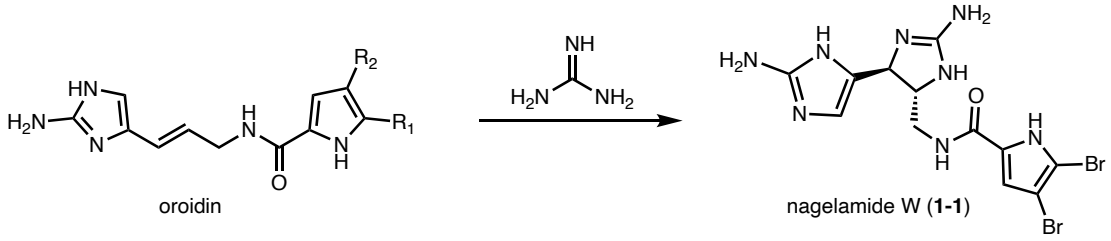

2.2 Results and Discussion

2.2.1 Unsuccessful attempt to synthesize nagelamide W

The initial approach to access nagelamide W (**2-1**) is shown in **Scheme 2.2**. In this retrosynthesis, nagelamide W could be accessed by hydrazine-mediated double deprotection of the pyrimidine part of the imidazo[1,2-*a*]pyrimidine core in **2-2**, using the heterocycle as a masked amino imidazolyl group.[20-21] Compound **2-2** can be obtained by series of chemical transformation of **2-5**. The key approach in this retrosynthesis was the proposed Friedel-Crafts like 1,4-addition of imidazo[1,2-*a*]pyrimidine and aldehyde **2-7**. At this step the two chiral centers in the natural product would be created, as well as the key imidazoline core of the natural product.

Scheme 2.2: Restrosynthesis of nagelamide W

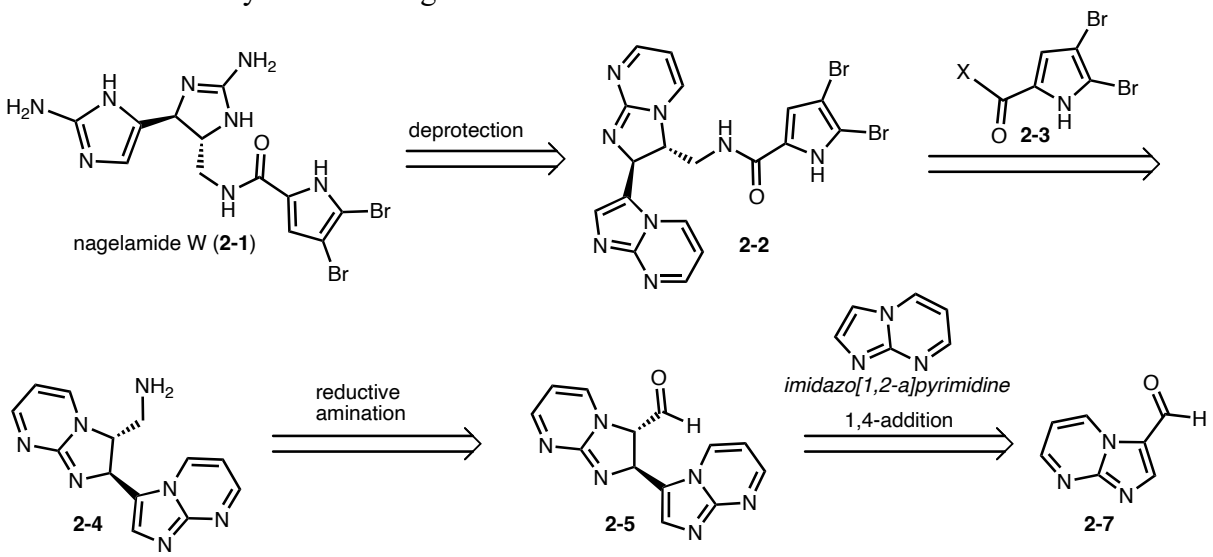

The closest example for the proposed Friedel-Craft like 1,4-addition step is based on the previous work done by the MacMillan group on the enantioselective alkylation of pyrrole and indole using MacMillan catalyst and α,β-unsaturated aldehydes (**Scheme 2.3**).[22-23] The reaction proceeds through the reversible formation of iminium ions with the chiral catalyst, which lowers the LUMO of the α,β-unsaturated aldehyde. Then, the conjugate addition of pyrrole or indole follows, resulting in the formation of the product. The reactions show to be efficient with yields

up to 90% and enantioselectivity up to 99% ee. While pyrrole and indole have been extensively studied, the reactivity of imidazo[1,2-*a*]pyrimidine remains unexplored. The first aim of the current approach to access nagelamide W became to first investigate the reactivity of imidazo[1,2-*a*]pyrimidine and aldehyde **2-7** in the Friedel-Crafts like 1,4-addition reaction that was pioneered by the MacMillan lab.

Scheme 2.3: Literature precedence on asymmetric Friedel-Craft alkylation with pyrrole and indole

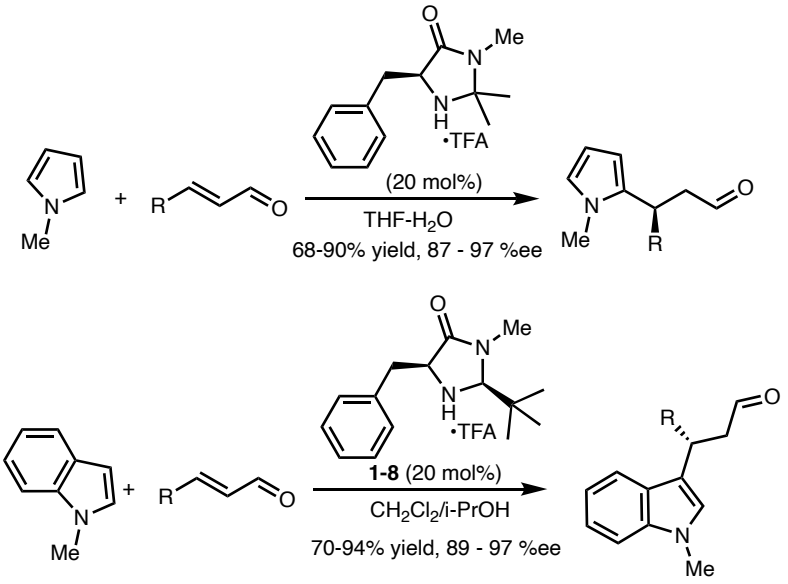

Following the proposed retrosynthesis, Vilsmeier-Haack formylation of imidazole[1,2-*a*]pyrimidine gave aldehyde **2-7** in moderate yield[24] and was used to explore the Friedel-Crafts like 1,4-addition. Initially, the reaction of imidazo[1,2-*a*]pyrimidine with aldehyde **2-7** in the presence of MacMillan catalyst gave no product (**Scheme 2.4**). This preliminary result led to the investigation of the nucleophilicity and electrophilicity of imidazo[1,2-*a*]pyrimidine and aldehyde **2-7** respectively to understand the underlying cause of the reactivity failure. It is also apparent that the electronics of the reactants, especially the aldehyde, is quite different from the one utilized by the MacMillan group. Exploring the limits of these reactants could reveal their limitation and perhaps how those limitation could be overcome.

Scheme 2.4: Attempt on Friedel-Craft like 1,4-addition

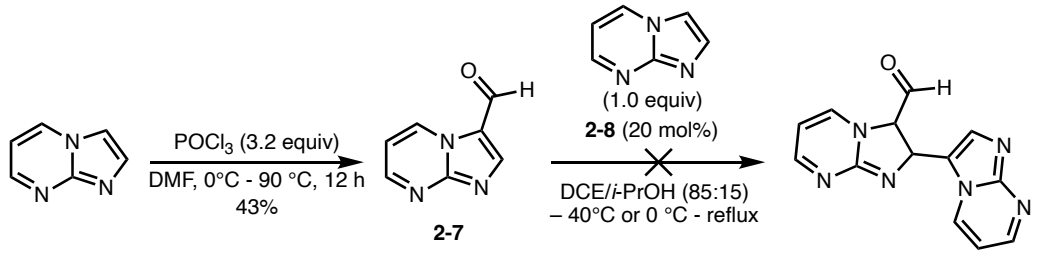

In order to understand the reactivity of imidazo[1,2-*a*]pyrimidine towards conjugate addition, crotonaldehyde and cyclohexenone were reacted with imidazo[1,2-*a*]pyrimidine using iminium catalyst as shown in **Scheme 2.5**. No products were obtained in any of the reactions, and in some instances, the starting materials decomposed upon heating to reflux. It was concluded that imidazo[1,2-*a*]pyrimidine is a weak nucleophile and does not undergo conjugate addition under the explored conditions, even when using highly reactive electrophiles such as crotonaldehyde.

Scheme 2.5: Investigation of the nucleophilicity of imidazo[1,2-*a*]pyrimidine

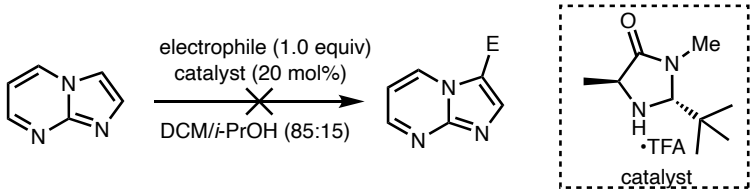

entry	E	temp	yield
1	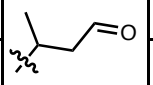	–40	0%
2		0 – rt	0%
3	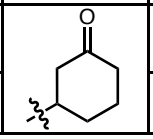	–40	0%
4		0 – rt	0%

Concurrent investigation of the electrophilicity of aldehyde **2-7** toward conjugate addition did not show promising result as well. Initially, the aldehyde's electrophilicity was assessed using the MacMillan catalyst and anisole as the nucleophile (**Scheme 2.6a**). The reaction gave no product even after being stirred at room temperature for up to 3 days. Increasing the temperature of the reaction also did not lead to the formation of any product. After this, stronger nucleophiles such as Gilman reagents were investigated (**Scheme 2.6b**), and they all gave no product. In addition,

attempt to increase the electrophilicity of the aldehyde by using different Lewis's acid did not facilitate the formation of any product. The aldehyde's lack of reactivity in conjugate addition was attributed to the anticipated loss of aromaticity in the imidazole ring upon the conjugate addition process.

Scheme 2.6: Investigation of the electrophilicity of aldehyde **2-7**

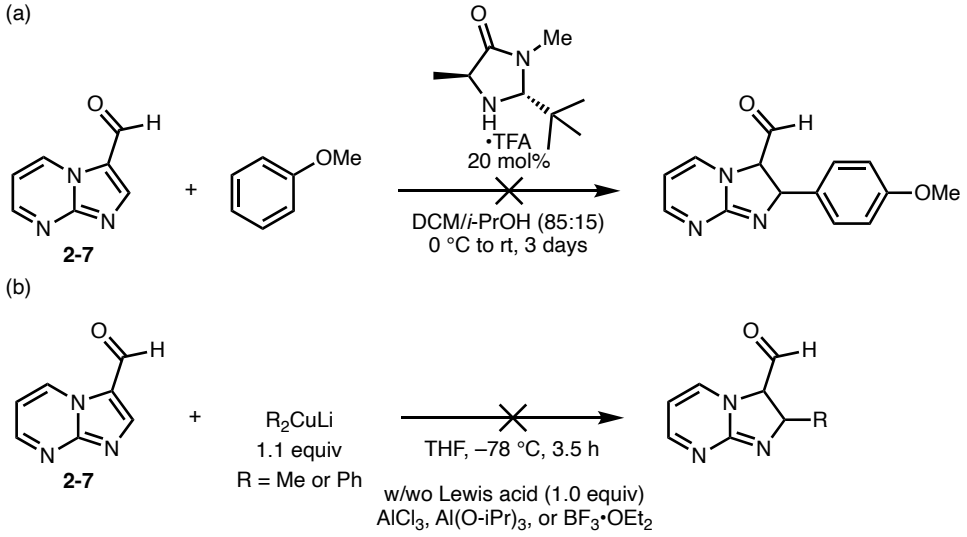

After encountering failure due to the lack of reactivity of both imidazo[1,2-a]pyrimidine and aldehyde **2-7** towards conjugate addition, it became imperative to reevaluate the proposed approach for the total synthesis of nagelamide W, leading to the conclusion that a different approach was warranted.

2.2.2 Alternate approach for the synthesis of nagelamide W

Based on the revised retrosynthetic analysis (**Scheme 2.7**), the proposed method for accessing the 2-aminoimidazole moiety of nagelamide W through a late-stage hydrazine-mediate deprotection[20-21] and amidation[25] of the amine (**2-10**) with dibromopyrrole carboxylate derivative remained unchanged. The 2-aminoimidazoline core in **2-10** can be obtained from 2-alkoxyimidazoline **2-11** through a nucleophilic displacement of the alkoxy group similarly to the approached used in the synthesis of dibromophakellin[26] and dragmacidin E[27] and the primary

amine can also be obtained through alcohol transformation. The key intermediate **2-11** in this total synthesis could be obtained through the functionalization of alkene **2-12** to access the key imidazoline core of the natural product.[28] Alkene **2-12** could be accessed from imidazo[1,2-a]pyrimidine which is readily available from commercial sources.

Scheme 2.7: Revised retrosynthetic analysis of nagelamide W

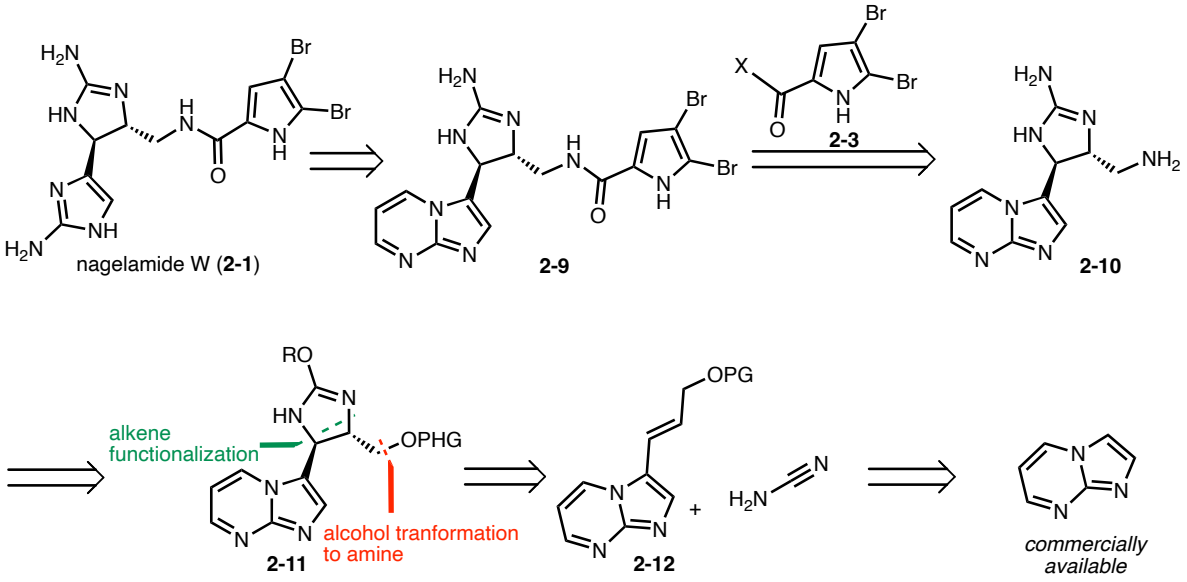

Following the new approach, alkene **2-13** was synthesized using the Horner–Wadsworth–Emmons (HWE) reaction from aldehyde **2-7** to give the desired product **2-13** in up to 89% yield (**Scheme 2.8**). The reduction of the conjugated ester **2-13** to allylic alcohol **2-14** was first carried out using diisobutylaluminium hydride (DIBAL-H). This reduction gave the desired product in 5-7% yield (**Table 2.1**). Mass spectrometry analysis of the crude reaction showed several other products which appeared to be over reduction product including the reduction of imidizo[1,2-*a*]pyrimidine ring and reduction of both ester and alkene. However, isolation of any these side products via column chromatography was unsuccessful. Different reaction conditions and hydride reagents were also investigated even though DIBAL-H is often used for this type of reduction. Other hydride sources such as $LiAlH_4$ (**Table 2.1**, **entry 5 – 7**), $NaBH_4$ (**Table 2.1**, **entry 8**), and $LiBH_4$ (**Table 2.1**, **entry 9**) failed to give the desired product. In some instances, starting materials

were recovered, while in others, complete decomposition occurring at higher equivalent of reducing agent and room temperature.

Scheme 2.8: Synthesis of alkene **2-13** and reduction attempts to allylic alcohol **2-14**

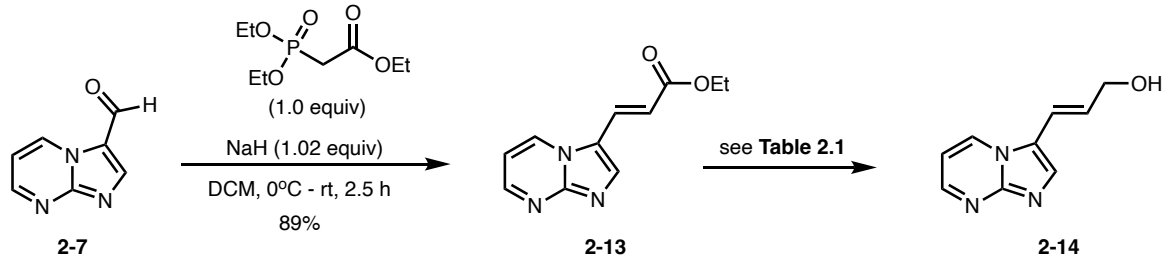

Table 2.1: Attempts on the reduction of **2-13** to **2-14**

Entry	Reagent (equiv.)	Conditions	Result
1	DIBAL-H (2.2 equiv)	THF, - 78 °C – rt, 2 h	5% product
2	DIBAL-H (4.2 equiv)	THF, - 78 °C, 3 h	ND, 45% RSM
3	DIBAL-H (3.0 equiv)	DCM, - 78 °C – rt, 2 h	7% product, 0% RSM
4	DIBAL-H (4.4 equiv)	DCM, - 78 °C – rt, 3 h	ND, 0% RSM
5	$LiAlH_4$ (1.1 equiv)	THF/DCM (1:1), 0 °C – rt, 3 h	ND, 75% RSM
6	$LiAlH_4$ (1.1 equiv)	THF, 0 °C – rt, 45 min	ND
7	$LiAlH_4$ (1.5 equiv) BnCl (1.5 equiv)	THF, rt, 2 h	ND
8	$NaBH_4$ (2.2 equiv)	THF, 0 °C – rt, 24 h	NR
9	$LiBH_4$	THF, 0 °C – rt, 0.5h	NR

Based on the evidence of imidazo[1,2-a]pyrimidine ring reduction observed through mass spectrometry, it was hypothesized that these side products could be prevented by initially removing the pyrimidine ring to obtain aminoimidazole. This aminoimidazole could then be protected before proceeding with the reduction of the conjugated ester to yield the allylic alcohol. The deprotection of the imidazoline ring was achieved using hydrazine hydrate and boc-protection of the free

nitrogens gave the desired triboc-product **2-15** in 64% yield over two steps. With the **2-15** at hand, the reduction of the ester to allylic alcohol was achieved using DIBAL-H in THF at – 78 °C in 84% yield (**Scheme 2.9**). While this approach diverged from the proposed method outlined in **Scheme 2.7** for accessing nagelamide W, it offered insights into the reductive behavior of imidazo[1,2-*a*]pyrimidine different from what is available in the literature[20,29] and provided a strategy for circumventing hydride reduction chemistry when this core is present.

Scheme 2.9: Alternate strategy for the reduction of ester **2-13** to allylic alcohol

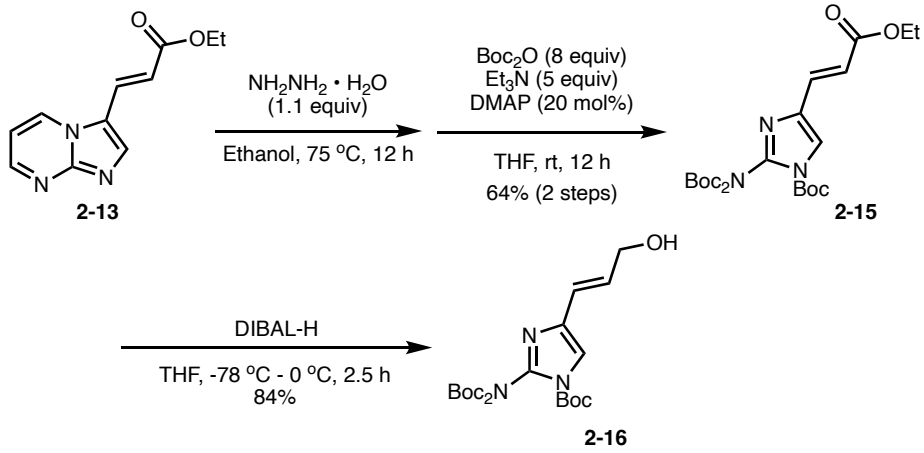

While we successfully obtained the allylic alcohol **2-16**, the absence of the imidazo[1,2-*a*]pyrimidine core as a masked amino imidazolyl group, along with the choice of protecting group, presents future challenges such as protecting group cleavage during alkene functionalization with acid. Therefore, it is necessary to reconsider an alternate approach to access the allylic alcohol while retaining the imidazo[1,2-*a*]pyrimidine core.

We envisioned using Suzuki coupling to access alkene **2-12.** Following previously reported procedures,[30] propargyl alcohol was benzylated to give benzyl propargyl ether **2-17**. The ether then underwent zirconium-mediated hydroboration using Schwartz's reagent and pinacolborane to give organoborane **2-18** in 93% yield.[31-32] Iodination of imidazo[1,2-*a*]pyrimidine with *N*-iodosuccinimide in anhydrous DMF gave **2-19** in good yield. We then utilized a palladium-

catalyzed Suzuki reaction, using aryl iodide **2-19** and organoborane **2-18** to give the desired alkene **2-12** in 75% yield.

Scheme 2.10: Synthesis of alkene **2-12** via Suzuki coupling

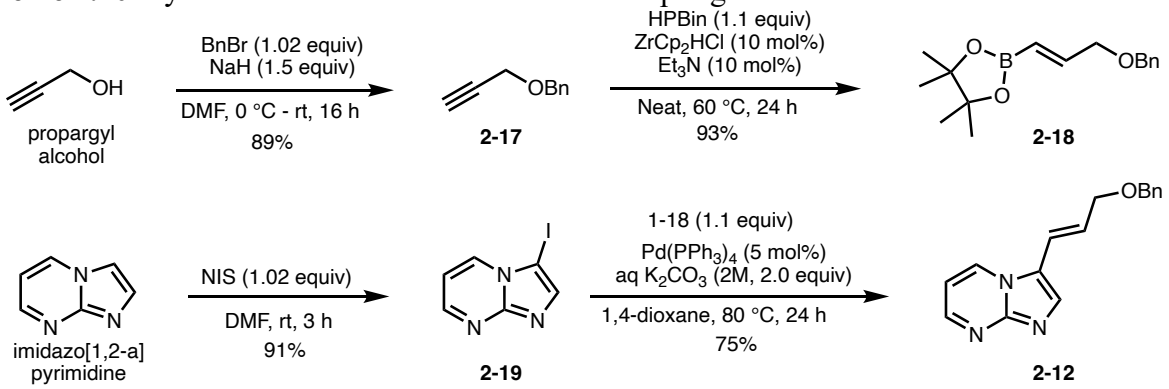

With alkene **2-12** at hand, we proceeded to synthesize the imidazoline core of nagelamide W. First, we treated compound **2-12** with *N*-bromosuccinimide (NBS) and cyanamide in dichloromethane (DCM) at room temperature to access cyanamide bromide **2-20**, but no desired product was obtained (**Table 2.2, Entry 1**).[28] When the solvent was changed to tetrahydrofuran (THF) and the reaction cooled to –78 °C, the desired cyanamide bromide product **2-20** was obtained but only 27% yield (*dr* = 3:1) (**Table 2.2, Entry 2**). To optimize the reaction, different conditions were investigated. Implementation of different bromonium sources such as 1,3-dibromo-5,5-dimethylhydantoin (DBDMH) and *N*-bromophthalimide gave similar results as NBS (**Table 2.2, Entries 3-4**). Then, the role of solvent was studied using NBS as the bromonium source. When DCM was used as solvent at –70 °C, no desired product was isolated probably due to the low solubility of cyanamide in DCM at this temperature (**Table 2.2, Entry 5**). We found that the use of DCM and hexafluoroisopropanol (HFIP) as co-solvent in a 5:1 ratio, gave the desired product **2-20** in 31% but also HFIP-adduct **2-21** as a side product in 37% yield (**Table 2.2, Entry 6**). Previous studies have shown that HFIP activates NBS by forming intermolecular hydrogen bonding with the carbonyl of NBS.[33-34] Additionally, HFIP helps solubilize cyanamide at this

cryogenic temperature. The combination of THF and HFIP did not seem to increase the yield of the desired product (**Table 2.2, Entry 9**), and we hypothesized that THF sequesters HFIP and prevents hydrogen bond formation between HFIP and NBS. The yield of **2-20** can be increased up to 63% when the ratio of DCM/HFIP was changed to 9:1 (**Table 2.2, Entry 7**) and the side product **2-21** can be minimized. A gram scale synthesis afforded 61% of the product **2-20** at –10 °C (**Table 2.2, Entry 8**).

Table 2.2: Synthesis and optimization of cyanamide bromide **2-20**

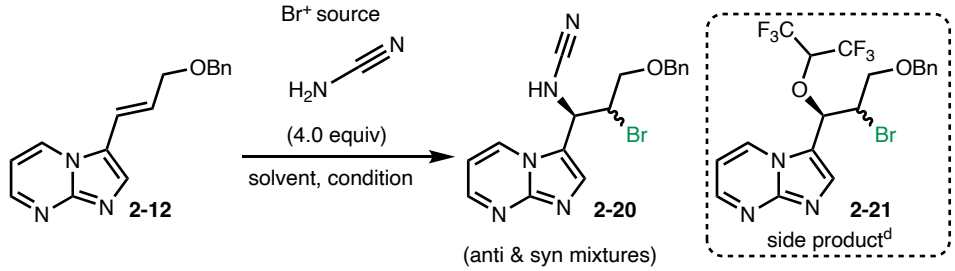

entry	Br^+ source (1.1 equiv)	solvent	conditions	yield of 10[b]
1	NBS	DCM	rt, 72 h	ND[c]
2	NBS	THF	–78 °C, 2 h	27% (dr = 3:1, anti:syn)
3	NBDMH	THF	–78 °C, 3 h	29% (dr = 3:1, anti:syn)
4	N-bromophthalimde	THF	–78 °C, 1 h	28% (dr = 3:1, anti:syn)
5	NBS	DCM	–78 °C - rt, 24 h	ND[c]
6[d]	NBS	DCM/HFIP (5:1)	0 °C, 3 h	31% (dr = 2:1, anti:syn)
7[e]	NBS	DCM/HFIP (9:1)	0 °C, 2 h	63% (dr = 2:1, anti:syn)
8[e,f]	NBS	DCM/HFIP (9:1)	–10 °C, 2 h	61% (dr = 2:1, anti:syn)
9	NBS	THF/HFIP (9:1)	0 °C, 3 h	34% (dr = 3:1, anti:syn)

[a]rt = room temperature, all reported yields are isolate yields.
[b]Diastereomeric ratio (dr) was assigned based on NMR coupling constant.
[c]ND = no product isolated. [d]Side product 1-21 was also isolated in 37% yield. [e]Reaction was ran at 0.075 M concentration. [f]Gram scale.

After the synthesis of **2-20** was optimized, we constructed the imidazoline core of nagelamide W in two steps by treating **2-20** with anhydrous ethanolic hydrogen chloride to give the isourea intermediate **2-22**. Treating intermediate **2-22** with triethylamine under reflux provided

imidazoline **2-23** as a single diastereomer (**Scheme 2.11**). Notably, the *trans*-imidazoline **2-23** was only obtained from *anti*-isomer of **2-22**. Hydrogenation of the benzyl ether group in **2-23** to give alcohol **2-24** was not feasible due to the potential hydrogenation of the imidazo[1,2-*a*]pyrimidine core.[29,35] We were able to achieve the debenzylation of **2-23** by treating the compound with 2.2 equivalents of boron trichloride to give the desired alcohol **2-24** in 80% yield. This debenzylation is concentration dependent and the best yield was obtained at [0.50 M]. At lower concentrations yields reduced significantly due to additional C-2 dealkylation of the ethyl group of the imidazoline to give the corresponding imidazolinone.

Scheme 2.11: Synthesis of imidazoline core and alcohol **2-24**

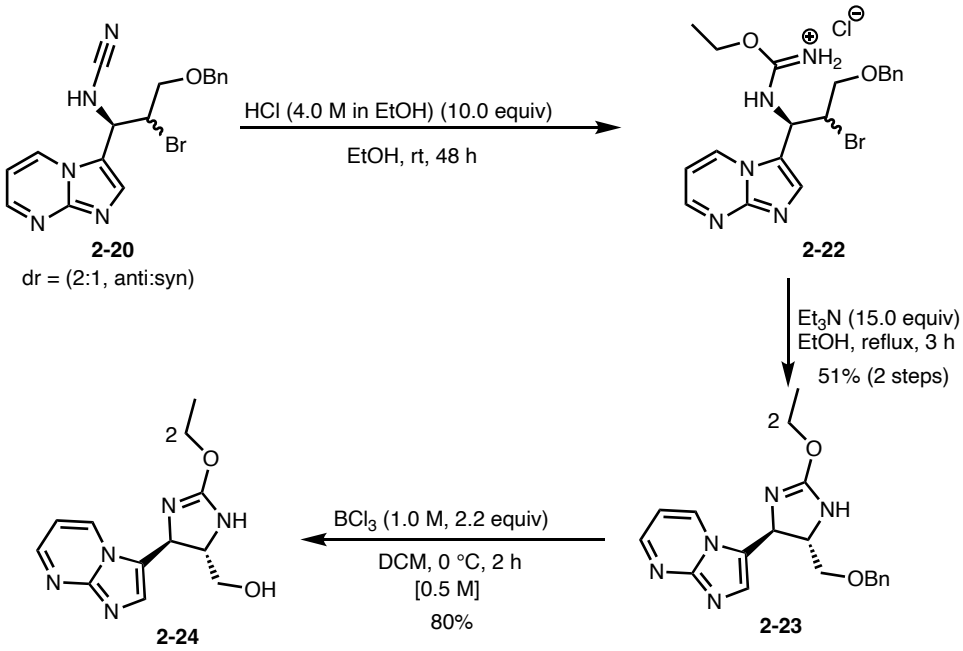

After obtaining alcohol **2-24**, we attempted the conversion of the hydroxyl group to primary amine, which proved to be more challenging than anticipated. A recent manuscript by Herath and Lovely[25] is a beautiful review that discuss various strategies that is used for the incorporation of pyrrole carboxamide in the total synthesis of pyrrole-imidazole alkaloids. We started by doing a Mitsunobu reaction using phthalimide, triphenylphosphine, and diethylazodicarboxylate with the aim of obtaining **2-25**, which we envisioned using to access **2-26**

upon treating with hydrazine (**Scheme 2.12**).[36] Using this approach, compound **2-24** was treated under Mitsunobu condition, however the desired imide product **2-25** was only observed in mass spectrometry and the isolated product was the [5,3]-fused imidazoline-aziridine **2-27** with 68% of alcohol starting material recovered after 16 hours (scheme **2.12**). Due to incomplete consumption of the alcohol **2-24**, the equivalent of phthalimide was increased to 2.3 and triphenylphosphine (PPh_3) and diethyl azodicarboxylate (DEAD) equivalents were increased to 2.2 each. Under the condition above, only the aziridine (**2-27**), was isolated in 28% yield. Also, an attempt to convert the hydroxyl group of **2-24** to chloride using thionyl chloride ($SOCl_2$) did not give the desired product. It was hypothesized that the formation of aziridine is due to the present of free N-H in **2-24** and protection of the N-H should not result in the formation of the aziridine product, and the desired imide should be obtained in good yield.

Scheme 2.12: Unsuccessful attempt to access imide **2-25**

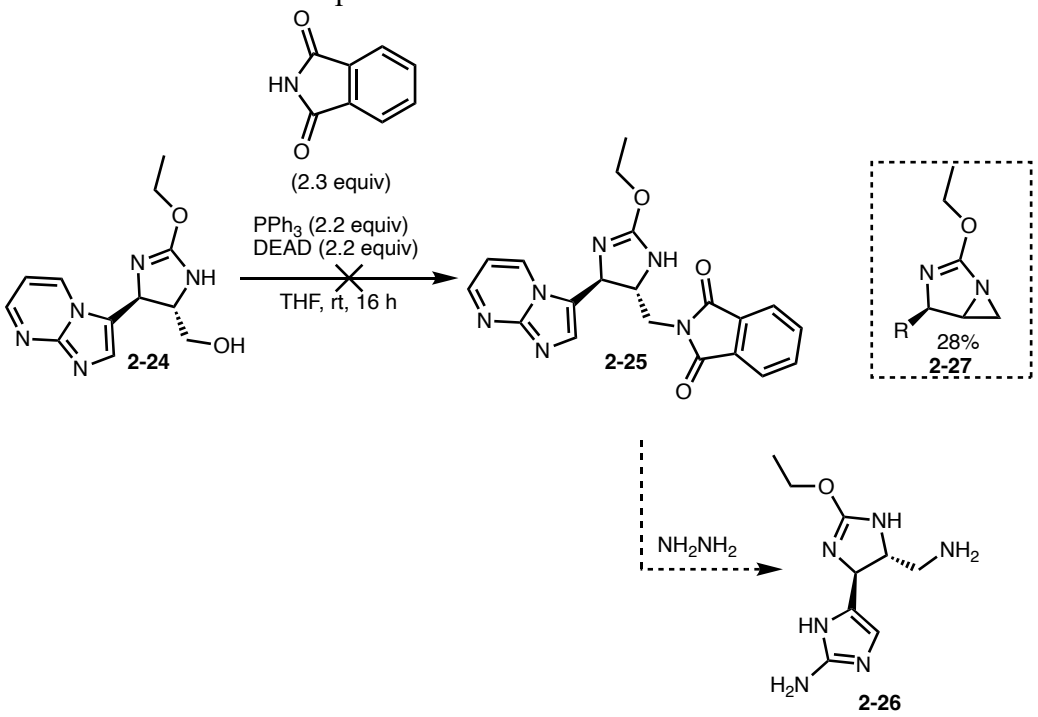

To test this theory, N-H protected imidazole was synthesized. The N-tosylated protected ether (**2-28**) was synthesized in 66% as a mixture of regioisomers from **2-24**. Treatment of

compound **2-28** with boron trichloride did not result the desired debenzylated product but instead gave the dealkylated imidazolone product (**2-29**) in 51% yield (**Scheme 2.13**). The failure to obtain the desired debenzylated product **2-30** led to the investigation of a different route to access the amine from the alcohol **2-24**.

Scheme 2.13: Unsuccessful attempt to access N-protected free alcohol **2-30**

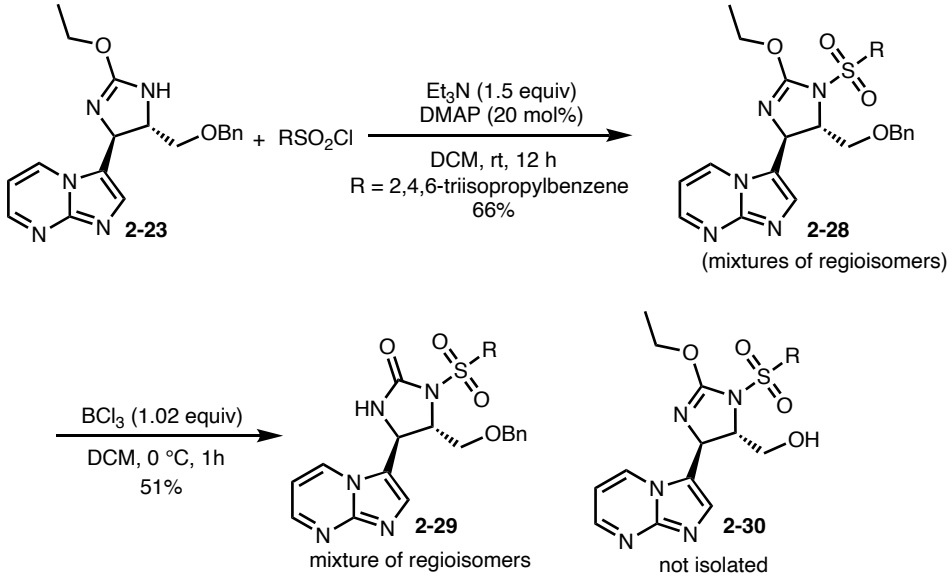

Alternatively, mesylating **2-24** provided **2-31** in 75% yield which then underwent a substitution reaction with potassium phthalimide to give **2-25** in good yield. We were able to obtain a crystal structure for compound **2-25** to confirm the *trans* stereochemistry originally assigned by NMR studies as shown in the scheme above. Treating **2-25** with hydrazine hydrate gave a complex mixture of products with **2-26** only being observed by mass spectrometry (**Scheme 2.14**).

Scheme 2.14: Unsuccessful attempt to access amine **2-26**

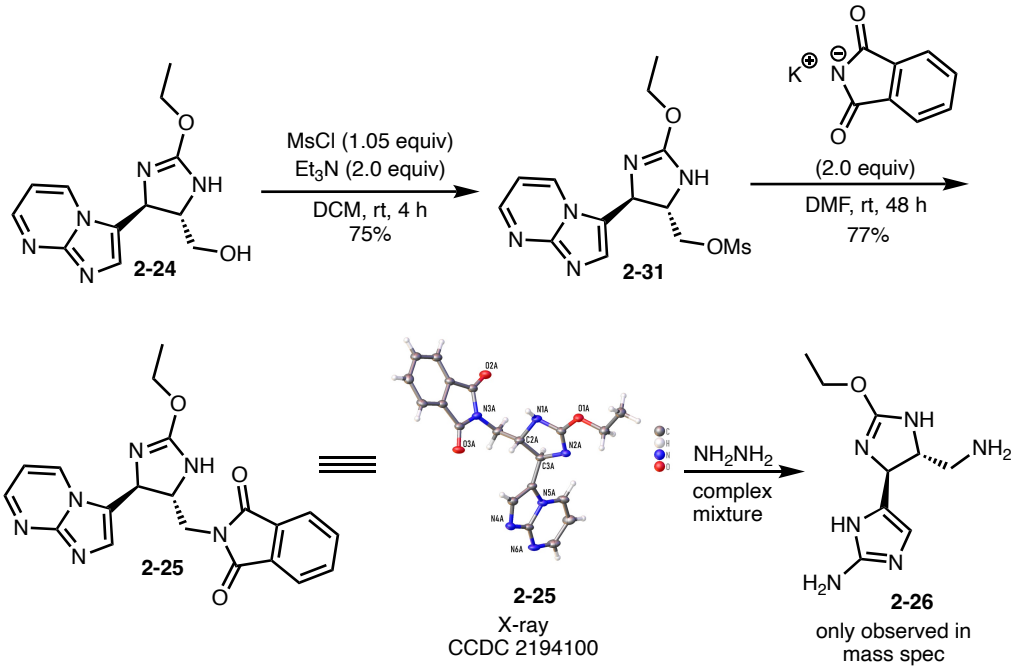

Following the failed attempts to convert alcohol **2-24** to amine using the Gabriel amine approach, we explored the Staudinger approach.[37] First, we converted **2-31** to azide **2-32** followed by Staudinger reduction with triphenylphosphine since hydrogenation was not feasible in the presence of imidazo[1,2-*a*]pyrimidine.[29] The desired amine **2-33** was obtained alongside imidazolone **2-34** as side product (**Scheme 2.15a**). We hypothesize that the imidazolone **2-34** was formed because of water as co-solvent in the reaction and at high temperature. When equivalent amount of water was used, there was no selectivity towards amine **2-33**. We also attempted Staudinger reduction at room temperature and the reaction resulted in no product formation. However, when catalytic amounts of triphenylphosphine and diphenyldisiloxane was used as reducing agent,[38] the desired product was obtained in low yield (**Scheme 2.15b**). Furthermore, direct ligation of azide **2-32** and carboxylic acid **2-37** using 2,2-Dipyridyl diselenide (PySeSePy) as catalyst and that resulted in no product formation (**Scheme 2.15c**).[39]

Scheme 2.15: Synthesis of compound **2-35**

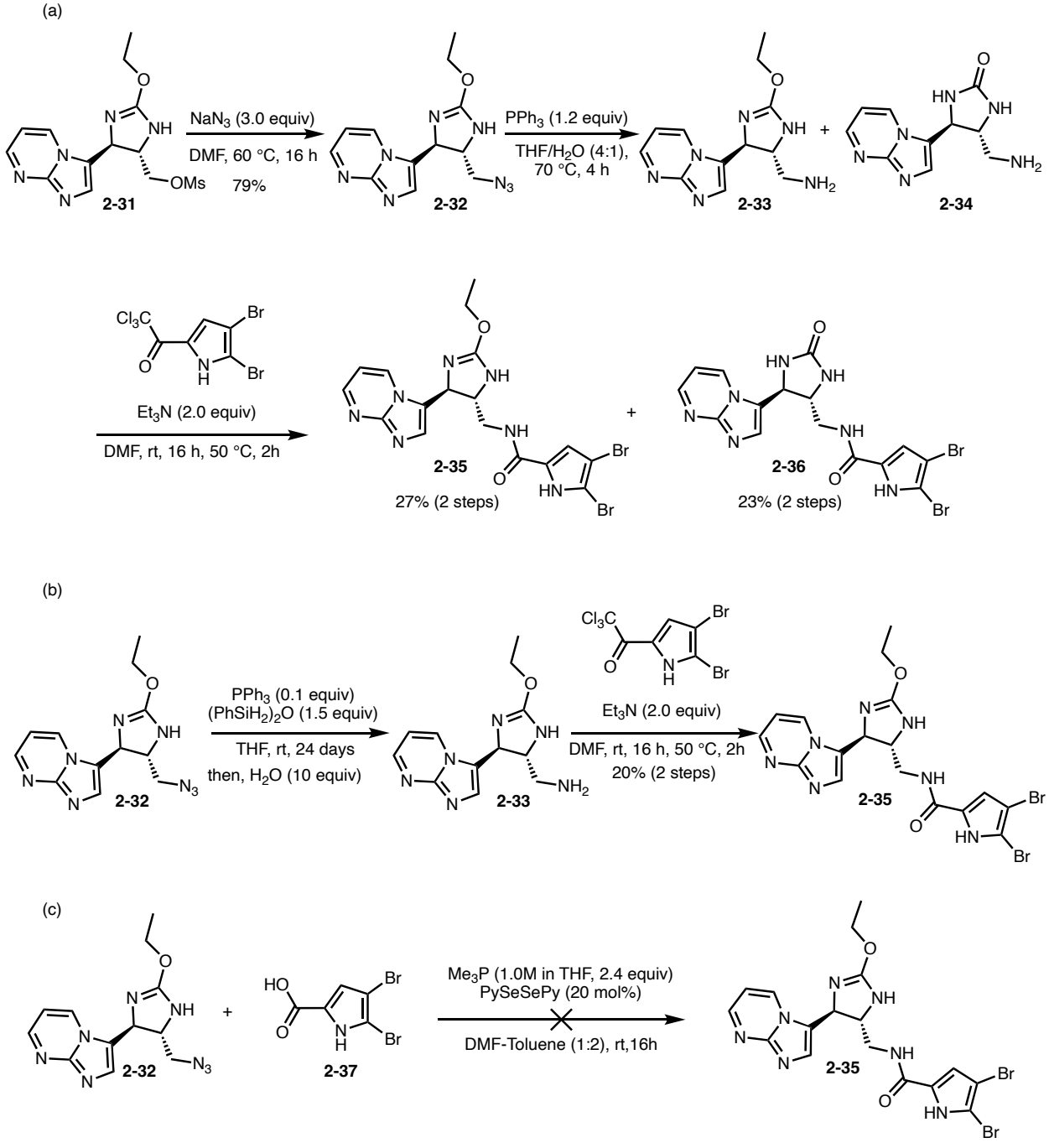

Since we planned on accessing the 2-aminoimidazoline group of the natural product from the 2-ethoxyimidazoline through nucleophilic displacement with ammonia, we thought of an alternate approach to access both 2-aminoimidazoline and primary amine from intermediate **2-31**. In this approach, **2-31** underwent two nucleophilic displacements with ammonia to give **2-38** as a

mesylate salt (**Scheme 2.16**). Amidation of the primary amine with 4,5-dibromotrichloroacetylpyrrole in the presence of triethylamine resulted in **2-39** as our final intermediate to nagelamide W.

Scheme 2.16: Completion of nagelamide W synthesis

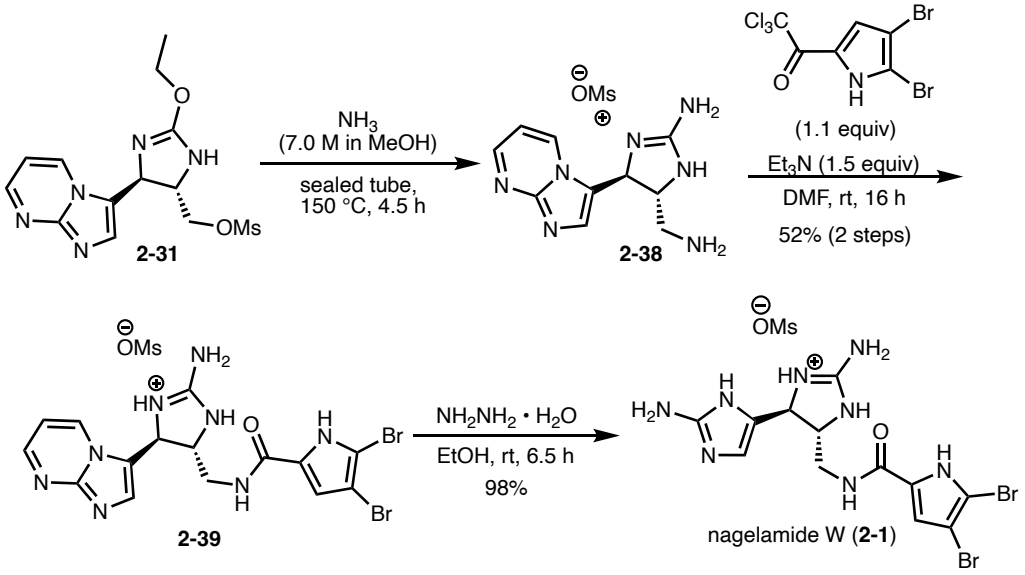

Once the synthesis of **2-39** was completed, we moved forward to the last step of the total synthesis. Herein, the imidazo[1,2-a]pyrimidine core of **2-39** was deprotected using hydrazine monohydrate affording the natural product, nagelamide W (**2-1**), as a mono-mesylated salt in 98% yield after column chromatography. To compare the NMR data for the synthetic sample with the isolated sample, bis-trifluoroacetate salt of **2-1** was prepared.

Spectroscopic data obtained from the synthesized nagelamide W is in full agreement with the spectra reported by Kobayashi *et. al's* (see **Table 2.3** and **Table 2.4** for comparison of nagelamide W to isolated natural product).[19] Slight changes in N-H ppm shift was observed and this is typically seen with exchangeable protons in in NMR. Additionally, the x-ray crystallographic of **2-25** also confirmed the *trans* stereochemistry that was previously assigned by NOE experiment.

Table 2.3: Comparison of [1]H-NMR data for isolated[19] and synthesized Nagelamide W (**2-1**)[40]

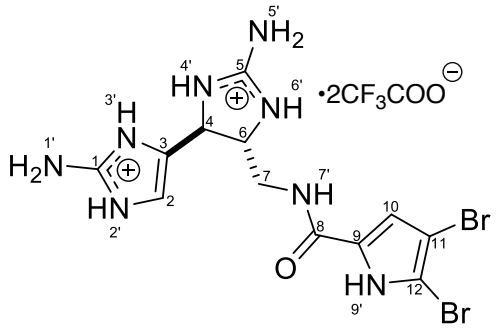

[1]H-#	*[1]H-NMR of Isolated, DMSO-d6*[3]	*[1]H-NMR of synthesized, 500 MHz, DMSO-d6*	*Δ[1]H-NMR*
1'-NH2	7.70 (2H, br s)	7.69 (2H, br s)	-0.01
2	6.83 (1H, s)	6.84 (1H, s)	0.01
2'-NH	12.27 (1H, br s)	12.16 (1H br s)	-0.11
3'-NH	12.86 (1H, br s)	12.82 (1H, br s)	-0.04
4	4.78 (1H, d, J = 7.0)	4.80 (1H, d, J = 7.4)	0.02
4'-NH	8.75 (1H, br s)	8.75 (1H, br s)	0.00
5'-NH2	8.14 (2H, br s)	8.13 (2H br s)	-0.01
6	3.98 (1H, q, J = 7.0)	3.98 (1H, q, J = 6.5)	0.00
6'-NH	8.79 (1H, br s)	8.61 (1H, br s)	-0.18
7	3.43 (2H, m)	3.45 (2H, m)	0.02
7'-NH	8.37 (1H, t, J = 6.0)	8.37 (1H, t, J = 6.0)	0.00
9'-NH	12.72 (1H, br s)	12.74 (1H, d, J = 2.8)	0.02
10	6.94 (1H, d, J = 1.8)	6.91 (1H, d, J = 2.4)	-0.03

Tables 2.4: Comparison of ^{13}C-NMR data for isolated[19] and synthesized Nagelamide W (**2-1**)[40]

^{13}C-#	***^{13}C-NMR of Isolated, DMSO-d6[3]***	***^{13}C-NMR of synthesized, 500 MHz, DMSO-d6***	***Δ^{13}C-NMR***
1	148.3	148.2	-0.1
2	113.2	113.2	0.0
3	124.5	124.6	0.1
4	53.2	53.3	0.1
5	158.8	158.7	-0.1
6	60.0	60.1	0.1
7	41.3	41.4	0.1
8	159.5	159.6	0.1
9	127.7	127.8	0.1
10	111.6	111.7	0.1
11	98.0	98.1	0.1
12	105.0	105.2	0.2

2.3 Conclusions

In conclusion, we have accomplished the first total synthesis of (±)-nagelamide W in 11 longest linear sequence with an overall yield of 6.0%. The structure described by Kobayashi *et. al's* in the isolation report[19] has been confirmed by NMR spectroscopy and the *trans* stereochemistry at the imidazoline core also confirmed by x-ray crystallography.

2.4 Experimental section

General Information

All flasks were oven-dried overnight and cooled under nitrogen. Reactions were carried out under a nitrogen atmosphere unless stated otherwise. All chemicals and solvents were purchased from commercial sources and used without further purification, unless otherwise mentioned. THF and ethanolic hydrogen chloride solution were dried over molecular sieves before use in the reaction. Dichloromethane was dried by passing it through packed column of alumina, and triethylamine was distilled over calcium hydride. N-bromosuccinimide was recrystallized in hot water before use and stored in the dark. Infrared spectra were recorded on a Jasco Series 6600 FTIR spectrometer. The mass spectrometer ionization method was ESI with a quadrupole detector. ^{1}H and ^{13}C NMR spectra were recorded on a 500 MHz spectrometer. Chemical shifts are reported relative to the residue peaks of the solvent: $CDCl_3$: 7.26 ppm for ^{1}H and 77.0 ppm for ^{13}C, CD_3OD: 3.31 ppm for ^{1}H and 47.6 ppm for ^{13}C, and DMSO-d6: 2.50 ppm for ^{1}H and 39.5 ppm for ^{13}C. Signal multiplicities are given as s (singlet), br (broad), d (doublet), t (triplet), dd (doublet of doublet), and m (multiplet). Reaction carried out at room temperature (rt) implies temperature range usually between 20 – 22 °C. Column chromatography was performed using a Teledyne ISCO CombiFlash® NextGen system with prepacked columns (RediSep® Normal-phase silica, 20-40 microns and RediSep® Rf Gold Reversed-Phase C18 silica, 20-40 microns). TLCs were performed on pre-coated 0.25 mm thick silica gel 60 F254 plates and pre-coated 150 um thick, C18 reverse phase F254 plates, visualized using UV light and iodine staining.

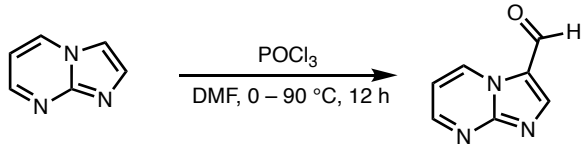

2-7

imidazo[1,2-*a*]pyrimidine-3-carbaldehyde (**2-7**): To a 50 mL round bottom flask equipped with a magnetic stirrer was added dimethylformamide (15 mL) and was cooled to 0 °C. Then, phosphorus oxychloride (5 mL, 53.7 mmol) was added and stirred at 0 °C for 30 mins. After that, imidazo-[1,2-*a*]-pyrimidine (2.0 g, 16.8 mmol) was added and the reaction was heated to 90 °C while stirring overnight. The reaction was cooled to room temperature and quenched with lithium bromide (15 mL). The pH of the reaction was adjusted to approximately 11 using 20% sodium hydroxide solution. The product was extracted with ethyl acetate (5 x 150 mL), and the organic layers were combined, dried over sodium sulfate, decanted, and concentrated. The crude was then purified using CombiFlash chromatography (silica gel, 20-40 microns, gradient 3% methanol/dichloromethane) to give **2-7** as yellow solid (1.07 g, 43%). mp = 196 – 198 °C. ^{1}H NMR (500 MHz, $CDCl_3$) δ 9.99 (s, 1H), 9.76 (dd, *J* = 6.8, 2.1 Hz, 1H), 8.86 (dd, *J* = 4.2, 2.1 Hz, 1H), 8.54 (s, 1H), 7.23 (dd, *J* = 6.8, 4.2 Hz, 1H). ^{13}C{^{1}H} NMR (125 MHz, $CDCl_3$) δ 178.8, 154.4, 151.7, 147.6, 136.3, 123.1, 111.6. IR (neat, cm^{-1}): 3109, 2847, 1646, 1613. HRMS (ESI-TOF) *m*/*z*: $[M + H]^+$ calcd for ($C_7H_6N_3O^+$) 148.0505; found 148.0536.

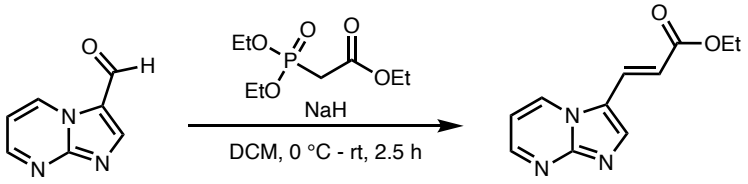

2-7 **2-13**

ethyl (*E*)-3-(imidazo[1,2-*a*]pyrimidin-3-yl)acrylate (**2-13**): Triethyl phosphonoacetate (1.40 mL, 6.79 mmol) was added dropwise under argon to a suspension of sodium hydride (NaH) (0.28 g, 6.93 mmol) in anhydrous dichloromethane (DCM) (8 mL) at 0 °C. The resulting solution was

stirred for 15 minutes until no hydrogen gas was released from the reaction. Then, a solution of imidazo[1,2-*a*]pyrimidine-3-carbaldehyde (1.0 g, 6.79 mmol) in anhydrous DCM (30 mL) was added dropwise over 20 minutes. The resulting solution was warmed slowly to room temperature and stirred for 2.5 h. The reaction was then quenched with ammonium chloride (20 mL), extracted with dichloromethane (3 x 40 mL). The organics were combined and washed with brine (50 mL). The organics was dried over sodium sulfate, concentrated, and titurated with cold diethyl ether to give the product as a yellow solid (1.31 g, 89%). mp = 192 – 194 °C. ^{1}H NMR (500 MHz, $CDCl_3$) δ 8.66 (dd, *J* = 6.9, 2.0 Hz, 1H), 8.63 (dd, *J* = 4.1, 2.0 Hz, 1H), 8.19 (s, 1H), 7.80 (d, *J* = 16.0 Hz, 1H), 7.08 (dd, *J* = 6.9, 4.1 Hz, 1H), 6.43 (d, *J* = 16.0 Hz, 1H), 4.26 (q, *J* = 7.1 Hz, 2H), 1.32 (t, *J* = 7.1 Hz, 3H). ^{13}C{^{1}H} NMR (125 MHz, $CDCl_3$) δ 166.7, 150.8, 150.4, 138.1, 132.0, 127.6, 120.2, 116.0, 110.0, 60.8, 14.3. FTIR (neat, cm^{-1}): 3063, 2977, 1699, 1626, 1516. HRMS (ESI-TOF) *m*/*z*: $[M+H]^+$ calcd for ($C_{11}H_{12}N_3O_2^+$) 218.0924; found 218.0982.

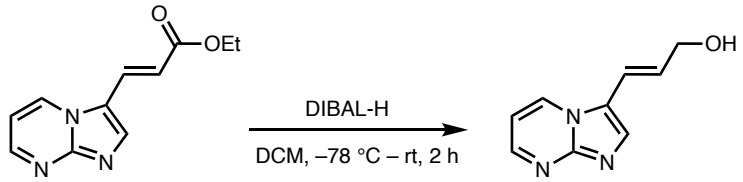

2-13 **2-14**

(*E*)-3-(imidazo[1,2-a]pyrimidin-3-yl)prop-2-en-1-ol (2-14): An oven-dried 25 mL round bottom flask equipped with stirrer bar was charged with **2-13** (0.060 g, 0.28 mmol) an anhydrous dichloromethane (8 mL). The solution was cooled to – 78 °C and diisobutylalluminium hydride DIBAL-H (1 M in hexane, 0.85 mL, 0.85 mmol) was added slowly via syringe. After that, the reaction was warmed to room temperature and stirred for 2 hours. The reaction was quenched with Rochelle's salt (5 mL) and the product extracted with DCM. The product was purified with CombiFlash chromatography (silica gel, 20-40 microns, gradient 0-5% methanol / dichloromethane) to give the product as a yellowish oil (3.5 mg, 7%). ^{1}H NMR (500 MHz,

CD_3OD) δ 8.92 (dd, *J* = 6.9, 1.7 Hz, 1H), 8.57 (dd, *J* = 4.1, 1.9 Hz, 1H), 7.92 (s, 1H), 7.13 (dd, *J* = 6.9, 4.1 Hz, 1H), 6.88 (d, *J* = 16.0 Hz, 1H), 6.54 (dt, *J* = 16.0, 5.2 Hz, 1H), 4.33 (dd, *J* = 5.2, 1.7 Hz, 2H). $^{13}C\{^1H\}$ NMR (125 MHz, $CDCl_3$) δ 149.3, 148.8, 133.3, 131.2, 130.9, 121.9, 114.4, 109.1, 63.2. FTIR (neat, cm^{-1}): 3351, 3061, 2970, 1685. HRMS (ESI-TOF) *m*/*z*: $[M+H]^+$ calcd for ($C_{11}H_{12}N_3O_2^+$) 176.0818; found 176.0824.

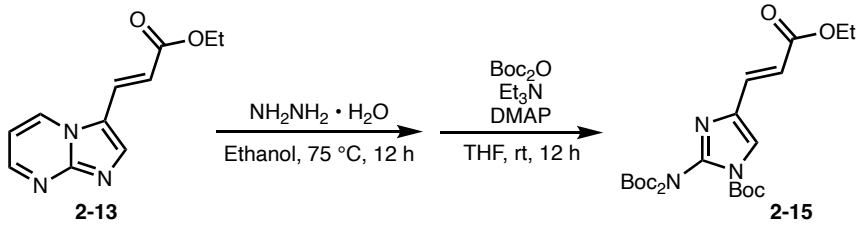

***tert*-butyl (*E*)-2-(bis(*tert*-butoxycarbonyl)amino)-4-(3-ethoxy-3-oxoprop-1-en-1-yl)-1H-imidazole-1-carboxylate (2-15):** To a suspension of **2-13** (0.22 g, 1.0 mmol) in ethanol (10 mL) was added hydrazine hydrate (50 µL, 1.1 mmol). The reaction was heated to 75 °C for 5 hours when TLC showed complete conversion of starting material. The reaction was stopped and cooled down to room temperature. The solvent was removed with rotary evaporator and tetrahydrofuran (15 mL), di-tert-butyl decarbonate Boc_2O (1.84 mL, 8.0 mmol), triethylamine (0.70 mL, 5.0 mmol), and dimethylaminopyridine DMAP (0.025 g, 0.2 mmol) were added. The reaction was the stirred overnight at room temperature. The reaction was quenched with ammonium chloride (20 mL) and the product was extracted with ethyl acetate (2 x 20 mL). The organic layers were combined and concentrated. The organics was dried over sodium sulfate and product was purified using CombiFlash chromatography (silica gel, 20-40 microns, gradient 20% ethyl acetate/hexane) to give the product has a yellow oil (0.31 g, 64%). ^1H NMR (500 MHz, $CDCl_3$) δ 7.50 (s, 1H), 7.42 (d, *J* = 15.6 Hz, 1H), 6.57 (d, *J* = 15.6 Hz, 1H), 4.20 (q, *J* = 7.1 Hz, 2H), 1.56 (s, 9H), 1.39 (s, 18H), 1.27 (t, *J* = 7.1 Hz, 3H). $^{13}C\{^1H\}$ NMR (125 MHz, $CDCl_3$) δ 166.8, 149.1, 145.8, 143.8, 139.2, 135.2, 134.3, 130.5, 119.3, 108.5, 86.5, 83.7, 60.2, 27.7, 27.6, 14.0. FTIR (neat, cm^{-1}): 3082,

2991, 1698, 1623. HRMS (ESI-TOF) *m/z:* $[M+H]^+$ calcd for ($C_{23}H_{36}N_3O_8^+$) 482.2497; found 482.2481.

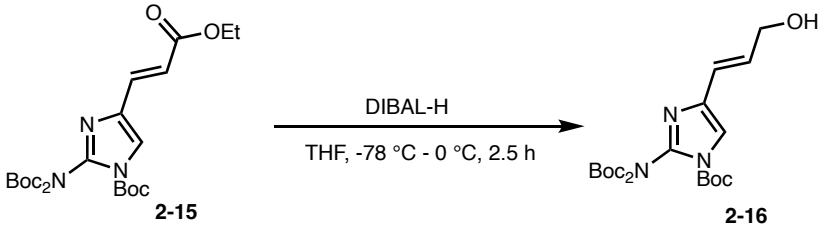

***tert*-butyl (*E*)-2-(*bis*(*tert*-butoxycarbonyl)amino)-4-(3-hydroxyprop-1-en-1-yl)-1H-imidazole-1-carboxylate (2-16):** To a solution of ester **2-15** (1.32 g, 2.74 mmol) in tetrahydrofuran (10 mL) at –78 °C was added diisobutylalluminium hydride DIBAL-H (1 M in hexane, 6.86 mL, 6.86 mmol). The reaction was stirred at –78 °C for 20 mins, then the reaction was stirred at 0 °C for 1 hour. The reaction was then cooled back down to –78 °C and 2 mL of methanol was added to destroy the excess DIBAL-H. The reaction was brought back to room temperature and diluted with ethyl acetate (20 mL) and Rochelle's salt (20 mL). The mixture was stirred for 3 hours, and organic layer was collected. The aqueous layer was extracted ethyl acetate (2 x 20 mL). The organics were combined, washed with brine, and dried with sodium sulfate. The product was then purified with CombiFlash chromatography (silica gel, 20-40 microns, gradient 40% ethyl acetate/hexane) to give the product has clear oil (1.01 g, 84%). ^{1}H NMR (500 MHz, $CDCl_3$) δ 7.26 (s, 1H), 6.53 (dt, J = 15.7, 5.3 Hz, 1H), 6.42 (dt, J = 15.7, 1.4 Hz, 1H), 4.30 (dd, J = 5.3, 1.4 Hz, 2H), 1.58 (s, 9H), 1.42 (s, 18H). ^{13}C{^{1}H} NMR (125 MHz, $CDCl_3$) δ 149.4, 146.3, 138.5, 136.9, 129.9, 121.1, 114.8, 86.0, 83.6, 63.2, 27.9, 27.8. FTIR (neat, cm^{-1}): 3348, 3021, 1621. HRMS (ESI-TOF) *m/z:* $[M+H]^+$ calcd for ($C_{21}H_{34}N_3O_7^+$) 440.2391; found 440.2484.

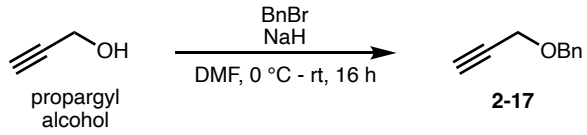

((prop-2-yn-1-yloxy)methyl)benzene (2-17): To a suspension of sodium hydride (60% in mineral oil, 4.40 g, 110 mmol) in anhydrous DMF (60 mL) at 0 °C was added propargyl alcohol (5.82 mL, 100 mmol) slowly via a syringe. After 15 mins, benzyl bromide (13.0 mL, 110 mmol) was added, and the reaction was stirred at room temperature overnight for 12 hours. The reaction was then diluted with ethyl acetate (200 mL) and washed with aqueous 1 M hydrochloric acid (200 mL). The organic layer was dried over sodium sulfate, decanted, and then concentrated and purified with CombiFlash chromatography (silica gel, 20-40 microns, gradient 0-5% ethyl acetate/hexane) to give the product as a clear oil (13.0 g, 89% yield). ^{1}H NMR (500 MHz, $CDCl_3$) δ 7.28 – 7.18 (m, 5H), 4.49 (s, 2H), 4.04 (d, J = 2.4 Hz, 2H), 2.40 (t, J = 2.4 Hz, 1H). $^{13}C\{^{1}H\}$ NMR (125 MHz, $CDCl_3$) δ 137.2, 128.2, 127.8, 127.6, 79.6, 74.6, 71.1, 56.7. FTIR (neat, cm^{-1}): 3289, 2854, 2150, 1495, 1072. Spectroscopy data is consistent with previous literature report.[30]

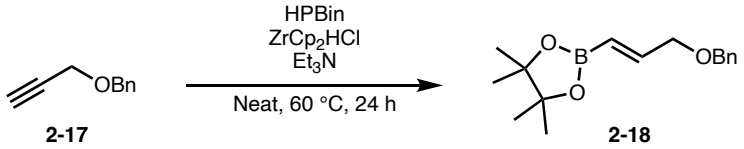

(*E*)-2-(3-(benzyloxy)prop-1-en-1-yl)-4,4,5,5-tetramethyl-1,3,2-dioxaborolane (**2-18**): A dry 250 mL round bottom flask equipped with magnetic stirrer bar was charged with alkyne **2-17** (9.0 g, 61.6 mmol), then zirconocene hydrochloride (1.59 g, 6.16 mmol) was added. The reaction was then purged with argon, and anhydrous triethylamine (0.86 mL, 6.16 mmol) was added followed by dropwise addition of pinacol borane (9.83 mL, 67.7 mmol). The reaction was then refluxed in a preheated aluminum beads at 60 °C for 24 hours. The reaction mixture was then cooled to room temperature and filtered through a short silica plug with diethyl ether/petroleum ether (1:4) as eluent. The filtrate was concentrated to give the crude product **2-18** as a clear oil (15.7 g, 93%).

The crude was used without further purification. ^{1}H NMR (500 MHz, $CDCl_3$) δ 7.38 – 7.25 (m, 5H), 6.69 (dt, *J* = 4.6, 9.2, 18.1 Hz, 1H), 5.82 – 5.74 (dt, *J* = 18.1, 3.5, 1.8 Hz, 1H), 4.54 (s, 2H), 4.12 (dd, *J* = 4.6, 1.8 Hz, 2H), 1.28 (s, 12H). ^{13}C{^{1}H} NMR (125 MHz, $CDCl_3$) δ 149.2, 138.3, 128.3, 127.6, 127.6, 83.3, 72.3, 71.7, 24.8 (the alkene CH next to boron was not observed due to quadrupolar coupling effect of the boron). FTIR (neat, cm^{-1}): 3085, 2977, 1643, 1322. Spectroscopy data is consistent with previous literature report.[31]

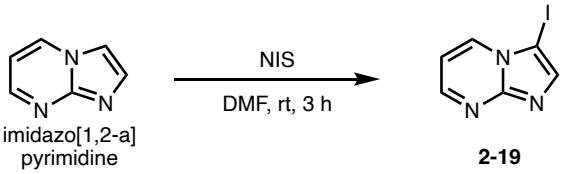

imidazo[1,2-a] pyrimidine

2-19

3-iodoimidazo[1,2-*a*]pyrimidine (2-19): To a solution of imidazo[1,2-*a*]pyrimidine (3.0 g, 25.18 mmol) in dimethylformamide (20 mL) at room temperature was added N-iodosuccinimide (5.78 g, 25.67 mmol) in the dark. The reaction was stirred in the dark for 3 hours then ethyl acetate (30 mL) was added. The product was filtered and washed with ethyl acetate (100 mL) to give a brown solid (5.6 g, 91% yield). mp = 187 °C (decomposed). ^{1}H NMR (500 MHz, DMSO-d_6) δ 8.78 (dd, *J* = 6.8, 1.9 Hz, 1H), 8.54 (dd, *J* = 4.1, 1.9 Hz, 1H), 7.90 (s, 1H), 7.18 (dd, *J* = 6.8, 4.1 Hz, 1H). ^{13}C{^{1}H} NMR (125 MHz, DMSO-d_6) δ 150.5, 150.0, 141.0, 135.0, 110.0, 64.1. FTIR (neat, cm^{-1}): 3115, 1669, 1495. HRMS (ESI-TOF) *m/z:* $[M+H]^+$ calcd for ($C_6H_5IN_3^+$) 245.9523; found: 245.9535.

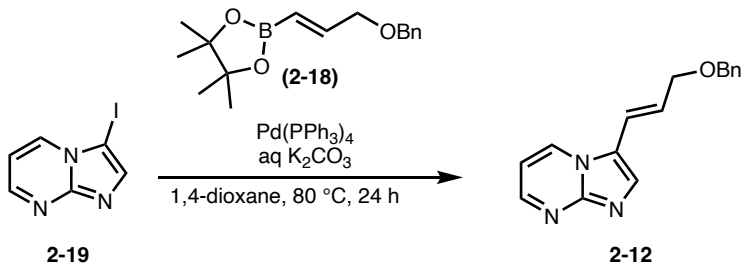

2-19 **2-12**

(*E*)-3-(3-(benzyloxy)prop-1-en-1-yl)imidazo[1,2-*a*]pyrimidine (2-12): 3-iodoimidazo[1,2-*a*]pyrimidine **2-19** (10.0 g, 40.81 mmol) was suspended in degassed 1,4-dioxane (100 mL) and **2-18** (15.4 g, 44.89 mmol) was added. Then, tetrakis(triphenylphosphine)palladium(0) (2.36 g, 2.04 mmol) was added followed by degassed aqueous potassium carbonate solution (2 M, 41.0 mL, 81.62 mmol). The reaction was purged with argon and refluxed in a preheated oil bath at 80 °C for 24 hours. The reaction was cooled to room temperature, diluted with water (100 mL) and then extracted with ethyl acetate (4 x 200 mL). The organics were combined, dried over sodium sulfate, and decanted. The organic was then concentrated and purified with CombiFlash chromatography (silica gel, 20-40 microns, gradient 0-3% methanol/dichloromethane) to give the product as a yellowish solid (8.1 g, 75% yield). mp = 95 °C. ^{1}H NMR (500 MHz, DMSO-d_6) δ 9.06 (dd, *J* = 6.8, 1.9 Hz, 1H), 8.53 (dd, *J* = 4.1, 1.9 Hz, 1H), 8.06 (s, 1H), 7.40 – 7.33 (m, 4H), 7.32 – 7.26 (m, 1H), 7.11 (dd, *J* = 6.8, 4.1 Hz, 1H), 6.98 (d, *J* = 16.0 Hz, 1H), 6.49 (dt, *J* = 16.0, 6.0 Hz, 1H), 4.56 (s, 2H), 4.22 (dd, J = 6.0, 1.5 Hz, 2H). ^{13}C{^{1}H} NMR (125 MHz, DMSO-d_6) δ 149.5, 148.1, 138.4, 133.0, 132.7, 128.3, 127.6, 127.5, 126.6, 121.5, 116.8, 109.0, 71.4, 70.2. FTIR (neat, cm^{-1}): 3085, 2891, 1654, 1263. HRMS (ESI-TOF) *m/z:* $[M+H]^+$ calcd for ($C_{16}H_{16}N_3O^+$) 266.1288; found 266.1292.

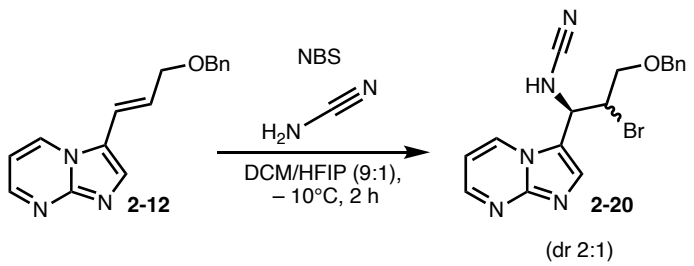

***N*-(3-(benzyloxy)-2-bromo-1-(imidazo[1,2-*a*]pyrimidin-3-yl)propyl)cyanamide (2-20).** Alkene **2-12** (1.28 g, 4.83 mmol) was dissolved in dichloromethane (58 mL) and hexafluoro-2-propanol (HFIP) (6.4 mL). Then, cyanamide (0.81 g, 19.32 mmol) was added and the solution was cooled to –10 °C. N-bromosuccinimide (0.95 g, 5.31 mmol) was added slowly at –10 °C and then stirred at that temperature for 2 hours in the dark. The reaction was warmed to room temperature and quenched with sodium thiosulfate (25 mL) and sodium bicarbonate (25 mL). The dichloromethane layer was collected, and the aqueous layer was further extracted with dichloromethane (2 x 50 mL). The organics were combined, dried over sodium sulfate and decanted. The organic was concentrated and purified with CombiFlash chromatography (silica gel, 20-40 microns, gradient 0-5% methanol/dichloromethane) to give the product as a foamy yellowish semi-solid (1.14 g, 61% yield (dr = 2:1 (*anti* : *syn*)). NMR data for major isomer (*anti*): ^{1}H NMR (500 MHz, CD_3OD) δ 8.90 (dd, *J* = 7.0, 1.9 Hz, 1H), 8.64 (m, 1H peak overlap with minor isomer), 7.97 (s, 1H), 7.30 – 7.21 (m, 5H, peak overlap with minor isomer), 7.14-7.10 (m, 1H, peak overlap with minor isomer), 5.39 (d, *J* = 6.6 Hz, 1H), 4.86 (m, 1H, peak overlap with minor isomer), 4.55 – 4.43 (m, 2H), 4.03 (dd, *J* = 10.8, 4.4 Hz, 1H), 3.73 (dd, *J* = 10.8, 6.2 Hz, 1H). ^{13}C{^{1}H} NMR (125 MHz, CD_3OD) δ 152.6, 149.9, 138.8, 134.9, 134.5, 129.4, 129.1, 129.0, 120.7, 116.0, 110.7, 74.3, 71.8, 52.8, 52.5. FTIR (neat, cm^{-1}): 3081, 3028, 2860, 1618, 1361. HRMS (ESI-TOF) *m/z:* $[M+H]^+$ calcd for ($C_{17}H_{17}BrN_5O^+$): 386.0611 & 388.0591; found 386.0609 & 388.0581.

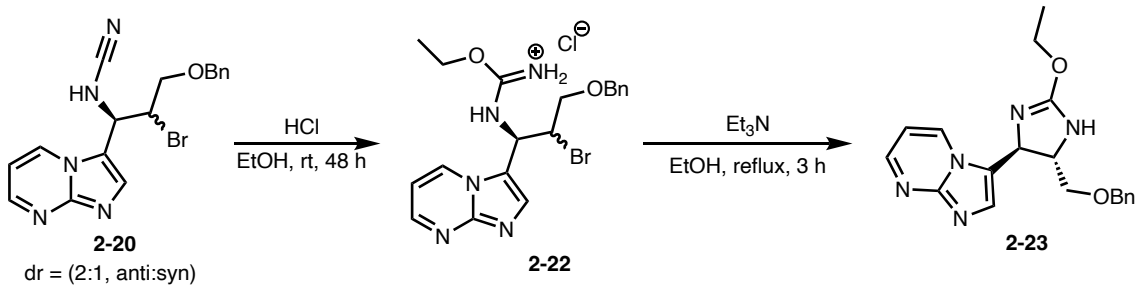

2-20
dr = (2:1, anti:syn)

2-22

2-23

3-(5-((benzyloxy)methyl)-2-ethoxy-4,5-dihydro-1*H*-imidazol-4-yl)imidazo[1,2-*a*]pyrimidine (**2-23**). Cyanamide bromide **2-20** (2.88 g, 7.46 mmol) was dissolved in anhydrous ethanol (15 mL) and anhydrous ethanolic hydrochloric acid (4.0 M, 18.7 mL, 74.61 mmol) was added. The reaction was stirred at room temperature for 48 hours to give intermediate **2-22**, then it was diluted with more anhydrous ethanol (15 mL) and cooled in an ice bath to 0 °C. Anhydrous triethylamine (15.6 mL, 111.92 mmol) was added slowly at 0 °C. Upon complete addition, the reaction was refluxed in a preheated aluminum beads at 80 °C for 3 hours and then cooled to room temperature. The solvent was then removed under reduced pressure. To the crude solid compound was added tetrahydrofuran (THF) (40 mL) and ethyl acetate (10 mL). The insoluble triethylammonium chloride salt was filtered and washed with THF (40 mL), and the filtrate was concentrated and purified with CombiFlash chromatography (silica gel, 20-40 microns, gradient 0-5% methanol/dichloromethane) to give the product as a yellowish foamy semi-solid (1.33 g, 51% yield). The relative *trans* configuration was assigned based on a 1D NOE NMR spectroscopy experiment which was further confirmed by X-ray crystallography of compound **2-25**. ^{1}H NMR (500 MHz, $CDCl_3$) δ 8.58 (dd, J = 7.0, 2.0 Hz, 1H), 8.41 (dd, J = 4.1, 2.0 Hz, 1H), 7.56 (s, 1H), 7.33 – 7.21 (m, 5H), 6.65 (dd, J = 7.0, 4.1 Hz, 1H), 5.0 (d, J = 6.0 Hz, 1H), 4.56 – 4.46 (m, 2H), 4.22 (m, 2H), 4.03 (q, J = 6.0 Hz, 1H), 3.56 (m, 2H), 1.26 (t, J = 7.1 Hz, 3H). ^{13}C{^{1}H} NMR (125 MHz, $CDCl_3$) δ 164.4, 149.4, 149.2, 137.6, 133.0, 132.5, 128.6, 128.1, 128.0, 123.7, 108.3, 73.6, 72.5, 65.4, 14.6 (the imidazoline methine carbons are not present in ^{13}C NMR due to rapid

tautomerism of the imidazoline). FTIR (neat, cm^{-1}): 3162, 3028, 2979, 1615, 1308. HRMS (ESI-TOF) *m/z:* $[M+H]^+$ calcd for ($C_{19}H_{22}N_5O_2^+$) 352.1768; found 352.1769.

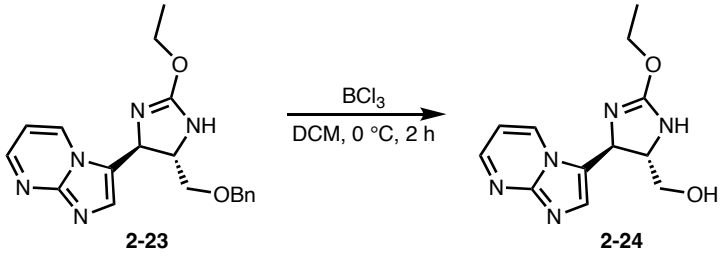

2-23 **2-24**

2-ethoxy-4-(imidazo[1,2-*a*]pyrimidin-3-yl)-4,5-dihydro-1*H*-imidazol-5-yl)methanol (**2-24**). To a solution of **2-23** (0.73 g, 2.07 mmol) in dichloromethane (4 mL) at 0 °C was added boron trichloride solution (1.0 M in dichloromethane, 4.60 mL, 4.55 mmol) dropwise. The reaction mixture was stirred at 0 °C for 2 hours. The reaction was quenched with methanol (5 mL) and basify with triethylamine until pH ≈ 7. The solvent was then removed at reduced pressure and the crude was purified with CombiFlash chromatography (basic alumina, 40-60 microns, gradient 3-10% methanol/dichloromethane) to give a foamy yellowish semi-solid (0.432g, 80% yield). ^{1}H NMR (500 MHz, CD_3OD) δ 8.86 (dd, *J* = 6.9, 2.0 Hz, 1H), 8.58 (dd, *J* = 4.2, 2.0 Hz, 1H), 7.68 (s, 1H), 7.10 (dd, *J* = 6.9, 4.2 Hz, 1H), 5.22 (d, *J* = 6.0 Hz, 1H), 4.25 (q, *J* = 7.1 Hz, 2H), 4.01 – 3.94 (m, 1H), 3.71 – 3.61 (m, 2H), 1.33 (t, *J* = 7.1 Hz, 3H). ^{13}C{^{1}H} NMR (125 MHz, CD_3OD) δ 167.1, 151.7, 150.2, 134.7, 132.3, 126.3, 110.2, 66.4, 64.9, 14.8 (the imidazoline methine carbons are not observed in ^{13}C NMR due to rapid tautomerism of the imidazoline). FTIR (cm^{-1}): 3162(br), 2975, 1614, 1494, 1263. HRMS (ESI-TOF) *m/z:* $[M+H]^+$ calcd for ($C_{12}H_{16}N_5O_2^+$) 262.1299; found 262.1304.

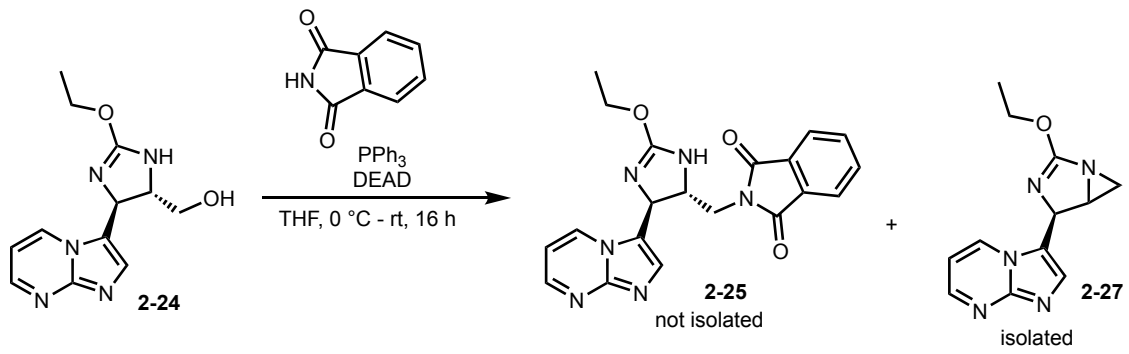

3-(2-ethoxy-1,3-diazabicyclo[3.1.0]hex-2-en-4-yl)imidazo[1,2-a]pyrimidine (2-27): To a solution of alcohol **2-24** (0.045 g, 0.17 mmol) in anhydrous tetrahydrofuran (THF) (4 mL) under argon at 0 °C was added triphenylphosphine (PPh_3) (0.097 g, 0.37 mmol) and phthalimide (0.057 g, 0.39 mmol). Then, diethyl azodicarboxylate (DEAD) (40% wt in toluene, 0.17 mL, 0.37 mmol) was added dropwise at 0 °C. The reaction was stirred at 0 °C for an hour and then room temperature overnight. The reaction was concentrated and purified with CombiFlash chromatography (basic alumina gel, gradient 0 - 5% methanol/dichloromethane) to give compound **2-27** as a clear oil (0.012 g, 28%). ^{1}H NMR (500 MHz, CD_3OD) δ 8.88 (dd, J = 6.9, 1.9 Hz, 1H), 8.62 (dd, J = 4.1, 1.9 Hz, 1H), 7.77 (s, 1H), 7.14 (dd, J = 6.9, 4.1 Hz, 1H), 5.65 – 5.61 (m, 1H), 4.25 – 4.15 (m, 2H), 3.50 (ddd, J = 5.4, 4.1, 1.6 Hz, 1H), 2.53 (d, J = 5.4 Hz, 1H), 2.15 (d, J = 4.1 Hz, 1H), 1.32 (t, J = 7.1 Hz, 3H). ^{13}C NMR (125 MHz, CD_3OD) δ 174.0, 150.7, 148.8, 133.3, 130.7, 124.2, 108.9, 66.7, 59.9, 43.0, 37.4, 13.0. FTIR (neat, cm^{-1}): 2961, 1713, 1618. HRMS (ESI-TOF) *m/z:* $[M+H]^+$ calcd for ($C_{12}H_{14}N_5O^+$) 244.1193; found: 244.1194.

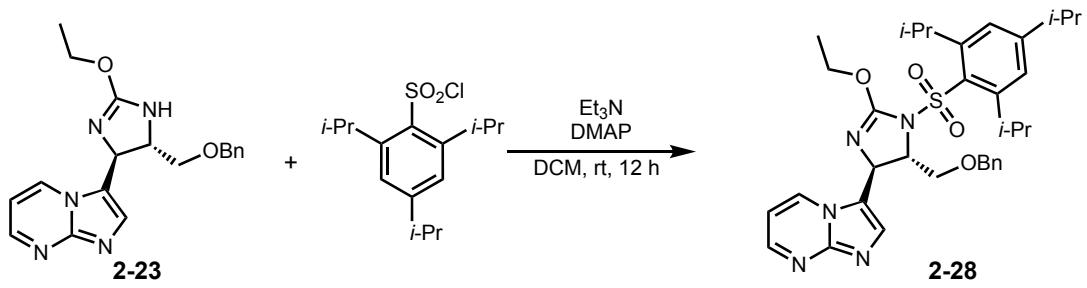

3-(5-((benzyloxy)methyl)-2-ethoxy-1-((2,4,6-triisopropylphenyl)sulfonyl)-4,5-dihydro-1H-imidazol-4-yl)imidazo[1,2-a]pyrimidine (**2-28**): To a solution of compound **2-23** (0.46 g, 1.32 mol) in dichloromethane (10 mL) was added 2,4,6-triisopropylbenzenesulfonyl chloride (0.44 g, 1.45 mmol), triethylamine (0.28 mL, 1.98 mmol) and 4-dimethylaminopyridine (0.032 g, 0.26 mmol). The reaction was stirred at room temperature overnight for 16 h. The reaction was quenched with ammonium chloride (10 mL) and extracted with dichloromethane (3 x 10 mL). The organic layers were combined, dried over sodium sulfate, concentrated under reduced pressure and then purified with CombiFlash chromatography (silica, 20-40 microns, gradient 1 – 2.5% methanol/dichloromethane) to give the titled compound as inseparable mixture of regioisomers as a foamy solid (0.54 g, 66%). ^{1}H NMR (500 MHz, $CDCl_3$) δ 8.76 (dd, J = 6.9, 2.0 Hz, 1H), 8.60 – 8.51 (m, 3H), 7.85 (s, 1H), 7.58 (d, J = 0.8 Hz, 1H), 7.37 (qd, J = 7.0, 3.6 Hz, 5H), 7.33 – 7.22 (m, 5H), 7.16 (s, 2H), 7.06 (s, 2H), 6.81 (dd, J = 6.9, 4.1 Hz, 1H), 6.65 (dd, J = 6.8, 4.0 Hz, 1H), 5.76 (d, J = 4.4 Hz, 1H), 5.32 – 5.27 (m, 1H), 4.71 – 4.58 (m, 4H), 4.49 (d, J = 11.9 Hz, 1H), 4.27 – 4.13 (m, 5H), 4.10 – 3.97 (m, 3H), 3.94 (dd, J = 9.2, 8.1 Hz, 1H), 3.76 – 3.65 (m, 3H), 3.55 (dd, J = 9.7, 8.2 Hz, 1H), 2.94 – 2.82 (m, 2H), 1.27 – 1.17 (m, 20H), 1.14 (d, J = 6.7 Hz, 7H), 1.08 (t, J = 7.1 Hz, 3H), 1.02 – 0.94 (m, 14H). ^{13}C NMR (125 MHz, $CDCl_3$) δ 157.2, 157.0, 154.4, 154.3, 151.4, 151.3, 149.8, 149.7, 148.9, 137.6, 137.2, 134.9, 132.8, 132.6, 131.4, 130.9, 128.6, 128.5, 128.2, 128.2, 127.9, 127.8, 123.8, 123.7, 122.4, 122.2, 108.5, 108.4, 73.9, 73.5, 71.7, 69.6, 67.2,

66.8, 66.8, 63.3, 58.7, 55.8, 34.3, 34.2, 29.4, 29.0, 24.8, 24.7, 24.1, 23.6, 23.5, 23.4, 13.8, 13.8. FTIR (cm^{-1}): 2957, 1656, 1325, 1152; HRMS (ESI-TOF) *m/z:* $[M+H]^+$ calcd for ($C_{34}H_{44}N_5O_4S^+$) 618.3109; found: 618.3110

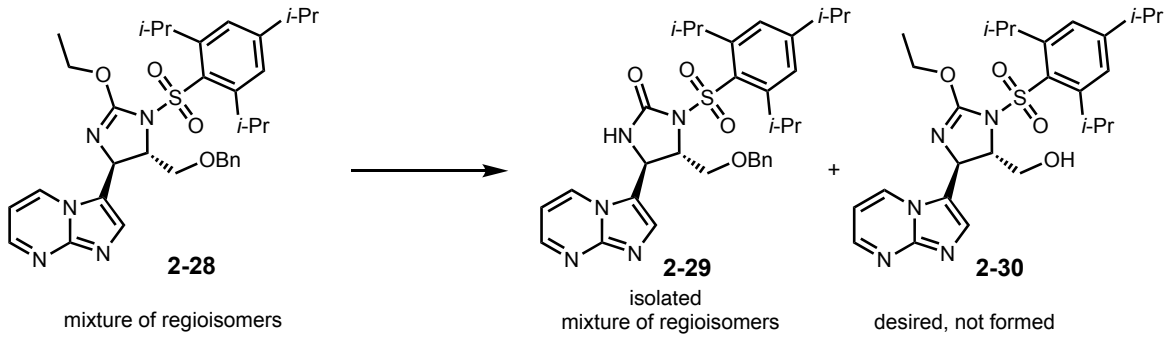

5-((benzyloxy)methyl)-4-(imidazo[1,2-a]pyrimidin-3-yl)-1-((2,4,6-triisopropylphenyl)sulfonyl)imidazolidin-2-one (**2-29**): To a solution of benzyl ether **2-28** (0.20 g, 0.32 mmol) in dichloromethane (8 mL) at 0 °C was added boron trichloride solution (1.0M in heptane, 0.33 mL, 0.33 mmol) slowly over 5 minutes. The reaction mixture was stirred at 0 °C for 3 hours. The reaction was quenched with methanol (5 mL) and triethylamine (1.5 mL). The solvent was then removed at high pressure and the crude was purified with CombiFlash chromatography (silica, 40-60 microns, gradient 3-10% methanol/dichloromethane) to give the titled compound as a yellowish oil (0.097 g, 51%). Major isomer: ^{1}H NMR (500 MHz, $CDCl_3$) δ 8.63 – 8.59 (m, 1H), 8.42 (dd, J = 4.1, 1.9 Hz, 1H), 7.51 (s, 1H), 7.43 – 7.35 (m, 5H), 7.12 (s, 2H), 6.49 (dd, J = 6.8, 4.1 Hz, 1H), 5.24 (t, J = 1.9 Hz, 1H), 4.66 (d, J = 1.8 Hz, 2H), 4.36 (dt, J = 9.5, 3.2 Hz, 1H), 4.23 (dd, J = 8.9, 3.7 Hz, 1H), 4.04 – 3.83 (m, 4H), 1.26 – 1.10 (m, 17H). ^{13}C NMR (125 MHz, $CDCl_3$) Messy carbon. FTIR (cm^{-1}): 3030, 2957, 2867, 1738. HRMS (ESI-TOF) *m/z:* $[M+H]^+$ calcd for ($C_{32}H_{40}N_5O_4S^+$) 590.2796; found: 590.2814.

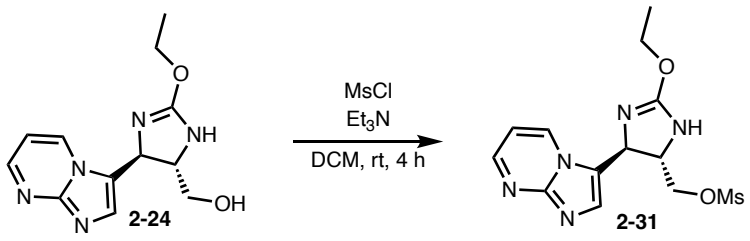

(2-ethoxy-4-(imidazo[1,2-a]pyrimidin-3-yl)-4,5-dihydro-1H-imidazol-5-yl)methyl methanesulfonate (**2-31**). Alcohol **2-24** (0.43 g, 1.65 mmol) was dissolved in dichloromethane (18 mL) in a 50 mL round bottom flask and then triethylamine (0.46 mL, 3.30 mmol) was added followed by dropwise addition of methanesulfonyl chloride (134 µL, 1.73 mmol). The reaction was then stirred at room temperature for 4 hours. The reaction was concentrated and purified with CombiFlash chromatography (basic alumina gel, gradient 0 - 4% methanol/dichloromethane) to give the desired product **2-31** as a foamy white semi-solid (0.422 g, 75%). ^{1}H NMR (500 MHz, CD_3OD) δ 8.77 (dd, *J* = 7.0, 2.0 Hz, 1H), 8.60 (dd, *J* = 4.2, 2.0 Hz, 1H), 7.73 (s, 1H), 7.13 (dd, *J* = 7.0, 4.2 Hz, 1H), 5.25 (d, *J* = 6.0 Hz, 1H), 4.38 – 4.29 (m, 3H), 4.29 – 4.24 (m, 2H), 3.14 (s, 3H), 1.34 (t, *J* = 7.1 Hz, 3H). ^{13}C{^{1}H} NMR (125 MHz, CD_3OD) δ 167.1, 152.0, 150.4, 134.8, 132.9, 125.1, 110.3, 72.0, 66.6, 37.3, 14.8 (the imidazoline methine carbons were not observed in ^{13}C-NMR due to rapid tautomerism of the imidazoline). FTIR (neat, cm^{-1}): 3170, 2981, 1617, 1345. HRMS (ESI-TOF) *m/z:* $[M+H]^+$ calcd for ($C_{13}H_{18}N_5O_4S^+$) 340.1074; found: 340.1071.

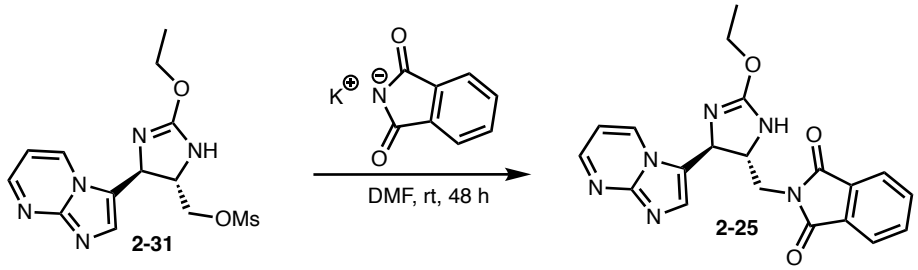

2-((2-ethoxy-4-(imidazo[1,2-a]pyrimidin-3-yl)-4,5-dihydro-1H-imidazol-5-yl)methyl)isoindoline-1,3-dione (**2-25**). To a solution of **2-31** (137 mg, 0.404 mmol) in dimethylformamide (3 mL) was added potassium phthalimide (150 mg, 0.808 mmol). The reaction

was stirred at room temperature for 48 hours after which TLC showed complete conversion of starting material. The solvent was removed under reduced pressure and the crude was purified with CombiFlash chromatography (basic alumina gel, gradient 0 - 5% methanol/dichloromethane) to give the desired product as white solid (122 mg, 77% yield). Crystallization from methanol via slow evaporation from 5ml vial over a period of 5 days gave a colorless crystal which was used for X-ray crystal structure. mp = 213 °C (decomposed). ^{1}H NMR (500 MHz, CD_3OD) δ 8.78 (dd, J = 7.0, 2.0 Hz, 1H), 8.55 (dd, *J* = 4.2, 2.0 Hz, 1H), 7.78 – 7.71 (m, 4H), 7.62 (s, 1H), 7.09 (dd, *J* = 7.0, 4.2 Hz, 1H), 5.22 (d, *J* = 7.2 Hz, 1H), 4.43 (q, *J* = 6.4 Hz, 1H), 4.18 (q, *J* = 7.2 Hz, 2H), 4.00 (dd, *J* = 14.1, 6.0 Hz, 1H), 3.90 (dd, *J* = 14.1, 6.0 Hz, 1H), 1.27 (t, *J* = 7.2 Hz, 3H). ^{13}C{^{1}H} NMR (125 MHz, CD_3OD): δ 169.9, 167.0, 164.8, 152.0, 150.2, 135.5, 134.8, 133.1, 132.6, 124.2, 110.3, 66.5, 42.9, 14.7 (the imidazoline methine carbons were not observed in ^{13}C-NMR due to rapid tautomerism of the imidazoline). FTIR (neat, cm^{-1}): 3144, 2934, 1769, 1715, 1613. HRMS (ESI-TOF) *m/z:* $[M+H]^+$ calcd for ($C_{20}H_{19}N_6O_3^+$) 391.1513; found: 391.1520.

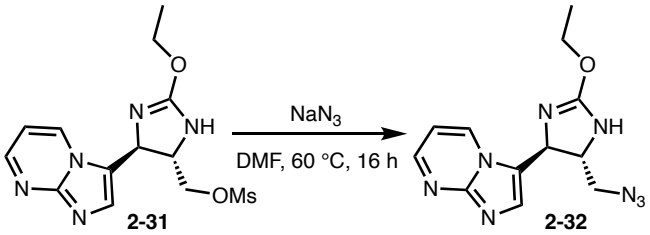

3-(5-(azidomethyl)-2-ethoxy-4,5-dihydro-1*H*-imidazol-4-yl)imidazo[1,2-*a*]pyrimidine (**2-32**): Compound **2-31** (0.18 g, 0.52 mmol) was dissolved in DMF (2.5 mL) in a 7.5 mL reaction vial and to the solution was added sodium azide (0.051 g, 0.78 mmol). The reaction was heated to 60 °C and stirred overnight. The DMF was removed under reduced pressure and the product was purified with CombiFlash chromatography (basic alumina gel, gradient 0 - 2% methanol/dichloromethane) to give the desired product as a foamy white solid (0.12 g, 79%). ^{1}H NMR (500 MHz, CD_3OD) δ 8.76 (d, *J* = 6.8 Hz, 1H), 8.59 (dd, *J* = 4.1, 1.9 Hz, 1H), 7.70 (s, 1H),

7.12 (dd, *J* = 6.8, 4.1 Hz, 1H), 5.18 (d, *J* = 6.4 Hz, 1H), 4.27 (q, *J* = 7.0 Hz, 2H), 4.18 (dd, *J* = 6.4, 4.9 Hz, 1H), 3.63 (dd, *J* = 12.6, 4.9 Hz, 1H), 3.45 (dd, *J* = 12.6, 4.5 Hz, 1H), 1.34 (t, *J* = 7.0 Hz, 3H). $^{13}C\{^{1}H\}$ NMR (125 MHz, CD_3OD) δ 165.6, 150.5, 149.0, 133.4, 131.4, 124.0, 108.9, 65.1, 54.2, 13.5 (the imidazoline methine carbons were not observed in ^{13}C-NMR due to rapid tautomerism of the imidazoline). FTIR (neat, cm^{-1}): 3140, 2931, 2103, 1615, 1345. HRMS (ESI-TOF) *m/z:* $[M+H]^+$ calcd for ($C_{12}H_{15}N_8O^+$) 287.1363; found: 287.1360.

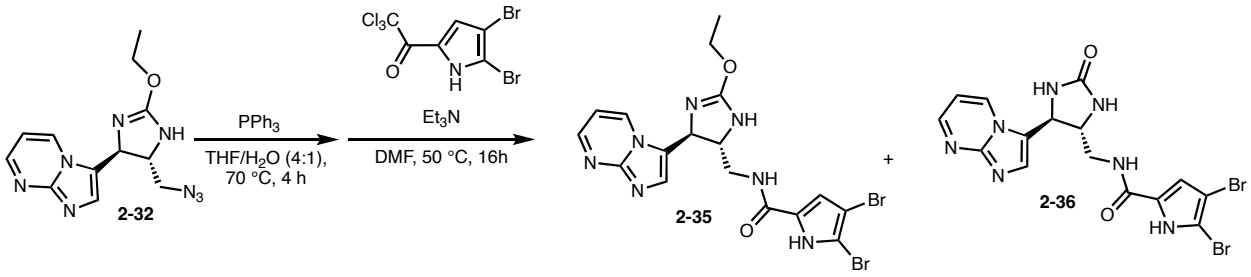

4,5-dibromo-*N*-((2-ethoxy-4-(imidazo[1,2-*a*]pyrimidin-3-yl)-4,5-dihydro-1*H*-imidazol-5-yl)methyl)-1*H*-pyrrole-2-carboxamide (2-35) and 4,5-dibromo-*N*-((5-(imidazo[1,2-*a*]pyrimidin-3-yl)-2-oxoimidazolidin-4-yl)methyl)-1*H*-pyrrole-2-carboxamide (2-36): Azide **2-32** (0.032 g, 0.11 mmol) was dissolved in THF (1 mL) and H_2O (0.25 mL), triphenylphosphine (0.045 g, 0.17 mmol) was added and the reaction was refluxed for 4 hours to give the corresponding amines. The reaction was concentrated, and the crude was dissolved in DMF (1 mL). Triethylamine (24 μL, 0.17 mmol) and 2,2,2-trichloro-1-(4,5-dibromo-1*H*-pyrrol-2-yl)ethan-1-one (0.063 g, 0.17 mmol) were added. The reaction was stirred at 50 °C overnight and then concentrated under reduced pressure. The crude was purified with CombiFlash chromatography (basic alumina gel, gradient 0 - 5% methanol/dichloromethane) to give **2-35** as white foamy solid (0.015 g, 27%) and **2-36** as white foamy solid (0.012 g, 23%).

2-35: ^{1}H NMR (500 MHz, CD_3OD) δ 9.29 (d, *J* = 6.8 Hz, 1H), 8.97 (d, *J* = 4.1 Hz, 1H), 8.34 (s, 1H), 7.53 (dd, *J* = 6.8, 4.1 Hz, 1H), 6.82 (s, 1H), 5.76 (d, *J* = 7.1 Hz, 1H), 4.72 – 4.63 (m, 1H),

4.55 (q, J = 7.0 Hz, 2H), 3.81 (dd, J = 14.4, 4.9 Hz, 1H), 3.72 (dd, J = 14.4, 4.9 Hz, 1H), 1.48 (t, J = 7.0 Hz, 3H). $^{13}C\{^{1}H\}$ NMR (126 MHz, CD_3OD) δ 163.5, 161.1, 155.9, 135.0, 133.4, 126.6, 113.4, 112.4, 105.6, 98.7, 71.1, 60.9, 51.8, 41.0, 13.0. HRMS (ESI-TOF) *m/z:* $[M+H]^+$ calcd for ($C_{17}H_{17}Br_2N_7O_2^+$) 509.9884, 511.9863 & 513.9843; found: 509.9825, 511.9867 & 513.9823.

2-36: ^{1}H NMR (500 MHz, cd_3od) δ 9.18 (d, J = 6.8 Hz, 1H), 8.95 (d, J = 4.1 Hz, 1H), 8.13 (s, 1H), 7.51 (dd, J = 6.8, 4.1 Hz, 1H), 6.81 (s, 1H), 5.23 (d, J = 6.1 Hz, 1H), 4.16 (m, 1H), 3.70 – 3.50 (m, 2H). HRMS (ESI-TOF) *m/z:* $[M + H]^+$ calcd for ($C_{17}H_{17}Br_2N_7O_2^+$) 481.9571, 483.9550, & 485.9530; found: 481.9597, 483.9584, & 485.9568.

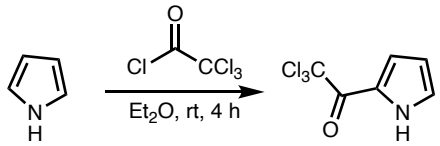

S2-1

2,2,2-trichloro-1-(1*H*-pyrrol-2-yl)ethan-1-one (**S2-1**). A 50 mL round bottom flask equipped with magnetic stirrer was charged with diethyl ether (20 mL) and trichloroacetyl chloride (2.50 mL, 22.0 mmol). Pyrrole (1.40 mL, 20.0 mmol) was added in portions every 10 minutes over 1 hour. Then, the reaction was further stirred at room temperature under nitrogen for 3 hours. The reaction was quenched with 5 mL of water followed by addition of 15 mL saturated aqueous potassium carbonate. The organic later was then collected and stirred with activated charcoal for 15 minutes. The mixture was filtered with celite plug and the resulting filtrate was concentrated under reduced pressure. The product was then recrystallized in hexane to give 2,2,2-trichloro-1-(1*H*-pyrrol-2-yl)ethan-1-one as a white solid (3.6 g, 85% yield). mp = 75 °C. ^{1}H NMR (500 MHz, CDCl3) δ 9.69 (s, br, 1H), 7.40 (ddd, J = 4.0, 2.5, 1.3 Hz, 1H), 7.21 – 7.16 (m, 1H), 6.39 (dt, J = 4.0, 2.5 Hz, 1H). $^{13}C\{1H\}$ NMR (125 MHz, CDCl3) δ 173.3, 127.3, 122.9, 121.3, 111.9, 94.9. FTIR (neat, cm-1): 3317, 1649, 1535. HRMS (ESI-TOF) m/z: $[M–H]^-$ calcd for ($C_6H_3Cl_3NO^-$): 209.9285, 211.9256, & 213.9226; found: 209.9286, 211.9244, & 213.9215.

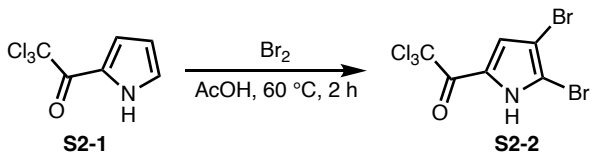

S2-1 S2-2

2,2,2-trichloro-1-(4,5-dibromo-1*H*-pyrrol-2-yl)ethan-1-one (S2-2): To a solution of **S2-1** (1.20 g, 5.65 mmol) in acetic acid (15 mL) was added bromine (0.58 mL, 11.30 mmol). The reaction was placed in a preheated aluminum beads at 60 °C and stirred for 2 hours. The reaction was then cooled to room temperature and stirred overnight. Then, water (10 mL) was added, and the pH of the solution was adjusted to 5 with 2M NaOH. The reaction was extracted with ethyl acetate (3 x 30 mL), and the organic layers were combined, dried over sodium sulfate, and filtered. The volatiles were removed, and the pure product was obtained by recrystallization with ethanol/water as a beige solid (1.7g 81%). mp: 138 °C. ^{1}H NMR (500 MHz, DMSO-d_6) δ 13.75 (s, 1H), 7.39 (s, 1H). ^{13}C{1H} NMR (125 MHz, DMSO-d_6) δ 171.4, 123.8, 122.9, 115.1, 101.3, 94.5. FTIR (neat, cm^{-1}): 3284, 1654, 1365. HRMS (ESI-TOF) *m/z:* [M–H]$^{-}$ calcd for ($C_6HBr_2Cl_3NO^{-}$): 365.7495, 367.7475, 369.7446, 371.7425, & 373.7396; found: 365.7489, 367.7473, 369.7451, 371.7417, & 373.7385.

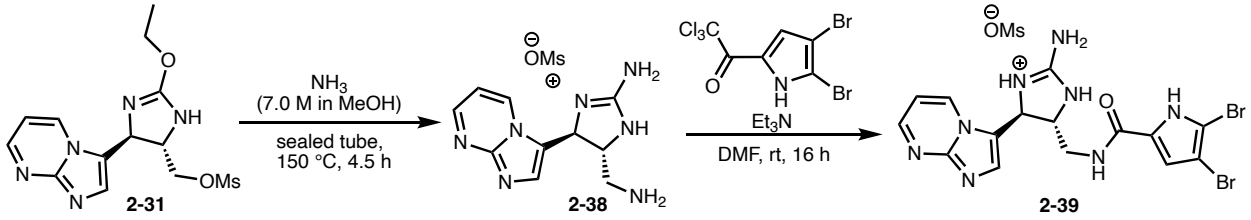

2-31 2-38 2-39

2-amino-5-((4,5-dibromo-1*H*-pyrrole-2-carboxamido)methyl)-4-(imidazo[1,2-*a*]pyrimidin-3-yl)-4,5-dihydro-1*H*-imidazol-3-ium methanesulfonate (**2-39**). Compound **2-31** (60.0 mg, 0.177 mmol) was dissolved in ammonia solution (7.0 M in methanol) (5 mL) in a sealed tube and was heated to 150 °C for 4.5 hours. The reaction was cooled to room temperature and the solvent evaporated to give **2-38**. The crude compound was redissolved in DMF (1.5 mL) and charged with

2,2,2-trichloro-1-(4,5-dibromo-1H-pyrrol-2-yl)ethan-1-one **S2-2** (79.0 mg, 0.212 mmol) and triethylamine (49.0 µL, 0.354 mmol) and the reaction was stirred for 24 hours at room temperature. The solvent was removed under reduced pressure and the product purified with CombiFlash chromatography (C18-derived rp silica, gradient 0 - 100% methanol/water) to give the desired product as white solid (53 mg, 52% yield). mp: 189 °C (decompose) ^{1}H NMR (500 MHz, CD_3OD) δ 8.82 (dd, *J* = 6.9, 2.0 Hz, 1H), 8.58 (dd, *J* = 4.2, 2.0 Hz, 1H), 7.86 (s, 1H), 7.06 (dd, *J* = 6.9, 4.2 Hz, 1H), 6.78 (s, 1H), 5.11 (d, *J* = 5.7 Hz, 1H), 4.33 (q, *J* = 5.7 Hz, 1H), 3.66 (dd, *J* = 5.7, 2.2 Hz, 2H), 2.70 (s, 3H) (mesylate proton). ^{13}C{^{1}H} NMR (125 MHz, CD_3OD) δ 162.2, 160.6, 153.0, 150.0, 146.4, 136.8, 128.4, 114.5, 110.80, 110.76, 106.5, 100.0, 63.3, 58.1, 43.0, 39.5 (mesylate carbon). FTIR (neat, cm^{-1}): 3107, 2924, 1685, 1618, 1561. HRMS (ESI-TOF) *m/z:* $[M+H]^+$ calcd for ($C_{15}H_{15}Br_2N_8O^+$) 480.9731, 482.9710, & 484.9690; found: 480.9743, 482.9726, & 484.9706.

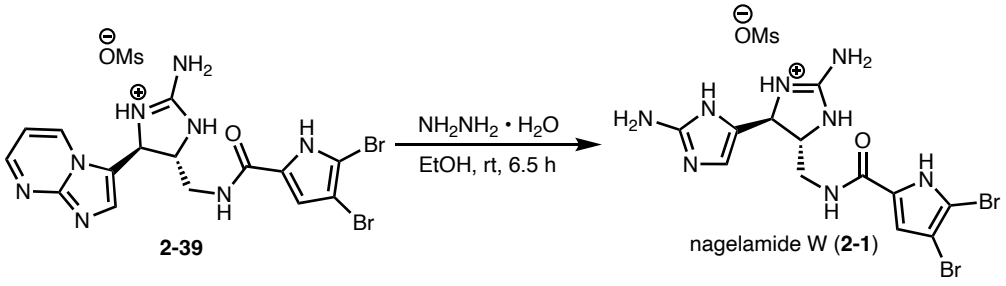

nagelamide W (**2-1**): Compound **2-39** (21.0 mg, 0.037 mmol) was dissolved in ethanol (2 mL) and hydrazine hydrate (1 mL) and stirred at room temperature for 6.5 hours. The solvent was then removed under reduced pressure and the product was purified with CombiFlash chromatography (C18-derived rp silica, gradient 0 - 100% methanol/water) to give nagelamide W as an off-white solid (19.7 mg, 98% yield). mp = 154-155°C. ^{1}H NMR (500 MHz, CD_3OD) δ 6.83 (s, 1H), 6.72 (s, 1H), 4.81 (d, *J* = 7.0 Hz, 1H), 4.15 (dt, *J* = 7.0, 5.5 Hz, 1H), 3.58 (t, *J* = 5.1 Hz, 2H), 2.72 (s, 2H). ^{13}C{^{1}H} NMR (125 MHz, CD_3OD) δ 160.8, 159.1, 149.7, 128.2, 127.0, 113.2, 110.9, 105.2, 98.6, 61.0, 54.9, 41.3, 38.1. FTIR (neat, cm^{-1}): 3175, 2928, 1682, 1559. HRMS (ESI-TOF) *m/z:*

$[M+H]^+$ calcd for ($C_{12}H_{15}Br_2N_8O^+$) 444.9731, 446.9710, & 448.9690; found: 444.9745, 446.9726, & 448.9708.

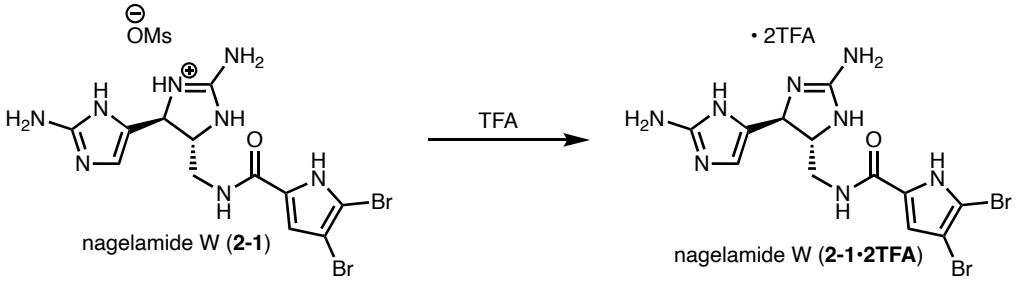

nagelamide W (**2-1 • 2TFA**): Nagelamide W (**2-1**) was dissolved in DMSO-d_6 and 2 equivalent of trifluoroacetic acid (TFA) was added to give the TFA salt which was directly used to obtain ^{1}H and ^{13}C-NMR. ^{1}H NMR (500 MHz, DMSO-d_6) δ 12.82 (s, 1H), 12.74 (d, *J* = 2.8 Hz, 1H), 12.16 (s, 1H), 8.75 (s, 1H), 8.61 (s, 1H), 8.37 (t, *J* = 6.0 Hz, 1H), 8.13 (s, 2H), 7.69 (s, 2H), 6.91 (d, *J* = 2.4 Hz, 1H), 6.84 (s, 1H), 4.80 (d, *J* = 7.4 Hz, 1H), 3.98 (q, *J* = 6.5 Hz, 1H), 3.50 – 3.41 (m, 2H). ^{13}C{^{1}H} NMR (125 MHz, DMSO-d_6) δ 159.6, 158.7, 148.2, 127.8, 124.6, 113.2, 111.7, 105.2, 98.1, 60.1, 53.3, 41.4.

REFERENCES

1. Buchanan, M. S.; Carroll, A. R.; Addepalli, R.; Avery, V. M.; Hooper, J. N. A.; Quinn, R. J., *J. Org. Chem.* **2007**, *72*, 2309-2317.

2. Rane, R. A.; Nandave, M.; Nayak, S.; Naik, A.; Shah, D.; Alwan, W. S.; Sahu, N. U.; Naphade, S. S.; Palkar, M. B.; Karunanidhi, S.; et al., *Arab. J. Chem.* **2017**, *10*, 458-464.

3. Tanaka, N.; Kusama, T.; Kashiwada, Y.; Kobayashi, J. i., *Chem. Pharm. Bull.* **2016**, *64*, 691-694.

4. Forte, B.; Malgesini, B.; Piutti, C.; Quartieri, F.; Scolaro, A.; Papeo, G. A Submarine Journey: The Pyrrole-Imidazole Alkaloids. In *Mar. Drugs*, 2009; Vol. 7, pp 705-753.

5. Chu, M.-J.; Li, M.; Ma, H.; Li, P.-L.; Li, G.-Q., *RSC Adv.* **2022**, *12*, 7789-7820.

6. Wang, X.; Ma, Z.; Wang, X.; De, S.; Ma, Y.; Chen, C., *Chem. Commun.* **2014**, *50*, 8628-8639.

7. Lindel, T. Chemistry and Biology of the Pyrrole–Imidazole Alkaloids. In *The Alkaloids: Chemistry and Biology*, Knölker, H.-J. Ed.; Vol. 77; Academic Press, 2017; pp 117-219.

8. Al Mourabit, A.; Potier, P., *Eur. J. Org. Chem.* **2001**, *2001*, 237-243.

9. Al-Mourabit, A.; Zancanella, M. A.; Tilvi, S.; Romo, D., *Nat. Prod. Rep.* **2011**, *28*, 1229-1260.

10. Genta-Jouve, G.; Cachet, N.; Holderith, S.; Oberhänsli, F.; Teyssié, J.-L.; Jeffree, R.; Al Mourabit, A.; Thomas, O. P., *ChemBioChem.* **2011**, *12*, 2298-2301.

11. Andrade, P.; Willoughby, R.; Pomponi, S. A.; Kerr, R. G., *Tetrahedron Lett.* **1999**, *40*, 4775-4778.

12. Das, J.; Bhandari, M.; Lovely, C. J. Chapter 10 - Isolation, Bioactivity, and Synthesis of Nagelamides. In *Stud. Nat. Prod. Chem.*, Atta ur, R. Ed.; Vol. 50; Elsevier, 2016; pp 341-371.

13. Endo, T.; Tsuda, M.; Okada, T.; Mitsuhashi, S.; Shima, H.; Kikuchi, K.; Mikami, Y.; Fromont, J.; Kobayashi, J., *J. Nat. Prod.* **2004**, *67*, 1262-1267.

14. Bhandari, M. R.; Sivappa, R.; Lovely, C. J., *Org. Lett.* **2009**, *11*, 1535-1538.

15. Bhandari, M. R.; Herath, A. K.; Rasapalli, S.; Yousufuddin, M.; Lovely, C. J., *J. Org. Chem.* **2020**, *85*, 12971-12987.

16. O'Malley, D. P.; Li, K.; Maue, M.; Zografos, A. L.; Baran, P. S., *J. Am. Chem. Soc.* **2007**, *129*, 4762-4775.

17. Tonsiengsom, S. Horne and Tongsiem have developed syntheses of nagelamides A and D but these work have only been decribed in dissertation till date. *Studies Towards the Total Synthesis of Nagelamide A and D, Agelastatin D, Dragmacidin A-C, Salacin and Almazoles*. Oregon State University, 2005.

18. Stout, E. P.; Morinaka, B. I.; Wang, Y.-G.; Romo, D.; Molinski, T. F., *J. Nat. Prod.* **2012**, *75*, 527-530.

19. Tanaka, N.; Kusama, T.; Takahashi-Nakaguchi, A.; Gonoi, T.; Fromont, J.; Kobayashi, J. i., *Tetrahedron Lett.* **2013**, *54*, 3794-3796.

20. Rasapalli, S.; Kumbam, V.; Dhawane, A. N.; Golen, J. A.; Lovely, C. J.; Rheingold, A. L., *Org. Biomol. Chem.* **2013**, *11*, 4133-4137.

21. Keel, K. L.; Tepe, J. J., *Org. Lett.* **2021**, *23*, 5368-5372.

22. Austin, J. F.; MacMillan, D. W., *J. Am. Chem. Soc.* **2002**, *124*, 1172-1173.

23. Paras, N. A.; MacMillan, D. W., *J. Am. Chem. Soc.* **2001**, *123*, 4370-4371.

24. Kamal, A.; Bharath Kumar, G.; Lakshma Nayak, V.; Reddy, V. S.; Shaik, A. B.; Rajender; Kashi Reddy, M., *MedChemComm* **2015**, *6*, 606-612.

25. Herath, A. K.; Lovely, C. J., *Org. Biomol. Chem.* **2021**, *19*, 2603-2621.

26. Feldman, K. S.; Fodor, M. D.; Skoumbourdis, A. P., *Synthesis* **2009**, *2009*, 3162-3173.

27. Feldman, K. S.; Ngernmeesri, P., *Org. Lett.* **2011**, *13*, 5704-5707.

28. Kohn, H.; Jung, S. H., *J. Am. Chem. Soc.* **1983**, *105*, 4106-4108.

29. Borisov, A. V.; Tolmachev, A. A.; Zavada, O. A.; Zhuravel', I. A.; Kovalenko, S. N., *Chem. Heterocycl. Compd.* **2013**, *49*, 704-711.

30. Farran, D.; Slawin, A. M. Z.; Kirsch, P.; O'Hagan, D., *J. Org. Chem.* **2009**, *74*, 7168-7171.

31. Martínez, J. I.; Smith, J. J.; Hepburn, H. B.; Lam, H. W., *Angew. Chem. Int. Ed.* **2016**, *55*, 1108-1112.

32. Wang, Y. D.; Kimball, G.; Prashad, A. S.; Wang, Y., *Tetrahedron Lett.* **2005**, *46*, 8777-8780.

33. Motiwala, H. F.; Armaly, A. M.; Cacioppo, J. G.; Coombs, T. C.; Koehn, K. R. K.; Norwood, V. M. I. V.; Aubé, J., *Chem. Rev.* **2022**, *122*, 12544-12747.

34. Tang, R.-J.; Milcent, T.; Crousse, B., *J. Org. Chem.* **2018**, *83*, 930-938.

35. Rival, Y.; Grassy, G.; Michel, G., *Chem. Pharm. Bull.* **1992**, *40*, 1170-1176.

36. Sen, S. E.; Roach, S. L., *Synthesis* **1995**, *1995*, 756-758.

37. Staudinger, H.; Meyer, J., *Helv. Chim. Acta* **1919**, *2*, 635-646.

38. Lenstra, D. C.; Wolf, J. J.; Mecinovic, J., *J. Org. Chem.* **2019**, *84*, 6536-6545.

39. Bures, J.; Martin, M.; Urpi, F.; Vilarrasa, J., *J. Org. Chem.* **2009**, *74*, 2203-2206.

40. George, D. E.; Tepe, J. J., *J. Org. Chem.* **2023**, *88*, 9306-9312.

APPENDIX

Figure 2.2: ^{1}H and $^{13}C\{1H\}$ NMR spectra of **2-7**

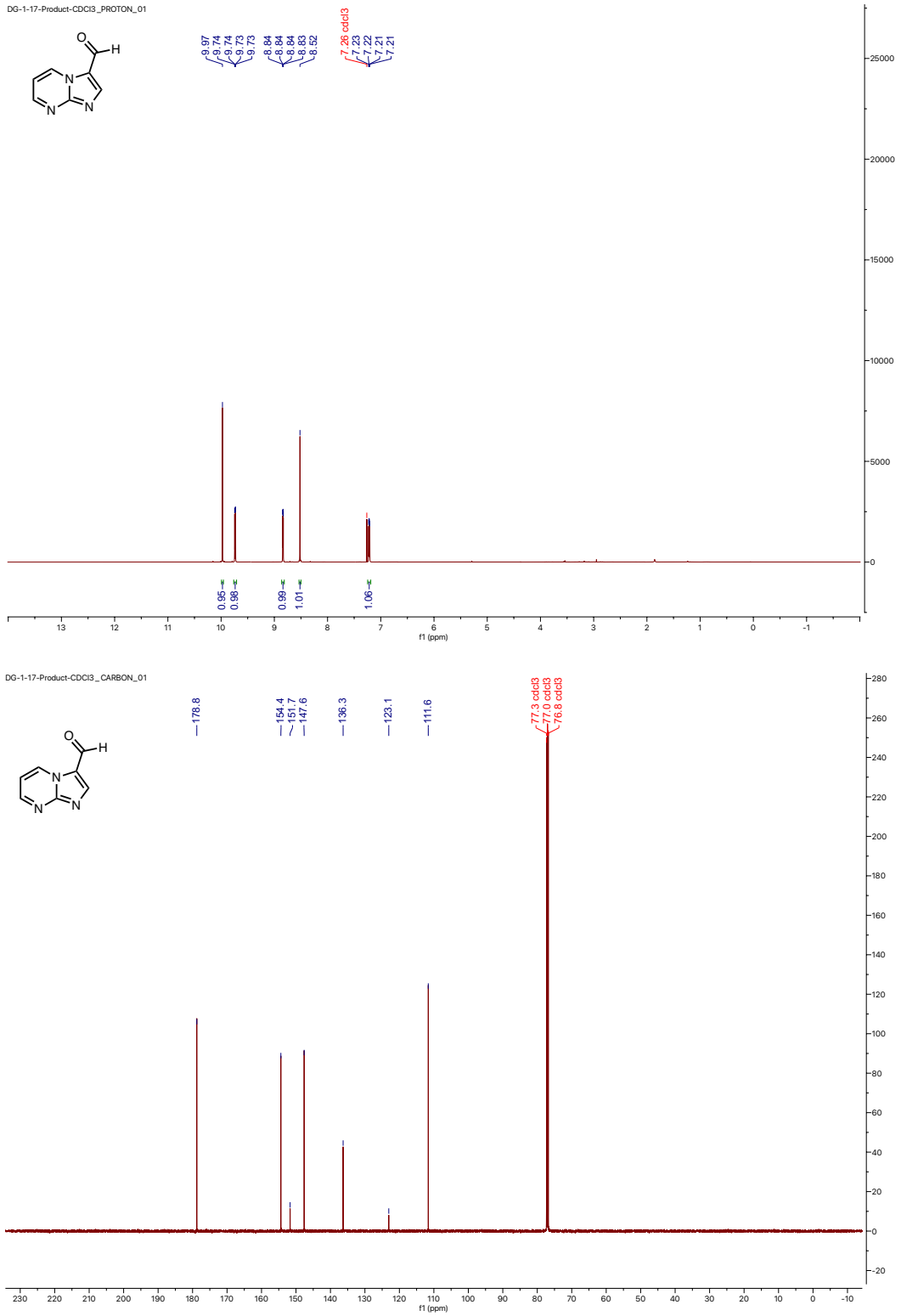

Figure 2.3: ^{1}H and $^{13}C\{1H\}$ NMR spectra of **2-13**

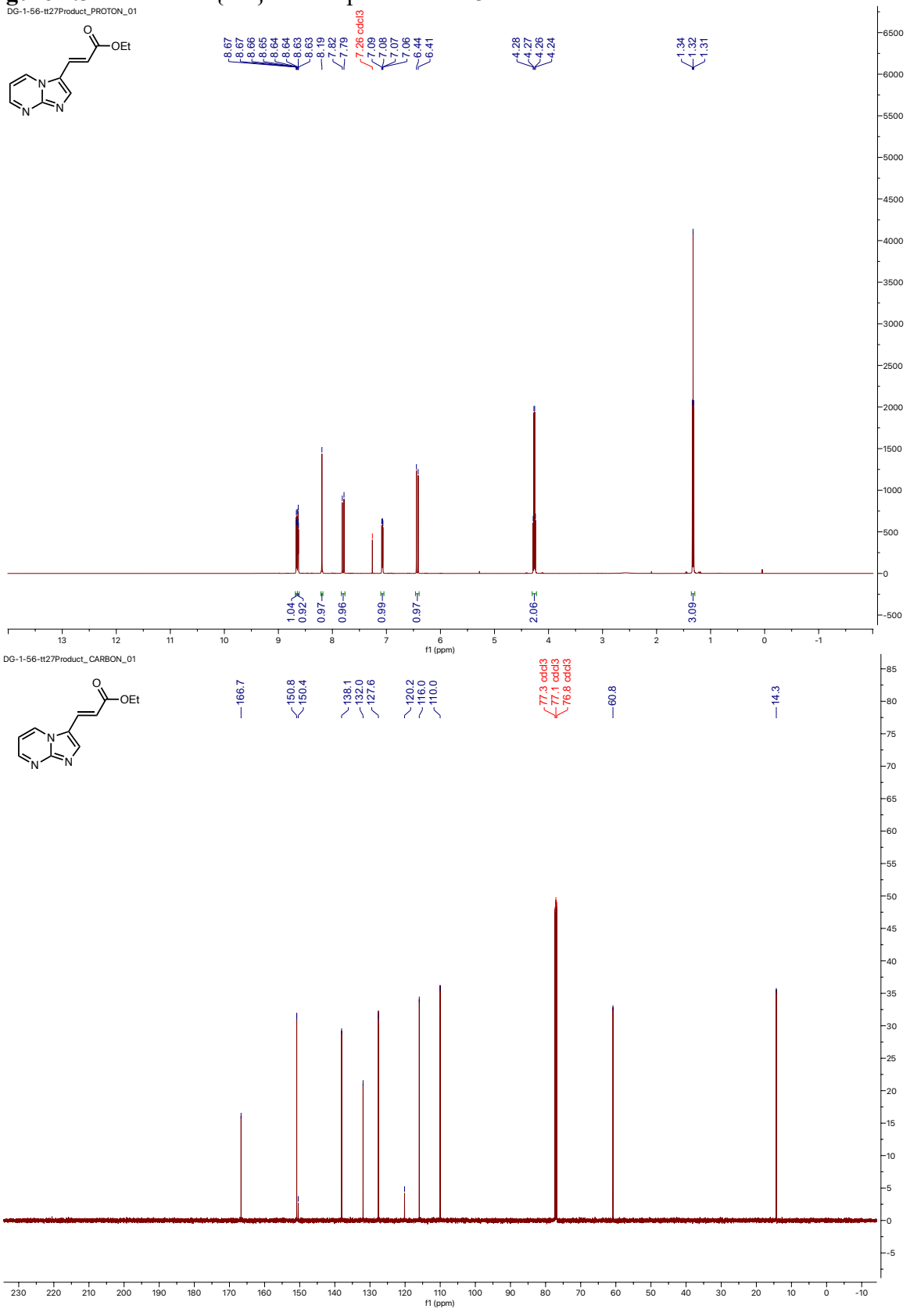

Figure 2.4: ^{1}H and $^{13}C\{1H\}$ NMR spectra of **2-14**

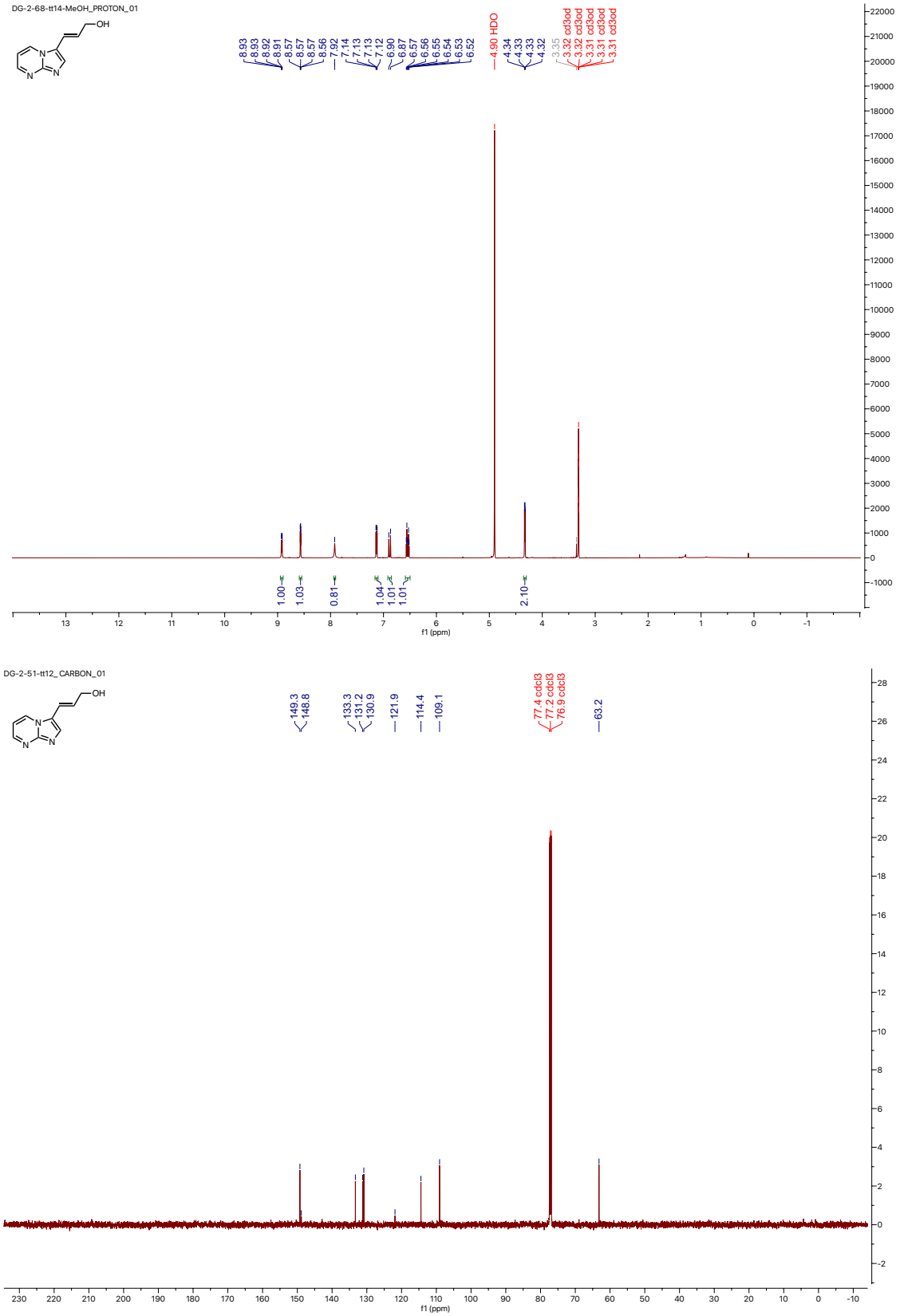

Figure 2.5: ^{1}H and $^{13}C\{1H\}$ NMR spectra of **2-15**

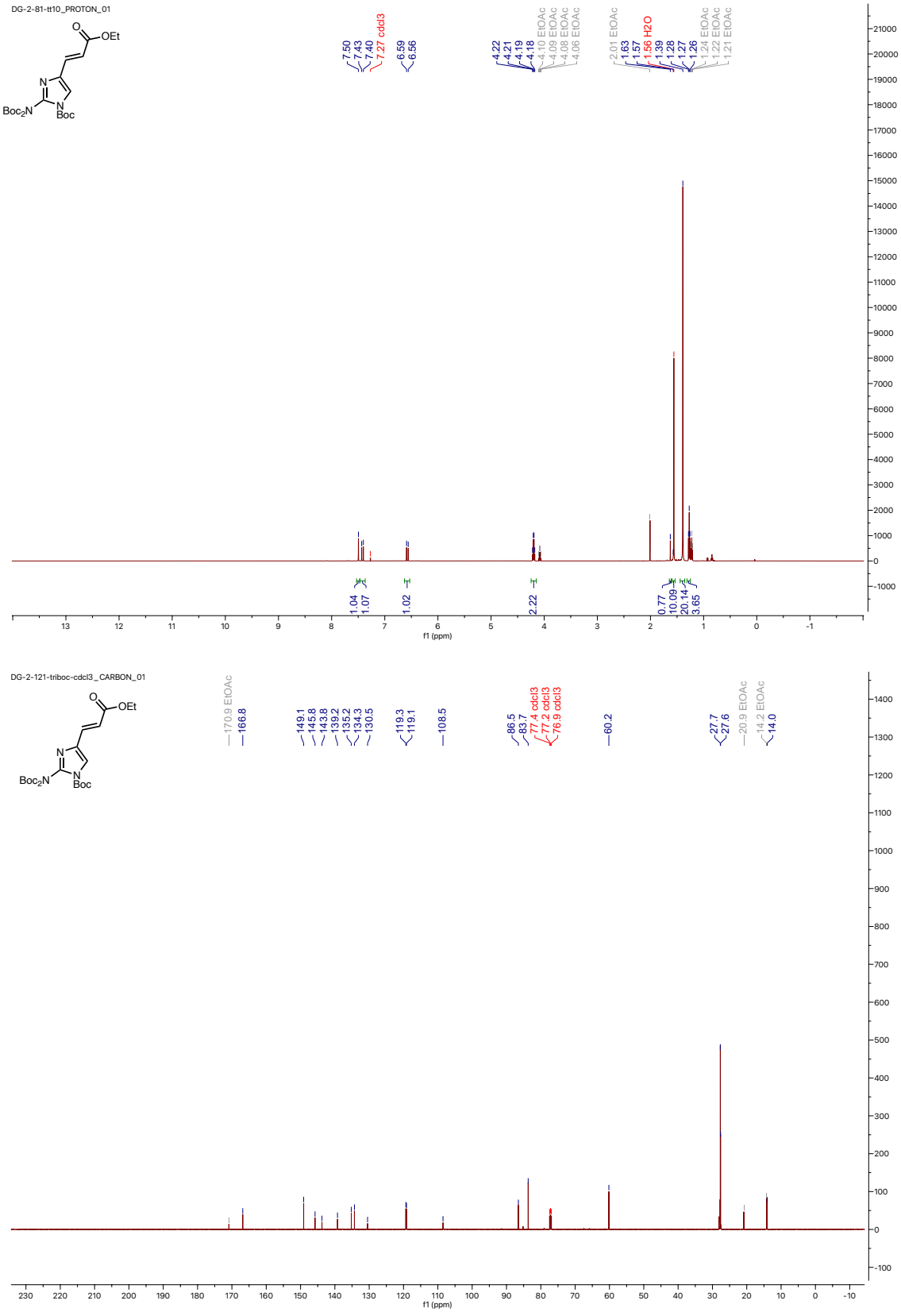

Figure 2.6: ^{1}H and $^{13}C\{1H\}$ NMR spectra of **2-16**

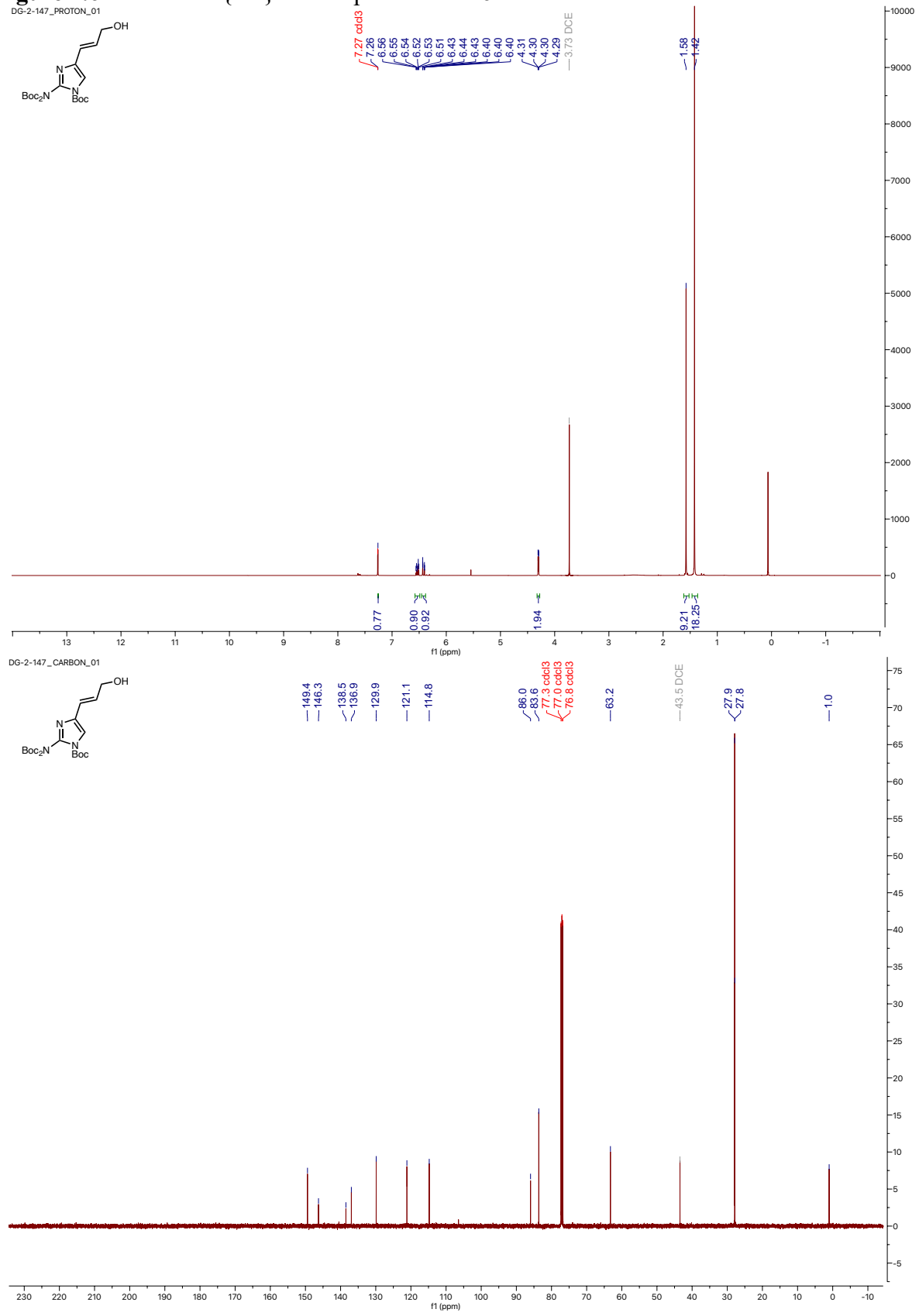

Figure 2.7: ^{1}H and $^{13}C\{1H\}$ NMR spectra of **2-17**

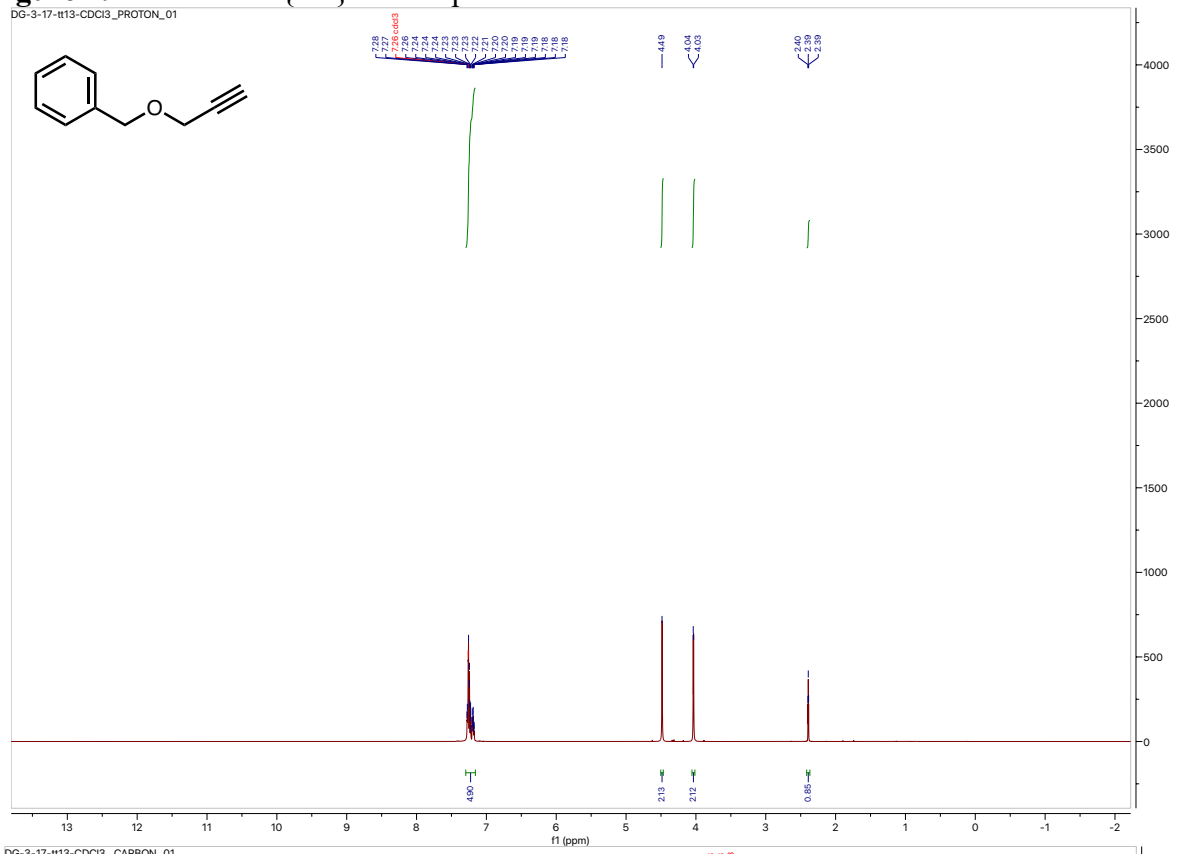

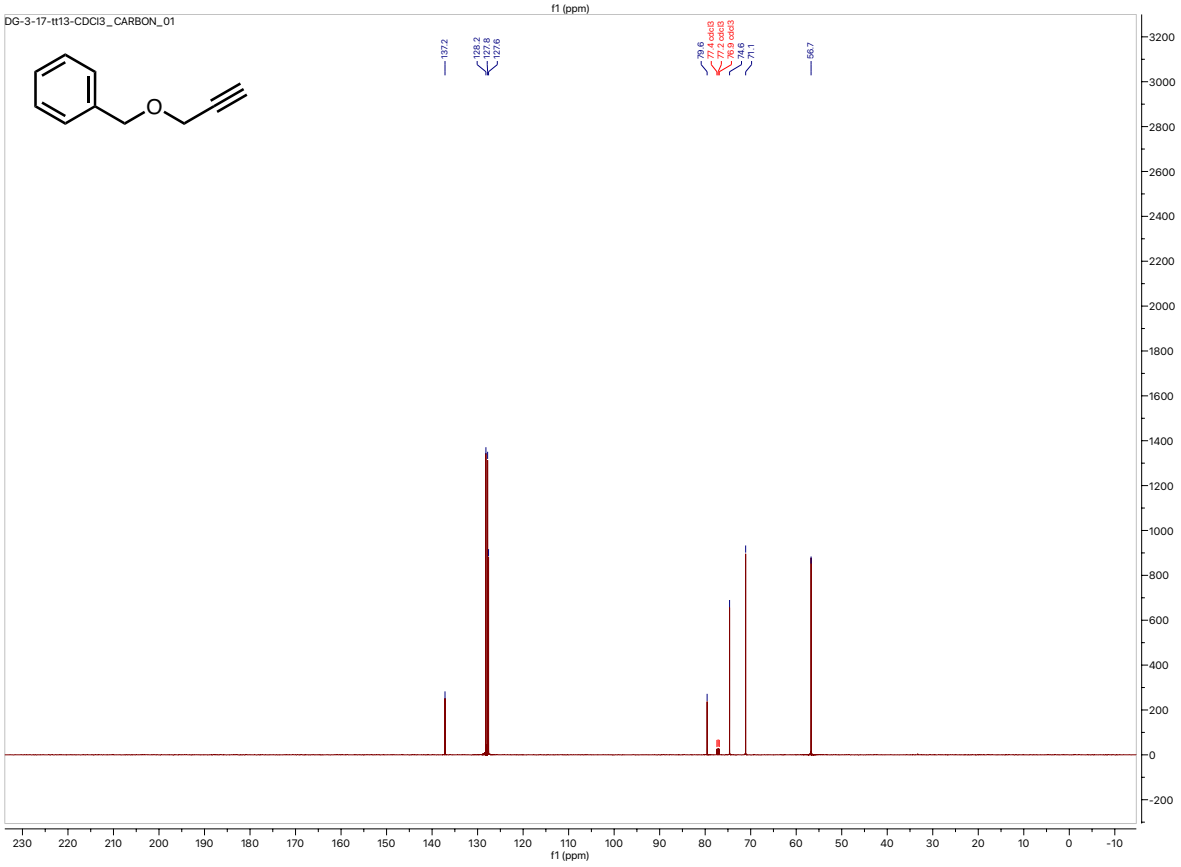

Figure 2.8: ^{1}H and $^{13}C\{1H\}$ NMR spectra of **2-18**

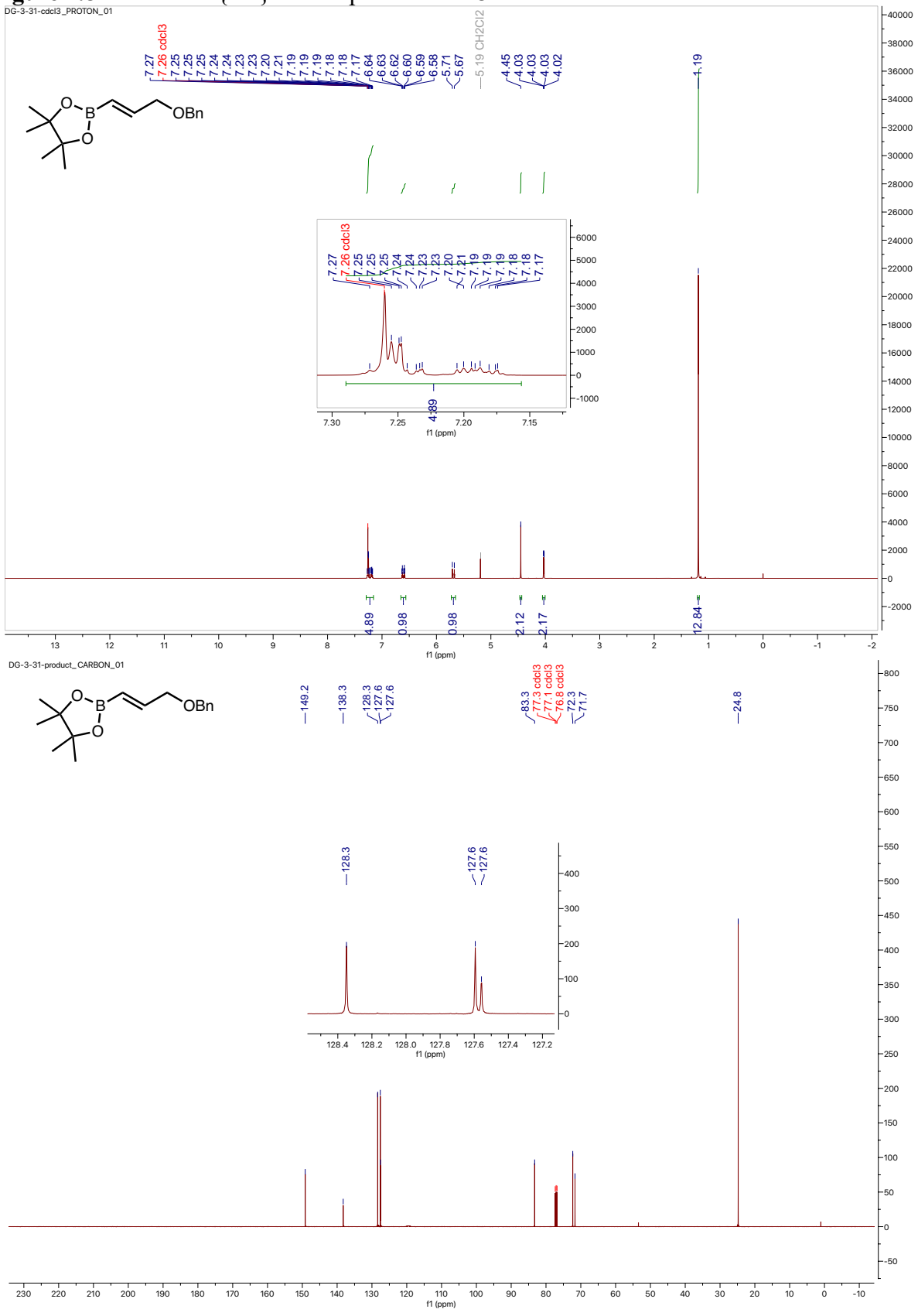

Figure 2.9: ^{1}H and $^{13}C\{1H\}$ NMR spectra of **2-19**

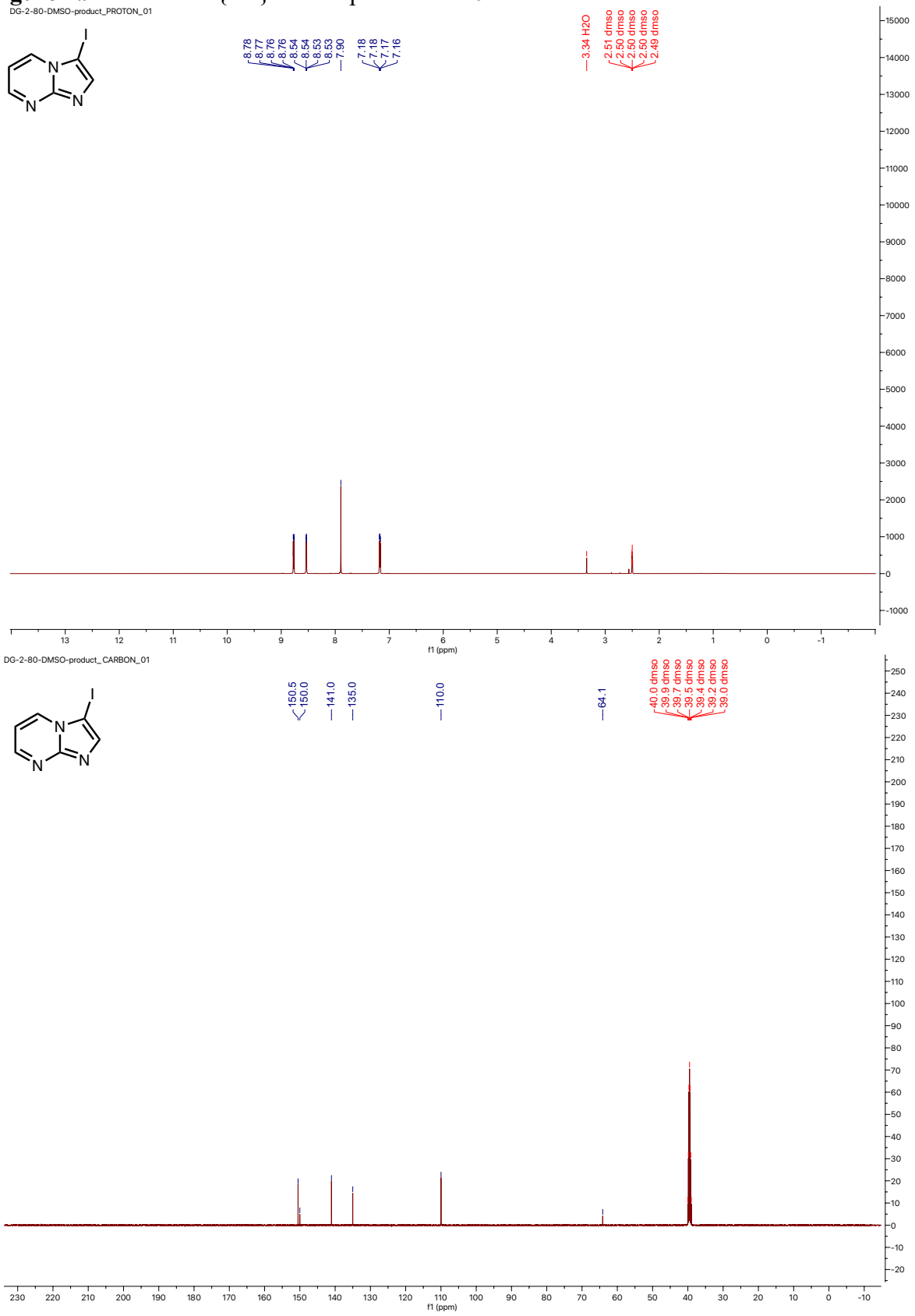

Figure 2.10: ^{1}H and $^{13}C\{1H\}$ NMR spectra of **2-12**

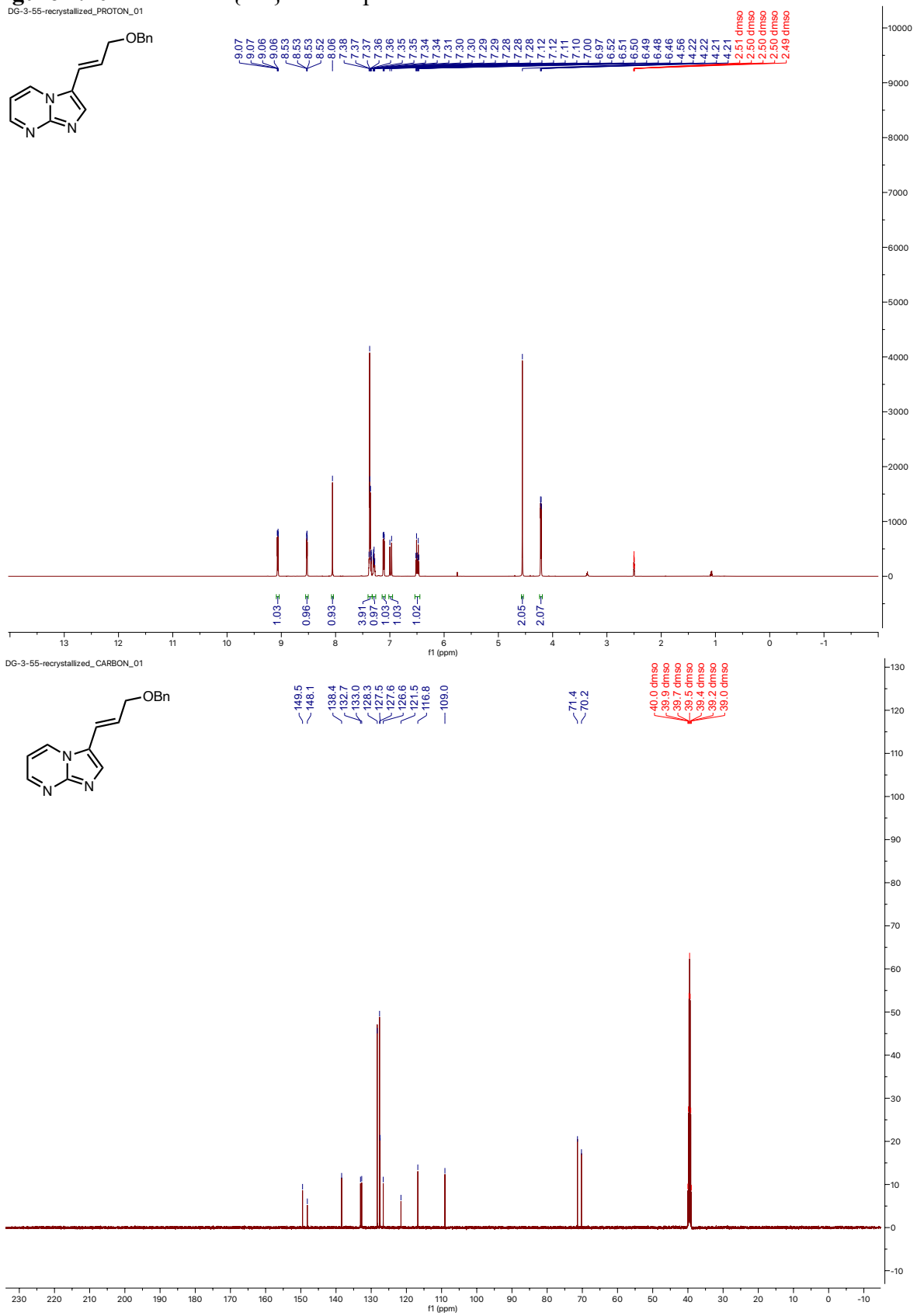

Figure 2.11: ^{1}H and $^{13}C\{1H\}$ NMR spectra of **2-20**

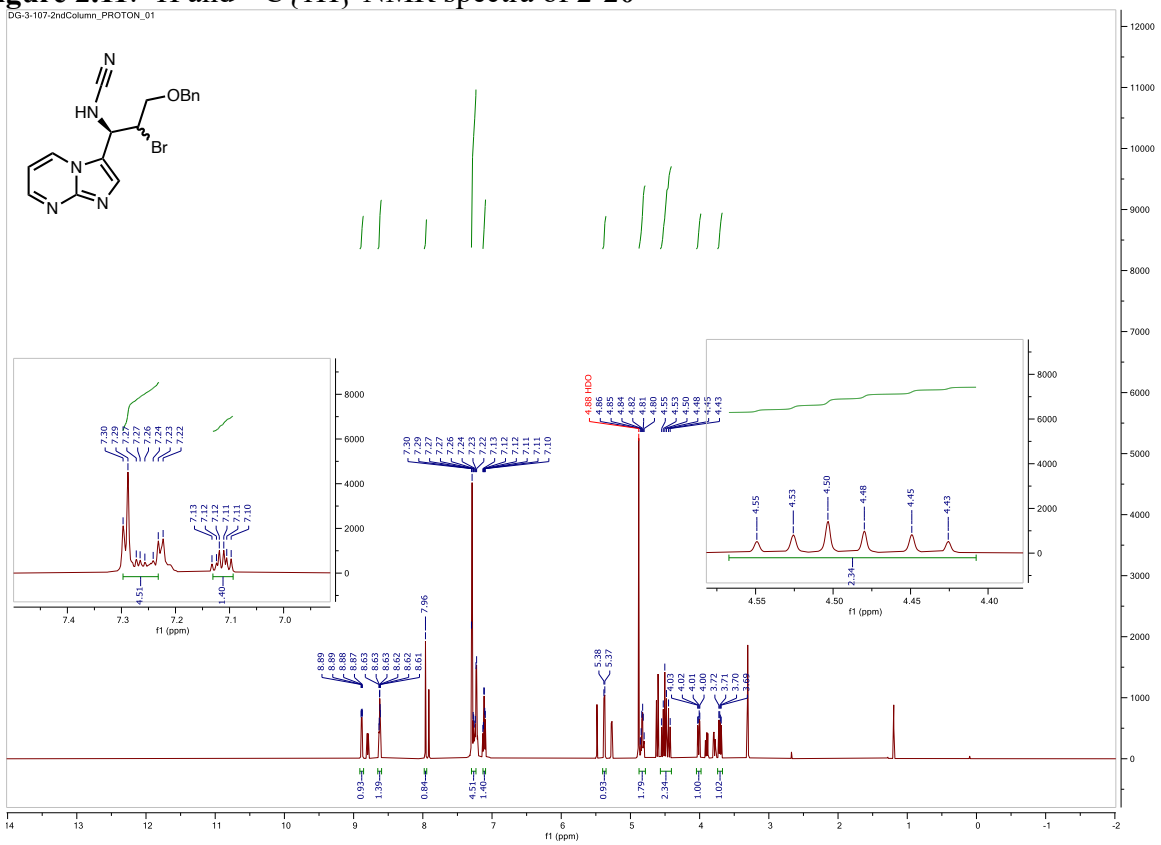

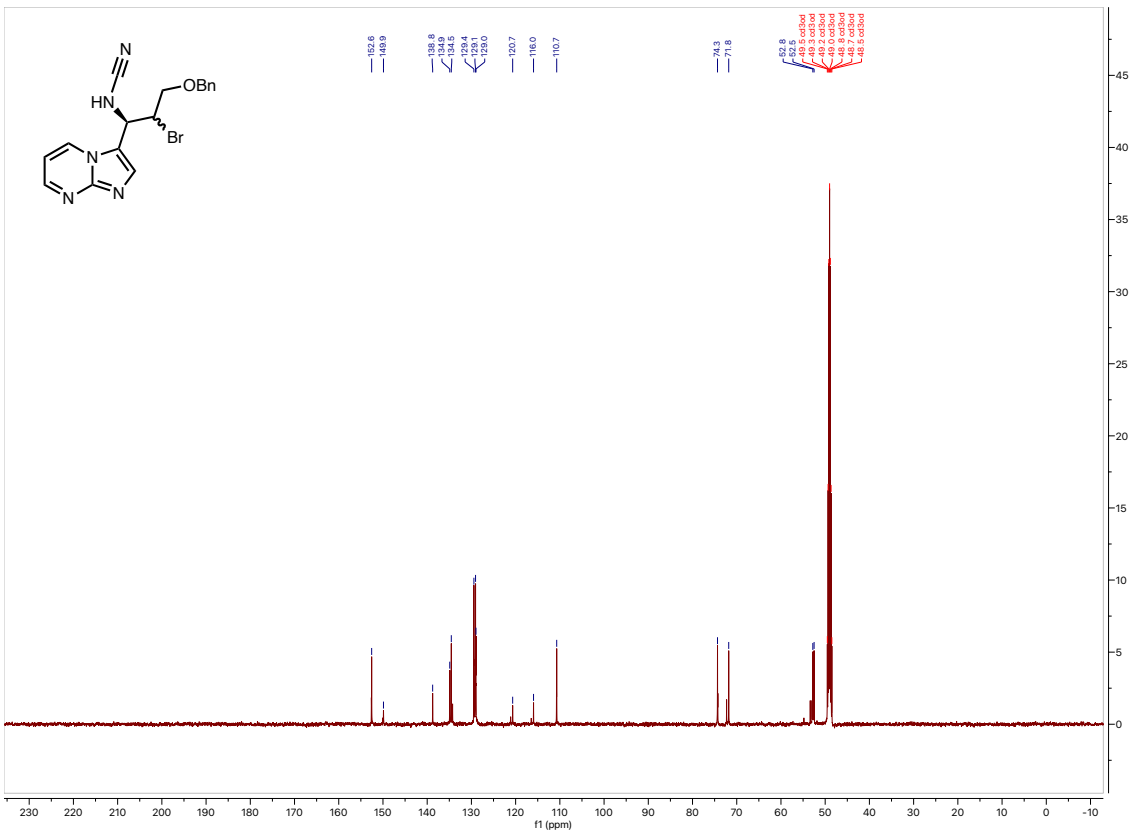

Figure 2.12: ^{1}H and $^{13}C\{1H\}$ NMR spectra of **2-23**

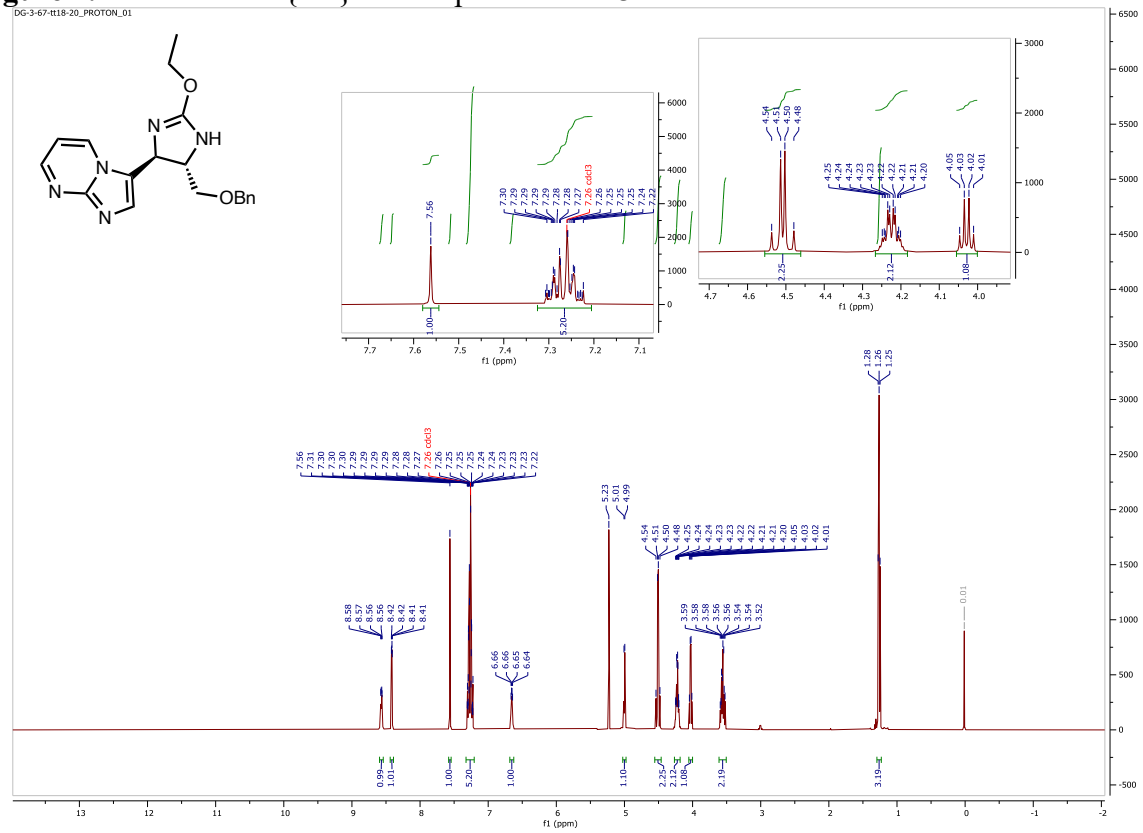

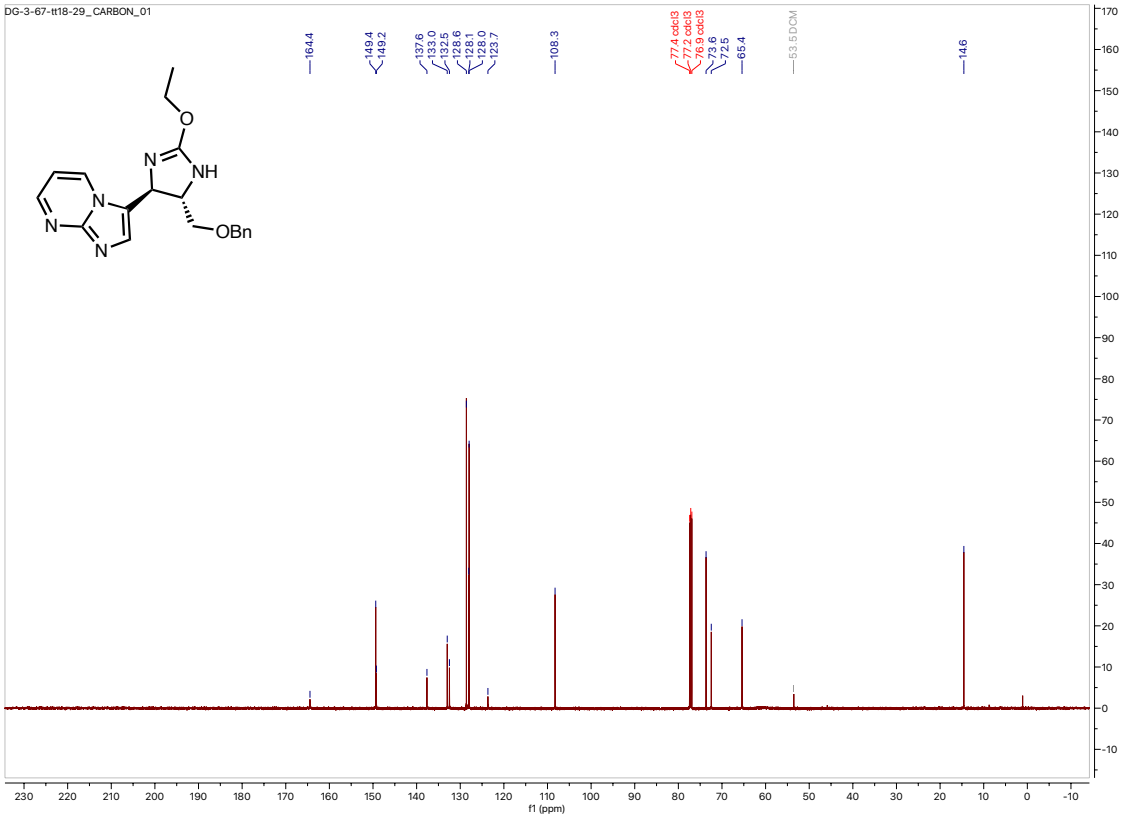

Figure 2.13: NOE spectra for compound 2-23

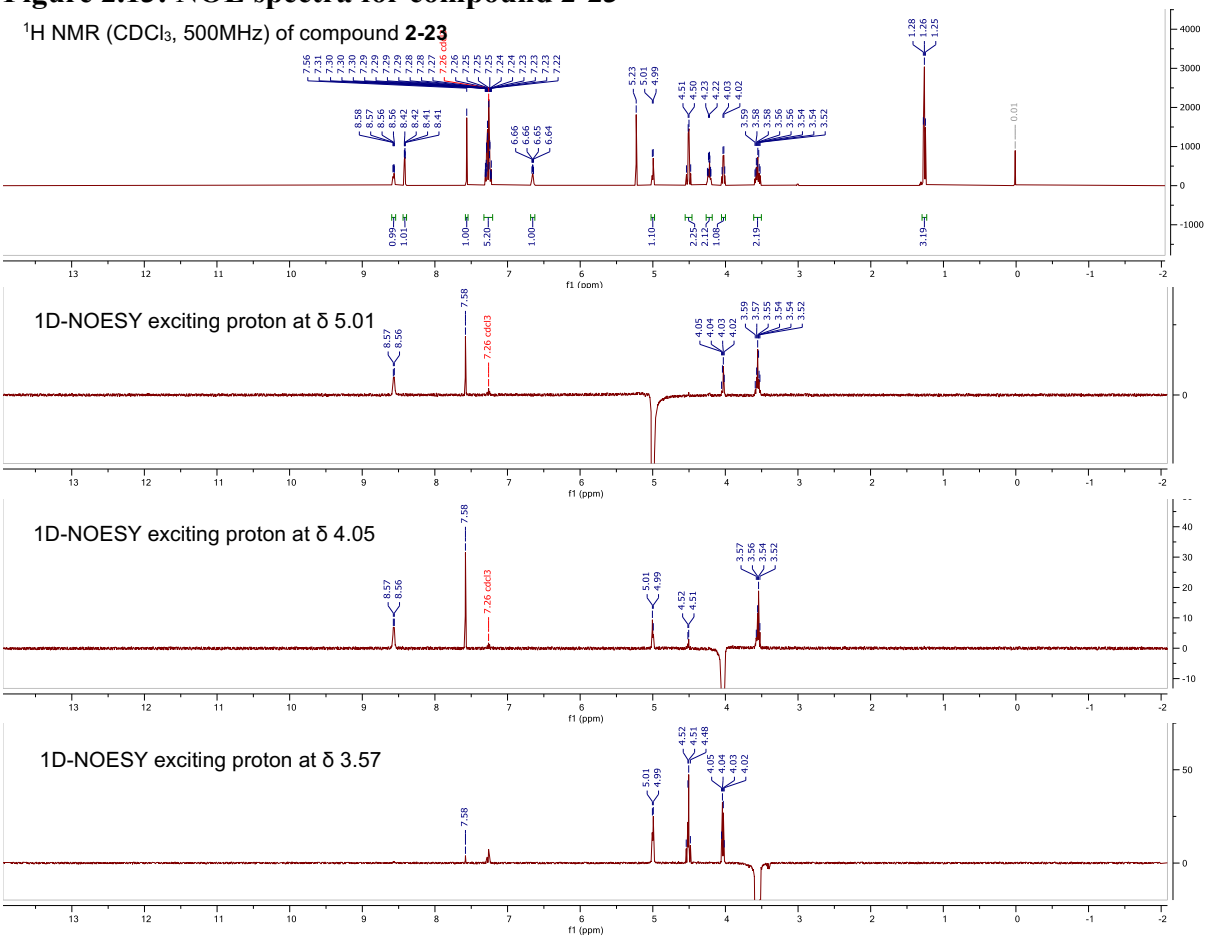

Figure 2.14: ^{1}H and $^{13}C\{1H\}$ NMR spectra of **2-24**

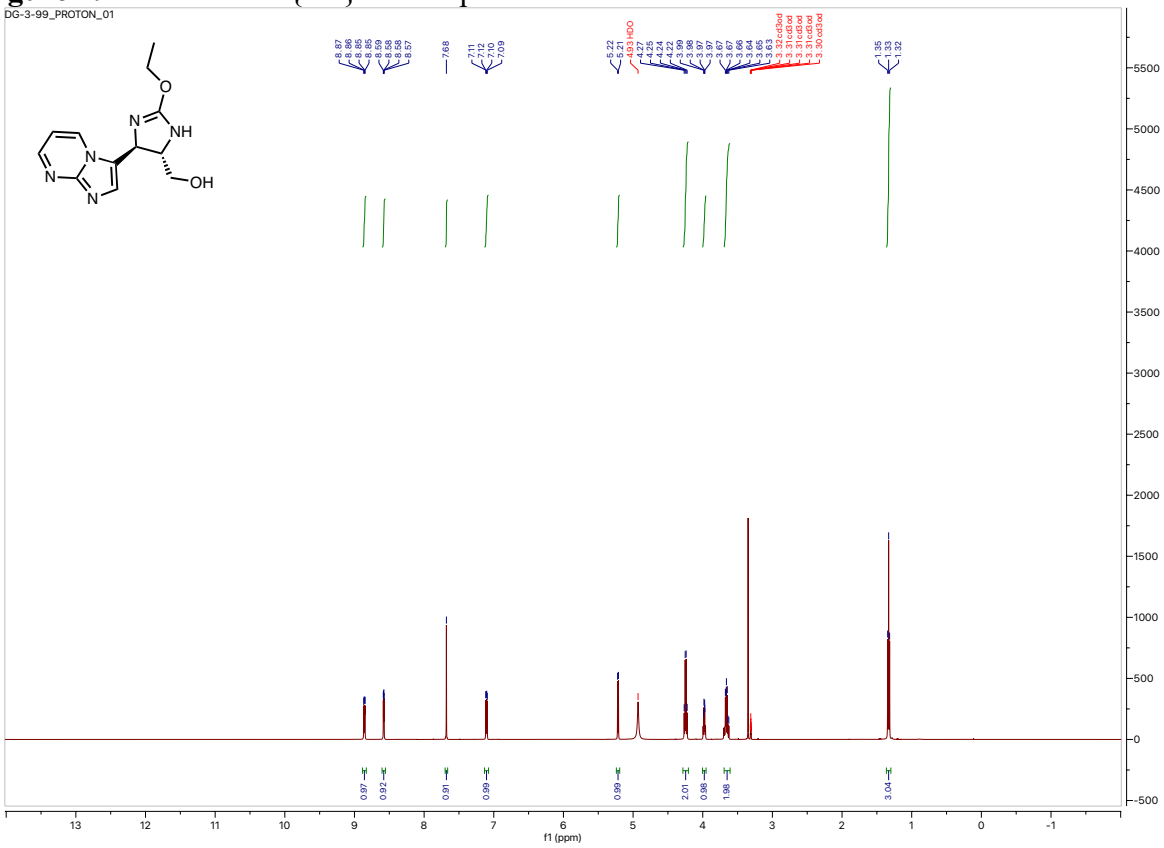

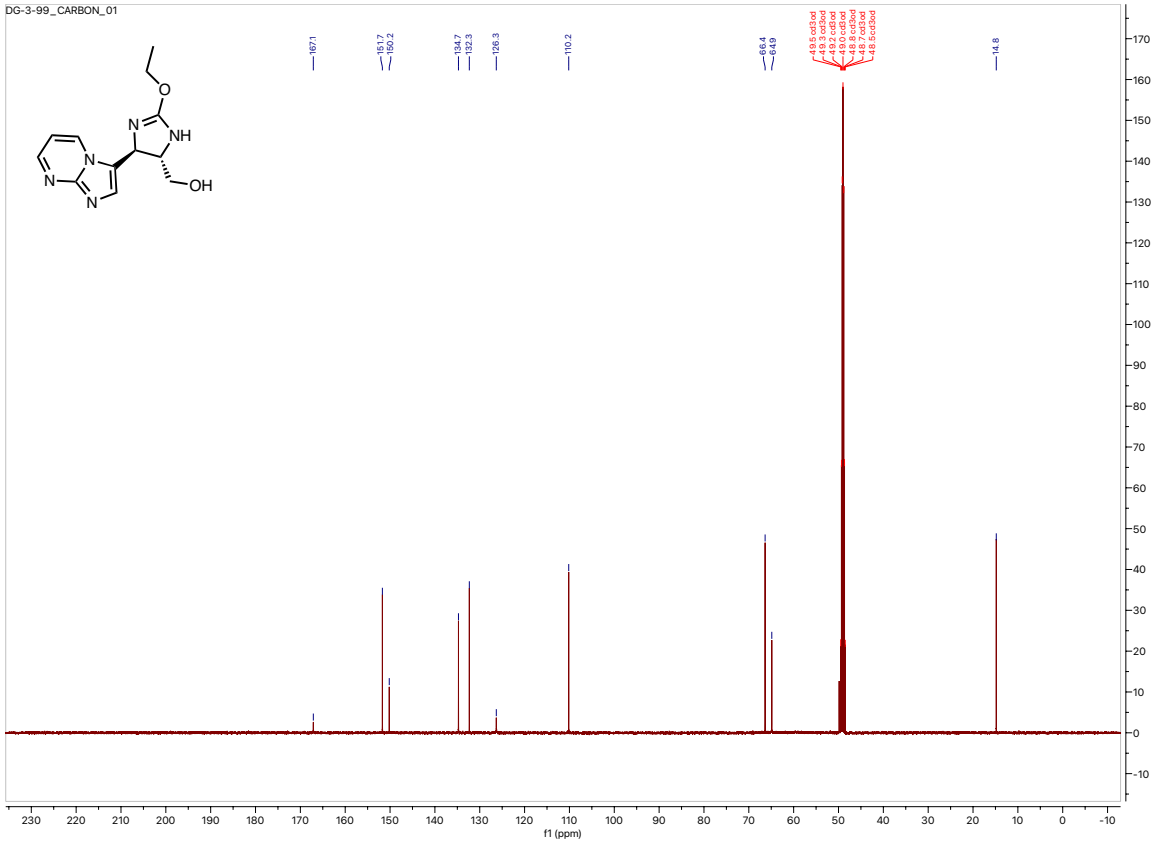

Figure 2.15: ^{1}H and $^{13}C\{1H\}$ NMR spectra of **2-27**

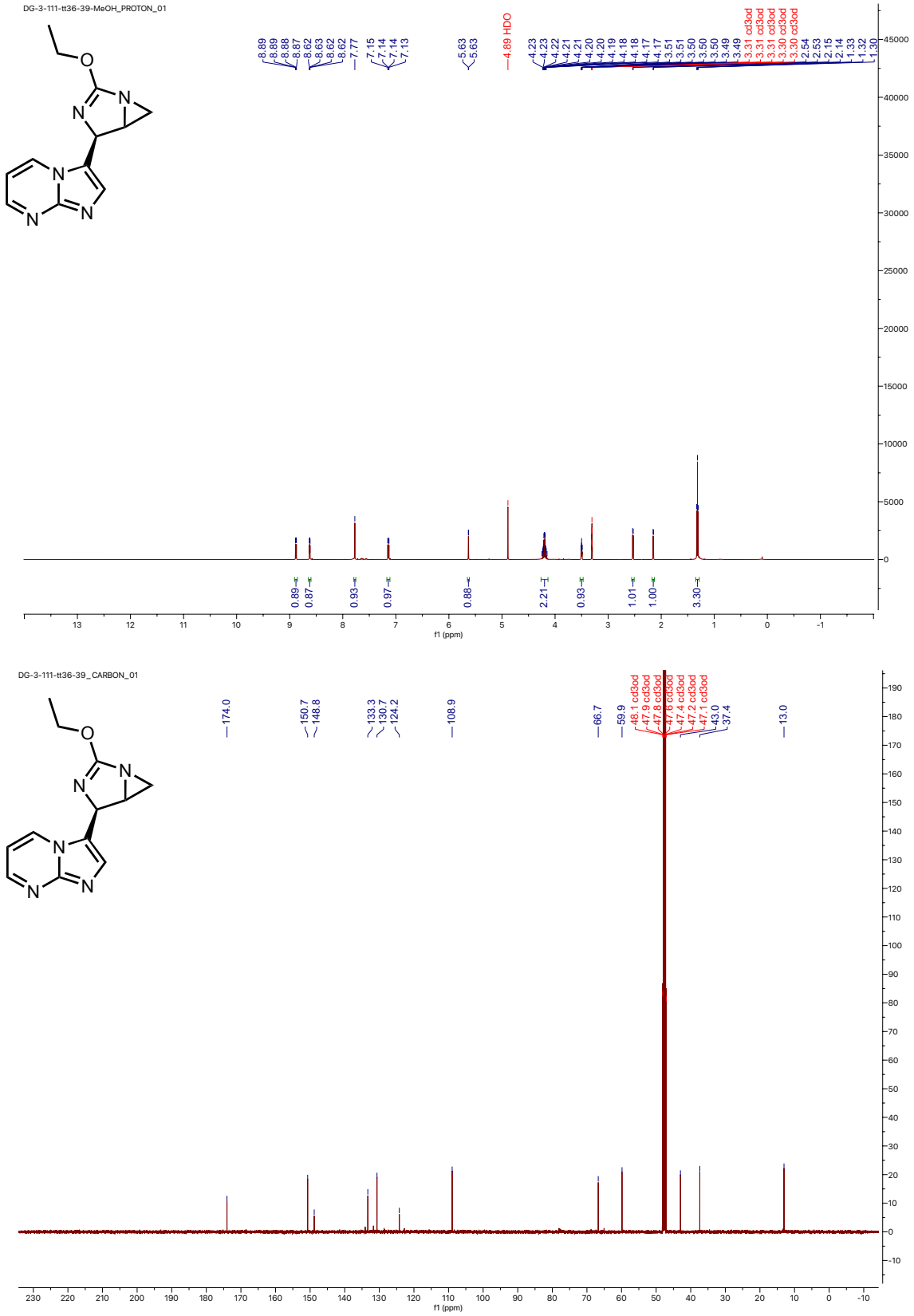

Figure 2.16: ^{1}H and $^{13}C\{1H\}$ NMR spectra of **2-28**

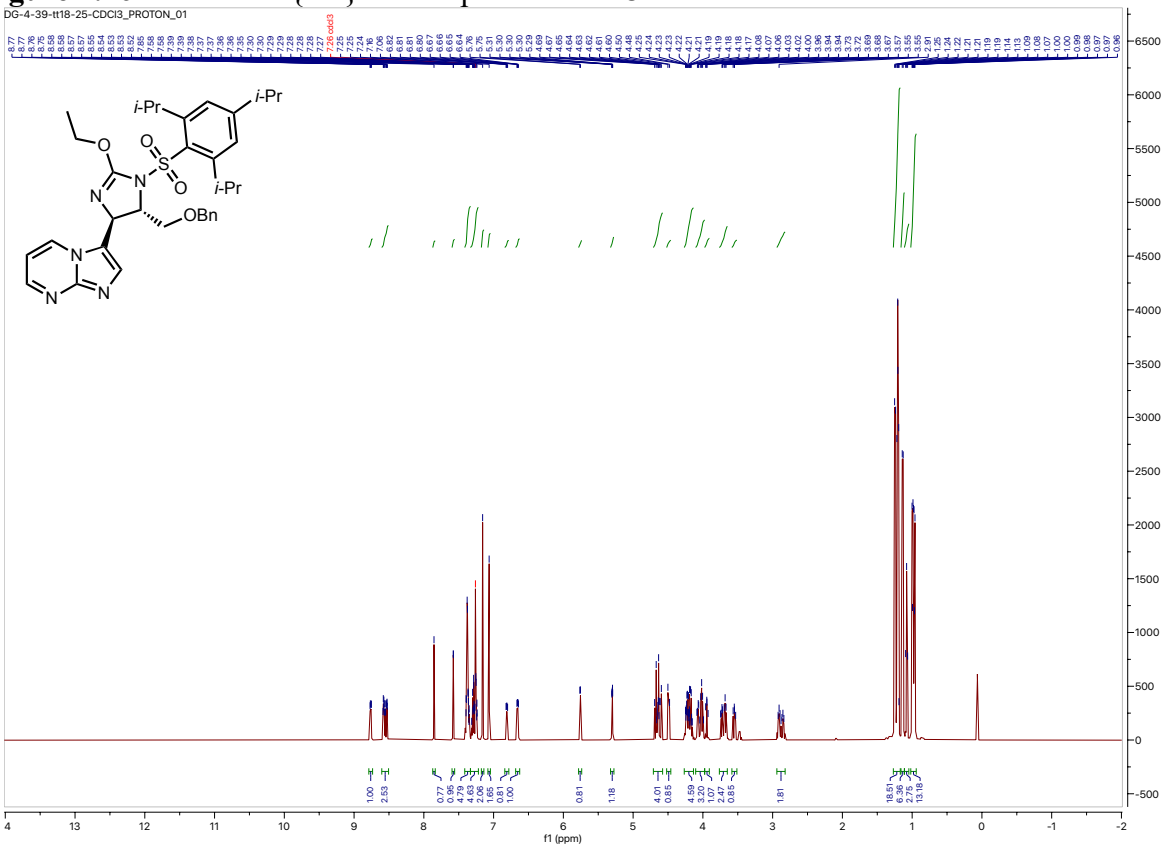

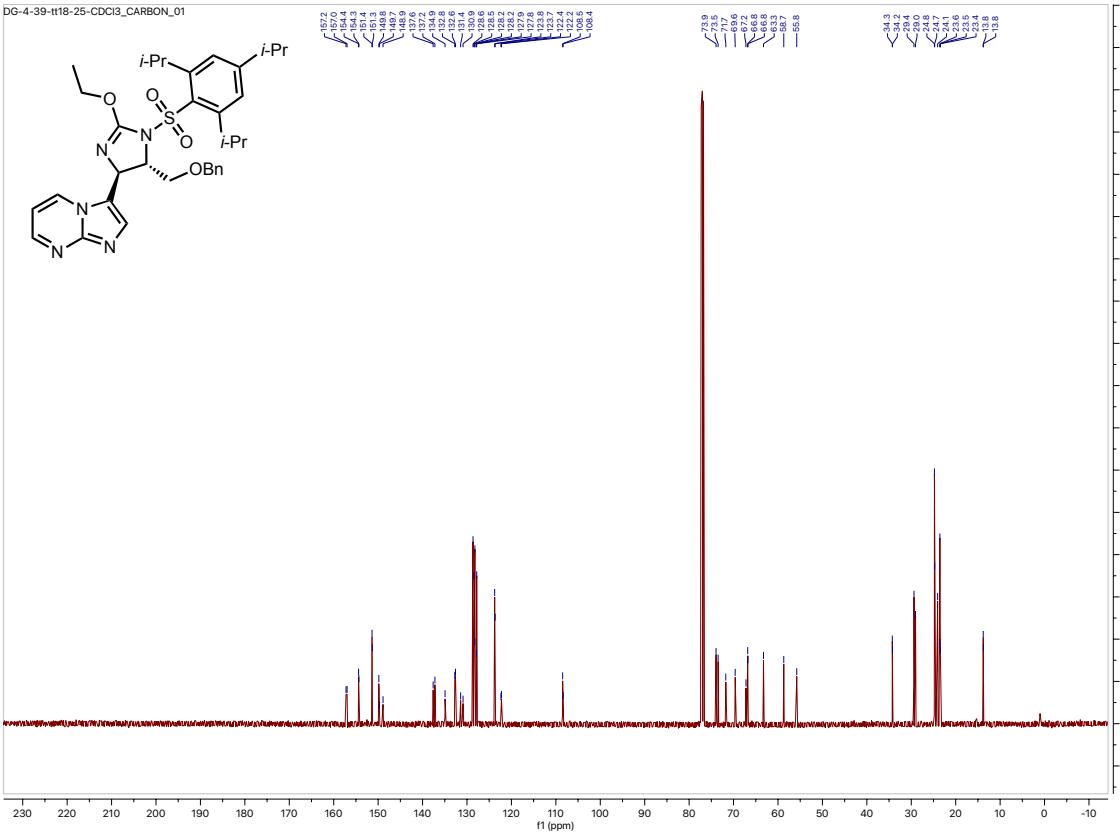

Figure 2.17: ^{1}H and $^{13}C\{1H\}$ NMR spectra of **2-29**

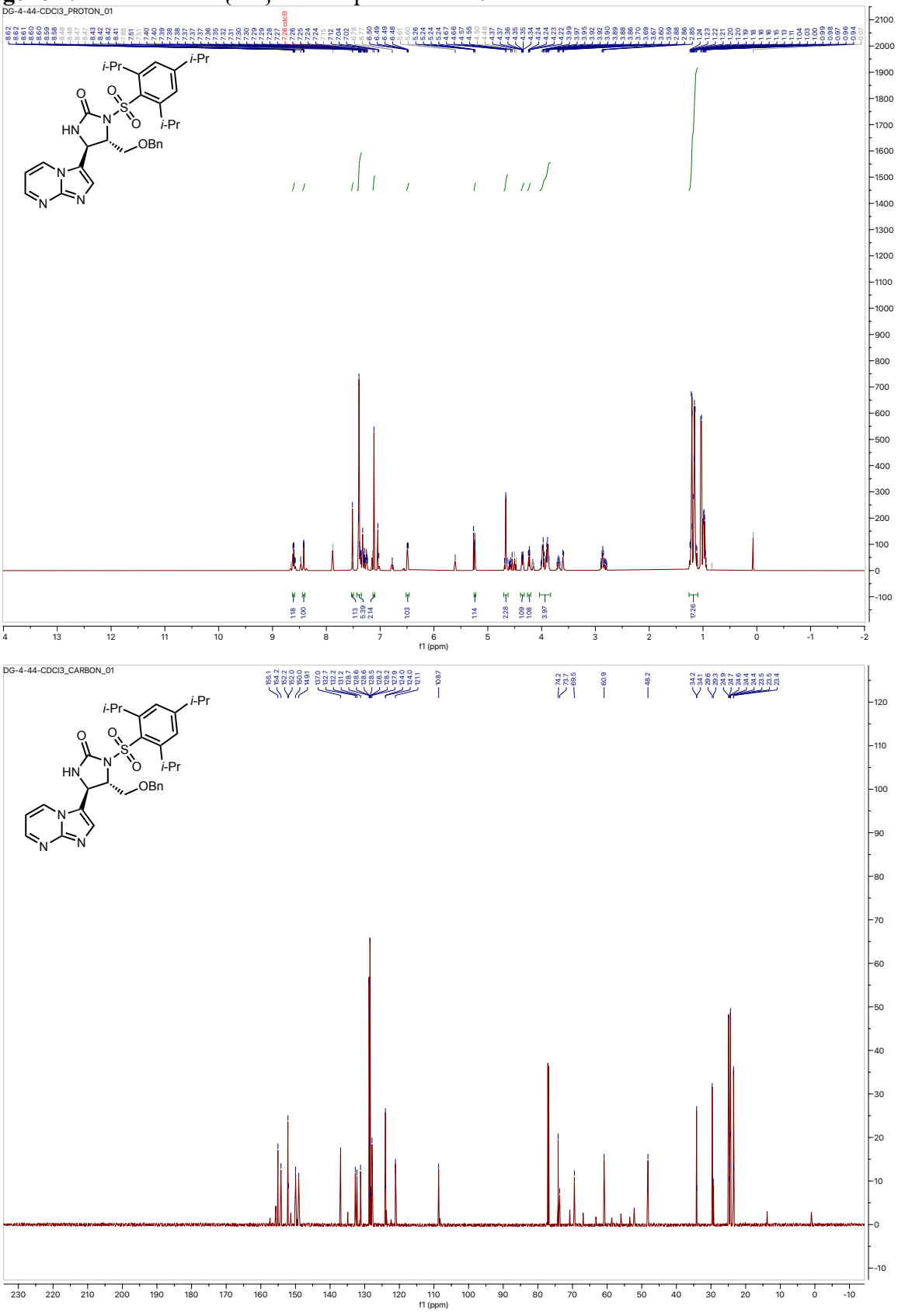

Figure 2.18: ^{1}H and $^{13}C\{1H\}$ NMR spectra of **2-31**

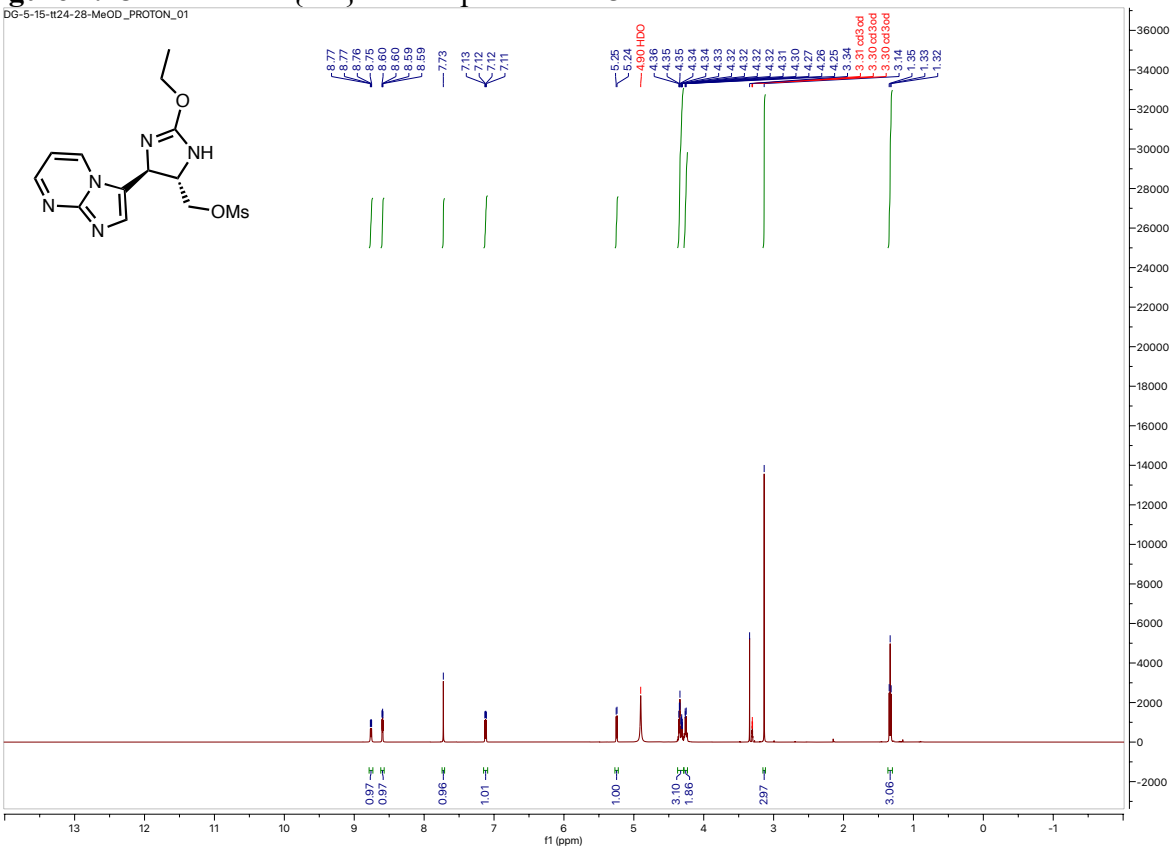

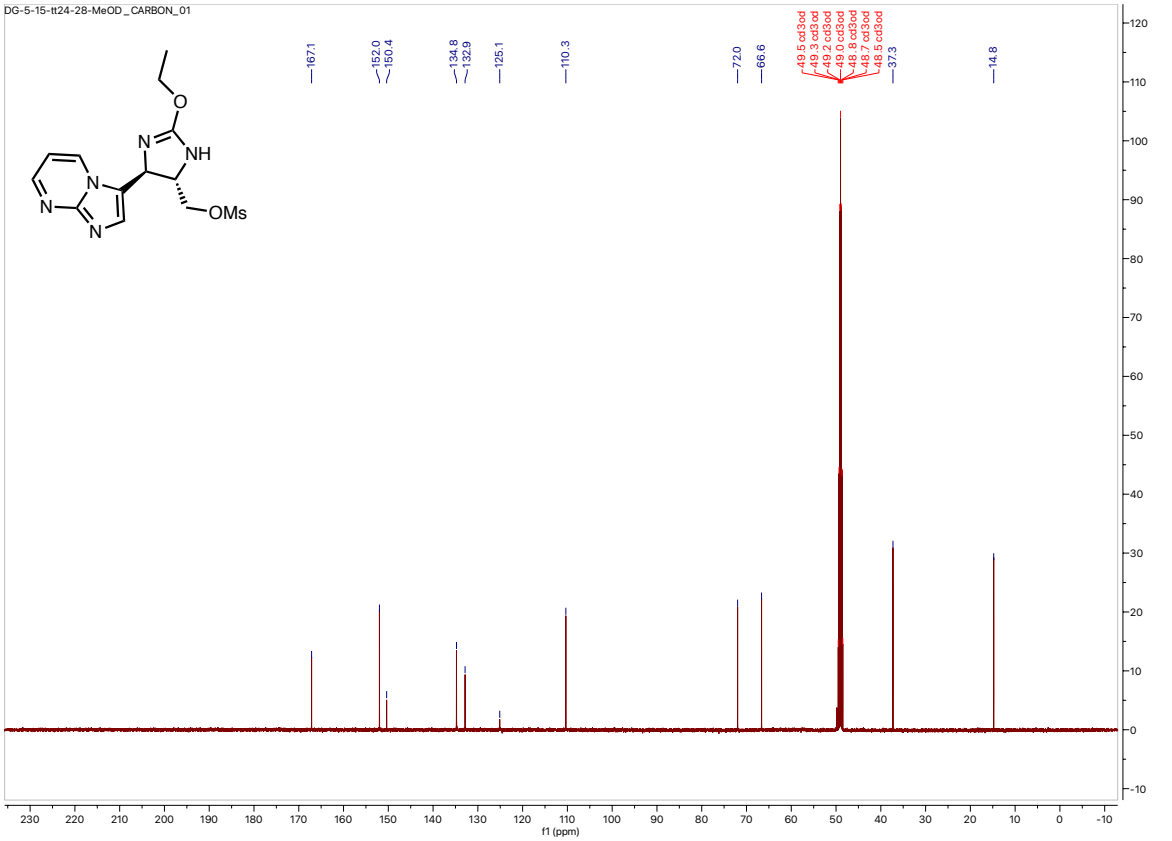

Figure 2.19: ^{1}H and $^{13}C\{1H\}$ NMR spectra of **2-25**

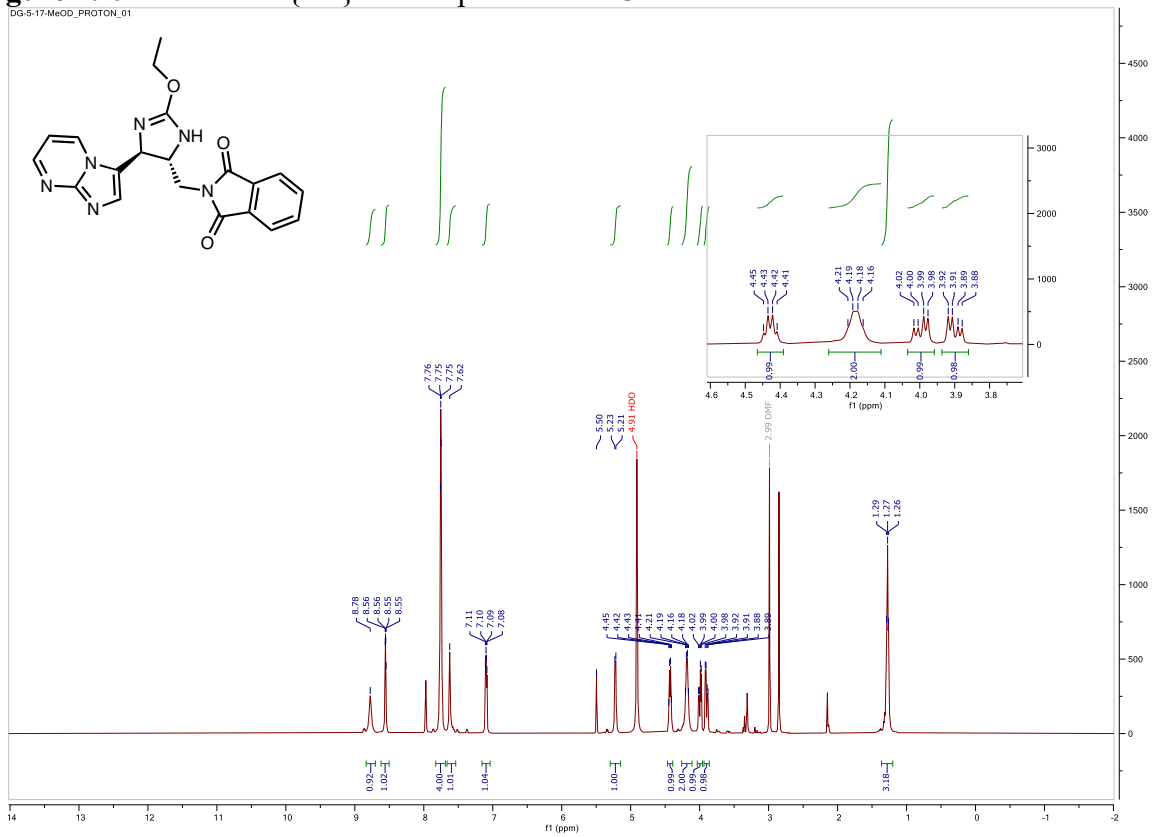

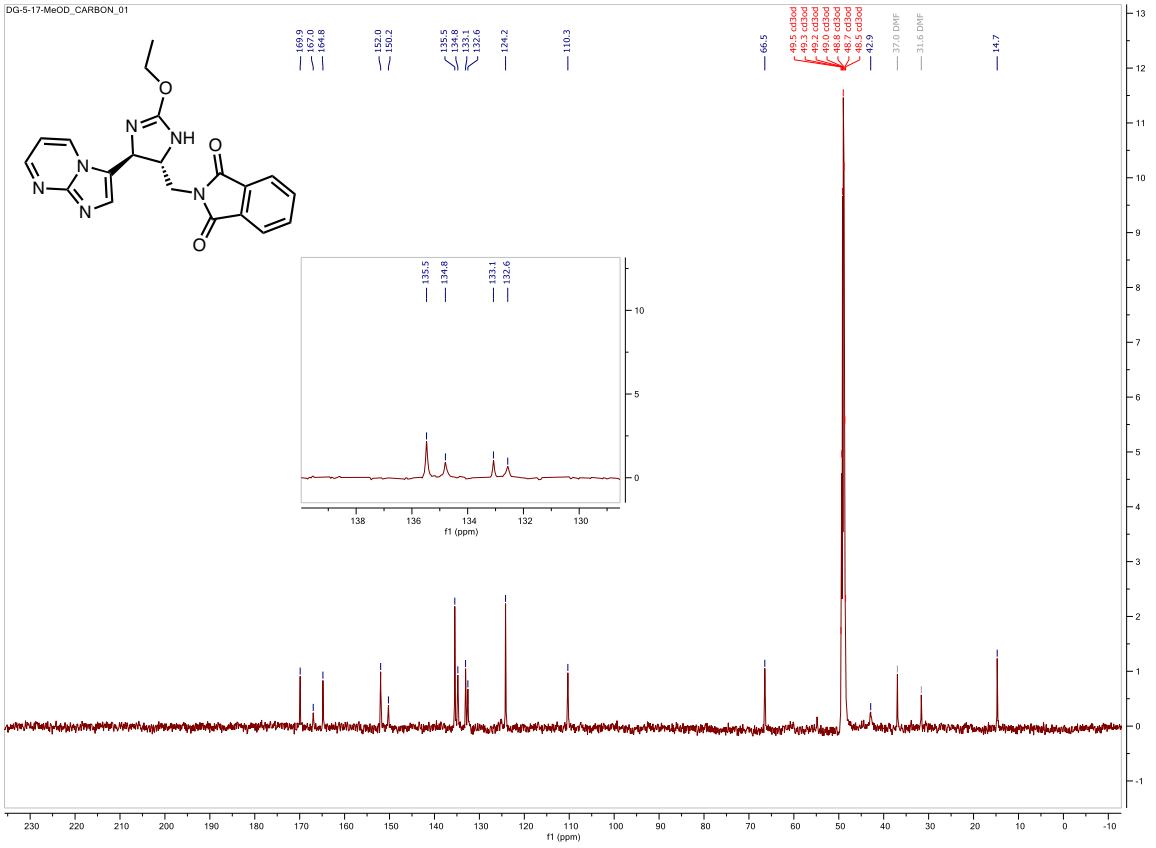

Figure 2.20: ^{1}H and $^{13}C\{1H\}$ NMR spectra of **2-32**

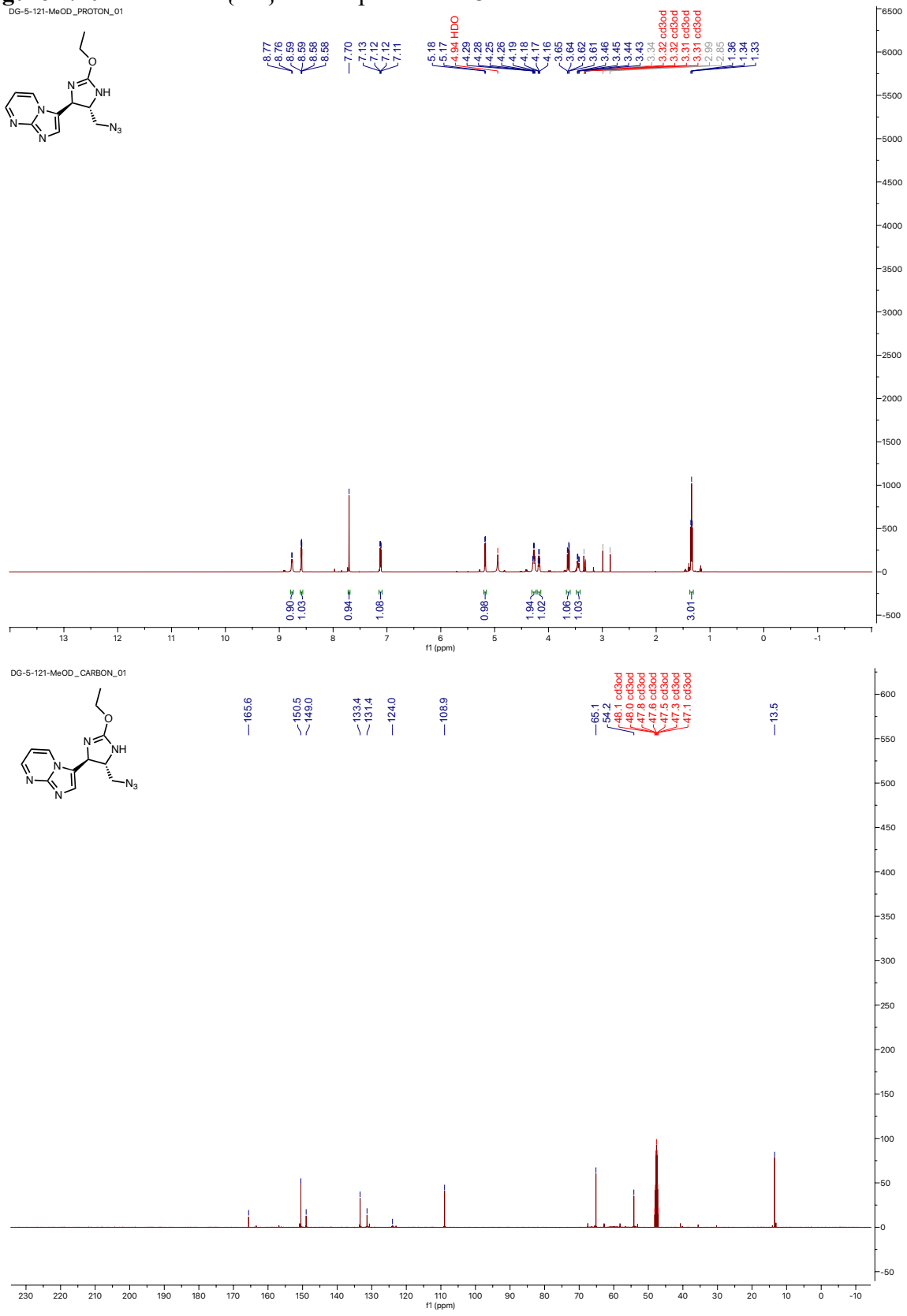

Figure 2.21: ^{1}H and $^{13}C\{1H\}$ NMR spectra of **2-35**

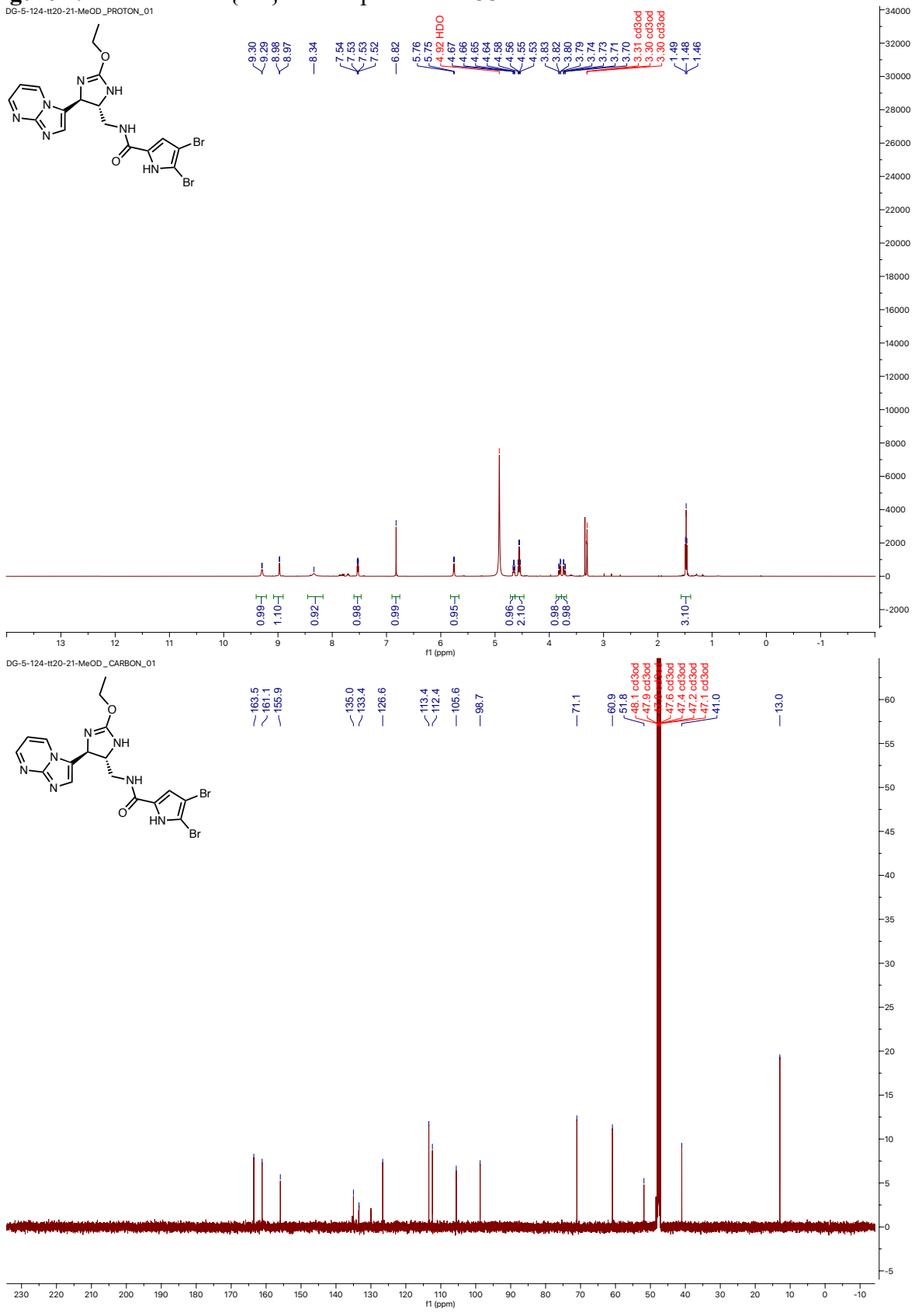

Figure 2.22: ^{1}H NMR spectra of **2-36**

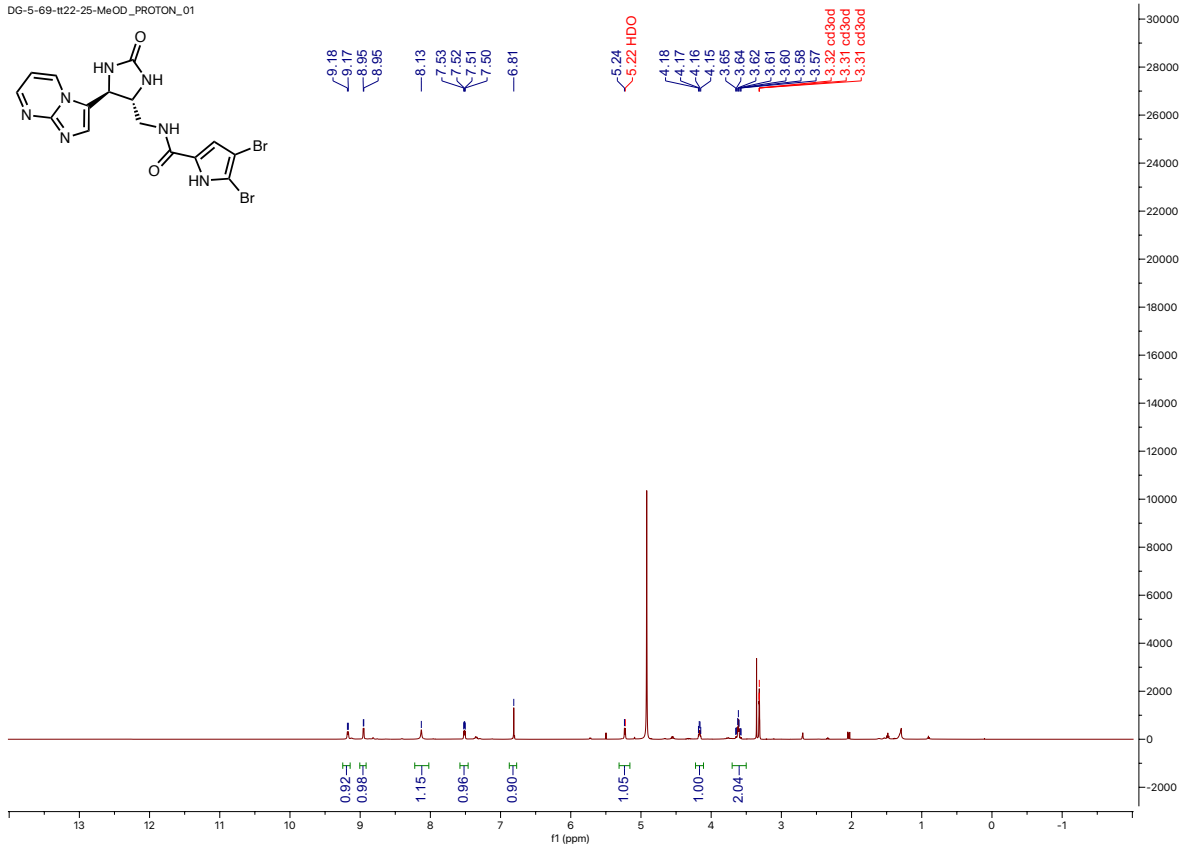

Figure 2.23: ^{1}H and $^{13}C\{1H\}$ NMR spectra of **S2-1**

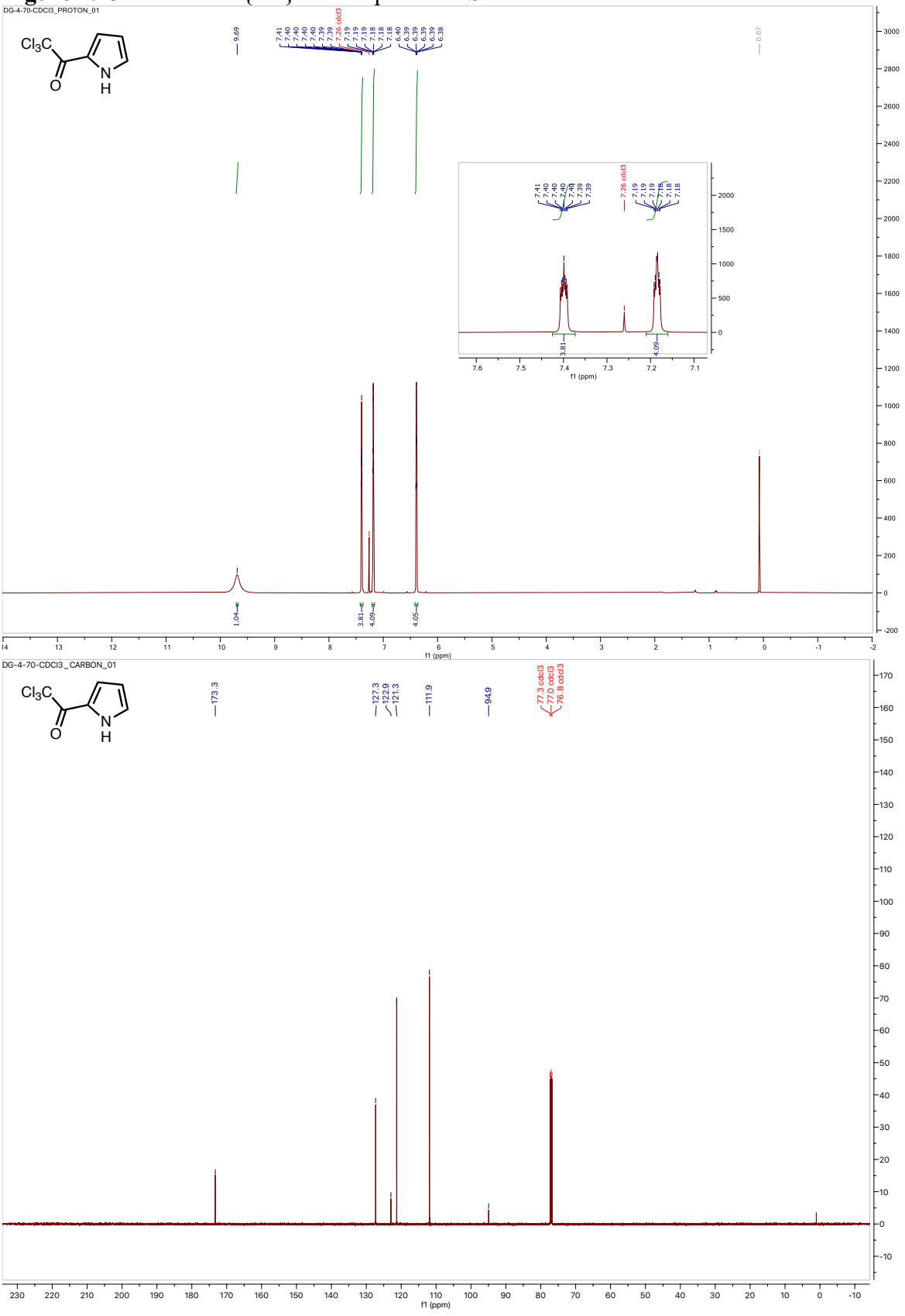

Figure 2.24: ^{1}H and $^{13}C\{1H\}$ NMR spectra of **S2-2**

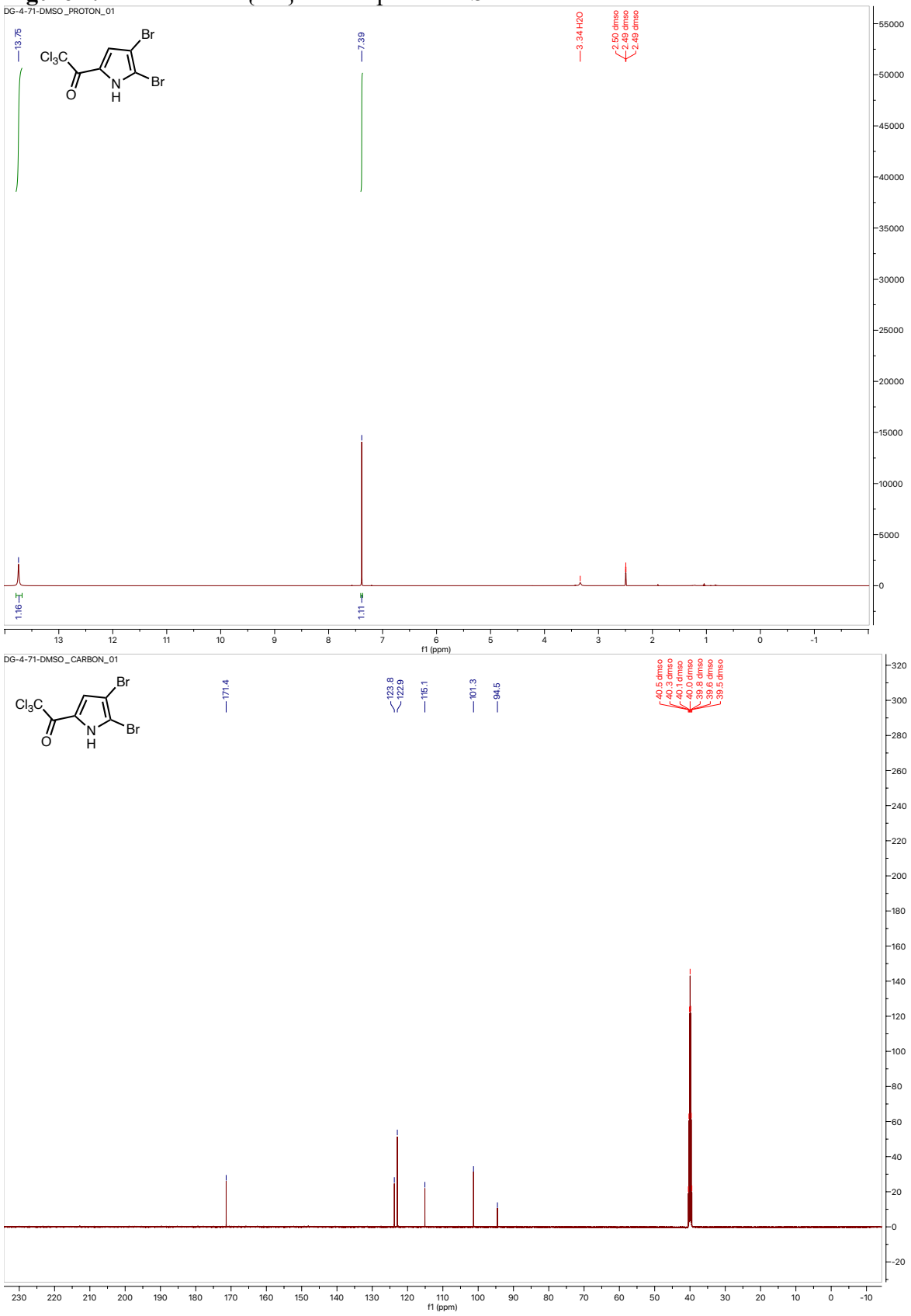

Figure 2.25: ^{1}H and $^{13}C\{1H\}$ NMR spectra of **2-39**

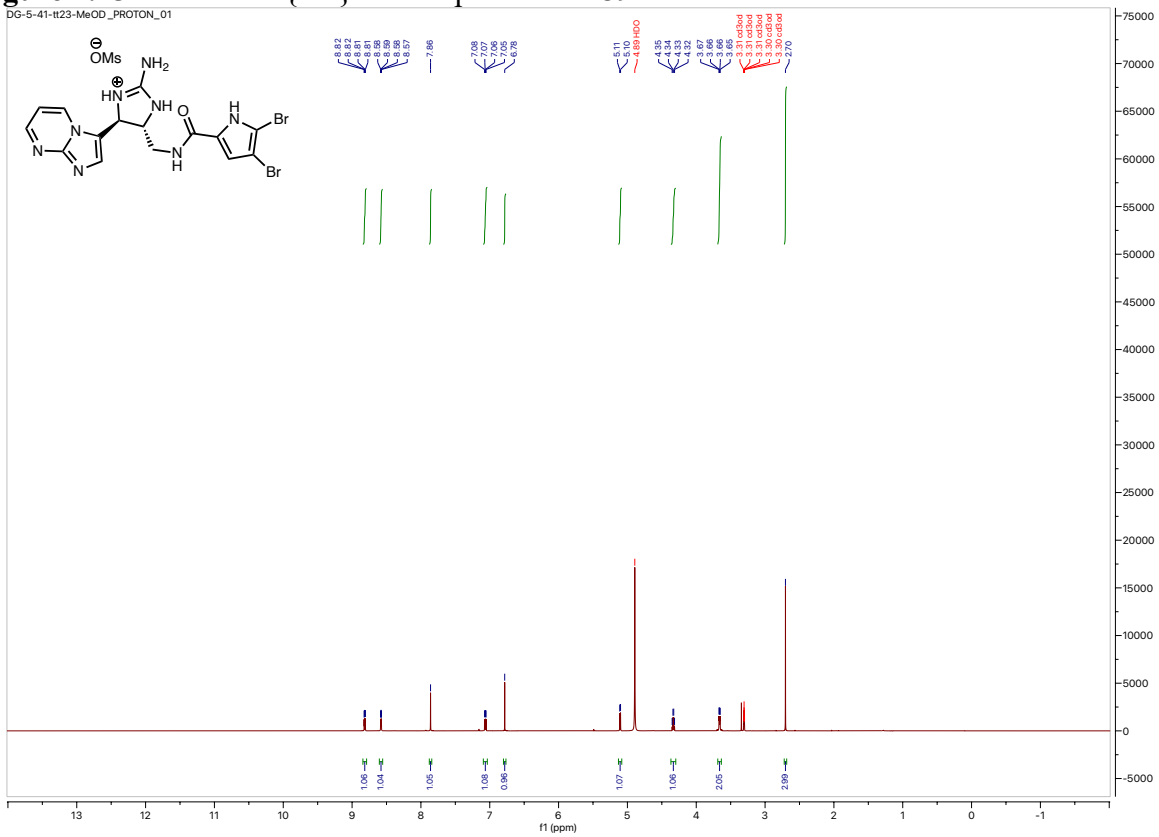

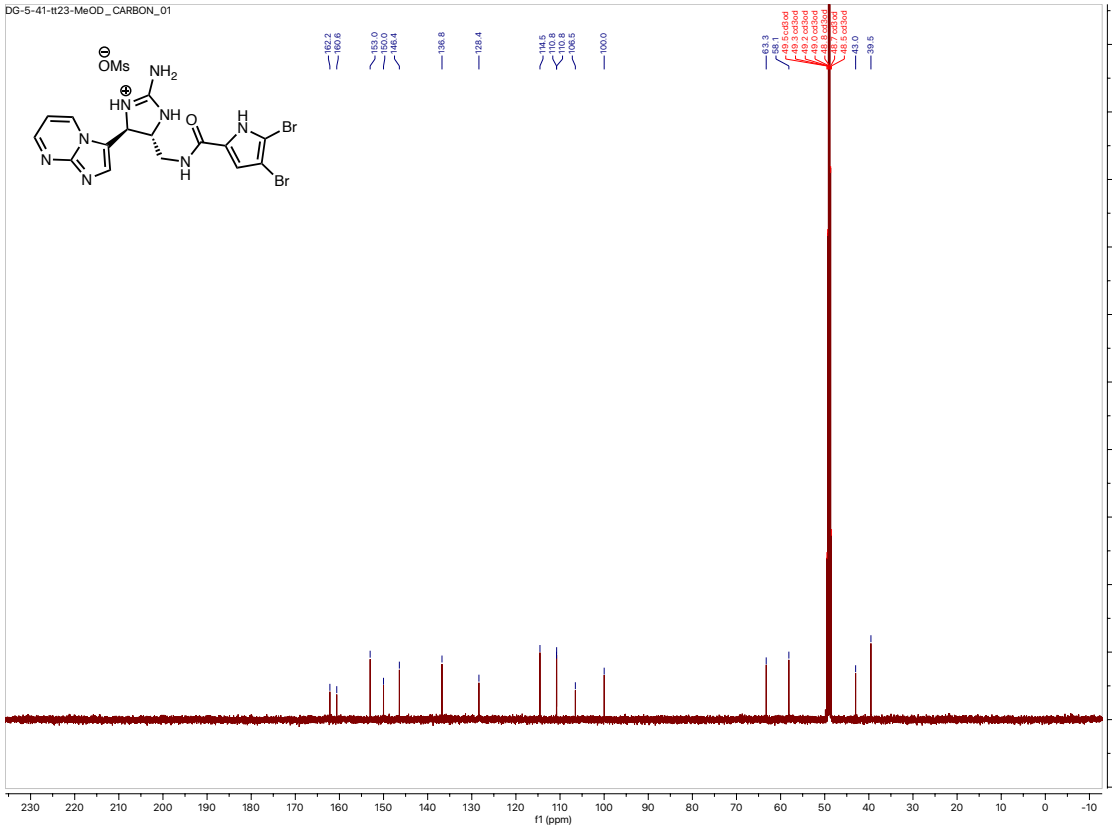

Figure 2.26: ^{1}H and $^{13}C\{1H\}$ NMR spectra of **2-1**

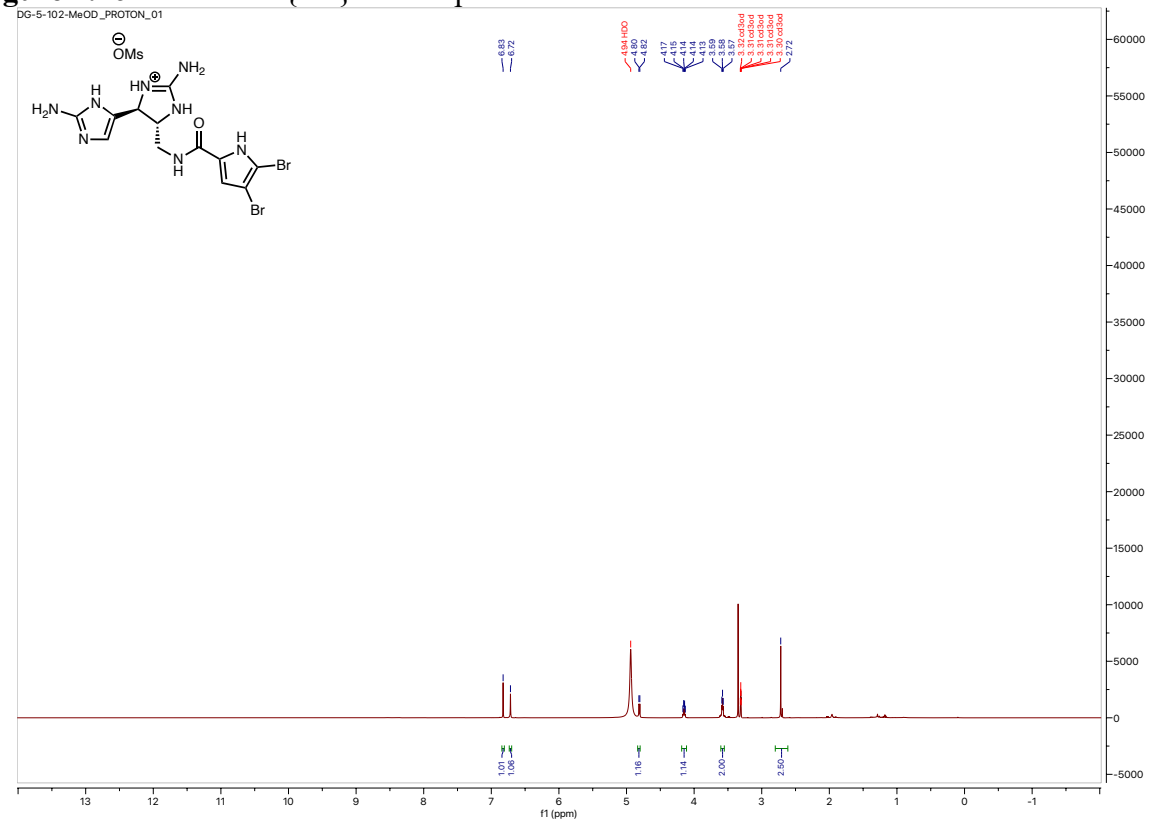

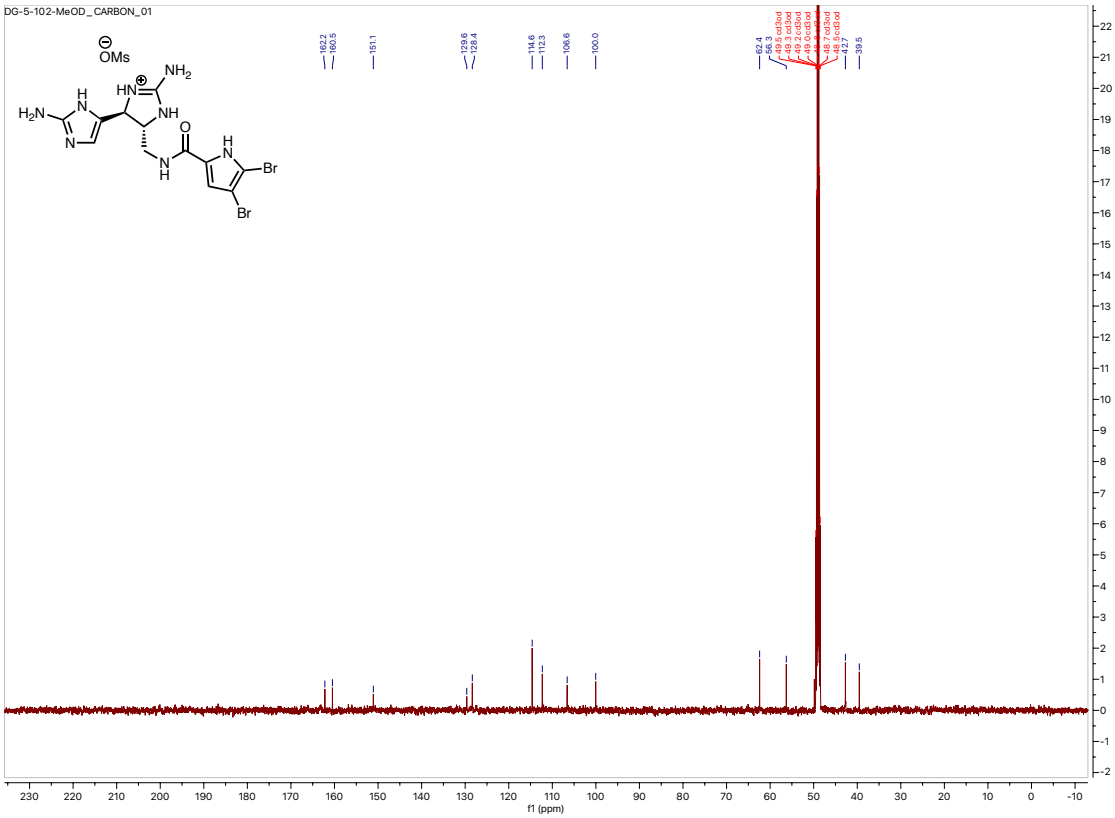

Figure 2.27: ^{1}H and $^{13}C\{1H\}$ NMR spectra of **2-1 • 2TFA**

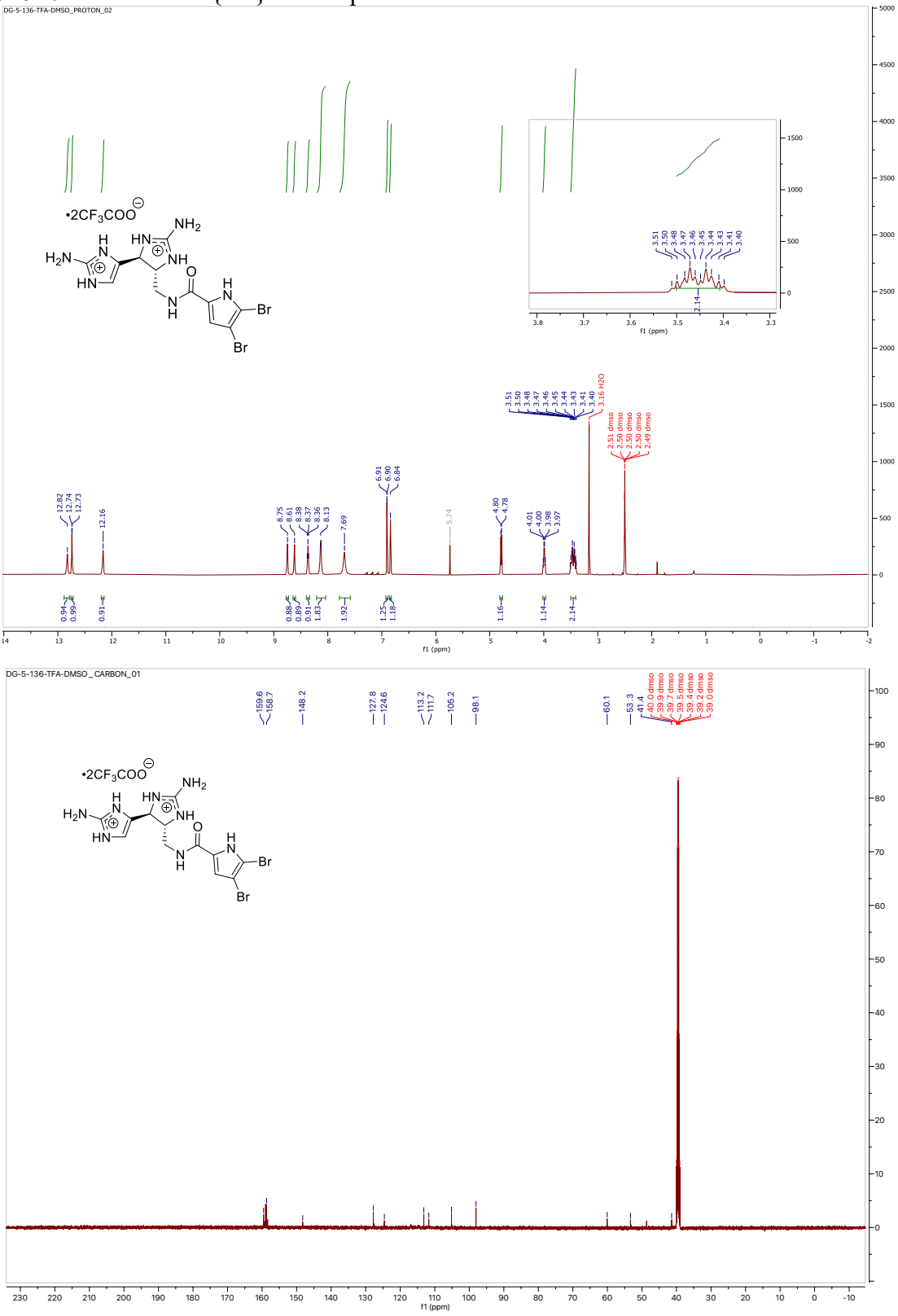

Crystal Data and Experimental

X-ray crystallographic analysis was performed by Dr. Richard Staples.

Figure 2.28: X-ray crystal structure of compound **2-25**

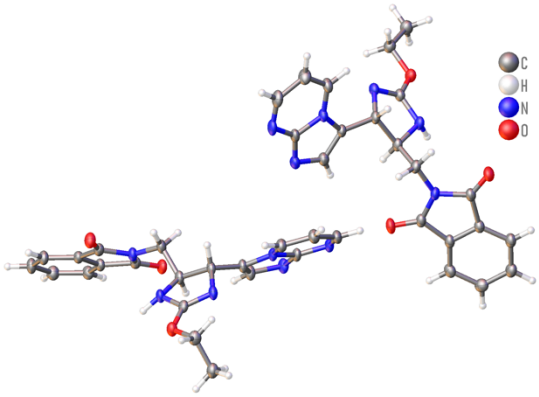

Experimental. Single colorless plate-shaped crystals of **JJT822A_twin1_hklf5** used as received. A suitable crystal with dimensions 0.19 × 0.12 × 0.07 mm^3 was selected and mounted on a nylon loop with paratone oil on a XtaLAB Synergy, Dualflex, HyPix diffractometer. The crystal was kept at a steady T = 100.01(12) K during data collection. The structure was solved with the **ShelXT** 2018/2 (Sheldrick, 2018) solution program using dual methods and by using **O.** V. Dolomanov, L. J. Bourhis, R. J. Gildea, J. A. K. Howard and H. Puschmann,Olex2: a complete structure solution, refinement and analysis program.J. Appl. Cryst. (2009). 42, 339-341. as the graphical interface. The model was refined with **ShelXL** 2018/3 (Sheldrick, 2015) using full matrix least squares minimisation on $\boldsymbol{F^2}$.

Crystal Data. $C_{20}H_{18}N_6O_3$, M_r = 390.40, monoclinic, $P2_1/c$ (No. 14), a = 15.6910(3) Å, b = 15.0668(2) Å, c = 15.2190(2) Å, b = 93.496(2)°, a = g = 90°, V = 3591.28(10) $Å^3$, T = 100.01(12) K, Z = 8, Z' = 2, m(Cu K_a) = 0.838, 16075 reflections measured, 16075 unique (R_{int} = .) which were used in all calculations. The final wR_2 was 0.2340 (all data) and R_1 was 0.0820 (I≥2 s(I)).

Table 2.5: Crystal data

Compound	**JJT822A_twin1_hklf5**
Formula	$C_{20}H_{18}N_6O_3$
CCDC	2194100
$D_{calc.}$/ g cm^{-3}	1.444
m/mm^{-1}	0.838
Formula Weight	390.40
Color	colorless
Shape	plate-shaped
Size/mm^3	0.19×0.12×0.07
T/K	100.01(12)
Crystal System	monoclinic
Space Group	$P2_1/c$
a/Å	15.6910(3)
b/Å	15.0668(2)
c/Å	15.2190(2)
a/°	90
b/°	93.496(2)
g/°	90
V/Å^3	3591.28(10)
Z	8
Z'	2

Table 2.5 (cont'd)

Wavelength/Å	1.54184
Radiation type	Cu K_a
$Q_{min}/^{\circ}$	2.821
$Q_{max}/^{\circ}$	80.341
Measured Refl's.	16075
Indep't Refl's	16075
Refl's I≥2 *s*(I)	14464
R_{int}	.
Parameters	534
Restraints	0
Largest Peak	0.495
Deepest Hole	-0.434
GooF	1.109
wR_2 (all data)	0.2340
wR_2	0.2311
R_1 (all data)	0.0867
R_1	0.0820

Table 2.6: Structure Quality Indicators

Reflections:	d min (Cu\a) 2Θ=160.7° 0.78	I/σ(I) 64.1	Rint n/a	Full 135.4° 99% to 160.7° 100
Refinement:	Shift 0.000	Max Peak 0.5	Min Peak -0.4	GooF 1.109

A colorless plate-shaped-shaped crystal with dimensions 0.19×0.12×0.07 mm^3 was mounted on a nylon loop with paratone oil. Data were collected using a XtaLAB Synergy, Dualflex, HyPix

diffractometer equipped with an Oxford Cryosystems low-temperature device, operating at T = 100.01(12) K.

MSU Data were measured using *w* scans using Cu K_a radiation (micro-focus sealed X-ray tube, 50 kV, 1 mA). The total number of runs and images was based on the strategy calculation from the program CrysAlisPro 1.171.42.64a (Rigaku OD, 2022). The achieved resolution was Q = 80.341.

Cell parameters were retrieved using the CrysAlisPro 1.171.42.64a (Rigaku OD, 2022) software and refined using CrysAlisPro 1.171.42.64a (Rigaku OD, 2022) on 23311 reflections, 145 % of the observed reflections. Data reduction was performed using the CrysAlisPro 1.171.42.64a (Rigaku OD, 2022) software which corrects for Lorentz polarization. The final completeness is 100.00 out to 80.341 in Q CrysAlisPro 1.171.42.64a (Rigaku Oxford Diffraction, 2022) Empirical absorption correction using spherical harmonics, implemented in SCALE3 ABSPACK scaling algorithm.

The structure was solved in the space group $P2_1/c$ (# 14) by using dual methods using the ShelXT (Sheldrick, 2015) structure solution program. The structure was refined by Least Squares ShelXL incorporated in Olex2 software program. All non-hydrogen atoms were refined anisotropically. Hydrogen atom positions were calculated geometrically and refined using the riding model, except for the hydrogen atom on the non-carbon atom(s) which were found by difference Fourier methods and refined isotropically when data permits.

CCDC 2194100 contains the supplementary crystallographic data for this paper. The data can be obtained free of charge from The Cambridge Crystallographic Data Centre via www.ccdc.cam.ac.uk/structures.

_twin_special_details: Component 2 rotated by -179.8461° around [1.00 -0.00 -0.03] (reciprocal)

or [1.00 -0.00 0.03] (direct).

The value of Z' is 2. This means that there are two independent molecules in the asymmetric unit.

Figure 2.29: Drawing at 50% ellipsoids showing the labeling scheme for compound **2-25**, where the model has Chirality at C2 (Centro SPGR) S, and Chirality at C3 (Centro SPGR) R

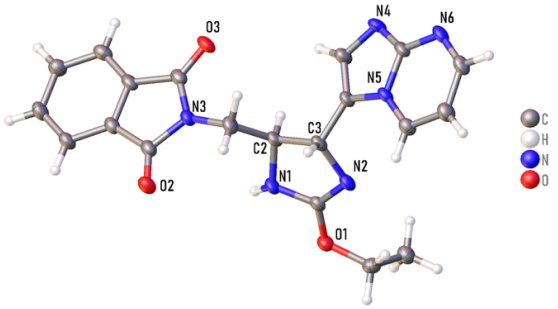

Figure 2.30: Drawing at 50% ellipsoids showing the labeling scheme, where the model has Chirality at C2A (Centro SPGR) S, and Chirality at C3A (Centro SPGR) R

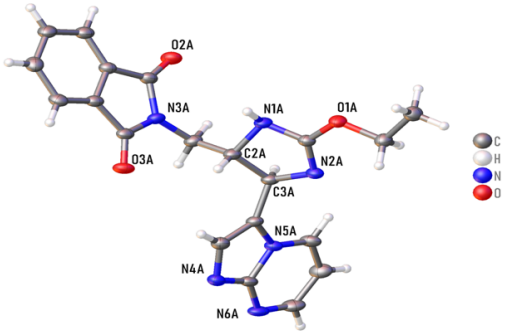

Figure 2.31: Packing diagram of JJT822A_twin1_hklf5

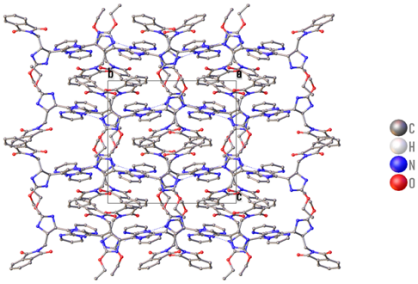

Figure 2.32: Data plots: Diffraction data

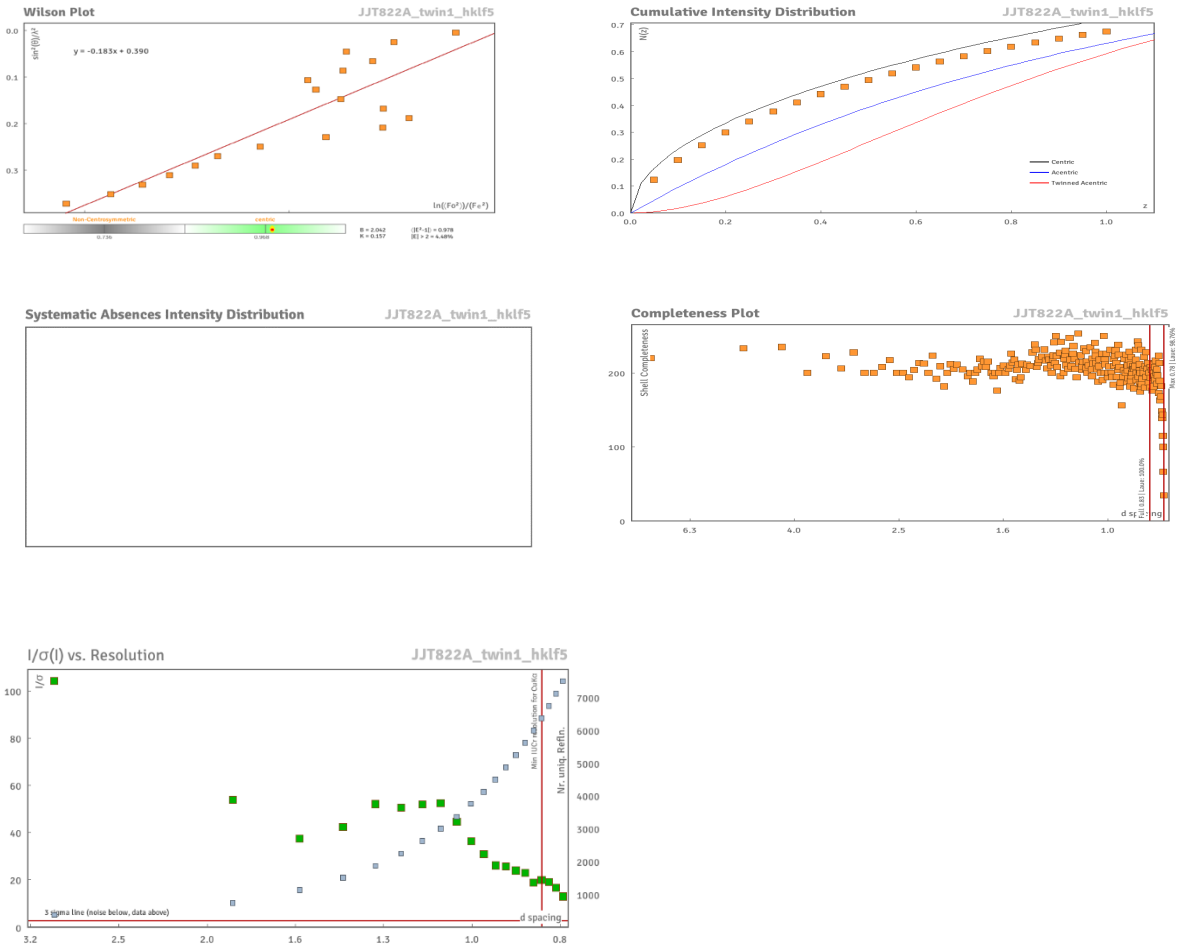

Figure 2.33: Data plots: Refinement and data

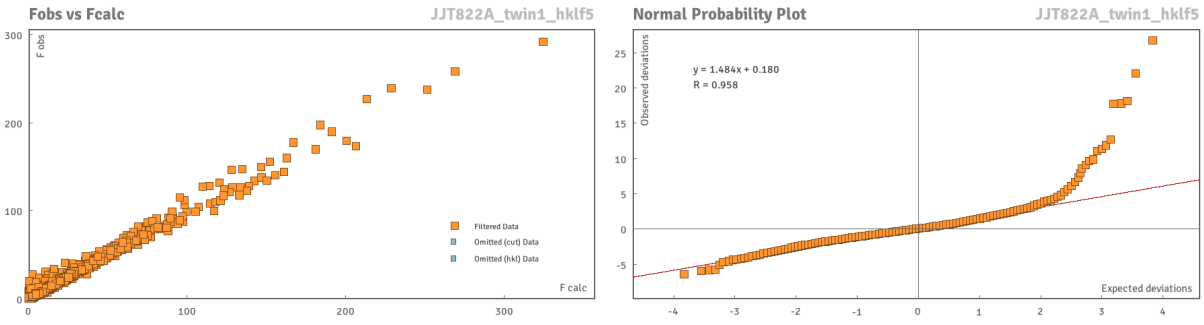

Table 2.7: Reflection Statistics

Total reflections (after filtering)	18680	Unique reflections	7775
Completeness	0.988	Mean I/*s*	16.8
hkl_{max} collected	(19, 19, 19)	hkl_{min} collected	(-20, -19, -19)
hkl_{max} used	(19, 19, 19)	hkl_{min} used	(-20, 0, 0)
Lim d_{max} collected	100.0	Lim d_{min} collected	0.77
d_{max} used	15.66	d_{min} used	0.78
Friedel pairs	3083	Friedel pairs merged	1
Inconsistent equivalents	0	R_{int}	0.0
R_{sigma}	0.0156	Intensity transformed	0
Omitted reflections	0	Omitted by user (OMIT hkl)	0
Multiplicity	(13016, 1513, 11)	Maximum multiplicity	0
Removed systematic absences	0	Filtered off (Shel/OMIT)	0

Figure 2.34: Selected Crystal Pictures

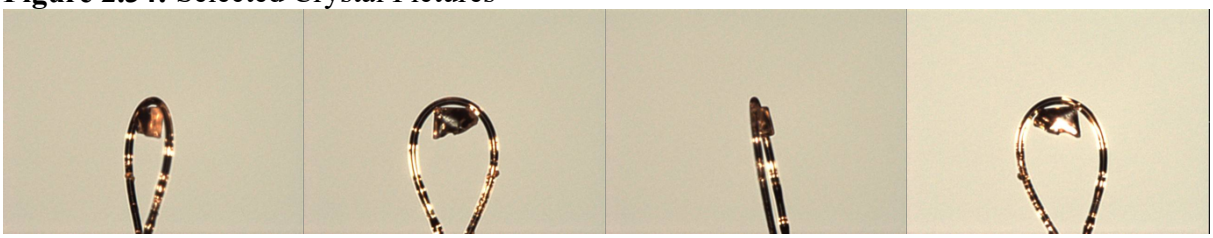

Table 2.8: Fractional Atomic Coordinates ($\times 10^4$) and Equivalent Isotropic Displacement Parameters ($Å^2 \times 10^3$) for **JJT822A_twin1_hklf5**. U_{eq} is defined as 1/3 of the trace of the orthogonalised U_{ij}

Atom	x	y	z	U_{eq}
O1	1087.0(18)	3924.2(16)	619.5(17)	28.2(6)
O2	886.5(18)	2685.6(17)	3996.5(19)	31.5(6)
O3	-784.7(18)	5152.9(16)	4208.2(18)	30.7(6)
N1	739(2)	4103.0(19)	2040(2)	25.3(6)
N2	1481(2)	5210.8(19)	1409(2)	26.4(6)
N3	172(2)	4033.6(19)	3959(2)	25.2(6)
N4	631(2)	7778.9(19)	2768(2)	28.5(7)
N5	1770(2)	7072.6(18)	2288(2)	23.7(6)
N6	1817(2)	8666.8(19)	2386(2)	28.2(7)
C1	1111(2)	4445(2)	1329(2)	23.6(7)
C2	667(2)	4836(2)	2657(2)	24.8(7)
C3	1367(2)	5459(2)	2335(2)	24.4(7)
C4	1564(3)	4228(3)	-117(3)	30.3(8)

Table 2.8 (cont'd)

C5	980(3)	4660(3)	-805(3)	33.6(9)
C6	842(3)	4577(2)	3612(2)	27.9(8)
C7	263(3)	3125(2)	4145(2)	26.0(7)
C8	-524(2)	2864(2)	4567(2)	25.1(7)
C9	-786(3)	2040(2)	4859(3)	28.4(8)
C10	-1571(3)	1999(2)	5237(3)	32.1(8)
C11	-2070(3)	2750(3)	5326(3)	30.5(8)
C12	-1809(3)	3574(2)	5026(3)	29.1(8)
C13	-1033(2)	3614(2)	4646(2)	25.7(7)
C14	-575(2)	4375(2)	4256(2)	25.7(7)
C15	1177(2)	6424(2)	2454(2)	24.1(7)
C16	498(3)	6877(2)	2746(3)	29.3(8)
C17	1400(3)	7888(2)	2495(2)	25.6(7)
C18	2569(3)	8613(2)	2060(3)	29.5(8)
C19	2972(3)	7804(3)	1833(3)	31.3(8)
C20	2552(2)	7027(2)	1954(3)	27.5(8)
O1A	5938.6(18)	10621.9(16)	4614.8(17)	27.9(6)
O2A	6072.8(18)	11698.3(17)	979.5(19)	32.7(6)
O3A	4122.7(18)	9442.4(17)	1055.6(18)	30.8(6)
N1A	5780(2)	10462.1(19)	3119(2)	25.8(6)
N2A	6350(2)	9305.5(19)	3939(2)	25.1(6)
N3A	5245(2)	10438.9(19)	1128(2)	24.7(6)

Table 2.8 (cont'd)

N4A	5619(2)	6782(2)	2296(2)	29.4(7)
N5A	6788.1(19)	7465.0(19)	2875(2)	23.2(6)
N6A	6898(2)	5914(2)	2534(2)	31.4(7)
C1A	6030(2)	10096(2)	3919(2)	24.2(7)
C2A	5698(2)	9693(2)	2525(2)	25.3(7)
C3A	6345(2)	9064(2)	2998(2)	24.3(7)
C4A	6185(3)	10234(2)	5464(2)	28.9(8)
C5A	6065(3)	10932(3)	6138(3)	32.5(8)
C6A	5890(2)	9878(2)	1587(2)	26.7(7)
C7A	5400(2)	11318(2)	861(2)	25.4(7)
C8A	4577(2)	11624(2)	421(2)	24.7(7)
C9A	4379(3)	12421(2)	13(3)	29.5(8)
C10A	3544(3)	12531(3)	-333(3)	30.6(8)
C11A	2931(3)	11869(3)	-271(3)	31.4(8)
C12A	3144(3)	11059(2)	146(3)	28.4(8)
C13A	3974(2)	10953(2)	480(2)	25.1(7)
C14A	4409(2)	10180(2)	919(2)	24.6(7)
C15A	6160(2)	8107(2)	2793(2)	23.2(7)
C16A	5463(3)	7664(2)	2444(3)	29.1(8)
C17A	6430(3)	6667(2)	2558(2)	26.2(7)
C18A	7700(3)	5963(3)	2849(3)	35.5(9)

Table 2.8 (cont'd)

C19A	8086(3)	6742(3)	3209(3)	35.3(9)
C20A	7618(3)	7495(2)	3219(3)	30.0(8)

Table 2.9: Anisotropic Displacement Parameters ($\times 10^4$) for **JJT822A_twin1_hklf5**. The anisotropic displacement factor exponent takes the form: $-2p^2[h^2a^{*2} \times U_{11} + ... + 2hka^* \times b^* \times U_{12}]$

Atom	U_{11}	U_{22}	U_{33}	U_{23}	U_{13}	U_{12}
O1	37.6(15)	18.5(12)	28.9(13)	-1.2(10)	5.5(11)	-1.5(10)
O2	33.3(15)	20.7(13)	41.2(16)	3.3(11)	6.9(12)	2.7(11)
O3	42.6(16)	13.5(12)	35.8(15)	0.0(10)	0.7(12)	2.1(10)
N1	34.6(17)	13.3(13)	28.2(16)	0.3(11)	3.2(12)	-4.3(12)
N2	30.7(16)	13.7(13)	35.2(17)	1.8(11)	4.6(13)	-1.6(11)
N3	33.4(17)	14.0(13)	28.5(15)	0.9(11)	4.4(12)	-1.8(12)
N4	34.1(18)	14.0(14)	37.9(18)	-2.4(12)	6.4(14)	4.5(12)
N5	30.5(16)	11.9(13)	28.7(15)	0.6(11)	1.4(12)	0.8(11)
N6	40.0(19)	13.2(14)	31.0(16)	0.7(11)	-1.6(13)	-1.9(12)
C1	26.8(18)	15.2(15)	28.9(18)	1.8(13)	2.3(14)	3.4(13)
C2	30.2(19)	13.0(15)	31.5(19)	-0.1(13)	4.1(14)	-0.1(13)
C3	26.7(18)	13.1(15)	33.7(19)	0.7(13)	2.8(14)	-1.0(13)
C4	34(2)	26.7(19)	30.7(19)	-2.3(15)	8.2(15)	2.4(15)
C5	41(2)	23.5(18)	36(2)	1.7(15)	5.2(17)	-0.3(16)
C6	36(2)	17.3(16)	30.8(19)	1.4(13)	3.8(15)	-5.7(14)
C7	34(2)	17.8(16)	25.9(18)	0.8(13)	0.8(14)	-1.0(14)

Table 2.9 (cont'd)

C8	32.1(19)	16.8(16)	26.2(18)	0.9(13)	-0.4(14)	-1.7(14)
C9	34(2)	15.8(16)	36(2)	2.2(14)	2.2(15)	0.7(14)
C10	38(2)	17.9(17)	41(2)	4.2(15)	5.1(17)	-2.5(15)
C11	30(2)	25.2(18)	36(2)	0.5(15)	5.4(15)	1.2(15)
C12	32(2)	19.2(17)	36(2)	-2.1(14)	1.1(15)	2.8(14)
C13	34(2)	14.3(15)	28.5(18)	-0.9(13)	-1.2(14)	-0.5(13)
C14	35(2)	17.4(16)	24.7(17)	-1.5(13)	-0.8(14)	-0.2(14)
C15	28.8(18)	13.5(15)	30.2(18)	0.7(13)	4.1(14)	-2.6(13)
C16	31(2)	17.5(17)	40(2)	0.7(14)	7.5(16)	0.3(14)
C17	38(2)	12.4(15)	26.5(18)	-0.5(12)	1.8(15)	-0.2(13)
C18	35(2)	18.0(17)	35(2)	2.8(14)	-1.7(16)	-6.2(14)
C19	32(2)	23.6(18)	39(2)	2.0(15)	2.8(16)	-3.9(15)
C20	28.7(19)	19.7(17)	34(2)	1.7(14)	1.6(15)	-0.2(14)
O1A	37.5(15)	17.9(12)	28.1(13)	-1.6(9)	0.9(11)	2.7(10)
O2A	33.6(15)	22.1(13)	42.2(16)	4.0(11)	1.9(12)	-5.8(11)
O3A	38.2(16)	16.2(12)	38.6(15)	0.8(10)	6.8(12)	-5.1(10)
N1A	35.1(18)	14.2(13)	28.1(16)	0.1(11)	2.5(13)	2.4(12)
N2A	29.0(16)	15.6(13)	30.5(16)	-0.9(11)	-0.6(12)	0.4(11)
N3A	31.5(16)	16.1(13)	26.7(15)	3.5(11)	3.1(12)	-0.7(11)
N4A	40.2(19)	17.5(14)	29.8(17)	-1.0(12)	-1.8(13)	-4.5(13)
N5A	26.3(15)	13.7(13)	29.9(16)	-0.8(11)	3.3(12)	-0.4(11)
N6A	47(2)	12.1(14)	35.3(18)	-1.2(12)	7.0(15)	-0.2(13)

Table 2.9 (cont'd)

C1A	27.9(18)	16.7(15)	28.1(18)	-1.3(13)	1.7(14)	-0.2(13)
C2A	34(2)	15.5(15)	27.1(18)	-0.2(13)	3.2(14)	1.3(13)
C3A	30.4(19)	13.9(15)	28.8(18)	0.5(13)	2.6(14)	0.3(13)
C4A	34(2)	23.9(18)	28.5(19)	0.7(14)	1.2(15)	2.6(15)
C5A	40(2)	27.4(19)	31(2)	-1.6(15)	4.2(16)	1.2(16)
C6A	33(2)	17.8(16)	29.8(19)	2.6(13)	2.4(15)	3.2(14)
C7A	31.8(19)	18.6(16)	26.1(18)	-0.4(13)	3.8(14)	-3.2(14)
C8A	29.4(19)	17.6(16)	27.2(18)	-1.1(13)	3.3(14)	-1.4(13)
C9A	39(2)	18.1(16)	32(2)	-1.2(14)	3.9(16)	-0.6(14)
C10A	41(2)	19.1(17)	32(2)	-1.2(14)	1.8(16)	3.3(15)
C11A	35(2)	26.6(19)	33(2)	-5.1(15)	-0.3(16)	6.2(15)
C12A	32(2)	19.6(17)	34(2)	-5.7(14)	2.9(15)	0.4(14)
C13A	33(2)	16.0(15)	26.8(18)	-1.6(13)	5.0(14)	-0.8(14)
C14A	35(2)	15.9(15)	23.3(17)	-1.7(12)	4.7(14)	-0.1(14)
C15A	28.5(18)	14.3(15)	26.9(18)	1.6(12)	2.4(14)	0.2(13)
C16A	34(2)	20.6(17)	32(2)	1.3(14)	0.6(15)	-2.5(14)
C17A	38(2)	13.7(15)	26.9(18)	-1.3(12)	2.6(15)	-2.7(14)
C18A	44(2)	17.8(17)	45(2)	1.0(15)	10.9(18)	5.9(16)
C19A	30(2)	25.9(19)	51(3)	2.6(17)	4.5(17)	5.7(16)
C20A	30(2)	17.7(17)	43(2)	-0.4(15)	3.6(16)	-3.2(14)

Table 2.10: Bond Lengths in Å for **JJT822A_twin1_hklf5**

Atom	Atom	Length/Å
O1	C1	1.334(4)
O1	C4	1.459(5)
O2	C7	1.214(5)
O3	C14	1.218(4)
N1	C1	1.362(5)
N1	C2	1.458(4)
N2	C1	1.294(5)
N2	C3	1.479(5)
N3	C6	1.456(5)
N3	C7	1.404(4)
N3	C14	1.383(5)
N4	C16	1.375(5)
N4	C17	1.311(5)
N5	C15	1.382(4)
N5	C17	1.403(4)
N5	C20	1.359(5)
N6	C17	1.358(5)
N6	C18	1.309(5)
C2	C3	1.547(5)
C2	C6	1.513(5)
C3	C15	1.497(5)

Table 2.10 (cont'd)

C4	C5	1.498(6)
C7	C8	1.478(5)
C8	C9	1.390(5)
C8	C13	1.393(5)
C9	C10	1.392(6)
C10	C11	1.386(5)
C11	C12	1.394(5)
C12	C13	1.380(6)
C13	C14	1.495(5)
C15	C16	1.362(5)
C18	C19	1.425(5)
C19	C20	1.363(5)
O1A	C1A	1.337(4)
O1A	C4A	1.449(4)
O2A	C7A	1.205(5)
O3A	C14A	1.222(4)
N1A	C1A	1.372(5)
N1A	C2A	1.470(4)
N2A	C1A	1.292(5)
N2A	C3A	1.478(5)
N3A	C6A	1.463(5)
N3A	C7A	1.410(4)

Table 2.10 (cont'd)

N3A	C14A	1.387(5)
N4A	C16A	1.372(5)
N4A	C17A	1.321(5)
N5A	C15A	1.381(4)
N5A	C17A	1.401(4)
N5A	C20A	1.374(5)
N6A	C17A	1.353(5)
N6A	C18A	1.321(6)
C2A	C3A	1.535(5)
C2A	C6A	1.503(5)
C3A	C15A	1.501(5)
C4A	C5A	1.489(5)
C7A	C8A	1.491(5)
C8A	C9A	1.380(5)
C8A	C13A	1.392(5)
C9A	C10A	1.392(6)
C10A	C11A	1.392(6)
C11A	C12A	1.407(5)
C12A	C13A	1.377(5)
C13A	C14A	1.487(5)
C15A	C16A	1.361(5)
C18A	C19A	1.416(6)

Table 2.10 (cont'd)

C19A	C20A	1.352(5)

Table 2.11: Bond Angles in ° for **JJT822A_twin1_hklf5**

Atom	**Atom**	**Atom**	**Angle/°**
C1	O1	C4	116.6(3)
C1	N1	C2	106.2(3)
C1	N2	C3	103.6(3)
C7	N3	C6	123.7(3)
C14	N3	C6	123.7(3)
C14	N3	C7	112.0(3)
C17	N4	C16	104.9(3)
C15	N5	C17	106.6(3)
C20	N5	C15	131.7(3)
C20	N5	C17	121.6(3)
C18	N6	C17	116.4(3)
O1	C1	N1	115.4(3)
N2	C1	O1	126.2(3)
N2	C1	N1	118.3(3)
N1	C2	C3	99.9(3)
N1	C2	C6	114.0(3)
C6	C2	C3	111.8(3)
N2	C3	C2	106.1(3)
N2	C3	C15	113.5(3)

Table 2.11 (cont'd)

C15	C3	C2	113.6(3)
O1	C4	C5	110.7(3)
N3	C6	C2	113.6(3)
O2	C7	N3	124.5(4)
O2	C7	C8	129.8(3)
N3	C7	C8	105.7(3)
C9	C8	C7	130.4(3)
C9	C8	C13	120.9(4)
C13	C8	C7	108.7(3)
C8	C9	C10	117.3(3)
C11	C10	C9	121.6(3)
C10	C11	C12	121.0(4)
C13	C12	C11	117.4(3)
C8	C13	C14	107.2(3)
C12	C13	C8	121.8(3)
C12	C13	C14	131.0(3)
O3	C14	N3	124.7(4)
O3	C14	C13	128.9(4)
N3	C14	C13	106.4(3)
N5	C15	C3	121.5(3)
C16	C15	N5	104.7(3)
C16	C15	C3	133.7(3)

Table 2.11 (cont'd)

C15	C16	N4	112.5(3)
N4	C17	N5	111.2(3)
N4	C17	N6	127.4(3)
N6	C17	N5	121.4(3)
N6	C18	C19	124.6(3)
C20	C19	C18	118.5(4)
N5	C20	C19	117.5(3)
C1A	O1A	C4A	115.6(3)
C1A	N1A	C2A	103.8(3)
C1A	N2A	C3A	103.0(3)
C7A	N3A	C6A	123.6(3)
C14A	N3A	C6A	124.4(3)
C14A	N3A	C7A	112.0(3)
C17A	N4A	C16A	104.9(3)
C15A	N5A	C17A	107.5(3)
C20A	N5A	C15A	131.7(3)
C20A	N5A	C17A	120.7(3)
C18A	N6A	C17A	116.8(3)
O1A	C1A	N1A	115.2(3)
N2A	C1A	O1A	126.0(3)
N2A	C1A	N1A	118.7(3)
N1A	C2A	C3A	99.7(3)

Table 2.11 (cont'd)

N1A	C2A	C6A	115.0(3)
C6A	C2A	C3A	113.2(3)
N2A	C3A	C2A	105.5(3)
N2A	C3A	C15A	115.3(3)
C15A	C3A	C2A	112.5(3)
O1A	C4A	C5A	106.9(3)
N3A	C6A	C2A	112.8(3)
O2A	C7A	N3A	124.7(4)
O2A	C7A	C8A	130.3(3)
N3A	C7A	C8A	105.1(3)
C9A	C8A	C7A	129.6(3)
C9A	C8A	C13A	121.8(4)
C13A	C8A	C7A	108.7(3)
C8A	C9A	C10A	117.0(4)
C9A	C10A	C11A	121.8(4)
C10A	C11A	C12A	120.4(4)
C13A	C12A	C11A	117.4(4)
C8A	C13A	C14A	107.5(3)
C12A	C13A	C8A	121.5(3)
C12A	C13A	C14A	130.9(3)
O3A	C14A	N3A	124.7(3)
O3A	C14A	C13A	128.7(4)

Table 2.11 (cont'd)

N3A	C14A	C13A	106.6(3)
N5A	C15A	C3A	121.7(3)
C16A	C15A	N5A	104.1(3)
C16A	C15A	C3A	133.9(3)
C15A	C16A	N4A	113.0(4)
N4A	C17A	N5A	110.4(3)
N4A	C17A	N6A	128.1(3)
N6A	C17A	N5A	121.4(3)
N6A	C18A	C19A	124.2(4)
C20A	C19A	C18A	118.7(4)
C19A	C20A	N5A	118.1(3)

Table 2.12: Torsion Angles in ° for **JJT822A_twin1_hklf5**

Atom	**Atom**	**Atom**	**Atom**	**Angle/°**
O2	C7	C8	C9	-4.5(7)
O2	C7	C8	C13	176.0(4)
N1	C2	C3	N2	23.0(3)
N1	C2	C3	C15	148.4(3)
N1	C2	C6	N3	-71.2(4)
N2	C3	C15	N5	-65.4(5)
N2	C3	C15	C16	117.2(5)
N3	C7	C8	C9	177.5(4)
N3	C7	C8	C13	-2.0(4)

Table 2.12 (cont'd)

N5	C15	C16	N4	0.3(5)
N6	C18	C19	C20	0.4(6)
C1	O1	C4	C5	-99.5(4)
C1	N1	C2	C3	-22.1(4)
C1	N1	C2	C6	-141.4(3)
C1	N2	C3	C2	-15.5(4)
C1	N2	C3	C15	-140.9(3)
C2	N1	C1	O1	-167.8(3)
C2	N1	C1	N2	15.0(5)
C2	C3	C15	N5	173.2(3)
C2	C3	C15	C16	-4.1(6)
C3	N2	C1	O1	-175.9(3)
C3	N2	C1	N1	0.9(4)
C3	C2	C6	N3	176.5(3)
C3	C15	C16	N4	177.9(4)
C4	O1	C1	N1	-173.2(3)
C4	O1	C1	N2	3.7(5)
C6	N3	C7	O2	-4.0(6)
C6	N3	C7	C8	174.1(3)
C6	N3	C14	O3	5.2(6)

Table 2.12 (cont'd)

C6	N3	C14	C13	-173.7(3)
C6	C2	C3	N2	143.9(3)
C6	C2	C3	C15	-90.7(4)
C7	N3	C6	C2	107.8(4)
C7	N3	C14	O3	176.8(4)
C7	N3	C14	C13	-2.2(4)
C7	C8	C9	C10	179.9(4)
C7	C8	C13	C12	-179.3(3)
C7	C8	C13	C14	0.7(4)
C8	C9	C10	C11	-0.4(6)
C8	C13	C14	O3	-178.1(4)
C8	C13	C14	N3	0.8(4)
C9	C8	C13	C12	1.1(6)
C9	C8	C13	C14	-178.8(3)
C9	C10	C11	C12	1.0(6)
C10	C11	C12	C13	-0.6(6)
C11	C12	C13	C8	-0.5(6)
C11	C12	C13	C14	179.4(4)
C12	C13	C14	O3	2.0(7)
C12	C13	C14	N3	-179.1(4)
C13	C8	C9	C10	-0.6(6)
C14	N3	C6	C2	-81.6(4)

Table 2.12 (cont'd)

C14	N3	C7	O2	-175.5(4)
C14	N3	C7	C8	2.6(4)
C15	N5	C17	N4	-0.3(4)
C15	N5	C17	N6	-178.7(3)
C15	N5	C20	C19	177.2(4)
C16	N4	C17	N5	0.4(4)
C16	N4	C17	N6	178.7(4)
C17	N4	C16	C15	-0.4(5)
C17	N5	C15	C3	-178.0(3)
C17	N5	C15	C16	0.0(4)
C17	N5	C20	C19	0.6(5)
C17	N6	C18	C19	-1.0(6)
C18	N6	C17	N4	-176.6(4)
C18	N6	C17	N5	1.5(5)
C18	C19	C20	N5	-0.1(6)
C20	N5	C15	C3	5.1(6)
C20	N5	C15	C16	-176.9(4)
C20	N5	C17	N4	177.0(3)
C20	N5	C17	N6	-1.3(5)
O2A	C7A	C8A	C9A	1.8(7)
O2A	C7A	C8A	C13A	-177.7(4)
N1A	C2A	C3A	N2A	29.1(3)

Table 2.12 (cont'd)

N1A	C2A	C3A	C15A	155.6(3)
N1A	C2A	C6A	N3A	-69.4(4)
N2A	C3A	C15A	N5A	-82.5(4)
N2A	C3A	C15A	C16A	104.2(5)
N3A	C7A	C8A	C9A	-177.7(4)
N3A	C7A	C8A	C13A	2.8(4)
N5A	C15A	C16A	N4A	-0.4(4)
N6A	C18A	C19A	C20A	-1.5(7)
C1A	O1A	C4A	C5A	178.0(3)
C1A	N1A	C2A	C3A	-27.5(4)
C1A	N1A	C2A	C6A	-148.9(3)
C1A	N2A	C3A	C2A	-19.6(4)
C1A	N2A	C3A	C15A	-144.3(3)
C2A	N1A	C1A	O1A	-163.6(3)
C2A	N1A	C1A	N2A	18.5(5)
C2A	C3A	C15A	N5A	156.6(3)
C2A	C3A	C15A	C16A	-16.8(6)
C3A	N2A	C1A	O1A	-176.5(3)
C3A	N2A	C1A	N1A	1.2(4)
C3A	C2A	C6A	N3A	176.8(3)
C3A	C15A	C16A	N4A	173.8(4)
C4A	O1A	C1A	N1A	178.8(3)

Table 2.12 (cont'd)

C4A	O1A	C1A	N2A	-3.4(5)
C6A	N3A	C7A	O2A	0.1(6)
C6A	N3A	C7A	C8A	179.6(3)
C6A	N3A	C14A	O3A	-3.5(6)
C6A	N3A	C14A	C13A	178.6(3)
C6A	C2A	C3A	N2A	151.8(3)
C6A	C2A	C3A	C15A	-81.8(4)
C7A	N3A	C6A	C2A	111.5(4)
C7A	N3A	C14A	O3A	177.6(3)
C7A	N3A	C14A	C13A	-0.2(4)
C7A	C8A	C9A	C10A	-178.9(4)
C7A	C8A	C13A	C12A	178.4(3)
C7A	C8A	C13A	C14A	-3.0(4)
C8A	C9A	C10A	C11A	0.2(6)
C8A	C13A	C14A	O3A	-175.7(4)
C8A	C13A	C14A	N3A	2.1(4)
C9A	C8A	C13A	C12A	-1.1(6)
C9A	C8A	C13A	C14A	177.5(3)
C9A	C10A	C11A	C12A	-0.3(6)
C10A	C11A	C12A	C13A	-0.2(6)
C11A	C12A	C13A	C8A	0.9(5)
C11A	C12A	C13A	C14A	-177.3(4)

Table 2.12 (cont'd)

C12A	C13A	C14A	O3A	2.7(7)
C12A	C13A	C14A	N3A	-179.6(4)
C13A	C8A	C9A	C10A	0.5(6)
C14A	N3A	C6A	C2A	-67.2(4)
C14A	N3A	C7A	O2A	179.0(4)
C14A	N3A	C7A	C8A	-1.5(4)
C15A	N5A	C17A	N4A	-0.6(4)
C15A	N5A	C17A	N6A	178.5(3)
C15A	N5A	C20A	C19A	179.7(4)
C16A	N4A	C17A	N5A	0.3(4)
C16A	N4A	C17A	N6A	-178.7(4)
C17A	N4A	C16A	C15A	0.1(4)
C17A	N5A	C15A	C3A	-174.5(3)
C17A	N5A	C15A	C16A	0.6(4)
C17A	N5A	C20A	C19A	2.6(6)
C17A	N6A	C18A	C19A	0.5(6)
C18A	N6A	C17A	N4A	-179.0(4)
C18A	N6A	C17A	N5A	2.1(5)
C18A	C19A	C20A	N5A	-0.1(6)
C20A	N5A	C15A	C3A	8.1(6)
C20A	N5A	C15A	C16A	-176.8(4)
C20A	N5A	C17A	N4A	177.1(3)

Table 2.12 (cont'd)

C20A	N5A	C17A	N6A	-3.7(5)

Table 2.13: Hydrogen Fractional Atomic Coordinates ($\times 10^4$) and Equivalent Isotropic Displacement Parameters ($Å^2 \times 10^3$) for **JJT822A_twin1_hklf5**. U_{eq} is defined as 1/3 of the trace of the orthogonalised U_{ij}

Atom	x	y	z	U_{eq}
H1	270(40)	3710(40)	1960(40)	54(16)
H2	93.8	5122.91	2570.71	30
H3	1911.61	5322.13	2684.07	29
H4A	1854.07	3716.59	-377.8	36
H4B	2007.04	4657.02	98.01	36
H5A	1315.51	4885.9	-1279.99	50
H5B	678.4	5153.34	-541.75	50
H5C	564.68	4224.28	-1044.94	50
H6A	1387.47	4245.9	3671.58	34
H6B	910.03	5122.72	3971.13	34
H9	-444.63	1524.95	4802.15	34
H10	-1769.77	1444.37	5438.46	38
H11	-2598.21	2701.16	5595.95	37
H12	-2151.03	4089.2	5081.03	35
H16	-10.53	6600.11	2914.4	35
H18	2866.89	9151.21	1969.57	35

Table 2.13 (cont'd)

H19	3521.09	7807.47	1601.5	38
H20	2796.64	6472.56	1809.94	33
H1A	5250(50)	10780(60)	3050(60)	110(30)
H2A	5111.25	9437.7	2541.83	30
H3A	6921.53	9205.01	2788.7	29
H4AA	6788.93	10041.32	5483.13	35
H4AB	5823.85	9711.75	5574.13	35
H5AA	6442.8	11435.05	6034.88	49
H5AB	6204.36	10687.91	6725.87	49
H5AC	5470.32	11133.33	6096.06	49
H6AA	6453.01	10174.34	1579.06	32
H6AB	5927	9308.47	1268.13	32
H9A	4793.83	12876.04	-30.28	35
H10A	3387.17	13071.76	-620.45	37
H11A	2365.47	11965.06	-510.84	38
H12A	2732.04	10602.16	195.49	34
H16A	4923.69	7936.97	2316.47	35
H18A	8039.7	5442.39	2832.59	43
H19A	8662.74	6736.18	3439.76	42
H20A	7855.58	8030.05	3456.91	36

Citations

CrysAlisPro (Rigaku, V1.171.42.64a, 2022)

CrysAlisPro (ROD), Rigaku Oxford Diffraction, Poland (?).

O.V. Dolomanov and L.J. Bourhis and R.J. Gildea and J.A.K. Howard and H. Puschmann,

Olex2: A complete structure solution, refinement and analysis program, *J. Appl. Cryst.*, (2009),

42, 339-341.

Sheldrick, G.M., Crystal structure refinement with ShelXL, *Acta Cryst.*, (2015), **C71**, 3-8.

The Rigaku Synergy S Diffractometer was purchased with Support from the MRI program by the National Science Foundation under Grant No. 1919565

Chapter 3: Advances in proteasome enhancement by small molecules

3.1 Introduction

The degradation of proteins is a continual process that is highly regulated by the two major proteolysis systems, the lysosomal degradation pathway, and the proteasome-mediated pathway. Protein degradation helps maintain biological homeostasis in cells which are needed for all cell functions and for maintaining optimal conditions for enzyme function[1]. The proteasome pathway is the major pathway for the degradation of misfolded, oxidatively damaged, and redundant proteins. Dysregulation of proteasome function has been identified in the pathogenesis of several neurodegenerative diseases including Parkinson's disease (PD)[2], Alzheimer's disease (AD), and other neurodegenerative diseases[3]. The proteasome pathway is also involved in the regulation of several other cellular processes such as cell cycle, stress signaling, gene expression regulation, inflammatory response, cell differentiation, and apoptosis, which makes it an appealing target in the treatment of other types of diseases, including cancer[4]. Due to the critical role of the proteasome-mediated degradation pathway in cell regulation, the modulation of proteasome proteolytic activity has become a valuable strategy in the pursuit of new therapeutics to treat several neurodegenerative diseases[5-8].

3.1.1 The Human Proteasome

The human proteasome is a large complex protein responsible for the intracellular degradation of unwanted and damaged proteins via a ubiquitin-dependent and ubiquitin-independent degradation pathway. The most common proteolytic clearance of proteins proceeds by tagging the protein with polyubiquitin, after which it is degraded into small peptides of seven to eight amino acids by the 26S proteasome[9]. Highly disordered proteins can also be degraded in a ubiquitin-independent manner by the 20S proteasome[10]. In this chapter, I will cover the use of

small molecules to enhance the proteolytic activity of both the 26S proteasome and the 20S proteasome.

3.1.2 Ubiquitin-Proteasome System

3.1.2.1 Ubiquitin

Ubiquitin (Ub) is a small protein (approximately 8600 Da) with 76 amino acid residues responsible for tagging a wide range of cellular proteins for proteolytic degradation. In the ubiquitin-proteasome system (UPS) (**Figure 3.1**), proteins are tagged for proteolysis by covalent ligation to ubiquitin[11]. Ubiquitination of proteins requires three enzymes in chronological order (**Figure 3.1a**). The E1 ubiquitin-activating enzyme, just like its name, activates the C-terminal glycine residue of the ubiquitin in an ATP-dependent manner. The binding of the ubiquitin to a cysteine residue of E1 forms a Ub-E1 complex via a thioester linkage. The E2 ubiquitin-conjugating enzymes transfer the ubiquitin from the Ub-E1 complex to itself via a trans-thioesterification to form the Ub-E2 complex and release the E1 enzyme from the system. Lastly, the ubiquitin ligases E3s are responsible for selecting proteins for ubiquitin-mediated proteolysis. Humans have two E1 enzymes, about 40 E2 enzymes, and are estimated to have about 500–1000 E3s[12].

Figure 3.1: Ubiquitin-proteasome system[13]. (a) Protein polyubiquitination process using the ubiquitin-activating enzyme E1, conjugating enzymes E2 and the E3 ligase; (b) Polyubiquitinated proteins are degraded by 26S proteasome into small peptides following its deubiquitination

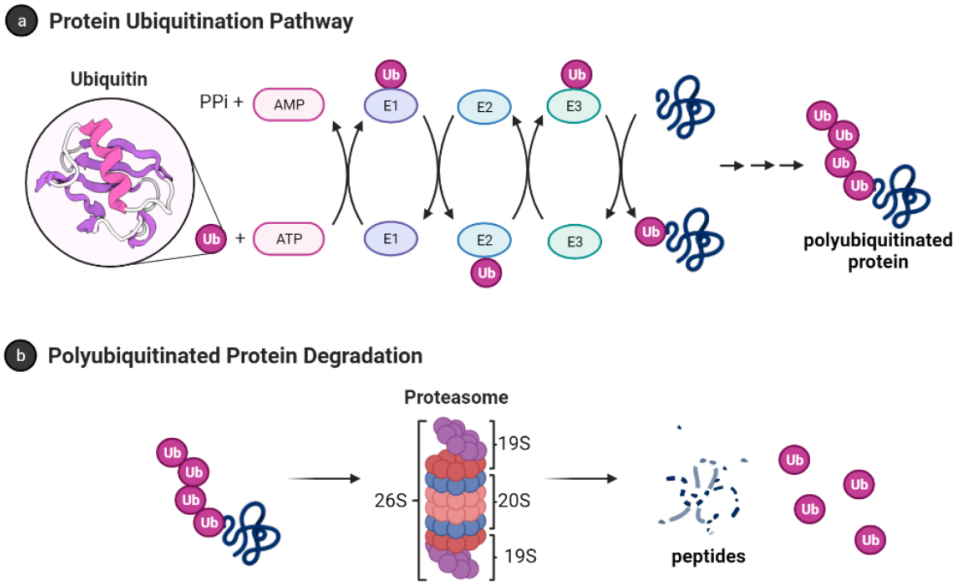

After monoubiquitination of the targeted protein, the C-terminus of each ubiquitin molecule can be linked to any of the other seven lysine residues (K6, K11, K27, K29, K33, K48, and K63) on the previous ubiquitin to extend the ubiquitin chain and form the polyubiquitinated tagged protein[14-15]. However, the signal for protein degradation by the proteasome usually involves the linking of Ub to the K48 of the previous Ub on the protein[16-17]. In addition, K11, K29, and K63 linked chains have also been shown to play a role in proteasomal degradation[17-18]. The 26S proteasome degrades polyubiquitinated proteins (**Figure 3.1b**), and a previous study shows that proteins marked for degradation must be tagged with at least four ubiquitin molecules to be recognized by the 26S proteasome[16,19]. However, shorter chains, monoubiquitinated and multiple monoubiquitinated proteins can also be targeted for degradation by the proteasome[20-23]. It is also important to note that the ubiquitination process is reversible, and the deubiquitinating enzymes (see Section 3.3.1.1) are present in the cell to remove ubiquitin-tagged proteins[24].

3.1.2.2 The 26S Proteasome

The 26S proteasome has a molecular weight of approximately 2.5MDa and it is made up of the 20S core particle (CP), and one or two 19S regulatory particle(s) (RP) attached to one or both end(s) of the CP[25]. The 19S RP (also known as PA700) binds to the 20S CP and facilitates the gate opening of the CP for proteolytic degradation of polyubiquitinated proteins[26]. The 19S RP is also responsible for recognizing, unfolding, and translocating polyubiquitinated protein into the 20S CP[27]. Cryo-EM studies have shown many conformation states of the 26S proteasome when engaged with substrate[28-35]. Some of these studies showed the processes by which substrate is engaged, deubiquitylated, unfolded, and translocated by the proteasome[28-29]. The proteasome is also referred to as the 30S proteasome when the 20S CP is capped at both ends with the 19S RP[36]. However, in this chapter, I will refer to the 26S proteasome without distinguishing between the singly or doubly capped CP.

3.1.3 The 20S Proteasome or Core Particle

The 20S proteasome is a 700 kDa protein with a cylindrical-like structure. The CP contains four heptameric rings stacked on each other in an $\alpha_{1-7}\beta_{1-7}\beta_{1-7}\alpha_{1-7}$ fashion. The outer α-rings form a gate, and they recognize regulatory particles that allow the opening and closing of the gate[37]. The inner β-rings contains six proteolytic sites, three on each β-ring (β1, β2, and β5), and are responsible for the proteolytic activity of the proteasome.

The three different proteolytic sites of the 20S CP exhibit different substrate preferences even though they all use N-terminal nucleophilic threonine to carry out their proteolytic activities. The β1 exhibits a caspase-like (C-L)/PGPH (peptidylglutamyl-peptide hydrolyzing) activity and preferentially cleaves after acidic residues. The β2 and β5 exhibit trypsin-like (T-L) and chymotrypsin-like (CT-L) activities, and they preferentially cleave after basic and hydrophobic

residues, respectively[38]. The 20S proteasome on its own degrades unstructured proteins using a ubiquitin-independent pathway.

3.1.4 Small Molecule Regulation of Proteasome Function

Due to the role of the proteasome in cellular functions, the regulation of proteasome has become a valuable target for the development of therapeutic molecules[39]. Proteasome inhibition is a therapeutic approach for the treatment of cancer. For example, bortezomib, a dipeptide boronate, was approved by the FDA in 2003 as an anticancer drug to treat mantle cell lymphoma and multiple myeloma[40-41]. Bortezomib inhibits the 26S proteasome by forming a covalent bond between its boron atom and threonine oxygen in the CT-L catalytic site of the 20S CP[40]. Molecules that inhibit the proteasome have also been shown to induce apoptosis in cell cultures and murine models of cancer. One of the proposed mechanisms is that proteasome inhibition prevents the degradation of the IκB, an NF-κB inhibitor, which prevents NF-κB nuclear translocation and consequently NF-κB mediated gene expression[42]. Proteasome inhibition results in the accumulation of IκB[43-48], cyclin-dependent kinase (CDK) inhibitor p21 [43,49-50], tumor suppressor p53, and other pro-apoptotic proteins[51-53]. The exceptional increase in apoptosis of certain multiple myeloma cells when treated with proteasome inhibitors has also been linked to an increase in protein unfolding and increasing substrate load on the proteasomes[54-55]. In addition, proteasome inhibition leads to lethal shortage of amino acids in the cells, which are the building blocks for cells to make new proteins. This amino acid scarcity caused by proteasome inhibition results in increasing ER stress and cell apoptosis[56]. Many reviews on proteasome inhibition have recently been published[57-66], including a recent review by our group on natural products scaffolds as inhibitors of the proteasome[67].

Proteasome activation by small molecules is a proposed strategy for the treatment of age-related diseases and several neurodegenerative diseases such as Parkinson's disease (PD), Alzheimer's Disease (AD), Huntington's Disease (HD), and Amyotrophic Lateral Sclerosis[8,68-72]. Increasing the proteolytic activity of proteasome enhances the degradation of specific intrinsically disordered proteins (IDPs) such as α-synuclein, β-amyloid, and tau, to mention a few, which are associated with the pathogenesis of these neurodegenerative diseases. This review will focus on the use of small molecule enhancers of proteasome-mediated proteolysis as a potential strategy for the treatment of various neurodegenerative diseases.

3.2 Proteasome Activity and Diseases

As humans age, there is a decline in proteasome function[3,73]. This reduction could be due to the reduction in the expression of proteasome subunits[74], oxidative damage of the protein[75-76], and disassembly of the 26S proteasome holocomplex[77-78]. The decrease in proteasome proteolytic function leads to lower rates of unwanted protein degradation which can induce toxic signaling upon accumulation and aggregation (**Figure 3.2**). In particular, the accumulation of specific intrinsically disordered proteins (IDPs), such as amyloid-β and α-synuclein, have been identified as a driving cause of many neurodegenerative diseases[79-98]. The exact mechanism by which these oligomers induce neurotoxicity is complex and still debated, but it is widely accepted that dysregulated IDPs accumulate, and the resulting soluble oligomeric forms of these protein aggregates are likely toxic species in disease pathogenesis[79,93,99-102]. These soluble oligomeric forms are also responsible for impairing proteasome function, which further drives disease progression [94,103-120]. Multiple studies have indicated that enhancing proteasome proteolytic activity prevents the accumulation of these IDPs, reduces brain damage and improves cognitive performance in mouse models , and may be a new therapeutic strategy to treat neurodegenerative

diseases[8,68-70,72,119,121-132]. More recently, it has been recognized that the 20S proteasome of the proteasome plays a critical role in maintaining proteostasis by the direct degradation of oxidatively damaged and highly disordered proteins[10,133-138]. The 20S proteasome, therefore, serves as the default protease to unremittently maintain low levels of these unwanted IDPs without the need for post-translation modifications, including protein ubiquitination[10,133]. Highly disordered proteins appear to be the main target of the 20S proteasome[139]. IDPs are also naturally short-lived, but basal levels are secured by forming proteolytically stable structured complexes with "nannies", chaperones, or other protein complexes[140]. However, when these IDPs production outpaces their degradation, they accumulate, oligomerize, and aggregate, resulting in the induction of downstream cytotoxic signaling events.

Figure 3.2: Accumulation of partially unfolded, misfolded, and dysregulated intrinsically disordered proteins (IDPs) such as amyloid-β and α-synuclein leads to neurotoxicity and neuronal cell death. The 20S proteasome degrades unwanted IDPs; however, small molecules can enhance the rate of proteasome-mediated degradation of these IDPs and prevent their accumulation

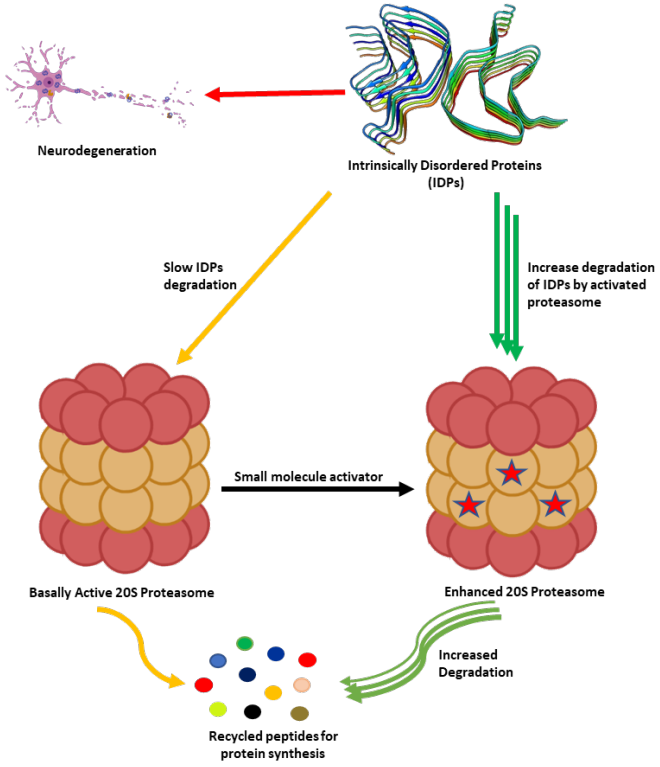

3.2.1 Aging

During aging, proteins are more susceptible to several types of modification, such as oxidation, glycoxidation, glycation, conjugation with peroxidation products, etc. These protein modifications can lead to decreased enzyme activity and thermodynamic stability[141-142], resulting in the accumulation of damaged proteins in the cell. Several models used to study proteasome proteolytic activity showed a decline in proteasomal activity as we age [143-144] and decreased degradation of oxidized proteins in cell cultures[145-146]. Reactive oxygen species accumulate during aging, resulting in an increase of oxidatively damaged proteins and an increased demand on the proteasome degradation system to eliminate these pathogenic aggregation-prone proteins[113].

Unfortunately, proteasome proteolytic activity declines as we age [3,73,75], resulting in the accumulation of oxidatively damaged proteins[147].

These unwanted protein aggregates interact with the proteasome and further reduce its proteolytic capacity[104-107,111,113]. This inhibition of proteasome leads to a compounding accumulation of more unwanted proteins and a vicious cycle of progressively worsening aggregation of oxidatively damaged proteins [94,104-107,116-119,148-150].

3.2.2 Neurodegenerative Diseases

3.2.2.1 Parkinson's Disease (PD)

Approximately 10 million people worldwide are affected by PD, making it the second most prevalent neurodegenerative disorder[151]. PD is characterized pathologically by the loss of dopaminergic neurons as a result of the accumulation of Lewy bodies in the substantia nigra pars compacta (SNc)[152]. Lewy bodies are the defining pathological hallmark of PD, and its major components are α-synuclein, ubiquitin, parkin, proteasomal components, and other UPS-related proteins. PD has been linked to various UPS proteins such as parkin and UCH-L1. Additionally, the expression of mutant α-synuclein in rat cells inhibits proteasome proteolytic activity, causing essential features common to PD such as inclusion body formation, accumulation of undegraded ubiquitinated protein, and cell death. Dysregulation of proteasome-mediated protein degradation has been associated with both familial and sporadic PD[153].

Different approaches have been used to determine the role of the proteasome in the pathology of PD. Rat models have been developed to display characteristics such as bradykinesia, tremor, and abnormal posture, which are similar to PD when treated with proteasome regulators[154]. In addition, α-synuclein and ubiquitin-containing inclusion resembling Lewy bodies were also present at the neurodegenerative sites of the rat neurons. However, other studies could not

reproduce similar output[155], which became controversial and indicated that proteasome inhibition is not a reliable model to study PD. As an alternative approach to study the development of PD, mouse models of proteasome subunits knock-out were generated. However, the removal of most proteasome genes causes embryonic lethality except for a few immune-related subunits[109,156]. The deletion of the proteasomal ATPase subunit Psmc1/Rpt2 in the dopaminergic neurons leads to intraneuronal α-synuclein and ubiquitin-positive inclusion, which resulted in neurodegeneration and thus resembling the human PD. This study provided direct support for the involvement of neuronal proteasome and Lewy-like inclusion seen in PD[157].

3.2.2.2 Alzheimer's Disease (AD)

AD is the most common cause of dementia, and it is ranked as the sixth leading cause of death in the United State as of 2019[158]. AD is associated with loss of cognitive functioning such as memory, thinking, and reasoning. It also impacts behavioral activities such as the ability to carry out daily life activities[159].

The pathogenesis of AD has been attributed to protein misfolding and aggregation[80-82,84,89]. It is characterized by the aggregation of extracellular β-amyloid plaques and intracellular accumulation of neurofibrillary tangles[160]. The neurofibrillary tangles (NFTs) are mostly composed of hyperphosphorylated microtubule-associated tau. Filamentous tau formation is triggered due to changes in the concentration of β-amyloid[160]. Although β-amyloid appears to be more specific to AD, tau is also associated with other neurodegenerative diseases such as corticobasal degeneration, chronic traumatic encephalopathy, argyrophilic grain disease, and progressive supranuclear palsy[161].

Different experimental and clinical data have shown that the main drivers of synaptic dysfunction, cognitive decline, and neuronal loss in AD patients are associated with soluble toxic

β-amyloid oligomers which impair proteasome proteolytic activity, rather than insoluble β-amyloid plaques[111,162-165].

The ubiquitin-dependent proteasome system is associated with AD and degradation of β-amyloid[120,166-168]. Studies showed that the activity of the proteasome decreases in some parts of the brain in AD patients[169]. Similarly, inhibition of the 26S proteasome by lactacystin resulted in the accumulation of β-amyloid in both astrocytes and neurons, suggesting that β-amyloid could be a substrate for proteasomal degradation[166]. These results indicate that enhancing proteasome proteolytic activity may alleviate some of the factors that drive the pathogenesis of AD.

3.2.2.3 Huntington's Disease (HD)

HD is a brain disorder caused by the mutations of the huntingtin (Htt) gene. HD affects mood, movement and also leads to progressive cognitive deterioration and psychosis as a result of changes in the central part of the brain. The disease is dominant, which implies that it is inheritable by children from their parents.

In HD the disorder of polyglutamine in the Htt protein results in toxic functions of mutant Htt, which consequently leads to neurodegeneration. The HD mutation is an unstable expansion of trinucleotide CAG repeats within the Htt gene, which causes polyglutamine stretch in the N-terminal of the protein and results in the formation of fibril and aggregates[170-171]. Remarkably, the mutant Htt still retains some of the functions of a normal Htt. The number of CAG repeats correlates to the progression of HD and the symptoms. Individuals with 36–40 CAG repeats may or may not develop HD symptoms. However, those with CAG repeats above 40 will eventually develop HD[172-173]. Greater than 50 long CAG repeats cause early onset of the disease (juvenile HD)[174]. Several studies suggest that mutant Htt aggregates impair the ubiquitin-proteasome system [104,116,175]. However, the actual mechanism of interaction between the mutant Htt aggregate and the

proteasome remains unclear. Interestingly, unlike the soluble Htt, the Htt aggregates have been found to be ubiquitinated, and those insoluble aggregates have also been shown not to impair the activity of the 26S proteasome[176-177]. The inclusions associated with HD have been proposed to be toxic and lead to neuronal death. But the exact mechanism of toxicity remains unsolved. Increasing proteasome-mediated substrate degradation has been shown to increase survival in HD patients' mutant huntingtin-expressing striatal and skin fibroblasts neurons. Over expression of PA28γ, a proteasome activator subunit also improved cell viability[178].

3.2.2.4 Amyotrophic Lateral Sclerosis (ALS)

ALS is another progressive neurodegenerative disease that affects the motoneurons in the brain and spinal cord. ALS is characterized by spasticity, muscle weakness, atrophy, and paralysis. The disease is often lethal within three to five years after diagnosis[179-181]. Like other neurodegenerative diseases, most ALS cases are sporadic (sALS), while about 10% could be familial (fALS) and result as a mutation in multiple genes[179]. Also, both sALS and fALS are clinically indistinguishable. Efforts at determining the mechanism underlying different fALS forms are thought to give insight into target identification and therapeutics development for both forms of diseases.

The first ALS-linked genetic mutation was found in 1993, and it was located in the gene coding of Cu-Zn superoxide dismutase 1 (SOD1)[182]. Since then, several ALS mutant genes have been identified[179,183-185]. The recently discovered C9orf72 gene mutation has been identified as the most common cause of fALS and frontotemporal dementia[186-187]. An expansion of a GGGGCC repeat in the C9orf72 gene translates into five dipeptide-repeats proteins: poly-GA, poly-GP, poly-GR, poly-PR, and poly-PA[188-192]. A study showed that poly-GA aggregates recruit numerous 26S

proteasome complexes which may affect neuronal proteasome-mediated proteostasis and the protein degradation process[193].

Both the sALS and fALS are often considered proteinopathies since they both tend to aggregate and accumulate misfolded and abnormal proteins generated in the damaged neurons[194-195]. The presence of ubiquitinated rich protein inclusions in motor neurons is a feature considered a common hallmark of not only human ALS but also in cellular and animal models of the disease[196-197]. The abundant accumulation of these ubiquitinated proteins suggests a significant contribution of the ubiquitin-proteasome system in these neuropathological features. In addition, the use of different cellular and animal models of ALS has provided substantial evidence of the involvement of the ubiquitin-proteasome system in the formation of inclusion and neuronal death[198].

3.3 Small Molecule Enhancers of 26S Proteasome Activity

The role of the proteasome in the regulation of cellular functions has made it an important target for the development of new treatments for cancer and neurodegenerative diseases. In addition, understanding proteasome regulation has allowed scientists to probe the mechanism of different cellular processes that involve the proteasome.

Small molecules that directly activate the 26S proteasome are rare and most of the well-studied approaches to enhance the 26S proteasome involve indirect activation by modulation of post-translational modification and by genetic manipulation. A recent review highlights some of the cellular mechanisms that activate 26S proteasomes[199]. In this review, we will focus on small molecules that activate the 26S proteasome.

3.3.1 Indirect Activation of 26S Proteasome

3.3.1.1 Inhibition of Deubiquitinase

Deubiquitinating enzymes (DUBs) play a critical role in the ubiquitin-proteasome system (UPS). The 19S RP of the proteasome uses deubiquitinase activity to remove and recycle polyubiquitin from protein substrates that are condemned for proteolysis[200]. There are three essential DUBs: RPN11, UCH37, and USP14 that are associated with the 19S RP of human proteasome [124,201-202]. The main function of these DUBs is to remove monoubiquitin and polyubiquitin chains from substrates tagged for proteasomal degradation[203-206]. USP14, a DUB of the cysteine protease class, interacts reversibly with the proteasome[124,207-209] and it cleaves the ubiquitin chain off the targeted protein before degradation by the proteasome[210-211], thereby inhibiting the degradation of ubiquitin-protein conjugates in vitro and in vivo[124]. Unlike USP14, the RPN11, a DUB of the metalloprotease class, is part of the 19S RP and cleaves the ubiquitin chain after degradation has been initiated by the proteasome[201]. The mechanism of action of UCH37 is not completely understood yet but this DUB could edit the ubiquitin chains and either prevent the protein from being degraded or enhance its degradation depending on the proteasome needs [201,212-213].

A study conducted in 2010 showed that USP14 inhibits protein degradation by the proteasome in murine embryonic fibroblasts. In the same study, the authors showed that inhibition of USP14 by 1-[1-(4-fluorophenyl)-2,5-dimethylpyrrol-3-yl]-2-pyrrolidin-1-ylethanone (IU1, **Figure 3.3**, compound **3-1**) drastically stimulate the degradation of oxidized proteins by the proteasome[124]. IU1 was identified as a USP14 inhibitor from high-throughput screening (HTS) of over sixty-three thousand compounds for their ability to inhibit USP14. From the HTS, 215 compounds were identified as true inhibitors of USP14, however, screening of the hit compounds

against several DUBs only provided three compounds as selective inhibitors of USP14. IU1 was found to be the most active of the three with IC_{50} of 4–5 μM[124]. Further optimization of IU1 has led to the discovery of more potent analogues such as IU1-47 (IC_{50} of 0.6 μM) (**Figure 3.3**, compound **3-2**)[214], IU1-248 (IC_{50} of 0.83 μM) (**Figure 3.3**, compound **3-3**)[215], and 1B10 and 1D18 (**Figure 3.3**, compound **3-4** & **3-5** respectively) which have better membrane permeability[216]. A recent review by Moon et al.[211], is focused on small molecules that inhibit proteasome-associated deubiquitinase and can be consulted for more information on DUB inhibitors.

Figure 3.3: Small molecules inhibitors of deubiquitinase enzymes (DUBs)

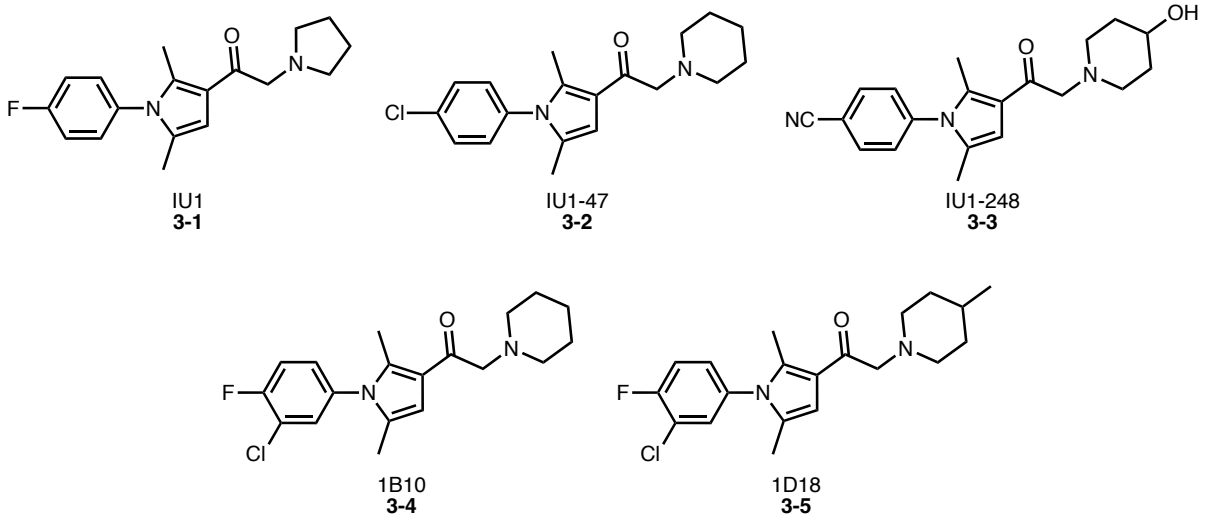

In a recent study by Kim et al.[217], proteasome-mediated proteolysis was increased by knocking down USP14 with small interfering RNA (siRNA) which led to a significant impairment of autophagic flux. This proteasome activation led to an increase in the microtubule-associated protein tau (MAPT) degradation and a decrease in the concentration of its oligomeric forms. This result is also consistent with Boselli et al.'s observation that USP14 inhibition enhances tau degradation in cultured neurons[214].

3.3.1.2 Modulation of cAMP-Dependent Protein Kinase A (PKA) and cGMP-Dependent Protein Kinase G

Phosphorylation of proteasome subunits was recently established as a promising way to proteasome regulation[218]. The phosphorylation of Ser-14 of Rpn6, a subunit of 19S regulatory particle, by cAMP-dependent PKA has been shown to enhance the hydrolysis of polyubiquitinated proteins and small peptides in cells and in vivo studies[219-222]. In addition, impeding the phosphorylation of Thr-25 of Rpt3 by dual-specificity tyrosine-regulated kinase 2 (DYRK2)[223-224] and Ser-120 of Rpt6 by calcium/calmodulin-dependent protein kinase II (CaMKII)[225-226] or PKA[119] have been shown to impair proteasome proteolytic capacity and impedes cell proliferation. Small molecules that raise cAMP have therapeutical promise because they enhance the capacity of cell cultures[221] and mouse brains[119,227] to degrade misfolded proteins such as tau, which has been implicated in the pathogenesis of Alzheimer's disease.

Small molecule inhibitors of phosphodiesterase have been found to increase proteasome function by cAMP/PKA-mediated phosphorylation. Rolipram (**Figure 3.4**, compound **3-6**) is an example of phosphodiesterase type-4 inhibitor (PDE4) that was developed as an antidepressant drug in the early 1990s[228]. A study shows that Rolipram decreases the level of insoluble tau and improves cognitive performance in mice by increasing proteasome function through activating cAMP-PKA signaling[119]. Cilostazol (**Figure 3.4**, compound **3-7**) is another phosphodiesterase type-3 inhibitor (PDE3). Administration of Cilostazol in rTg4510 mice also showed improved cognitive performance and increased proteasome function through the cAMP/PKA pathway[227]. This small molecule was approved by the FDA to treat intermittent claudication and can also be used for secondary stroke prevention[229]. In late 2020, the FDA completed the clinical trial to determine the therapeutical use of cilostazol for patients with mild cognitive impairment[230].

Figure 3.4: Rolipram (3-6) and Cilostazol (3-7) are examples of phosphodiesterase type-4 (PDE4) inhibitors. Molecules that inhibit PDE4 raise cAMP/PKA-mediated phosphorylation which increases the rate of degradation of IDPs and misfolded proteins in cellular assays and animal models. Sildenafil (3-8), Tadalafil (3-9), BAY41-2272 (3-10), and Cinaciguat (3-11) are molecules that raise cGMP level and induce cGMP-mediated proteasome activation

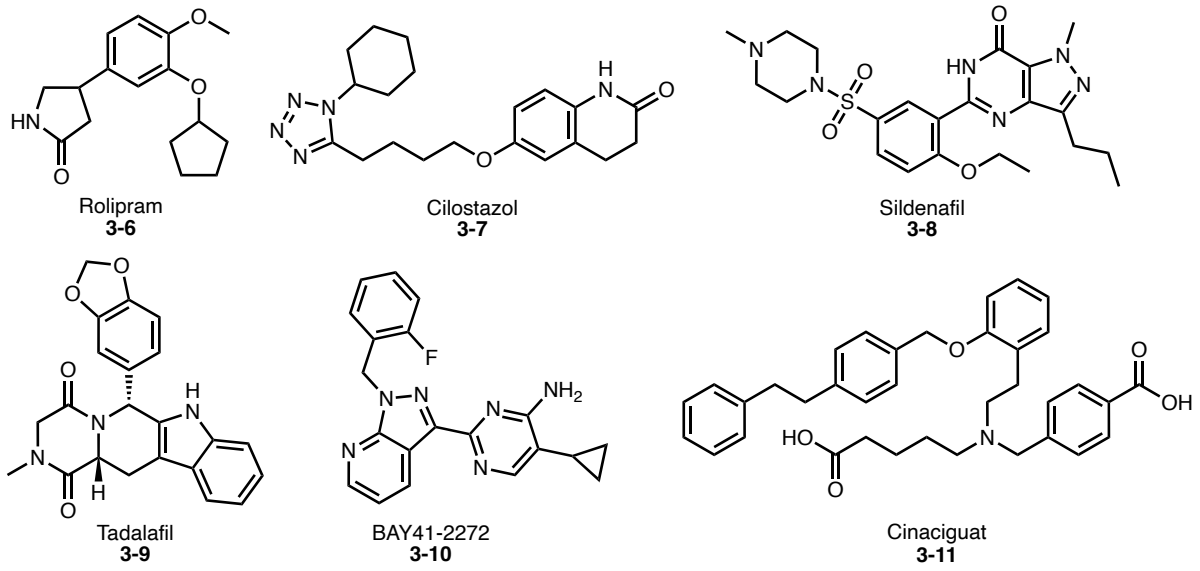

Like cAMP-mediated modulation of 26S proteasome, small molecules that raise cGMP and activate PKG were recently shown to enhance proteasome proteolytic activity without affecting lysosomal degradation and increase the rate of degradation of both short-lived and long-lived proteins, including tau and mutant Htt.[199,231]. In the study conducted by VerPlank et al.[231], treatment of human neuroblast cells (SH-SY5Y) with molecules that raises cGMP such as sildenafil (**Figure 3.4**, compound **3-8**) or tadalafil (**Figure 3.4**, compound **3-9**) which are phosphodiesterase type-5 inhibitors (PDE5), or BAY41-2272 (**Figure 3.4**, compound **3-10**) and cinaciguat, (**Figure 3.4**, compound **3-11**) which are stimulators of soluble guanylyl cyclases, led to a rapid increase in proteasomal activity in cell lysates. However, unlike phosphorylation of Rpn6 by PKA[221-222], Rpt3 by DYRK2[223-224], or Rpt6 by CaMKII)[225-226] or PKA[119], phosphorylation of Rpn6, Rpt3, or Rpt6 subunit was not observed in the PKG pathway[231]. Overexpression of PKG in SH-SY5Y and HEK293 cells led to an increase in the level of phosphorylated proteins compared

to cells that were transfected with empty vectors during proteasome preparations. Thus, the 26S proteasome subunit or an associated protein that is phosphorylated in the cGMP-mediated proteasome activation is still unknown and the mechanism of action remains unclear.

3.3.1.3 Inhibition of p38 Mitogen-Activated Protein Kinase (MAPK)

MAPKs are enzymes that phosphorylate the hydroxyl group of threonine and serine residues in proteins. These kinases play an important role in the control of cell proliferation and apoptosis. The p38 MAPK is involved in a signaling pathway that regulates various biological functions including biosynthesis of cytokinesis such as interleukin-1β (IL-1β) and tumor necrosis factor-α (TNF-α)[232-233]. The activation of the p38 MAPK pathway as a defense to osmotic stress has been shown to lead to phosphorylation of 19S RP at Thr-273 of the Rpn2 subunit, which resulted in the inhibition of the 26S proteasome proteolytic activity[234].

In ALS and AD, the over-activation of the p38 MAPK pathway has been reported in animal models and postmortem brains of AD patients[196,235-237]. The activation of the p38 MAPK pathway in cell lines and animal models has led to tau phosphorylation, neuroinflammation, neurotoxicity, and synaptic dysfunction, which are events associated with Alzheimer's disease. Therefore, the search for p38 MAPK inhibitors became a novel approach for targeting neurodegenerative diseases[238].

In 2017, Leestemaker et al.[122] discovered imidazole inhibitors of p38 MAPK as enhancers of 26S proteasome proteolytic activity. The compounds were identified from high-throughput screening of over 2750 compounds using a proteasome activity-based probe (Me_4BodipyFLAhx$_3$L$_3$VS) that covalently binds to proteasome catalytic sites in an activity-dependent manner in living cells. The group found that PD169316 (**Figure 3.5**, compound **3-12**), a known inhibitor of p38 MAPK and its structural analogues, SB202190 (**Figure 3.5**, compound

3-13), and SB203580 (**Figure 3.5**, compound **3-14**), increases the proteolytic activity of the proteasome in a dose-dependent manner in MelJuSo cells. Further characterization of these compounds showed that they increase proteasome proteolytic activity by inhibiting the p38 MAPK pathway without affecting cell viability, subunits abundance, and the overall level of ubiquitinated proteins[122]. Similarly, Huang et al.[239], demonstrated that treatment of HAP 40 depleted cells with p38 MAPK inhibitor, PD169316, increases the CT-L activity of the proteasome and enhances degradation of both soluble and aggregated forms of mutant Htt in a Huntington's disease model. These data suggest that the regulation of the p38 MAPK pathway could be a potential way of modulating proteasome-mediated proteolytic activity.

Figure 3.5: Imidazole inhibitors of p38 MAPK that enhances proteasome activities

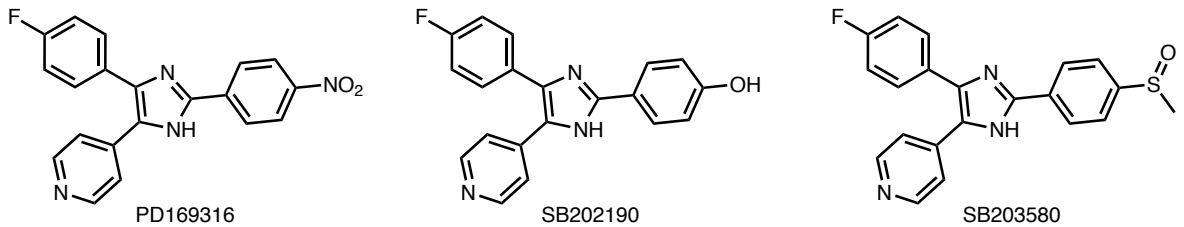

3.3.1.4 Proteasome Activation by Genetic Manipulation

Another approach to enhancing proteasome proteolytic activity is by proteasome subunit overexpression. Overexpression of β5i subunit in HeLa cells and lymphoblasts has led to an increase in the CT-L and T-L activities of the proteasome[240-241]. Previous studies also showed that stable overexpression of the β5 subunit in human fibroblast cell lines increased the level of other β subunits, increasing the overall proteolytic activity of the three catalytic sites[242]. Furthermore, overexpression of the 19S RP subunit PSMD11/Rpn6 increases proteasome assembly and proteolytic activity in human embryonic stem cells[243].

Small molecule activation of the transcription factor NRF2, nuclear factor erythroid 2-related factor 2, enhances the expression of the 20S and 19S proteasome particles and increases

the proteolytic activity of the proteasome in cells containing NRF2. 18α-glycyrrhetinic acid (18α-GA) has been shown to increase proteasome proteolytic activities from 1.5- to 1.8-fold, with the activity of the caspase-like site being the most affected in wide-type HFL-1 human fibroblasts. In addition, the increase in the proteasome proteolytic activity was not observed when NRF2 was knockdown using siRNA in HFL-1 cells and the cells were treated with 18α-GA, further confirming the upregulation of proteasome proteolytic activity through NRF2 activation[244]. The activation of NRF2 increases the level of 20S proteasome subunits: α4, β1, β2, and β5 in both human fibroblasts[244] and mice liver[245], and the 19S subunits: Rpt2, Rpt5, and Rpn11 in mice liver[245]. The expression of antioxidant enzymes such as UDP-glucuronosyltransferase (UGT)[246], glutathione S-transferase (GST)[247], and NAD(P)H quinone oxidoreductase 1[248], to name a few, are also controlled by this transcription factor. Activation of NRF2 by *tert*-Butylhydroquinone (t-BHQ) and sulforaphane increases proteasome proteolytic activity in human embryonic stem cells (hESCs)[249] and also protects against oxidative stress[250].

3.4 Small Molecule Enhancers of 20S Proteasome Activity

3.4.1 Sodium Dodecyl Sulfate (SDS)

SDS (sodium dodecyl sulfate), also known as SLS (sodium lauryl sulfate), is a synthetic organosulfate salt used in cleaning, pharmaceutical, and food products. In 1988, Tanaka et al.[251] showed that 20S proteasome proteolytic activity could be enhanced at a low concentration of SDS (0.04–0.08%) in biochemical assays. However, at higher SDS concentrations, the activity of the proteasome is lost, and the SDS inhibits the proteasome[252]. SDS is an invaluable in vitro tool that is used by most researchers to activate the proteasome as means to test compounds for subsequent proteasome inhibition. It is believed that SDS induces gate opening of the proteasome by partial denaturation of the 20S to facilitate substrate entrance into the catalytic core. However, the actual

mechanism of SDS proteasome activation is still unclear and considering that SDS is a detergent, it should not really be considered as a small molecule activator of the 20S proteasome.

3.4.2 Natural Product-Based Activators

Several natural products have been identified as 20S proteasome activators, some of which include betulinic acid (**Figure 3.6**, compound **3-15**)[253], ursolic acid (**Figure 3.6**, compound **3-16**)[127], and oleuropein (**Figure 3.6**, compound **3-17**)[254]. Betulinic acid is a triterpene isolated from the bark of *Betula pubescens* (commonly known as white birch). It was reported as a selective inhibitor of human melanoma and it has been demonstrated to induce programmed cell death in human neuroblastoma and neuroectodermal tumor cells[255]. Betulinic acid is one of the first reported enhancers of the 20S proteasome. A small peptide assay using Suc-Leu-Leu-Val-Tyr-AMC (used to determine the CT-L activity of the proteasome) showed that's betulinic acid enhances the CT-L activity of the proteasome with EC_{50} of approximately 2.5 μg/mL. Unfortunately, several chemical modifications to enhance the activity of betulinic acid resulted in compounds that inhibit the proteasome[253]. Like betulinic acid, ursolic acid is another triterpenoid that enhances the activity of the 20S proteasome. Ursolic acid is similar in structurally to betulinic acid, and they both enhance the CT-L activity of the 20S proteasome[127,253]. Although both betulinic acid and ursolic acid showed good activity in small peptide assay, unfortunately, betulinic acid did not show any activity for the turnover of misfolded proteins in vitro and in vivo [72].

Figure 3.6: Natural product-based activators of 20S proteasome

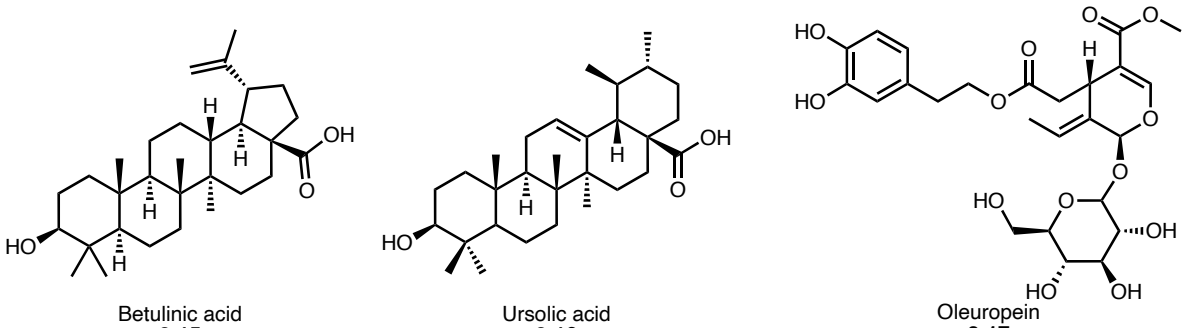

In addition, other natural compounds have been identified as 20S proteasome agonists. Some of these compounds include lipids[256] and fatty acids[257]. In 1993, Ruiz de Mena et al.[256] studied the effect of phospholipids on the T-L, CT-L, and C-L activities of the proteasome in rat liver. In the study, the team identified cardiolipin (diphosphatidylglycerol) as a strong CT-L enhancer (up to 60-fold enhancement) and C-L enhancer (up to 30-fold enhancement). SDS and cardiolipin activation was shown to be additive and at either optimal or suboptimal concentrations of both compounds. Furthermore, fatty acids such as oleic, linoleic, and linolenic acids isolated from spinach leaves were found to increase proteasome-mediated substrate degradation by enhancing CT-L and C-L activities at about one-third to one-sixth the required concentration of SDS. Unlike SDS, at extremely low concentration (0.0007–0.0025%, ~25–90 μM), the T-L catalytic site is inhibited and the degradation of Boc-L-R-R-AMC is prevented[257].

3.4.3 AM-404 and MK-886

Although many compounds show increased peptide cleavage activities using the standard aminomethyl coumarin tagged small peptide substrates, most have failed to demonstrate an increase in proteolytic activity under physiological conditions. One likely explanation is that the small peptide probes, used for detection of in vitro proteasome proteolytic activity, may be small enough to inadvertently enter the CP-proteolytic cavity following minor conformational changes

to the gate. Trader and Kodadek developed a follow-up assay that uses larger peptides with a single cleavage site and uses LC-MS to monitor proteasome proteolytic activity over time. They also validated molecules from LC-MS assay for their ability to turnover of α-synuclein in cells by monitoring the appearance of free GFP which correlates to the number of α-synuclein that was degraded. Using these assays, the lab was able to identify small molecules capable of increasing 20S mediated proteolytic activity [72]. The authors screened 726 compounds in the NIH Clinical Collection and identified AM-404 (**Figure 3.7**, compound **3-18**) and MK-886 (**Figure 3.7**, compound **3-19**) as "true" proteasome enhancers. The study showed both compounds increase the proteolytic activity of the 20S proteasome by 3- to 4-folds with an EC_{50} of 32 μM, and they also enhance the degradation of α-synuclein in cell culture[72].

Figure 3.7: Structure of AM-404 and MK-886

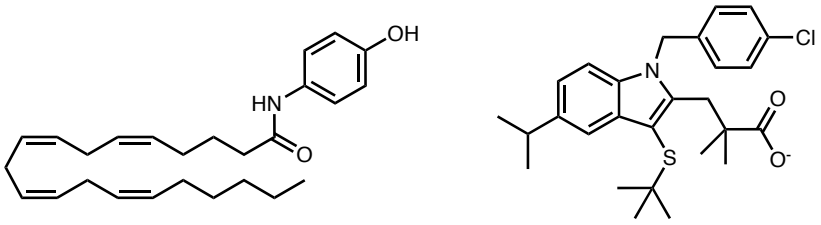

AM-404
3-18

MK-886
3-19

Recently, the Trader's lab investigated the structural component of AM-404 needed to enhance the proteasome proteolytic activity. In the study, they synthesized various derivatives of AM-404 by varying the aliphatic chain length, degree of unsaturation, and substitutions. They illustrated the importance of the aliphatic chain length and the *cis*-alkene at C8 of the aliphatic chain in stimulating the 20S proteasome[126].

3.4.4 Imidazolines

Imidazolines are an important class of compounds that are found in various natural and synthetic bioactive molecules[258-259]. This class of compounds displays a wide range of biological activities including proteasome and NF-κB modulation[260-262], and therapeutic significance such as antifungi[263], antitumor[264], antihelminthics[265], antihyperglycemic[266], and antihypertensive activity[267].

Our lab reported the imidazoline, TCH-165 (**Figure 3.8**, compound **3-20**), as a 20S proteasome enhancer as a low (1.5 μM) activator of the 20S proteasome [70]. TCH-165 enhanced 20S mediated degradation of IDPs such as α-synuclein, tau, ornithine decarboxylase, and c-Fos in cell cultures. However, it does not affect the degradation of structured proteins such as GAPDH. Treatment of HEK293T cells with TCH-165 showed a time-dependent disassembling of both the singly and doubly capped 26S proteasome and showed an increase in the free 20S CP. TCH-165 prevents the binding of the 19S RP to the 20S proteasome suggesting that the molecule binds directly on the α-ring of the 20S CP and shifts the equilibrium between 26S and 20S proteasomes towards an activated 20S CP. To gain insight into the mechanism of 20S proteasome activation, atomic force microscopy (AFM) imaging revealed that the ratio of open to closed 20S proteasome increases in a dose-dependent manner when treated with TCH-165 at concentrations as low as 200nM[70]. This further supports that TCH-165 induces the open gate conformation of the 20S CP. It is also important to note that this is the only small molecule with biophysical data (atomic force microscopy (AFM) imaging) that support gate opening of the 20S proteasome[70].

Figure 3.8: Imidazoline TCH-165 enhances proteasome activities and degrades intrinsically disordered proteins

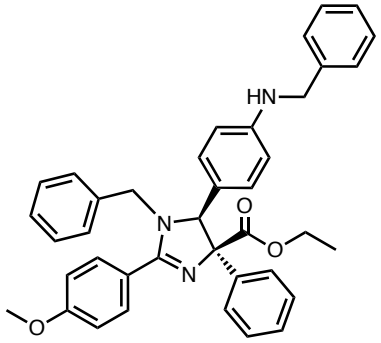

TCH-165
3-20

3.4.5 Chlorpromazines

During the search for proteasome activators, our lab screened the NIH Clinical Collection and Prestwick libraries, where we identified chlorpromazine (Figure 3.9, compound 3-21) and related phenothiazines as 20S proteasome activators inducing up to 20-fold activity[69]. Chlorpromazine is an FDA-approved drug that is used in the treatment of schizophrenia or manic-depression in adults. Chlorpromazine is believed to be a dopamine antagonist with some antiserotonergic and antihistaminergic properties[268].

Figure 3.9: Structure of chlorpromazine and a chlorpromazine analogue 8

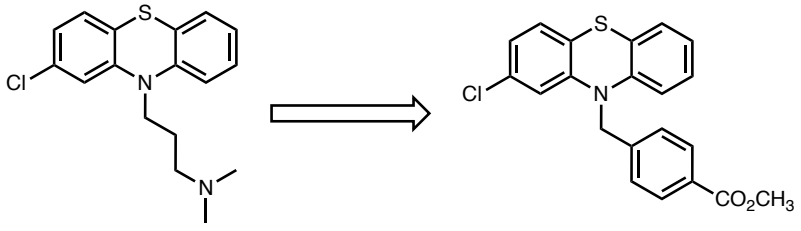

Chlorpromazine
3-21

Analogue 8
3-22

Chlorpromazine and related phenothiazines preferentially enhance the CT-L activity of the proteasome and promote degradation of IDPs, such as α-synuclein and tau but not structured proteins in in vitro assays. Chemical modification of chlorpromazine abrogated its dopamine D2R receptor activity while preserving its ability to enhance the 20S proteolytic activity. Analogue 8

(Figure 3.9, compound 3-22), an analogue of chlorpromazine with physiological insignificant potency for dopamine receptor ($K_i \geq 250$ μM) showed better efficacy with about 10-fold maximum enhancement and EC_{200} (concentration where the 20S mediated proteolysis is increased by 2-fold or 200%) of 13.5 μM.

Interestingly, a structural analogue of chlorpromazine, methylene blue, was also found to enhance the CT-L and T-L activity of the 20S proteasome. Methylene blue was also found to decrease the level of β-amyloid and increase learning and memory in 3xTg-AD mouse model but does not affect tau phosphorylation in vivo[269]. A recent study also showed that methylene blue inhibits caspase-6-induced neurodegeneration, decreases neuroinflammation, and prevents cognitive impairment in mice[270].

3.4.6 Dihydroquinazolines

The 3,4-dihroquinazoline compounds are found in several natural products and synthetic compounds with various biological properties. Members of this class of compounds have biological properties that includes antifungal[271], antiparasitic[272], antitumor[273-279], and antiviral activities[280-281].

In 2021, Mosey et al. synthesized and evaluated several dihydroquinoline analogues as 20S proteasome enhancers[125,282]. In this study, they were able to identify several promising 20S activators with the most potent being dihydroquinazoline **18** (**Figure 3.10**, compound **3-23**), doubling proteasome proteolytic activity at 1.3 μM (EC_{200} 1.3 μM). The dihydroquinazolines enhance the three catalytic sites activity of the 20S proteasome and increase the degradation of α-synuclein, the IDP identified in the pathogenesis of Parkinson's disease.

Figure 3.10: Structure of dihydroquinoline scaffold and dihydroquinoline 18 (compound 3-23)

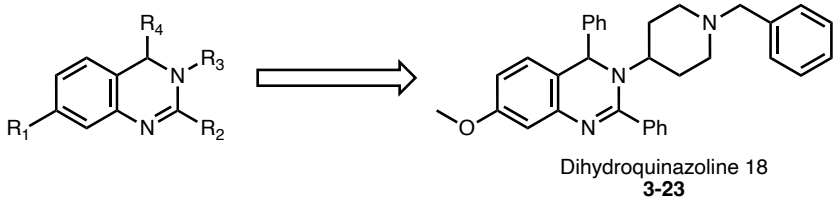

Dihydroquinazoline 18
3-23

3.4.7 Fluspirilene and Acylfluspirilene

In 2021, the Tepe group identified fluspirilene (**Figure 3.11**, compound **3-24**) and its synthetic analogues which were capable of enhancing 20S proteasome proteolytic activity and even restoring the proteolytic activity of 20S proteasome impaired by IDP oligomers[132]. Fluspirilene and its amide derivative, acylfluspirilene (**Figure 3.11**, compound **3-25**) activate the three catalytic sites of 20S CP and prevent IDP aggregation and oligomerization. Interestingly, acylfluspirilene exhibits more potency (EC_{200} 1.9 μM) compared to fluspirilene and a better maximum fold enhancement of greater than 20-fold. Furthermore, molecular docking shows that fluspirilene and acylfluspirilene bind to the α2-3 intersubunit pocket of the 20S CP, which is different from the previously reported 20S enhancers, TCH-165, dihydroquinoline, and chlorpromazine, which bind in the α1-2 pocket of the proteasome. In silico and in vitro structure-activity relationship (SAR) studies indicated the importance of the in-pocket binding interactions of these molecules with the 20S proteasome. This group of molecules does not enhance the proteolytic activity of the 26S proteasome and may therefore be used to selectively prevent the accumulation of dysregulated intrinsically disordered proteins without affecting regular ubiquitin-dependent protein degradation [132].

Figure 3.11: Structure of Fluspirilene and Acylfluspirilene

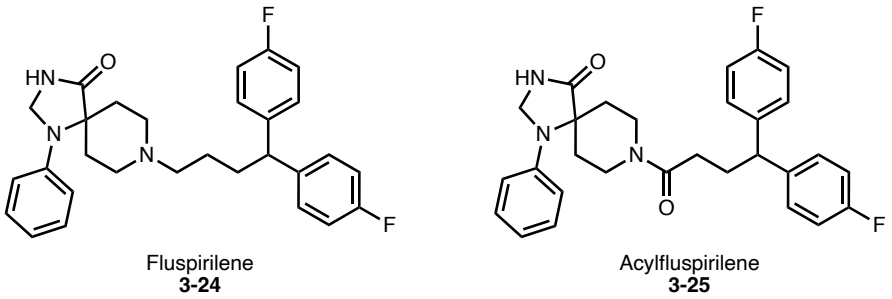

3.4.8 Pyrazolones

Pyrazolones are a rare class of compounds that enhance proteasome activation. This class of molecule was first discovered as proteasome activator in 2014 by the Silverman group and as potential compounds for the treatment of ALS[71]. The pyrazolones (**Figure 3.12**, compound **3-26**–**3-28**) were shown to protect neurons in PC12-SOD1^{G93A} cells in cellular models of ALS. The compounds also increased ALS transgenic mouse survival by 13%, further confirming their potential in the development of ALS therapeutics. During the mechanistic investigation of CMB-087229 (Figure 12, compound **3-27**), the compound was found to antagonize G protein-coupled receptor metabotropic glutamate receptor 5 ($mGluR_5$), a previously identified target in ALS therapeutic[283], to about 65% at 10 μM concentration. The group investigated if $mGluR_5$ was the target of the pyrazolones by screening known $mGluR_5$ antagonists in their cell-based assay. However, the screened $mGluR_5$ receptor antagonists (including MPEP and fenobam) showed no activity in the assay. Based on the result, it was concluded that the antagonism of the $mGluR_5$ is unlikely to be the mode of action of the pyrazolones. Pull down experiments indicated several 26S proteasome regulatory subunits as a possible target for the pyrazolones. The pyrazolones were able to reverse bortezomib-induced cytotoxicity in the PC12 cells, further supporting evidence that their mechanism of action involved proteasome activation[284].

Figure 3.12: Structure of pyrazolones that have been shown to increase proteasome activities

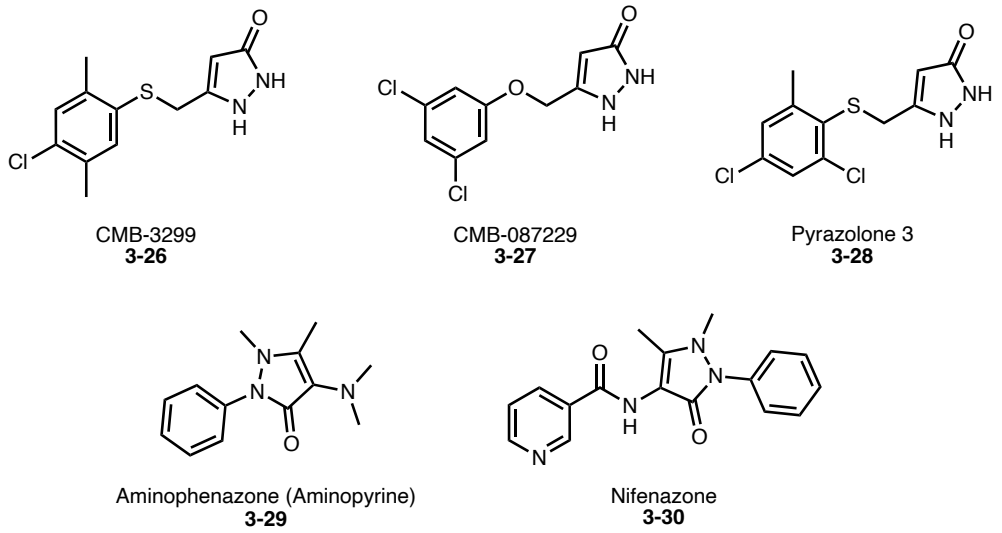

Following up on Silverman's discovery, Santoro et al.[285] screened a small library of structurally-related pyrazolones for proteasome enhancement and neuroprotection against amyloid-induced toxicity in neuroblastoma SH-SY5Y cells. The group reported that the aminopyrine analogue (Figure 12, compound **3-29**) and nifenazone (Figure 12, compound **3-30**) displayed up to twofold induction of 26S proteasome proteolytic activity in cells. Using docking studies coupled with Saturation Transfer Difference (STD) NMR experiments, the group proposed that aminopyrine enhances the 20S proteasome by a mechanism involving binding to the α-ring surfaces of the proteasome; however, only a marginal increase in activity was observed (<30% increase at 10 μM) in a purified proteasome assay.

3.5 Conclusions

Efficient proteasome function is critical in maintaining healthy cellular homeostasis. Dysregulation of protein or proteasome impairment can result in a toxic accumulation of unwanted proteins, which is observed in the pathogenesis of different neurodegenerative diseases and aging. Enhancing the proteolytic activity of the proteasome by increasing its capacity, accessibility, or the rate at which it degrades has long been hypothesized as a means to prevent the accumulation

of dysregulated IDPs. More recently, researchers from various labs have explored the use of small molecules to induce protein proteolysis. Small molecule proteasome agonists can enhance the proteolytic clearance of unwanted proteins and restore homeostasis. Small molecule enhancers of the 26S proteasome are described herein which mainly induce enhanced 26S-mediated proteolysis of ubiquitinated proteins via an indirect mechanism of proteasome activation.

Small molecule inhibitors of deubiquitinases prevent proteins marked for ubiquitin-dependent degradation fromescaping their fate. Even though there are no approved therapies yet based on deubiquitinating enzyme (DUB) inhibitors, this is an emerging field with great significance. Small molecule regulation of upstream signaling pathways, including cAMP-depending protein kinase A and c-GMP-dependent protein kinase G, affect the phosphorylation of the proteasome regulatory particles. As a result, small molecule regulators of phosphodiesterase type-3 (PDE3) can therefore indirectly increase the rate of substrate degradation by the proteasome. Small molecules that directly interact with the 26S proteasome and enhance the rate of 26S proteasome-mediated protein degradation are less known and likely a fruitful field for exploration.

Whereas the 26S proteasome targets ubiquitinylated protein substrates, the 20S proteasome is limited to the degradation of only disordered proteins. Several small molecule enhancers of 20S proteasome-mediated protein degradation have been identified in the literature. We summarized herein several different classes of small molecule 20S proteasome enhancers that induce 20S—mediated degradation of dysregulated intrinsically disordered proteins by direct interaction with the 20S core particle.

The activation of the proteasome by small molecules is a relatively new field in science. Its potential as a therapeutic approach is still unknown and the consequences of chronic exposure

to proteasome enhancers are not known. However, considering the possibility of treating multiple disorders for which there are currently no treatment options available, this approach has enormous potential. However, as in all new fields, the approach still needs further validation, in vivo studies in particular, to fully understand its therapeutic potential and limitation. In addition, more studies are needed to elucidate the mechanistic details of small molecule proteasome activation and its overall cellular consequences.

REFERENCES

1. Hetz, C.; Glimcher, L. H., *Curr. Opin. Cell. Biol.* **2011**, *23*, 123-125.

2. McNaught, K. S. P.; Olanow, C. W.; Halliwell, B.; Isacson, O.; Jenner, P., *Nat. Rev. Neurosci.* **2001**, *2*, 589-594.

3. Saez, I.; Vilchez, D., *Curr. Genomics* **2014**, *15*, 38-51.

4. LaPlante, G.; Zhang, W., *Cancers (Basel)* **2021**, *13*, 3079.

5. Momtaz, S.; Memariani, Z.; El-Senduny, F. F.; Sanadgol, N.; Golab, F.; Katebi, M.; Abdolghaffari, A. H.; Farzaei, M. H.; Abdollahi, M., *Front Physiol.* **2020**, *11*, 361.

6. Rao, G.; Croft, B.; Teng, C.; Awasthi, V., *J. Drug. Metab. Toxicol.* **2015**, *6*, 187.

7. Huang, Q.; Figueiredo-Pereira, M. E., *Apoptosis* **2010**, *15*, 1292-1311.

8. Njomen, E.; Tepe, J. J., *J. Med. Chem.* **2019**, *62*, 6469-6481.

9. Kisselev, A. F.; Akopian, T. N.; Woo, K. M.; Goldberg, A. L., *J. Biol. Chem.* **1999**, *274*, 3363-3371.

10. Kumar Deshmukh, F.; Yaffe, D.; Olshina, M. A.; Ben-Nissan, G.; Sharon, M., *Biomolecules* **2019**, *9*, 190.

11. Hershko, A.; Ciechanover, A., *Annu. Rev. Biochem* **1998**, *67*, 425-479.

12. Stewart, M. D.; Ritterhoff, T.; Klevit, R. E.; Brzovic, P. S., *Cell Res.* **2016**, *26*, 423-440.

13. *Adapted from "Ubiquitin Proteasome System", by BioRender.com*. https://app.biorender.com/biorender-templates (accessed 2021 19 October 2021).

14. Komander, D., *Biochem. Soc. Trans.* **2009**, *37*, 937-953.

15. Peng, J.; Schwartz, D.; Elias, J. E.; Thoreen, C. C.; Cheng, D.; Marsischky, G.; Roelofs, J.; Finley, D.; Gygi, S. P., *Nat. Biotechnol.* **2003**, *21*, 921-926.

16. Chau, V.; Tobias, J. W.; Bachmair, A.; Marriott, D.; Ecker, D. J.; Gonda, D. K.; Varshavsky, A., *Science* **1989**, *243*, 1576-1583.

17. Tracz, M.; Bialek, W., *Cell. Mol. Biol. Lett.* **2021**, *26*, 1.

18. Komander, D.; Rape, M., *Annu. Rev. Biochem* **2012**, *81*, 203-229.

19. Thrower, J. S.; Hoffman, L.; Rechsteiner, M.; Pickart, C. M., *EMBO J.* **2000**, *19*, 94-102.

20. Dimova, N. V.; Hathaway, N. A.; Lee, B.-H.; Kirkpatrick, D. S.; Berkowitz, M. L.; Gygi, S. P.; Finley, D.; King, R. W., *Nat. Cell Biol.* **2012**, *14*, 168-176.

21. Shabek, N.; Herman-Bachinsky, Y.; Buchsbaum, S.; Lewinson, O.; Haj-Yahya, M.; Hejjaoui, M.; Lashuel, Hilal A.; Sommer, T.; Brik, A.; Ciechanover, A., *Mol. Cell* **2012**, *48*, 87-97.

22. Kravtsova-Ivantsiv, Y.; Ciechanover, A., *J. Cell Sci.* **2012**, *125*, 539-548.

23. Martinez-Fonts, K.; Davis, C.; Tomita, T.; Elsasser, S.; Nager, A. R.; Shi, Y.; Finley, D.; Matouschek, A., *Nat. Commun.* **2020**, *11*, 477-477.

24. Komander, D.; Clague, M. J.; Urbé, S., *Nat. Rev. Mol. Cell Biol.* **2009**, *10*, 550-563.

25. Peters, J. M.; Cejka, Z.; Harris, J. R.; Kleinschmidt, J. A.; Baumeister, W., *J. Mol. Biol.* **1993**, *234*, 932-937.

26. da Fonseca, P. C.; Morris, E. P., *J. Biol. Chem.* **2008**, *283*, 23305-23314.

27. Orlowski, M.; Wilk, S., *Arch. Biochem. Biophys.* **2000**, *383*, 1-16.

28. Dong, Y.; Zhang, S.; Wu, Z.; Li, X.; Wang, W. L.; Zhu, Y.; Stoilova-McPhie, S.; Lu, Y.; Finley, D.; Mao, Y., *Nature* **2019**, *565*, 49-55.

29. Finley, D.; Chen, X.; Walters, K. J., *Trends Biochem. Sci* **2016**, *41*, 77-93.

30. Peña, A. H. d. l.; Goodall, E. A.; Gates, S. N.; Lander, G. C.; Martin, A., *Science* **2018**, *362*, eaav0725.

31. Eisele, M. R.; Reed, R. G.; Rudack, T.; Schweitzer, A.; Beck, F.; Nagy, I.; Pfeifer, G.; Plitzko, J. M.; Baumeister, W.; Tomko, R. J.; et al., *Cell Rep.* **2018**, *24*, 1301-1315.e1305.

32. Ding, Z.; Fu, Z.; Xu, C.; Wang, Y.; Wang, Y.; Li, J.; Kong, L.; Chen, J.; Li, N.; Zhang, R.; et al., *Cell Res.* **2017**, *27*, 373-385.

33. Huang, X.; Luan, B.; Wu, J.; Shi, Y., *Nat. Struct. Mol. Biol.* **2016**, *23*, 778-785.

34. Chen, S.; Wu, J.; Lu, Y.; Ma, Y.-B.; Lee, B.-H.; Yu, Z.; Ouyang, Q.; Finley, D. J.; Kirschner, M. W.; Mao, Y., *Proc. Natl. Acad. Sci.* **2016**, *113*, 12991.

35. Ding, Z.; Xu, C.; Sahu, I.; Wang, Y.; Fu, Z.; Huang, M.; Wong, C. C. L.; Glickman, M. H.; Cong, Y., *Mol. Cell* **2019**, *73*, 1150-1161.e1156.

36. Vilchez, D.; Saez, I.; Dillin, A., *Nat. Commun.* **2014**, *5*, 5659.

37. Bochtler, M.; Ditzel, L.; Groll, M.; Hartmann, C.; Huber, R., *Annu. Rev. Biophys. Biomol. Struct.* **1999**, *28*, 295-317.

38. Huber, E. M.; Heinemeyer, W.; Li, X.; Arendt, C. S.; Hochstrasser, M.; Groll, M., *Nat. Commun.* **2016**, *7*, 10900.

39. Huang, L.; Chen, C. H., *Curr. Med. Chem.* **2009**, *16*, 931-939.

40. Kane, R. C.; Bross, P. F.; Farrell, A. T.; Pazdur, R., *Oncologist* **2003**, *8*, 508-513.

41. Bruna, J.; Udina, E.; Alé, A.; Vilches, J. J.; Vynckier, A.; Monbaliu, J.; Silverman, L.; Navarro, X., *Exp. Neurol.* **2010**, *223*, 599-608.

42. Gilmore, T. D.; Herscovitch, M., *Oncogene* **2006**, *25*, 6887-6899.

43. Hideshima, T.; Richardson, P.; Chauhan, D.; Palombella, V. J.; Elliott, P. J.; Adams, J.; Anderson, K. C., *Cancer Res.* **2001**, *61*, 3071-3076.

44. Russo, S. M.; Tepper, J. E.; Baldwin, A. S., Jr.; Liu, R.; Adams, J.; Elliott, P.; Cusack, J. C., Jr., *Int. J. Radiat. Oncol. Biol. Phys.* **2001**, *50*, 183-193.

45. Sunwoo, J. B.; Chen, Z.; Dong, G.; Yeh, N.; Crowl Bancroft, C.; Sausville, E.; Adams, J.; Elliott, P.; Van Waes, C., *Clin. Cancer. Res.* **2001**, *7*, 1419-1428.

46. Hideshima, T.; Chauhan, D.; Richardson, P.; Mitsiades, C.; Mitsiades, N.; Hayashi, T.; Munshi, N.; Dang, L.; Castro, A.; Palombella, V.; et al., *J. Biol. Chem.* **2002**, *277*, 16639-16647.

47. Tan, C.; Waldmann, T. A., *Cancer Res.* **2002**, *62*, 1083-1086.

48. Ma, M. H.; Yang, H. H.; Parker, K.; Manyak, S.; Friedman, J. M.; Altamirano, C.; Wu, Z. Q.; Borad, M. J.; Frantzen, M.; Roussos, E.; et al., *Clin. Cancer. Res.* **2003**, *9*, 1136-1144.

49. Shah, S. A.; Potter, M. W.; McDade, T. P.; Ricciardi, R.; Perugini, R. A.; Elliott, P. J.; Adams, J.; Callery, M. P., *J. Cell. Biochem.* **2001**, *82*, 110-122.

50. Yang, Y.; Ikezoe, T.; Saito, T.; Kobayashi, M.; Koeffler, H. P.; Taguchi, H., *Cancer Sci.* **2004**, *95*, 176-180.

51. Williams, S. A.; McConkey, D. J., *Cancer Res.* **2003**, *63*, 7338-7344.

52. Li, B.; Dou, Q. P., *Proc. Natl. Acad. Sci. U S A* **2000**, *97*, 3850-3855.

53. Breitschopf, K.; Zeiher, A. M.; Dimmeler, S., *J. Biol. Chem.* **2000**, *275*, 21648-21652.

54. Bianchi, G.; Oliva, L.; Cascio, P.; Pengo, N.; Fontana, F.; Cerruti, F.; Orsi, A.; Pasqualetto, E.; Mezghrani, A.; Calbi, V.; et al., *Blood* **2009**, *113*, 3040-3049.

55. Sha, Z.; Goldberg, A. L., *Proc. Natl. Acad. Sci. U S A* **2020**, *117*, 21588.

56. Suraweera, A.; Münch, C.; Hanssum, A.; Bertolotti, A., *Mol. Cell* **2012**, *48*, 242-253.

57. Aliabadi, F.; Sohrabi, B.; Mostafavi, E.; Pazoki-Toroudi, H.; Webster, T. J., *Open Biol.* **2021**, *11*, 200390.

58. Fricker, L. D., *Annu. Rev. Pharmacool. Toxicol.* **2020**, *60*, 457-476.

59. Gandolfi, S.; Laubach, J. P.; Hideshima, T.; Chauhan, D.; Anderson, K. C.; Richardson, P. G., *Cancer Metastasis Rev.* **2017**, *36*, 561-584.

60. Ito, S., *Cancers* **2020**, *12*, 265.

61. Kaplan, G. S.; Torcun, C. C.; Grune, T.; Ozer, N. K.; Karademir, B., *Free Radical Biol. Med.* **2017**, *103*, 1-13.

62. Manasanch, E. E.; Orlowski, R. Z., *Nat. Rev. Clin. Oncol* **2017**, *14*, 417-433.

63. Narayanan, S.; Cai, C.-Y.; Assaraf, Y. G.; Guo, H.-Q.; Cui, Q.; Wei, L.; Huang, J.-J.; Ashby, C. R.; Chen, Z.-S., *Drug Resist. Updat.* **2020**, *48*, 100663.

64. Roeten, M. S. F.; Cloos, J.; Jansen, G., *Cancer Chemother. Pharmacol.* **2018**, *81*, 227-243.

65. Sherman, D. J.; Li, J., *Molecules* **2020**, *25*, 671.

66. Zhang, X.; Linder, S.; Bazzaro, M., *Cancers* **2020**, *12*, 902.

67. Hubbell, G. E.; Tepe, J. J., *RSC Chem. Biol.* **2020**, *1*, 305-332.

68. Jones, C. L.; Tepe, J. J., *Molecules* **2019**, *24*, 2841.

69. Jones, C. L.; Njomen, E.; Sjogren, B.; Dexheimer, T. S.; Tepe, J. J., *ACS Chem. Biol.* **2017**, *12*, 2240-2247.

70. Njomen, E.; Osmulski, P. A.; Jones, C. L.; Gaczynska, M.; Tepe, J. J., *Biochemistry* **2018**, *57*, 4214-4224.

71. Trippier, P. C.; Zhao, K. T.; Fox, S. G.; Schiefer, I. T.; Benmohamed, R.; Moran, J.; Kirsch, D. R.; Morimoto, R. I.; Silverman, R. B., *ACS Chem. Neurosci.* **2014**, *5*, 823-829.

72. Trader, D. J.; Simanski, S.; Dickson, P.; Kodadek, T., *Biochim. Biophys. Acta* **2017**, *1861*, 892-899.

73. López-Otín, C.; Blasco, M. A.; Partridge, L.; Serrano, M.; Kroemer, G., *Cell* **2013**, *153*, 1194-1217.

74. Lee, C.-K.; Klopp, R. G.; Weindruch, R.; Prolla, T. A., *Science* **1999**, *285*, 1390-1393.

75. Bulteau, A.-L.; Lundberg, K. C.; Humphries, K. M.; Sadek, H. A.; Szweda, P. A.; Friguet, B.; Szweda, L. I., *J. Biol. Chem.* **2001**, *276*, 30057-30063.

76. Wang, X.; Yen, J.; Kaiser, P.; Huang, L., *Sci. Signal.* **2010**, *3*, ra88.

77. Tonoki, A.; Kuranaga, E.; Tomioka, T.; Hamazaki, J.; Murata, S.; Tanaka, K.; Miura, M., *Mol. Cell. Biol.* **2009**, *29*, 1095-1106.

78. Bajorek, M.; Finley, D.; Glickman, M. H., *Curr. Biol.* **2003**, *13*, 1140-1144.

79. Kayed, R.; Dettmer, U.; Lesné, S. E., *J. Parkinsons Dis.* **2020**, *10*, 791-818.

80. Ono, K., *Neurochem. Int.* **2018**, *119*, 57-70.

81. Mroczko, B.; Groblewska, M.; Litman-Zawadzka, A.; Kornhuber, J.; Lewczuk, P., *J. Neural Transm.* **2018**, *125*, 177-191.

82. Gulisano, W.; Maugeri, D.; Baltrons, M. A.; Fà, M.; Amato, A.; Palmeri, A.; D'Adamio, L.; Grassi, C.; Devanand, D.; Honig, L. S., *J. Alzheimer's Dis.* **2018**, *64*, S611-S631.

83. Ghag, G.; Bhatt, N.; Cantu, D. V.; Guerrero-Munoz, M. J.; Ellsworth, A.; Sengupta, U.; Kayed, R., *Protein Sci.* **2018**, *27*, 1901-1909.

84. Forloni, G.; Balducci, C., *J. Alzheimer's Dis.* **2018**, *62*, 1261-1276.

85. Cline, E. N.; Bicca, M. A.; Viola, K. L.; Klein, W. L., *J. Alzheimer's Dis.* **2018**, *64*, S567-S610.

86. Choi, M. L.; Gandhi, S., *The FEBS journal* **2018**, *285*, 3631-3644.

87. Castillo-Carranza, D. L.; Guerrero-Muñoz, M. J.; Sengupta, U.; Gerson, J. E.; Kayed, R., *Biol. Psychiatry* **2018**, *84*, 499-508.

88. Shafiei, S. S.; Guerrero-Muñoz, M. J.; Castillo-Carranza, D. L., *Front. aging neurosci.* **2017**, *9*, 83.

89. Sengupta, U.; Nilson, A. N.; Kayed, R., *EBioMedicine* **2016**, *6*, 42-49.

90. Ingelsson, M., *Front. Neurosci.* **2016**, *10*, 408.

91. Cárdenas-Aguayo, M. a. d. C.; Gómez-Virgilio, L.; DeRosa, S.; Meraz-Ríos, M. A., *ACS Chem. Neurosci.* **2014**, *5*, 1178-1191.

92. Katzmarski, N.; Ziegler-Waldkirch, S.; Scheffler, N.; Witt, C.; Abou-Ajram, C.; Nuscher, B.; Prinz, M.; Haass, C.; Meyer-Luehmann, M., *Brain Pathol.* **2020**, *30*, 36-45.

93. Haass, C.; Selkoe, D. J., *Nat. Rev. Mol. Cell Biol.* **2007**, *8*, 101-112.

94. Smith, D. M., *J. Exp. Neurosci.* **2018**, *12*, 1179069518794675.

95. Gerson, J. E.; Farmer, K. M.; Henson, N.; Castillo-Carranza, D. L.; Murillo, M. C.; Sengupta, U.; Barrett, A.; Kayed, R., *Mol. Neurodegener.* **2018**, *13*, 1-14.

96. Gerson, J. E.; Sengupta, U.; Kayed, R. Tau oligomers as pathogenic seeds: preparation and propagation in vitro and in vivo. In *Tau Protein*, Springer, 2017; pp 141-157.

97. Bengoa-Vergniory, N.; Roberts, R. F.; Wade-Martins, R.; Alegre-Abarrategui, J., *Acta Neuropathol.* **2017**, *134*, 819-838.

98. Gerson, J. E.; Mudher, A.; Kayed, R., *Crit. Rev. Biochem. Mol. Biol.* **2016**, *51*, 482-496.

99. Brettschneider, J.; Del Tredici, K.; Lee, V. M.; Trojanowski, J. Q., *Nat. Rev. Neurosci.* **2015**, *16*, 109-120.

100. Rubinsztein, D. C., *Nature* **2006**, *443*, 780-786.

101. Selkoe, D. J., *Nature* **2003**, *426*, 900-904.

102. Selkoe, D. J.; Hardy, J., *EMBO Mol. Med.* **2016**, *8*, 595-608.

103. Cecarini, V.; Bonfili, L.; Amici, M.; Angeletti, M.; Keller, J. N.; Eleuteri, A. M., *Brain Res.* **2008**, *1209*, 8-18.

104. Díaz-Hernández, M.; Valera, A. G.; Morán, M. A.; Gómez-Ramos, P.; Alvarez-Castelao, B.; Castaño, J. G.; Hernández, F.; Lucas, J. J., *J. Neurochem.* **2006**, *98*, 1585-1596.

105. Gregori, L.; Fuchs, C.; Figueiredo-Pereira, M. E.; Van Nostrand, W. E.; Goldgaber, D., *J. Biol. Chem.* **1995**, *270*, 19702-19708.

106. Lindersson, E.; Beedholm, R.; Højrup, P.; Moos, T.; Gai, W.; Hendil, K. B.; Jensen, P. H., *J. Biol. Chem.* **2004**, *279*, 12924-12934.

107. Bence, N. F.; Sampat, R. M.; Kopito, R. R., *Science* **2001**, *292*, 1552-1555.

108. Oh, S.; Hong, H. S.; Hwang, E.; Sim, H. J.; Lee, W.; Shin, S. J.; Mook-Jung, I., *Mech. Ageing Dev.* **2005**, *126*, 1292-1299.

109. Tanaka, K.; Matsuda, N., *Biochim. Biophys. Acta* **2014**, *1843*, 197-204.

110. Tanaka, Y.; Engelender, S.; Igarashi, S.; Rao, R. K.; Wanner, T.; Tanzi, R. E.; Sawa, A.; L. Dawson, V.; Dawson, T. M.; Ross, C. A., *Hum. Mol. Genet.* **2001**, *10*, 919-926.

111. Tseng, B. P.; Green, K. N.; Chan, J. L.; Blurton-Jones, M.; LaFerla, F. M., *Neurobiol. Aging* **2008**, *29*, 1607-1618.

112. Emmanouilidou, E.; Stefanis, L.; Vekrellis, K., *Neurobiol. Aging* **2010**, *31*, 953-968.

113. Deriziotis, P.; André, R.; Smith, D. M.; Goold, R.; Kinghorn, K. J.; Kristiansen, M.; Nathan, J. A.; Rosenzweig, R.; Krutauz, D.; Glickman, M. H., *The EMBO journal* **2011**, *30*, 3065-3077.

114. Deriziotis, P.; Tabrizi, S. J., *Biochim. Biophys. Acta* **2008**, *1782*, 713-722.

115. Kristiansen, M.; Deriziotis, P.; Dimcheff, D. E.; Jackson, G. S.; Ovaa, H.; Naumann, H.; Clarke, A. R.; van Leeuwen, F. W.; Menéndez-Benito, V.; Dantuma, N. P., *Mol. Cell* **2007**, *26*, 175-188.

116. Thibaudeau, T. A.; Anderson, R. T.; Smith, D. M., *Nat. Commun.* **2018**, *9*, 1097.

117. Zondler, L.; Kostka, M.; Garidel, P.; Heinzelmann, U.; Hengerer, B.; Mayer, B.; Weishaupt, J. H.; Gillardon, F.; Danzer, K. M., *PloS one* **2017**, *12*, e0184040.

118. Ruegsegger, C.; Saxena, S., *Brain Res.* **2016**, *1648*, 571-579.

119. Myeku, N.; Clelland, C. L.; Emrani, S.; Kukushkin, N. V.; Yu, W. H.; Goldberg, A. L.; Duff, K. E., *Nat. Med.* **2016**, *22*, 46-53.

120. Papanikolopoulou, K.; Skoulakis, E. Altered proteostasis in neurodegenerative tauopathies. In *Proteostasis and Disease*, Barrio, R., Sutherland, J. D., Rodriguez, M. S. Eds.; Springer International Publishing, 2020; pp 177-194.

121. Choi, W. H.; De Poot, S. A.; Lee, J. H.; Kim, J. H.; Han, D. H.; Kim, Y. K.; Finley, D.; Lee, M. J., *Nat. Commun.* **2016**, *7*, 1-12.

122. Leestemaker, Y.; de Jong, A.; Witting, K. F.; Penning, R.; Schuurman, K.; Rodenko, B.; Zaal, E. A.; van de Kooij, B.; Laufer, S.; Heck, A. J., *Cell Chem. Biol.* **2017**, *24*, 725-736.

123. Leestemaker, Y.; Ovaa, H., *Drug Discov. Today Technol.* **2017**, *26*, 25-31.

124. Lee, B.-H.; Lee, M. J.; Park, S.; Oh, D.-C.; Elsasser, S.; Chen, P.-C.; Gartner, C.; Dimova, N.; Hanna, J.; Gygi, S. P., *Nature* **2010**, *467*, 179-184.

125. Fiolek, T. J.; Magyar, C. L.; Wall, T. J.; Davies, S. B.; Campbell, M. V.; Savich, C. J.; Tepe, J. J.; Mosey, R. A., *Bioorg. Med. Chem. Lett.* **2021**, *36*, 127821.

126. Coleman, R. A.; Muli, C. S.; Zhao, Y.; Bhardwaj, A.; Newhouse, T. R.; Trader, D. J., *Bioorg. Med. Chem. Lett.* **2019**, *29*, 420-423.

127. Coleman, R. A.; Trader, D. J., *ACS Comb. Sci.* **2018**, *20*, 269-276.

128. Giżyńska, M.; Witkowska, J.; Karpowicz, P.; Rostankowski, R.; Chocron, E. S.; Pickering, A. M.; Osmulski, P.; Gaczynska, M.; Jankowska, E. b., *J. Med. Chem.* **2019**, *62*, 359-370.

129. Njomen, E.; Lansdell, T.; Vanecek, A.; Benham, V.; Bernard, M.; Yang, Y.-T.; Schall, P.; Isaac, D.; Alkharabsheh, O.; Al-Janadi, A., *bioRxiv* **2020.08.24.265470**.

130. Chondrogianni, N.; Georgila, K.; Kourtis, N.; Tavernarakis, N.; Gonos, E. S., *The FASEB Journal* **2015**, *29*, 611-622.

131. Gonos, E., *Free Radical Biol. Med.* **2014**, *75*, S7.

132. Fiolek, T. J.; Keel, K. L.; Tepe, J. J., *ACS Chem. Neurosci.* **2021**, *12*, 1438-1448.

133. Ben-Nissan, G.; Sharon, M., *Biomolecules* **2014**, *4*, 862-884.

134. Njomen, E.; Tepe, J. J., *Cell Chem. Biol.* **2019**, *26*, 1283-1294.

135. Asher, G.; Reuven, N.; Shaul, Y., *Bioessays* **2006**, *28*, 844-849.

136. Korovila, I.; Hugo, M.; Castro, J. P.; Weber, D.; Höhn, A.; Grune, T.; Jung, T., *Redox Biol.* **2017**, *13*, 550-567.

137. Höhn, T. J.; Grune, T., *Redox Biol.* **2014**, *2*, 388-394.

138. Chondrogianni, N.; Petropoulos, I.; Grimm, S.; Georgila, K.; Catalgol, B.; Friguet, B.; Grune, T.; Gonos, E. S., *Mol. Aspects Med.* **2014**, *35*, 1-71.

139. Myers, N.; Olender, T.; Savidor, A.; Levin, Y.; Reuven, N.; Shaul, Y., *Proteomics* **2018**, *18*, e1800076.

140. Tsvetkov, P.; Reuven, N.; Shaul, Y., *Nat. Chem. Biol.* **2009**, *5*, 778-781.

141. Oliver, C. N.; Ahn, B. W.; Moerman, E. J.; Goldstein, S.; Stadtman, E. R., *J. Biol. Chem.* **1987**, *262*, 5488-5491.

142. Carrard, G.; Dieu, M.; Raes, M.; Toussaint, O.; Friguet, B., *Int. J. Biochem. Cell Biol.* **2003**, *35*, 728-739.

143. Keller, J. N.; Huang, F. F.; Markesbery, W. R., *Neuroscience* **2000**, *98*, 149-156.

144. Giannini, C.; Kloß, A.; Gohlke, S.; Mishto, M.; Nicholson, T. P.; Sheppard, P. W.; Kloetzel, P. M.; Dahlmann, B., *PLoS One* **2013**, *8*, e64042.

145. Merker, K.; Sitte, N.; Grune, T., *Arch. Biochem. Biophys.* **2000**, *375*, 50-54.

146. Sitte, N.; Merker, K.; von Zglinicki, T.; Grune, T., *Free Radical Biol. Med.* **2000**, *28*, 701-708.

147. Reeg, S.; Grune, T., *Antioxid. Redox Signal.* **2014**, *23*, 239-255.

148. Deger, J. M.; Gerson, J. E.; Kayed, R., *Aging Cell* **2015**, *14*, 715-724.

149. McKinnon, C.; Goold, R.; Andre, R.; Devoy, A.; Ortega, Z.; Moonga, J.; Linehan, J. M.; Brandner, S.; Lucas, J. J.; Collinge, J.; et al., *Acta Neuropathol.* **2016**, *131*, 411-425.

150. Otero, A.; Betancor, M.; Erana, H.; Fernandez Borges, N.; Lucas, J. J.; Badiola, J. J.; Castilla, J.; Bolea, R., *Int. J. Mol. Sci.* **2021**, *22*, 465.

151. *Parkinson's Disease Foundation*. https://www.parkinson.org/Understanding-Parkinsons/Statistics (accessed 2021 17 October 2021).

152. Moore, D. J.; Dawson, V. L.; Dawson, T. M., *Neuromolecular Med.* **2003**, *4*, 95-108.

153. McNaught, K. S. P.; Jenner, P., *Neurosci. Lett.* **2001**, *297*, 191-194.

154. McNaught, K. S.; Perl, D. P.; Brownell, A. L.; Olanow, C. W., *Ann. Neurol.* **2004**, *56*, 149-162.

155. Matsuda, N.; Tanaka, K., *J. Alzheimer's Dis.* **2010**, *19*, 1-9.

156. Kincaid, E. Z.; Che, J. W.; York, I.; Escobar, H.; Reyes-Vargas, E.; Delgado, J. C.; Welsh, R. M.; Karow, M. L.; Murphy, A. J.; Valenzuela, D. M.; et al., *Nat. Immunol.* **2012**, *13*, 129-135.

157. Bedford, L.; Hay, D.; Devoy, A.; Paine, S.; Powe, D. G.; Seth, R.; Gray, T.; Topham, I.; Fone, K.; Rezvani, N., *J. Neurosci.* **2008**, *28*, 8189-8198.

158. *FastStats - Leading Causes of Death*. https://www.cdc.gov/nchs/fastats/leading-causes-of-death.htm (accessed 17 October 2021).

159. *Alzheimer's & Dementia* **2019**, *15*, 321-387.

160. Tiwari, S.; Atluri, V.; Kaushik, A.; Yndart, A.; Nair, M., *Int. J. Nanomedicine* **2019**, *14*, 5541-5554.

161. Goedert, M., *Science* **2015**, *349*, 1255555.

162. Ferreira, S.; Lourenco, M.; Oliveira, M.; De Felice, F., *Front. cell. neurosci.* **2015**, *9*, 191.

163. Cleary, J. P.; Walsh, D. M.; Hofmeister, J. J.; Shankar, G. M.; Kuskowski, M. A.; Selkoe, D. J.; Ashe, K. H., *Nat. Neurosci.* **2005**, *8*, 79-84.

164. Balducci, C.; Beeg, M.; Stravalaci, M.; Bastone, A.; Sclip, A.; Biasini, E.; Tapella, L.; Colombo, L.; Manzoni, C.; Borsello, T., *Proc. Natl. Acad. Sci. U S A* **2010**, *107*, 2295-2300.

165. Shankar, G. M.; Li, S.; Mehta, T. H.; Garcia-Munoz, A.; Shepardson, N. E.; Smith, I.; Brett, F. M.; Farrell, M. A.; Rowan, M. J.; Lemere, C. A., *Nat. Med.* **2008**, *14*, 837-842.

166. Lopez Salon, M.; Pasquini, L.; Besio Moreno, M.; Pasquini, J. M.; Soto, E., *Exp. Neurol.* **2003**, *180*, 131-143.

167. Hong, L.; Huang, H. C.; Jiang, Z. F., *Neurol. Res.* **2014**, *36*, 276-282.

168. Wang, H.; Saunders, A. J., *Discov Med* **2014**, *18*, 41-50.

169. Riederer, B. M.; Leuba, G.; Vernay, A.; Riederer, I. M., *Exp. Biol. Med.* **2011**, *236*, 268-276.

170. Vonsattel, J. P.; DiFiglia, M., *J. Neuropathol. Exp. Neurol.* **1998**, *57*, 369-384.

171. MacDonald, M. E.; Ambrose, C. M.; Duyao, M. P.; Myers, R. H.; Lin, C.; Srinidhi, L.; Barnes, G.; Taylor, S. A.; James, M.; Groot, N.; et al., *Cell* **1993**, *72*, 971-983.

172. Sánchez, I.; Mahlke, C.; Yuan, J., *Nature* **2003**, *421*, 373-379.

173. Snell, R. G.; MacMillan, J. C.; Cheadle, J. P.; Fenton, I.; Lazarou, L. P.; Davies, P.; MacDonald, M. E.; Gusella, J. F.; Harper, P. S.; Shaw, D. J., *Nat. Genet.* **1993**, *4*, 393-397.

174. Nance, M. A.; Myers, R. H., *Ment. Retard. Dev. Disabil. Res. Rev.* **2001**, *7*, 153-157.

175. Dantuma, N. P.; Bott, L. C., *Front. Mol. Neurosci.* **2014**, *7*, 70.

176. Hipp, M. S.; Patel, C. N.; Bersuker, K.; Riley, B. E.; Kaiser, S. E.; Shaler, T. A.; Brandeis, M.; Kopito, R. R., *J. Cell Biol.* **2012**, *196*, 573-587.

177. Kalchman, M. A.; Graham, R. K.; Xia, G.; Koide, H. B.; Hodgson, J. G.; Graham, K. C.; Goldberg, Y. P.; Gietz, R. D.; Pickart, C. M.; Hayden, M. R., *J. Biol. Chem.* **1996**, *271*, 19385-19394.

178. Seo, H.; Sonntag, K. C.; Kim, W.; Cattaneo, E.; Isacson, O., *PLoS One* **2007**, *2*, e238.

179. Taylor, J. P.; Brown, R. H.; Cleveland, D. W., *Nature* **2016**, *539*, 197-206.

180. Al-Chalabi, A.; Hardiman, O., *Nat. Rev. Neurol.* **2013**, *9*, 617-628.

181. Turner, M. R.; Hardiman, O.; Benatar, M.; Brooks, B. R.; Chio, A.; de Carvalho, M.; Ince, P. G.; Lin, C.; Miller, R. G.; Mitsumoto, H.; et al., *Lancet Neurol.* **2013**, *12*, 310-322.

182. Rosen, D. R.; Siddique, T.; Patterson, D.; Figlewicz, D. A.; Sapp, P.; Hentati, A.; Donaldson, D.; Goto, J.; O'Regan, J. P.; Deng, H. X.; et al., *Nature* **1993**, *362*, 59-62.

183. Sreedharan, J.; Blair, I. P.; Tripathi, V. B.; Hu, X.; Vance, C.; Rogelj, B.; Ackerley, S.; Durnall, J. C.; Williams, K. L.; Buratti, E.; et al., *Science* **2008**, *319*, 1668-1672.

184. Vance, C.; Rogelj, B.; Hortobágyi, T.; De Vos, K. J.; Nishimura, A. L.; Sreedharan, J.; Hu, X.; Smith, B.; Ruddy, D.; Wright, P.; et al., *Science* **2009**, *323*, 1208-1211.

185. Deng, H. X.; Chen, W.; Hong, S. T.; Boycott, K. M.; Gorrie, G. H.; Siddique, N.; Yang, Y.; Fecto, F.; Shi, Y.; Zhai, H.; et al., *Nature* **2011**, *477*, 211-215.

186. DeJesus-Hernandez, M.; Mackenzie, I. R.; Boeve, B. F.; Boxer, A. L.; Baker, M.; Rutherford, N. J.; Nicholson, A. M.; Finch, N. A.; Flynn, H.; Adamson, J.; et al., *Neuron* **2011**, *72*, 245-256.

187. Renton, A. E.; Majounie, E.; Waite, A.; Simón-Sánchez, J.; Rollinson, S.; Gibbs, J. R.; Schymick, J. C.; Laaksovirta, H.; van Swieten, J. C.; Myllykangas, L.; et al., *Neuron* **2011**, *72*, 257-268.

188. Ash, Peter E. A.; Bieniek, Kevin F.; Gendron, Tania F.; Caulfield, T.; Lin, W.-L.; DeJesus-Hernandez, M.; van Blitterswijk, Marka M.; Jansen-West, K.; Paul, Joseph W.; Rademakers, R.; et al., *Neuron* **2013**, *77*, 639-646.

189. Gendron, T. F.; Bieniek, K. F.; Zhang, Y.-J.; Jansen-West, K.; Ash, P. E. A.; Caulfield, T.; Daughrity, L.; Dunmore, J. H.; Castanedes-Casey, M.; Chew, J.; et al., *Acta Neuropathol.* **2013**, *126*, 829-844.

190. Mori, K.; Arzberger, T.; Grässer, F. A.; Gijselinck, I.; May, S.; Rentzsch, K.; Weng, S.-M.; Schludi, M. H.; van der Zee, J.; Cruts, M.; et al., *Acta Neuropathol.* **2013**, *126*, 881-893.

191. Mori, K.; Weng, S.-M.; Arzberger, T.; May, S.; Rentzsch, K.; Kremmer, E.; Schmid, B.; Kretzschmar Hans, A.; Cruts, M.; Van Broeckhoven, C.; et al., *Science* **2013**, *339*, 1335-1338.

192. Zu, T.; Liu, Y.; Bañez-Coronel, M.; Reid, T.; Pletnikova, O.; Lewis, J.; Miller, T. M.; Harms, M. B.; Falchook, A. E.; Subramony, S. H.; et al., *Proc. Natl. Acad. Sci.* **2013**, *110*, E4968.

193. Guo, Q.; Lehmer, C.; Martínez-Sánchez, A.; Rudack, T.; Beck, F.; Hartmann, H.; Pérez-Berlanga, M.; Frottin, F.; Hipp, M. S.; Hartl, F. U.; et al., *Cell* **2018**, *172*, 696-705.e612.

194. Kato, S., *Acta Neuropathol.* **2008**, *115*, 97-114.

195. Strong, M. J.; Kesavapany, S.; Pant, H. C., *J. Neuropathol. Exp. Neurol.* **2005**, *64*, 649-664.

196. Bendotti, C.; Atzori, C.; Piva, R.; Tortarolo, M.; Strong, M. J.; Debiasi, S.; Migheli, A., *J. Neuropathol. Exp. Neurol.* **2004**, *63*, 113-119.

197. Leigh, P. N.; Whitwell, H.; Garofalo, O.; Buller, J.; Swash, M.; Martin, J. E.; Gallo, J. M.; Weller, R. O.; Anderton, B. H., *Brain* **1991**, *114*, 775-788.

198. Bendotti, C.; Marino, M.; Cheroni, C.; Fontana, E.; Crippa, V.; Poletti, A.; De Biasi, S., *Prog. Neurobiol.* **2012**, *97*, 101-126.

199. Goldberg, A. L.; Kim, H. T.; Lee, D.; Collins, G. A., *Biomolecules* **2021**, *11*, 779.

200. Verma, R.; Aravind, L.; Oania, R.; McDonald, W. H.; Yates, J. R., 3rd; Koonin, E. V.; Deshaies, R. J., *Science* **2002**, *298*, 611-615.

201. Shin, J. Y.; Muniyappan, S.; Tran, N. N.; Park, H.; Lee, S. B.; Lee, B. H., *Int. J. Mol. Sci.* **2020**, *21*, 5312.

202. Finley, D., *Annu. Rev. Biochem* **2009**, *78*, 477-513.

203. Yao, T.; Cohen, R. E., *Nature* **2002**, *419*, 403-407.

204. Nijman, S. M.; Luna-Vargas, M. P.; Velds, A.; Brummelkamp, T. R.; Dirac, A. M.; Sixma, T. K.; Bernards, R., *Cell* **2005**, *123*, 773-786.

205. Lee, M. J.; Lee, B. H.; Hanna, J.; King, R. W.; Finley, D., *Mol. Cell. Proteomics* **2011**, *10*, R110.003871.

206. Koulich, E.; Li, X.; DeMartino, G. N., *Mol. Biol. Cell* **2008**, *19*, 1072-1082.

207. Kim, H. T.; Goldberg, A. L., *J. Biol. Chem.* **2017**, *292*, 9830-9839.

208. Aufderheide, A.; Beck, F.; Stengel, F.; Hartwig, M.; Schweitzer, A.; Pfeifer, G.; Goldberg, A. L.; Sakata, E.; Baumeister, W.; Förster, F., *Proc. Natl. Acad. Sci. U.S.A* **2015**, *112*, 8626-8631.

209. Kuo, C. L.; Goldberg, A. L., *Proc. Natl. Acad. Sci. U S A* **2017**, *114*, E3404-e3413.

210. Lee, B. H.; Lu, Y.; Prado, M. A.; Shi, Y.; Tian, G.; Sun, S.; Elsasser, S.; Gygi, S. P.; King, R. W.; Finley, D., *Nature* **2016**, *532*, 398-401.

211. Moon, S.; Muniyappan, S.; Lee, S.-B.; Lee, B.-H., *Int. J. Mol. Sci.* **2021**, *22*, 6213.

212. Lam, Y. A.; Xu, W.; DeMartino, G. N.; Cohen, R. E., *Nature* **1997**, *385*, 737-740.

213. Deol, K. K.; Crowe, S. O.; Du, J.; Bisbee, H.; Guenette, R. G.; Strieter, E. R., *Mol. Cell* **2020**, *80*, 796-809.

214. Boselli, M.; Lee, B. H.; Robert, J.; Prado, M. A.; Min, S. W.; Cheng, C.; Silva, M. C.; Seong, C.; Elsasser, S.; Hatle, K. M.; et al., *J. Biol. Chem.* **2017**, *292*, 19209-19225.

215. Wang, Y.; Jiang, Y.; Ding, S.; Li, J.; Song, N.; Ren, Y.; Hong, D.; Wu, C.; Li, B.; Wang, F.; et al., *Cell Res.* **2018**, *28*, 1186-1194.

216. Palmer, A. L.; de Jong, A.; Leestemaker, Y.; Geurink, P. P.; Wijdeven, R. H.; Ovaa, H.; Dolan, B. P., *J. Immun.* **2018**, *200*, 928-936.

217. Kim, E.; Park, S.; Lee, J. H.; Mun, J. Y.; Choi, W. H.; Yun, Y.; Lee, J.; Kim, J. H.; Kang, M. J.; Lee, M. J., *Cell Rep.* **2018**, *24*, 732-743.

218. VerPlank, J. J.; Goldberg, A. L., *Biochem. J.* **2017**, *474*, 3355-3371.

219. Zhang, F.; Hu, Y.; Huang, P.; Toleman, C. A.; Paterson, A. J.; Kudlow, J. E., *J. Biol. Chem.* **2007**, *282*, 22460-22471.

220. Asai, M.; Tsukamoto, O.; Minamino, T.; Asanuma, H.; Fujita, M.; Asano, Y.; Takahama, H.; Sasaki, H.; Higo, S.; Asakura, M.; et al., *J Mol Cell Cardiol* **2009**, *46*, 452-462.

221. Lokireddy, S.; Kukushkin, N. V.; Goldberg, A. L., *Proc. Natl. Acad. Sci. U S A* **2015**, *112*, E7176-E7185.

222. VerPlank, J. J.; Lokireddy, S.; Zhao, J.; Goldberg, A. L., *Proc. Natl. Acad. Sci. U S A* **2019**, *116*, 4228-4237.

223. Banerjee, S.; Ji, C.; Mayfield, J. E.; Goel, A.; Xiao, J.; Dixon, J. E.; Guo, X., *Proc. Natl. Acad. Sci.* **2018**, *115*, 8155.

224. Guo, X.; Wang, X.; Wang, Z.; Banerjee, S.; Yang, J.; Huang, L.; Dixon, J. E., *Nat. Cell Biol.* **2016**, *18*, 202-212.

225. Djakovic, S. N.; Schwarz, L. A.; Barylko, B.; DeMartino, G. N.; Patrick, G. N., *J. Biol. Chem.* **2009**, *284*, 26655-26665.

226. Djakovic, S. N.; Marquez-Lona, E. M.; Jakawich, S. K.; Wright, R.; Chu, C.; Sutton, M. A.; Patrick, G. N., *J. Neurosci.* **2012**, *32*, 5126.

227. Schaler, A. W.; Myeku, N., *Transl. Res.* **2018**, *193*, 31-41.

228. Zhu, J.; Mix, E.; Winblad, B., *CNS Drug Rev.* **2001**, *7*, 387-398.

229. ASHP. *Cilostazol Monographs for Professionals*. https://www.drugs.com/monograph/cilostazol.html (accessed 2021 4 August 2021).

230. *A Trial of Cilostazol in Patients With Mild Cognitive Impairment (COMCID)*. https://clinicaltrials.gov/ct2/show/NCT02491268 (accessed 4 August 2021).

231. VerPlank, J. J. S.; Tyrkalska, S. D.; Fleming, A.; Rubinsztein, D. C.; Goldberg, A. L., *Proc. Natl. Acad. Sci. U S A* **2020**, *117*, 14220.

232. Yokota, T.; Wang, Y., *Gene* **2016**, *575*, 369-376.

233. Li, H. N.; Yang, Q. Q.; Wang, W. T.; Tian, X.; Feng, F.; Zhang, S. T.; Xia, Y. T.; Wang, J. X.; Zou, Y. W.; Wang, J. Y.; et al., *J. Neuroinflammation* **2021**, *18*, 150.

234. Lee, S.-H.; Park, Y.; Yoon, S. K.; Yoon, J.-B., *J. Biol. Chem.* **2010**, *285*, 41280-41289.

235. Zhu, X.; Rottkamp, C. A.; Boux, H.; Takeda, A.; Perry, G.; Smith, M. A., *J. Neuropathol. Exp. Neurol.* **2000**, *59*, 880-888.

236. Atzori, C.; Ghetti, B.; Piva, R.; Srinivasan, A. N.; Zolo, P.; Delisle, M. B.; Mirra, S. S.; Migheli, A., *J. Neuropathol. Exp. Neurol.* **2001**, *60*, 1190-1197.

237. Tortarolo, M.; Veglianese, P.; Calvaresi, N.; Botturi, A.; Rossi, C.; Giorgini, A.; Migheli, A.; Bendotti, C., *Mol. Cell. Neurosci.* **2003**, *23*, 180-192.

238. Munoz, L.; Ammit, A. J., *Neuropharmacology* **2010**, *58*, 561-568.

239. Huang, Z.-N.; Chen, J.-M.; Huang, L.-C.; Fang, Y.-H.; Her, L.-S., *Mol. Neurobiol.* **2021**, *58*, 2704-2723.

240. Gaczynska, M.; Rock, K. L.; Spies, T.; Goldberg, A. L., *Proc. Natl. Acad. Sci. U S A* **1994**, *91*, 9213-9217.

241. Gaczynska, M.; Goldberg, A. L.; Tanaka, K.; Hendil, K. B.; Rock, K. L., *J. Biol. Chem.* **1996**, *271*, 17275-17280.

242. Chondrogianni, N.; Tzavelas, C.; Pemberton, A. J.; Nezis, I. P.; Rivett, A. J.; Gonos, E. S., *J. Biol. Chem.* **2005**, *280*, 11840-11850.

243. Vilchez, D.; Boyer, L.; Morantte, I.; Lutz, M.; Merkwirth, C.; Joyce, D.; Spencer, B.; Page, L.; Masliah, E.; Berggren, W. T.; et al., *Nature* **2012**, *489*, 304-308.

244. Kapeta, S.; Chondrogianni, N.; Gonos, E. S., *J. Biol. Chem.* **2010**, *285*, 8171-8184.

245. Kwak, M.-K.; Wakabayashi, N.; Greenlaw Jennifer, L.; Yamamoto, M.; Kensler Thomas, W., *Mol. Cell. Biol.* **2003**, *23*, 8786-8794.

246. Yueh, M. F.; Tukey, R. H., *J. Biol. Chem.* **2007**, *282*, 8749-8758.

247. Hayes, J. D.; Chanas, S. A.; Henderson, C. J.; McMahon, M.; Sun, C.; Moffat, G. J.; Wolf, C. R.; Yamamoto, M., *Biochem. Soc. Trans.* **2000**, *28*, 33-41.

248. Venugopal, R.; Jaiswal, A. K., *Proc. Natl. Acad. Sci. U S A* **1996**, *93*, 14960.

249. Jang, J.; Wang, Y.; Kim, H. S.; Lalli, M. A.; Kosik, K. S., *Stem Cells* **2014**, *32*, 2616-2625.

250. Kwak, M. K.; Cho, J. M.; Huang, B.; Shin, S.; Kensler, T. W., *Free Radic Biol Med* **2007**, *43*, 809-817.

251. Tanaka, K.; Yoshimura, T.; Kumatori, A.; Ichihara, A.; Ikai, A.; Nishigai, M.; Kameyama, K.; Takagi, T., *J. Biol. Chem.* **1988**, *263*, 16209-16217.

252. Tanaka, K.; Yoshimura, T.; Ichihara, A., *J. Biochem.* **1989**, *106*, 495-500.

253. Huang, L.; Ho, P.; Chen, C. H., *FEBS Lett.* **2007**, *581*, 4955-4959.

254. Katsiki, M.; Chondrogianni, N.; Chinou, I.; Rivett, A. J.; Gonos, E. S., *Rejuvenation Res.* **2007**, *10*, 157-172.

255. Tan, Y.; Yu, R.; Pezzuto, J. M., *Clin. Cancer. Res.* **2003**, *9*, 2866-2875.

256. Ruiz de Mena, I.; Mahillo, E.; Arribas, J.; Castaño, J. G., *Biochem. J.* **1993**, *296 (Pt 1)*, 93-97.

257. Watanabe, N.; Yamada, S., *Plant Cell Physiol.* **1996**, *37*, 147-151.

258. Liu, H.; Du, D.-M., *Adv. Synth. Catal.* **2009**, *351*, 489-519.

259. Mehedi, M. S. A.; Tepe, J. J., *Adv. Synth. Catal.* **2020**, *362*, 4189-4225.

260. Sharma, V.; Peddibhotla, S.; Tepe, J. J., *J. Am. Chem. Soc.* **2006**, *128*, 9137-9143.

261. Kahlon, D. K.; Lansdell, T. A.; Fisk, J. S.; Hupp, C. D.; Friebe, T. L.; Hovde, S.; Jones, A. D.; Dyer, R. D.; Henry, R. W.; Tepe, J. J., *J. Med. Chem.* **2009**, *52*, 1302-1309.

262. Kahlon, D. K.; Lansdell, T. A.; Fisk, J. S.; Tepe, J. J., *Biorg. Med. Chem.* **2009**, *17*, 3093-3103.

263. Sztanke, K.; Pasternak, K.; Sidor-Wójtowicz, A.; Truchlińska, J.; Jóźwiak, K., *Biorg. Med. Chem.* **2006**, *14*, 3635-3642.

264. Sharma, V.; Lansdell, T. A.; Peddibhotla, S.; Tepe, J. J., *Chem. Biol.* **2004**, *11*, 1689-1699.

265. Brewer, M. D.; Dorgan, R. J. J.; Manger, B. R.; Mamalis, P.; Webster, R. A. B., *J. Med. Chem.* **1987**, *30*, 1848-1853.

266. Crane, L.; Anastassiadou, M.; Hage, S. E.; Stigliani, J. L.; Baziard-Mouysset, G.; Payard, M.; Leger, J. M.; Bizot-Espiard, J.-G.; Ktorza, A.; Caignard, D.-H.; et al., *Biorg. Med. Chem.* **2006**, *14*, 7419-7433.

267. Szabo, B., *Pharmacol. Ther.* **2002**, *93*, 1-35.

268. Savelyeva, M. V.; Baldenkov, G. N.; Kaverina, N. V., *Biomed Biochim Acta* **1988**, *47*, 1085-1087.

269. Medina, D. X.; Caccamo, A.; Oddo, S., *Brain Pathol* **2011**, *21*, 140-149.

270. Zhou, L.; Flores, J.; Noël, A.; Beauchet, O.; Sjöström, P. J.; LeBlanc, A. C., *Acta Neuropathol. Commun.* **2019**, *7*, 210.

271. Li, W.-J.; Li, Q.; Liu, D.-L.; Ding, M.-W., *J. Agric. Food Chem.* **2013**, *61*, 1419-1426.

272. Patterson, S.; Alphey, M. S.; Jones, D. C.; Shanks, E. J.; Street, I. P.; Frearson, J. A.; Wyatt, P. G.; Gilbert, I. H.; Fairlamb, A. H., *J. Med. Chem.* **2011**, *54*, 6514-6530.

273. Lee, J. Y.; Park, S. J.; Park, S. J.; Lee, M. J.; Rhim, H.; Seo, S. H.; Kim, K.-S., *Bioorg. Med. Chem. Lett.* **2006**, *16*, 5014-5017.

274. Heo, J. H.; Seo, H. N.; Choe, Y. J.; Kim, S.; Oh, C. R.; Kim, Y. D.; Rhim, H.; Choo, D. J.; Kim, J.; Lee, J. Y., *Bioorg. Med. Chem. Lett.* **2008**, *18*, 3899-3901.

275. Al-Obaid, A. M.; Abdel-Hamide, S. G.; El-Kashef, H. A.; Alaa, A.-M.; El-Azab, A. S.; Al-Khamees, H. A.; El-Subbagh, H. I., *Eur. J. Med. Chem.* **2009**, *44*, 2379-2391.

276. Jung, S. Y.; Lee, S. H.; Kang, H. B.; Park, H. A.; Chang, S. K.; Kim, J.; Choo, D. J.; Oh, C. R.; Kim, Y. D.; Seo, J. H., *Bioorg. Med. Chem. Lett.* **2010**, *20*, 6633-6636.

277. Kang, H. B.; Rim, H.-K.; Park, J. Y.; Choi, H. W.; Choi, D. L.; Seo, J.-H.; Chung, K.-S.; Huh, G.; Kim, J.; Choo, D. J., *Bioorg. Med. Chem. Lett.* **2012**, *22*, 1198-1201.

278. Rim, H.-K.; Lee, H.-W.; Choi, I. S.; Park, J. Y.; Choi, H. W.; Choi, J.-H.; Cho, Y.-W.; Lee, J. Y.; Lee, K.-T., *Bioorg. Med. Chem. Lett.* **2012**, *22*, 7123-7126.

279. Jang, S. J.; Choi, H. W.; Choi, D. L.; Cho, S.; Rim, H.-K.; Choi, H.-E.; Kim, K.-S.; Huang, M.; Rhim, H.; Lee, K.-T., *Bioorg. Med. Chem. Lett.* **2013**, *23*, 6656-6662.

280. Goldner, T.; Hewlett, G.; Ettischer, N.; Ruebsamen-Schaeff, H.; Zimmermann, H.; Lischka, P., *J. Virol.* **2011**, *85*, 10884-10893.

281. Marschall, M.; Stamminger, T.; Urban, A.; Wildum, S.; Ruebsamen-Schaeff, H.; Zimmermann, H.; Lischka, P., *Antimicrob. Agents Chemother.* **2012**, *56*, 1135-1137.

282. Magyar, C. L.; Wall, T. J.; Davies, S. B.; Campbell, M. V.; Barna, H. A.; Smith, S. R.; Savich, C. J.; Mosey, R. A., *Org. Biomol. Chem.* **2019**, *17*, 7995-8000.

283. Vermeiren, C.; de Hemptinne, I.; Vanhoutte, N.; Tilleux, S.; Maloteaux, J. M.; Hermans, E., *J. Neurochem.* **2006**, *96*, 719-731.

284. Benmohamed, R.; Arvanites, A. C.; Kim, J.; Ferrante, R. J.; Silverman, R. B.; Morimoto, R. I.; Kirsch, D. R., *Amyotroph. Lateral. Scler.* **2011**, *12*, 87-96.

285. Santoro, A. M.; Lanza, V.; Bellia, F.; Sbardella, D.; Tundo, G. R.; Cannizzo, A.; Grasso, G.; Arizzi, M.; Nicoletti, V. G.; Alcaro, S.; et al., *ChemMedChem* **2020**, *15*, 302-316.

Chapter 4: Synthesis of pyrazolo[1,5-*b*]pyridazines analogs as potential 20S proteasome activator

4.1 Introduction

Protein structures span a broad spectrum, from those with well-defined shapes to proteins that lack a define tertiary structure. Proteins with no tertiary structure are often referred to as intrinsically disordered proteins (IDPs).[1] Intrinsically disordered proteins (IDPs) serve a range of critical functions in biological systems and their flexibility and adaptability enable them to participate in diverse cellular processes. IDPs play key roles in signal transduction, gene expression, scaffolding large protein complexes, and driving cell cycle progression.[2-3] Although, IDPs are essential in several cellular process, their accumulation and aggregation have been shown to induce toxic signaling.[4-5] Accumulation of IDPs such as α-synuclein, amyloid-β and tau, are classic hallmarks of Parkinson's and Alzheimer's disease respectively.[6] The build-up of these proteins has been shown to disrupt cellular proteostasis, ultimately leading to neuronal death and the further progression of the disease.[7-8]

Small molecule activation of the proteasome has been proposed as a potential strategy to treat neurodegenerative diseases by targeted degradation of these IDPs.[9-14] In **Chapter 3**, I discussed the structure of the proteasome and examine the link between its proteolytic activity, aging, and several neurodegenerative conditions. Additionally, I provided an overview of the different classes of compounds that are capable of enhancing the proteasome-mediated protein degradation, either directly or indirectly.[15]

The Tepe lab and other labs have identified various molecules that can enhance the proteolytic activity of the 20S proteasome.[9-14] Some of the identified activators from the Tepe's lab are shown in **Figure 4.1**. It is hypothesized that these small molecule activators binds to the α-

ring of the 20S proteasome to induce a ring-opening conformation and enhance the rate of proteolytic degradation of intrinsically disordered protein (IDPs) by increasing access to the catalytic core of the proteasome.

Figure 4.1: Structure of some known 20S proteasome activators from the Tepe's lab

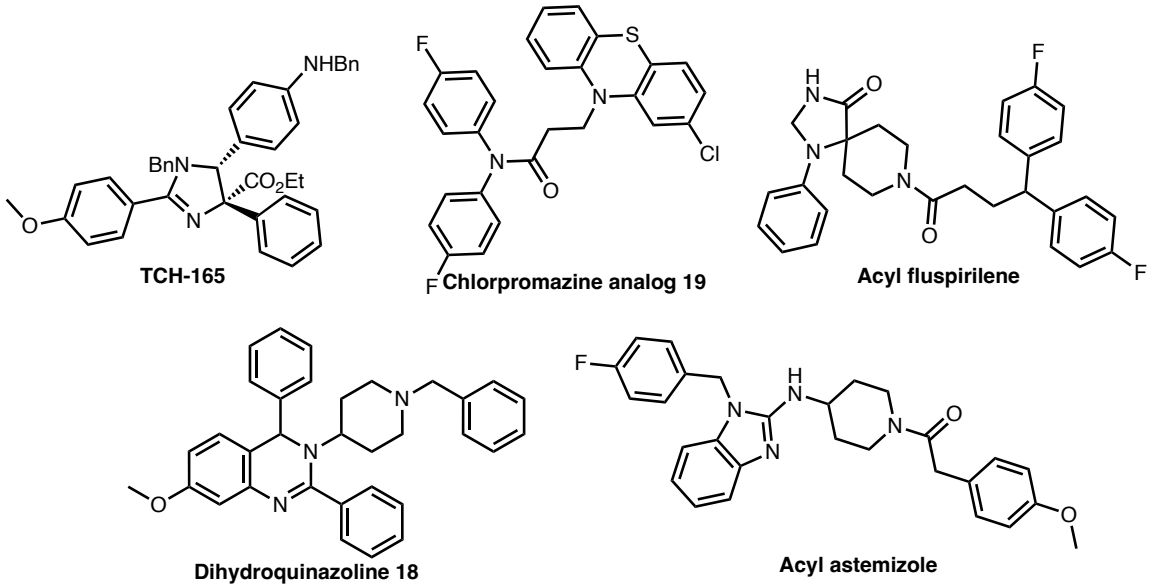

While some small molecule proteasome activators have been discovered, many exhibit only moderate potency, typically in the micromolar range, therefore limiting the clinical potential of these molecules. To thoroughly assess the feasibility of targeting the proteasome in vivo and to explore the clinical potential of this therapeutic strategy, more potent 20S proteasome enhancers are needed. These would enable a deeper investigation into the utility of proteasome activation in treating various neurodegenerative diseases.

Lipinski's Rule of Five is a set of guidelines derived from the observation that most orally available small-molecule drugs exhibit common chemical and physical traits. According to Lipinski, a typical small-molecule drug has a molecular weight (MW) under 500 g/mol, an octanol-water partition coefficient (cLog P) not exceeding 5, and a maximum of 5 hydrogen bond donors and 10 hydrogen bond acceptors.[16] These characteristics are associated with small molecules that can cross biological membranes to interact with target receptors. In the search for more potent 20S

proteasome enhancers that also adhere to Lipinski's rule of five, the Tepe lab conducted a cell-based high throughput screen of the Prestwick and NIH Clinical library.[17] From the 25,000 compounds screened in this library, compound **4-1** (also called **MSU-7**) was identified as a 20S proteasome enhancer (**Figure 4.2**).

Figure 4.2: Structure of compound **4-1 (MSU-7)**

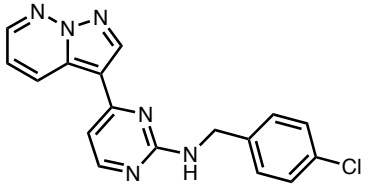

Compound **4-1** and its analogs has been previously identified as human kinase inhibitor, specifically GSK-3β, CDK-2, and CDK-4 with the potential of using this class of compounds for the treatment of solid tumors.[18] Several compounds of this class has also been studied with the goal of repurposing them for the treatment of human African trypanosomiasis.[19] We embark on the study of pyrazolo[1,5-*b*]pyridazine scaffolds with the goal of evaluating them as 20S proteasome enhancers and also discovering a more potent analog of this class of compound.

4.2 Results and Discussion

We started by first synthesizing compound **4-1** to verify its 20S proteasome activity. Using a previously establish approach[19-20], **4-1** was synthesized in 5 steps starting from dichloropyrimidine **4-2** (**Scheme 4.1**). Sonogashira coupling of **4-2** with trimethylsilylacetylene yielded the desired TMS-protected alkyne **4-3** which then underwent a TMS deprotection with potassium hydroxide to give the free alkyne **4-4** in good yield. Pyridazine **4-5** was also reacted with hydroxylamine-O-sulfonic acid (HOSA) to generate 1-aminopyridazin-1-ium iodide **4-6** in 87% yield. A [3+2] cycloaddition reaction between **4-6** and alkyne **4-3** provided the pyrazolo[1,5-*b*]pyridazines scaffold **4-7** as the final intermediate to the desired analog. Nucleophilic aromatic substitution with 4-chlorobenzylamine gave compound **4-1** (**MSU-7)** in 82% yield.

Scheme 4.1: Synthesis of compound **4-1** (**MSU-7**)

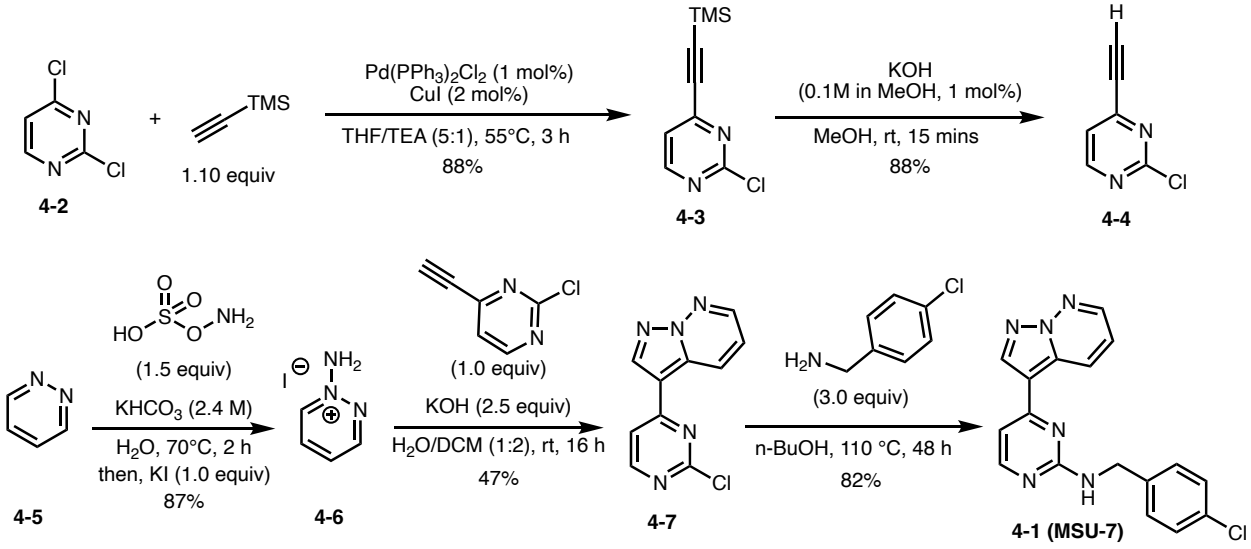

After the synthesis of **4-1** was achieved, its 20S proteasomal activity was validated by Sophia Staerz and Shannon Cartwright using western blot to measure the impact of **4-1** on purified IDP degradation by the 20S proteasome, in this case, α-synuclein degradation (**Figure 4.3a**). The cytotoxicity of compound **4-1** in H929 cells, a multiple myeloma cell line was also performed by Shannon Cartwright and the CC_{50} of compound **4-1** was determined to be 2.4 μM (**Figure 4.3b**). CC_{50} is the concentration at which 50% of the cancer cells were dead. From these preliminary data, I started the synthesis of different fragments of compound **4-1** to identify the fragment(s) that is important for the compound to maintain its 20S proteasomal activities.

Figure 4.3: (a) In vitro α-synuclein degradation with 20S proteasome using TCH as control N=3. (b) Cell viability assay of compound **4-1** in H929 cells. N=3

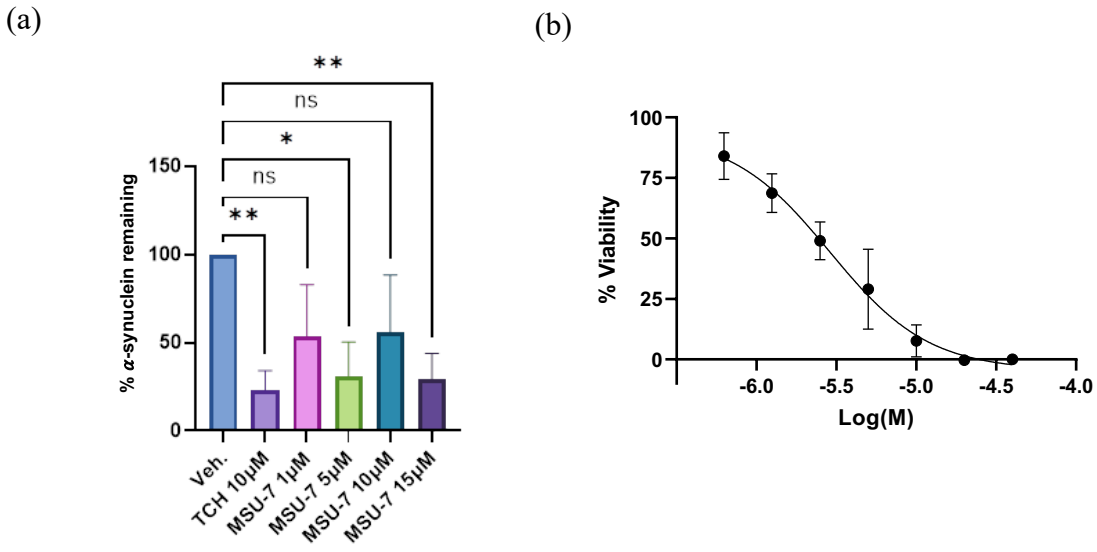

4.2.1 Investigation of different fragments of compound 4-1 for proteasome activity

4.2.1.1 Synthesis of fragments of compound 4-1 (MSU-7)

Following the synthesis and validation of **4-1** as 20S proteasome enhancer, I embarked on the synthesis of fragments of **4-1** with the goal of identifying the fragment needed to maintain proteolytic activity or if the entire structure of **4-1** is needed for activity. Compound **4-7** appears to be a good fragment that can be used to explore the effect of the 4-chlorobenzylamine on the activity of the hit compound. In addition to intermediate **4-7**, compounds **4-8** – **4-10** were also synthesized to investigate the important of the 4-chlorobenzyl fragment of **4-1**. Compounds **4-8** and **4-9** were synthesized using the approach outlined in **Scheme 4.2**. Compound **4-8** was accessed in 36% yield by heating **4-7** in excess ethanolic ammonia solution and **4-9** was synthesized by refluxing **4-7** with three equivalents of dimethylamine in *n*-butanol at 110 °C for 16 hours (**Scheme 4.2**). Unlike compounds **4-8** and **4-9**, accessing **4-10** was a little bit challenging. My initial approach to access **4-10** in a similar fashion for the synthesis of **4-7** using compound **4-6** and phenylacetylene gave no desired product. I hypothesize that the reaction failed because

phenylacetylene is an electron-rich alkyne; previous literature on the [3+2] cycloaddition has demonstrated success only with electron-deficient alkynes. Alternatively, following a slightly modified procedure from the literature (**Scheme 4.3**),[19] **4-10** was accessed starting from [3+2] cycloaddition of **4-6** with methyl propiolate to give ester **4-11**. Base hydrolysis of **4-11** gave carboxylic acid **4-12** in 96% yield, this was then followed by NBS-mediated Hunsdiecker reaction to give aryl bromide **4-13** in 77%. Suzuki coupling of **4-13** with phenylboronic acid gave the desired analog **4-10** in 86% yield.

Scheme 4.2: Synthesis of compound **4-8** and **4-9**

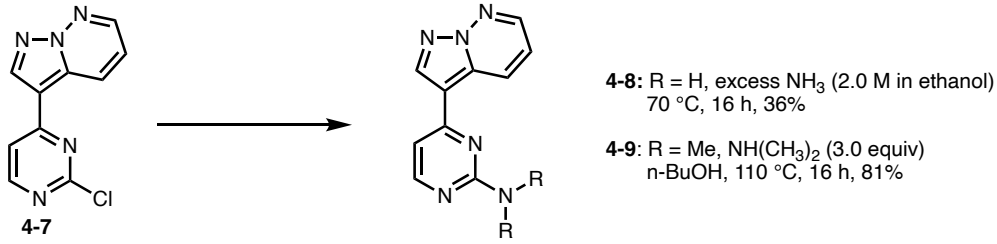

Scheme 4.3: Synthesis of **4-10**

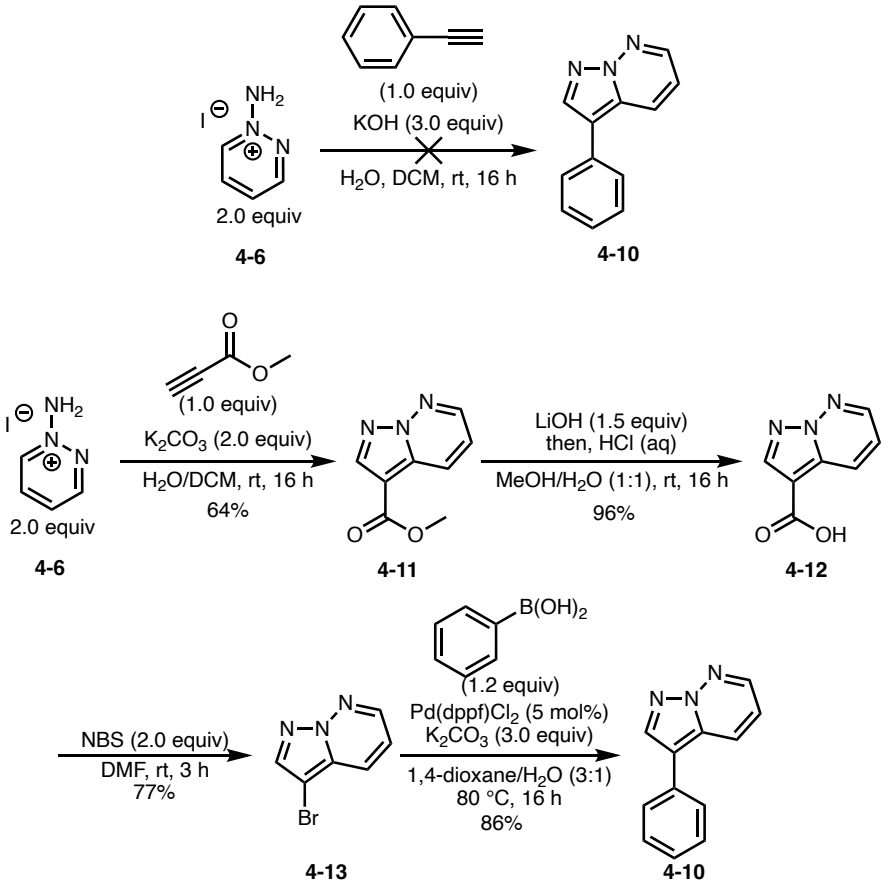

After the synthesis of **4-8** – **4-10** were achieved, I set out to synthesize molecules to investigate the importance of the triazole core in the proteasomal activity of **4-1**. Initially, the triazole core was replaced with a phenyl or indole to give **4-15** and **4-17,** respectively. Compound **4-15** was synthesized in two steps, first by a Suzuki coupling of **4-2** with phenylboronic acid to give **4-14** in 66% yield, followed by nucleophilic aromatic substitution with 4-chlorobenzylamine to give the desired analog **4-15** in 82% yield (**Scheme 4.4**). Using a slightly different approach, the indole analog **4-17** was synthesized by deprotonating 1*H*-indole using phenylmagnesium bromide. The deprotonated indole was then reacted with **4-2** under reflux for 48 hours, resulting in **4-16**. Nucleophilic aromatic substitution of **4-16** with 4-chlorobenzylamine yielded **4-17** in up

to 74% yield. The final analog **4-19** was also synthesized to probe the effect of the absence of any aromatic substituent at the triazole position in compound **4-1**.

Scheme 4.4: Synthesis of analog **4-15**, **4-17**, and **4-19**

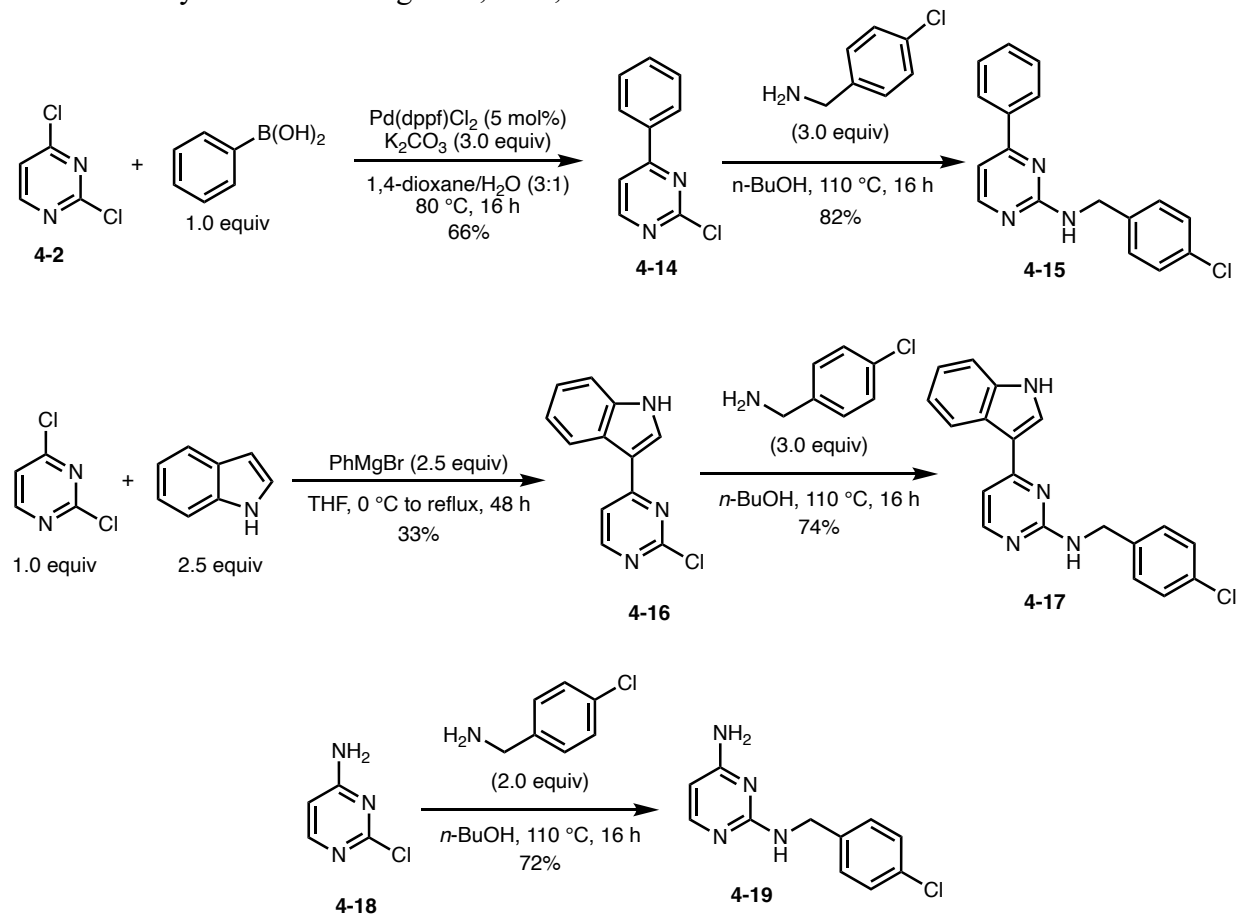

4.2.1.2 Evaluation of compound 4-1 (MSU-7) fragments towards the 20S proteasome

The activity of compound **4-7** – **4-10**, **4-15**, **4-17**, and **4-19** towards the 20S proteasome were determined by Shannon Cartwright. The assay utilizes fluorogenic 7-amino-methylcoumarin (AMC) conjugated small peptides that correspond to each of the three catalytic sites of the 20S proteasome. The three fluorogenic small peptides that were used are Suc-LLVY-AMC, Boc-LRR-AMC, and Z-LLE-AMC corresponding to the chymotrypsin-like (CT-L), trypsin-like (T-L), and caspase-like (Casp-L) sites of the 20S proteasome, respectively. Typically, purified human 20S proteasome is pretreated with varying concentration of compounds followed by the three

fluorogenic probes. Cleavage of the peptides by 20S proteasome results in the release of AMC which is then measured over time to quantify the proteolytic activity of the 20S proteasome. From this experiment, the concentration required to increase the activity of 20S proteasome by 200% (EC_{200}) and maximum fold enhancement (Max fold increase) over vehicle are usually determined.

Table 4.1: Small peptide activity of compound **4-1** (**MSU-7**) fragments

Compound	Molecular Weight (g/mol)	cLogP	EC_{200}	Max Fold Increase at 80 µM
4-8	210.24	2.19	-	-
4-9	240.27	0.79	ND	1.2
4-10	195.23	3.41	-	-
4-15	295.77	2.91	ND	1.8
4-17	334.81	2.90	-	-
4-19	234.69	-0.42	ND	1.1

From the table shown above, fragments of compound **4-1** that were tested in the small peptide assay showed no proteasome activity with no EC_{200} due to the compound not attaining 200% activity over vehicle. Since the elimination the benzyl group (**4-9**) or the triazole core (**4-19**) resulted in inactive compounds, we hypothesized that both the triazole core and the benzyl fragment of compound **4-1** are necessary to maintain its proteasomal activity.

4.2.2 Synthesis of analogs of compound 4-1 (MSU-7) with focus on the tail piece

After using a fragment-based approach to determine which fragment of **4-1** is necessary to maintain proteasomal activity, the results showed that the entire structure might be needed for activity. I focused on synthesizing new analogs of **4-1** by first focusing on the tail end of the molecule. Analogs **4-20** to **4-28** were synthesized by three different types of chemistries. Compound **4-20** – **4-25** were accessed by nucleophilic aromatic substitution of **4-7** with

benzylamines or anilines (**Scheme 4.5**). While this approach is robust with various amines and anilines, anilines containing tertiary amines did not give the desired product due to the higher reactivity of the tertiary amine over the aniline group (**Scheme 4.5**, **a1** & **a2**).

Scheme 4.5: Synthesis of analog **4-20** – **4-45** by nucleophilic aromatic substitution and limitations

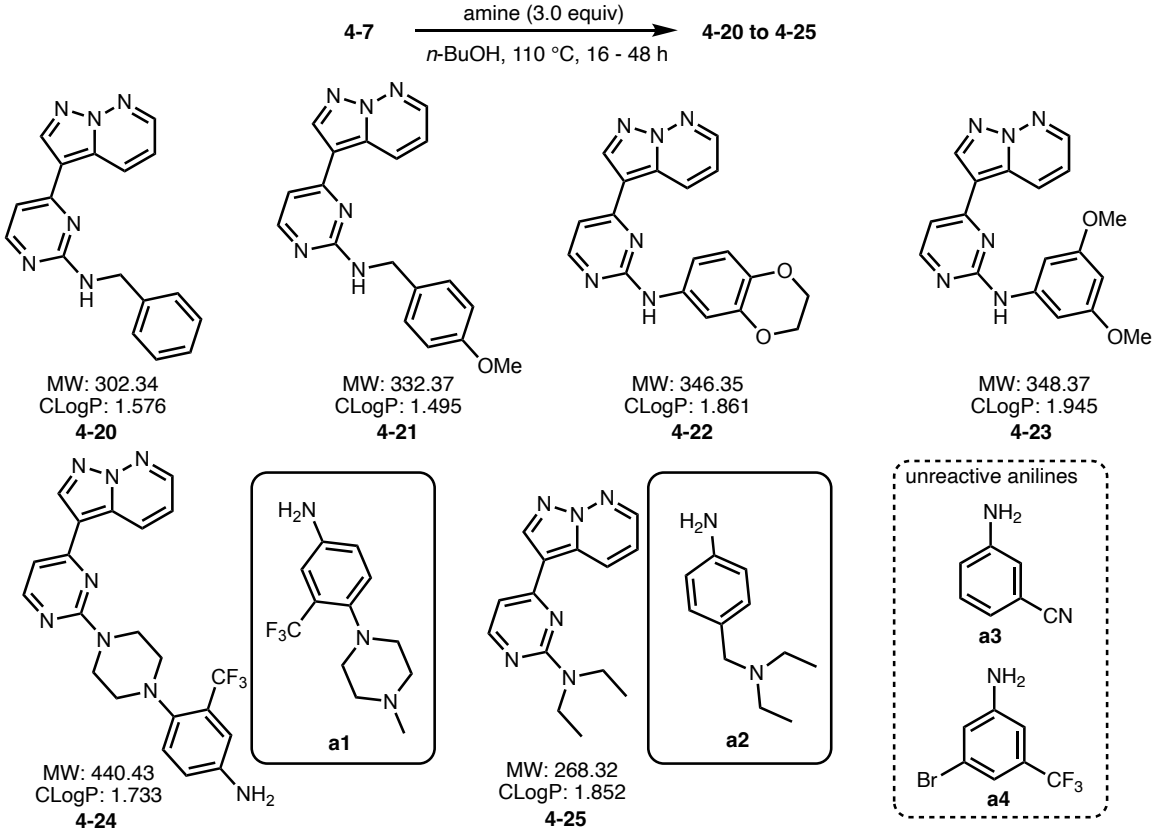

Additionally, nucleophilic aromatic substitution failed for electron deficient aniline (**Scheme 4.5**, compound **a3** & **a4**) and resulted in no product formation. Electron deficient aniline analogs such as **a3** can be accessed using Buchward-Hartwig coupling of the **a3** with **4-7** (**Scheme 4.6**). While this approach afforded analog **4-26**, anilines containing tertiary amine such as **a1** and **a2** did not give the desired product.

Scheme 4.6: Synthesis of analog **4-26** by Buchward-Hartwig coupling

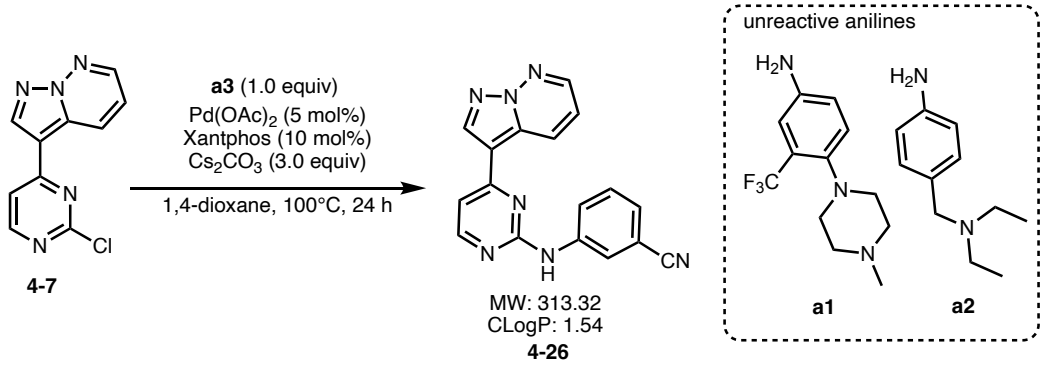

Analogs of anilines containing tertiary amines that could not be synthesized through either the nucleophilic substitution reaction or Buchward-Hartwig coupling were synthesized using a different approach shown in **Scheme 4.7.**[18,21] The reaction of 1-aminopyridazin-1-ium iodide with 3-butyn-2-one afforded compound **4-29** in 86%. The subsequent reaction of **4-29** with N,N-dimethylformamide dimethyl acetal (DMF-DMA) gave β-amino-α,β-enone **4-30** in 77% yield. Analogs **4-27** and **4-28** were then access by reacting **4-30** with the corresponding guanidine.

Scheme 4.7: Synthesis of analogs **4-27** and **4-28**

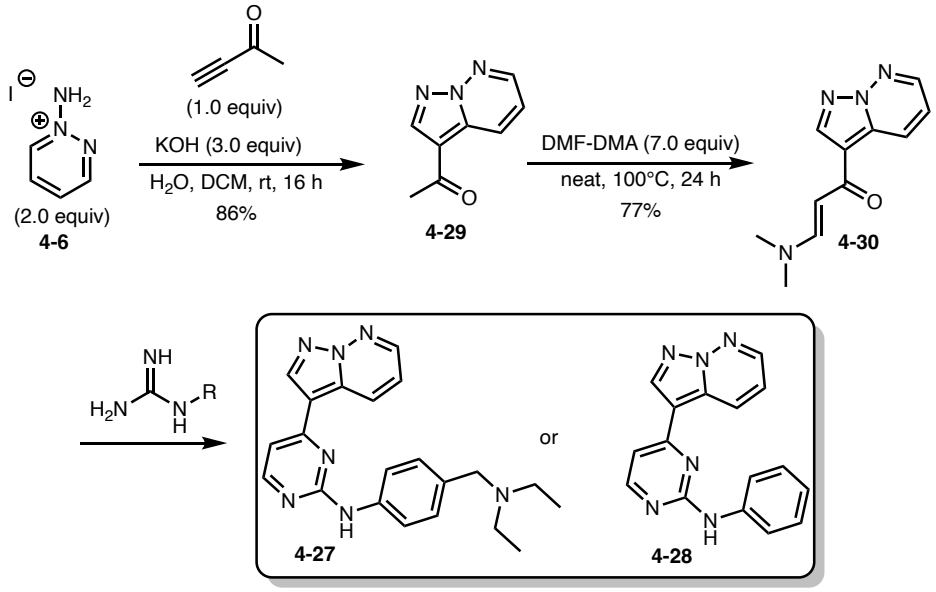

Following the synthesis of these analogs, their proteasomal activity were explored using the small peptide assay described in section **4.2.1.2** above by Shannon Cartwright. From this

experiment, inconsistent results were obtained for the compounds indicating that something else was affecting the activity. It was hypothesized that the pyrazolo[1,5-*b*]pyridazines exhibit inherent fluorescence that might be interfering with the fluorescence in the assay read-out. To test the hypothesis, Shannon took fluorescence readings comparing compound **4-1** (**MSU-7**) with TCH-165. TCH-165 is a known proteasome activator from our lab and has been used as control in most of our lab assays. **Figure 4.4** showed the fluorescence reading of TCH-165 + 20S proteasome, MSU-7 + 20S proteasome, Blank + MSU-7, and vehicle. TCH-165 + 20S proteasome and MSU-7 + 20S proteasome samples contains the compound, 20S proteasome, and substrate. Blank + MSU-7 contains buffer, compound, and substrate. From the data shown in **Figure 4.4**, we could conclude that MSU-7 has inherent fluorescence that affect the fluorescence readings in the assay.

Figure 4.4: Fluorescent readings (time = 0) of small peptide assay comparing MSU-7 and TCH-165 at different concentration. Data obtained by Shannon Cartwright

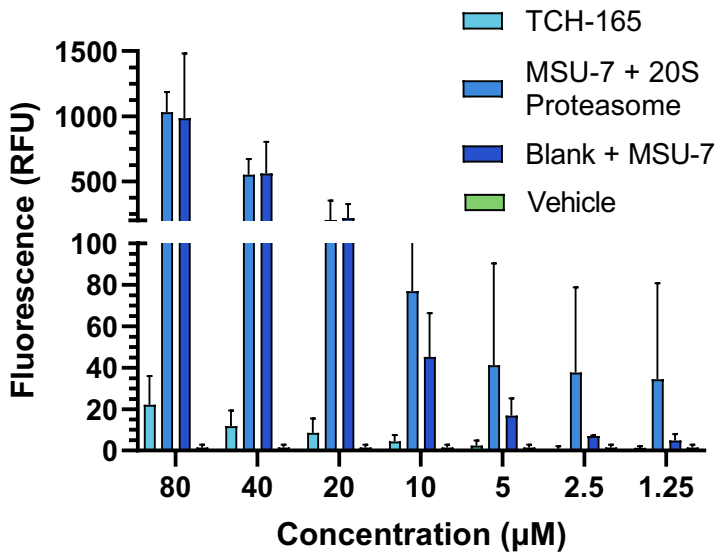

To further confirm the hypothesis of the fluorescence of MSU-7 interfering the small peptide assay, the absorption and emission of MSU-7 compared to free, and peptide bound AMC were determined. The data showed that MSU-7 absorbs and emits at a wavelength that overlaps

with both free and peptide bound AMC probe (suc-LLVY-AMC) making it difficult to accurately determine the 20S proteasome activity of MSU-7 or it's analogs using small peptide AMC probes.

Figure 4.5: Absorbance and emission measurements of MSU-7, suc-LLVY-AMC, and free AMC. Data obtained by Shannon Cartwright

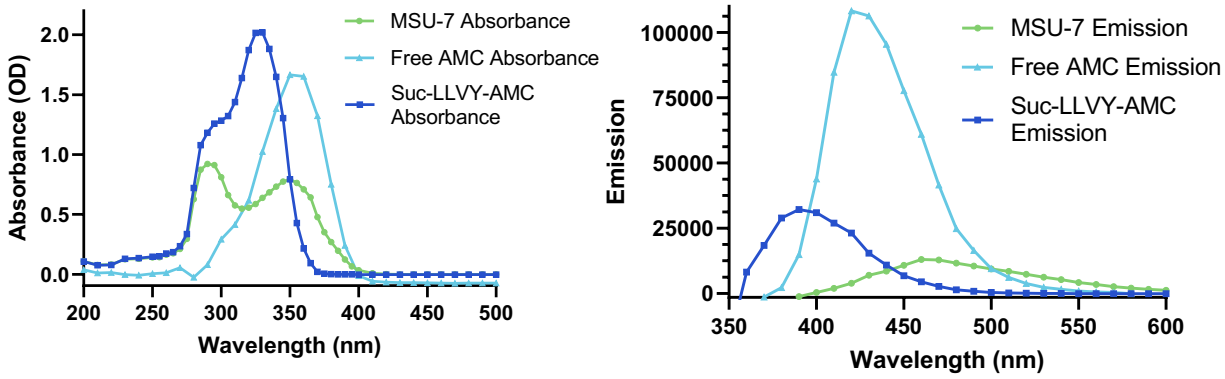

From a structural perspective, I hypothesized that the inherent fluorescence of MSU-7 could be attributed to the conjugation of the triazole core to the pyrimidine and the planarity of the molecule. To address this fluorescence problem from a synthesis perspective, I designed new scaffold similar to that of MSU-7. In the new scaffold, the triazole core was replaced with indole and the indole was conjugated with the pyrimidine through the nitrogen (**Figure 4.6**). The N-conjugated indole pyrimidine would prevent electron donation from the indole to the pyrimidine and ultimately reducing the fluorescence of the new analogs. It is also important to mention that C-3 conjugated indole pyrimidine did not eliminate the fluorescence of the molecule as expected.

Figure 4.6: Proposed approach proposed to reduce fluorescence of the analogs

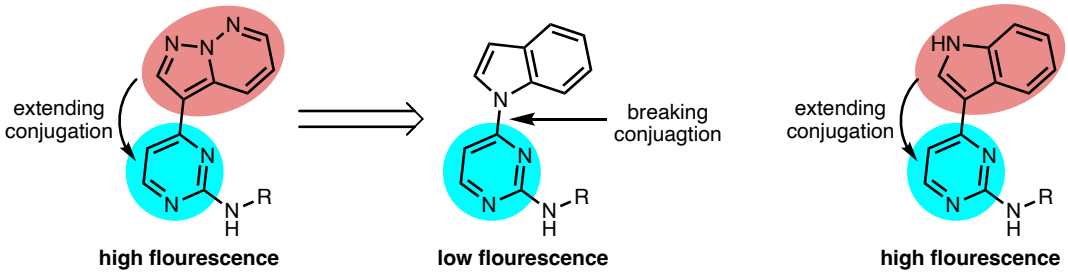

To access the N-conjugated indole pyrimidine analog of MSU-7, indole was deprotonated with sodium hydride and treated with 2,3-dichloropyrimidine to give compound **4-31**. Nucleophilic addition of 4-chlorobenzylamine to **4-31** gave analog **4-32**. As hypothesized, compound **4-32** showed low fluorescence and was able to be tested in the small peptide assay. Unfortunately, the compound showed no proteasomal activity in the assay.

Scheme 4.8: Synthesis of low fluorescence MSU-7 analog **4-32**

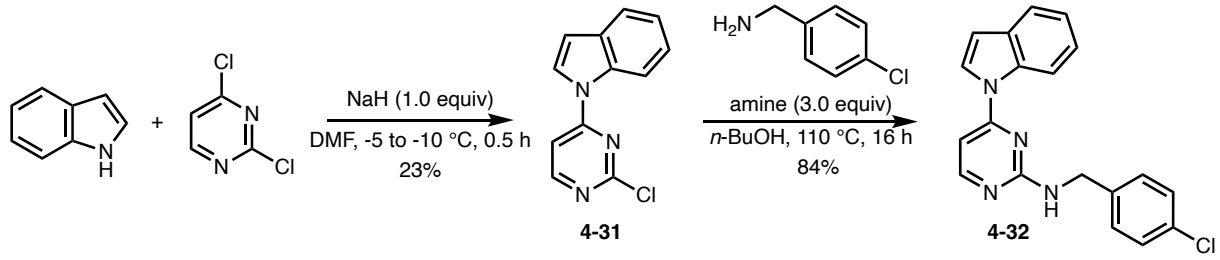

4.3 Conclusion

Although several analogs of pyrazolo[1,5-*b*]pyridazines were synthesized, the potential of these compounds as 20S proteasome enhancers still remains unexplored. The compounds could not be studied for 20S proteasome activation due to their inherent fluorescence that interfere with the fluorescence being measured in the small peptide assay. One potential solution to study these molecules would involve the utilization of non-fluorescence assay. This study is still ongoing and the proteasomal activity of the synthesized analogs would be evaluated when suitable assay becomes available in the lab.

4.4 Experimental

General information

All flasks were oven-dried overnight and cooled under nitrogen. Reactions were carried out under a nitrogen atmosphere unless stated otherwise. All chemicals and solvents were purchased from commercial sources and used without further purification, unless otherwise mentioned. THF and DCM were dried by passing it through packed column of alumina or over activated 3Å molecular sieves. Infrared spectra were recorded on a Jasco Series 6600 FTIR spectrometer. The mass spectrometer ionization method was ESI with a quadrupole detector. ^{1}H and ^{13}C NMR spectra were recorded on a 500 MHz spectrometer. Chemical shifts are reported relative to the residue peaks of the solvent: $CDCl_3$: 7.26 ppm for ^{1}H and 77.0 ppm for ^{13}C, CD_3OD: 3.31 ppm for ^{1}H and 47.6 ppm for ^{13}C, and DMSO-d_6: 2.50 ppm for ^{1}H and 39.5 ppm for ^{13}C. Signal multiplicities are given as s (singlet), br (broad), d (doublet), t (triplet), dd (doublet of doublet), and m (multiplet). Reaction carried out at room temperature (rt) implies temperature range usually between 20 – 22 °C. Column chromatography was performed using a Teledyne ISCO CombiFlash® NextGen system with prepacked columns (RediSep® Normal-phase silica, 20-40 microns). TLCs were performed on pre-coated 0.25 mm thick silica gel 60 F254 plates and pre-coated 150 um thick, visualized using UV light and iodine staining.

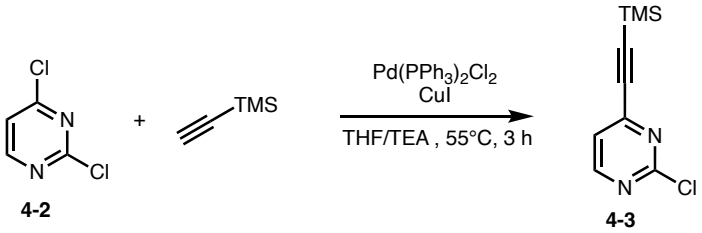

2-chloro-4-((trimethylsilyl)ethynyl)pyrimidine (4-3): To a solution of 2,4-dichloropyrimidine **4-2** (4.47 g, 30.0 mmol) in degassed tetrahydrofuran (50 mL) and degassed triethylamine (10 mL) was added bis(triphenylphosphine)palladium(II) dichloride $PdCl_2(PPh_3)_2$ (1 mol%, 0.21 g, 0.30

mmol). Then, copper(I) iodide (2 mol%, 0.114 g, 0.60 mmol) and trimethylsilylacetylene (4.38 mL, 33.0 mmol) was added. A color change from orange to dark brown was observed after adding the alkyne. The reaction was then heated to 55 °C for 3 hours and then cooled to room temperature. The triethylammonium salt was filtered out and washed with ethyl acetate. The filtrate was concentrated and purified with CombiFlash chromatography (silica gel, 20-40 microns, gradient 0-10% ethyl acetate/hexane) to give the product as a brown solid (5.56 g, 88%). ^{1}H NMR (500 MHz, $CDCl_3$) δ 8.54 (d, J = 5.0 Hz, 1H), 7.27 (d, J = 5.0 Hz, 1H), 0.20 (s, 9H). $^{13}C\{^{1}H\}$ NMR (125 MHz, $CDCl_3$) δ 161.4, 159.5, 152.6, 121.9, 103.4, 100.0, -0.7. The spectroscopy data are consistent with previous literature reports.[19]

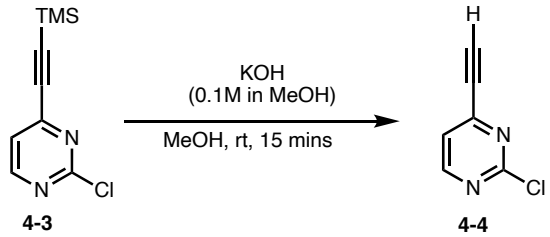

4-3 **4-4**

2-chloro-4-ethynylpyrimidine (4-4): A 50 mL round bottom flask equipped with stirrer bar was charged with **4-3** (4.0 g, 18.98 mmol), then methanol (20 mL) was added. Potassium hydroxide (0.1M in MeOH, 0.99 mL, 0.095 mmol) was added and the reaction was stirred for 15 minutes at room temperature after which TLC shows complete conversion. The reaction was stopped, and the solvent was evaporated. The crude was then purified with CombiFlash chromatography (silica gel, 20-40 microns, gradient 5% ethyl acetate/hexane) to give the product as off-white solid (2.31 g, 88%). ^{1}H NMR (500 MHz, $CDCl_3$) δ 8.63 (d, J = 5.0 Hz, 1H), 7.37 (d, J = 5.0 Hz, 1H), 3.47 (s, 1H). $^{13}C\{^{1}H\}$ NMR (125 MHz, CDCl3) δ 161.6, 159.8, 152.2, 122.2, 83.8, 79.6. The spectroscopy data are consistent with previous literature reports.[19]

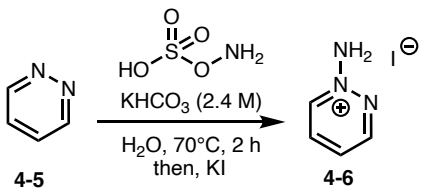

4-5 4-6

1-aminopyridazin-1-ium iodide (4-6): To a solution of hydroxylamine-O-sulfonic acid, HOSA, (7.01 g, 61.98 mmol) in water (15 mL) was added aqueous potassium bicarbonate $KHCO_3$ (2.4M) until the pH is approximately 5. Then, pyridazine **4-5** (3.0 g, 41.32 mmol) was added. The reaction was placed in pre-heated oil bath at 70 °C and stirred for 1.5 hours. The reaction was neutralized with 2.4 M aqueous $KHCO_3$ until pH is approximately 7. The reaction was cooled to 60 °C and potassium iodide (6.87 g, 41.32 mmol) in water (15 mL) was added and the reaction was further stirred for 1 hour. The reaction was concentrated to remove the water and a solution of 5% MeOH in EtOH (50 mL) was then added to the residue. The product was filtered and dried under vacuum to give the desired product as a yellow solid (8.05 g, 87%). ^{1}H NMR (500 MHz, DMSO-d_6) δ 9.80 (s, 2H), 9.26 – 9.21 (m, 1H), 9.09 (dt, J = 6.2, 1.0 Hz, 1H), 8.46 (ddd, J = 8.2, 6.2, 2.1 Hz, 1H), 8.10 (ddd, J = 8.2, 5.2, 1.0 Hz, 1H). ^{13}C{^{1}H} NMR (125 MHz, DMSO-d_6) δ 153.3, 137.4, 135.3, 129.4. The spectroscopy data are consistent with previous literature reports.[19]

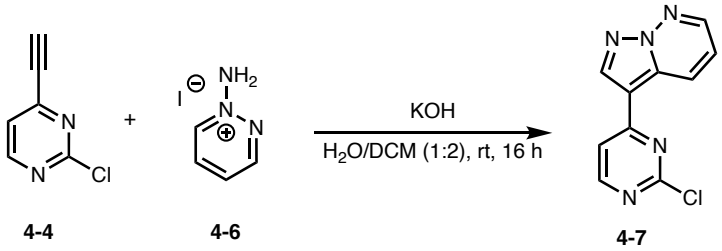

4-4 4-6 4-7

3-(2-chloropyrimidin-4-yl)pyrazolo[1,5-*b*]pyridazine (4-7): Alkyne **4-4** (0.91 g, 6.60 mmol) was added to a slurry of **4-6** (2.94 g, 13.20 mmol) in DCM/H_2O (2:1) (39 mL) followed by potassium hydroxide KOH (0.93 g, 16.50 mmol). The reaction was then stirred at room temperature overnight for 16 hours. The reaction was diluted with dichloromethane (15 mL) and

water (20 mL) and the organic layer was collected. The aqueous layer was further extracted with dichloromethane (3 x 30 mL) and the organics were combined, dried over sodium sulfate, filtered, concentrated, and purified with CombiFlash chromatography (silica gel, 20-40 microns, gradient 2% methanol/dichloromethane) to give the product as off-white solid (0.72 g, 47%). ^{1}H NMR (500 MHz, DMSO-d_6) δ 9.02 (s, 1H), 8.88 (d, J = 9.0 Hz, 1H), 8.74 – 8.65 (m, 2H), 8.05 (d, J = 5.4 Hz, 1H), 7.56 (dd, J = 9.0, 4.5 Hz, 1H). ^{13}C{^{1}H} NMR (125 MHz, DMSO-d_6) δ 160.2, 144.6, 140.7, 128.9, 120.3, 115.4 (Quaternary carbons were not observed in the C-13 NMR). HRMS (ESI-TOF) *m/z:* $[M+H]^+$ calcd for ($C_{10}H_7ClN_5^+$) 232.0385 & 234.0355; found 232.0387 & 234.0358. The spectroscopy data are consistent with previous literature reports.[19]

General procedure for nucleophilic aromatic substitution

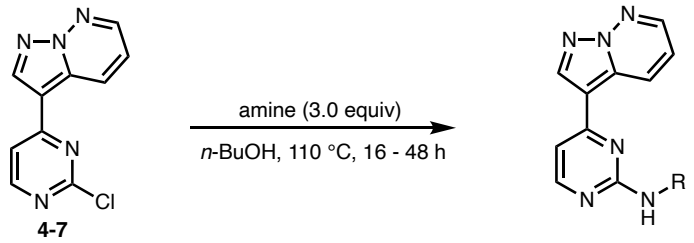

4-7

To a suspension of compound **4-7** (1.0 equiv) in *n*-butanol (3 mL) in a sealed tube was added amine (3.0 equiv). The mixture was placed in a pre-heated oil bath at 110 °C and stirred for 16 – 48 hours. The reaction was cooled to room temperature and the solvent was removed under pressure. The mixture was purified with CombiFlash chromatography to give the product.

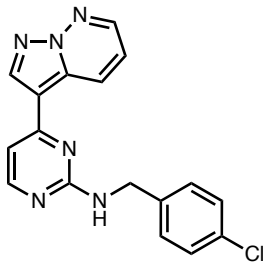

***N*-(4-chlorobenzyl)-4-(pyrazolo[1,5-*b*]pyridazin-3-yl)pyrimidin-2-amine (4-1):** Synthesized according to the general procedure for nucleophilic aromatic substitution with **4-7** (0.18 g, 0.78

mmol), 4-chlorobenzylamine (0.29 mL, 2.34 mmol) and *n*-butanol (5 mL) for 48 hours. Purified with CombiFlash chromatography (silica gel, 20-40 microns, gradient 2% methanol/dichloromethane) to give a white solid (0.22 g, 82%). mp = 182 – 183 °C. ^{1}H NMR (500 MHz, $CDCl_3$) δ 8.45 (s, 1H), 8.34 (dd, *J* = 4.5, 1.9 Hz, 1H), 8.29 (d, *J* = 5.2 Hz, 1H), 7.38 – 7.30 (m, 4H), 7.02 (s, 1H), 6.93 (d, *J* = 5.3 Hz, 1H), 5.68 (s, 1H), 4.69 (d, *J* = 5.9 Hz, 2H). ^{13}C{^{1}H} NMR (125 MHz, $CDCl_3$) δ 162.2, 160.0, 158.1, 142.9, 139.3, 137.8, 133.0, 132.9, 129.5, 128.7, 128.5, 117.6, 110.8, 106.7, 45.1. FTIR (neat, cm^{-1}): 3243, 3071, 2974, 1620. HRMS (ESI-TOF) *m/z:* $[M+H]^+$ calcd for ($C_{17}H_{14}ClN_6^+$) 337.0963 & 339.0934 ; found 337.0964 & 339.0939.

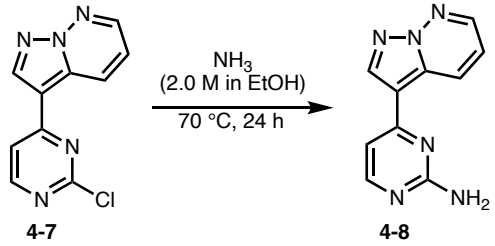

4-7 **4-8**

4-(pyrazolo[1,5-*b*]pyridazin-3-yl)pyrimidin-2-amine (4-8): Compound **4-7** (0.05 g, 0.22 mmol) was suspended in ethanolic ammonia solution (2.0 M, 2.5 mL) and the reaction was stirred for 24 hours. After 24 hours, TLC showed incomplete conversion and addition ethanolic ammonia solution (2.0 M, 2.0 mL) was added. The reaction was further stirred for 24 hours and the product was then concentrated and purified with CombiFlash chromatography (silica gel, 20-40 microns, gradient 0-5% methanol/dichloromethane) to give a white solid (0.017 g, 36%). ^{1}H NMR (500 MHz, DMSO-d_6) δ 9.15 (dd, *J* = 9.0, 1.8 Hz, 1H), 8.79 (s, 1H), 8.57 (dd, *J* = 4.3, 1.8 Hz, 1H), 8.23 (d, *J* = 5.2 Hz, 1H), 7.41 (dd, *J* = 9.0, 4.4 Hz, 1H), 7.10 (d, *J* = 5.2 Hz, 1H), 6.67 (s, 2H). ^{13}C{^{1}H} NMR (125 MHz, DMSO-d_6) δ 164.0, 159.7, 158.8, 144.4, 139.9, 132.9, 130.3, 118.9, 110.6, 105.8. The spectroscopy data are consistent with previous literature reports.[19]

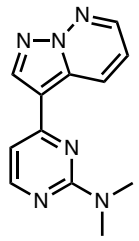

***N*,*N*-dimethyl-4-(pyrazolo[1,5-*b*]pyridazin-3-yl)pyrimidin-2-amine (4-9):** Synthesized according to the general procedure for nucleophilic aromatic substitution with **4-7** (0.40 g, 1.73 mmol), dimethylamine (2.6 mL, 5.17 mmol) and *n*-butanol (1 mL) for 16 hours. Purified with CombiFlash chromatography (silica gel, 20-40 microns, gradient 0–3% methanol/dichloromethane) to give a white solid (0.34 g, 81%). ^{1}H NMR (500 MHz, DMSO-d_6) δ 8.90 (d, *J* = 8.9 Hz, 1H), 8.80 (s, 1H), 8.58 – 8.54 (m, 1H), 8.31 (d, *J* = 5.0 Hz, 1H), 7.41 (dd, *J* = 8.9, 4.3 Hz, 1H), 7.09 (d, *J* = 5.0 Hz, 1H), 3.17 (s, 6H). ^{13}C{^{1}H} NMR (125 MHz, DMSO-d_6) δ 162.3, 159.3, 158.4, 144.3, 140.1, 132.7, 129.6, 119.4, 110.9, 105.0, 37.4. The spectroscopy data are consistent with previous literature reports.[19]

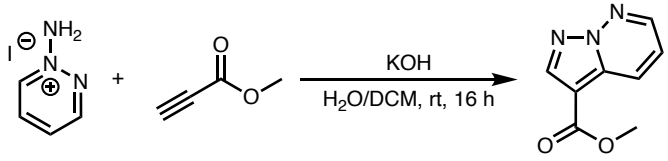

4-6 **4-11**

methyl pyrazolo[1,5-*b*]pyridazine-3-carboxylate (4-11): To a slurry of **4-6** (1.0 g, 4.48 mmol) in DCM (10 mL) was added methyl propiolate (0.20 mL, 2.24 mmol) and cooled to 0 °C. Then, K_2CO_3 (6.19 g, 4.48 mmol) in H_2O (5 mL) was added. The reaction was warmed to room temperature and stirred for 16 hours. The reaction was diluted with dichloromethane (5 mL) and water (10 mL) and the organic layer was collected. The aqueous layer was further extracted with dichloromethane (3 x 15 mL) and the organics were combined, dried over sodium sulfate, filtered, concentrated, and purified with CombiFlash chromatography (silica gel, 20-40 microns, gradient 0-100% ethyl acetate/hexane) to give the product as light-yellow solid (0.51 g, 64%). ^{1}H NMR

(500 MHz, $CDCl_3$) δ 8.52 (dd, *J* = 9.0, 1.9 Hz, 1H), 8.45 (s, 1H), 8.41 (dd, *J* = 4.4, 1.9 Hz, 1H), 7.25 (dd, *J* = 9.0, 4.4 Hz, 1H), 3.91 (s, 3H). $^{13}C\{^1H\}$ NMR (125 MHz, $CDCl_3$) δ 163.1, 143.2, 142.4, 135.0, 128.1, 119.2, 104.2, 51.6. The spectroscopy data are consistent with previous literature reports.[22]

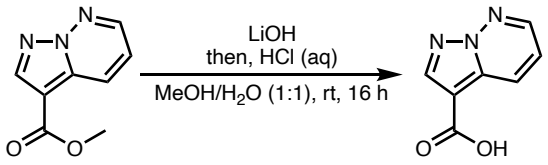

4-11 **4-12**

pyrazolo[1,5-*b*]pyridazine-3-carboxylic acid (4-12): To a solution of ester **4-11** (0.50 g, 2.82 mmol) in methanol (3 mL) at room temperature was added lithium hydroxide (0.10 g, 4.28 mmol) in H_2O (3 mL). The reaction was stirred at room temperature for 16 hours and then diluted with H_2O (10 mL). The reaction was cooled to 0 °C and quenched with 1.0 M HCl solution (10 mL), the product precipitated out and was filtered and washed with water to give a white solid (0.44 g, 96%). ^1H NMR (500 MHz, DMSO-d_6) δ 12.85 (s, 1H), 8.64 (dd, *J* = 4.4, 1.7 Hz, 1H), 8.53 (dd, *J* = 9.0, 1.7 Hz, 1H), 8.49 (s, 1H), 7.50 (dd, *J* = 9.0, 4.4 Hz, 1H). $^{13}C\{^1H\}$ NMR (125 MHz, DMSO-d_6) δ 164.0, 144.8, 142.5, 135.0, 128.3, 120.7, 104.9. The spectroscopy data are consistent with previous literature reports.[22]

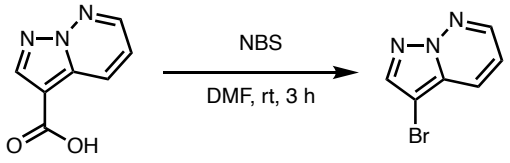

4-12 **4-13**

3-bromopyrazolo[1,5-*b*]pyridazine (4-13): Carboxylic acid **4-12** (0.36 g, 2.21 mmol) was dissolved in DMF (4 mL) and NBS (0.79 g, 4.42 mmol) was added. The reaction was stirred at room temperature for 3 hours and the solvent was removed under reduced pressure. The crude was purified with CombiFlash chromatography (silica gel, 20-40 microns, gradient 0-20% ethyl

acetate/hexane) to give the product as white solid (0.34 g, 77%). ^{1}H NMR (500 MHz, $CDCl_3$) δ 8.29 (dd, *J* = 4.4, 1.7 Hz, 1H), 8.01 (s, 1H), 7.92 (dd, *J* = 9.0, 1.7 Hz, 1H), 7.06 (dd, *J* = 9.0, 4.4 Hz, 1H). ^{13}C{^{1}H} NMR (125 MHz, $CDCl_3$) δ 142.6, 139.8, 131.9, 125.8, 116.5, 84.8. The spectroscopy data are consistent with previous literature reports.[22]

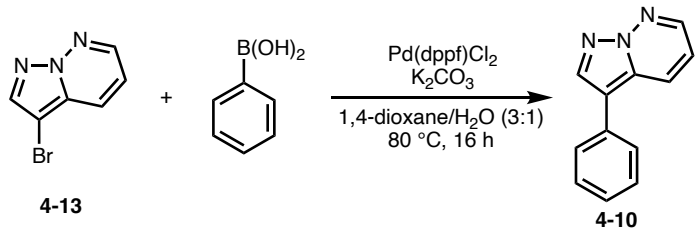

3-phenylpyrazolo[1,5-*b*]pyridazine (4-10): To a solution of arylbromide (0.10 g, 0.50 mmol) in degassed 1,4-dioxane/H_2O (3:1) (8 mL) was added phenylboronic acid (0.073 g, 0.60 mmol), Pd(dppf)Cl_2 (5 mol%, 0.018 g, 0.025 mmol), and K_2CO_3 (0.15 g, 1.50 mmol). The solution was purge with argon and stirred in preheated oil bath at 80 °C for 16 hours. The reaction was cooled to room temperature, diluted with water (8 mL) and then extracted with ethyl acetate (3 x 10 mL). The organics were combined, dried over sodium sulfate, concentrated, and purified with CombiFlash chromatography (silica gel, 20-40 microns, gradient 0-20% ethyl acetate/hexane) to give the product as white solid (0.084 g, 86%). ^{1}H NMR (500 MHz, $CDCl_3$) δ 8.30 (dd, *J* = 4.2, 1.7 Hz, 1H), 8.23 (s, 1H), 8.21 – 8.14 (m, 1H), 7.64 – 7.52 (m, 2H), 7.48 (t, *J* = 7.5 Hz, 2H), 7.35 (t, *J* = 7.5 Hz, 1H), 7.04 (dd, *J* = 9.0, 4.2 Hz, 1H). FTIR (neat, cm^{-1}): 3094, 1601, 1541. HRMS (ESI-TOF) *m/z:* $[M+H]^+$ calcd for ($C_{12}H_{10}N_3^+$) 196.0870; found 196.0886. The spectroscopy data are consistent with previous literature reports.[19]

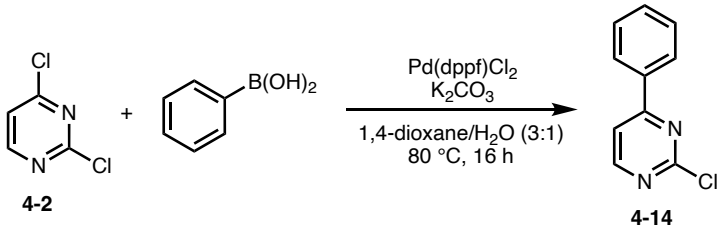

2-chloro-4-phenylpyrimidine (4-14): To a solution of **4-2** (0.50 g, 3.36 mmol) in degassed 1,4-dioxane/H_2O (3:1) (12 mL) was added phenylboronic acid (0.41 g, 3.36 mmol), Pd(dppf)Cl_2 (5 mol%, 0.12 g, 0.17 mmol), and K_2CO_3 (0.99 g, 10.08 mmol). The solution was purge with argon and stirred in preheated oil bath at 80 °C for 16 hours. The reaction was cooled to room temperature, diluted with water (10 mL) and then extracted with ethyl acetate (3 x 10 mL). The organics were combined, dried over sodium sulfate, concentrated, and purified with CombiFlash chromatography (silica gel, 20-40 microns, gradient 0-20% ethyl acetate/hexane) to give the product as white solid (0.43 g, 66%). ^{1}H NMR (500 MHz, $CDCl_3$) δ 8.63 (d, *J* = 5.2 Hz, 1H), 8.12 – 8.06 (m, 2H), 7.65 (d, *J* = 5.2 Hz, 1H), 7.59 – 7.48 (m, 3H). $^{13}C\{^1H\}$ NMR (125 MHz, $CDCl_3$) δ 167.2, 161.9, 159.9, 135.0, 131.9, 129.1, 127.4, 115.2. The spectroscopy data are consistent with previous literature reports.[23]

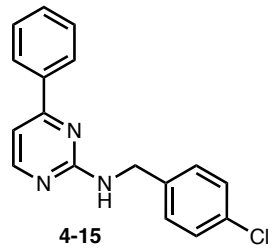

4-15

***N*-(4-chlorobenzyl)-4-phenylpyrimidin-2-amine (4-15):** Synthesized according to the general procedure for nucleophilic aromatic substitution with **4-14** (0.03 g, 0.16 mmol), 4-chlorobenzylamine (57 µL, 0.47 mmol) and 2-methoxylethanol (2 mL) for 16 hours. Purified with CombiFlash chromatography (silica gel, 20-40 microns, gradient 0-100% ethylacetate/hexane) to give a white solid (0.041 g, 89%). ^{1}H NMR (500 MHz, $CDCl_3$) δ 8.27 (s, 1H), 8.01 (dd, *J* = 6.5, 2.9 Hz, 2H), 7.46 (dd, *J* = 5.2, 1.8 Hz, 3H), 7.34 – 7.26 (m, 4H), 6.99 (d, *J* = 5.2 Hz, 1H), 6.07 (s, 1H), 4.68 (d, *J* = 6.0 Hz, 2H). $^{13}C\{^1H\}$ NMR (125 MHz, $CDCl_3$) δ 164.9, 162.5, 158.6, 138.1, 137.3, 132.8, 130.6, 128.9, 128.7, 128.6, 127.0, 106.9, 44.8. FTIR (neat, cm^{-1}): 3260, 3065, 2916,1561. HRMS (ESI-TOF) *m/z:* $[M+H]^+$ calcd for ($C_{17}H_{15}ClN_3^+$) 296.0950; found 296.0977.

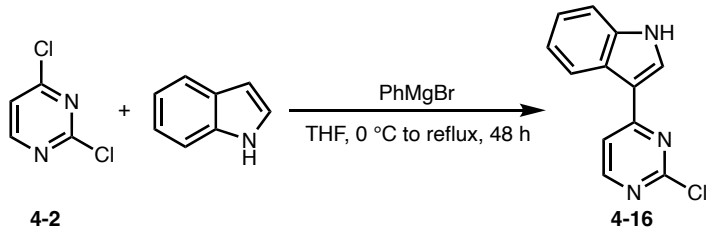

4-2 4-16

3-(2-chloropyrimidin-4-yl)-1*H*-indole (4-16): 1*H*-Indole (0.88 g, 7.5 mmol) was dissolved in anhydrous THF (20 mL) and cooled to 0 °C. Then, phenylmagnesium bromide (3M in Et_2O, 2.5 mL, 7.5 mmol) was added slowly and stirred for 15 minutes. A solution of 2,4-dichloropyrimidine (0.45 g, 3.0 mmol) in anhydrous THF (10 mL) was added slowly and the solution was reflux for 48 hours. The reaction was then cooled to room temperature and quenched with 1 M HCl (25 mL). The reaction was extracted with ethyl acetate (3 x 30 mL). The organics were combined, dried over sodium sulfate, concentrated, and purified with CombiFlash chromatography (silica gel, 20-40 microns, gradient 20-50% ethyl acetate/hexane) to give the product as yellow solid (0.23 g, 33%). mp = 215 – 217 °C. ^{1}H NMR (500 MHz, DMSO-d_6) δ 12.09 (s, 1H), 8.52 (d, *J* = 5.3 Hz, 2H), 8.43 – 8.41 (m, 1H), 7.91 (d, *J* = 5.3 Hz, 1H), 7.51 – 7.49 (m, 1H), 7.25 – 7.21 (m, 2H). ^{13}C{^{1}H} NMR (125 MHz, DMSO-d_6) δ 165.5, 160.7, 159.0, 137.7, 131.6, 125.5, 123.2, 122.1, 121.8, 115.0, 112.8, 112.3. FTIR (neat, cm^{-1}): 3144, 3047, 2915, 1573. HRMS (ESI-TOF) *m/z:* $[M+H]^+$ calcd for ($C_{12}H_9ClN_3^+$) 230.0480; found: 230.0485.

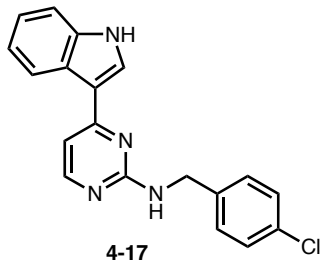

4-17

***N*-(4-chlorobenzyl)-4-(1*H*-indol-3-yl)pyrimidin-2-amine (4-17):** Synthesized according to the general procedure for nucleophilic aromatic substitution with **4-16** (0.05 g, 0.22 mmol), 4-chlorobenzylamine (80 µL, 0.65 mmol) and *n*-butanol (3 mL) for 16 hours. Purified with

CombiFlash chromatography (silica gel, 20-40 microns, gradient 0–30% ethyl acetate/hexane) to give a yellow solid (0.054 g, 74%). mp = 190 – 191 °C. ^{1}H NMR (500 MHz, DMSO-d$_6$) δ 11.67 (s, 1H), 8.19 (s, 1H), 8.13 (d, *J* = 5.3 Hz, 1H), 7.58 (t, *J* = 5.9 Hz, 1H), 7.44 – 7.32 (m, 5H), 7.13 (t, *J* = 7.2 Hz, 1H), 7.02 (d, *J* = 5.3 Hz, 2H), 4.58 (s, 2H). ^{13}C{^{1}H} NMR (125 MHz, DMSO-d$_6$) δ 162.6, 162.3, 156.9, 140.1, 137.0, 130.9, 128.8, 128.5, 128.1, 125.3, 122.2, 122.0, 120.3, 113.7, 111.8, 105.5, 43.6. FTIR (neat, cm^{-1}): 3407, 3215, 3032, 2990, 1594. HRMS (ESI-TOF) *m/z:* [M+H]$^{+}$ calcd for ($C_{19}H_{16}ClN_4^{+}$) 335.1058; found: 335.1067

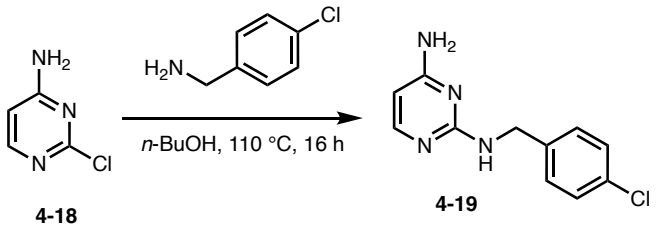

***N*^{2}-(4-chlorobenzyl)pyrimidine-2,4-diamine (4-19):** Synthesized according to the general procedure for nucleophilic aromatic substitution with **4-18** (0.50 g, 3.86 mmol), 4-chlorobenzylamine (0.94 mL, 7.72 mmol) and *n*-butanol (5 mL) for 16 hours. Purified with CombiFlash chromatography (silica gel, 20-40 microns, gradient 20–100% ethyl acetate/hexane) to give a yellow solid (0.65g, 72%). ^{1}H NMR (500 MHz, DMSO-d$_6$) δ 7.63 (d, *J* = 5.7 Hz, 1H), 7.34 – 7.25 (m, 4H), 6.91 (s, 1H), 6.30 (s, 2H), 5.68 (d, *J* = 5.7 Hz, 1H), 4.39 (d, *J* = 6.5 Hz, 2H). ^{13}C{^{1}H} NMR (125 MHz, DMSO-d$_6$) δ 164.4, 162.0, 155.1, 140.6, 131.3, 129.3, 128.4, 95.9, 43.5. FTIR (neat, cm^{-1}): 3466, 3170, 2952, 1638, 1572. HRMS (ESI-TOF) *m/z:* [M+H]$^{+}$ calcd for ($C_{11}H_{12}ClN_4^{+}$) 234.0745 & 237.0716; found: 235.0688 & 237.0660.

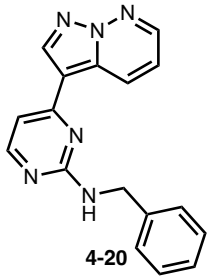

4-20

***N*-benzyl-4-(pyrazolo[1,5-*b*]pyridazin-3-yl)pyrimidin-2-amine (4-20):** Synthesized according to the general procedure for nucleophilic aromatic substitution with **4-7** (0.060 g, 0.26 mmol), benzylamine (85 µL, 0.78 mmol) and *n*-butanol (3 mL) for 16 hours. Purified with CombiFlash chromatography (silica gel, 20-40 microns, gradient 2% methanol/dichloromethane) to give a white solid (0.061 g, 78%). mp = 211 – 212 °C. ^{1}H NMR (500 MHz, DMSO-d_6) δ 8.78 (s, 1H), 8.53 (s, 1H), 8.28 (d, *J* = 5.2 Hz, 1H), 7.80 (t, *J* = 6.2 Hz, 1H), 7.37 (d, *J* = 7.1 Hz, 2H), 7.31 (m, 2H), 7.20 (t, *J* = 7.1 Hz, 1H), 7.11 (d, *J* = 5.2 Hz, 1H), 4.57 (d, *J* = 4.6 Hz, 2H). ^{13}C{^{1}H} NMR (125 MHz, DMSO-d_6) δ 162.3, 159.1, 158.3, 143.9, 140.4, 139.5, 132.4, 128.3, 127.3, 126.9, 126.6, 118.5, 110.2, 105.6, 44.3. FTIR (neat, cm^{-1}): 3240, 3032, 2879, 1623, 1565. HRMS (ESI-TOF) *m/z:* $[M+H]^+$ calcd for ($C_{17}H_{15}N_6^+$) 303.1353; found: 303.1362.

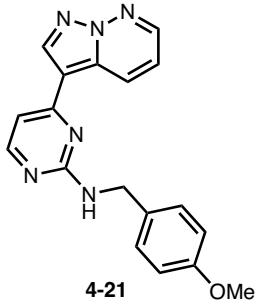

4-21

***N*-(4-methoxybenzyl)-4-(pyrazolo[1,5-*b*]pyridazin-3-yl)pyrimidin-2-amin(4-21):** Synthesized according to the general procedure for nucleophilic aromatic substitution with **4-7** (0.060 g, 0.26 mmol), 4-methoxybenzylamine (0.10 mL, 0.78 mmol) and *n*-butanol (3 mL) for 16 hours. Purified with CombiFlash chromatography (silica gel, 20-40 microns, gradient 2% methanol/dichloromethane) to give a yellow solid (0.074 g, 85%). mp = 188 – 189 °C. ^{1}H NMR

(500 MHz, DMSO-d_6) δ 8.78 (s, 1H), 8.54 (s, 1H), 8.27 (d, *J* = 5.2 Hz, 1H), 7.72 (t, *J* = 6.0 Hz, 1H), 7.29 (d, *J* = 7.9 Hz, 3H), 7.10 (d, *J* = 5.2 Hz, 1H), 6.87 (d, *J* = 8.6 Hz, 2H), 4.49 (s, 2H), 3.68 (s, 3H). $^{13}C\{^1H\}$ NMR (125 MHz, DMSO-d_6) δ 162.3, 158.4, 158.1, 143.9, 139.5, 132.4, 132.3, 128.7, 128.0, 118.5, 113.7, 110.2, 105.5, 55.0, 43.7. FTIR (neat, cm^{-1}): 3224, 3032, 2956, 1584. HRMS (ESI-TOF) *m/z:* $[M+H]^+$ calcd for ($C_{18}H_{17}N_6O^+$) 333.1458; found: 333.1467.

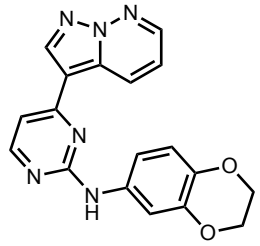

4-22

***N*-(2,3-dihydrobenzo[*b*][1,4]dioxin-6-yl)-4-(pyrazolo[1,5-*b*]pyridazin-3-yl)pyrimidin-2-amine (4-22):** Synthesized according to the general procedure for nucleophilic aromatic substitution with **4-7** (0.040 g, 0.17 mmol), 2,3-dihydrobenzo[*b*][1,4]dioxin-6-amine (64 µL, 0.51 mmol) and *n*-butanol (3 mL) for 16 hours. Purified with CombiFlash chromatography (silica gel, 20-40 microns, gradient 0-5% methanol/dichloromethane) to give a yellow solid (0.020 g, 34%). mp = 215 – 217 °C. ^1H NMR (500 MHz, DMSO-d_6) δ 9.37 (s, 1H), 9.13 (d, *J* = 7.2 Hz, 1H), 8.86 (s, 1H), 8.59 (dd, *J* = 4.4, 2.0 Hz, 1H), 8.41 (d, *J* = 5.2 Hz, 1H), 7.42 (dd, *J* = 9.0, 4.4 Hz, 1H), 7.36 (d, *J* = 2.0 Hz, 1H), 7.30 (d, *J* = 5.2 Hz, 1H), 7.09 (dd, *J* = 8.7, 2.4 Hz, 1H), 6.80 (d, *J* = 8.7 Hz, 1H), 4.26 – 4.18 (m, 4H). $^{13}C\{^1H\}$ NMR (125 MHz, DMSO-d_6) δ 160.5, 159.6, 158.5, 144.5, 143.4, 140.2, 138.8, 134.5, 132.9, 130.0, 119.2, 117.1, 113.3, 110.5, 109.2, 107.7, 64.7, 64.4. FTIR (neat, cm^{-1}): 3257, 3081, 2942, 1625, 1573. HRMS (ESI-TOF) *m/z:* $[M+H]^+$ calcd for ($C_{18}H_{15}N_6O_2^+$) 347.1251; found: 347.1257.

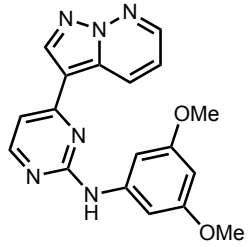

4-23

***N*-(3,5-dimethoxyphenyl)-4-(pyrazolo[1,5-*b*]pyridazin-3-yl)pyrimidin-2-amine (4-23):** Synthesized according to the general procedure for nucleophilic aromatic substitution with **4-7** (0.030 g, 0.13 mmol), 3,5-dimethoxyaniline (60 mg, 0.39 mmol) and *n*-butanol (3 mL) for 48 hours. Purified with CombiFlash chromatography (silica gel, 20-40 microns, gradient 0-5% methanol/dichloromethane) to give a yellow solid (0.026 g, 57%). mp = 196 – 197 °C. ^{1}H NMR (500 MHz, DMSO-d_6) δ 9.53 (s, 1H), 9.21 (d, *J* = 8.9 Hz, 1H), 8.89 (s, 1H), 8.60 (dd, *J* = 4.4, 1.8 Hz, 1H), 8.47 (d, *J* = 5.2 Hz, 1H), 7.43 (dd, *J* = 8.9, 4.4 Hz, 1H), 7.37 (d, *J* = 5.2 Hz, 1H), 7.04 (t, *J* = 2.2 Hz, 2H), 6.15 (t, *J* = 2.2 Hz, 1H), 3.73 (s, 6H). FTIR (neat, cm^{-1}): 3333, 3055, 2993, 1612, 1587. HRMS (ESI-TOF) *m/z:* $[M+H]^+$ calcd for ($C_{18}H_{17}N_6O_2^+$) 349.1408; found 349.1407. The spectroscopy data are consistent with previous literature reports.[21]

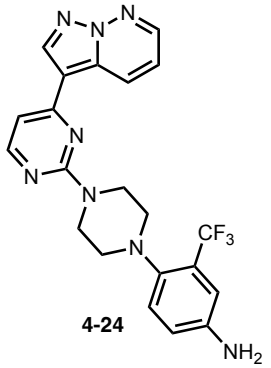

4-24

4-(4-(4-(pyrazolo[1,5-*b*]pyridazin-3-yl)pyrimidin-2-yl)piperazin-1-yl)-3-(trifluoromethyl)aniline (4-24): Synthesized according to the general procedure for nucleophilic aromatic substitution with **4-7** (0.030 g, 0.13 mmol), 4-(4-methylpiperazin-1-yl)-3-(trifluoromethyl)aniline (0.10 mg, 0.39 mmol) and *n*-butanol (3 mL) for 48 hours. Purified with

CombiFlash chromatography (silica gel, 20-40 microns, gradient 0-10% methanol/dichloromethane) to give a white solid (0.036 g, 63%). mp = 80 – 83 °C. ^{1}H NMR (500 MHz, CD_3OD) δ 8.71 (dd, *J* = 9.1, 1.7 Hz, 1H), 8.49 (s, 1H), 8.37 (dd, *J* = 4.4, 1.7 Hz, 1H), 8.20 (d, *J* = 5.2 Hz, 1H), 7.23 (dd, *J* = 9.1, 4.4 Hz, 1H), 7.18 (d, *J* = 8.5 Hz, 1H), 6.94 (d, *J* = 2.5 Hz, 1H), 6.89 (d, *J* = 5.2 Hz, 1H), 6.83 (dd, *J* = 8.5, 2.5 Hz, 1H), 4.15 – 3.53 (m, 4H), 2.85 (t, *J* = 4.8 Hz, 4H). ^{13}C{^{1}H} NMR (125 MHz, CD_3OD) δ 163.0, 160.9, 158.8, 147.0, 144.7, 140.3, 133.9, 130.3, 129.4 (q, *J* = 27.8 Hz), 126.7 (q, *J* = 270.7 Hz), 126.f4, 119.8, 119.8, 113.6 (q, *J* = 5.4 Hz), 112.3, 106.5, 68.6, 45.9. FTIR (neat, cm^{-1}): 3341, 3102, 2846, 1618, 1568. HRMS (ESI-TOF) *m/z:* $[M+H]^+$ calcd for ($C_{21}H_{20}F_3N_8^+$) 441.1758; found 441.1759.

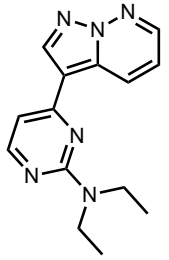

4-25

***N*,*N*-diethyl-4-(pyrazolo[1,5-*b*]pyridazin-3-yl)pyrimidin-2-amine (4-25):** Synthesized according to the general procedure for nucleophilic aromatic substitution with **4-7** (0.030 g, 0.13 mmol), 4-((diethylamino)methyl)aniline (0.041 mg, 0.23 mmol) and *n*-butanol (2 mL) for 24 hours. Purified with CombiFlash chromatography (silica gel, 20-40 microns, gradient 0-5% methanol/dichloromethane) to give a white solid (0.020 g, 57%). mp = 82 – 84 °C. ^{1}H NMR (500 MHz, cd_3od) δ 8.83 (dd, *J* = 9.1, 2.0 Hz, 1H), 8.54 (s, 1H), 8.41 (dd, *J* = 4.4, 1.9 Hz, 1H), 8.19 (d, *J* = 5.2 Hz, 1H), 7.27 (dd, *J* = 9.1, 4.4 Hz, 1H), 6.90 (d, *J* = 5.2 Hz, 1H), 3.65 (q, *J* = 7.1 Hz, 4H), 1.22 (t, *J* = 7.1 Hz, 6H). ^{13}C{^{1}H} NMR (125 MHz, CD_3OD) δ 160.6, 159.5, 157.3, 143.4, 138.8, 132.5, 128.8, 118.2, 111.1, 104.0, 42.0, 12.1. FTIR (neat, cm^{-1}): 3100, 2973, 1619. HRMS (ESI-TOF) *m/z:* $[M+H]^+$ calcd for ($C_{14}H_{17}N_6^+$) 269.1509; found 269.1511.

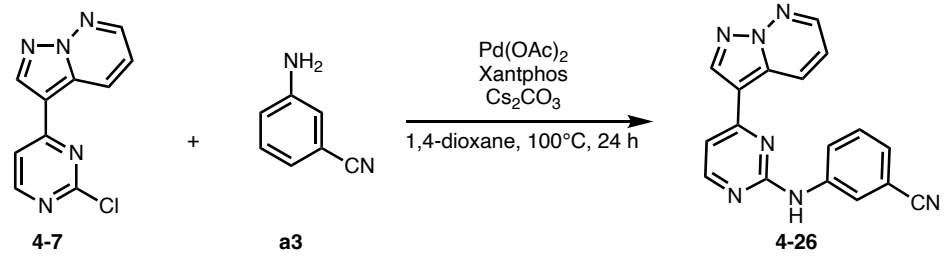

3-((4-(pyrazolo[1,5-*b*]pyridazin-3-yl)pyrimidin-2-yl)amino)benzonitrile (4-26): To a suspension of **4-7** (0.070 g, 0.30 mmol) in degassed anhydrous dioxane (5 mL) was added cesium carbonate (0.29 g, 0.90 mmol), palladium acetate (5 mol%, 3.4 mg, 0.015 mmol), xantphos (10 mol%, 0.058 g, 0.030 mmol) and 3-aminobenzonitrile (0.035 g, 0.30 mmol). The reaction was purged with argon and refluxed at 100 °C for 18 hours. The reaction was then cooled to room temperature and the solvent was removed under pressure. The reaction was purified with CombiFlash chromatography (silica gel, 20-40 microns, gradient 0 - 10% methanol/dichloromethane) to give a yellow solid (0.053 g, 56%). mp = >250 °C. ^{1}H NMR (500 MHz, DMSO-d$_6$) δ 9.95 (s, 1H), 9.13 (d, *J* = 8.8 Hz, 1H), 8.91 (s, 1H), 8.63 (d, *J* = 2.7 Hz, 1H), 8.54 (d, *J* = 5.2 Hz, 1H), 8.37 (s, 1H), 7.93 (d, *J* = 8.2 Hz, 1H), 7.53 (t, *J* = 7.9 Hz, 1H), 7.54 – 7.40 (m, 2H), 7.41 (d, *J* = 7.5 Hz, 1H). ^{13}C{^{1}H} NMR (125 MHz, DMSO-d$_6$) δ 160.0, 160.0, 158.6, 144.6, 141.9, 140.5, 133.0, 130.5, 129.8, 125.2, 123.9, 121.7, 119.6, 119.5, 111.8, 110.3, 109.1. FTIR (neat, cm^{-1}): 3109, 2920, 2255, 1618. HRMS (ESI-TOF) *m/z:* [M+H]$^{+}$ calcd for ($C_{17}H_{12}N_7^{+}$) 314.1149; found 314.1143.

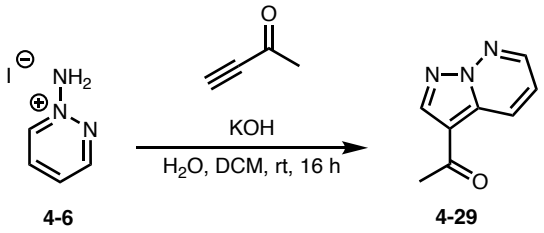

1-(pyrazolo[1,5-*b*]pyridazin-3-yl)ethan-1-one (4-29): To a slurry of 1-aminopyridazin-1-ium iodide **4-6** (2.0 g, 8.97 mmol) in dichloromethane (25 mL), 3-butyn-2-one (0.35 mL, 4.48 mmol)

was added. The reaction was cooled to 0 °C and potassium hydroxide (0.63 g, 11.20 mmol) in water (12.7 mL) was added. The reaction was brought to room temperature and stirred for 16 hours. The organic layer was separated and collected, and the aqueous layer was further extracted with dichloromethane (2 x 25 mL). The organics were combined, dried over sodium sulfate and purified with CombiFlash chromatography (silica gel, 20-40 microns, gradient 40 – 100% ethyl acetate/hexane) to give reddish black solid (0.62 g, 86%). ^{1}H NMR (500 MHz, $CDCl_3$) δ 8.73 (dd, *J* = 9.0, 2.0 Hz, 1H), 8.46 (dd, *J* = 4.4, 1.9 Hz, 1H), 8.42 (s, 1H), 7.30 (dd, *J* = 9.0, 4.4 Hz, 1H), 2.58 (s, 3H). ^{13}C{^{1}H} NMR (125 MHz, $CDCl_3$) δ 192.3, 143.8, 142.3, 134.4, 129.0, 120.0, 113.1, 27.9. The spectroscopic data are consistent with previous literature reports.[22]

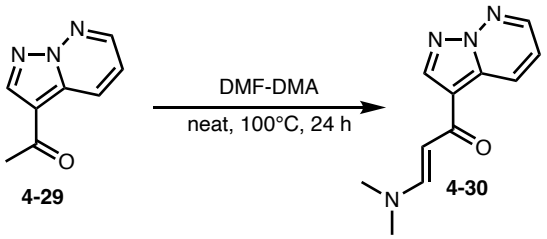

(*E*)-3-(dimethylamino)-1-(pyrazolo[1,5-*b*]pyridazin-3-yl)prop-2-en-1-one (4-30)

A 15 mL sealed tube equipped with magnetic stirrer was charged with ketone **4-29** (0.61 g, 3.80 mmol) and N,N-dimethylformamide dimethyl acetal DMF-DMA (3.54 mL, 26.58 mmol) was added. The reaction was placed in pre-heated oil bath at 100 °C and stirred for 16 hours overnight. The reaction was concentrated and purified with CombiFlash chromatography (silica gel, 20-40 microns, gradient 2 – 5% methanol/dichloromethane) to give yellowish solid (0.63 g, 77%). ^{1}H NMR (500 MHz, $CDCl_3$) δ 8.78 (dd, *J* = 9.0, 2.0 Hz, 1H), 8.32 (q, *J* = 2.0 Hz, 2H), 7.75 (d, *J* = 12.3 Hz, 1H), 7.14 (dd, *J* = 9.0, 4.5 Hz, 1H), 5.59 (d, *J* = 12.3 Hz, 1H), 3.10 (s, 3H), 2.90 (s, 3H). ^{13}C{^{1}H} NMR (125 MHz, $CDCl_3$) δ 182.4, 152.8, 143.1, 139.9, 134.4, 129.7, 118.3, 114.5, 92.9, 45.0, 37.3. The spectroscopic data are consistent with previous literature reports.[22]

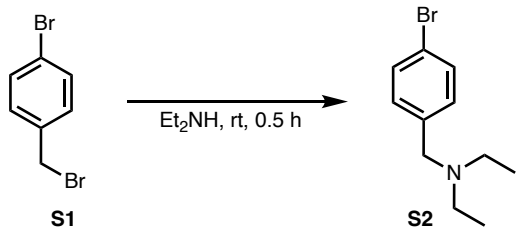

N-(4-bromobenzyl)-N-ethylethanamine (S2): A 50 mL round bottom flask equipped with magnetic stirrer was charged with 4-bromobenzylbromide **S1** (1.0 g, 4.0 mmol) and diethylamine (5 mL) was added. The reaction was stirred at room temperature for 30 minutes (TLC shows complete conversion) and the reaction was stopped, diluted with 30 mL ethyl acetate. The organics was washed with 1 M potassium hydroxide (2 x 10 mL) and brine (10 mL). The organic was concentrated, dried over sodium sulfate, and concentrated to give the desired product as a colorless oil (0.96 g, 99%). ^{1}H NMR (500 MHz, $CDCl_3$) δ 7.42 (d, J = 8.4 Hz, 2H), 7.22 (d, J = 8.4 Hz, 2H), 3.50 (s, 2H), 2.50 (q, J = 7.1 Hz, 4H), 1.03 (t, J = 7.1 Hz, 6H). ^{13}C{^{1}H} NMR (125 MHz, $CDCl_3$) δ 139.3, 131.3, 130.6, 120.5, 57.0, 46.9, 11.9. The spectroscopy data are consistent with previous literature.[24]

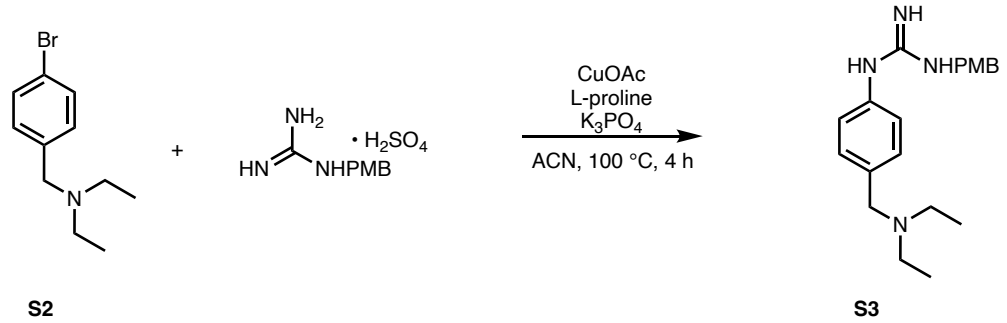

1-(4-((diethylamino)methyl)phenyl)-3-(4-methoxybenzyl)guanidine (S3): Aryl halide **S2** (0.24 g, 1 mmol), PMB-guanidine hemisulfate (0.23 g, 1 mmol), CuOAc (10 mol%, 0.10 mmol), l-proline (10 mol%, 0.20 mmol), and K_3PO_4 (1.27 g, 6.0 mmol) were mixed in a pressure tube with a magnetic stir bar and anhydrous acetonitrile (6 mL) was added. The reaction was heated to 100 °C for 4 h. After complete consumption of the starting material, ethyl acetate (30 mL) and H_2O

(30 mL) were added. The separated aqueous layer was extracted with ethyl acetate (2 × 30 mL). The combined organic layers were washed with brine (40 mL), dried over sodium sulfate, and concentrated. The residue was purified with CombiFlash chromatography (silica gel) to give the desired product **S3** (0.20 g, 58%). ^{1}H NMR (500 MHz, DMSO-d$_6$) δ 7.27 (d, *J* = 8.0 Hz, 2H), 7.09 (d, *J* = 7.8 Hz, 2H), 6.89 (d, *J* = 8.0 Hz, 3H), 6.71 (d, *J* = 6.6 Hz, 2H), 5.76 (s, 1H), 4.90 (s, 1H), 4.26 (s, 2H), 3.73 (s, 3H), 3.41 (s, 2H), 2.43 (q, *J* = 6.8 Hz, 4H), 0.96 (t, *J* = 6.8 Hz, 6H). ^{13}C{^{1}H} NMR (125 MHz, DMSO-d$_6$) δ 158.1, 151.1, 132.7, 131.1, 129.1, 128.7, 122.5, 113.6, 56.6, 55.0, 45.8, 43.6, 11.7, (missing guanidine carbon).

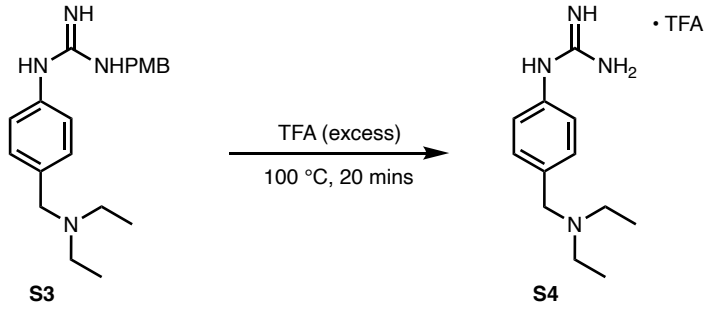

1-(4-((diethylamino)methyl)phenyl)guanidine triflate salt (S4): A 15 mL pressured tube equipped with magnetic stirrer bar was charged with compound **S3** (0.15 g, 0.44 mmol), then trifloroacetic acid (2 mL) was added. The reaction was sealed with teflon cap and placed in a preheated oil bath at 100 °C and then stirred for 20 minutes. The reaction was cooled to room temperature and the solvent removed under reduced pressure. The crude product was used directly without further purification.

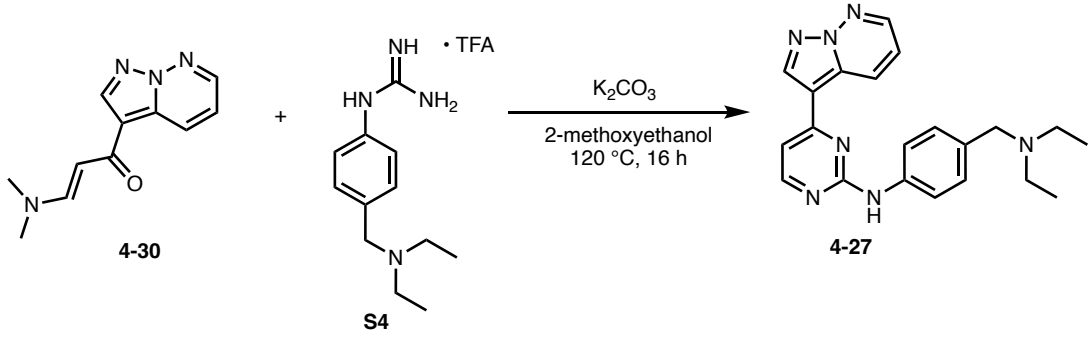

Compound **4-30** (0.048 g, 0.22 mmol) was dissolved in 2-methoxyethanol (3 mL) and to the solution was added crude guanidine **S4** (0.44 mmol) and potassium carbonate (0.091 g, 0.66 mmol). The solution was placed in a preheated oil bath and refluxed at 120 °C overnight. The reaction was then cooled down to room temperature, concentrated and product purified with CombiFlash chromatography (silica gel, 20-40 microns, gradient 0 – 5% methanol/dichloromethane) to give the desired product as a yellowish solid (0.041 g, 50%). mp = 124 – 125 °C. ^{1}H NMR (500 MHz, CD_3OD) δ 8.97 (d, *J* = 9.0 Hz, 1H), 8.56 (s, 1H), 8.42 – 8.38 (m, 1H), 8.29 (d, *J* = 5.3 Hz, 1H), 7.58 (d, *J* = 8.4 Hz, 2H), 7.27 (d, *J* = 8.4 Hz, 2H), 7.20 (dd, *J* = 9.0, 4.4 Hz, 1H), 7.11 (d, *J* = 5.3 Hz, 1H), 3.57 (s, 2H), 2.56 (q, *J* = 7.2 Hz, 4H), 1.09 (t, *J* = 7.2 Hz, 6H). ^{13}C{^{1}H} NMR (125 MHz, CD_3OD) δ 160.4, 159.8, 157.6, 143.5, 139.2, 138.9, 132.8, 131.6, 129.7, 129.6, 119.9, 118.3, 110.6, 107.1, 56.3, 45.9, 9.9. FTIR (neat, cm^{-1}): 3255, 3064, 2963,1609, 1570. HRMS (ESI-TOF) *m/z:* $[M+H]^+$ calcd for ($C_{21}H_{24}N_7^+$) 374.2088; found: 374.2091.

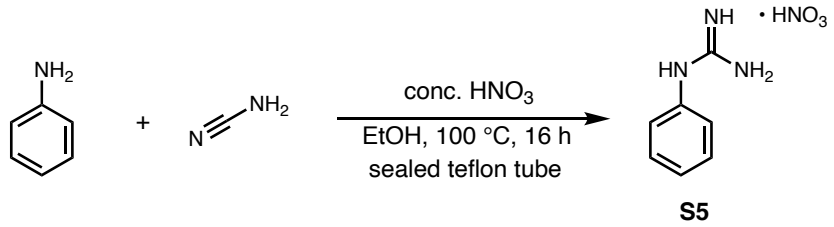

S5

1-phenylguanidine nitrate salt (**S5**): To a pressure tube equipped with stirrer bar was added aniline (0.91 mL, 10.0 mmol), ethanol (5 mL), cyanamide (50% in water, 1.20 mL, 15.0 mmol) and nitric acid (0.63 mL, 10.0 mmol). The tube was sealed and placed in a preheated oil bath at 100 °C and was allowed to stir for 16 h. The reaction was stopped, cooled to room temperature, and concentrated to give the crude product which was used directly for the next step without further purification.

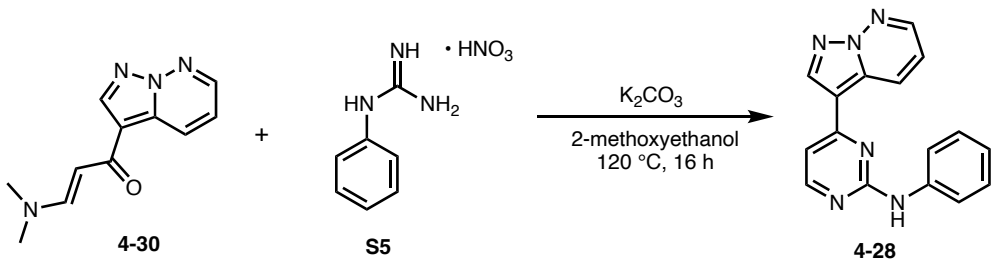

N-phenyl-4-(pyrazolo[1,5-b]pyridazin-3-yl)pyrimidin-2-amine (**4-28**): Compound **4-30** (0.10 g, 0.46 mmol) was dissolved in 2-methoxyethanol (4 mL) and to the solution was added crude phenylguanide **S5** (0.18 g, 0.92 mmol) and potassium carbonate (0.19 g, 1.38 mmol). The solution was placed in a preheated oil bath and refluxed at 120 °C overnight. The reaction was then cooled down to room temperature, concentrated, and product purified with CombiFlash chromatography (silica gel, 20-40 microns, gradient 2% methanol/dichloromethane) to give the desired product as yellowish solid (0.073 g, 55%). ^{1}H NMR (500 MHz, DMSO-d_6) δ 9.57 (s, 1H), 9.16 (d, J = 8.7 Hz, 1H), 8.88 (s, 1H), 8.59 (dd, J = 4.4, 1.9 Hz, 1H), 8.45 (d, J = 5.2 Hz, 1H), 7.74 (d, J = 7.7 Hz, 2H), 7.44 (dd, J = 9.1, 4.4 Hz, 1H), 7.37 – 7.28 (m, 3H), 6.97 (t, J = 7.3 Hz, 1H). ^{13}C{^{1}H} NMR (125 MHz, DMSO-d_6) δ 160.5, 159.8, 158.5, 144.5, 140.9, 140.3, 132.9, 130.0, 129.0, 122.0, 119.8, 119.2, 110.4, 108.1. The spectroscopy data are consistent with previous literature[19]

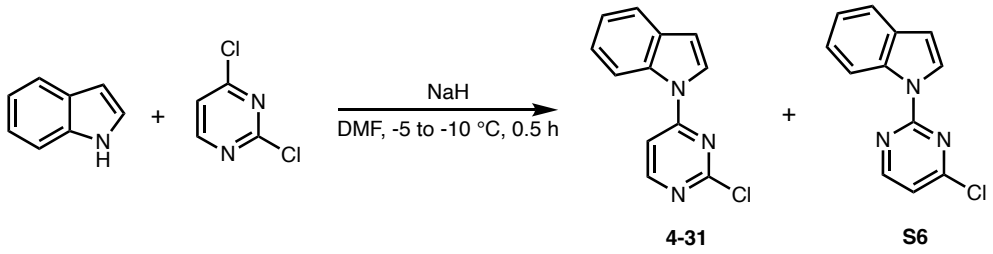

1-(2-chloropyrimidin-4-yl)-1*H*-indole (**4-31**): To a solution of indole (1.17 g, 10.0 mmol) and 2,4-dichloropyrimidine (1.52 g, 10.20 mmol) in dimethylformamide (30 mL) between -5 to -10 °C was added a sodium hydride (60 wt% in mineral oil, 0.40 g, 10.0 mmol) slowly. The reaction was stirred for 30 minutes and then quenched with water (35 mL). The white solid was filtered and

purified CombiFlash chromatography (silica, 40-60 microns, gradient 5-30% ethyl acetate/hexane) to give **4-31** as white solid (0.53 g, 23%) and **S6** as white solid (0.34 g, 15%).

4-31: mp = 128 – 129 °C. ^{1}H NMR (500 MHz, $CDCl_3$) δ 8.54 – 8.49 (m, 2H), 7.68 – 7.59 (m, 2H), 7.39 (ddd, *J* = 8.5, 7.1, 1.3 Hz, 1H), 7.32 – 7.23 (m, 2H), 6.78 (dd, *J* = 3.7, 0.9 Hz, 1H). ^{13}C{^{1}H} NMR (125 MHz, $CDCl_3$) δ 161.0, 159.7, 159.3, 135.2, 131.2, 124.8, 124.1, 123.3, 121.4, 115.7, 109.7, 106.8. FTIR (neat, cm^{-1}): 3142, 3114, 1574. HRMS (ESI-TOF) *m/z:* $[M+H]^+$ calcd for ($C_{12}H_9ClN_3^+$) 230.0480; found: 230.0484.

S6: mp = 84 – 85 °C. ^{1}H NMR (500 MHz, $CDCl_3$) δ 8.79 – 8.74 (m, 1H), 8.54 (d, *J* = 5.2 Hz, 1H), 8.22 (d, *J* = 3.7 Hz, 1H), 7.63 (d, *J* = 7.7 Hz, 1H), 7.37 (ddd, *J* = 8.4, 7.3, 1.2 Hz, 1H), 7.30 – 7.24 (m, 1H), 7.05 (d, *J* = 5.2 Hz, 1H), 6.72 (dd, *J* = 3.7, 0.6 Hz, 1H). ^{13}C NMR (125 MHz, $CDCl_3$) δ 161.6, 159.1, 157.4, 135.3, 131.4, 125.7, 124.0, 122.7, 120.9, 116.4, 115.9, 107.9. FTIR (neat, cm^{-1}): 3153, 3047, 1562, 1545. HRMS (ESI-TOF) *m/z:* $[M+H]^+$ calcd for ($C_{12}H_9ClN_3^+$) 230.0480; found: 230.0486.

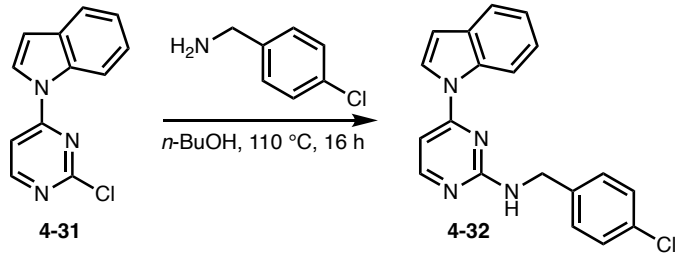

4-31 **4-32**

Synthesized according to the general procedure for nucleophilic aromatic substitution with **4-31** (0.060 g, 0.26 mmol), 4-chlorobenzylamine (95 µL, 0.78 mmol) and *n*-butanol (3 mL) for 16 hours. Purified with CombiFlash chromatography (silica gel, 20-40 microns, gradient 0-100% hexane/ethyl acetate) to give a white solid (0.073 g, 84%). mp = 194 – 195 °C. ^{1}H NMR (500 MHz, DMSO-d_6) δ 8.30 (s, 1H), 8.11 – 7.90 (m, 2H), 7.58 (s, 1H), 7.38 (s, 4H), 7.26 – 7.07 (m, 2H), 6.96 (s, 1H), 6.74 (s, 1H), 4.57 (s, 2H). ^{13}C{^{1}H} NMR (125 MHz, DMSO-d_6) δ 162.2, 159.8,

158.7, 139.4, 134.7, 131.1, 130.4, 129.0, 128.5, 128.2, 125.8, 123.3, 122.0, 120.8, 107.1, 97.9, 43.6. FTIR (neat, cm^{-1}): 3222, 3142, 2990, 1611. HRMS (ESI-TOF) *m/z:* $[M+H]^+$ calcd for ($C_{19}H_{16}ClN_4^+$) 335.1058; found: 335.1064.

REFERENCES

1. Dunker, A. K.; Lawson, J. D.; Brown, C. J.; Williams, R. M.; Romero, P.; Oh, J. S.; Oldfield, C. J.; Campen, A. M.; Ratliff, C. M.; Hipps, K. W.; et al., *J. Mol. Graphics Model.* **2001**, *19*, 26-59.

2. Dyson, H. J.; Wright, P. E., *Nat. Rev. Mol. Cell Biol.* **2005**, *6*, 197-208.

3. DeForte, S.; Uversky, V. N., *Molecules* **2016**, *21*.

4. Babu, M. M.; van der Lee, R.; de Groot, N. S.; Gsponer, J., *Curr. Opin. Struct. Biol.* **2011**, *21*, 432-440.

5. Uversky, V. N.; Oldfield, C. J.; Dunker, A. K., *Annu. Rev. Biophys.* **2008**, *37*, 215-246.

6. Catalgol, B.; Grune, T., *Prog. Mol. Biol. Transl. Sci.* **2012**, *109*, 397-414.

7. Korsak, M.; Kozyreva, T. Beta Amyloid Hallmarks: From Intrinsically Disordered Proteins to Alzheimer's Disease. In *Intrinsically Disordered Proteins Studied by NMR Spectroscopy*, Felli, I. C., Pierattelli, R. Eds.; Springer International Publishing, 2015; pp 401-421.

8. Ciechanover, A.; Brundin, P., *Neuron* **2003**, *40*, 427-446.

9. Njomen, E.; Osmulski, P. A.; Jones, C. L.; Gaczynska, M.; Tepe, J. J., *Biochemistry* **2018**, *57*, 4214-4224.

10. Trader, D. J.; Simanski, S.; Dickson, P.; Kodadek, T., *Biochimica et Biophysica Acta (BBA) - General Subjects* **2017**, *1861*, 892-899.

11. Lansdell, T. A.; Hurchla, M. A.; Xiang, J.; Hovde, S.; Weilbaecher, K. N.; Henry, R. W.; Tepe, J. J., *ACS Chem. Biol.* **2013**, *8*, 578-587.

12. Jones, C. L.; Njomen, E.; Sjogren, B.; Dexheimer, T. S.; Tepe, J. J., *ACS Chem. Biol.* **2017**, *12*, 2240-2247.

13. Fiolek, T. J.; Keel, K. L.; Tepe, J. J., *ACS Chem. Neurosci.* **2021**, *12*, 1438-1448.

14. Staerz, S. D.; Jones, C. L.; Tepe, J. J., *J. Med. Chem.* **2022**, *65*, 6631-6642.

15. George, D. E.; Tepe, J. J. Advances in Proteasome Enhancement by Small Molecules. In *Biomolecules*, 2021; Vol. 11.

16. Lipinski, C. A.; Lombardo, F.; Dominy, B. W.; Feeney, P. J., *Adv. Drug Del. Rev.* **2001**, *46*, 3-26.

17. Staerz, S. D.; Lisabeth, E. M.; Njomen, E.; Dexheimer, T. S.; Neubig, R. R.; Tepe, J. J., *ACS Omega* **2023**, *8*, 15650-15659.

18. Stevens, K. L.; Reno, M. J.; Alberti, J. B.; Price, D. J.; Kane-Carson, L. S.; Knick, V. B.; Shewchuk, L. M.; Hassell, A. M.; Veal, J. M.; Davis, S. T.; et al., *Bioorg. Med. Chem. Lett.* **2008**, *18*, 5758-5762.

19. Tear, W. F.; Bag, S.; Diaz-Gonzalez, R.; Ceballos-Pérez, G.; Rojas-Barros, D. I.; Cordon-Obras, C.; Pérez-Moreno, G.; García-Hernández, R.; Martinez-Martinez, M. S.; Ruiz-Perez, L. M.; et al., *J. Med. Chem.* **2020**, *63*, 756-783.

20. Schaenzer, A. J.; Wlodarchak, N.; Drewry, D. H.; Zuercher, W. J.; Rose, W. E.; Ferrer, C. A.; Sauer, J.-D.; Striker, R., *ACS Infect. Dis.* **2018**, *4*, 1508-1518.

21. Tavares, F. X.; Boucheron, J. A.; Dickerson, S. H.; Griffin, R. J.; Preugschat, F.; Thomson, S. A.; Wang, T. Y.; Zhou, H.-Q., *J. Med. Chem.* **2004**, *47*, 4716-4730.

22. Henderson, S. H.; Sorrell, F.; Bennett, J.; Fedorov, O.; Hanley, M. T.; Godoi, P. H.; Ruela de Sousa, R.; Robinson, S.; Ashall-Kelly, A.; Hopkins Navratilova, I.; et al., *J. Med. Chem.* **2021**, *64*, 11709-11728.

23. Zhang, H.; Wei, Z.; Zhang, A. H.; Yu, S., *Org. Lett.* **2020**, *22*, 7315-7320.

24. Yao, W.; Fang, H.; He, Q.; Peng, D.; Liu, G.; Huang, Z., *J. Org. Chem.* **2019**, *84*, 6084-6093.

APPENDIX

Figure 4.7: ^{1}H and $^{13}C\{1H\}$ NMR spectra of **4-3**

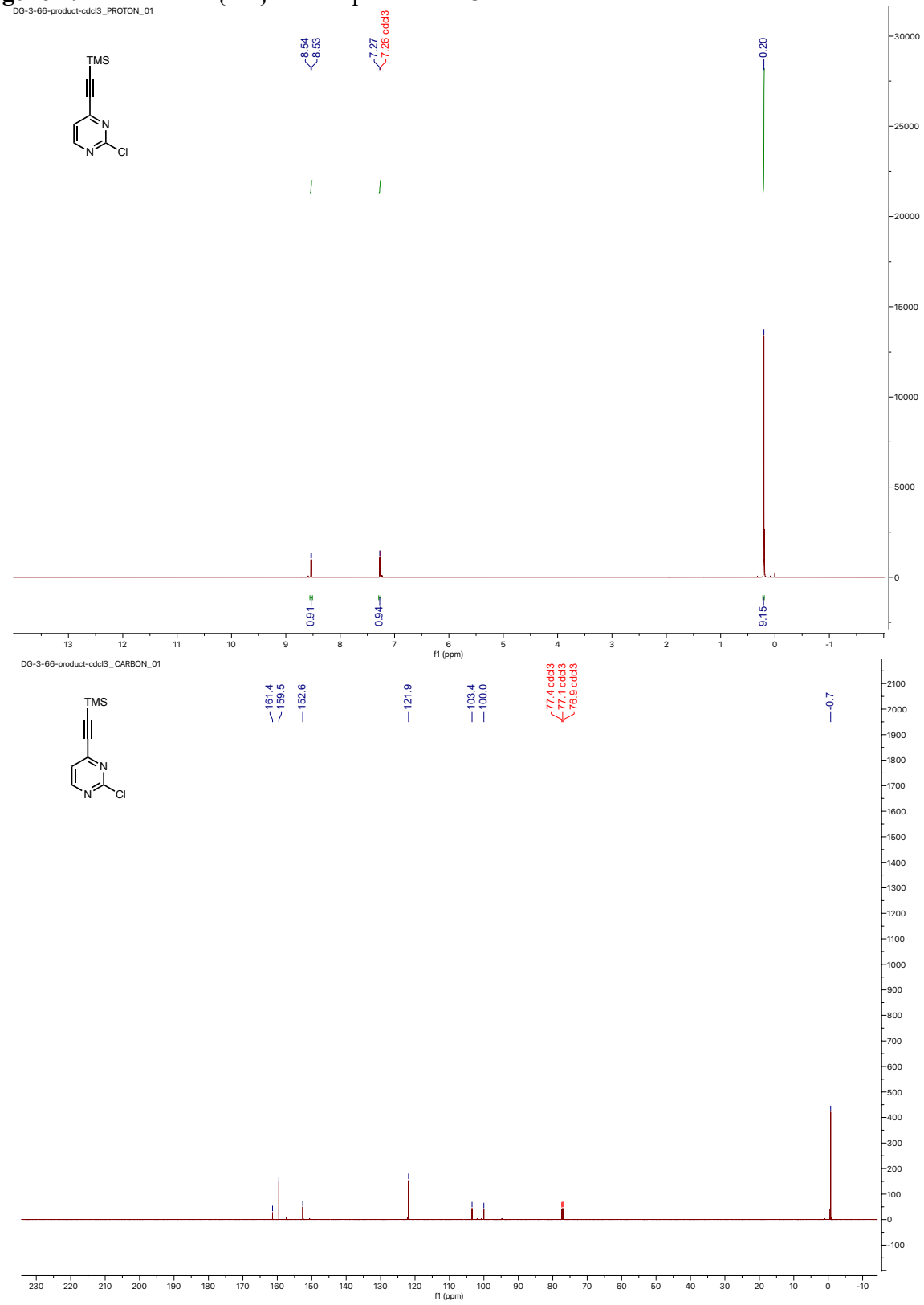

Figure 4.8: ^{1}H and $^{13}C\{1H\}$ NMR spectra of **4-4**

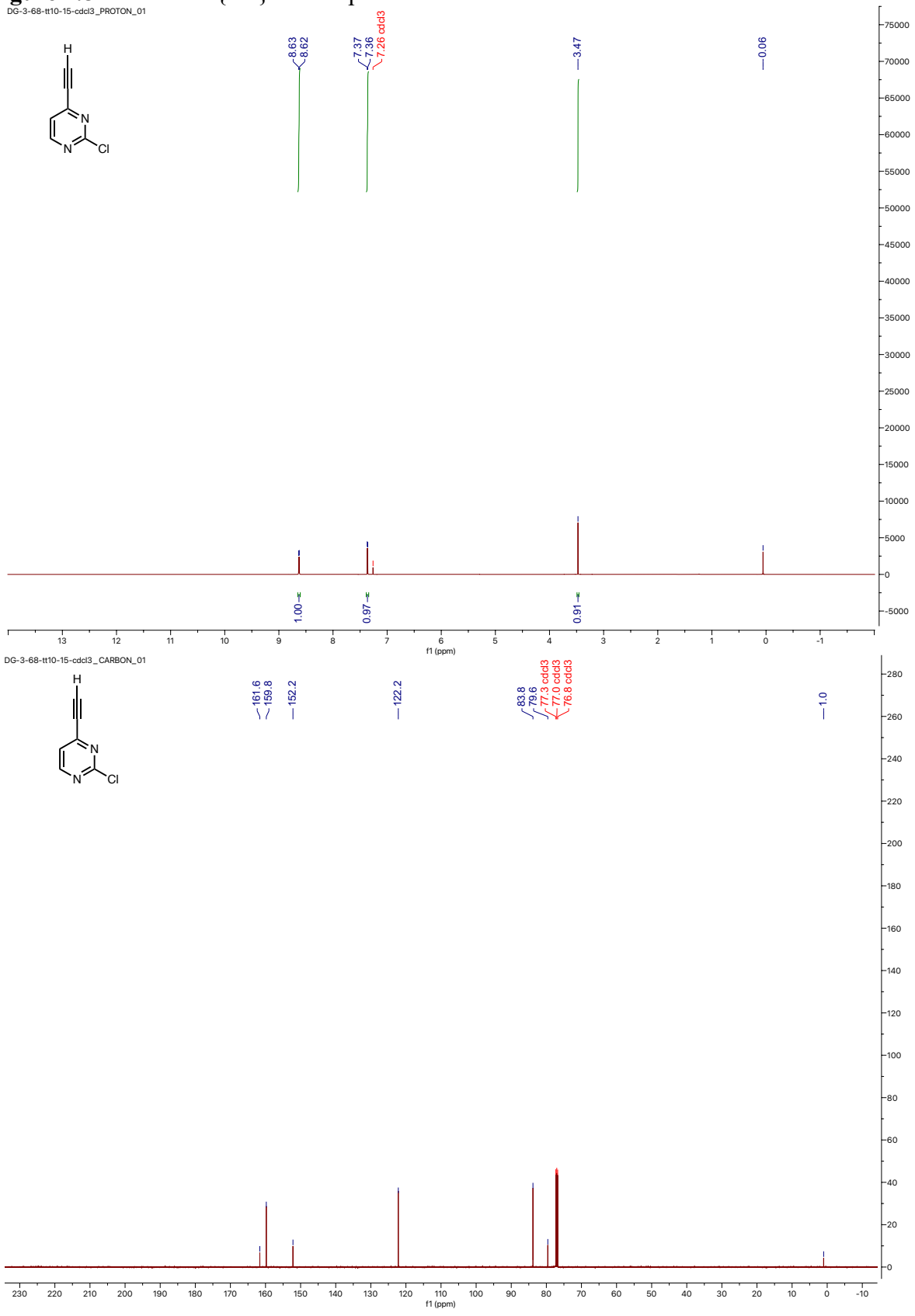

Figure 4.9: ^{1}H and $^{13}C\{1H\}$ NMR spectra of **4-6**

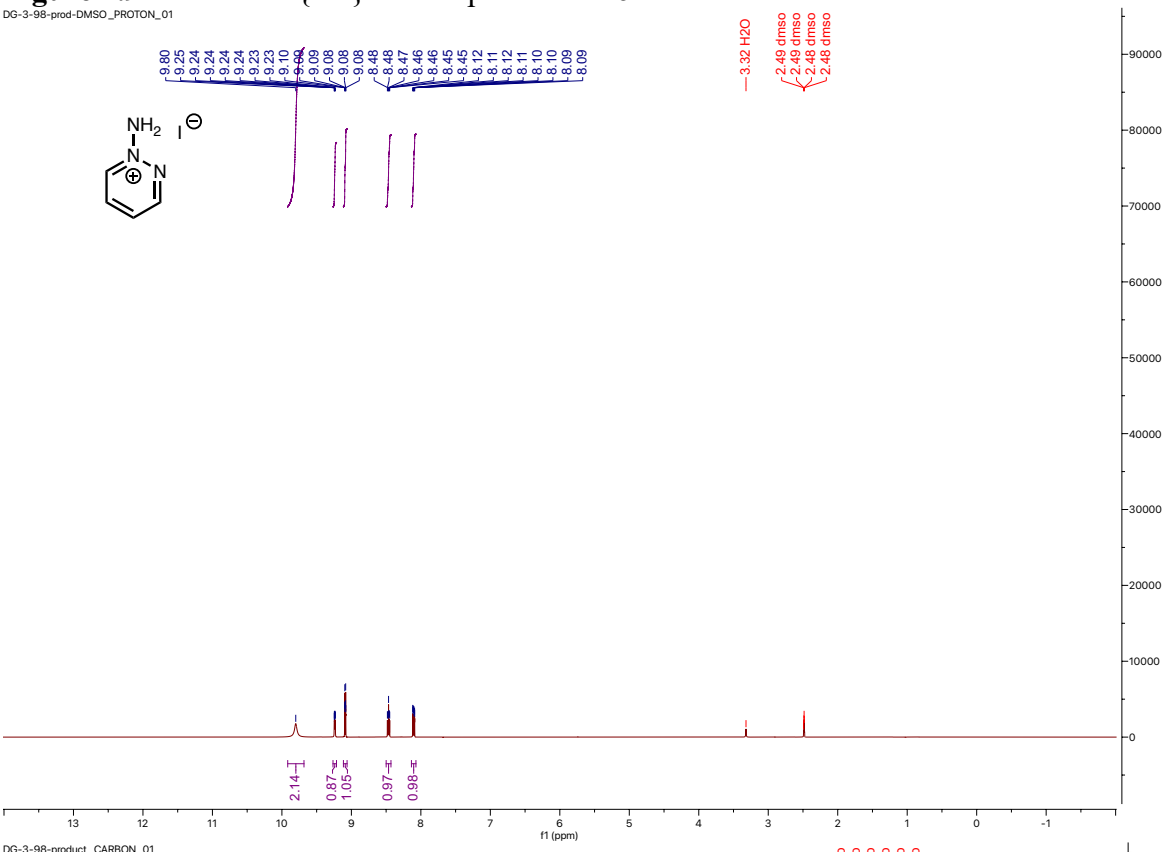

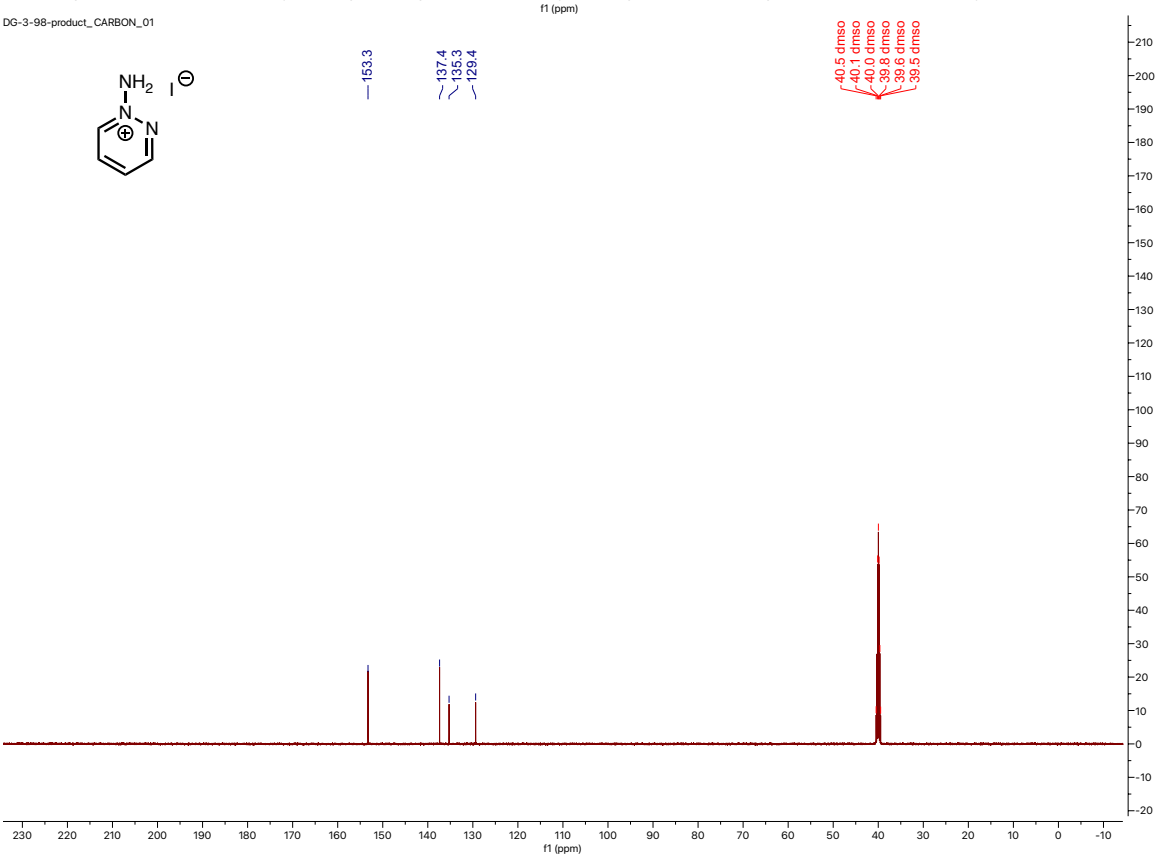

Figure 4.10: ^{1}H and $^{13}C\{1H\}$ NMR spectra of **4-7**

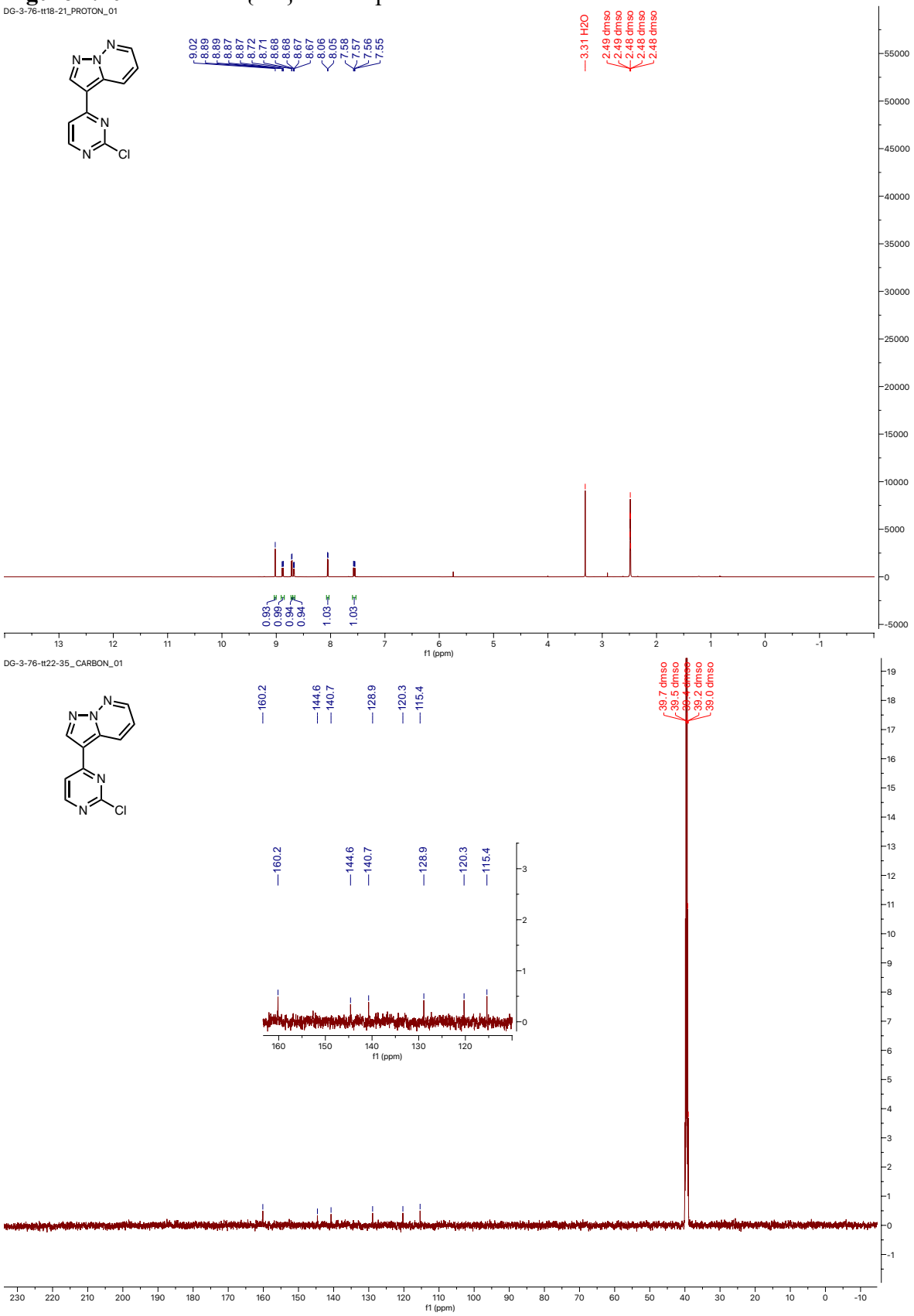

Figure 4.11: ^{1}H and $^{13}C\{1H\}$ NMR spectra of **4-1**

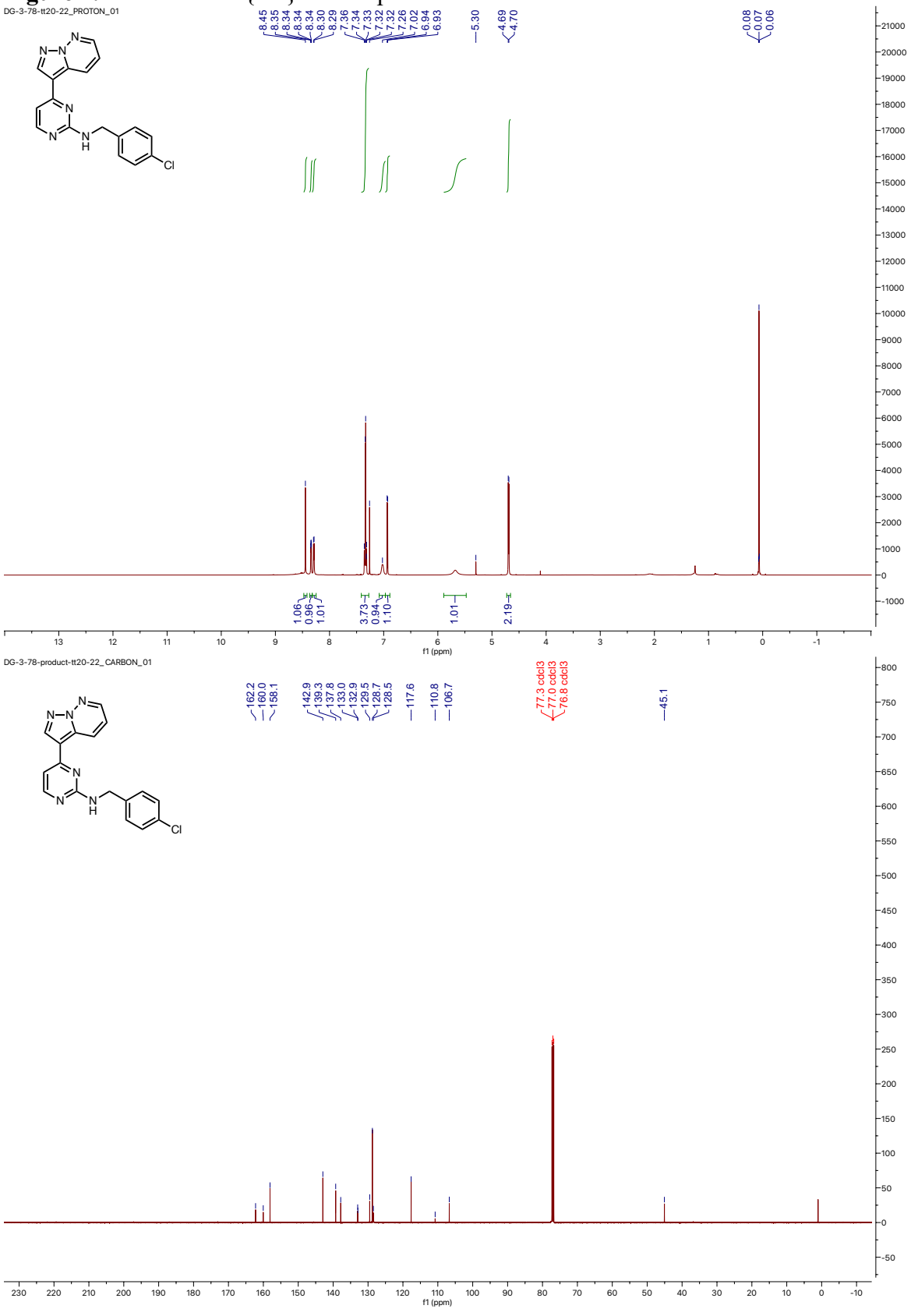

Figure 4.12: ^{1}H and $^{13}C\{1H\}$ NMR spectra of **4-8**

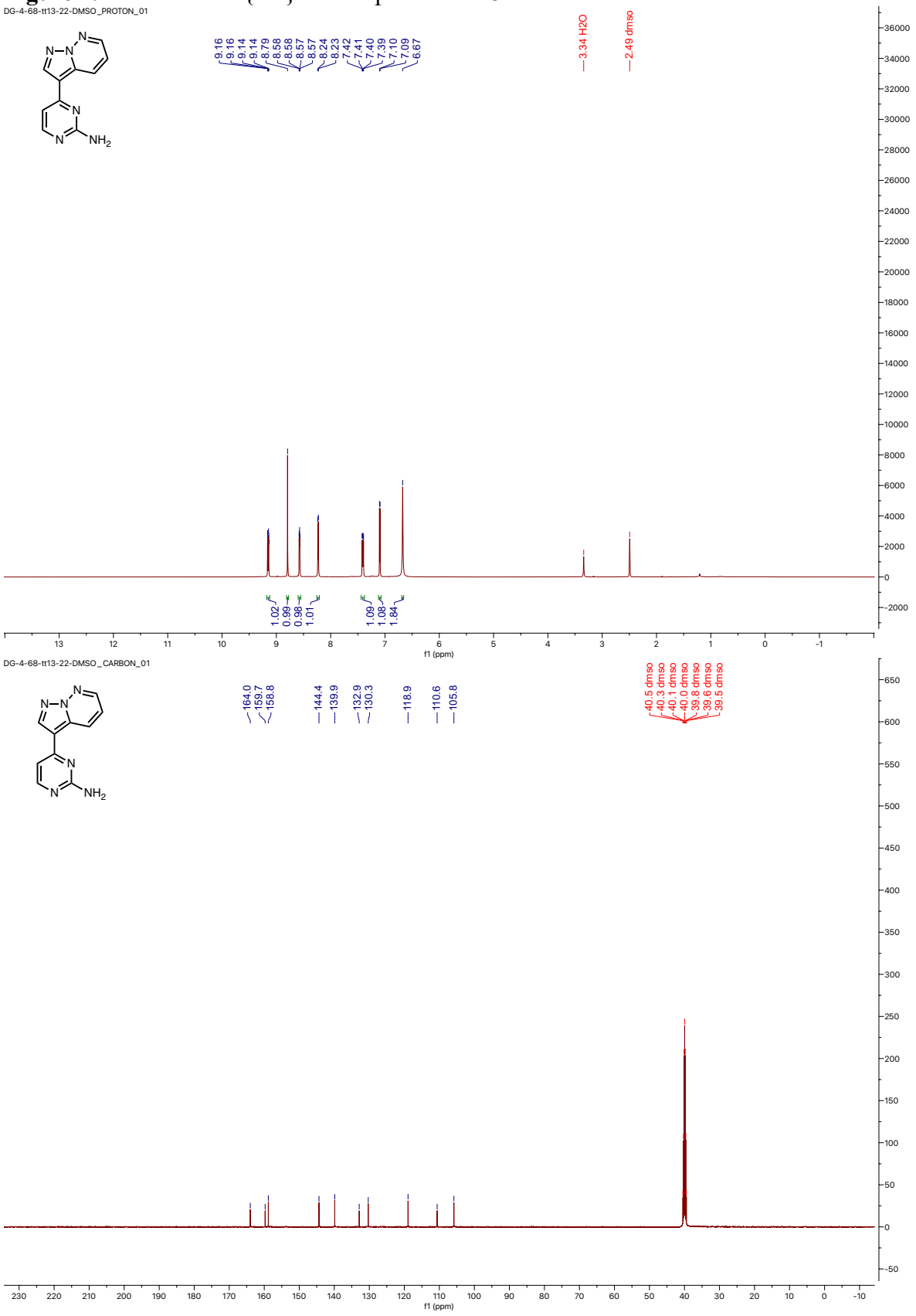

Figure 4.13: ^{1}H and $^{13}C\{1H\}$ NMR spectra of **4-9**

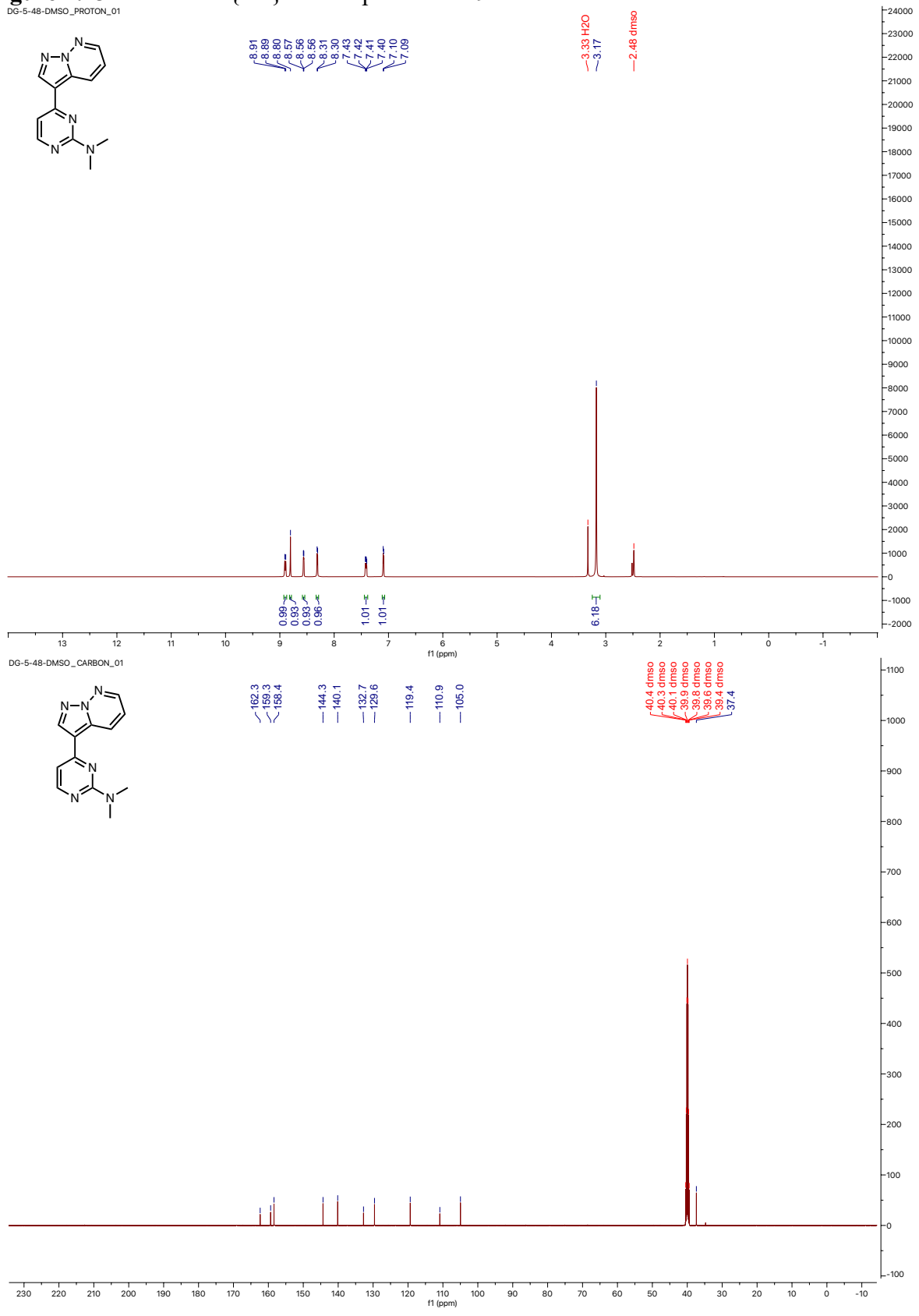

Figure 4.14: ^{1}H and $^{13}C\{1H\}$ NMR spectra of **4-11**

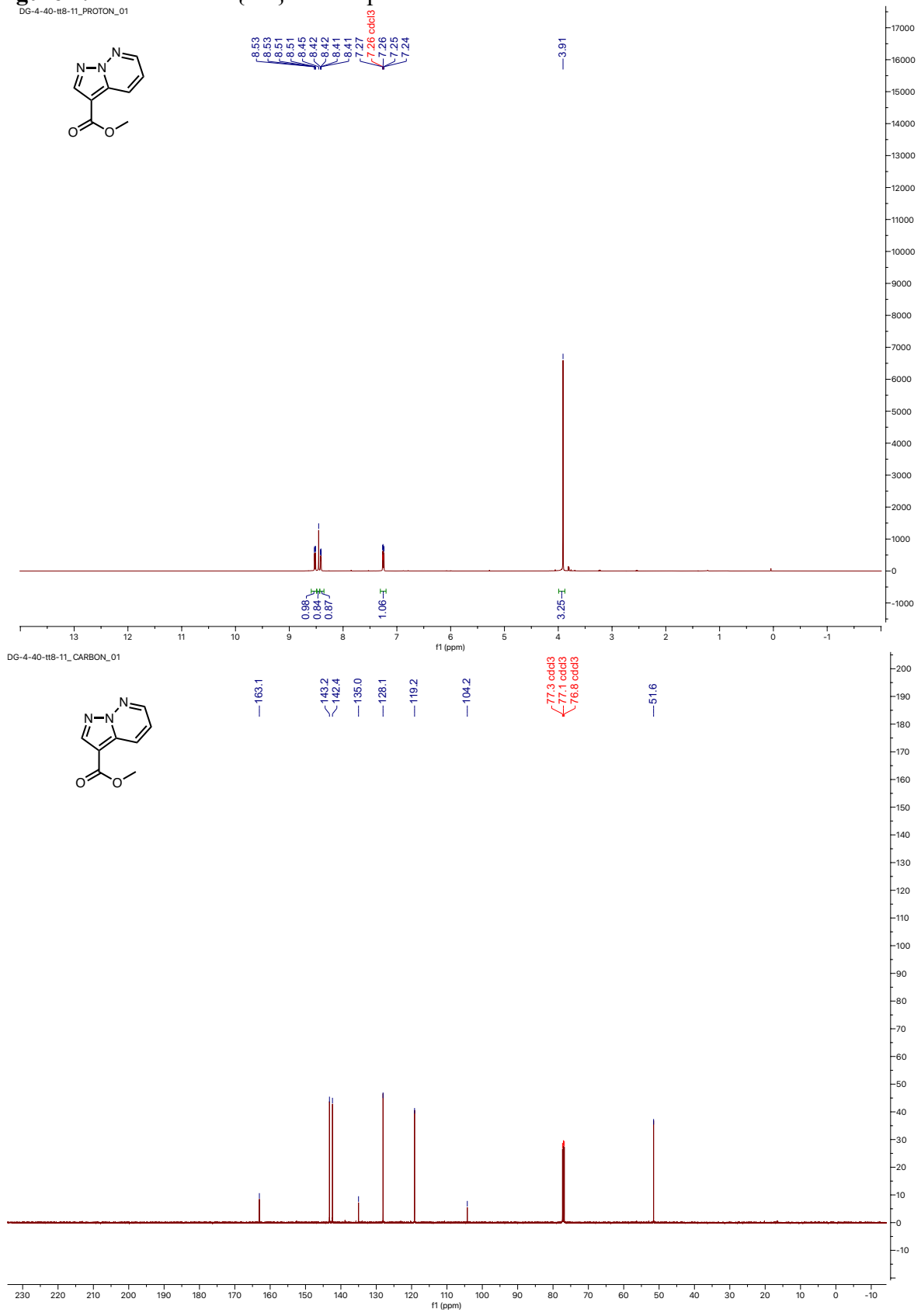

Figure 4.15: ^{1}H and $^{13}C\{1H\}$ NMR spectra of **4-12**

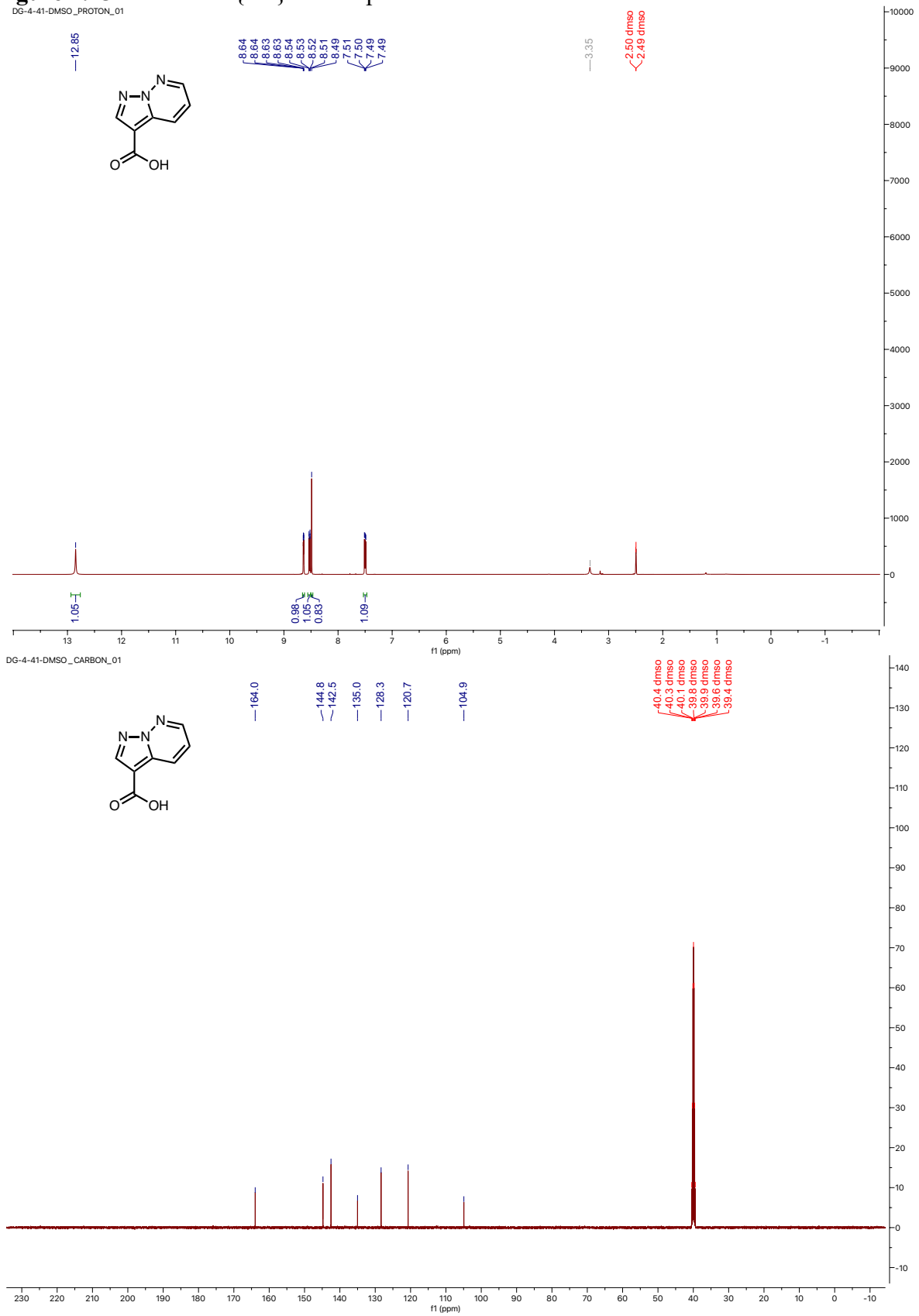

Figure 4.16: ^{1}H and $^{13}C\{1H\}$ NMR spectra of **4-13**

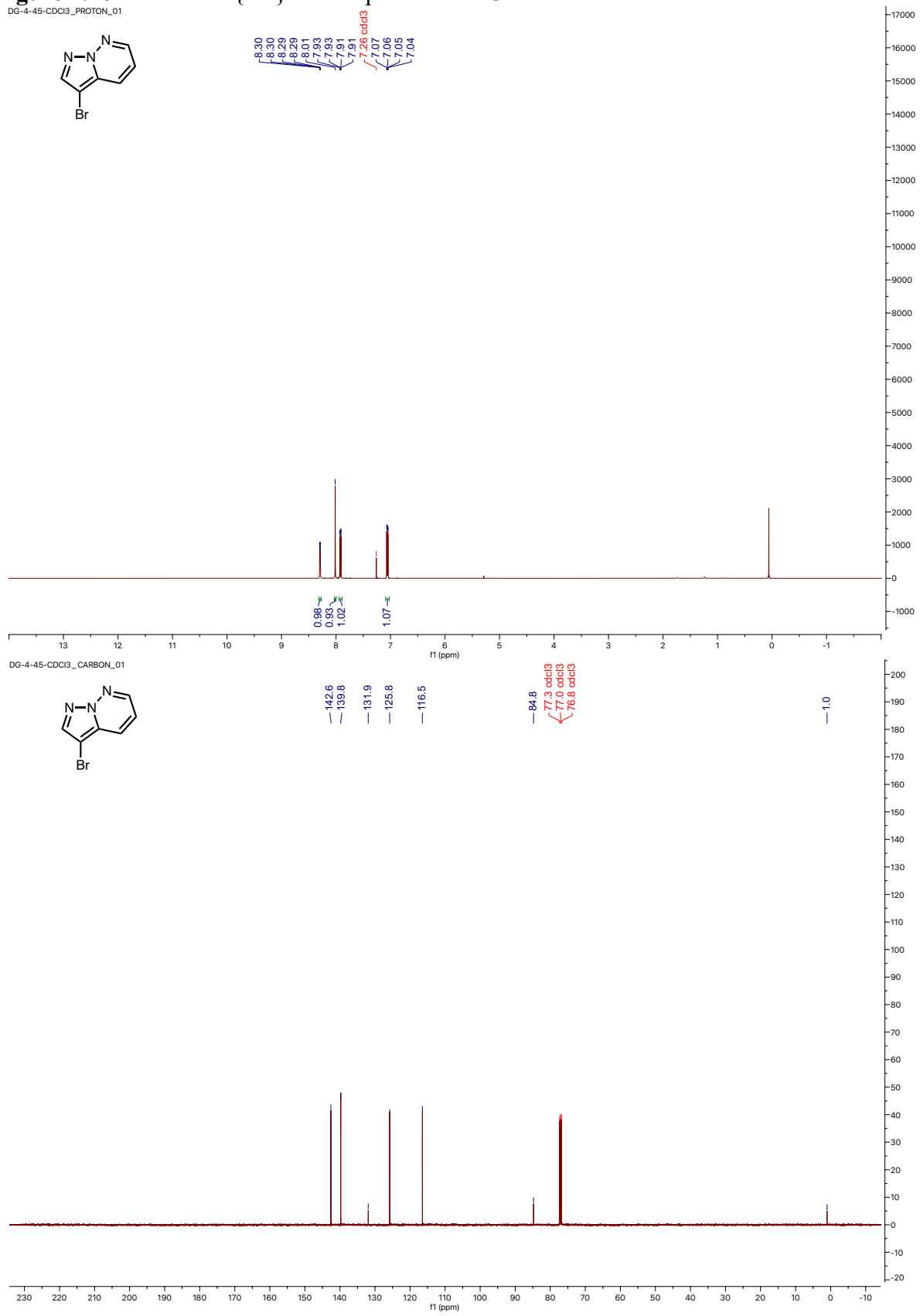

Figure 4.17: ^{1}H NMR spectra of **4-10**

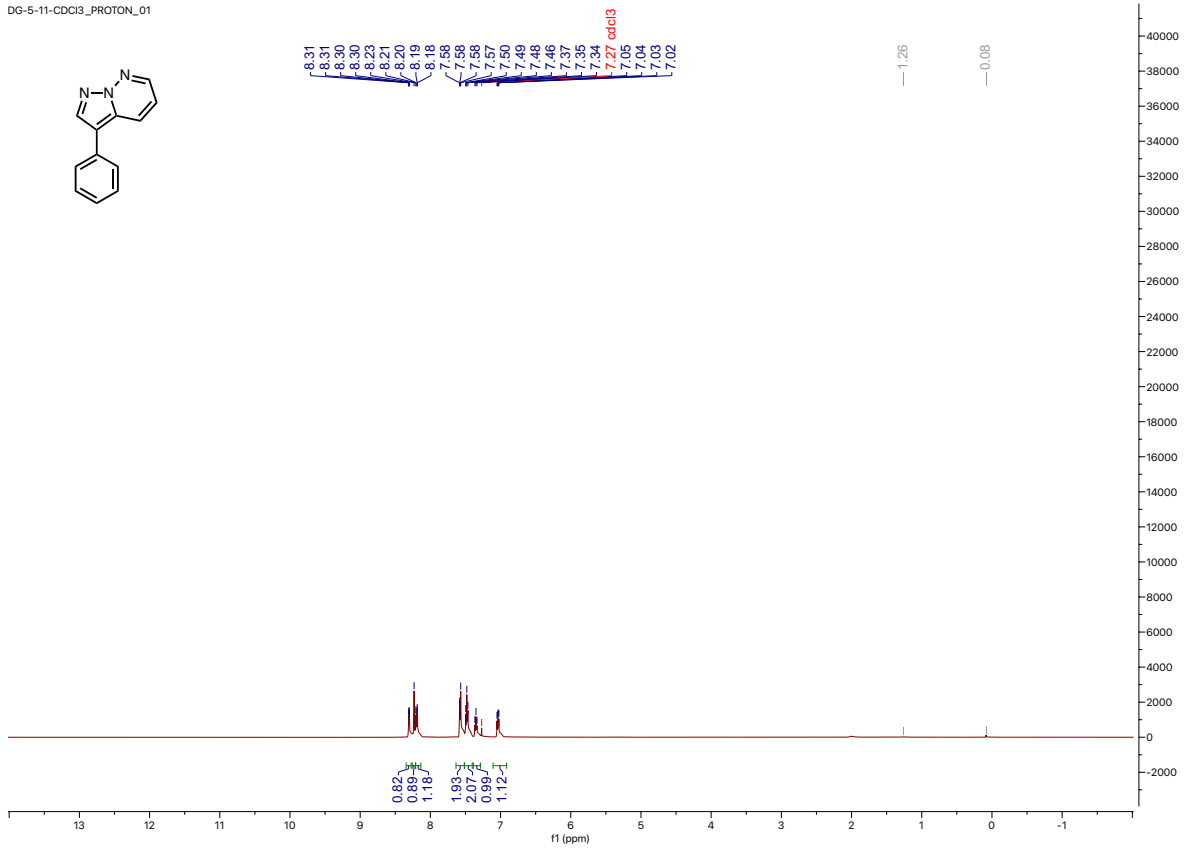

Figure 4.18: ^{1}H and $^{13}C\{1H\}$ NMR spectra of **4-14**

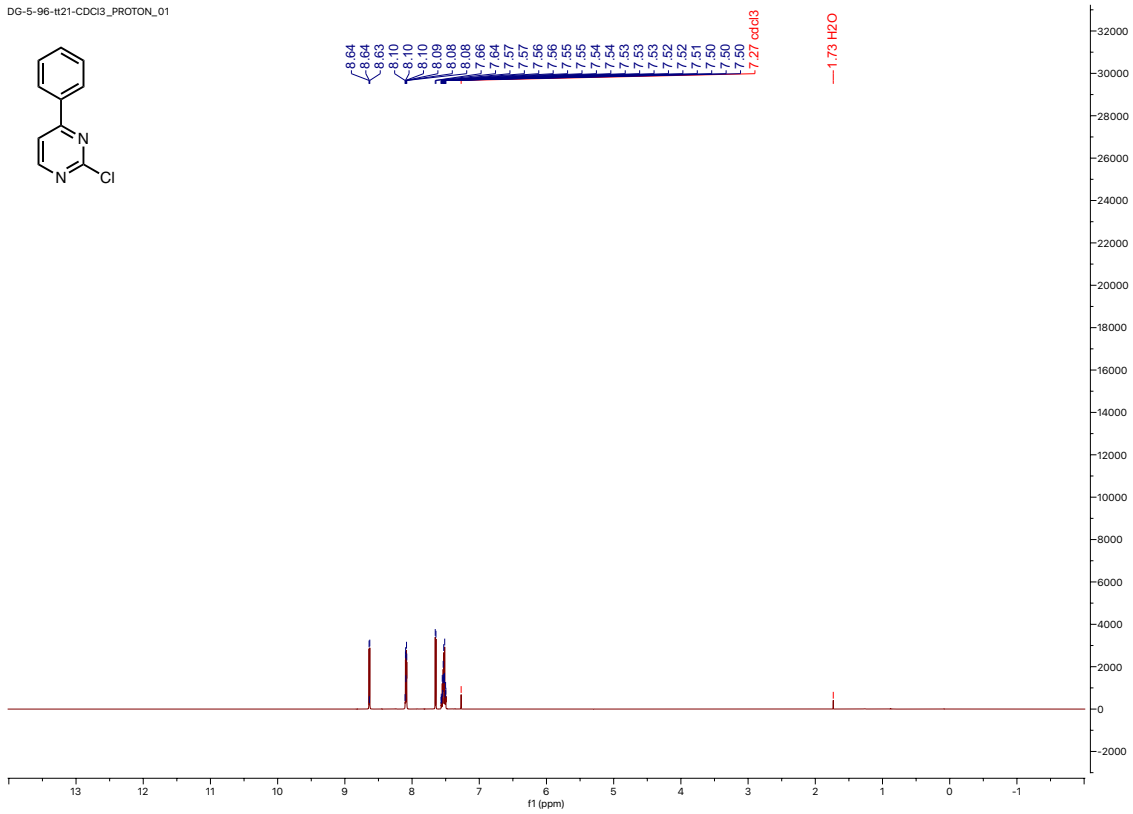

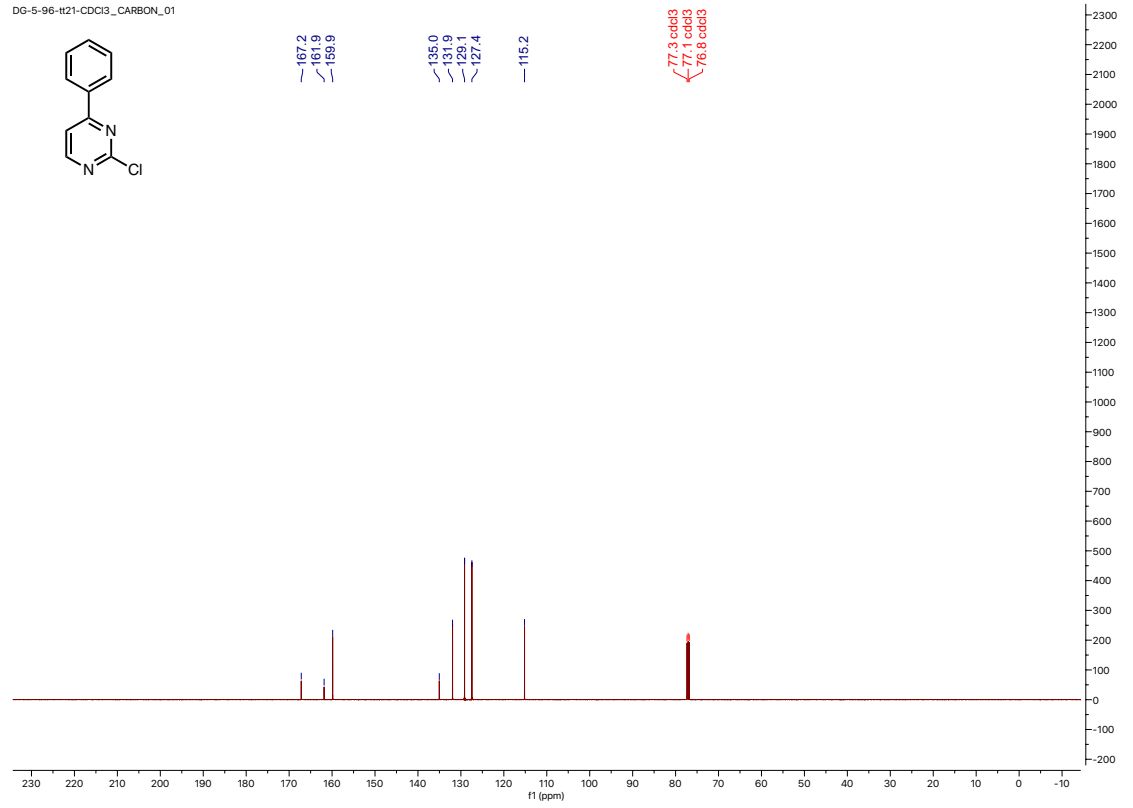

Figure 4.19: ^{1}H and $^{13}C\{1H\}$ NMR spectra of **4-15**

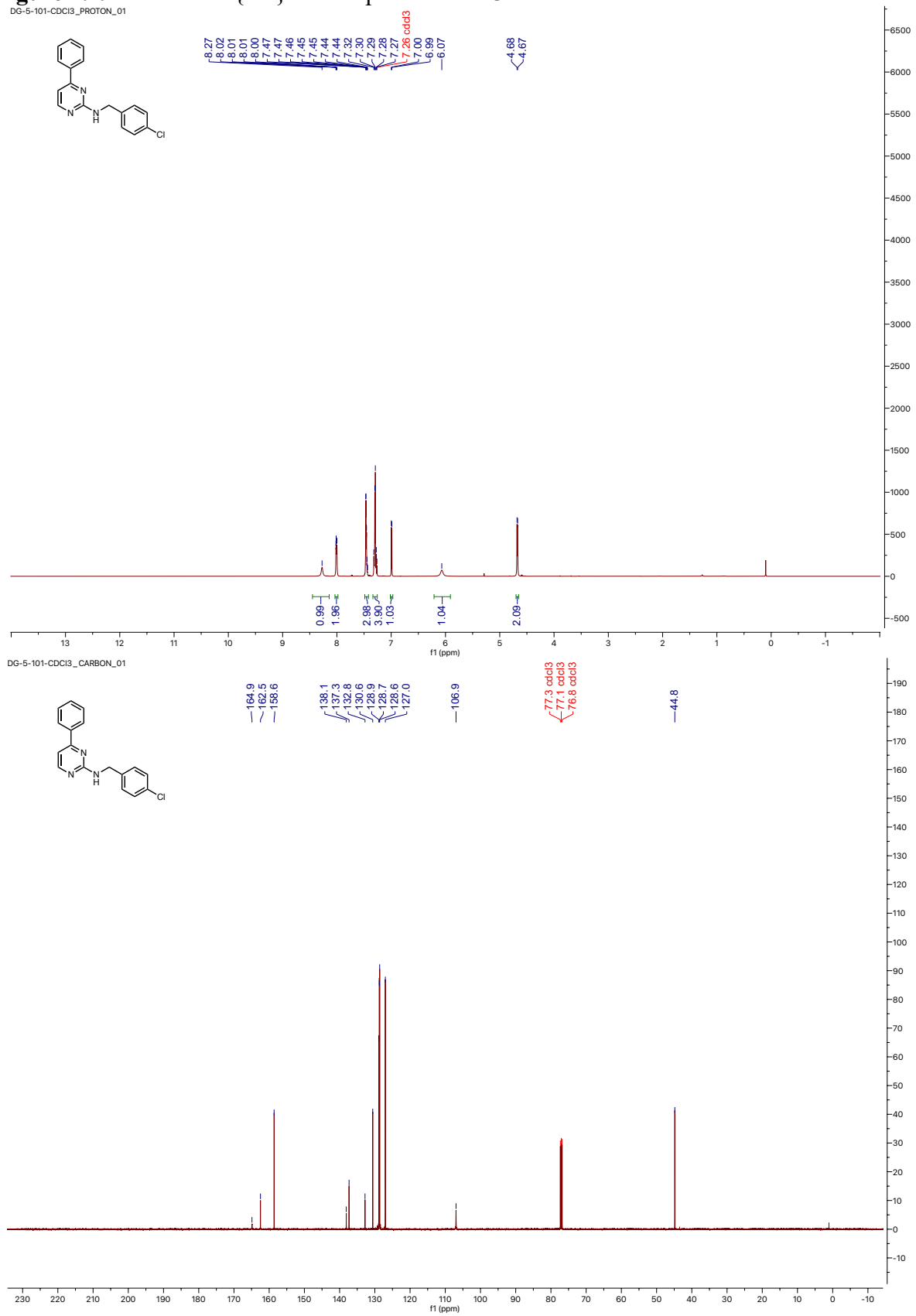

Figure 4.20: ^{1}H and $^{13}C\{1H\}$ NMR spectra of **4-16**

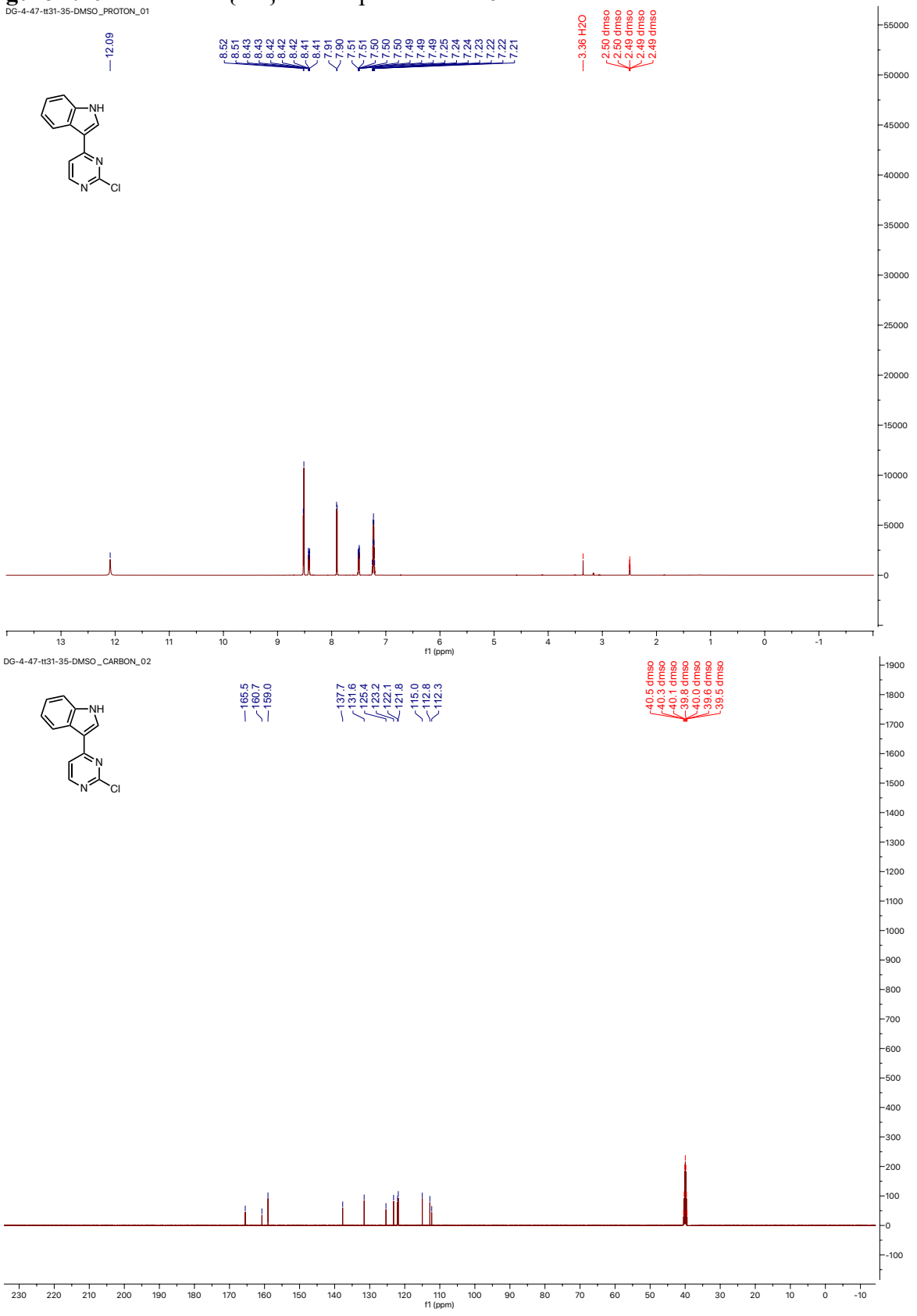

Figure 4.21: ^{1}H and $^{13}C\{1H\}$ NMR spectra of **4-17**

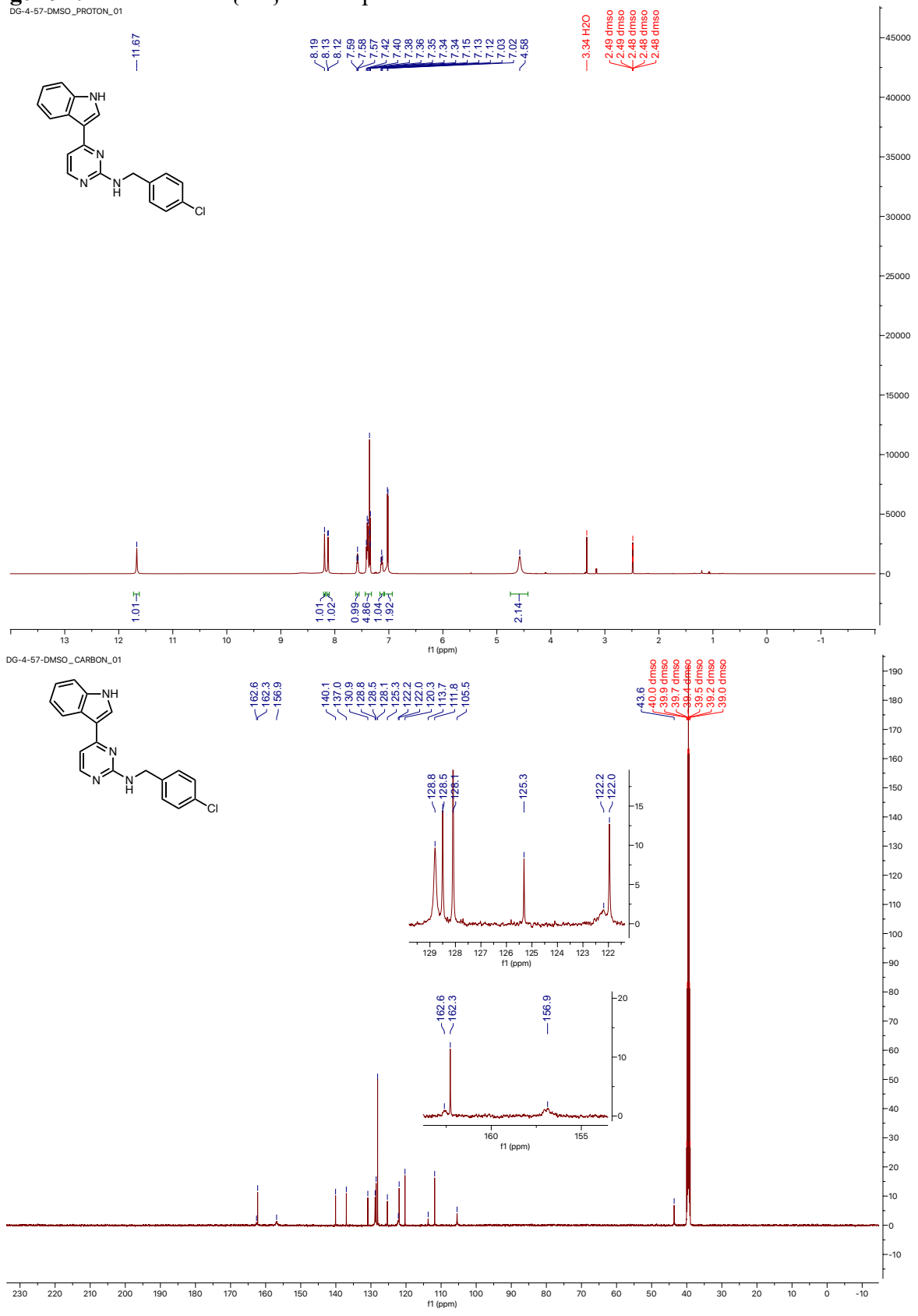

Figure 4.22: ^{1}H and $^{13}C\{1H\}$ NMR spectra of **4-17**

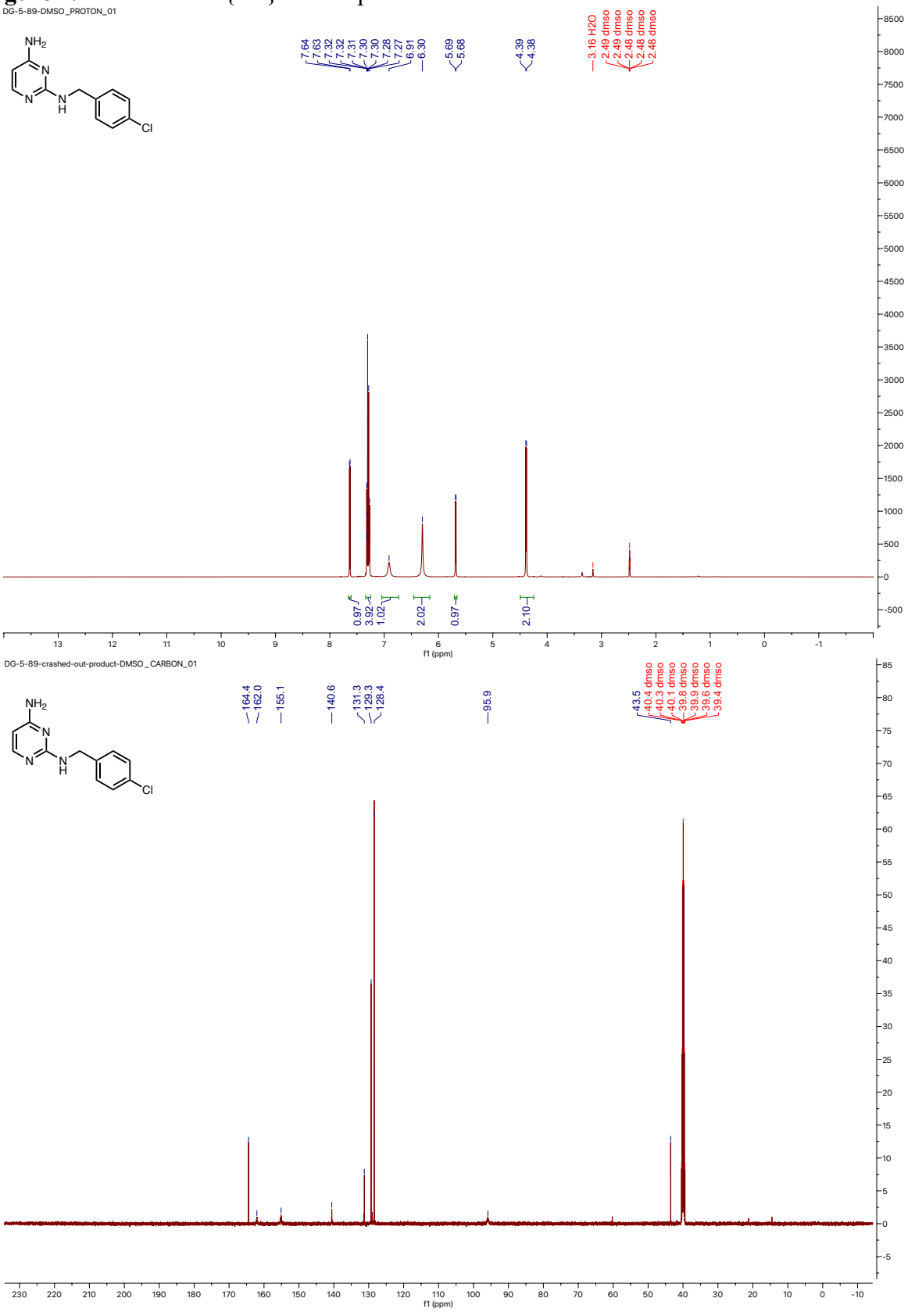

Figure 4.23: ^{1}H and $^{13}C\{1H\}$ NMR spectra of **4-20**

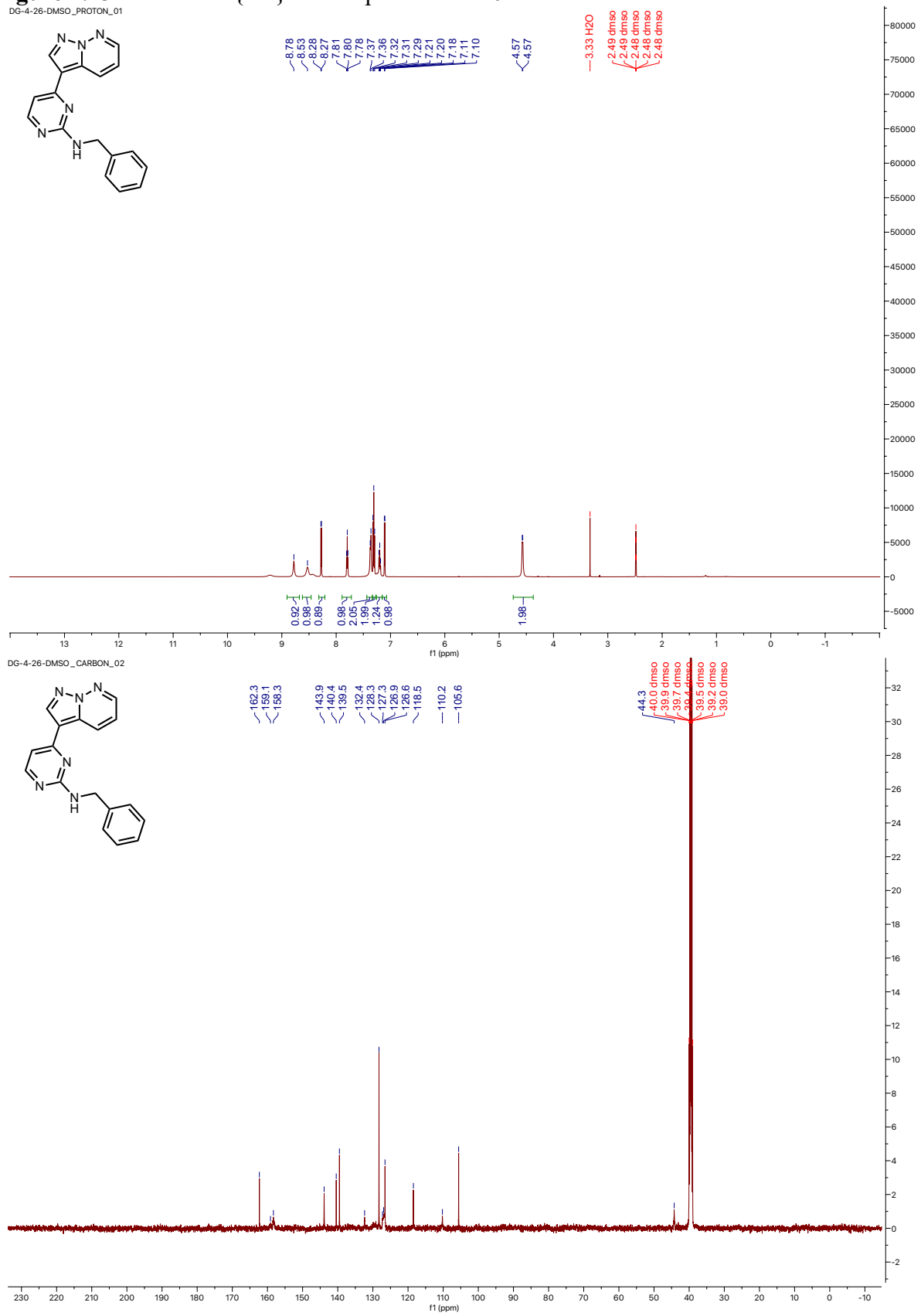

Figure 4.24: ^{1}H and $^{13}C\{1H\}$ NMR spectra of **4-21**

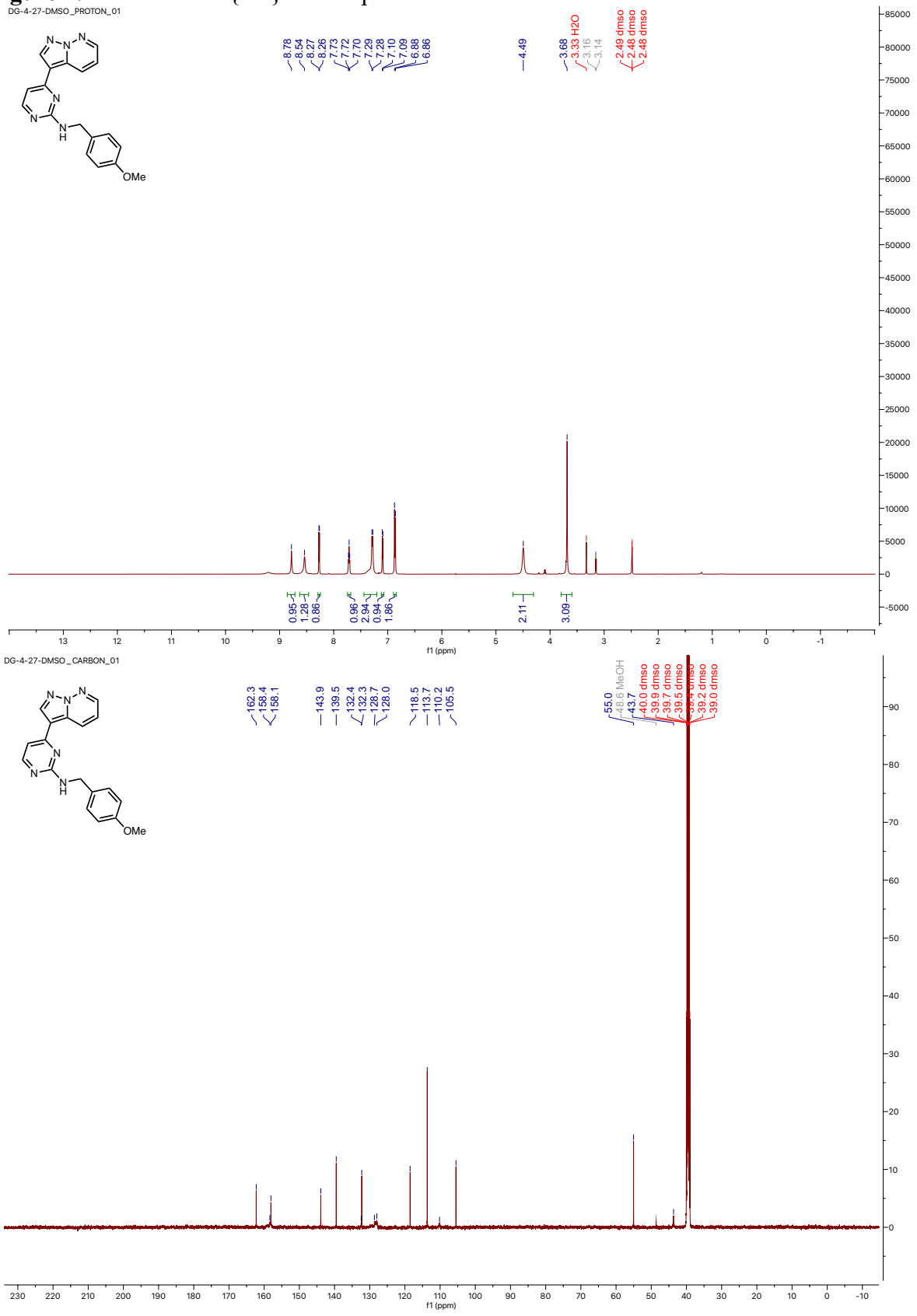

Figure 4.25: ^{1}H and $^{13}C\{1H\}$ NMR spectra of **4-22**

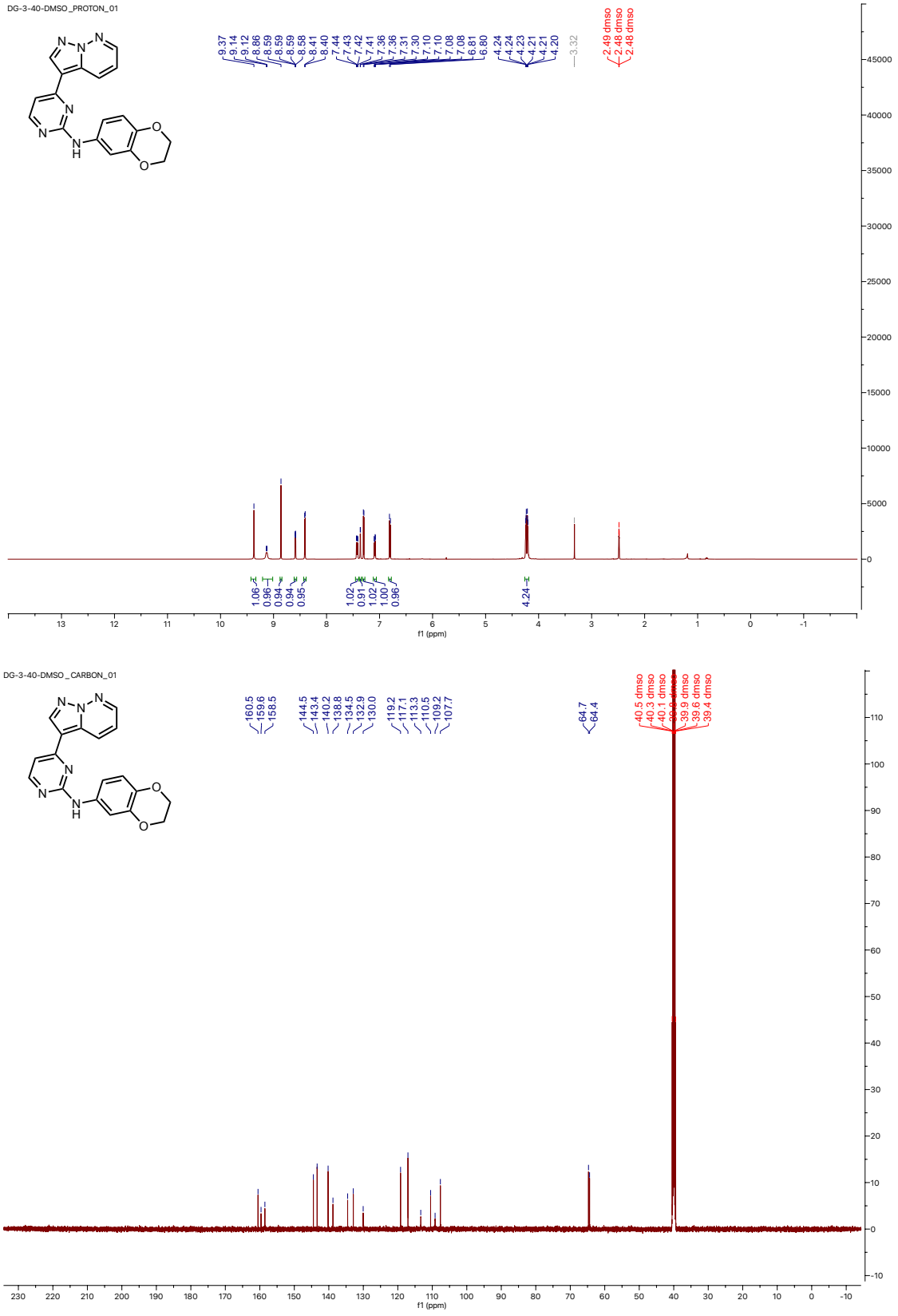

Figure 4.26: ^{1}H and $^{13}C\{1H\}$ NMR spectra of **4-23**

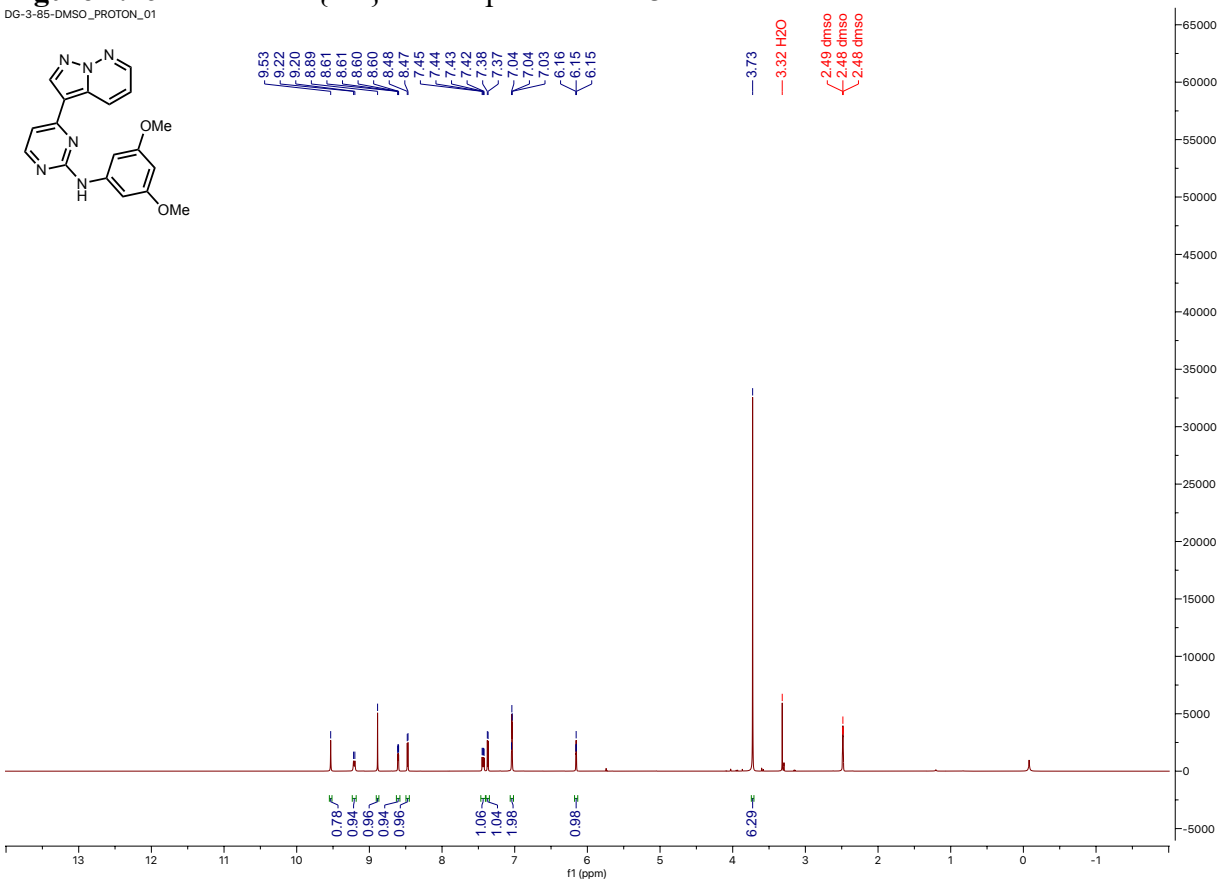

Figure 4.27: ^{1}H and $^{13}C\{1H\}$ NMR spectra of **4-24**

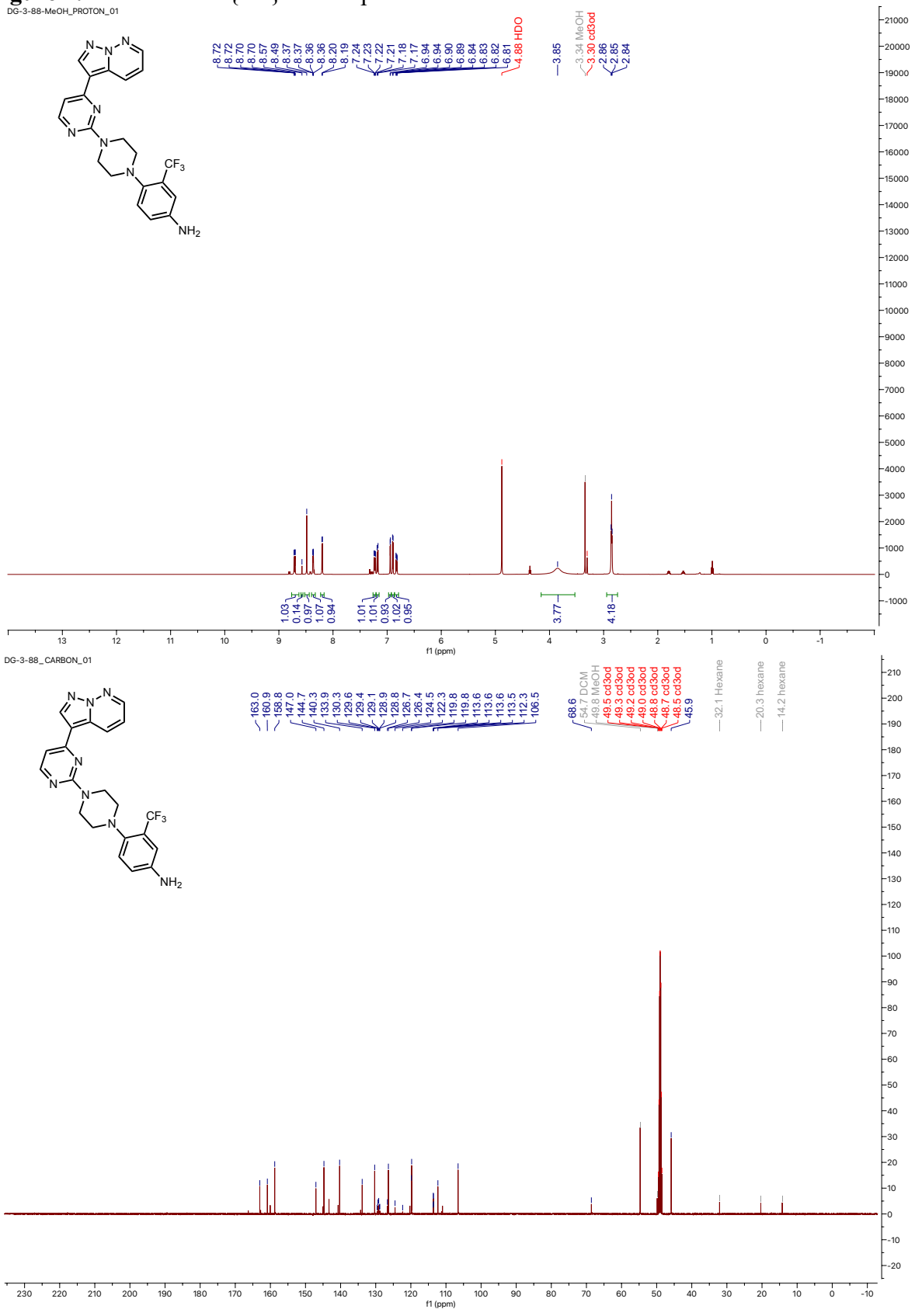

Figure 4.28: ^{1}H and $^{13}C\{1H\}$ NMR spectra of **4-25**

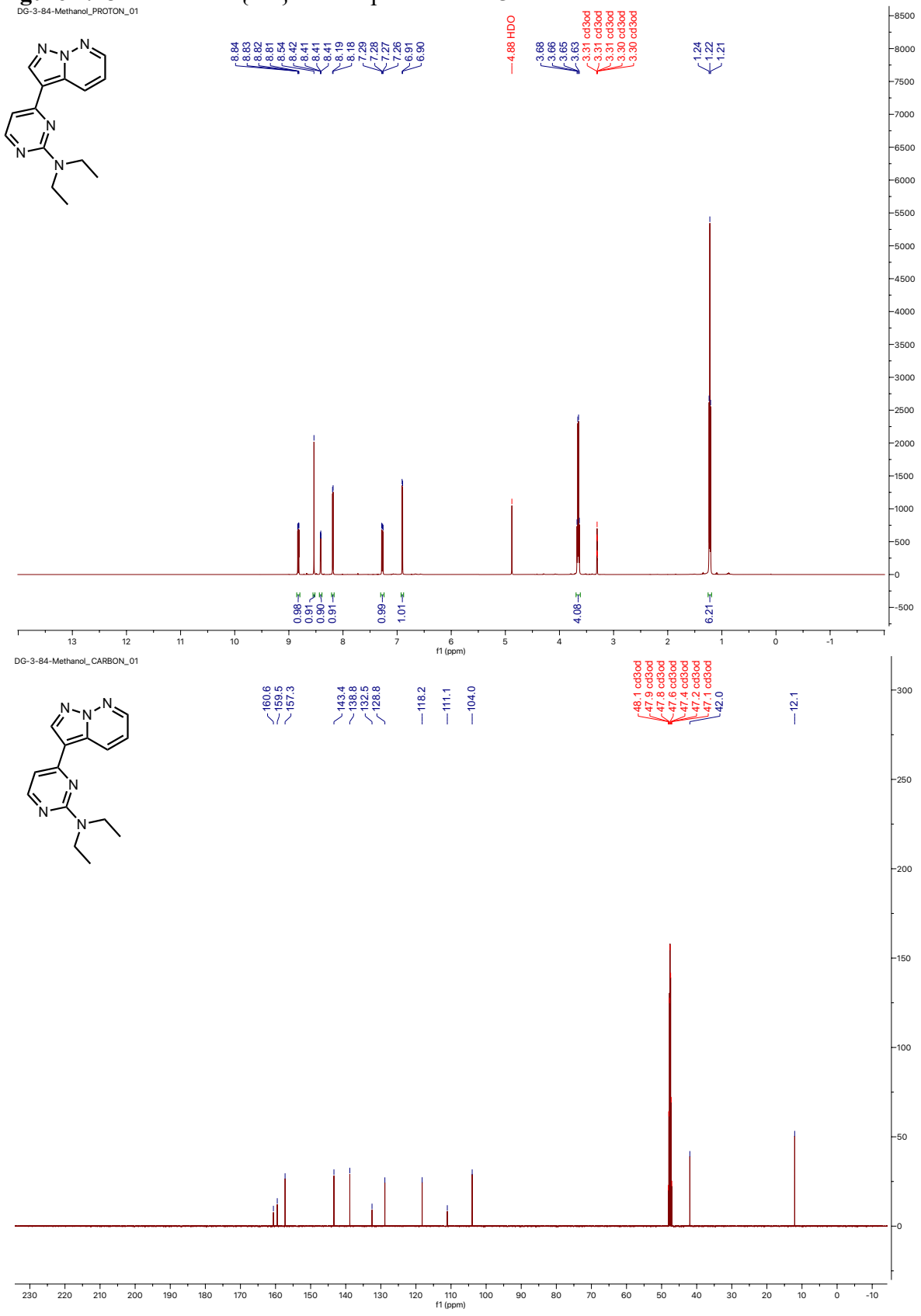

Figure 4.29: ^{1}H and $^{13}C\{1H\}$ NMR spectra of **4-26**

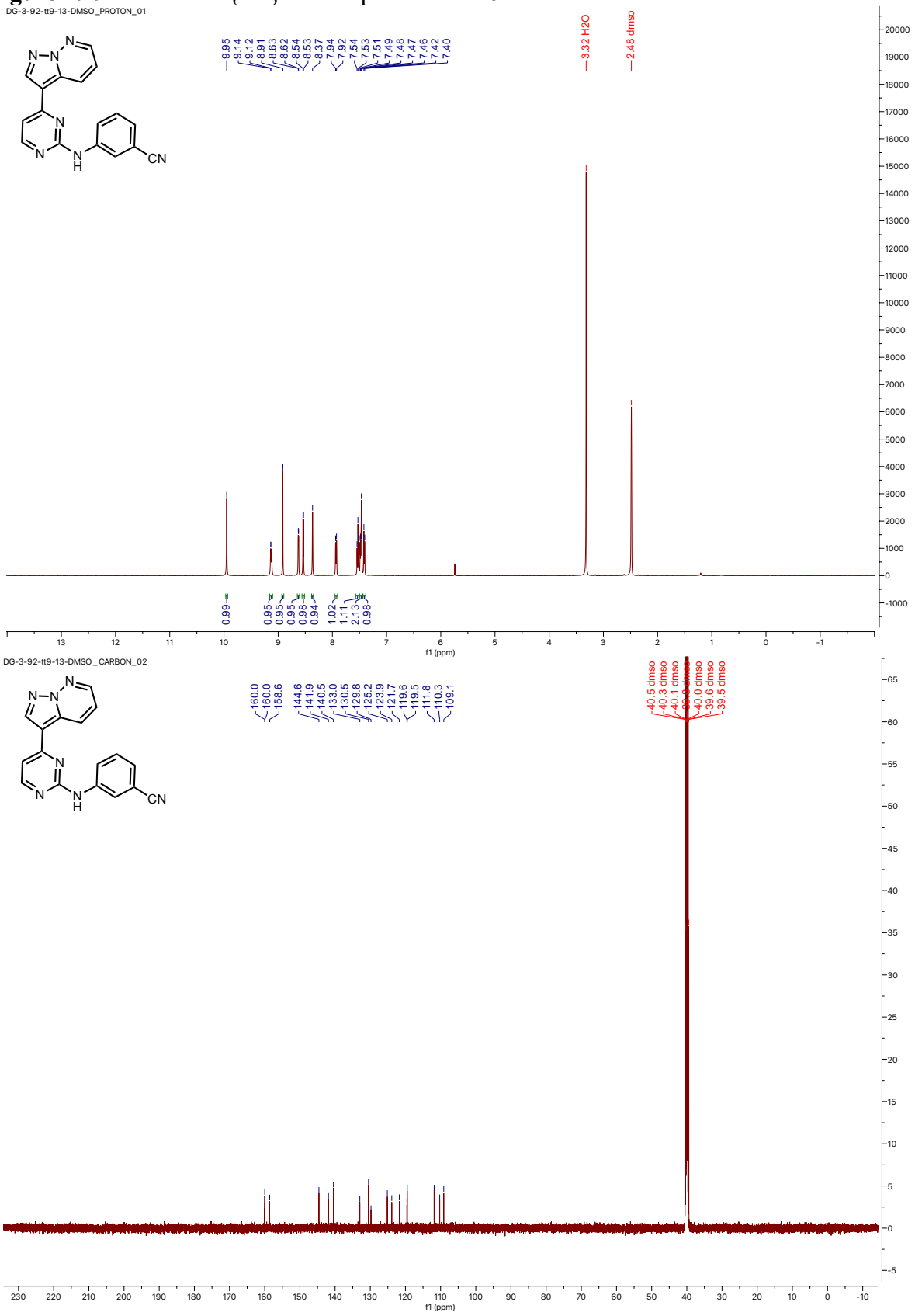

Figure 4.30: ^{1}H and $^{13}C\{1H\}$ NMR spectra of **4-29**

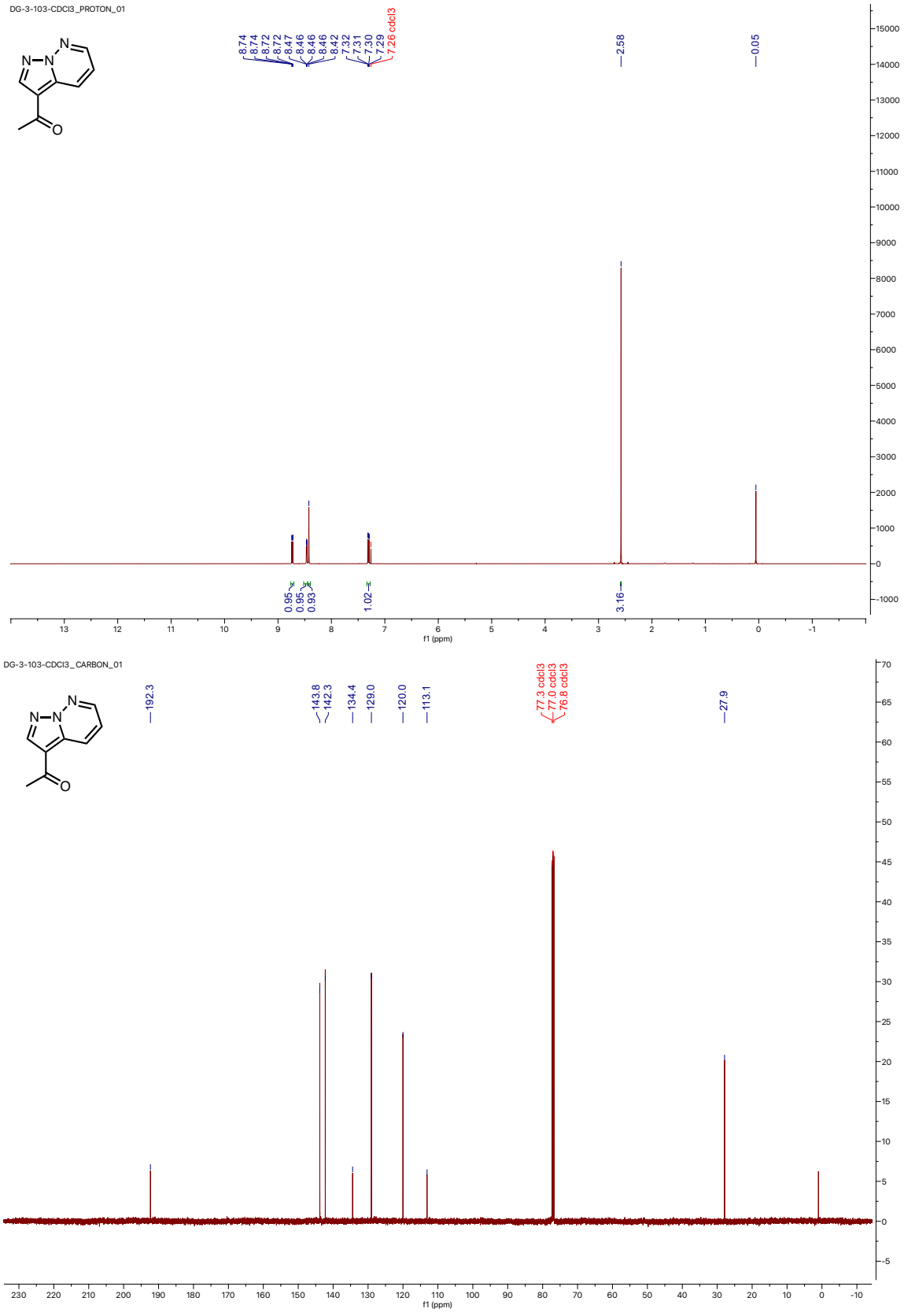

Figure 4.31: ^{1}H and $^{13}C\{1H\}$ NMR spectra of **4-30**

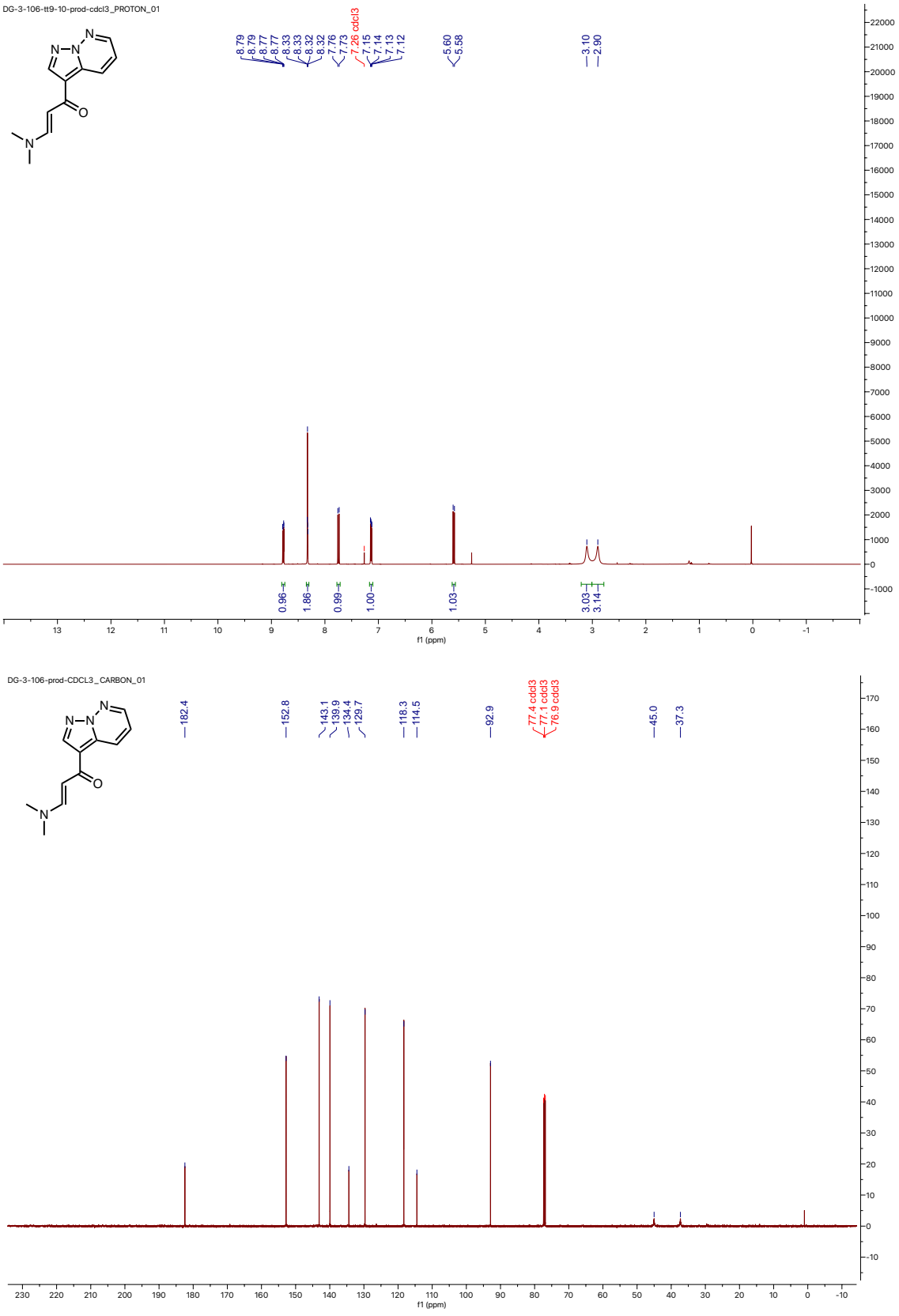

Figure 4.32: ^{1}H and $^{13}C\{1H\}$ NMR spectra of **S2**

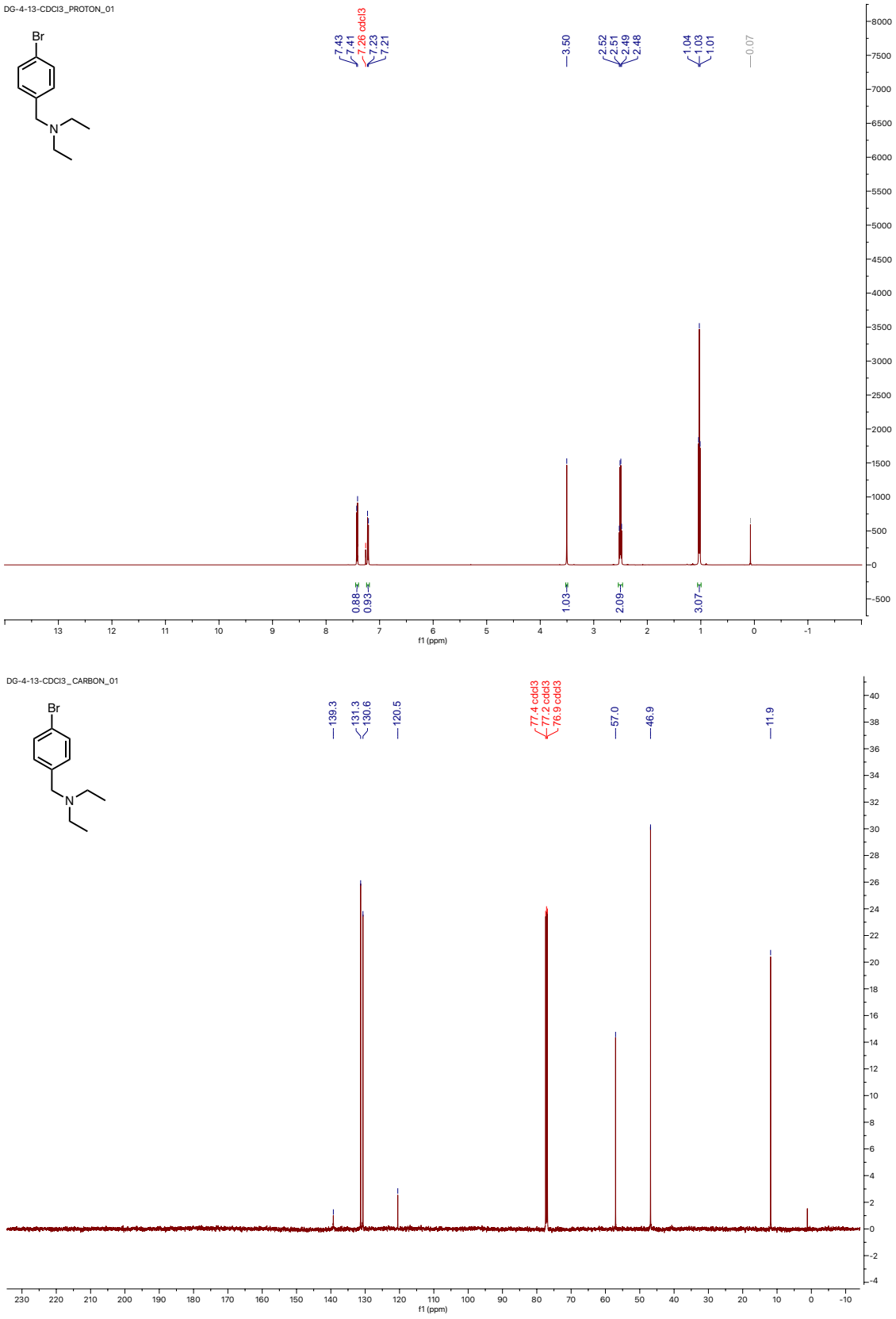

Figure 4.33: ^{1}H and $^{13}C\{1H\}$ NMR spectra of **S3**

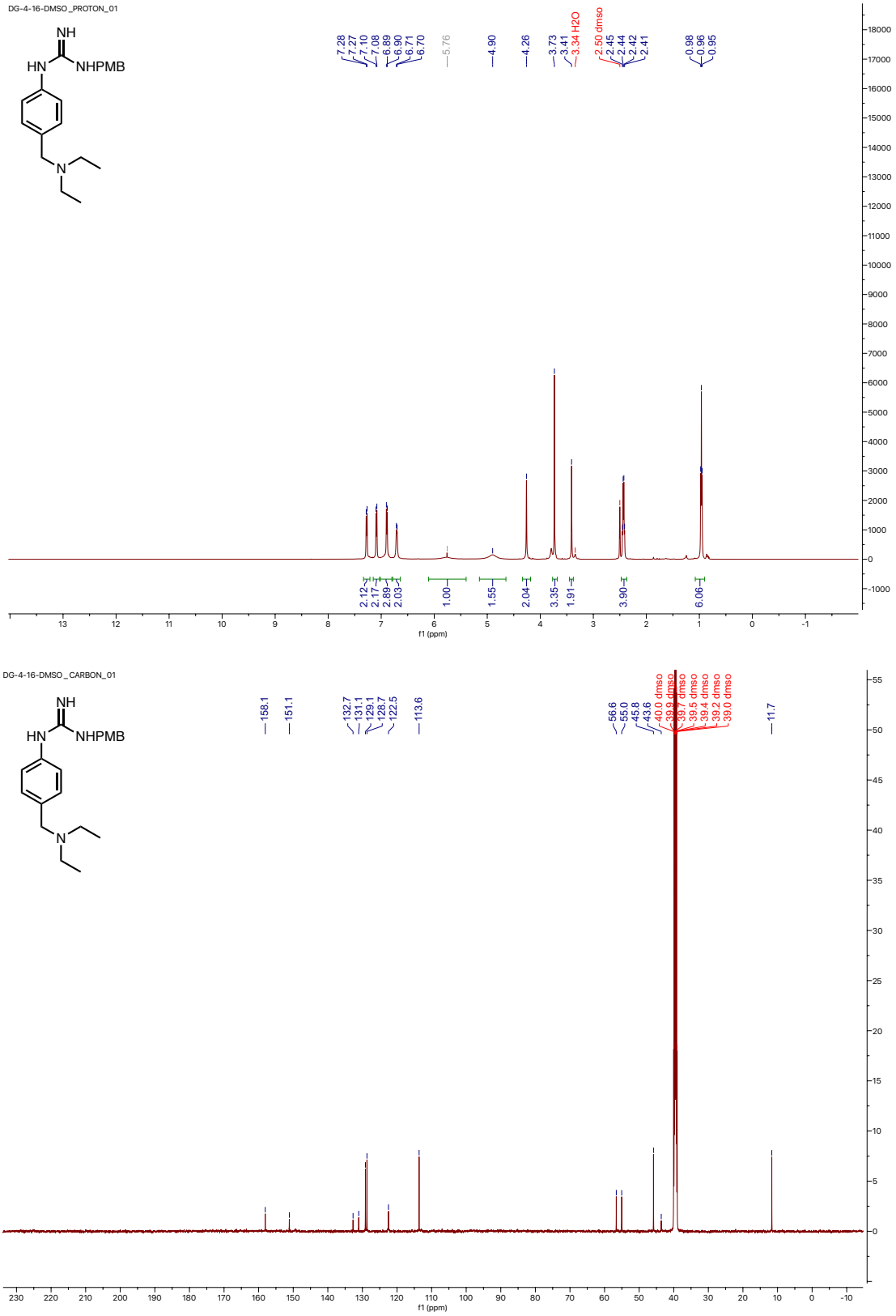

Figure 4.34: ^{1}H and $^{13}C\{1H\}$ NMR spectra of **4-27**

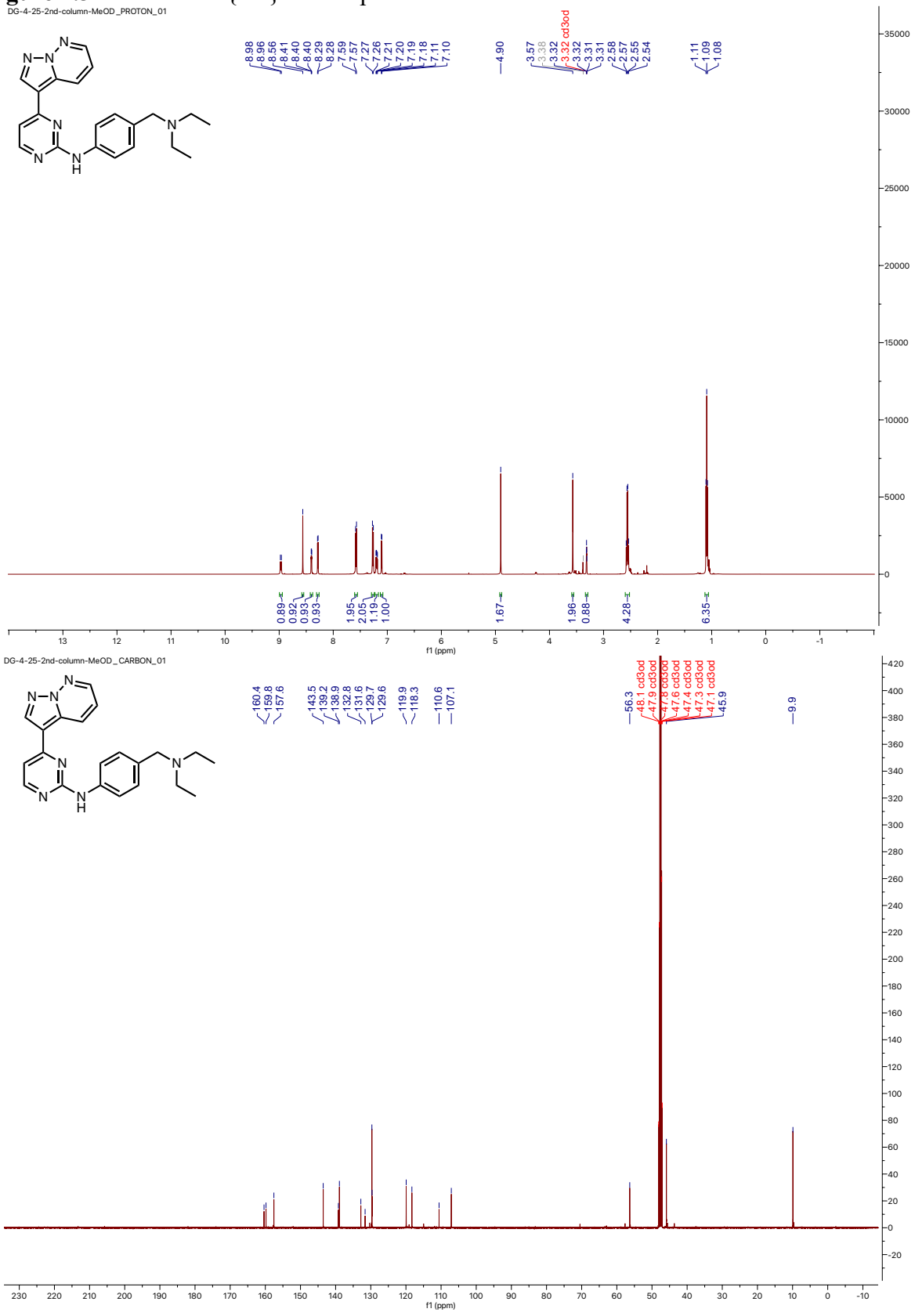

Figure 4.35: ^{1}H and $^{13}C\{1H\}$ NMR spectra of **4-28**

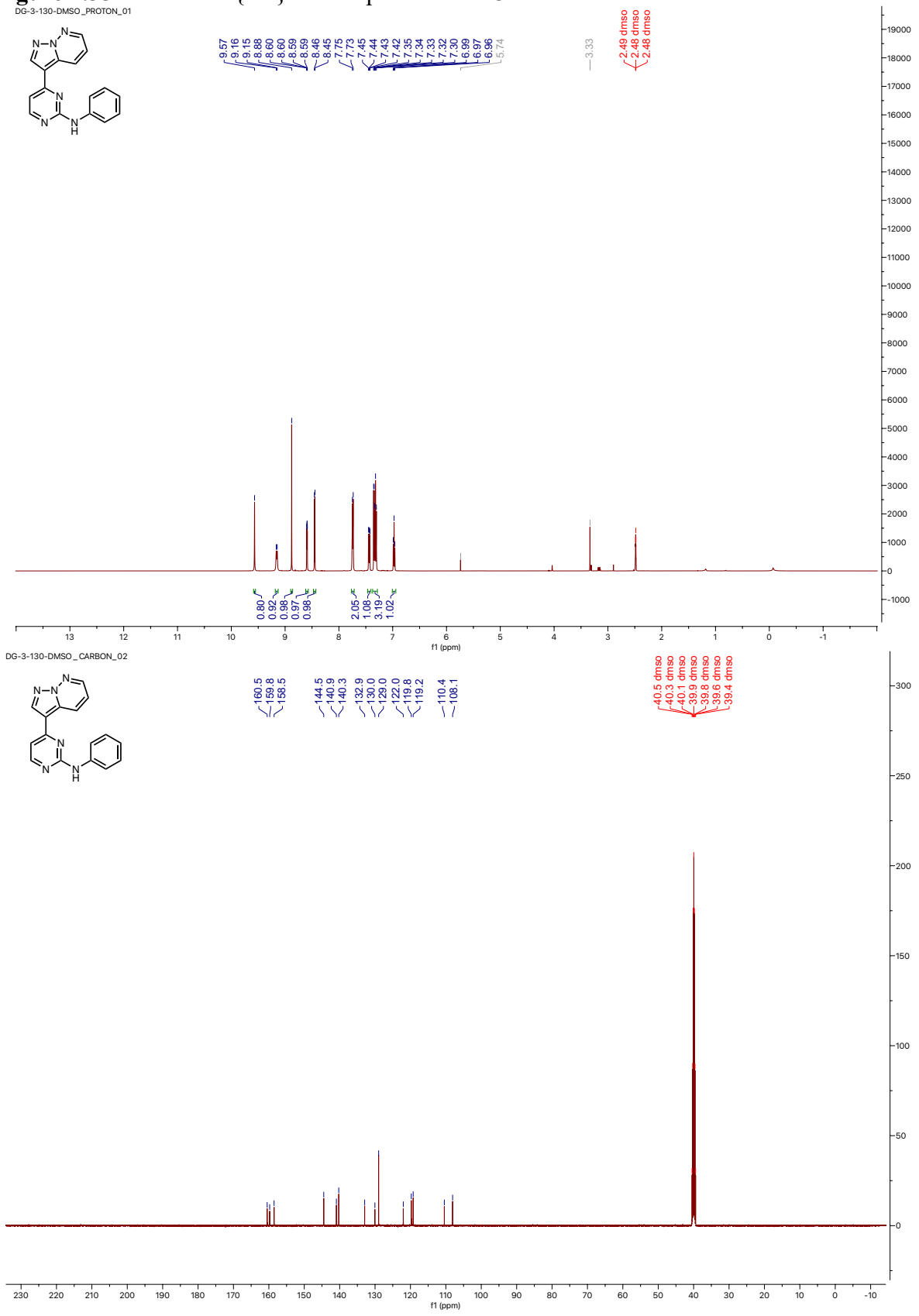

Figure 4.36: ^{1}H and $^{13}C\{1H\}$ NMR spectra of **4-31**

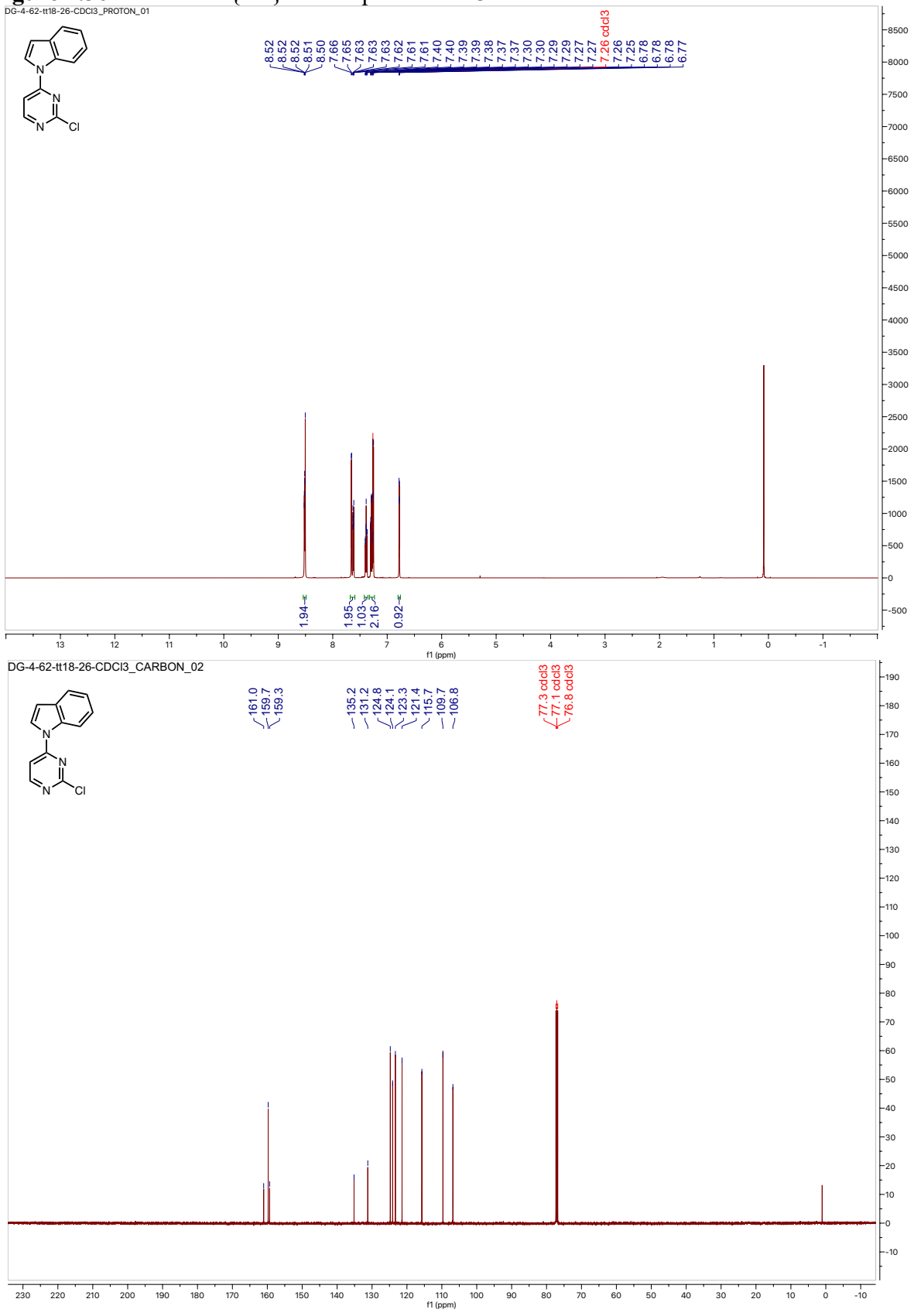

Figure 4.37: ^{1}H and $^{13}C\{1H\}$ NMR spectra of **S6**

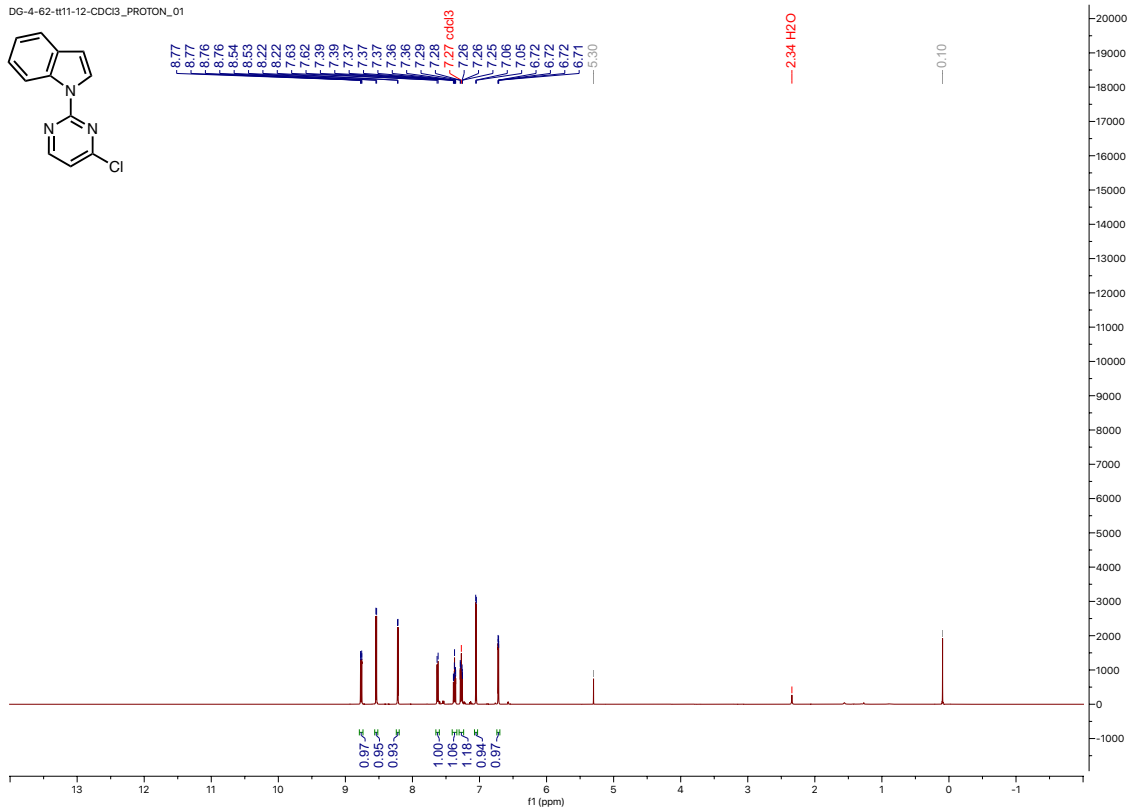

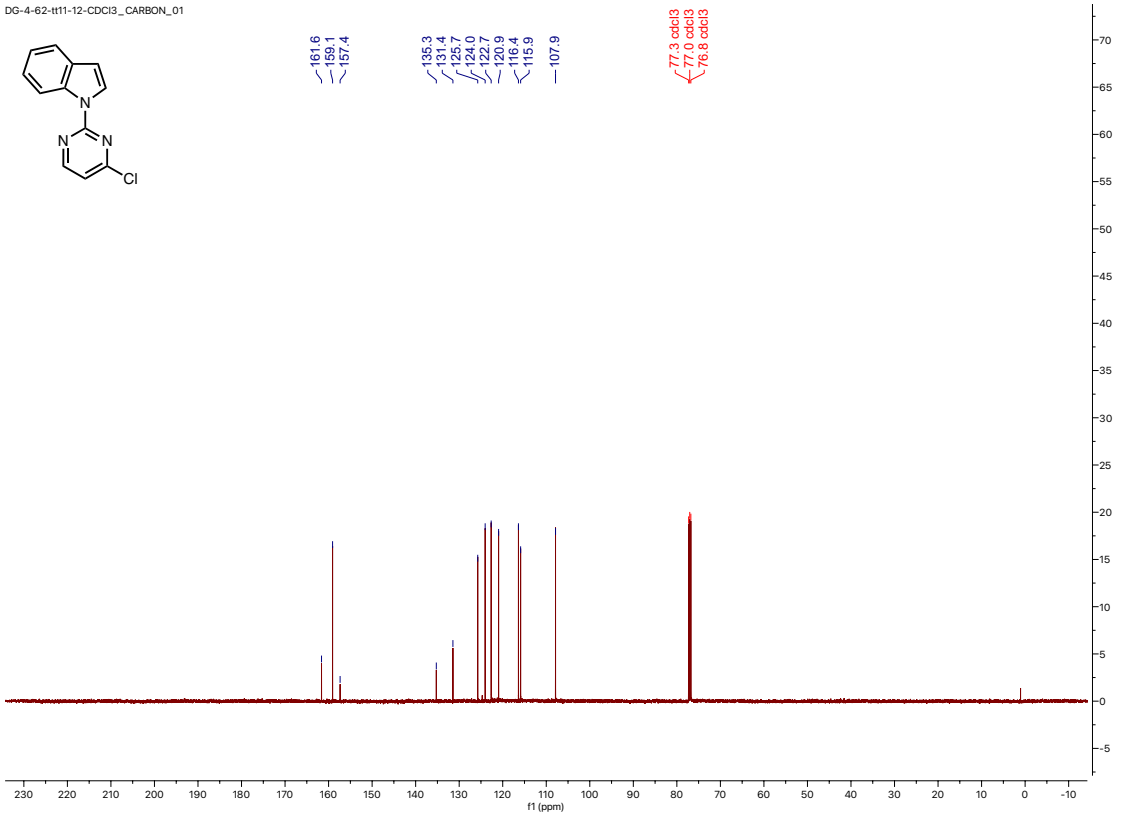

Figure 4.38: ^{1}H and $^{13}C\{1H\}$ NMR spectra of **4-32**

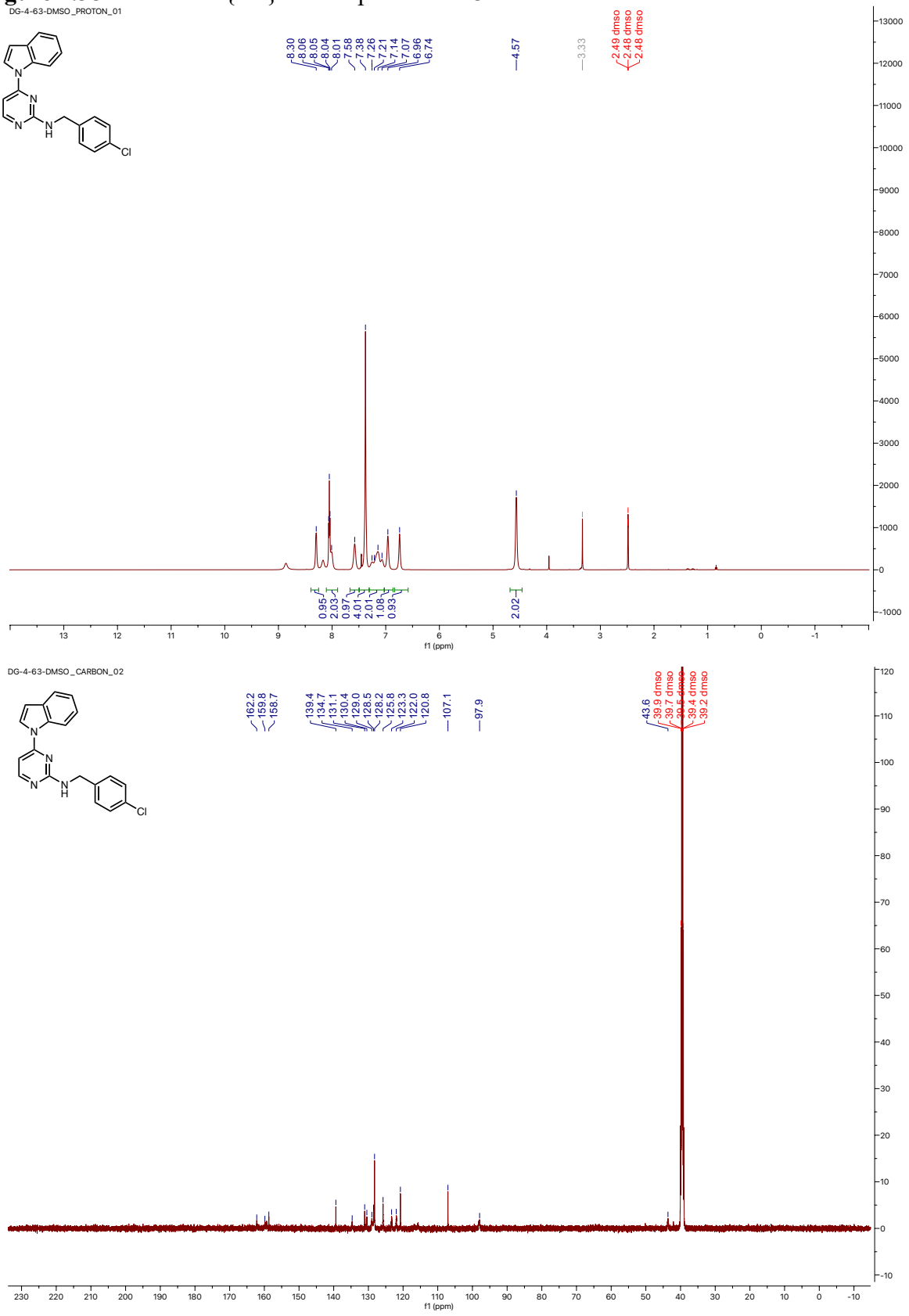

Chapter 5: Progress towards the design and synthesis of molecular proteasome staples and probes

5.1 Introduction

Proteasomes are intricate protein complexes responsible for the degradation and recycling of damaged or unwanted proteins within cells. These cellular "recycling centers" play a vital role in maintaining protein homeostasis and regulating various cellular processes, including cell cycle progression, DNA repair, and immune response.[1] Among the various types of proteasomes, the human 20S proteasome has gained significant attention due to its central role in protein degradation. The 20S proteasome is composed of four stacked rings, each containing seven distinct subunits, forming a barrel-shaped structure (**Figure 5.1**). It possesses three types of proteolytic activities: caspase-like, trypsin-like, and chymotrypsin-like, enabling the proteasome to cleave proteins at different sites.[2] The 20S proteasome can be divided into two distinct rings: the outer alpha rings and the inner beta rings (**Figure 5.1a**).[3] The alpha ring of the 20S proteasome forms the outermost layer of the complex and provides structural stability. It consists of seven distinct alpha subunits (α1-α7) arranged in a circular manner (**Figure 5.1c**). These alpha subunits share a conserved proteasome-activating nucleotidase (PAN) domain, which contributes to the overall assembly and stability of the 20S proteasome complex. Additionally, specific alpha subunits within the alpha ring have specialized functions. For example, α1 and α2 subunits are involved in regulating the opening and closing of the proteasome gate for substrate entry and exit, while the α3 subunit contributes to the assembly and integrity of the complex, and the α4 subunit plays a role in substrate recognition and processing.[4-5]

Figure 5.1: Overview of the structure of 20S proteasome

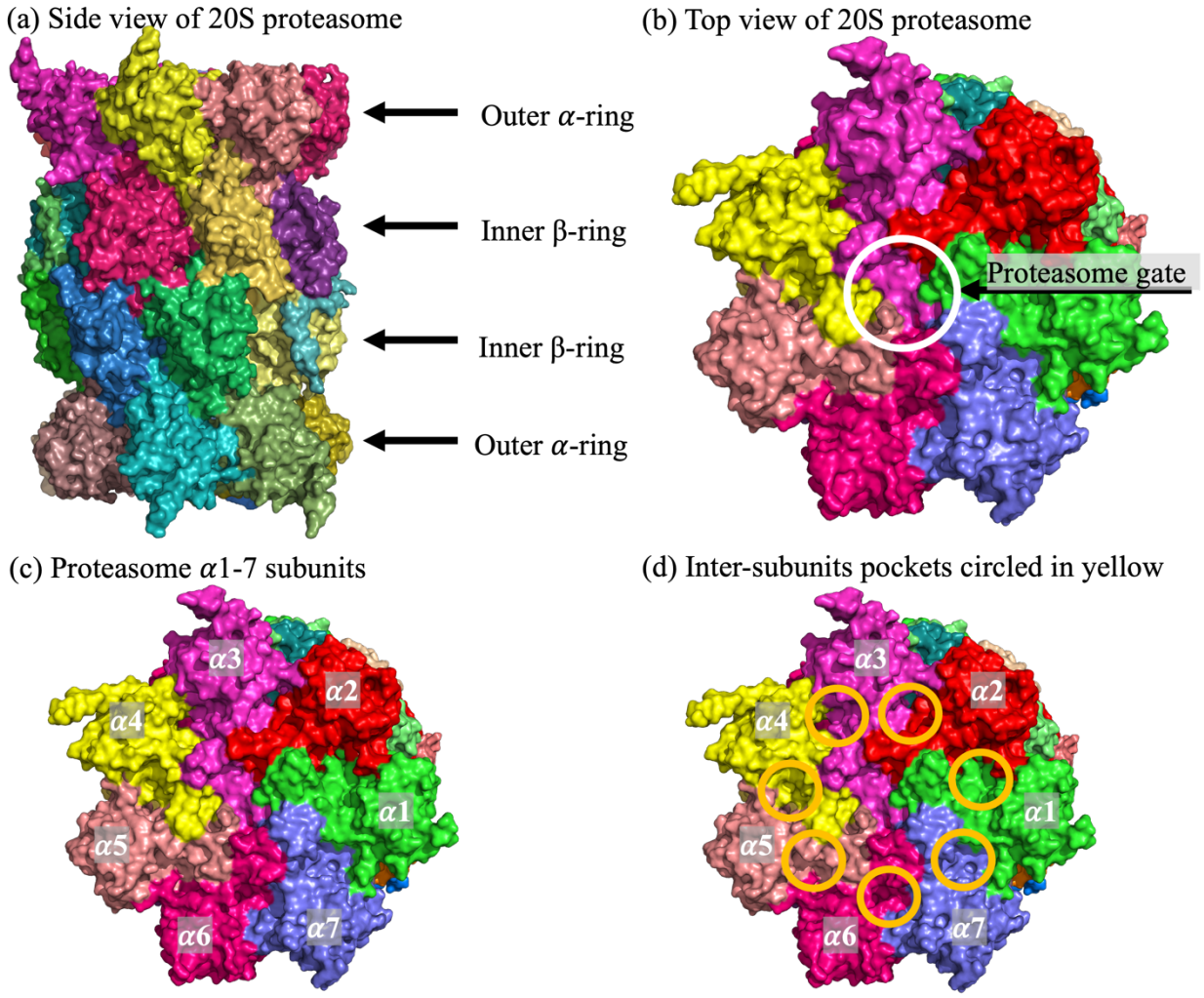

Dysregulation of proteasome activity has been implicated in several diseases, including cancer, neurodegenerative disorders, and autoimmune conditions (see Chapter 3).[6-7] Consequently, the development of proteasome modulators has been proposed as a novel strategy to treat these neurodegenerative diseases.[8-13]

Our lab and others have identified various activators of the 20S proteasome that are hypothesized to interact directly the α-ring of the 20S proteasome to induce an open gate conformation.[8,11-13] To understand the mechanism of activation of 20S proteasome by our small molecules, atomic force microscopy (AFM) imaging was used to study the gate opening dynamics

of 20S proteasome with TCH-165 (a known 20S proteasome activator).[8] While AFM imaging showed that there was a significant increase in the population of open gate 20S proteasome particles in treated sample compared to control, binding mechanism could not be elucidated using this technique. In addition, previous computational studies from our lab showed that the small molecule activators of 20S proteasome interact with the inter-subunit pockets on the α-ring of the 20S proteasome to induce the open gate conformation, however, the binding mode of this small molecules still remain unclear via molecular docking.[8,11-13] Identification of ligands binding site, especially the important subunits and residues needed to induce 20S proteasome gate opening would have a huge impact on the designing of future proteasome activators. Furthermore, if the small molecule binding site is determined to be the inter-subunit pockets on the α-rings, this would validate the molecular docking approach currently being used to predict the small molecule binding to the 20S proteasome.

Several attempts have been made over the years in the group to identify the binding the binding site of small molecule activators of 20S proteasome using mass spectrometry and Cryo-EM. These attempts have failed partially due to the significant size difference between the 20S proteasome, which is approximately 750,000 Da, and the much smaller ligands used in the study, which are about 500 Da. In recent Cryo-EM attempts by Allison Vanecek, from the Tepe group, to obtain the structure of 20S proteasome bound to small molecule activator (SS-4-15, EC_{200} = 1.2 ± 0.6 μM) of the 20S proteasome, the structure of the ligand-bound 20S proteasome could not be obtained, likely due to the low proportion of ligand-bound 20S proteasomes complex compared to unbound ones. The 3D structure is reconstructed by averaging various 2D classes, so if only a small fraction of 20S proteasomes have a ligand bound, the electron density of the ligand may be

averaged out in the final 3D structure. Additional, high concentration of compound (~200 μM) was used and resulted in denaturing of the 20S proteasome during sample preparation.

We proposed we could overcome these challenges by utilizing more potent small molecule binders of the 20S proteasome. These compounds would have lower off rate and would increase the chance of obtaining a ligand-bound 20S proteasome. We hypothesized that we could design molecules that would target multiple binding pockets on the 20S proteasome since crystal structure and cryo-EM showed that the 20S proteasome have seven binding pockets on each α-ring. We called these molecules "proteasome staples". The proteasome staples are also hypothesized to be better binders of the 20S proteasome and lock the 20S proteasome in a more rigid conformation that would enable image collection during cryo-EM studies better. The proteasome staples are also expected to have higher potency than traditional proteasome modulators, as they target multiple binding sites simultaneously. However, translating these molecules into therapeutics would be challenging due to their large size and their violation of Lipinski's Rule of Five for oral drugs. Nonetheless, they could serve as valuable tools for understanding how 20S proteasome activators bind to the protein.

5.2 Results and Discussion

5.2.1 Designing molecules i.e. "proteasome staples" that target multiple inter-subunit pockets on the α-rings of the 20S proteasome

The proteasome staples are made of two main components: small molecule proteasome modulators and a linker (**Figure 5.2**). Proteasome modulators are compounds hypothesized to target the inter-subunit pockets of the 20S proteasome. Each proteasome modulator at each end of the linker is designed to target a different but adjacent inter-subunit pocket. When designing the staples, there were series of things that were considered. The first thing was identifying the

proteasome modulator of choice from the list of proteasome activators from our lab. A good choice of molecule would be one that have non-specific binding on the proteasome inter-subunit pocket i.e. the molecule should bind on multiple binding pockets on the α-ring, preferrable adjacent binding pockets. This would avoid having to use two different molecules to target different inter-subunit pocket on the 20S proteasome. Also, the molecule of choice should be easily functionalized with a handle that would allow easy coupling to any linker of choice.

Figure 5.2: Generic structure for the 20S proteasome staples

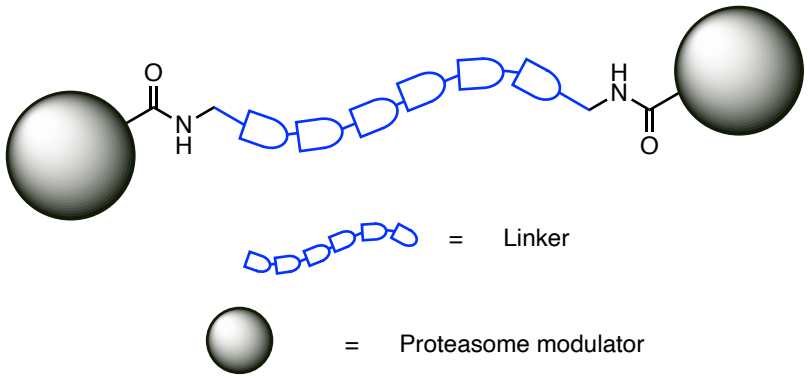

Among all the known proteasome activators in our lab, we selected compound **5-1** (**Figure 5.3**). Compound **5-1** was selected as a molecule of choice because it has an indole moiety that could be easily functionalized at the C-3 position as a handle to incorporate a linker of choice. Although, docking studies predicted that 4 out of 9 preferred modes of **5-1** bind to the α1-2 inter-subunit pocket on the 20S proteasome and no other inter-subunit pocket. Interestingly, the derivatives of **5-1** such as the carboxylic acid **5-2** and amide derivatives **5-3** & **5-4** predominantly bind to both the α1-2 and α2-3 inter-subunits pockets making them a promising candidate for the proteasome staple design. Compounds **5-3** and **5-4** were used to mimic how one end of the proteasome staple would bind to the 20S proteasome.

Figure 5.3: Structure **5-1** and derivatives

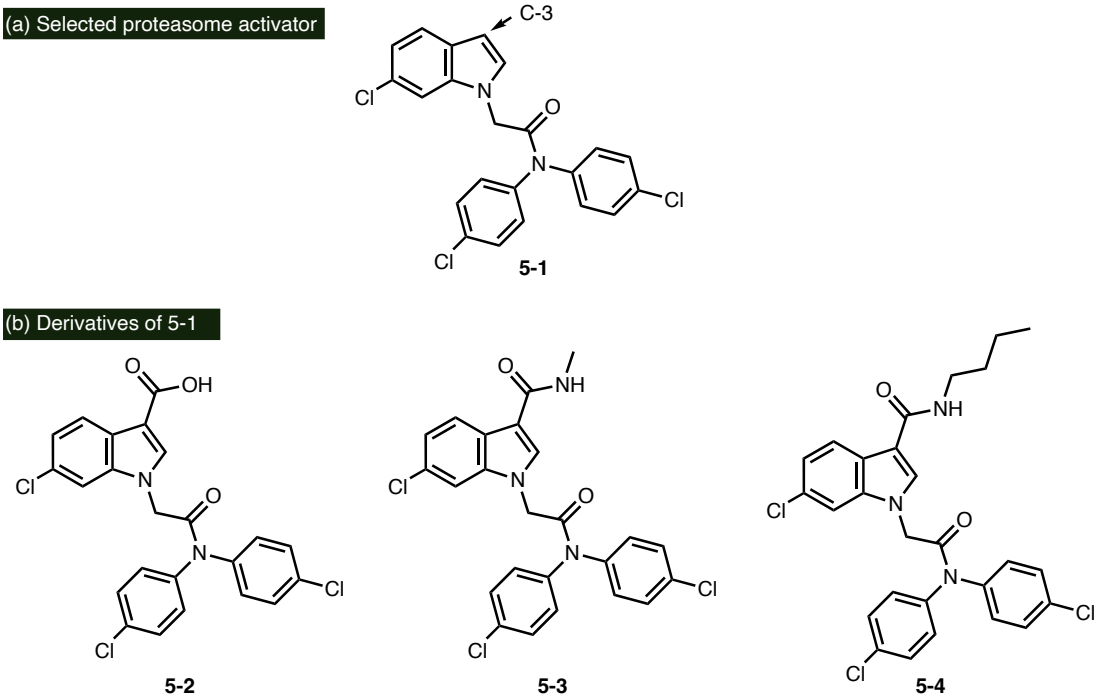

Compound **5-1** was also selected because docking studies showed the C-3 position in the indole moiety to be exposed (**Figure 5.4a**), thereby indicating that there would be high possibility of maintaining similar binding pose even after functionalization with a linker. Similar result was seen with compound **5-3** in the α1-2 inter-subunit pocket of the 20S proteasome (**Figure 5.4b**). Both docking results further support the possibility of the compound maintaining its current binding pose in the proteasome after functionalizing with a linker and also allow the linker to extended outside of the binding pocket into the adjacent inter-subunit pocket for the other end of the staple to bind.

Figure 5.4: Docking pose of compounds **5-1** and **5-3** in 20S proteasome inter-subunit binding site

(a) Docking of compound **5-1**

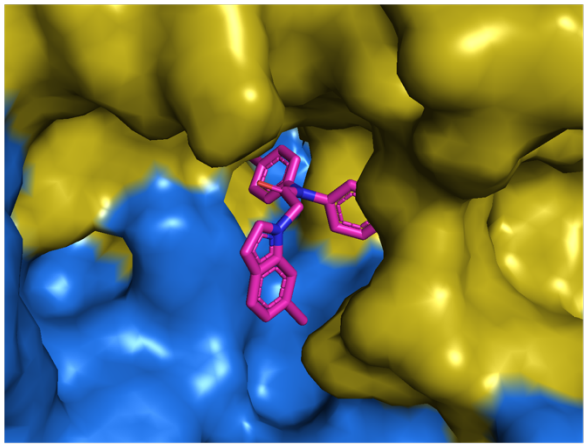

(b) Docking of compound **5-3**

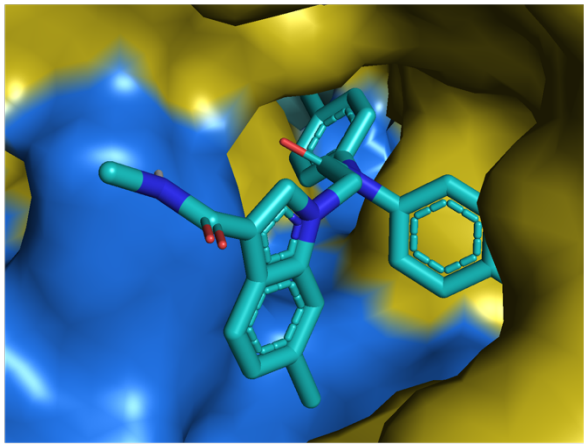

Another important information to mention is that compound **5-3** and **5-4** maintained proteasome activity with EC_{200} of 3.1 µM and 2.4 µM respectively when compared to **5-1** with EC_{200} = 3.1 µM, indicating that the additional functionality at the C-3 position of the indole does not significantly impact the binding of the molecule to the 20S proteasome, which is desirable for eventual functionalization with a linker.

Following the selection of the proteasome modulator, the next thing was selecting the linker of choice. Polyethylene glycol was selected as a linker of choice due to its water solubility and great biocompatibility.[14] The biggest challenge after identifying the linker of choice was determining the suitable PEG length. To get an insight into the approximate number of PEG needed for compounds to reach both the α1-2 and α2-3 inter-subunit pockets, the distance between these two inter-subunit pockets was measured using Pymol and was determined to be between 28 Å – 30 Å (**Figure 5.5**) which is equivalent to about 5-6 PEG units. Although this length only indicates the straight distance between the two inter-subunit pockets, it does not account for folding or extra PEG units that would be needed within each of the inter-subunit pocket to extend to the outside of the proteasome. To account for folding and extra PEG units, more than 6 PEG units would be

needed to reach both the α1-2 and α2-3 inter-subunit pockets of the proteasome. Hence, several staples with varying PEG length were synthesized as discussed in section **5.2.3**.

Figure 5.5: Distance between the α1-2 and α2-3 inter-subunit pockets in Å

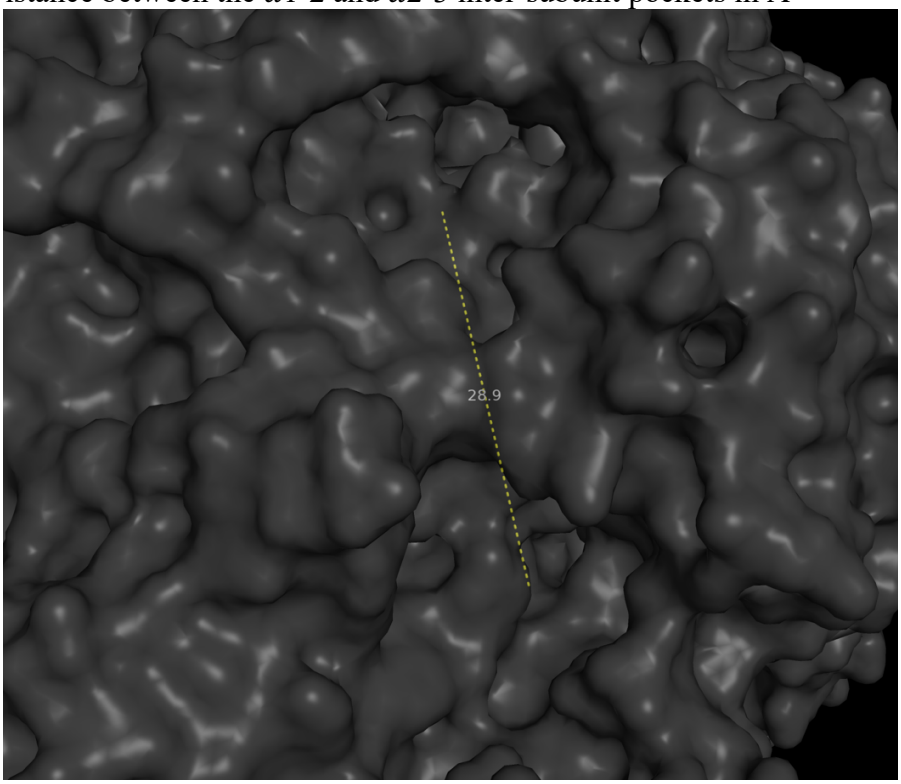

5.2.2 Synthesis of compound 5-1 and derivatives

Compound **5-1** was synthesized in two steps starting from **5-5**. Compound **5-5** was first acylated with chloroacetyl chloride to give amide **5-6** which was then alkylated with 6-chloroindole to give the desired compound **5-1** in 83% yield (**Scheme 5.1**). Vilsmeier-Haack reaction on **5-1** gave aldehyde **5-7** which was then oxidized with potassium permanganate to give carboxylic acid **5-2** in 55% yield. Alternatively, the carboxylic acid **5-2** can be synthesized from amide **5-6** by direct alkylation with 6-chloroindole-3-carboxylic acid in 87% yield, making compound **5-2** accessible in two steps from commercially available starting material **5-5** (**Scheme 5.1**).

Scheme 5.1: Synthesis of compound **5-1** and **5-2**

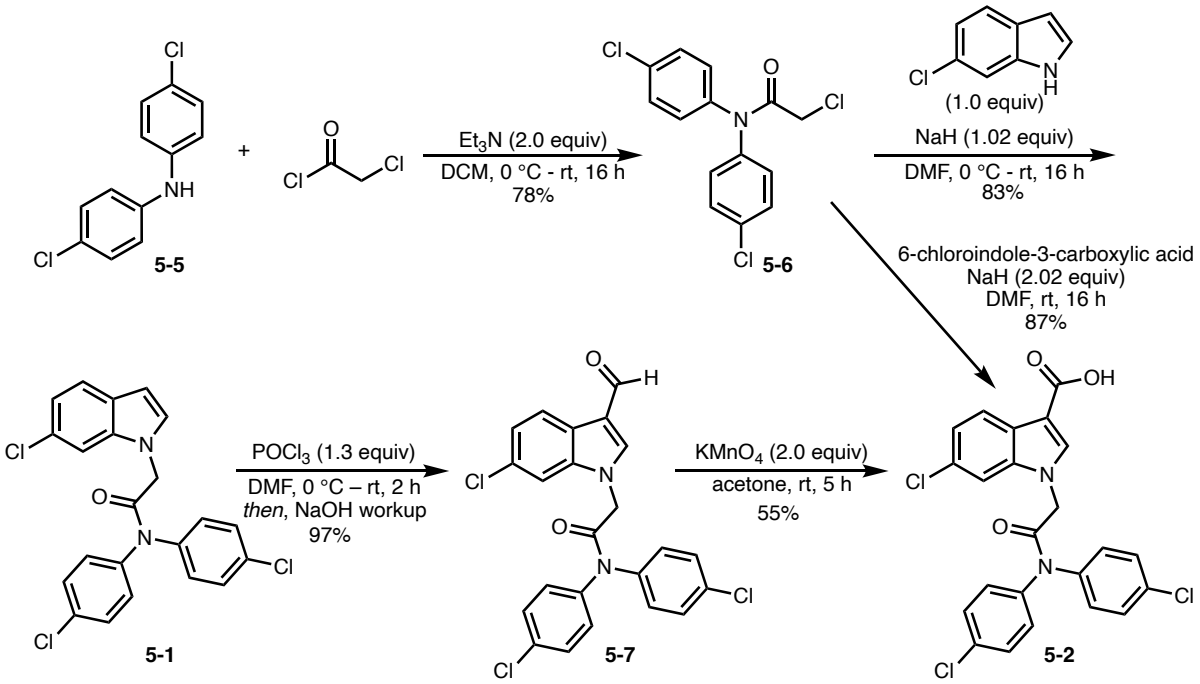

Following the synthesis of **5-2**, compounds **5-3** and **5-4** were synthesized through HBTU coupling of the carboxylic with the corresponding amine. Compound **5-3** was synthesized in 61% yield and **5-4** in 81% yield.

Scheme 5.2: Synthesis of amide **5-3** and **5-4**

5.2.3 Synthesis and evaluation of proteasome activity of the 20S proteasome staples

From section **5.2.1**, we determined that more than six PEG units is needed in the proteasome staple to be able to reach the α1-2 and α2-3 inter-subunit pockets. This number does not account for the folding and extra PEG units that would be needed within each of the inter-

subunit pocket to extend to the outside of the proteasome. I synthesized various staples with PEG units ranging from 5 to 21 to determine the optimal number of PEG units needed to maximize the activity of the staples, using compound **5-1** as the proteasome modulator.

Carboxylic acid **5-2** was first coupled with PEG-5 (five PEG units) and PEG-8 (eight PEG units) amine via HBTU coupling, producing amides **5-8** and **5-9**, respectively (**Scheme 5.3**). Boc deprotection of the protected end of the linkers in compound **5-8** with trifluoroacetic acid (TFA) yielded amine **5-10** in 87% over two steps. Similarly, **5-9** was deprotected to yield amine **5-11** in 67% over two steps. Compounds **5-10** and **5-11** were then reacted with carbonyl diimidazole (CDI) to give the proteasome staples **5-12** and **5-13** with 10 and 16 PEG units respectively.

Scheme 5.3: Synthesis of proteasome staples **5-10** & **5-11**

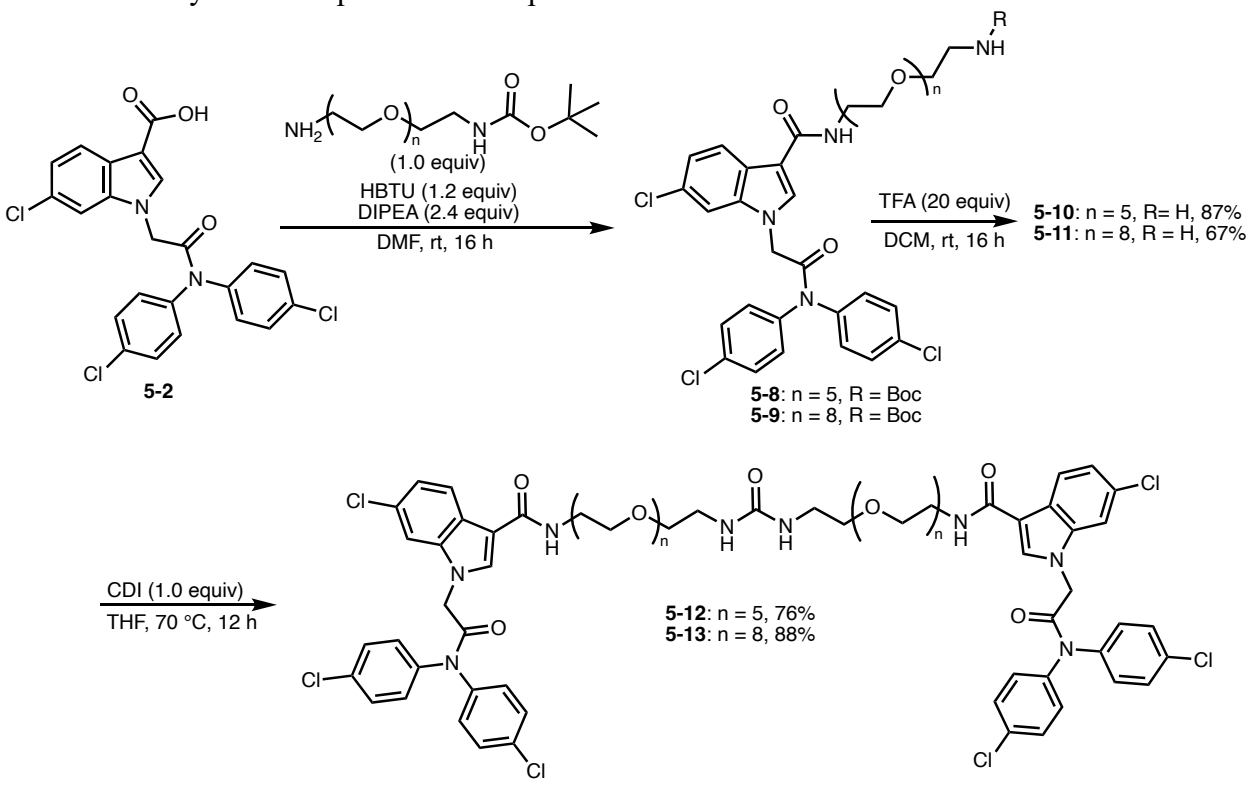

Additionally, the length of the PEG units could be increased to 21 PEG units by reacting compound **5-10** with dicarboxylic acid **5-14** to give staple **5-15** in 57% yield.

Scheme 5.4: Synthesis of proteasome staples **5-15**

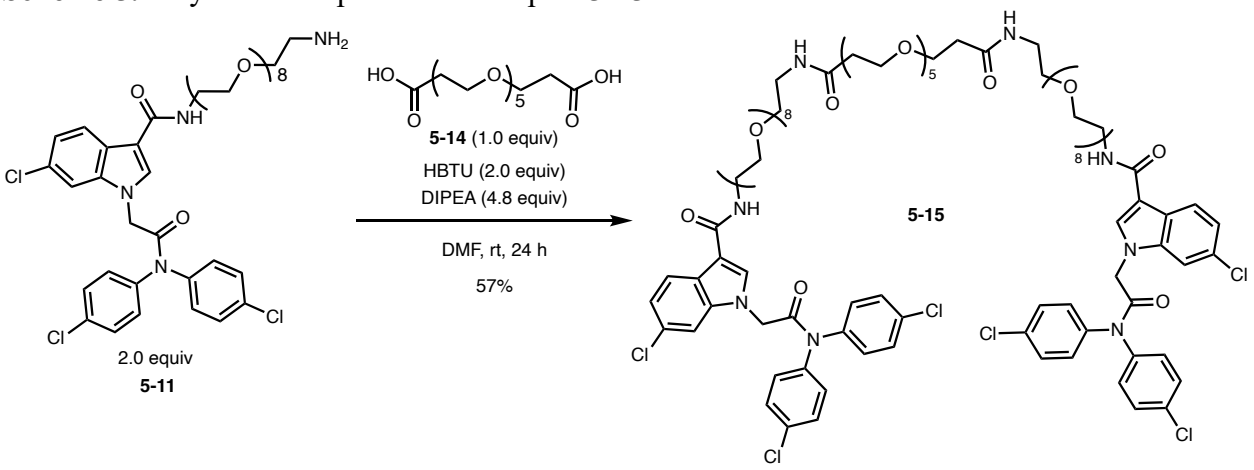

When evaluating the proteasome activity of these compounds, we envisioned that the staples could either bind to the α-ring of the 20S proteasome and activate the proteasome by inducing an open gate conformation or stabilize the closed conformation and therefore acting as a proteasome inhibitor. Following the synthesis of the three proteasome staples above, **5-12**, **5-13**, & **5-15**, they were evaluated in both the 20S proteasome activation and inhibition assay by Allison Vanecek using fluorogenic 7-amino-methylcoumarin (AMC) conjugated small peptides assay. The experiment showed that compounds **5-12**, **5-13**, & **5-15** are inactive in the proteasome activation assay, even showing that there is a slight decrease in the activity of the 20S proteasome when compared to that of the vehicle. The result of this experiment is summarized in **Figure 5.6A**. However, when the compounds were tested in proteasome inhibition assay, they showed inhibition of the 20S proteasome at nanomolar concentration. Compound **5-12** with 10 PEG units showed the best activity with $IC_{50} = 111 \pm 2$ nM. Compound **5-13** with 16 PEG units have an $IC_{50} = 124 \pm 2$ nM and compound **5-15** with 21 PEG units have an IC_{50} 196 ± 5 nM (**Figure 5.6B**). Also, when comparing the proteasome inhibition activity of **5-15** to **5-12**, the enormous reduction in the activity could be the result of the length of the PEG linker which is significantly longer than needed.

Figure 5.6: Proteasome activation and inhibition assays with proteasome staples. Data obtained by Allison Vanecek

A

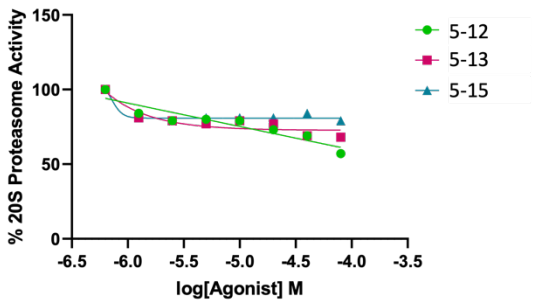

Percent 20S Proteasome Activity

	5-12	5-13	5-15
80 µM	57	68	79
40 µM	69	69	84
20 µM	73	77	81
10 µM	79	79	81
5 µM	80	77	81
2.5 µM	79	79	79
1.25 µM	84	81	81
Vehicle	100	100	100
EC_{200} (µM)	**N/A**	**N/A**	**N/A**

B

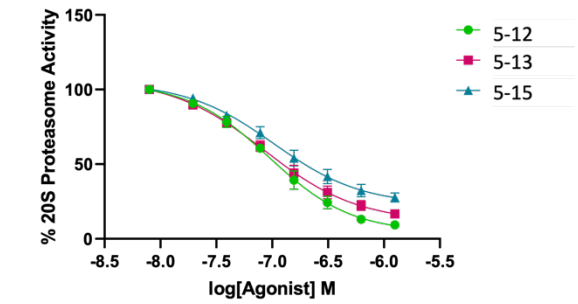

Percent 20S Proteasome Activity

	5-12	5-13	5-15
1250 nM	9	16	28
625 nM	13	22	32
313 nM	24	31	42
156 nM	39	44	54
78 nM	60	62	71
39 nM	78	78	83
20 nM	91	89	94
Vehicle	100	100	100
IC_{50} (µM)	**0.111 ± 0.02**	**0.124 ± 0.02**	**0.196 ± 0.05**

To understand if the staples target two binding pockets on the α-ring has intended during the design of the compounds, compound **5-16** with 5 PEG units which would be too short to bridge the distance between the two inter-subunit pockets was also synthesized. Compound **5-16** should show little to no activity since more than 6 PEG units is needed for activity as determined in section **5.2.1**. Compound **5-16** was synthesized from **5-10** through HBTU coupling with carboxylic **5-2** to yield the desired product in 78% yield (**Scheme 5.5**). As expected, **5-16** was inactive in the proteasome inhibition assay with $IC_{50} > 20$ µM further confirming the important of the right linker length for the staples.

Scheme 5.5: Synthesis of compound **5-16**

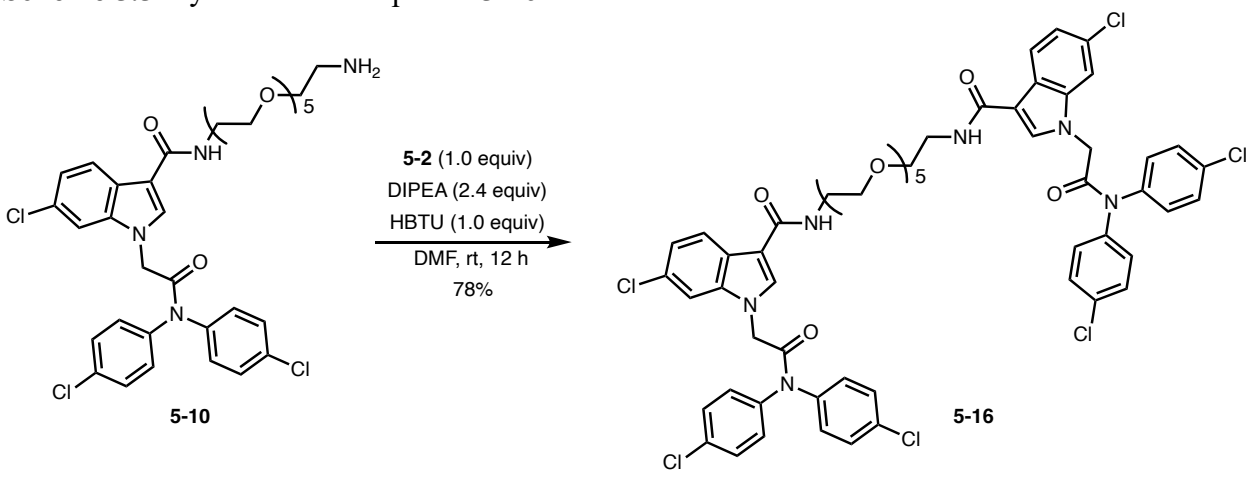

Following the synthesis of the three staples, I set out to investigate the effect of using a less active compound on both ends of the linker and how that would translate to the activity of the staples. Previous unpublished SAR studies on similar scaffolds showed that removing the chlorine on the parent molecule would lead to a significant loss in proteasome activity. I synthesized compound **5-17** which has no chlorine on either the phenyl rings or indole in two steps according to **Scheme 5.6**. As expected, compound **5-17** have an EC_{200} = 29 μM, which is about 10-fold less active than compound **5-1** with EC_{200} = 3.1 μM.

Scheme 5.6: Synthesis of control compound **5-17**

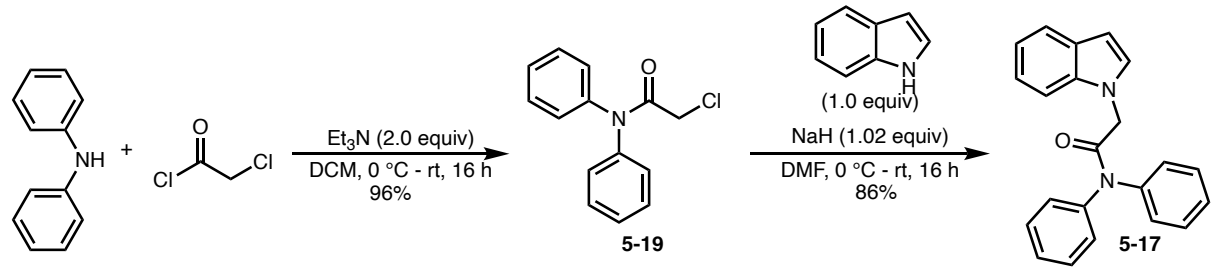

After the identification of **5-17** as a less active proteasome enhancer (compared to **5.1**) of the same class, proteasome staple **5-18** was synthesized using this compound as the proteasome modulator. The staple, **5-18** was synthesized similarly to the synthesis of **5-12** as shown in **Scheme 5.7** and was evaluated in proteasome inhibition assay. Compound **5-18** have an IC_{50} = 1200 nM

which is also about 10-fold less active when compared to it chlorinated counterpart **5-12** with IC_{50} = 111 nM. This was an exciting result that showed that the activity of the proteasome modulator directly translates to the activity of the proteasome staple and also support that the staples most likely interact with the inter-subunit pockets on the α-rings of the 20S proteasome.

Scheme 5.7: Synthesis of proteasome staple **5-18**

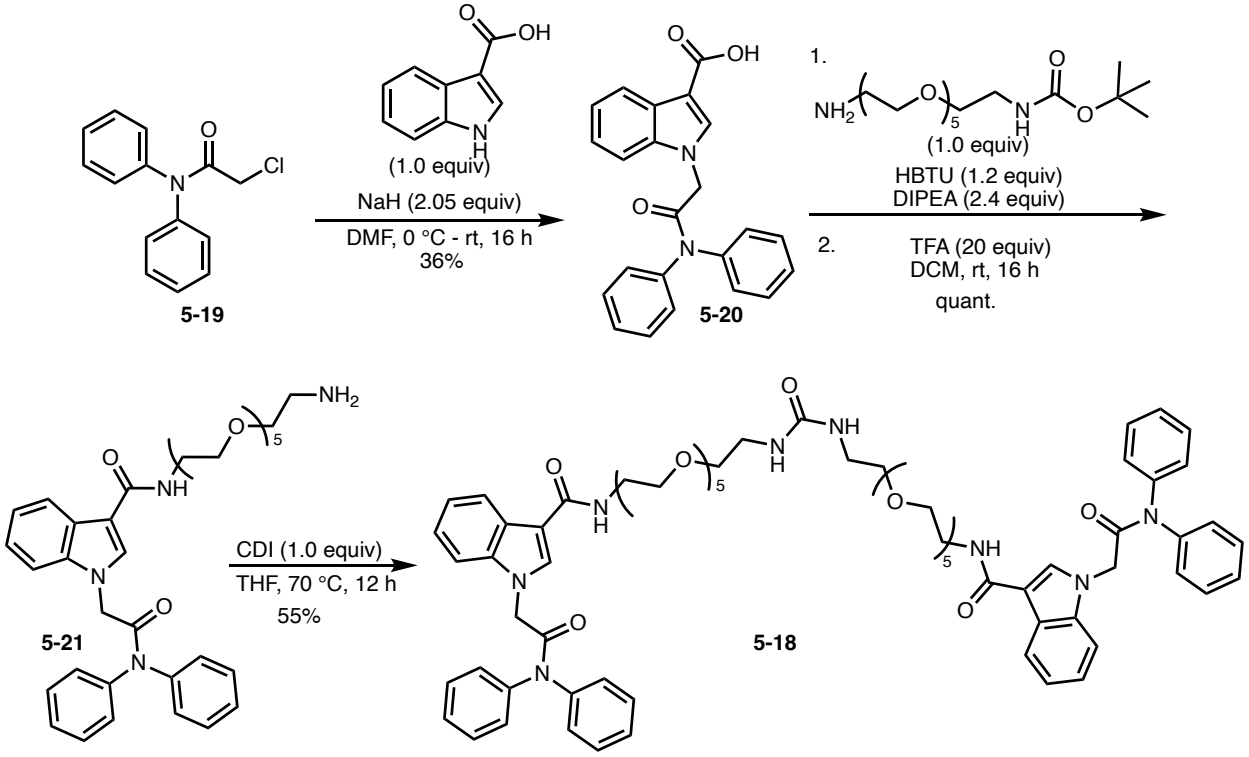

To verify the direct interaction of the proteasome staples with the 20S proteasome, I used surface plasmon resonance (SPR) to investigate the direct binding of the staple with the proteasome. The SPR experiments were done in collaboration with Miracle Olatunde and Erica Lisabeth at the MSU drug discovery core. The Surface Plasmon Resonance (SPR) assay is a straightforward, label-free optical technique utilized for detecting biomolecular interactions and determining the dissociation constant (K_D) of proteins and their ligands. It operates by detecting changes in mass on the chip surface. In this method, a metal surface, typically composed of gold or silver, is coated with carboxymethylated dextran or streptavidin. The protein or ligand of interest

is immobilized onto the metal surface, and a solution containing the analyte in an appropriate buffer is passed over it. Binding between the protein and analyte leads to alterations in the refractive index of light passing through the prism, resulting in a reduction in intensity. These changes are monitored in real-time, and the data is graphed as response units (RU) over time, known as a sensogram. Due to the enormous size of the proteasome, we choose to immobilize the staple on a streptavidin chip and flow the proteasome on the chip. The interaction between the staple and the proteasome should lead to a significant change in the mass which can be easily detected.

Compound **5-24**, an analogue of proteasome staple **5-12** that is functionalized with biotin, was first synthesized. Biotin is needed to immobilize the compound on the streptavidin chip for SPR experiment. HBTU coupling of **5-10** with dicarboxylic acid **5-22** followed by deprotection to give the desired compound **5-23** which was then used to synthesize the biotinylated compound **5-24** (**Scheme 5.8**). SPR study of compound **5-24** after immobilization on streptavidin coated chip showed no interaction with the 20S proteasome when the proteasome was flowed over the chip at varying concentrations. I hypothesized that it could be due to the short linker length between the biotin-streptavidin on the surface of the chip and the proteasome staple, leading to the molecule being too close to the chip and not enough distance for the proteasome to interact with the molecule.

Scheme 5.8: Synthesis of biotinylated proteasome staple **5-24**

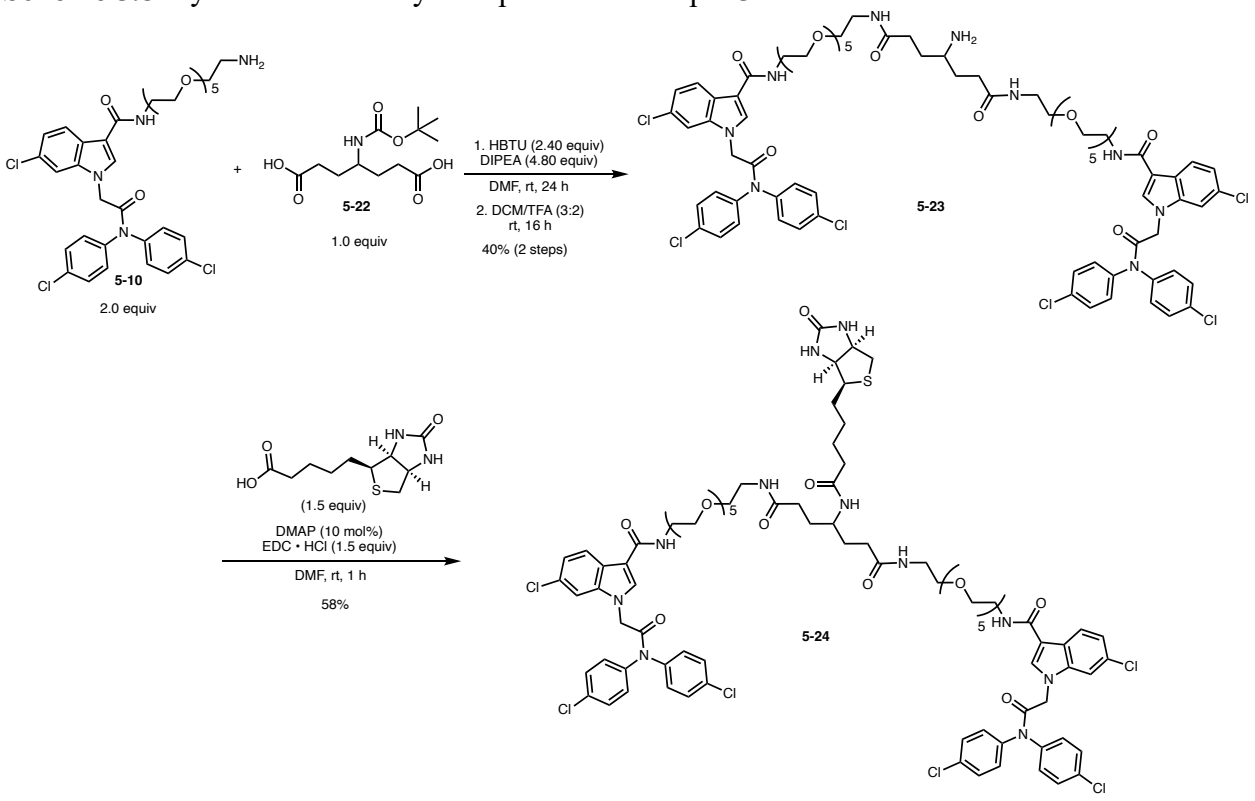

To test this hypothesis, I redesigned compound **5-24** to compound **5-27** which include 4 PEG units between the biotin and the rest of the staple to allow room for interaction with the proteasome. Compound **5-27** was synthesized following a similar approach for the synthesis of compound **5-24**. It is important to note that, I switched from N-boc-dicarboxylic acid linker **5-22** ($312 / 0.10 g from A2B Chemical), to a cheaper linker **5-25** ($30 / 100 g) during the synthesis of compound **5-27** to allow access to more materials at a cheaper cost (**Scheme 5.9**). Compound **5-31** was also synthesized according to **scheme 5.10** as a less active control for the SPR experiment.

Scheme 5.9: Synthesis of compound **5-27**

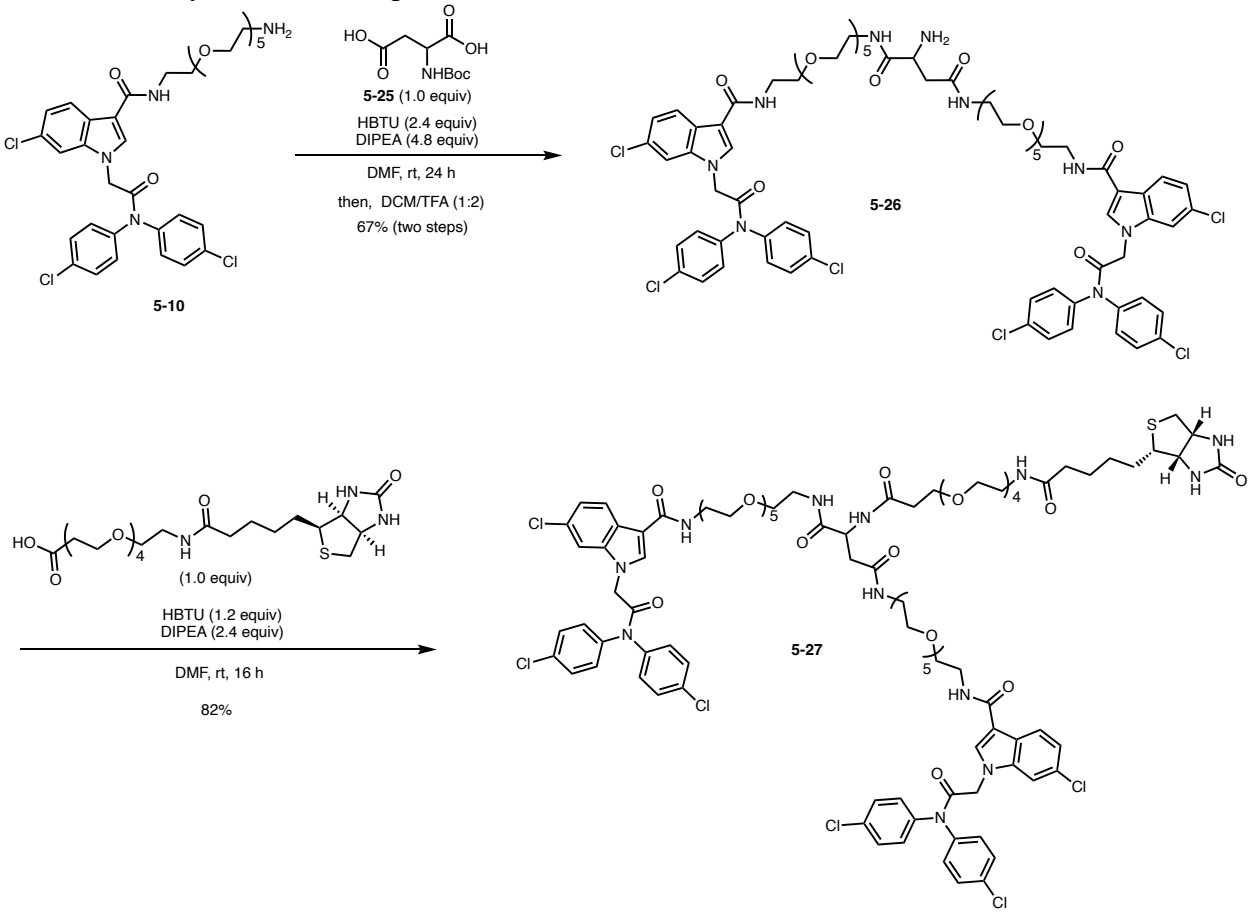

Following the synthesis of **5-27** and **5-31**, the two compounds were evaluated in the proteasome inhibition assay. Compound **5-27** showed proteasome activity with IC_{50} = 254 nM and the **5-31** lost its proteasome activity as expected with IC_{50} > 20 μM. The SPR study was then conducted using **5-27** and **5-31**. Compound **5-27** was immobilized on channel 1 and 2 while compound **5-31** was immobilized on channel 3 of the streptavidin coated chip (**Figure 5.7a**). A serial dilution of purified 20S proteasome in PBS buffer was then flowed over all three channels and a sensogram showing increase in response units (RUs) with increase in concentration of proteasome over time was generated for both compounds **5-27** (**Figure 5.7b**) and **5-31** (**Figure 5.7c**). The sensogram was then converted into a graph of RUs against log of concentration as shown in **Figure 5.7d** and **Figure 5.7e** respectively. From this study, the K_D of compound **5-27**

was determined to be between 0.031 nM – 0.80 nM and the control compound **5-31** ranged between 0.51 nM – 15000 nM.

Scheme 5.10: Synthesis of less active compound **5-31**

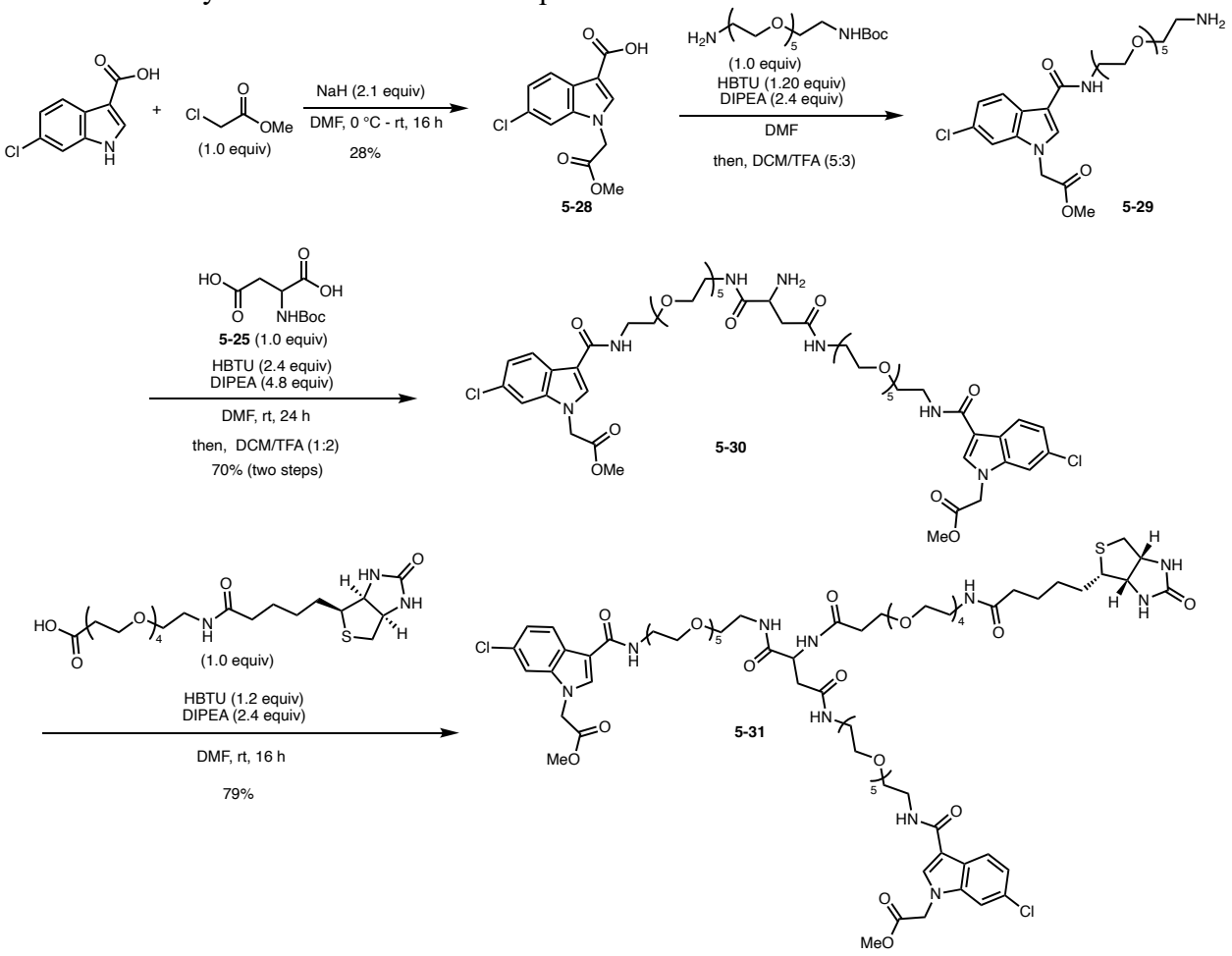

From the SPR experiment, I was able to get binding with the proteasome with both compound **5-27** and the control **5-31** unlike compound **5-24** where proteasome binding was not observed. This supports that the short distance between the chip surface and the binding staple in compound **5-24** may be preventing the binding of the staple to the proteasome. In addition, the control compound **5-31** has a higher and wider range of K_D when compared to the active compound **5-27** indicating that the compound have less binding to the proteasome.

Figure 5.7: (**a**) Sensogram showing the immobilization of compound **5-27** on channel 1 (red) and 2 (pink) and control compound **5-31** on channel 3 (blue). (**b**) Sensogram showing increase in RUs with increase in concentration of proteasome over time on channel 1 & 2 for compound **5-27** (**DG-6-136**) (**c**) Sensogram showing increase in RUs with increase in concentration of proteasome over time channel 3 for compound **5-31** (**DG-6-137**). (**d**) A graph of RU against (log) concentration of proteasome for compound **5-27** (**DG-6-136**). (**e**) A graph of RU against (log) concentration of proteasome for compound **5-31** (**DG-6-137**)

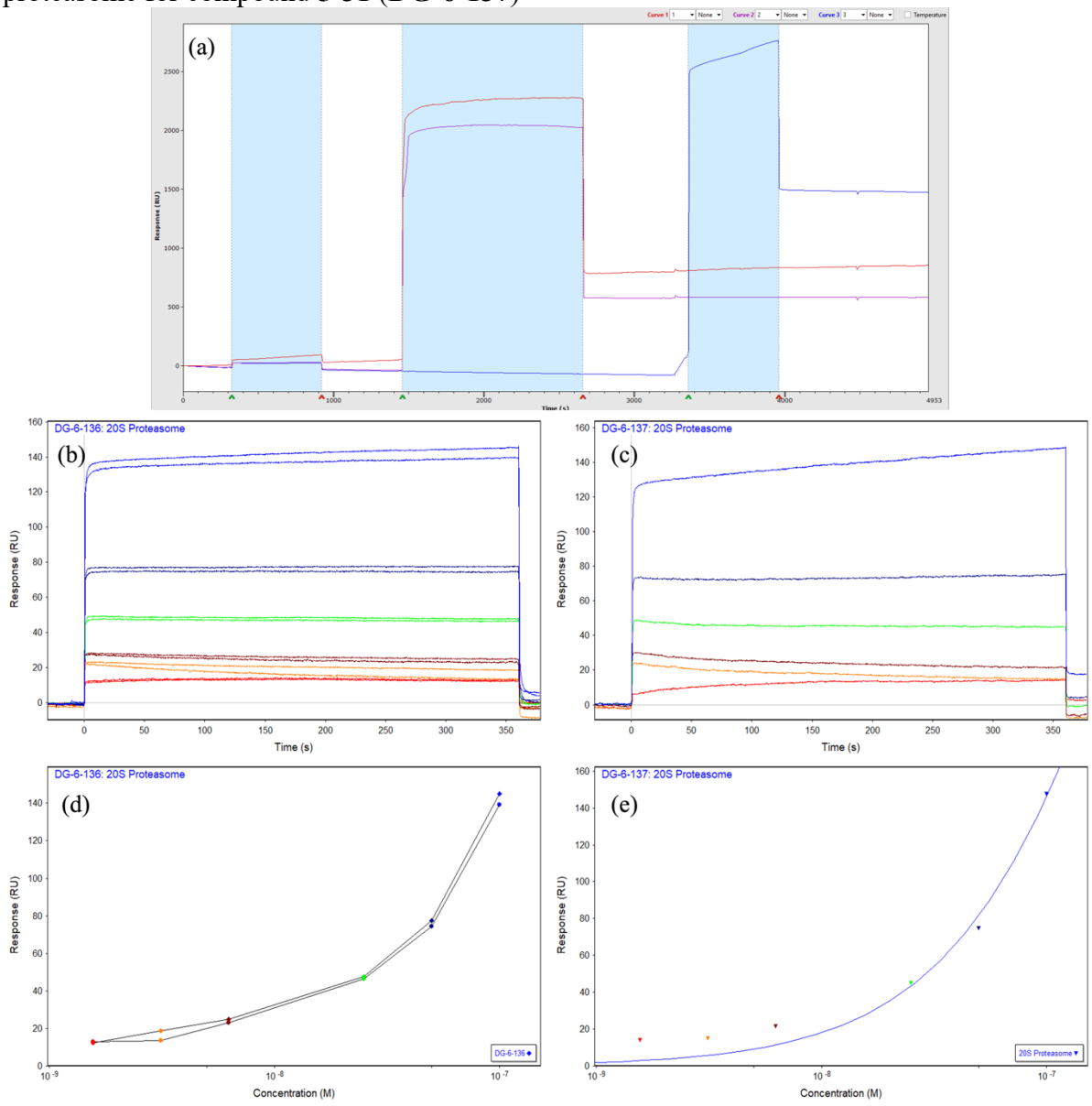

After verifying the interaction between proteasome staples and 20S proteasome using the in vitro inhibition assay and SPR, we decided to use photoaffinity labelling (PAL) to study the interaction between the proteasome staples and the proteasome with the goal of determining the

subunit(s) on the α-ring that the staples interact with. Photoaffinity labelling (PAL) is a sophisticated method for studying interaction between small molecules and protein. Usually, a molecule of interest is functionalized with photoreactive group and upon photolysis, the molecule traps its binding partner, usually a protein, covalently.[15] When PAL is combined with analytical techniques such as mass spectrometry, a wide range of studies can be conducted. This enables the mapping of interactions between small molecules and proteins, as well as the determination of the small molecule's binding site on the protein.[16] Among the photoreactive groups utilized in photoaffinity labeling, diazirines have attracted considerable attention. This is owing to their small size, long irradiation wavelength (350–355 nm), which minimizes damage to biological systems, and their short lifetime upon irradiation, thus diminishing nonspecific binding.[17] Upon irradiation of diazirines with light, they generates carbene with then covalently bind with the nearest target molecule through C–C, O–H and X–H (X = N,S) insertions.

Only few studies have been done in the literature on photoaffinity labelling of the proteasome. In 2010, Geurink et. al. used a combination of photoreactive group and a bio-orthogonal ligation handle incorporated into peptides to identify the β-subunits the peptide was binding to in the proteasome.[18] Similarly, Zhu et al. employed PAL to identify the α-subunits to which peptides binding to the 20S proteasome, inducing an open gate conformation, were binding.[19] While these two studies involved PAL and 20S proteasome, none of them used small molecule regulators of the 20S proteasome. I started by first synthesizing compound **5-33** by functionalizing the proteasome staple with amine handle **5-26** with probe **5-32** (**Scheme 5.11**). Probe **5-32** contains diazirine for photo crosslinking and an alkyne for click chemistry with reporter tags. Probe **5-32** has be used significantly in the literature for proteomic profiling,[20-25] photoaffinity based fragment screening,[26-28] and ligand mapping[29-32]. Probe **5-32** is also

commercially available but quite expensive ($436 for 100 mg from A2B) and published synthetic approach to access the compound requires significant synthetic effort to obtain the product in good yield.[20,27] I have developed a novel approach to synthesize **5-32** in fewer steps and with a higher overall yield. The manuscript detailing this work is currently being prepared.

Scheme 5.11: Syntheses of diazirine functionalized proteasome staples as probes for photoaffinity labelling of the 20S proteasome

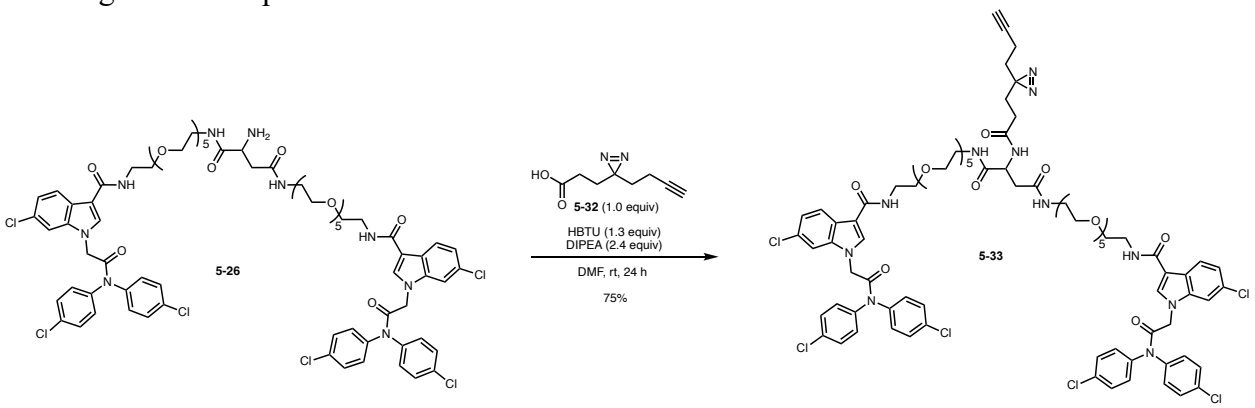

5.3 Future direction

Following the synthesis of **5-33**, Sydney Cobb is currently exploring its use in photoaffinity labeling studies with the 20S proteasome. We aim to covalently bind **5-33** to the 20S proteasome, then determine which subunit the compound interacts with by using SDS-PAGE after tagging the alkyne handle with a BODIPY probe. After successful result with SDS-PAGE, the subunit interacting with the staple can be purified by clicking the alkyne handle with a biotin and the subunit purified by a streptavidin column. The purified subunit(s) can then be characterized using mass spectrometry to determine their identities.

Following the failed attempts in obtaining cryo-EM structure of small molecule bound 20S proteasome complex using previous small molecules from our lab, **5-33** could be the suitable compound needed for the cryo-EM experiments, considering its potent and unique binding interaction. Furthermore, **5-33** can covalently bind to the proteasome through the diazirine functionality and thereby eliminate the off rate of ligand when obtaining cryo-EM analysis. Since

another challenge that was faced while obtaining cryo-EM structure is sorting ligand bound 20S proteasome from unbound 20S proteasome, the alkyne handle in **5-33** can undergo a click reaction with an azide conjugated Au nanoparticle which would allow better sorting of ligand bound and unbound 20S proteasome.

5.4 Conclusion

In this study, bivalent compounds called the "proteasome staples" that targets multiple inter-subunit pockets were developed. The proteasome staples are made up of a PEG linker and 20S proteasome modulators at each end of the linker. The effect of the linker length and the activity of the proteasome modulator were investigated on the 20S proteasome inhibition activity of the staples. The proteasome staples exhibit 20S proteasome inhibition activity at nM concentration and the binding activity of the most active proteasome staple was also verified using SPR studies. In addition, the most active staple was functionalized with a diazirine group which would allow future studies of the compound interaction with 20S proteasome using photoaffinity labelling studies and ultimately obtaining a cryo-EM structure of small molecule bound 20S proteasome. This would allow identification and characterization of the inter-subunit pocket(s) being targeted by small molecule modulators of the 20S proteasome.

5.5 Experimental

General Information

All flasks were oven-dried overnight and cooled under nitrogen. Reactions were carried out under a nitrogen atmosphere unless stated otherwise. All chemicals and solvents were purchased from commercial sources and used without further purification, unless otherwise mentioned. THF and DCM were dried by passing it through packed column of alumina or over activated 3Å molecular sieves. Infrared spectra were recorded on a Jasco Series 6600 FTIR spectrometer. The mass

spectrometer ionization method was ESI with a quadrupole detector. ^{1}H and ^{13}C NMR spectra were recorded on a 500 MHz spectrometer. Chemical shifts are reported relative to the residue peaks of the solvent: $CDCl_3$: 7.26 ppm for ^{1}H and 77.0 ppm for ^{13}C, CD_3OD: 3.31 ppm for ^{1}H and 47.6 ppm for ^{13}C, and DMSO-d6: 2.50 ppm for ^{1}H and 39.5 ppm for ^{13}C. Signal multiplicities are given as s (singlet), br (broad), d (doublet), t (triplet), dd (doublet of doublet), and m (multiplet). Reaction carried out at room temperature (rt) implies temperature range usually between 20 – 22 °C. Column chromatography was performed using a Teledyne ISCO CombiFlash® NextGen system with prepacked columns (RediSep® Normal-phase silica, 20-40 microns). TLCs were performed on pre-coated 0.25 mm thick silica gel 60 F254 plates and pre-coated 150 um thick, visualized using UV light and iodine staining.

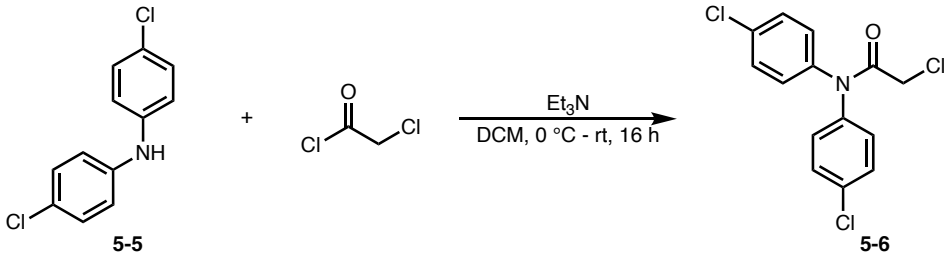

2-chloro-*N*,*N*-bis(4-chlorophenyl)acetamide (**5-6**): An 100 mL round bottom flask equipped with magnetic stirrer was charged with bis(4-chlorophenyl)amine (3.0 g, 12.60 mmol) and dichloromethane (50 mL). The resulting solution was cooled to 0 °C and then triethylamine (3.5 mL, 25.20 mmol) was added. A solution of chloroacetyl chloride (1.1 mL, 13.86 mmol) in dichloromethane (1.5 mL) was added slowly over 15 mins. After 4 hours, additional solution of chloroacetyl chloride (1.1 mL, 13.86 mmol) in dichloromethane (1.5 mL) was added. The reaction was then warmed up to room temperature and allowed to stirred overnight. The reaction was then diluted with sodium carbonate (50 mL) and the organic layer was collected. The aqueous phase was further extracted with dichloromethane (2 x 50 mL) and the organic phases were combined. The organics were dried over sodium sulfate, decanted and concentrated under reduced pressure

to give the crude product. The crude was then recrystallized in ethylacetate/hexane (4:1) to give the pure product has a pink solid (3.10 g, 78% yield). mp = 103 °C. ^{1}H NMR (500 MHz, $CDCl_3$) δ 7.39 (br, m, 4H), 7.23 (br, m, 4H), 4.01 (s, 2H). $^{13}C\{^{1}H\}$ NMR (125 MHz, $CDCl_3$) δ 166.2, 140.2, 130.5, 129.7, 127.3, 42.5. FTIR (cm^{-1}): 3094, 2989, 1670, 1486. HRMS (ESI-TOF) *m/z*: $[M+H]^+$ calcd for ($C_{14}H_{11}Cl_3NO^+$), 313.9901; found: 313.9932 and 315.9904.

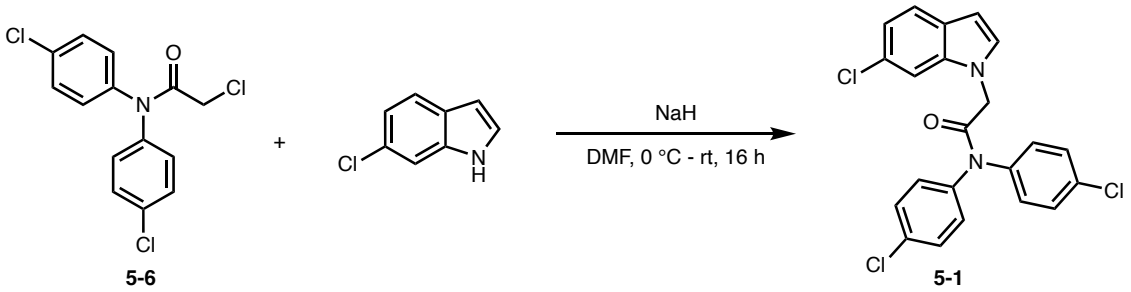

2-(6-chloro-1*H*-indol-1-yl)-*N*,*N*-bis(4-chlorophenyl)acetamide (5-1): Sodium hydride (60% in mineral oil, 0.13 g, 3.24 mmol) was suspended in anhydrous *N,N*-dimethylformamide (5 mL) and cooled to 0 °C, then a solution of 6-chloroindole (0.48 g, 3.18 mmol) in *N,N*-dimethylformamide (5 mL) was added slowly via syringe. After 10 mins, a solution of *α*-chloroamide **5-6** (1.0 g, 3.18 mmol) in *N,N*-dimethylformamide (5 mL) was added in one-portion and the reaction was warmed up to room temperature and stirred overnight. Then, ethyl acetate (50 mL) and 1 M hydrochloric acid (30 mL) was added, and the organic layer was collected. The organic was further washed with 1 M hydrochloric acid (2 x 30 mL). The organic was dried over sodium sulfate, decanted and concentrated under reduced pressure to give the crude product which was used without further purification. mp = 174 °C. ^{1}H NMR (500 MHz, $CDCl_3$) δ 7.51(d, J = 8.7 Hz, 1H), 7.40 (s, 2H), 7.29 (s, 2H), 7.14 (d, J = 8.7 Hz, 4H), 7.08 (d, J = 7.7 Hz, 2H), 6.90 (d, J = 3.2 Hz, 1H), 6.47 (d, J = 3.2 Hz, 1H), 4.75 (s, 2H). $^{13}C\{^{1}H\}$ NMR (125 MHz, $CDCl_3$) δ 167.1, 136.7, 130.7, 129.6, 129.2, 129.0, 127.9, 127.0, 126.8, 122.0, 120.6, 109.0, 102.7, 49.4. FTIR (neat, cm^{-1}): 3062, 2939,

1668, 1490. HRMS (ESI-TOF) *m/z*: $[M+H]^+$ calcd for ($C_{22}H_{16}Cl_3N_2O^+$), 429.0323, 431.0294 & 433.0264; found: 429.0341, 431.0290, & 433.0287.

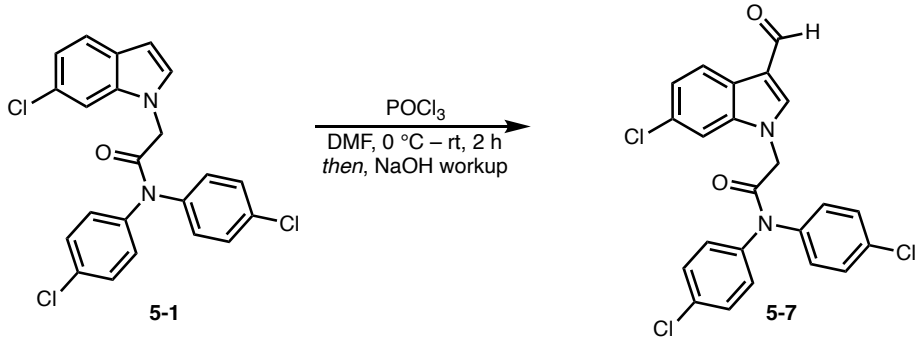

2-(6-chloro-3-formyl-1*H*-indol-1-yl)-*N*,*N*-bis(4-chlorophenyl)acetamide (**5-7**): A 100 mL round bottom flask equipped with magnetic stirrer was charged with *N,N*-dimethylformamide (5 mL) and cooled to 0 °C , then phosphorus oxychloride (0.39 mL, 4.13 mmol) was added slowly. The reaction was stirred for 15 mins, and a solution of the indole amide **5-1** (1.39 g, 3.18 mmol) in *N,N*-dimethylformamide (10 mL) was added. The reaction was stirred for 2 hours, diluted with water (30 mL) and basify with sodium hydroxide until pH ≈ 7 – 8. The reaction was extracted with ethyl acetate (3 x 30 mL) and the organics were combined and washed with lithium bromide (3 x 30 mL). The organic was dried over sodium sulfate, concentrated and recrystallized in ethyl acetate to give the desired product as a yellow foamy solid (1.45 g, quantitative). ^{1}H NMR (500 MHz, DMSO-d_6) δ 9.91 (s, 1H), 8.26 (s, 1H), 8.06 (d, *J* = 8.4 Hz, 1H), 7.83 (d, *J* = 1.8 Hz, 1H), 7.78 (s, 2H), 7.64 (s, 2H), 7.43 (s, 2H), 7.35 (s, 2H), 7.27 (dd, *J* = 8.4, 1.8 Hz, 1H), 5.08 (s, 2H). ^{13}C{^{1}H} NMR (125 MHz, DMSO-d_6) δ 185.3, 166.6, 143.2, 139.0, 130.6, 129.4, 128.7 (overlaps with a broad aromatic carbon), 123.5, 123.1, 122.4, 117.7, 112.2, 49.8. FTIR (neat, cm^{-1}): 3094, 2924, 1660, 1489. HRMS (ESI-TOF) *m/z*: $[M+H]^+$ calcd for ($C_{23}H_{16}Cl_3N_2O_2^+$), 457.0272; found, 457.0295 and 459.0269.

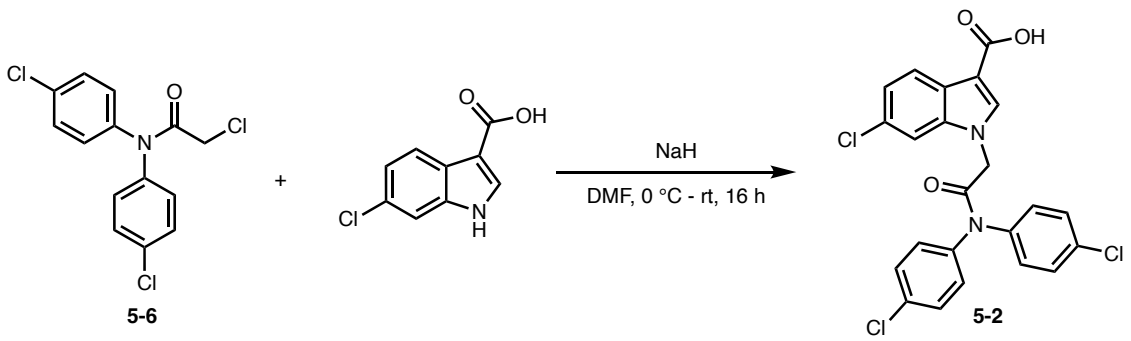

1-(2-(bis(4-chlorophenyl)amino)-2-oxoethyl)-6-chloro-1*H*-indole-3-carboxylic acid (5-2): Sodium hydride (60% in mineral oil, 0.42 g, 10.49 mmol) was suspended in anhydrous *N,N*-dimethylformamide (5 mL) and cooled to 0 °C, then a solution of 6-chloroindole-3-carboxylic acid (0.93 g, 4.77 mmol) in *N,N*-dimethylformamide (10 mL) was added slowly via syringe. After 10 mins, a solution of α-chloroamide **5-6** (1.50 g, 4.77 mmol) in *N,N*-dimethylformamide (10 mL) was added in one-portion and the reaction was warmed up to room temperature and stirred overnight. Then, ethyl acetate (50 mL) and 1 M hydrochloric acid (30 mL) was added, and the organic layer was collected. The organic was further washed with 1 M hydrochloric acid (2 x 30 mL). The organic was dried over sodium sulfate, decanted and concentrated under reduced pressure. The crude was recrystallized in ethyl acetate to give the product as white solid (1.96 g, 87% yield). mp = 242 – 243 °C. ^{1}H NMR (500 MHz, DMSO-d_6) δ 12.15 (s, 1H), 8.04 (s, 1H), 7.95 (d, J = 8.5 Hz, 1H), 7.75 (d, J = 2.0 Hz, 3H), 7.62 (s, 2H), 7.42 (s, 2H), 7.32 (s, 2H), 7.18 (dd, J = 8.5, 1.9 Hz, 1H), 5.00 (s, 2H). ^{13}C{^{1}H} NMR (125 MHz, DMSO-d_6) δ 166.8, 165.7, 138.4, 138.0, 131.6, 130.5, 129.4, 128.6, 127.6, 125.3, 122.3, 122.0, 111.7, 107.5, 49.5. FTIR (neat, cm^{-1}): 3056, 2925, 1671, 1490. HRMS (ESI-TOF) *m/z*: [M+H]$^{+}$ calcd for ($C_{23}H_{16}Cl_3N_2O_3^{+}$), 473.0221; found: 473.0245 and 475.0219.

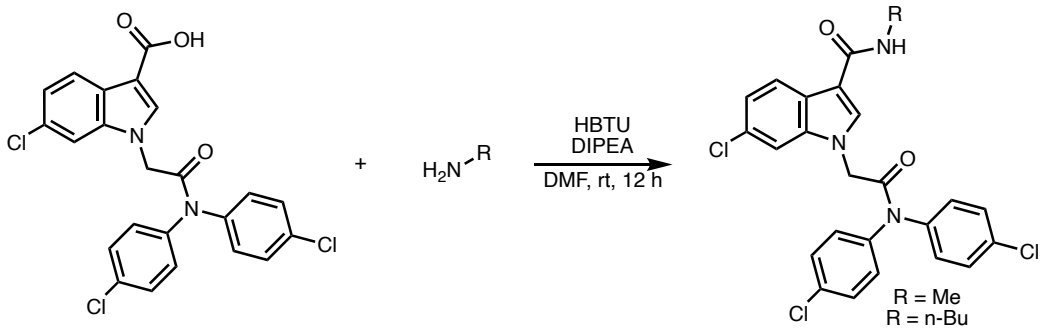

In a 7mL vial, carboxylic acid (1.0 equiv, 0.127 mmol) was dissolved in *N,N*-dimethylformamide (1.5 mL) and HBTU (1.2 equiv, 0.152 mmol) and DIPEA (2.4 equiv, 0.305 mmol) were added. The reaction was stirred at room temperature for 10 mins, then amine (1.0 equiv, 0.127 mmol) was added and the reaction was stirred overnight for 12 hours. The solvent was removed under reduced pressure and the product was purified with CombiFlash chromatography (silica gel, 20−40 μm, gradient 20 – 70% ethyl acetate/hexane).

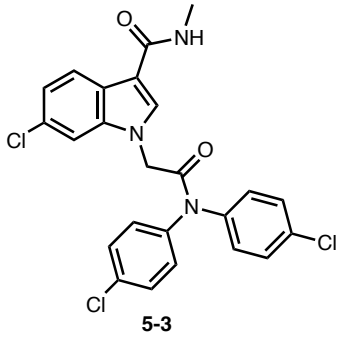

5-3

1-(2-(bis(4-chlorophenyl)amino)-2-oxoethyl)-6-chloro-*N*-methyl-1*H*-indole-3-carboxamide (**5-3**): Synthesized according to the procedure approach. Isolated as white solid (yield: 0.038 g, 61% yield). mp = 95 – 96 °C. ^{1}H NMR (500 MHz, CD_3OD) δ 8. 00 (d, *J* = 8.6 Hz, 1H), 7.57 (s, 1H), 7.43 (s, 4H), 7.33 (d, *J* = 1.8 Hz, 3H), 7.22 (s, 2H), 7.12 (dd, *J* = 8.6, 1.8 Hz, 1H), 4.91 (s, 2H), 2.89 (s, 3H). ^{13}C{^{1}H} NMR (125 MHz, CD_3OD) δ 167.4, 166.4, 137.5, 132.0, 130.2, 129.9, 128.9, 128.4, 127.6, 124.7, 121.8, 121.4, 110.9, 109.8, 37.5, 25.0. FTIR (neat, cm^{-1}): 3340, 3087,

2929, 1676, 1618, 1489. HRMS (ESI-TOF) *m/z*: $[M+H]^+$ calcd for ($C_{24}H_{19}Cl_3N_3O_2^+$), 486.0537; found: 486.0558 and 488.0532.

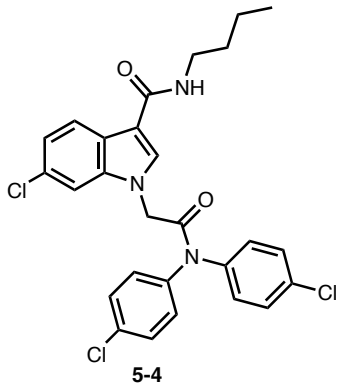

5-4

1-(2-(bis(4-chlorophenyl)amino)-2-oxoethyl)-*N*-butyl-6-chloro-1*H*-indole-3-carboxamide (**5-4**): Synthesized according to the procedure approach. Isolated as off-white solid (yield: 0.054 mg, 81% yield). mp = 78 – 79 °C. ^{1}H NMR (500 MHz, CD_3OD) δ 8.01 (d, *J* = 8.6 Hz, 1H), 7.61 (s, 1H), 7.54 – 7.17 (m, 9H), 7.12 (dd, *J* = 8.6 1.8 Hz, 1H), 4.90 (s, 2H), 3.34 (t, *J* = 7.2 Hz, 2H), 1.57 (q, *J* = 7.6 Hz, 2H), 1.40 (h, *J* = 7.4 Hz, 2H), 0.96 (t, *J* = 7.4 Hz, 3H). ^{13}C{^{1}H} NMR (125 MHz, CD_3OD) δ 167.4, 165.8, 137.5, 132.0, 130.2, 129.9, 128.8, 128.4, 127.6, 124.9, 121.9, 121.4, 111.1, 109.8, 48.9, 38.8, 31.5, 19.9, 12.8. FTIR (neat, cm^{-1}): 3295, 2926, 1673, 1609, 1489. HRMS (ESI-TOF) *m/z*: $[M+H]^+$ calcd for ($C_{27}H_{25}Cl_3N_3O_2^+$), 528.1007; found, 528.1032 and 530.1007.

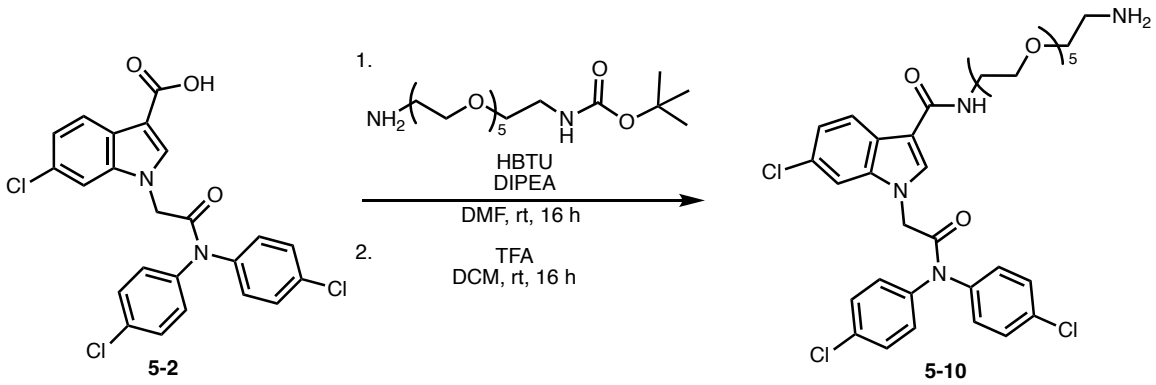

5-2 **5-10**

***N*-(17-amino-3,6,9,12,15-pentaoxaheptadecyl)-1-(2-(bis(4-chlorophenyl)amino)-2-oxoethyl)-6-chloro-1*H*-indole-3-carboxamide (5-10)**: To a solution of indole carboxylic acid **5-2** (0.20 g,

0.422 mmol) in *N,N*-dimethylformamide (1.0 mL) at room temperature was added HBTU (0.19 g, 0.507 mmol) and DIPEA (0.18 mL, 1.01 mmol). The reaction was stirred for 15 mins and a solution of the PEG linker (0.16 g, 0.422 mmol) in *N,N*-dimethylformamide (0.5 mL) was added. The reaction was further stirred at room temperature overnight. Then, the solvent was removed under reduced pressure to give the crude N-boc product.

The crude product was dissolved in dichloromethane (3 mL) and trifluoroacetic acid (0.65 mL, 8.44 mmol) and stirred overnight. The reaction was quenched with sodium carbonate (10 mL). The reaction was extracted with dichloromethane (3 x 10 mL) and the organics were combined and dried over sodium sulfate. The organic was then concentrated and purified with CombiFlash chromatography (silica gel, 20−40 μm, gradient 0−8% methanol (5% Et_3N)/dichloromethane) to give the product as a white foamy solid (0.27 g, 87%). ^1H NMR (500 MHz, CD_3OD) δ 8.02 (d, *J* = 8.6 Hz, 1H), 7.73 (s, 1H), 7.48 (s, 4H), 7.35 (d, *J* = 1.8 Hz, 1H), 7.27 (s, 2H), 7.21 (s, 2H), 7.11 (dd, *J* = 8.6, 1.8 Hz, 1H), 4.90 (s, 2H), 3.65 – 3.45 (m, 22H), 2.80 (t, *J* = 5.2 Hz, 2H). $^{13}C\{^1H\}$ NMR (125 MHz, CD_3OD) δ 167.2, 165.8, 137.6, 132.4, 130.3, 130.1, 128.9, 128.4, 127.7, 124.9, 121.9, 121.5, 110.8, 109.9, 70.2, 70.1, 70.1, 70.0, 70.0, 70.0, 69.9, 69.8, 69.7, 69.5, 65.5, 40.2, 38.9. FTIR (neat, cm^{-1}): 3418, 2868, 1680, 1618, 1488. HRMS (ESI-TOF) *m/z*: $[M+H]^+$ calcd for ($C_{35}H_{42}Cl_3N_4O_7^+$), 735.2114; found, 735.2117, 736.2178, 737.2238, 738.2212, 739.2228, 740.2214, 741.2198.

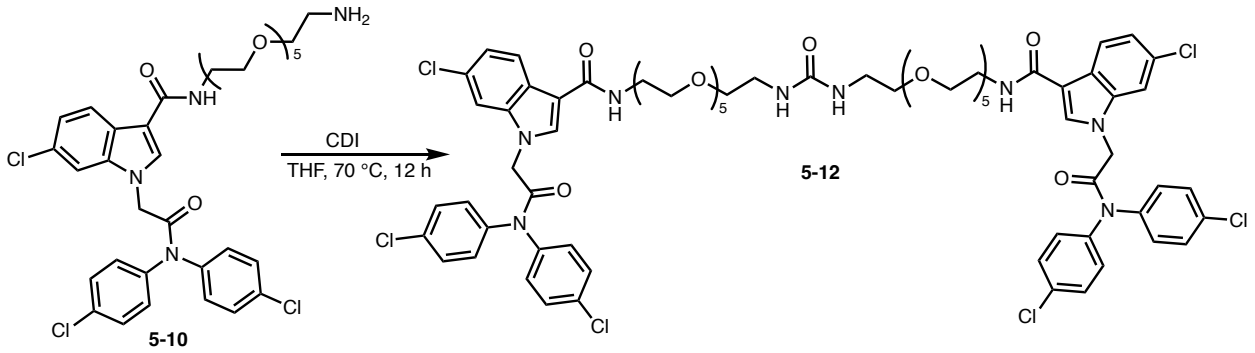

***N*,*N*'-(19-oxo-3,6,9,12,15,23,26,29,32,35-decaoxa-18,20-diazaheptatriacontane-1,37-diyl)bis(1-(2-(bis(4-chlorophenyl)amino)-2-oxoethyl)-6-chloro-1*H*-indole-3-carboxamide)** (**5-12**): Amine **5-10** (0.049 g, 0.067 mmol) was dissolved in tetrahydrofuran (1 mL) in a 15 mL pressure tube. Then carbonyldiimidazole CDI (5.4 mg, 0.034 mmol) was added. The reaction was placed in a preheated aluminum beads at 70 °C and stirred for 12 hours. The reaction was diluted with ethyl acetate (5 mL) and washed with 1 N hydrochloric acid (2 x 3 mL). The organic layer was collected, dried over sodium sulfate, decanted, and concentrated under reduced pressure. The reaction was then purified with CombiFlash chromatography (silica gel, 20−40 μm, gradient 0−8% methanol/dichloromethane) to give the product as a white foamy solid (0.039 g, 76%). ^{1}H NMR (500 MHz, $CDCl_3$) δ 8.03 (d, *J* = 8.5 Hz, 1H), 7.56 (s, 1H), 7.44 (s, 2H), 7.22 (s, 4H), 7.16 (dd, *J* = 8.5, 1.6 Hz, 1H), 7.11 (s, 2H), 7.06 (d, *J* = 1.6 Hz, 1H), 4.70 (d, *J* = 7.6 Hz, 1H), 3.67 – 3.50 (m, 20H), 3.45 (t, *J* = 5.2 Hz, 2H), 3.29 (t, *J* = 5.2 Hz, 2H). ^{13}C{^{1}H} NMR (125 MHz, $CDCl_3$) δ 166.3, 164.5, 158.8, 137.1, 131.9, 130.8, 129.7, 129.2, 128.8, 126.9, 124.8, 122.4, 122.3, 111.9, 109.4, 70.6, 70.5, 70.4, 70.4, 70.4, 70.3, 70.3, 70.1, 70.0, 49.3, 45.7, 39.9, 39.1. FTIR (neat, cm^{-1}): 3313, 3081, 2866, 1687, 1629. HRMS (ESI-TOF) *m/z*: $[M+H]^+$ calcd for ($C_{71}H_{81}Cl_6N_8O_{15}^+$), 1495.3948; found, 1495.3877, 1496.3909, 1497.3861, 1498.3882, 1499.3843, 1500.3857, 1501.3833, 1502.3842.

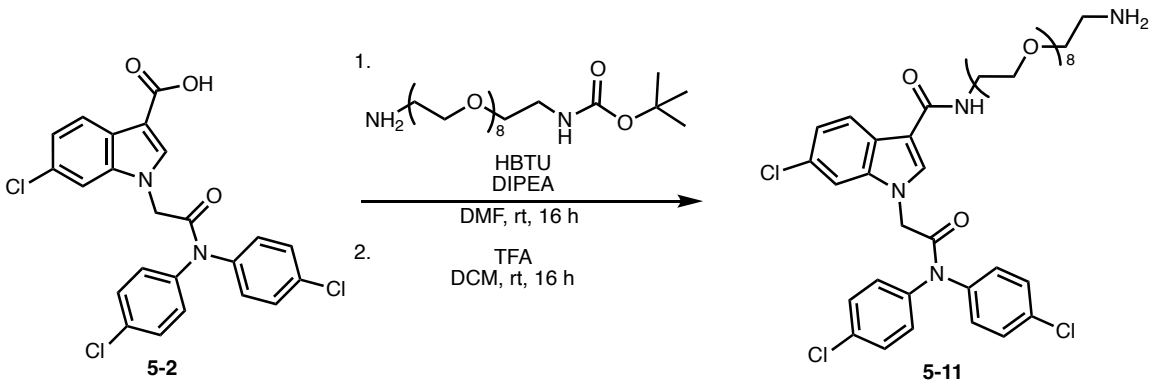

***N*-(26-amino-3,6,9,12,15,18,21,24-octaoxahexacosyl)-1-(2-(bis(4-chlorophenyl)amino)-2-oxoethyl)-6-chloro-1*H*-indole-3-carboxamide** (**5-11**): To a solution of the indole-carboxylic acid **5-2** (0.20 g, 0.422 mmol) in *N,N*-dimethylformamide (1.0 mL) at room temperature was added HBTU (0.19 g, 0.507 mmol) and DIPEA (0.18 mL, 1.01 mmol). The reaction was stirred for 15 mins and a solution of the PEG linker (0.22 g, 0.422 mmol) in *N,N*-dimethylformamide (0.5 mL) was added. The reaction was further stirred at room temperature overnight. Then, the solvent was removed under reduced pressure to give the crude product.

The crude product was dissolved in dichloromethane (3 mL) and trifluoroacetic acid (0.65 mL, 8.44 mmol) and stirred overnight. The reaction was quenched with sodium carbonate (10 mL). The reaction was extracted with dichloromethane (3 x 10 mL) and the organics were combined and dried over sodium sulfate. The organic was then concentrated and purified with CombiFlash chromatography (silica gel, 20−40 μm, gradient 0−8% methanol (5% Et_3N)/dichloromethane) to give the product as a clear oil (0.24 g, 67%). ^{1}H NMR (500 MHz, CD_3OD) δ 8.03 (d, *J* = 8.5 Hz, 1H), 7.72 (s, 1H), 7.49 (s, 4H), 7.36 (s, 1H), 7.30 (s, 4H), 7.13 (dd, *J* = 8.6, 1.8 Hz, 1H), 4.92 (d, *J* = 6.8 Hz, 1H), 4.85 (s, 2H, overlap with H_2O), 3.67 – 3.43 (m, 36H), 2.74 (t, *J* = 5.1 Hz, 2H, NH_2). ^{13}C{^{1}H} NMR (125 MHz, CD_3OD) δ 168.5, 167.1, 138.9, 133.8, 131.6, 131.4, 130.2, 129.7, 129.0, 126.3, 123.3, 122.9, 112.2, 111.3, 73.2, 71.5, 71.5, 71.4, 71.4, 71.4, 71.4, 71.3, 71.2, 70.8,

66.9, 42.0, 40.3. FTIR (neat, cm^{-1}): 3354, 3085, 2867, 1687, 1631. HRMS (ESI-TOF) *m/z*: $[M+H]^+$ calcd for ($C_{41}H_{54}Cl_3N_4O_{10}^+$), 867.2900; found, 867.2891 and 869.2870.

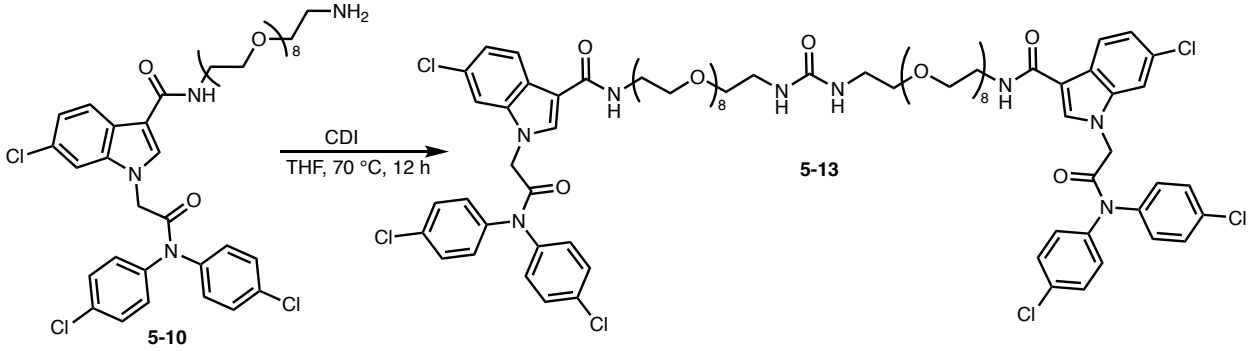

***N*,*N*'-(28-oxo-3,6,9,12,15,18,21,24,32,35,38,41,44,47,50,53-hexadecaoxa-27,29-diazapentapentacontane-1,55-diyl)bis(1-(2-(bis(4-chlorophenyl)amino)-2-oxoethyl)-6-chloro-1*H*-indole-3-carboxamide)** (**5-13**): Amine **5-10** (33 mg, 0.038 mmol) was dissolved in tetrahydrofuran (1 mL) in a 15 mL pressure tube. Then carbonyldiimidazole CDI (3.0 mg, 0.019 mmol) was added. The reaction was placed in a preheated aluminum beads at 70 °C and stirred for 12 hours. The reaction was diluted with ethyl acetate (5 mL) and washed with 1 N hydrochloric acid (2 x 3 mL). The organic layer was collected, dried over sodium sulfate, decanted, and concentrated under reduced pressure. The reaction was then purified with CombiFlash chromatography (silica gel, 20−40 μm, gradient 0−8% methanol/dichloromethane) to give the product as a white foamy solid (29 mg, 88%). ^{1}H NMR (500 MHz, CD_2Cl_2) δ 7.91 (d, *J* = 8.4 Hz, 1H), 7.47 (s, 1H), 7.36 (s, 2H), 7.16 (s, 4H), 7.04 (d, *J* = 10.1 Hz, 4H), 6.62 (d, *J* = 5.9 Hz, 1H, NH), 4.62 (s, 2H), 3.65 – 3.34 (m, 36H). ^{13}C{^{1}H} NMR (126 MHz, cd_2cl_2) δ 166.1, 164.2, 158.5, 137.2, 132.0, 130.8, 130.0, 129.0, 128.6, 127.1, 124.8, 122.4, 121.9, 111.9, 109.6, 70.6, 70.4, 70.4, 70.4, 70.3, 70.3, 70.2, 70.1, 70.0, 49.3, 40.0, 39.1. FTIR (cm^{-1}): 3338, 3089, 2868, 1685, 1633, 1488. HRMS (ESI-TOF) *m/z*: $[M+H]^+$ calcd for ($C_{83}H_{105}Cl_6N_8O_{21}^+$), 1759.5520; found, 1759.5155, 1760.5183, 1761.5134, 1762.5154, 1763.5120, 1764.5131, 1765.5116, 1766.5118.

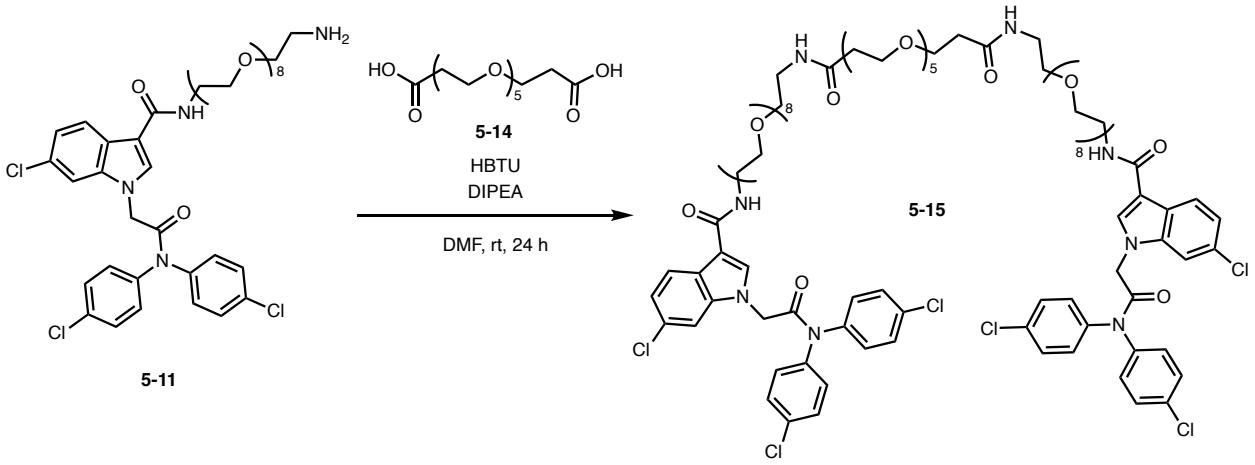

***N*[1],*N*[19]-bis(1-(1-(2-(bis(4-chlorophenyl)amino)-2-oxoethyl)-6-chloro-1*H*-indol-3-yl)-1-oxo-5,8,11,14,17,20,23,26-octaoxa-2-azaoctacosan-28-yl)-4,7,10,13,16-pentaoxanonadecanediamide** (**5-15**): To a solution of the dicarboxylic acid **5-14** (8 mg, 0.023 mmol) in *N,N*-dimethylformamide (1.0 mL) at room temperature was added HBTU (17 mg, 0.046 mmol) and DIPEA (19 μL, 0.110 mmol). The reaction was stirred for 15 mins and a solution of the amine **5-11** (40 mg, 0.046 mmol) in *N,N*-dimethylformamide (1 mL) was added. The reaction was further stirred at room temperature overnight. Then, the solvent was removed under reduced pressure and purified with CombiFlash chromatography (silica gel, 20−40 μm, gradient 0−8% methanol/dichloromethane) to give the product as a clear oil (27 mg, 57%). ^{1}H NMR (500 MHz, CD_2Cl_2) δ 8.03 (d, *J* = 8.7 Hz, 1H), 7.63 (s, 1H), 7.57 – 7.04 (m, 10H), 6.77 (s, 2H), 4.76 (s, 2H), 3.80 – 3.27 (m, 46H), 2.40 (t, *J* = 5.6 Hz, 2H). ^{13}C{^{1}H} NMR (125 MHz, CD_2Cl_2) δ 171.3, 166.1, 164.3, 137.3, 132.0, 130.8, 130.0, 129.0, 128.6, 127.1, 124.8, 122.3, 122.0, 111.9, 109.6, 70.4, 70.4, 70.3, 70.2, 70.2, 70.1, 70.0, 69.7, 67.1, 49.3, 39.1, 36.7. FTIR (neat, cm^{-1}): 3322, 3092, 2866, 1689, 1539. HRMS (ESI-TOF) *m/z*: $[M+H]^+$ calcd for ($C_{96}H_{129}Cl_6N_8O_{27}^+$), 2038.7097; found, 2038.7106.

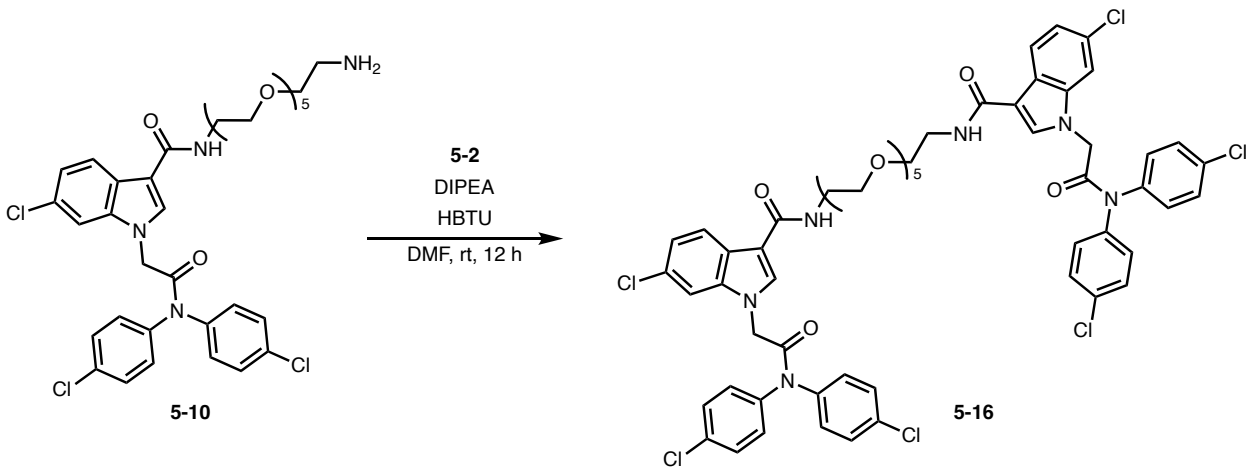

***N,N'*-(3,6,9,12,15-pentaoxaheptadecane-1,17-diyl)bis(1-(2-(bis(4-chlorophenyl)amino)-2-oxoethyl)-6-chloro-1*H*-indole-3-carboxamide) (5-16)**: To a solution of the indole-carboxylic acid **5-2** (52 mg, 0.109 mmol) in *N,N*-dimethylformamide (1.5 mL) at room temperature was added HBTU (42 mg, 0.111 mmol) and DIPEA (46 μL, 0.262 mmol). The reaction was stirred for 15 mins and a solution of the amine **5-10** (80 mg, 0.109 mmol) in *N,N*-dimethylformamide (1.5 mL) was added. The reaction was further stirred at room temperature overnight. Then, the solvent was removed under reduced pressure and purified with CombiFlash chromatography (silica gel, 20−40 μm, gradient 0−8% methanol/dichloromethane) to give the product as a yellow foamy solid (101 mg, 78%). ^{1}H NMR (500 MHz, CD_2Cl_2) δ 8.05 (d, J = 9.3 Hz, 1H), 7.65 (s, 1H), 7.50 (s, 2H), 7.40 – 7.11 (m, 8H), 4.74 (s, 2H), 3.76 – 3.43 (m, 13H). ^{13}C{^{1}H} NMR (125 MHz, CD_2Cl_2) δ 166.2, 164.2, 137.2, 132.0, 130.8, 129.9, 129.0, 128.5, 127.0, 124.8, 122.4, 121.9, 111.8, 109.5, 70.4, 70.4, 70.4, 70.1, 69.9, 49.2, 39.1. FTIR (neat, cm^{-1}): 2875, 1676, 1631, 1549. HRMS (ESI-TOF) *m/z*: $[M+H]^+$ calcd for ($C_{58}H_{55}Cl_6N_6O_9^+$), 1189.2156; found,1189.2139, 1190.2173, 1191.2120, 1192.2152, 1193.2103, 1194.2125, 1195.2094, 1196.2094.

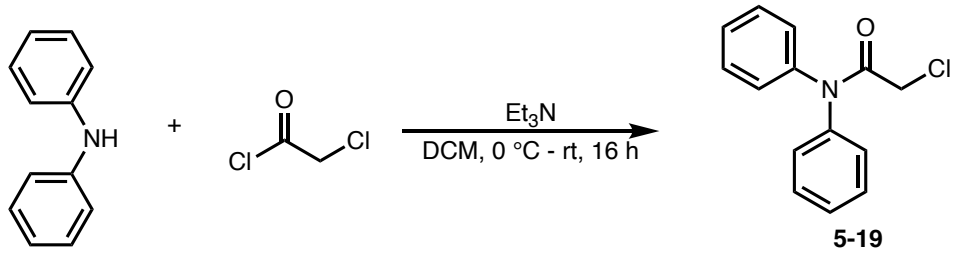

2-chloro-*N*,*N*-diphenylacetamide (**5-19**): A 100 mL round bottom flask equipped with magnetic stirrer was charged with diphenylamine (2.0 g, 11.82 mmol) and dichloromethane (30 mL). The resulting solution was cooled to 0 °C and then triethylamine (3.29 mL, 23.64 mmol) was added. A solution of chloroacetyl chloride (1.03 mL, 13.00 mmol) in dichloromethane (1.5 mL) was added slowly over 15 mins. After 4 hours, additional solution of chloroacetyl chloride (1.03 mL, 13.00 mmol) in dichloromethane (1.5 mL) was added. The reaction was then warmed up to room temperature and allowed to stirred overnight. The reaction was then diluted with sodium carbonate (50 mL) and the organic layer was collected. The aqueous phase was further extracted with dichloromethane (2 x 50 mL) and the organic phases were combined. The organics were dried over sodium sulfate, decanted and concentrated under reduced pressure to give the crude product as yellow solid (2.78g, 96%). mp: 116 – 117 °C. ^{1}H NMR (500 MHz, DMSO-d_6) δ 7.60 – 7.28 (m, br, 10H), 4.19 (s, 2H). ^{13}C{^{1}H} NMR (125 MHz, DMSO-d_6) δ 165.4, 129.8, 129.1, 128.6, 126.7, 43.2. FTIR (neat, cm^{-1}): 3005, 2945, 1676, 1490. HRMS (ESI-TOF) *m/z*: [M+H]$^{+}$ calcd for ($C_{14}H_{13}ClNO^{+}$), 246.0680; found, 246.0712 and 248.0685.

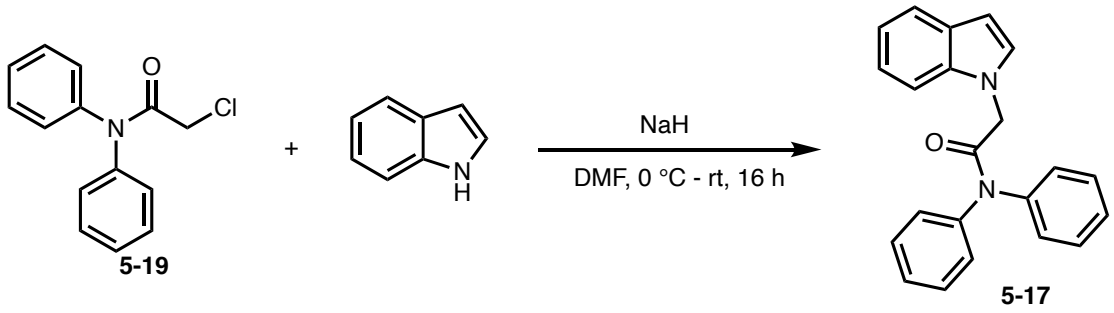

2-(1*H*-indol-1-yl)-*N*,*N*-diphenylacetamide (**5-17**): Sodium hydride (60% in mineral oil, 166 mg, 4.15 mmol) was suspended in anhydrous *N,N*-dimethylformamide (10 mL) and cooled to 0 °C, then a solution of indole (0.48 g, 4.07 mmol) in *N,N*-dimethylformamide (5 mL) was added slowly via syringe. After 10 mins, a solution of the α-chloroamide **5-19** (1.0 g, 4.07 mmol) in *N,N*-dimethylformamide (5 mL) was added in one-portion and the reaction was warmed up to room temperature and stirred overnight. Then, ethyl acetate (50 mL) and 1 M hydrochloric acid (30 mL) was added, and the organic layer was collected. The organic was further washed with 1 M hydrochloric acid (2 x 30 mL). The organic was dried over sodium sulfate, decanted, and concentrated under reduced pressure. The product was purified with CombiFlash chromatography (silica gel, 20−40 μm, gradient 5 – 15% ethyl acetate/hexane) to give a yellow foamy solid (1.15 g, 86% yield). ^{1}H NMR (500 MHz, DMSO-d_6) δ 7.83 – 7.16 (m, 13H), 7.13 (t, J = 7.5 Hz, 1H), 7.02 (t, J = 7.5 Hz, 1H), 6.40 (d, J = 3.2 Hz, 1H), 4.89 (s, 2H). ^{13}C{^{1}H} NMR (125 MHz, DMSO-d_6) δ 167.5, 136.8, 130.6, 130.3, 129.4, 128.5, 127.0, 121.5, 120.7, 119.5, 110.1, 101.2, 48.9 (one of the broad phenyl carbon was not observed). FTIR (neat, cm^{-1}): 3054, 2944, 1687, 1485. HRMS (ESI-TOF) *m/z*: $[M+H]^+$ calcd for ($C_{22}H_{19}N_2O^+$), 327.1492; found, 327.1524.

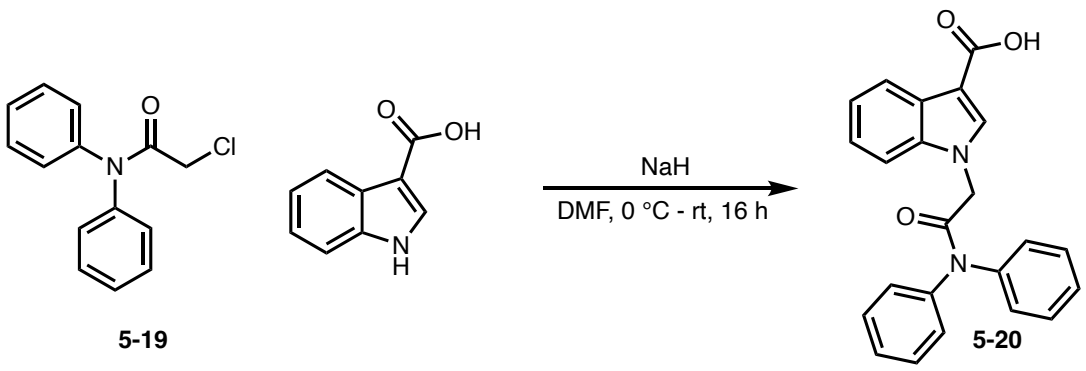

5-19 5-20

1-(2-(diphenylamino)-2-oxoethyl)-1*H*-indole-3-carboxylic acid (**5-20**): Sodium hydride (60% in mineral oil, 163 mg, 4.07 mmol) was suspended in anhydrous *N,N*-dimethylformamide (5 mL) and cooled to 0 °C, then a solution of indole-3-carboxylic acid (327 mg, 2.03 mmol) in *N,N*-dimethylformamide (5 mL) was added slowly via syringe. After 10 mins, a solution of α-chloroamide (500 mg, 2.03 mmol) in *N,N*-dimethylformamide (5 mL) was added in one-portion and the reaction was warmed up to room temperature and stirred overnight. Then, ethyl acetate (30 mL) and 1 M hydrochloric acid (20 mL) was added and the organic layer was collected. The organic was further washed with 1 M hydrochloric acid (2 x 30 mL). The organic was dried over sodium sulfate, decanted and concentrated under reduced pressure. The product was purified with CombiFlash chromatography (silica gel, 20−40 μm, gradient 20 – 40% ethyl acetate/hexane) to give a yellow solid (267 mg, 36% yield). mp: 222 – 223 °C. ^{1}H NMR (500 MHz, DMSO-d_6) δ 11.99 (s, 1H), 7.99 (s, 1H), 7.83 – 7.26 (m, 11H), 7.27 – 7.12 (m, 3H), 4.98 (s, 2H). ^{13}C{^{1}H} NMR (125 MHz, DMSO-d_6) δ 166.8, 166.1, 137.5, 137.2, 130.5, 129.4, 127.0, 126.7, 122.7, 121.7, 121.1, 111.2, 107.2, 49.3 (one of the broad phenyl carbon was not observed). FTIR (neat, cm^{-1}): 3056, 2933, 1677, 1655, 1490. HRMS (ESI-TOF) *m/z*: [M+H]$^{+}$ calcd for ($C_{23}H_{19}N_2O_3^{+}$), 371.1390; found, 371.1415.

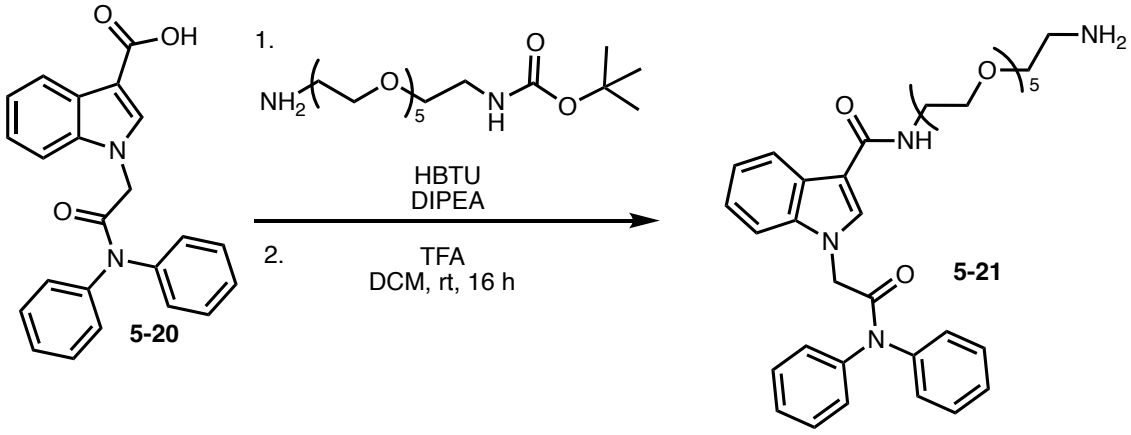

***N*-(17-amino-3,6,9,12,15-pentaoxaheptadecyl)-1-(2-(diphenylamino)-2-oxoethyl)-1*H*-indole-3-carboxamide** (**5-21**): To a solution of the indole-carboxylic acid (100 mg, 0.270 mmol) in *N,N*-dimethylformamide (1.0 mL) at room temperature was added HBTU (104 mg, 0.275 mmol) and DIPEA (112 μL, 0.650 mmol). The reaction was stirred for 10 mins and a solution of the PEG linker (103 mg, 0.270 mmol) in *N,N*-dimethylformamide (1.0 mL) was added. The reaction was further stirred at room temperature overnight. Then, the solvent was removed under reduced pressure to give the crude N-boc product.

The crude product was dissolved in dichloromethane (3 mL) and trifluoroacetic acid (0.41 mL, 5.40 mmol) and stirred overnight. The reaction was quenched with sodium carbonate (10 mL). The reaction was extracted with dichloromethane (3 x 10 mL) and the organics were combined and dried over sodium sulfate. The organic was then concentrated and purified with CombiFlash chromatography (silica gel, 20−40 μm, gradient 0−8% methanol (5% Et_3N)/dichloromethane) to give the product as a clear oil (193 mg, quantitative). ^{1}H NMR (500 MHz, CD_3OD) δ 8.12 (d, J = 7.9 Hz, 1H), 7.77 (s, 1H), 7.64 – 7.08 (m, 14H), 4.92 (s, 2H), 3.68 – 3.43 (m, 24H), 2.91 (t, J = 5.1 Hz, 2H). ^{13}C{^{1}H} NMR (125 MHz, CD_3OD) δ 168.8, 167.7, 138.4, 133.5, 131.5, 130.1, 129.7, 127.7, 127.6, 123.9, 122.4, 122.2, 111.6, 110.9, 71.3, 71.2, 71.1, 71.1, 71.0, 70.9, 70.8, 68.9, 50.1,

40.7, 40.0. FTIR (neat, cm^{-1}): 3343, 3050, 2872, 1682, 1626. HRMS (ESI-TOF) *m/z*: $[M+H]^+$ calcd for ($C_{35}H_{45}N_4O_7^+$), 633.3283; found, 633.3313.

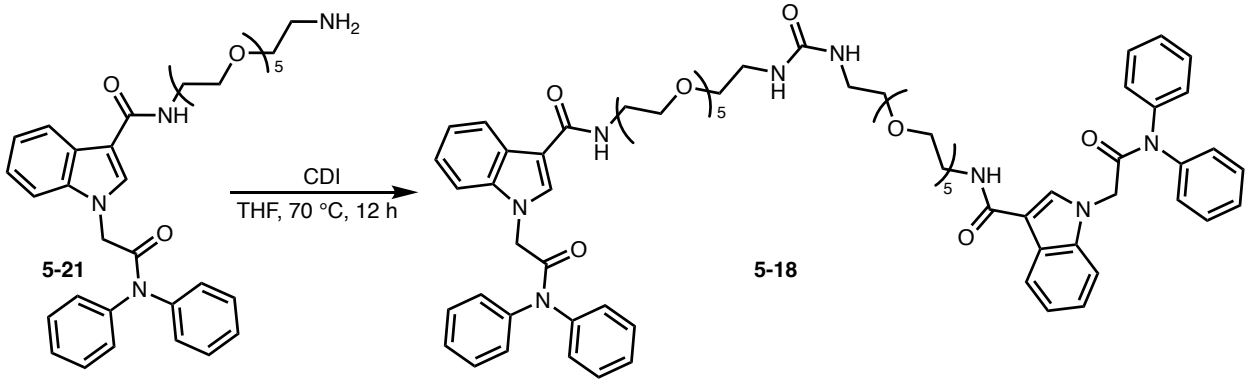

***N*,*N*'-(19-oxo-3,6,9,12,15,23,26,29,32,35-decaoxa-18,20-diazaheptatriacontane-1,37-diyl)bis(1-(2-(diphenylamino)-2-oxoethyl)-1*H*-indole-3-carboxamide)** (**5-18**): Amine **5-21** (50 mg, 0.079 mmol) was dissolved in tetrahydrofuran (1 mL) in a 15 mL pressure tube. Then carbonyldiimidazole CDI (6.4 mg, 0.040 mmol) was added. The reaction was placed in a preheated aluminum beads at 70 °C and stirred for 12 hours. The reaction was diluted with ethyl acetate (5 mL) and washed with 1 N hydrochloric acid (2 x 3 mL). The organic layer was collected, dried over sodium sulfate, decanted, and concentrated under reduced pressure. The reaction was then purified with CombiFlash chromatography (silica gel, 20−40 μm, gradient 0−8% methanol/dichloromethane) to give the product as a foamy white solid (29 mg, 55%). ^{1}H NMR (500 MHz, CD_3OD) δ 8.08 (d, *J* = 7.9 Hz, 1H), 7.69 (s, 1H), 7.62 – 7.12 (m, 13H), 4.93 (s, 2H), 3.66 – 3.47 (m, 20H), 3.40 (t, *J* = 5.4 Hz, 2H), 3.21 (t, *J* = 5.3 Hz, 2H). ^{13}C{^{1}H} NMR (125 MHz, CD_3OD) δ 169.0, 167.7, 161.0, 138.4, 133.5, 131.5, 130.2, 129.8, 127.6, 127.6, 123.9, 122.5, 122.2, 111.8, 110.9, 71.5, 71.5, 71.4, 71.4, 71.4, 71.3, 71.2, 70.9, 50.3, 40.9, 40.3.

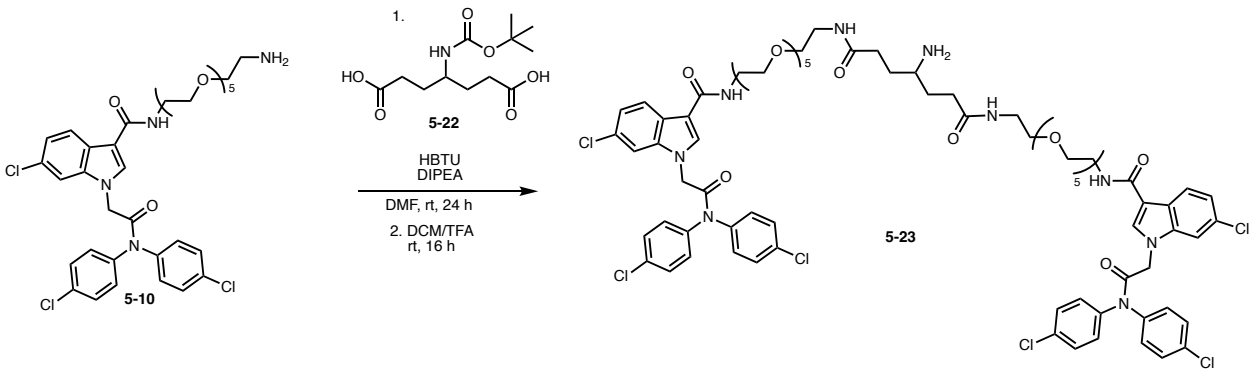

4-amino-*N*1,*N*7-bis(1-(1-(2-(bis(4-chlorophenyl)amino)-2-oxoethyl)-6-chloro-1*H*-indol-3-yl)-1-oxo-5,8,11,14,17-pentaoxa-2-azanonadecan-19-yl)heptanediamide (**5-23**): To a solution of the dicarboxylic acid **5-22** (19 mg, 0.068 mmol) in *N,N*-dimethylformamide (1.0 mL) at room temperature was added HBTU (62 mg, 0.163 mmol) and DIPEA (57 µL, 0.326 mmol). The reaction was stirred for 15 mins at room temperature and a solution of the amine **5-10** (100 mg, 0.136 mmol) in *N,N*-dimethylformamide (2.0 mL) was added. The reaction was further stirred at room temperature for 24 hours. Then, the solvent was removed under reduced pressure and the crude N-boc product was used directly for the next step.

The crude N-boc product was dissolved in dichloromethane (1.5 mL) and trifluoroacetic acid (1.0 mL) and stirred overnight. The reaction was quenched with sodium carbonate (18 mL). The reaction was extracted with dichloromethane (3 x 15 mL) and the organics were combined and dried over sodium sulfate. The organic was then concentrated and purified with CombiFlash chromatography (silica gel, 20−40 µm, gradient 0−8% methanol (5% Et_3N)/dichloromethane) to give the product as a foamy white solid (43.4 mg, 40% yield). ^1H NMR (500 MHz, CD_2Cl_2) δ 8.08 (d, J = 8.4 Hz, 1H), 7.73 (s, 1H), 7.59 – 7.42 (m, 2H), 7.41 – 7.13 (m, 8H), 7.03 (t, J = 5.5 Hz, 1H, NH), 6.88 (t, J = 5.6 Hz, 1H, NH), 4.79 (s, 2H), 3.73 – 3.50 (m, 22H), 3.46 (q, J = 5.7 Hz, 2H), 3.32 (q, J = 5.4 Hz, 2H), 2.55 (q, J = 7.2 Hz, 1H), 2.21 (hept, J = 7.3 Hz, 2H), 1.70 (dq, J = 12.2, 7.4 Hz, 1H), 1.53 (dq, J = 12.2, 7.4 Hz, 1H). $^{13}C\{^1H\}$ NMR (125 MHz, CD_2Cl_2) δ 173.3, 166.6,

164.6, 137.6, 132.5, 131.1, 130.4, 129.4, 128.9, 127.5, 125.3, 122.8, 122.3, 112.2, 109.9, 70.8, 70.8, 70.7, 70.4, 70.4, 70.3, 70.0, 51.0, 49.7, 46.4, 39.5, 39.4, 33.2, 33.1. FTIR (neat, cm^{-1}): 3287, 3063, 2868, 1685. HRMS (ESI-TOF) *m/z*: $[M+H]^+$ calcd for ($C_{77}H_{92}Cl_6N_9O_{16}^+$), 1608.4685; found, 1608.4606, 1609.4633, 1610.4592, 1611.4615, 1612.4583, 1613.4601, 1614.4575, 1615.4580, 1616.4565.

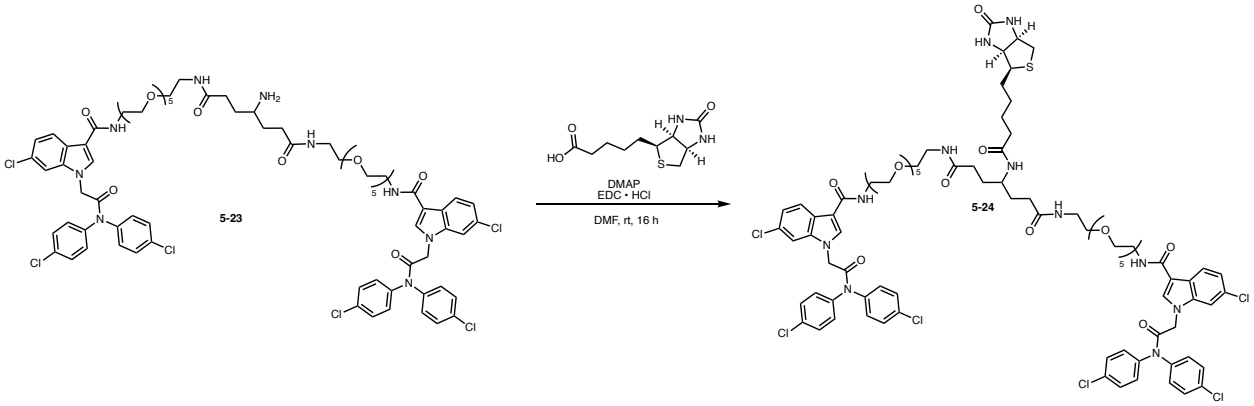

***N*^{1},*N*^{7}-bis(1-(1-(2-(bis(4-chlorophenyl)amino)-2-oxoethyl)-6-chloro-1*H*-indol-3-yl)-1-oxo-5,8,11,14,17-pentaoxa-2-azanonadecan-19-yl)-4-(5-((3a*S*,4*S*,6a*R*)-2-oxohexahydro-1*H*-thieno[3,4-*d*]imidazol-4-yl)pentanamido)heptanediamide** (**5-24**): A 15 mL round bottom flask equipped with magnetic stirrer bar was charged with amine **5-23** (31 mg, 0.019 mmol) and dimethylformamide (DMF) (2 mL). To the resulting solution was added biotin (7.1mg, 0.029 mmol), dimethylaminopyridine (DMAP) (10 mol%), and N-(3-Dimethylaminopropyl)-N′-ethylcarbodiimide hydrochloride (EDC•HCl) (6 mg, 0.029 mmol). The solution was further stirred at room temperature for 16 hours before the solvent was removed under reduced pressure. The crude was then purified with CombiFlash chromatography (silica gel, 20−40 μm, gradient 0−8% methanol/dichloromethane) to give the product as a white foamy solid (20.3 mg, 58%). ^{1}H NMR (500 MHz, CD_2Cl_2) δ 8.08 (d, *J* = 8.5 Hz, 2H), 7.69 (d, *J* = 1.9 Hz, 2H), 7.58 – 7.06 (m, 20H), 7.03 – 6.87 (m, 4H), 6.80 (d, *J* = 8.5 Hz, 1H), 6.42 (s, 1H), 5.79 (s, 1H), 4.79 (s, 4H), 4.41 (dd, *J* = 8.0, 4.9 Hz, 1H), 4.21 (dd, *J* = 8.0, 4.5 Hz, 1H), 3.70 – 3.51 (m, 43H), 3.48 (t, *J* = 5.4 Hz, 4H),

3.42 – 3.25 (m, 5H), 2.19 – 2.08 (m, 4H), 2.10 – 2.03 (m, 2H), 1.75 – 1.60 (m, 6H), 1.55 (q, J = 7.3 Hz, 3H). $^{13}C\{^{1}H\}$ NMR (125 MHz, CD_2Cl_2) δ 173.4, 173.1, 173.0, 166.3, 164.3, 163.9, 137.2, 132.1, 130.8, 130.0, 129.1, 128.5, 127.1, 124.9, 122.5, 121.9, 111.9, 109.5, 70.4, 70.4, 70.4, 70.2, 70.1, 70.1, 70.0, 69.7, 69.7, 61.7, 60.1, 55.6, 49.3, 48.9, 40.5, 39.3, 39.2, 35.5, 32.9, 30.8, 27.9, 27.8, 25.3. FTIR (neat, cm^{-1}): 3297, 2869, 1640, 1540. HRMS (ESI-TOF) *m/z*: $[M+H]^+$ calcd for ($C_{87}H_{106}Cl_6N_{11}O_{18}S^+$), 1836.5535, 1837.5568, 1838.5505, 1839.5539; found 1836.5425, 1837.5443, 1838.5410, 1839.5427.

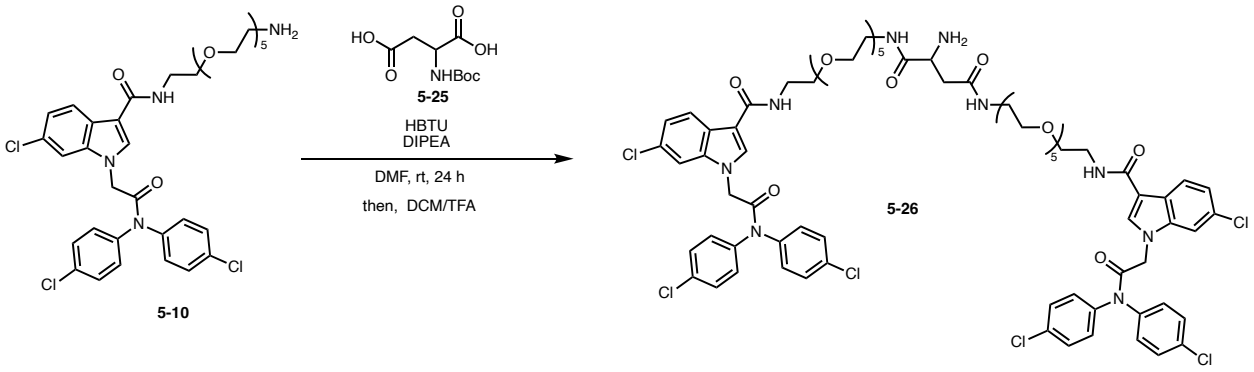

2-amino-*N*^{1},*N*^{4}-bis(1-(1-(2-(bis(4-chlorophenyl)amino)-2-oxoethyl)-6-chloro-1*H*-indol-3-yl)-1-oxo-5,8,11,14,17-pentaoxa-2-azanonadecan-19-yl)succinimide (**5-26**): To a solution of amine **5-10** (100 mg, 0.136 mmol) in DMF (2 mL) was added dicarboxylic acid (14 mg, 0.062 mmol) followed by HBTU (56 mg, 0.149 mmol) and DIPEA (52 µL, 0.062 mmol). The solution was then stirred overnight and then concentrated under reduced pressure to give the crude N-boc protected product.

The crude N-boc protected amine was redissolved in DCM (2 mL) and TFA (1 mL) and was stirred for another 16 hours. The reaction was diluted with DCM (5 mL) and quenched with sodium carbonate until pH ≈ 7. The DCM layer was collected, and the aqueous layer was further extracted with DCM (2 x 5 mL). The organics were combined, dried over sodium sulfate, decanted and then concentrated to give the crude amine. The crude was then purified with CombiFlash

chromatography (silica gel, 20−40 μm, gradient 0−10% methanol/dichloromethane) to give the product as off-white foamy solids (64 mg, 67%). ^{1}H NMR (500 MHz, CD_2Cl_2) δ 8.12 – 8.06 (m, 2H), 7.71 (d, *J* = 8.2 Hz, 2H), 7.67 (t, *J* = 6.0 Hz, 1H), 7.53 – 7.15 (m, 20H), 7.07 (q, *J* = 5.5 Hz, 2H), 7.01 (t, *J* = 5.5 Hz, 1H), 4.78 (d, *J* = 2.6 Hz, 4H), 3.67 – 3.51 (m, 43H), 3.46 (dt, *J* = 8.4, 5.3 Hz, 4H), 3.34 (dh, *J* = 9.9, 5.2 Hz, 4H). ^{13}C{^{1}H} NMR (125 MHz, CD_2Cl_2) δ 174.2, 171.2, 166.3, 166.2, 164.3, 164.3, 137.2, 132.2, 132.1, 130.7, 130.0, 129.0, 128.5, 128.5, 127.1, 125.0, 125.0, 122.5, 122.5, 121.9, 111.8, 111.8, 109.5, 70.4, 70.4, 70.3, 70.3, 70.2, 70.2, 70.1, 70.1, 70.1, 69.6, 52.6, 49.3, 45.8, 40.9, 39.1, 39.1, 39.0. FTIR (neat, cm^{-1}): 3302, 2922, 1670, 1544, 1275. HRMS (ESI-TOF) *m/z*: $[M+2H]^{2+}$ calcd for ($C_{74}H_{87}Cl_6N_9O_{16}^{2+}$), 784.7181, 785.2198, 785.7166, 786.2183; found 784.7188, 785.2202, 785.7183, 786.2192

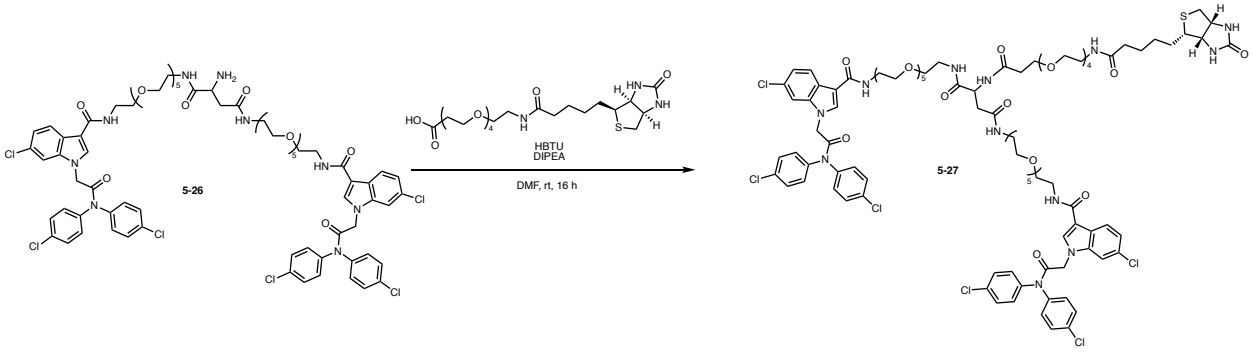

To a solution of amine (64 mg, 0.0408 mmol) in DMF (3 mL) was added carboxylic acid (22 mg, 0.0449 mmol) followed by HBTU (19 mg, 0.0489 mmol) and DIPEA (17 μL, 0.0979 mmol). The solution was then stirred overnight and then concentrated under reduced pressure to give the crude product. The crude was then purified with CombiFlash chromatography (silica gel, 20−40 μm, gradient 0−10% methanol/dichloromethane) to give the product as a foamy white solid (68 mg, 82%). ^{1}H NMR (500 MHz, CD_2Cl_2) δ 8.09 (d, *J* = 8.5 Hz, 2H), 7.76 (d, *J* = 7.8 Hz, 1H), 7.69 (d, *J* = 8.5 Hz, 2H), 7.61 – 7.09 (m, 20H), 7.02 (m, 2H), 6.89 (s, 1H), 6.24 (s, 1H), 5.62 (s, 1H), 5.35 (d, *J* = 6.0 Hz, 1H), 4.80 (s, 4H), 4.72 (q, *J* = 6.0 Hz, 1H), 4.50 – 4.38 (m, 1H), 4.37 – 4.17 (m,

1H), 4.00 – 3.21 (m, 66H), 3.11 (d, J = 4.5 Hz, 1H), 3.02 – 2.37 (m, 9H), 2.15 (t, J = 7.1 Hz, 2H), 1.61 (m, 4H), 1.39 (s, 2H). $^{13}C\{^{1}H\}$ NMR (125 MHz, CD_2Cl_2) δ 173.0, 171.4, 170.8, 166.4, 166.3, 164.3, 164.3, 163.8, 137.2, 132.2, 132.1, 130.7, 130.0, 129.0, 128.5, 127.2, 125.0, 122.5, 121.9, 111.8, 109.5, 70.4, 70.4, 70.4, 70.4, 70.3, 70.3, 70.2, 70.2, 70.1, 70.0, 69.9, 69.6, 69.5, 67.2, 61.8, 60.1, 55.7, 50.3, 49.3, 40.5, 39.3, 39.2, 39.2, 39.2, 37.6, 36.8, 35.5, 28.1, 28.0, 25.5. FTIR (neat, cm^{-1}): 3296, 2864, 1642, 1538, 1278. HRMS (ESI-TOF) *m/z*: $[M+H]^+$ calcd for ($C_{95}H_{121}Cl_6N_{12}O_{23}S^+$), 2041.6485, 2042.6518, 2043.6455, 2044.6489; found: 2041.6473, 2042.6494, 2043.6476, 2044.6476.

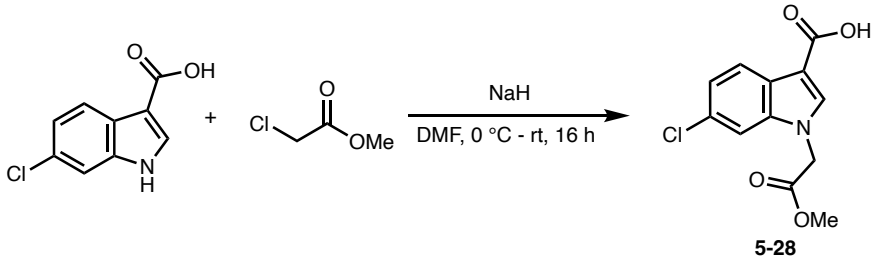

5-28

6-chloro-1-(2-methoxy-2-oxoethyl)-1*H*-indole-3-carboxylic acid (**5-28**): To a suspension of NaH (60% in mineral oil, 2.1 equiv, 429 mg) in DMF (10 mL) at 0 °C was slowly added 6-chloroindole-3-carboxylic acid (1.0 equiv, 1.0 g). The solution was stirred for 15 minutes and methyl chloroacetate (1.0 equiv, 0.45 mL) was added. The reaction was then allowed to warm up to room temperature and stirred for 16 hours. Then, ethyl acetate (50 mL) and 1 M hydrochloric acid (30 mL) was added and the organic layer was collected. The organic was further washed with 1 M hydrochloric acid (2 x 30 mL). The organic was dried over sodium sulfate, decanted, and concentrated under reduced pressure to give the crude products. The crude was then purified with CombiFlash chromatography (silica gel, 20−40 μm, gradient 20−60% ethylacetate/hexane) to give the products as white solids (0.38 g, 28%). ^{1}H NMR (500 MHz, acetone) δ 8.13 (d, J = 8.5 Hz, 1H), 8.12 (s, 1H), 7.63 (d, J = 1.8 Hz, 1H), 7.26 (dd, J = 8.5, 1.8 Hz, 1H), 5.27 (s, 2H), 3.75 (s,

3H). $^{13}C\{^{1}H\}$ NMR (125 MHz, acetone) δ 168.4, 164.8, 137.9, 136.9, 128.3, 125.6, 122.4, 122.1, 110.6, 107.8, 51.9, 47.4. FTIR (neat, cm^{-1}): 3057, 2955, 1730, 1701. HRMS (ESI-TOF) *m/z*: $[M+H]^+$ calcd for ($C_{12}H_{11}ClNO_4^+$), 268.0372 & 270.0342; found: 268.0374 & 270.0359.

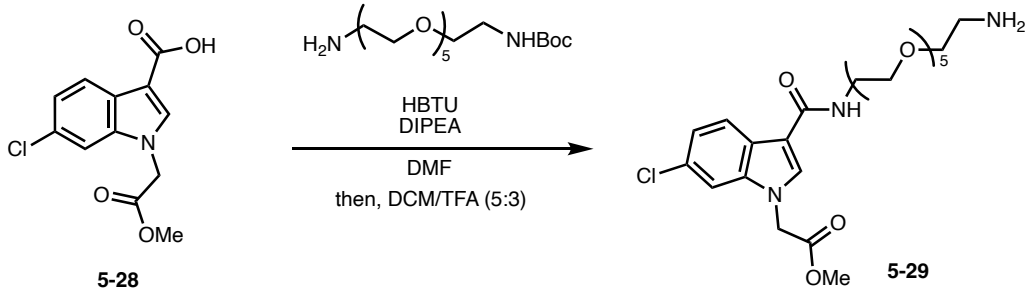

methyl 2-(3-((17-amino-3,6,9,12,15-pentaoxaheptadecyl)carbamoyl)-6-chloro-1*H*-indol-1-yl)acetate (**5-29**): To a solution of indole carboxylic acid **5-28** (200 mg, 0.75 mmol) in *N,N*-dimethylformamide (2.0 mL) at room temperature was added HBTU (341 mg, 1.20 mmol) and DIPEA (0.31 mL, 1.8 mmol). The reaction was stirred for 15 mins and a solution of the PEG linker (284 mg, 0.75 mmol) in *N,N*-dimethylformamide (1.0 mL) was added. The reaction was further stirred at room temperature overnight. Then, the solvent was removed under reduced pressure to give the crude product.

The crude product was dissolved in dichloromethane (5 mL) and trifluoroacetic acid (3 mL) and stirred overnight. The reaction was quenched with sodium carbonate (10 mL). The reaction was extracted with dichloromethane (3 x 10 mL) and the organics were combined and dried over sodium sulfate. The organic was then concentrated and purified with CombiFlash chromatography (silica gel, 20−40 μm, gradient 0−8% methanol (5% Et_3N)/dichloromethane) to give the product as a white foamy solid (252 mg, 63%). ^{1}H NMR (500 MHz, CD_2Cl_2) δ 8.22 (d, *J* = 8.5 Hz, 1H), 8.20 (s, 1H), 8.12 (t, *J* = 5.6 Hz, 1H), 7.88 (s, 2H), 7.26 (d, *J* = 1.8 Hz, 1H), 7.18 (dd, *J* = 8.5, 1.8 Hz, 1H), 4.87 (s, 2H), 3.75 (s, 3H), 3.72 – 3.47 (m, 24H). $^{13}C\{^{1}H\}$ NMR (125 MHz, CD_2Cl_2) δ 168.6, 164.6, 137.7, 132.1, 129.2, 125.5, 122.9, 122.5, 112.7, 110.1, 73.6, 70.9, 70.9, 70.9, 70.9,

70.8, 70.6, 70.6, 70.5, 48.2, 42.1, 39.6. FTIR (neat, cm^{-1}): 3313, 2925, 1657, 1545, 1382. HRMS (ESI-TOF) *m/z*: $[M+H]^+$ calcd for ($C_{24}H_{37}ClN_3O_8^+$), 530.2264 & 532.2235; found 530.2284 & 532.2267.

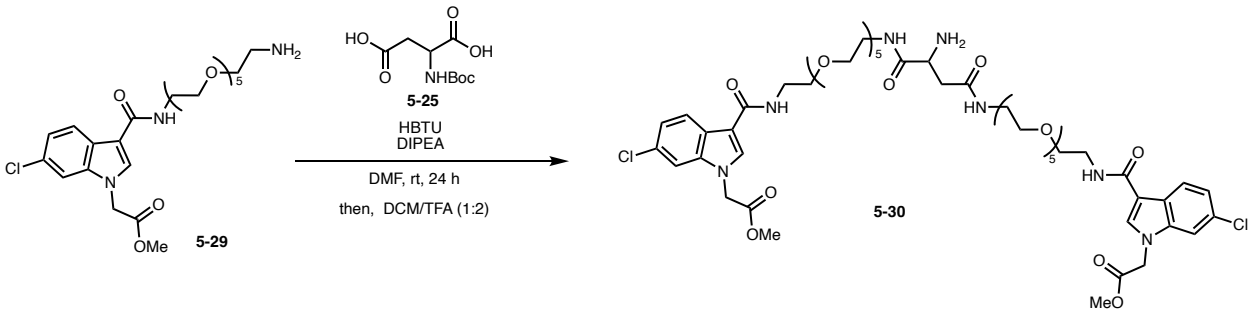

dimethyl 2,2'-((22-amino-21,24-dioxo-5,8,11,14,17,28,31,34,37,40-decaoxa-2,20,25,43-tetraazatetratetracontanedioyl)bis(6-chloro-1*H*-indole-3,1-diyl))diacetate (**5-30**): To a solution of amine (195 mg, 0.368 mmol) in DMF (3 mL) was added dicarboxylic acid (39mg, 0.167 mmol) followed by HBTU (152 mg, 0.401 mmol) and DIPEA (140 µL, 0.802 mmol). The solution was then stirred overnight and then concentrated under reduced pressure to give the crude boc protected product.

The crude boc protected amine was redissolved in DCM (5 mL) and TFA (3 mL) and was stirred for another 16 hours. The reaction was diluted with DCM (10 mL) and quenched with sodium carbonate until pH ≈ 7. The DCM layer was collected, and the aqueous layer was further extracted with DCM (2 x 10 mL). The organics were combined, dried over sodium sulfate, decanted and then concentrated to give the crude amine. The crude was then purified with CombiFlash chromatography (silica gel, 20−40 µm, gradient 0−8% methanol/dichloromethane) to give the product as a white foamy solid (135 mg, 70%). ^{1}H NMR (500 MHz, CD_2Cl_2) δ 8.12 (dd, *J* = 8.5, 2.8 Hz, 2H), 7.80 (d, *J* = 7.6 Hz, 2H), 7.70 (t, *J* = 5.4 Hz, 1H), 7.28 (d, *J* = 1.6 Hz, 2H), 7.20 (dd, *J* = 8.5, 1.6 Hz, 2H), 7.11 (t, *J* = 5.2 Hz, 1H), 7.08 (t, *J* = 5.2 Hz, 1H), 7.02 (t, *J* = 5.2 Hz, 1H), 4.91 – 4.88 (m, 4H), 3.75 (s, 6H), 3.72 – 3.51 (m, 43H), 3.51 – 3.45 (m, 4H), 3.42 – 3.29 (m, 4H).

$^{13}C\{^{1}H\}$ NMR (125 MHz, CD_2Cl_2) δ 174.1, 171.4, 168.6, 168.6, 164.6, 164.6, 137.6, 132.2, 132.2, 129.0, 125.4, 125.4, 122.9, 122.8, 122.3, 112.4, 112.3, 110.0, 70.7, 70.7, 70.7, 70.7, 70.7, 70.5, 70.5, 70.5, 70.4, 70.4, 70.3, 69.9, 69.9, 53.0, 52.9, 48.0, 40.9, 39.5, 39.4, 39.3. FTIR (neat, cm^{-1}): 3311, 2922, 1653, 1543, 1384. HRMS (ESI-TOF) *m/z*: $[M+H]^+$ calcd for ($C_{52}H_{76}Cl_2N_7O_{18}^+$), 1156.4619, 1157.4652, 1158.4589; found: 1156.4667, 1157.4702, 1158.463.

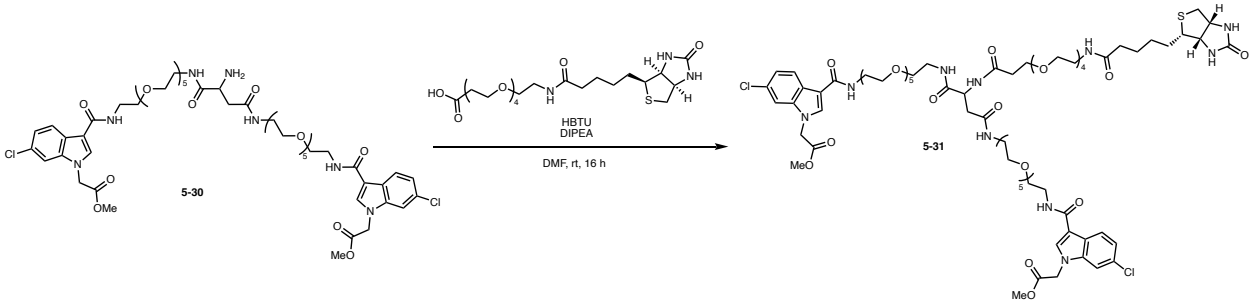

dimethyl 2,2'-((21,24-dioxo-22-(17-oxo-21-((3a*S*,4*S*,6a*R*)-2-oxohexahydro-1*H*-thieno[3,4-*d*]imidazol-4-yl)-4,7,10,13-tetraoxa-16-azahenicosanamido)-5,8,11,14,17,28,31,34,37,40-decaoxa-2,20,25,43-tetraazatetratetracontanedioyl)bis(6-chloro-1*H*-indole-3,1-diyl))diacetate (**5-31**): To a solution of amine (135 mg, 0.117 mmol) in DMF (3 mL) was added carboxylic acid (63 mg, 0.129 mmol) followed by HBTU (53 mg, 0.140 mmol) and DIPEA (49 μL, 0.281 mmol). The solution was then stirred overnight and then concentrated under reduced pressure to give the crude product. The crude was then purified with CombiFlash chromatography (silica gel, 20−40 μm, gradient 0−8% methanol/dichloromethane) to give the product as a white foamy solid (151 mg, 79%). ^{1}H NMR (500 MHz, CD_2Cl_2) δ 8.13 (d, *J* = 8.3 Hz, 2H), 7.79 (m, 3H), 7.43 (s, 1H), 7.30 (s, 3H), 7.23 – 7.11 (m, 4H), 6.98 (s, 1H), 6.40 (s, 1H), 5.88 (s, 1H), 5.35 (d, *J* = 5.3 Hz, 1H), 4.92 (s, 4H), 4.78 – 4.63 (m, 1H), 4.45 (s, 1H), 4.26 (s, 1H), 3.94 – 3.02 (m, 81H), 2.87 (d, *J* = 8.5 Hz, 1H), 2.74 (m, 2H), 2.66 – 2.54 (m, 1H), 2.48 (s, 2H), 2.17 (s, 2H), 1.64 (d, *J* = 35.0 Hz, 4H), 1.40 (s, 2H). $^{13}C\{^{1}H\}$ NMR (125 MHz, CD_2Cl_2) δ 173.1, 171.4, 170.8, 168.4, 164.3, 164.0, 137.3, 132.0, 132.0, 128.6, 125.1, 122.6, 122.0, 111.9, 109.7, 70.4, 70.3, 70.3, 70.2,

70.2, 70.1, 70.1, 70.0, 69.9, 69.6, 69.5, 67.2, 61.8, 60.2, 55.7, 52.7, 50.2, 47.7, 40.5, 39.3, 39.2, 39.2, 39.2, 37.6, 36.8, 35.6, 28.2, 28.1, 25.5. FTIR (neat, cm^{-1}): 3308, 2864, 1749, 1639, 1544. HRMS (ESI-TOF) *m/z*: $[M+H]^+$ calcd for ($C_{73}H_{112}Cl_2N_{10}O_{25}S^{2+}$), 815.3444, 815.8460, 816.3429, 816.8446; found: 815.3436, 815.8456, 816.3438, 816.8447.

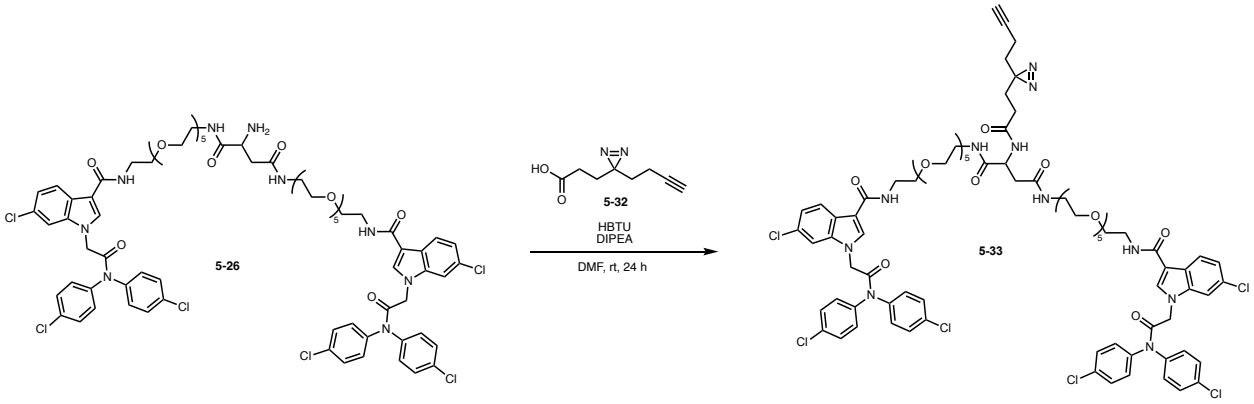

***N*^{1},*N*^{4}-bis(1-(1-(2-(bis(4-chlorophenyl)amino)-2-oxoethyl)-6-chloro-1*H*-indol-3-yl)-1-oxo-5,8,11,14,17-pentaoxa-2-azanonadecan-19-yl)-2-(3-(3-(but-3-yn-1-yl)-3*H*-diazirin-3-yl)propanamido)succinimide** (**5-33**): Amine **5-26** (208 mg, 0.133 mmol) was dissolved in DMF (2 mL) and diazirine **5-32** (26.5 mg, 0.159 mmol) was added. Then, HBTU (66 mg, 0.173 mmol) and DIPEA (56 µL, 0.319 mmol) were added. The reaction was stirred in the dark and at room temperature for 24 hours. The reaction was diluted with DCM (20 mL) and 10% LiBr solution (10 mL). The DCM layer was collected and washed with 10% LiBr solution (3 x 10 mL). The organic layer was dried using sodium sulfate, concentrated, and purified with CombiFlash chromatography (silica gel, 20−40 µm, gradient 0−8% methanol/dichloromethane) to give the product as a white foamy solid (171 mg, 75%). ^{1}H NMR (400 MHz, CD_2Cl_2) δ 8.14 – 8.04 (m, 2H), 7.71 (d, *J* = 10.4 Hz, 2H), 7.62 – 6.95 (m, 25H), 4.79 (d, *J* = 2.0 Hz, 4H), 3.57 (m, 41H), 3.42 (dd, *J* = 4.9, 2.8 Hz, 4H), 3.31 (dt, *J* = 5.6, 3.1 Hz, 4H), δ 2.06 (t, *J* = 2.6 Hz, 1H), 1.97 (m, 4H), 1.73 (t, *J* = 7.7 Hz, 2H), 1.57 (t, *J* = 7.5 Hz, 2H), 1.41 (d, *J* = 6.6 Hz, 2H). ^{13}C{^{1}H} NMR (101 MHz, CD_2Cl_2) δ 171.5, 171.2, 170.8, 166.4, 166.4, 164.5, 164.5, 137.2, 132.3, 132.3, 130.7, 130.0, 129.0, 128.5, 127.2,

125.0, 125.0, 122.5, 121.9, 111.7, 111.7, 109.5, 82.9, 70.3, 70.3, 70.3, 70.2, 70.2, 70.1, 70.1, 70.0, 70.0, 69.9, 69.5, 69.5, 69.1, 50.3, 49.3, 39.3, 39.2, 39.1, 37.6, 32.1, 29.9, 28.1, 28.0, 13.1. FTIR (neat, cm^{-1}): 3262, 2895, 1639, 1538, 1268. HRMS (ESI-TOF) *m/z*: $[M+H]^+$ calcd for ($C_{82}H_{95}Cl_6N_{11}O_{17}^{2+}$), 858.7499, 859.2516, 859.7485, 860.2501; found: 858.7490, 859.2501, 859.7485, 860.2490.

REFERENCES

1. Hetz, C.; Glimcher, L. H., *Current Opinion in Cell Biology* **2011**, *23*, 123-125.

2. Huber, E. M.; Heinemeyer, W.; Li, X.; Arendt, C. S.; Hochstrasser, M.; Groll, M., *Nature Communications* **2016**, *7*, 10900.

3. Coux, O.; Tanaka, K.; Goldberg, A. L., *Annu. Rev. Biochem* **1996**, *65*, 801-847.

4. Eisele, M. R.; Reed, R. G.; Rudack, T.; Schweitzer, A.; Beck, F.; Nagy, I.; Pfeifer, G.; Plitzko, J. M.; Baumeister, W.; Tomko, R. J., Jr.; et al., *Cell Reports* **2018**, *24*, 1301-1315.e1305.

5. Sahu, I.; Bajorek, M.; Tan, X.; Srividya, M.; Krutauz, D.; Reis, N.; Osmulski, P. A.; Gaczynska, M. E.; Glickman, M. H. A Role for the Proteasome Alpha2 Subunit N-Tail in Substrate Processing. In *Biomolecules*, 2023; Vol. 13.

6. McNaught, K. S. P.; Olanow, C. W.; Halliwell, B.; Isacson, O.; Jenner, P., *Nature Reviews Neuroscience* **2001**, *2*, 589-594.

7. Saez, I.; Vilchez, D., *Curr. Genomics* **2014**, *15*, 38-51.

8. Njomen, E.; Osmulski, P. A.; Jones, C. L.; Gaczynska, M.; Tepe, J. J., *Biochemistry* **2018**, *57*, 4214-4224.

9. Trader, D. J.; Simanski, S.; Dickson, P.; Kodadek, T., *Biochimica et Biophysica Acta (BBA) - General Subjects* **2017**, *1861*, 892-899.

10. Lansdell, T. A.; Hurchla, M. A.; Xiang, J.; Hovde, S.; Weilbaecher, K. N.; Henry, R. W.; Tepe, J. J., *ACS Chem. Biol.* **2013**, *8*, 578-587.

11. Jones, C. L.; Njomen, E.; Sjogren, B.; Dexheimer, T. S.; Tepe, J. J., *ACS Chem. Biol.* **2017**, *12*, 2240-2247.

12. Fiolek, T. J.; Keel, K. L.; Tepe, J. J., *ACS Chem. Neurosci.* **2021**, *12*, 1438-1448.

13. Staerz, S. D.; Jones, C. L.; Tepe, J. J., *J. Med. Chem.* **2022**, *65*, 6631-6642.

14. Tedeschini, T.; Campara, B.; Grigoletto, A.; Bellini, M.; Salvalaio, M.; Matsuno, Y.; Suzuki, A.; Yoshioka, H.; Pasut, G., *J. Controlled Release* **2021**, *337*, 431-447.

15. Hashimoto, M.; Hatanaka, Y., *Eur. J. Org. Chem.* **2008**, *2008*, 2513-2523.

16. Smith, E.; Collins, I., *Future Med. Chem.* **2015**, *7*, 159-183.

17. Dubinsky, L.; Krom, B. P.; Meijler, M. M., *Biorg. Med. Chem.* **2012**, *20*, 554-570.

18. Geurink, P. P.; Florea, B. I.; Van der Marel, G. A.; Kessler, B. M.; Overkleeft, H. S., *Chem. Commun.* **2010**, *46*, 9052-9054.

19. Zhu, Y.; Shigeyoshi, K.; Hayakawa, Y.; Fujiwara, S.; Kishida, M.; Ohki, H.; Horibe, T.; Shionyu, M.; Mizukami, T.; Hasegawa, M. Acceleration of Protein Degradation by 20S Proteasome-Binding Peptides Generated by In Vitro Artificial Evolution. In *Int. J. Mol. Sci.*, 2023; Vol. 24.

20. Li, Z.; Hao, P.; Li, L.; Tan, C. Y.; Cheng, X.; Chen, G. Y.; Sze, S. K.; Shen, H. M.; Yao, S. Q., *Angew. Chem. Int. Ed. Engl.* **2013**, *52*, 8551-8556.

21. Zhang, P.; Liu, X.; Abegg, D.; Tanaka, T.; Tong, Y.; Benhamou, R. I.; Baisden, J.; Crynen, G.; Meyer, S. M.; Cameron, M. D.; et al., *J. Am. Chem. Soc.* **2021**, *143*, 13044-13055.

22. Korovesis, D.; Rufo, N.; Derua, R.; Agostinis, P.; Verhelst, S. H. L., *ACS Chem. Biol.* **2020**, *15*, 3106-3111.

23. Voorneveld, J.; Florea, B. I.; Bakkum, T.; Mendowicz, R. J.; van der Veer, M. S.; Gagestein, B.; van Kasteren, S. I.; van der Stelt, M.; Overkleeft, H. S.; Filippov, D. V., *ChemBioChem* **2020**, *21*, 2431-2434.

24. Howard, R. T.; Hemsley, P.; Petteruti, P.; Saunders, C. N.; Molina Bermejo, J. A.; Scott, J. S.; Johannes, J. W.; Tate, E. W., *ACS Chem. Biol.* **2020**, *15*, 325-333.

25. Gao, C. L.; Hou, G. G.; Liu, J.; Ru, T.; Xu, Y. Z.; Zhao, S. Y.; Ye, H.; Zhang, L. Y.; Chen, K. X.; Guo, Y. W.; et al., *Angew. Chem. Int. Ed. Engl.* **2020**, *59*, 2429-2439.

26. Grant, E. K.; Fallon, D. J.; Hann, M. M.; Fantom, K. G. M.; Quinn, C.; Zappacosta, F.; Annan, R. S.; Chung, C. W.; Bamborough, P.; Dixon, D. P.; et al., *Angew. Chem. Int. Ed. Engl.* **2020**, *59*, 21096-21105.

27. Parker, C. G.; Galmozzi, A.; Wang, Y.; Correia, B. E.; Sasaki, K.; Joslyn, C. M.; Kim, A. S.; Cavallaro, C. L.; Lawrence, R. M.; Johnson, S. R.; et al., *Cell* **2017**, *168*, 527-541 e529.

28. Ma, H.; Murray, J. B.; Luo, H.; Cheng, X.; Chen, Q.; Song, C.; Duan, C.; Tan, P.; Zhang, L.; Liu, J.; et al., *RSC Med. Chem.* **2022**, *13*, 1341-1349.

29. Wang, Y.; Dix, M. M.; Bianco, G.; Remsberg, J. R.; Lee, H. Y.; Kalocsay, M.; Gygi, S. P.; Forli, S.; Vite, G.; Lawrence, R. M.; et al., *Nat. Chem.* **2019**, *11*, 1113-1123.

30. Burton, N. R.; Kim, P.; Backus, K. M., *Org. Biomol. Chem.* **2021**, *19*, 7792-7809.

31. Balaratnam, S.; Rhodes, C.; Bume, D. D.; Connelly, C.; Lai, C. C.; Kelley, J. A.; Yazdani, K.; Homan, P. J.; Incarnato, D.; Numata, T.; et al., *Nat. Commun.* **2021**, *12*, 5856.

32. Miyajima, R.; Sakai, K.; Otani, Y.; Wadatsu, T.; Sakata, Y.; Nishikawa, Y.; Tanaka, M.; Yamashita, Y.; Hayashi, M.; Kondo, K.; et al., *ACS Chem. Biol.* **2020**, *15*, 2364-2373.

APPENDIX

Figure 5.8: ^{1}H and $^{13}C\{1H\}$ NMR spectra of **5-6**

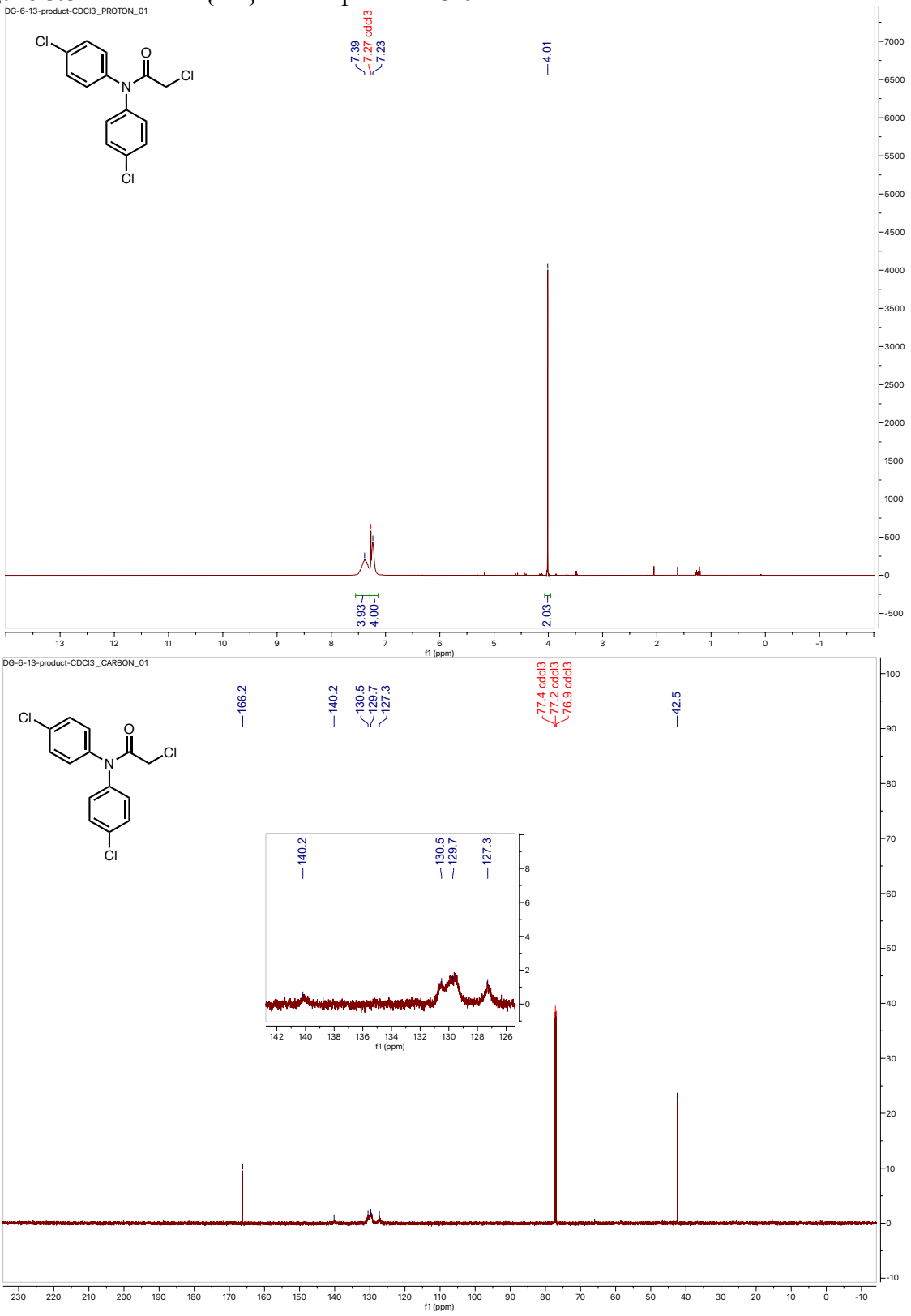

Figure 5.9: ^{1}H and $^{13}C\{1H\}$ NMR spectra of **5-1**

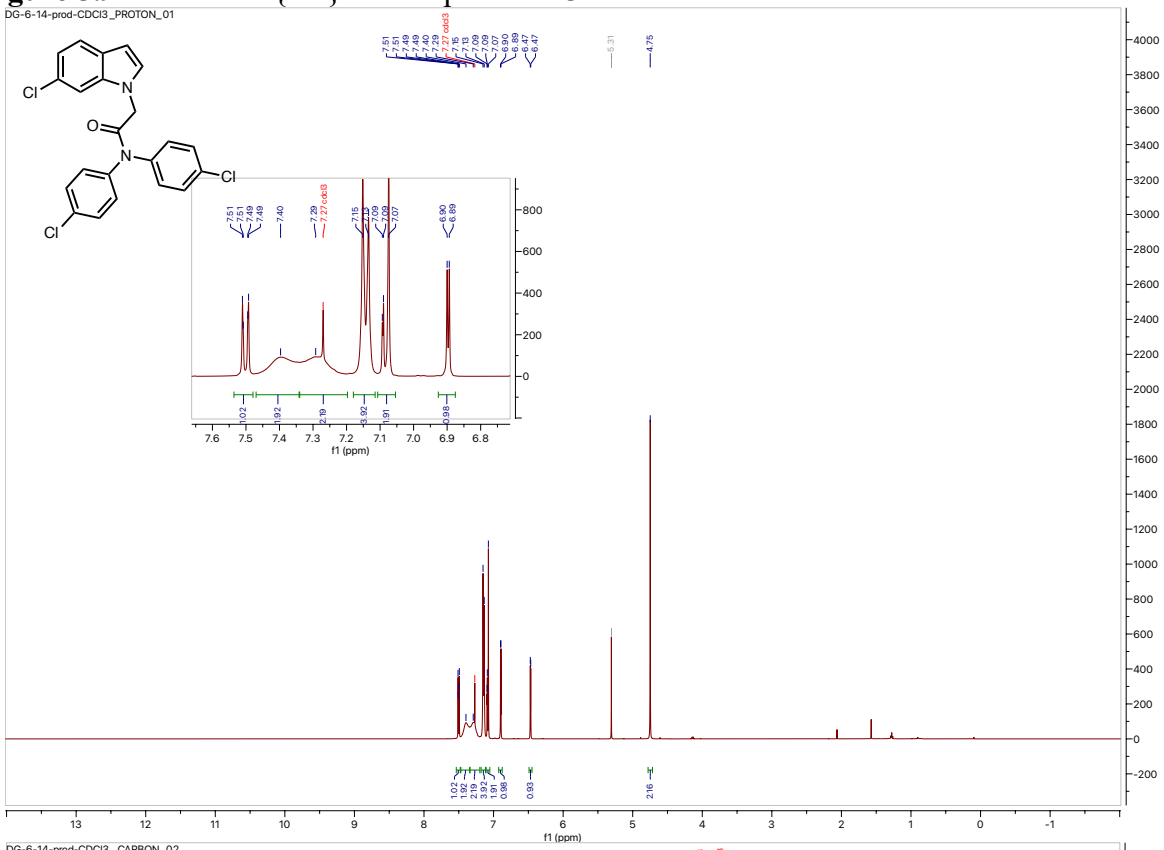

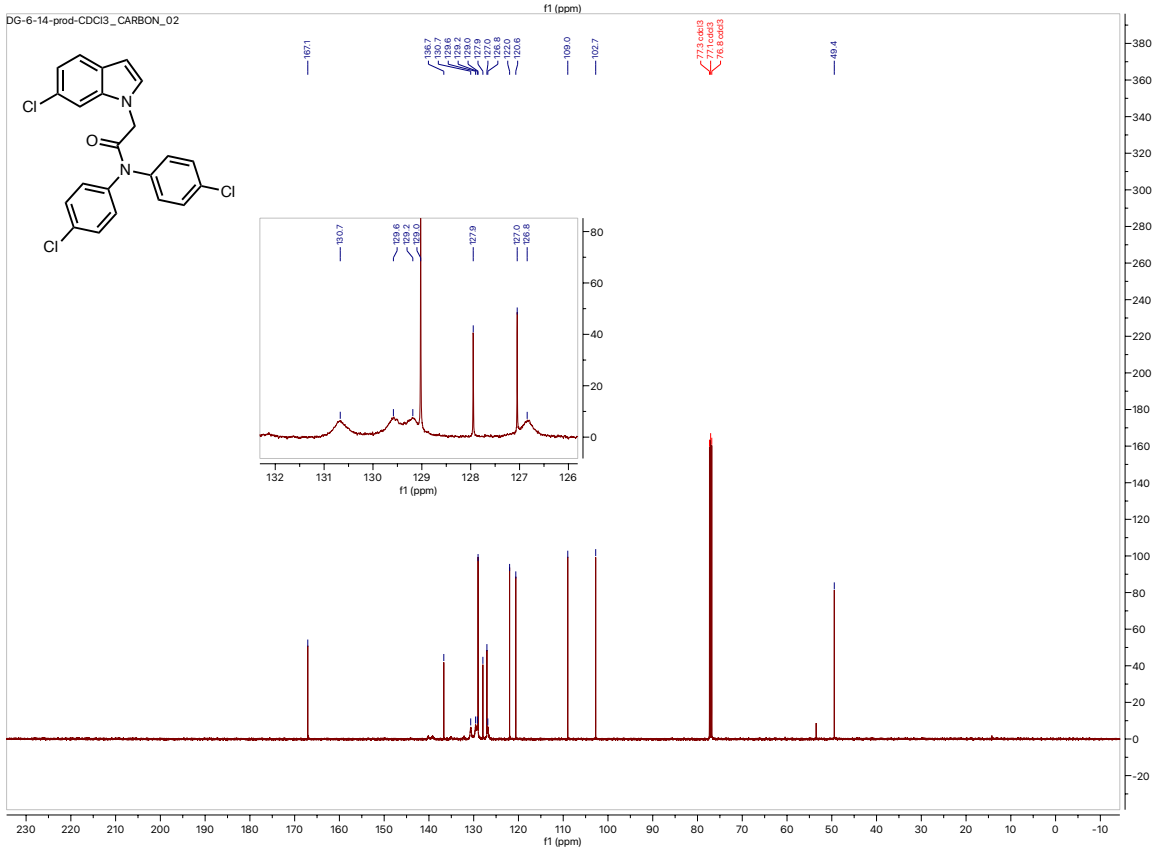

Figure 5.10: ^{1}H and $^{13}C\{1H\}$ NMR spectra of **5-7**

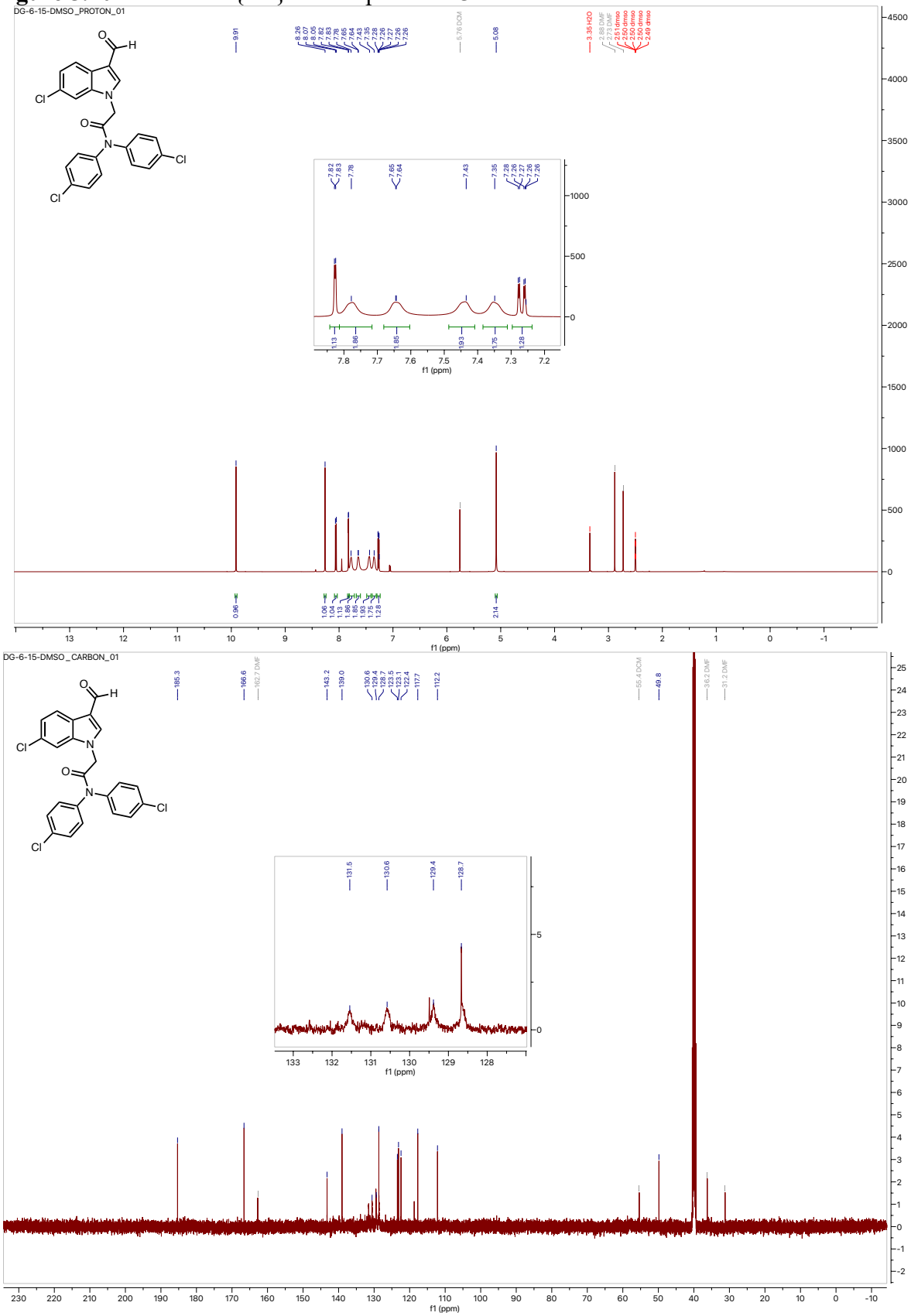

Figure 5.11: ^{1}H and $^{13}C\{1H\}$ NMR spectra of **5-2**

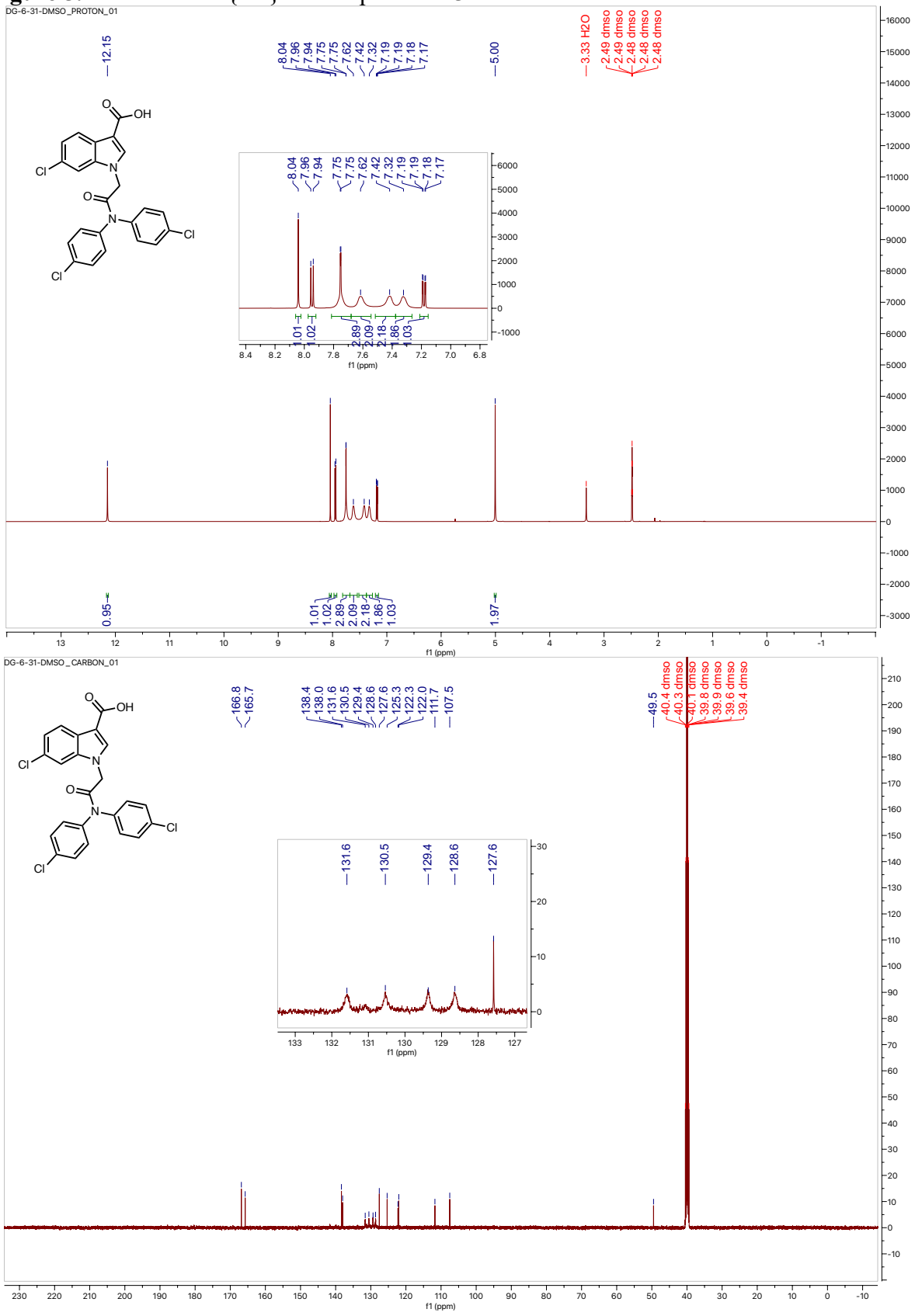

Figure 5.12: ^{1}H and $^{13}C\{1H\}$ NMR spectra of **5-3**

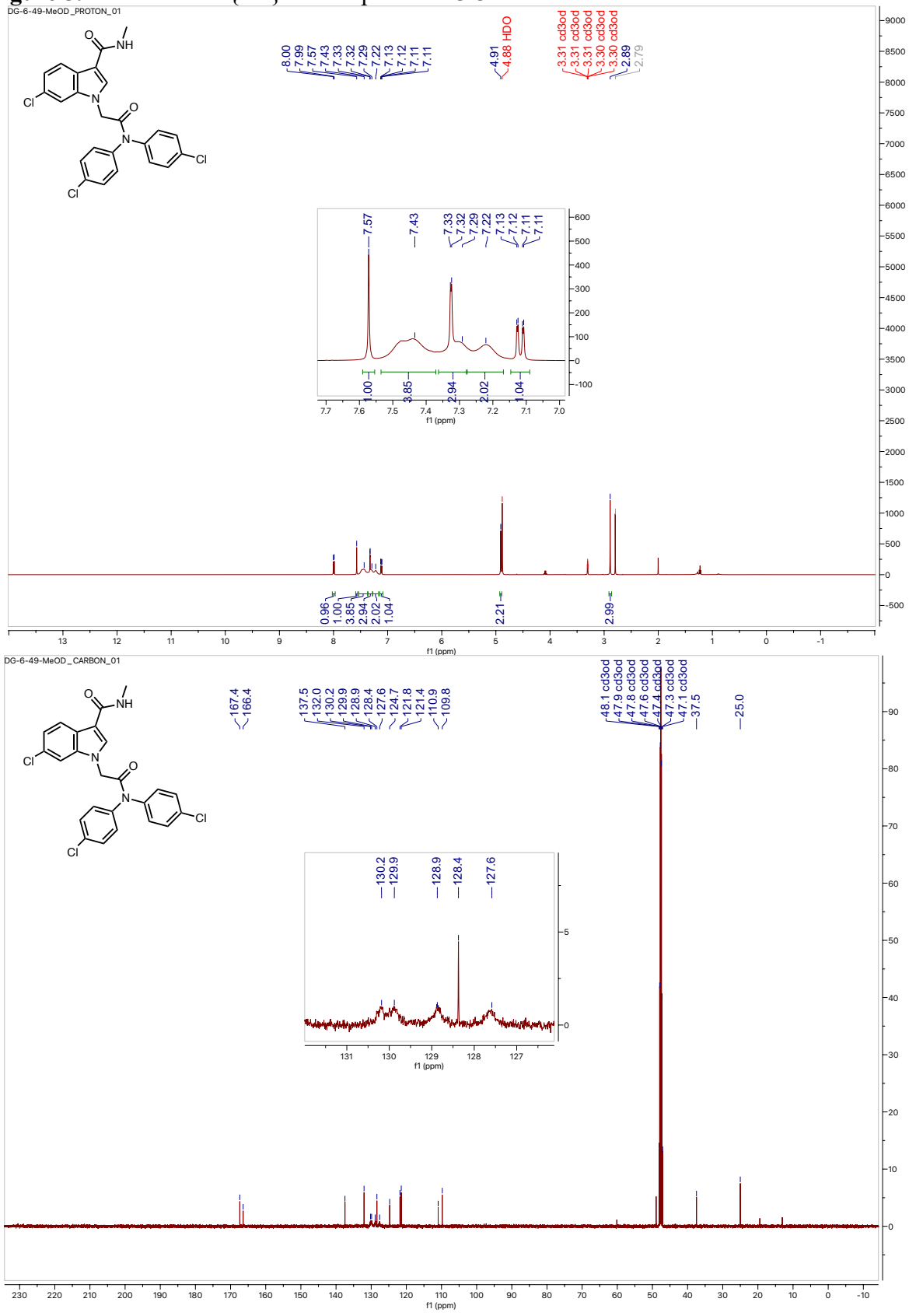

Figure 5.13: ^{1}H and $^{13}C\{1H\}$ NMR spectra of **5-4**

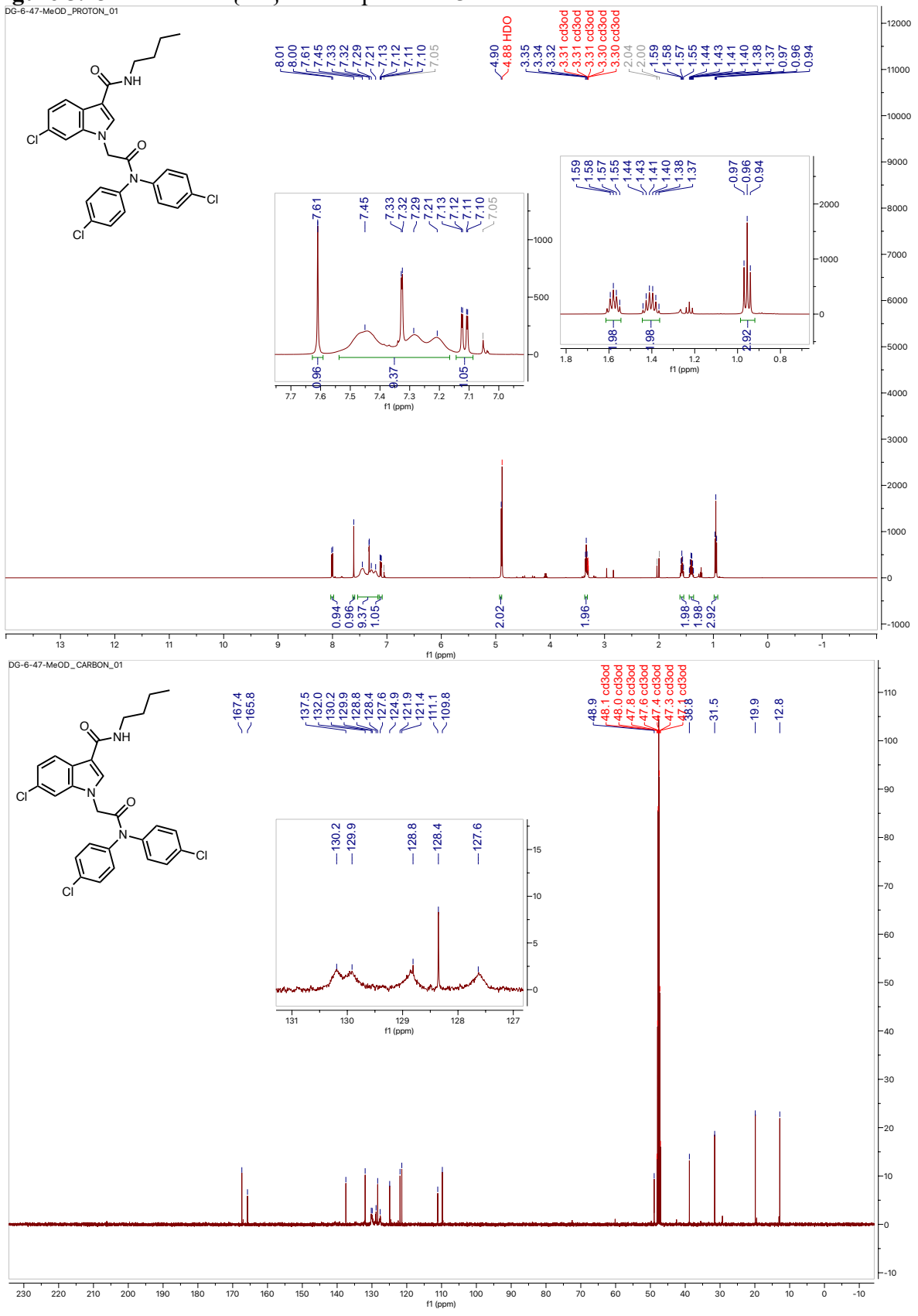

Figure 5.14: ^{1}H and $^{13}C\{1H\}$ NMR spectra of **5-10**

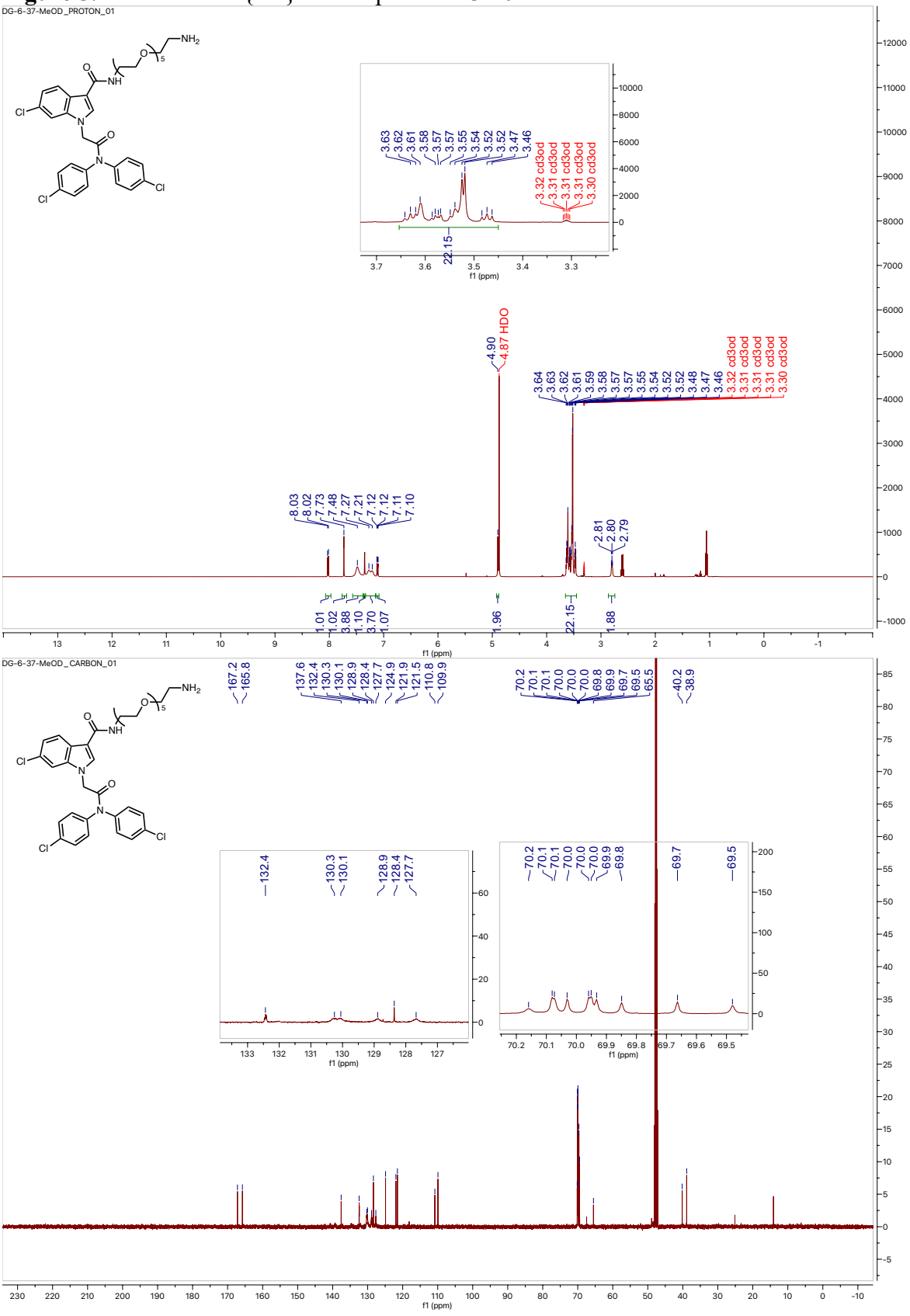

Figure 5.15: ^{1}H and $^{13}C\{1H\}$ NMR spectra of **5-12**

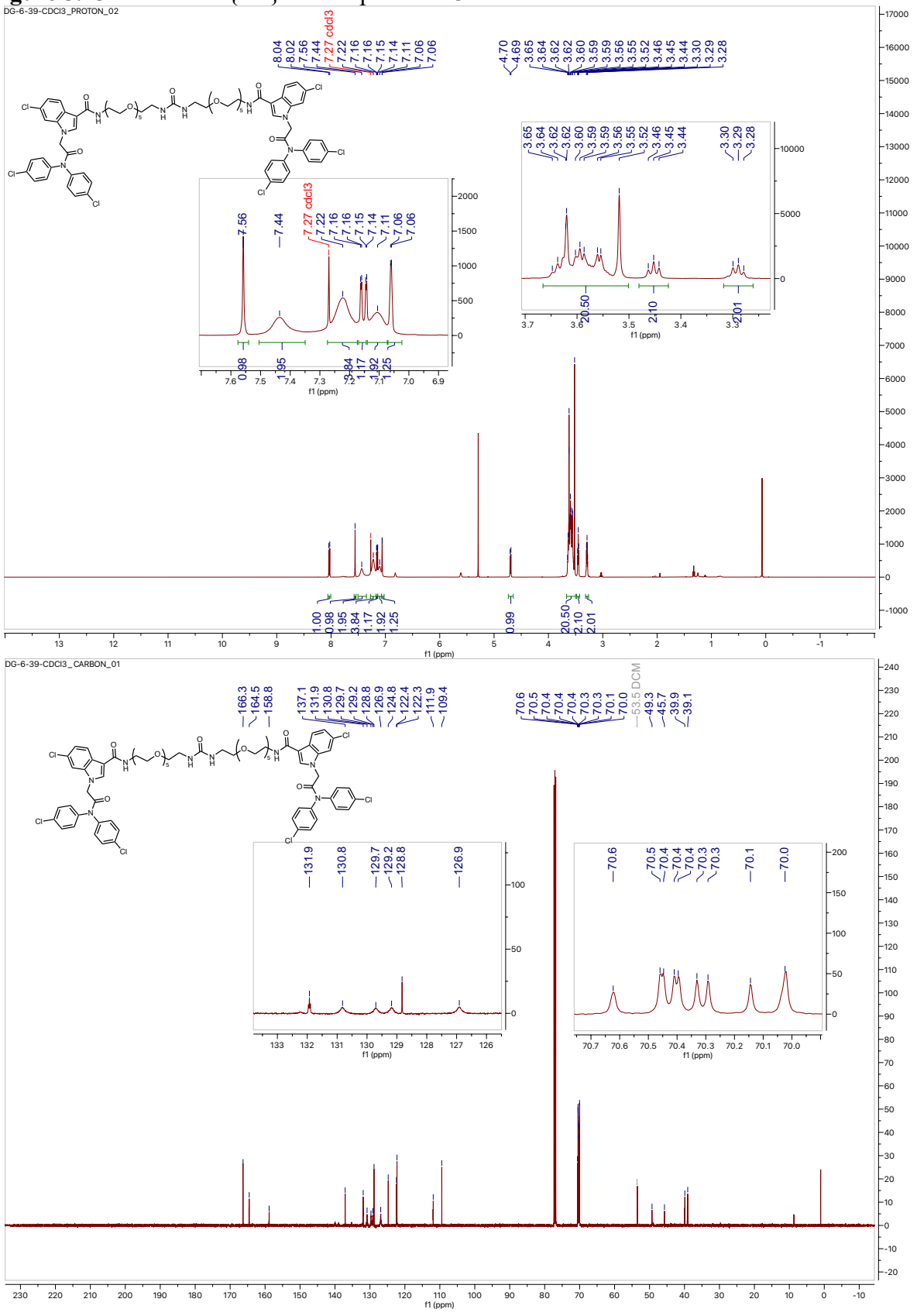

Figure 5.16: ^{1}H and $^{13}C\{1H\}$ NMR spectra of **5-11**

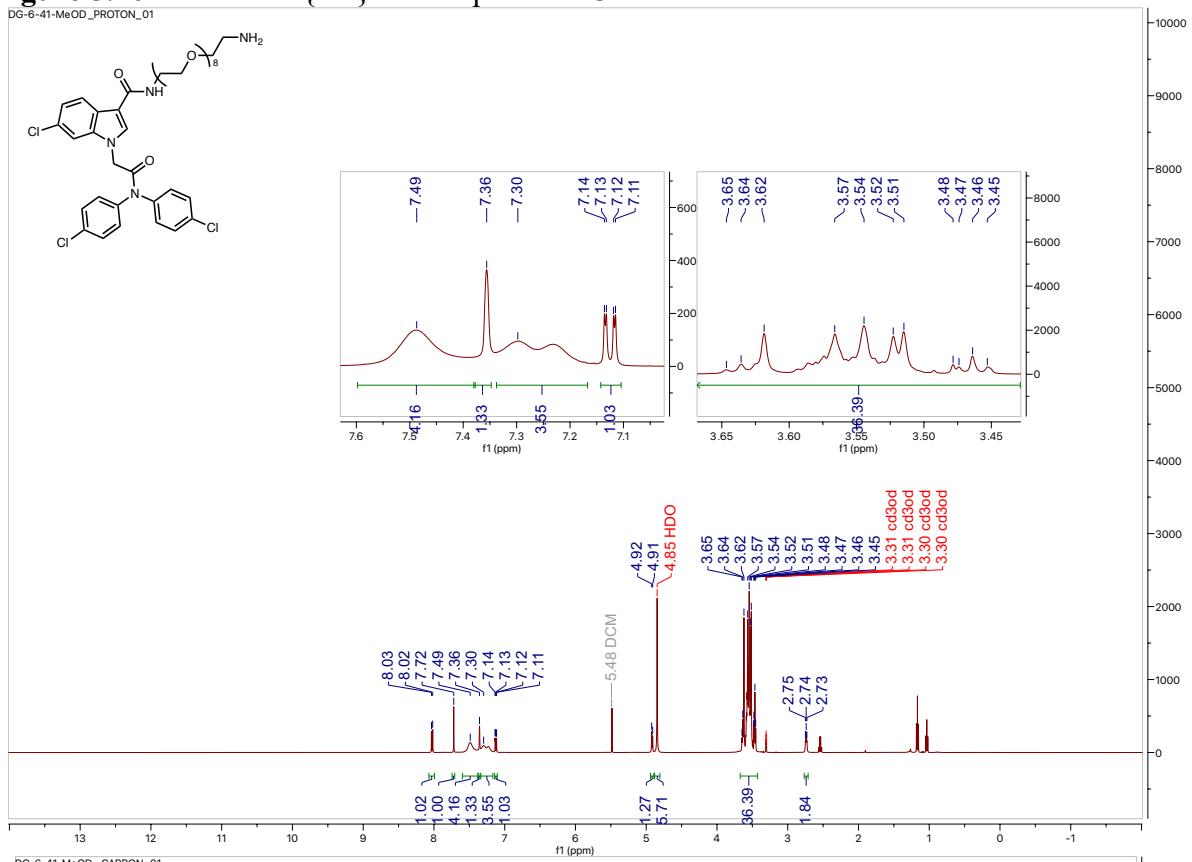

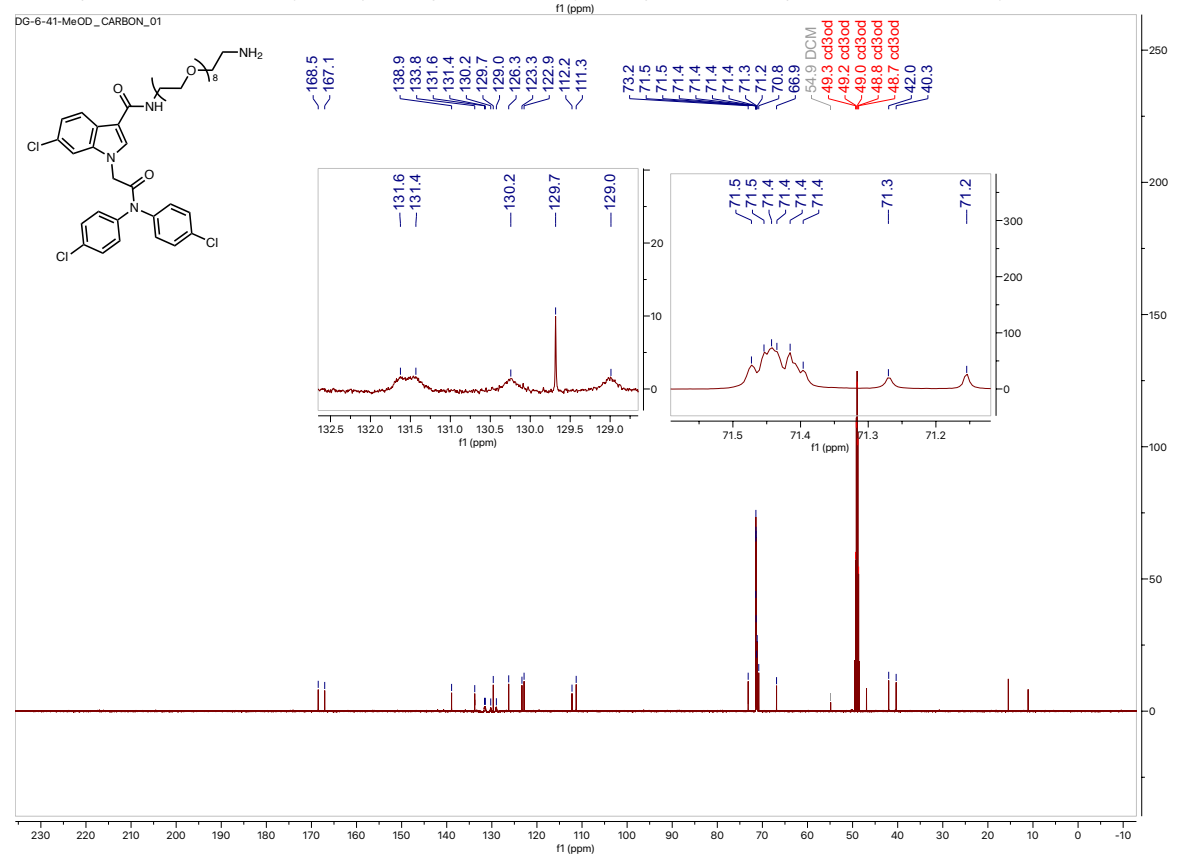

Figure 5.17: ^{1}H and $^{13}C\{1H\}$ NMR spectra of **5-13**

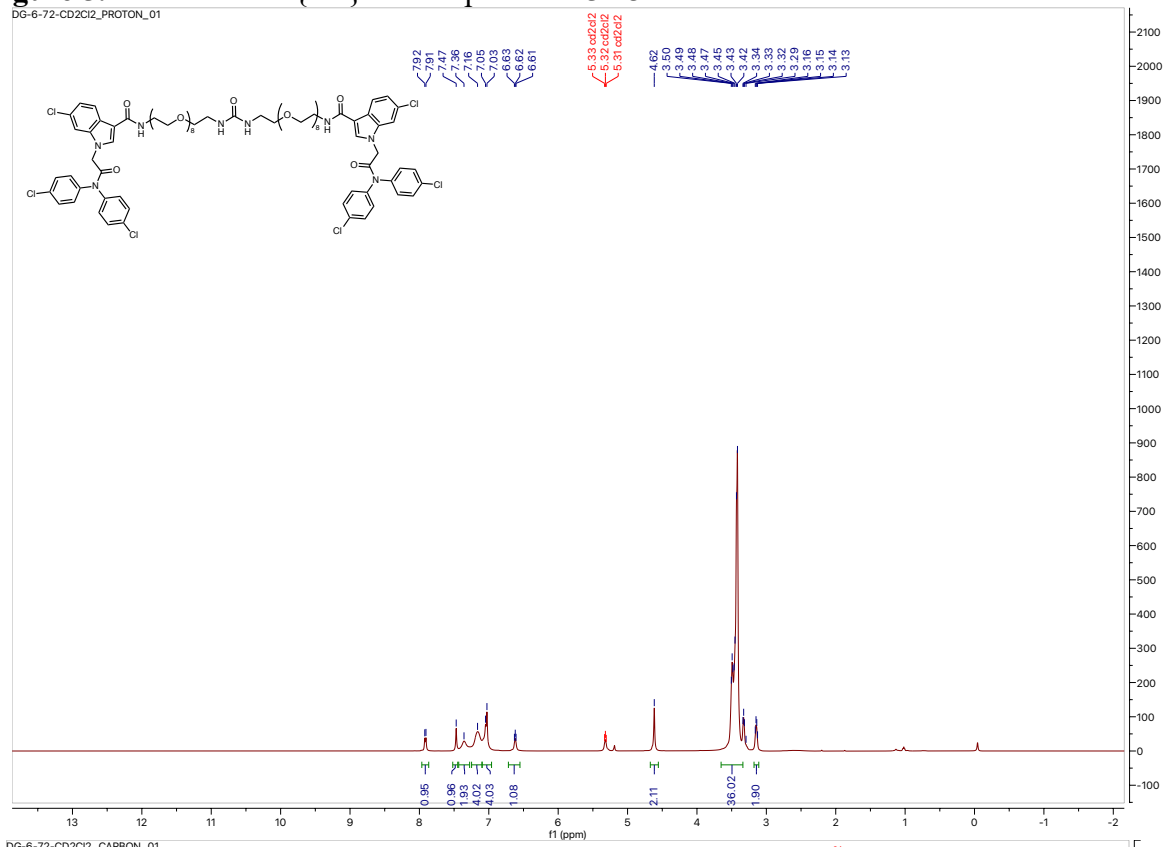

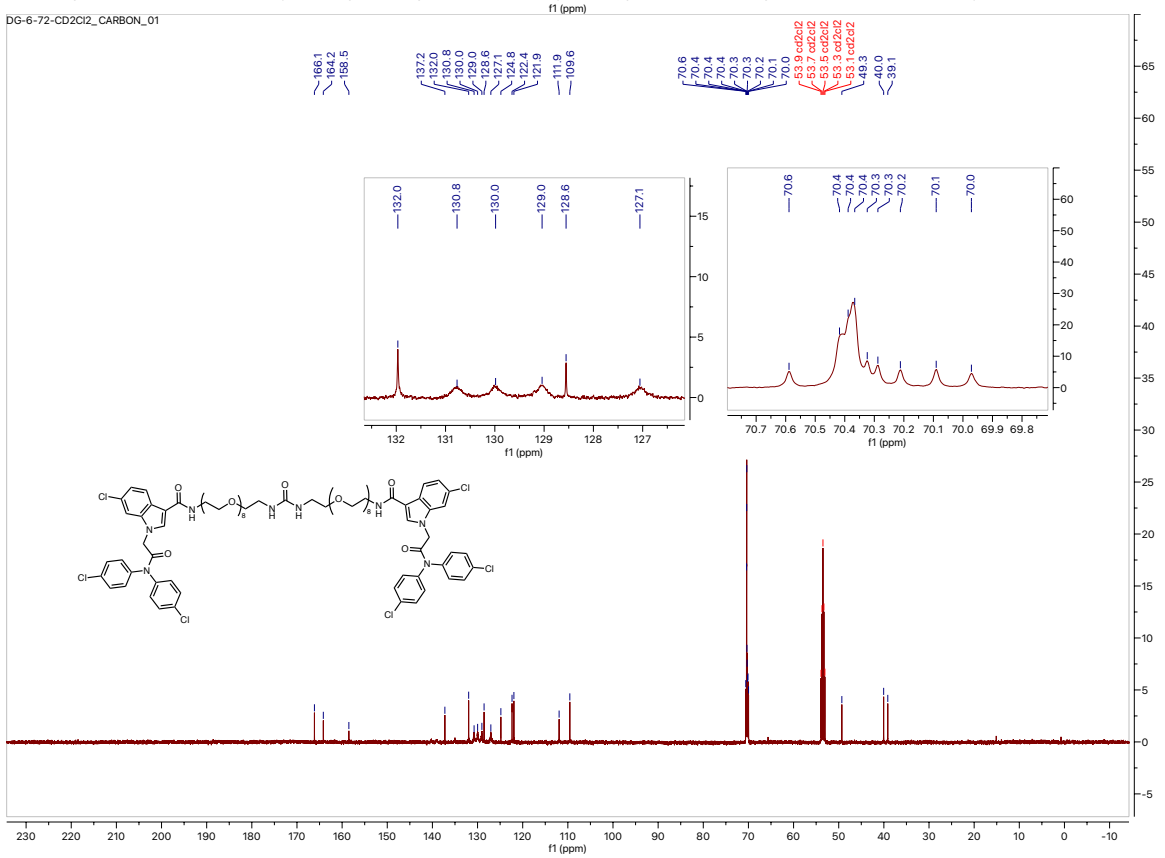

Figure 5.18: ^{1}H and $^{13}C\{1H\}$ NMR spectra of **5-15**

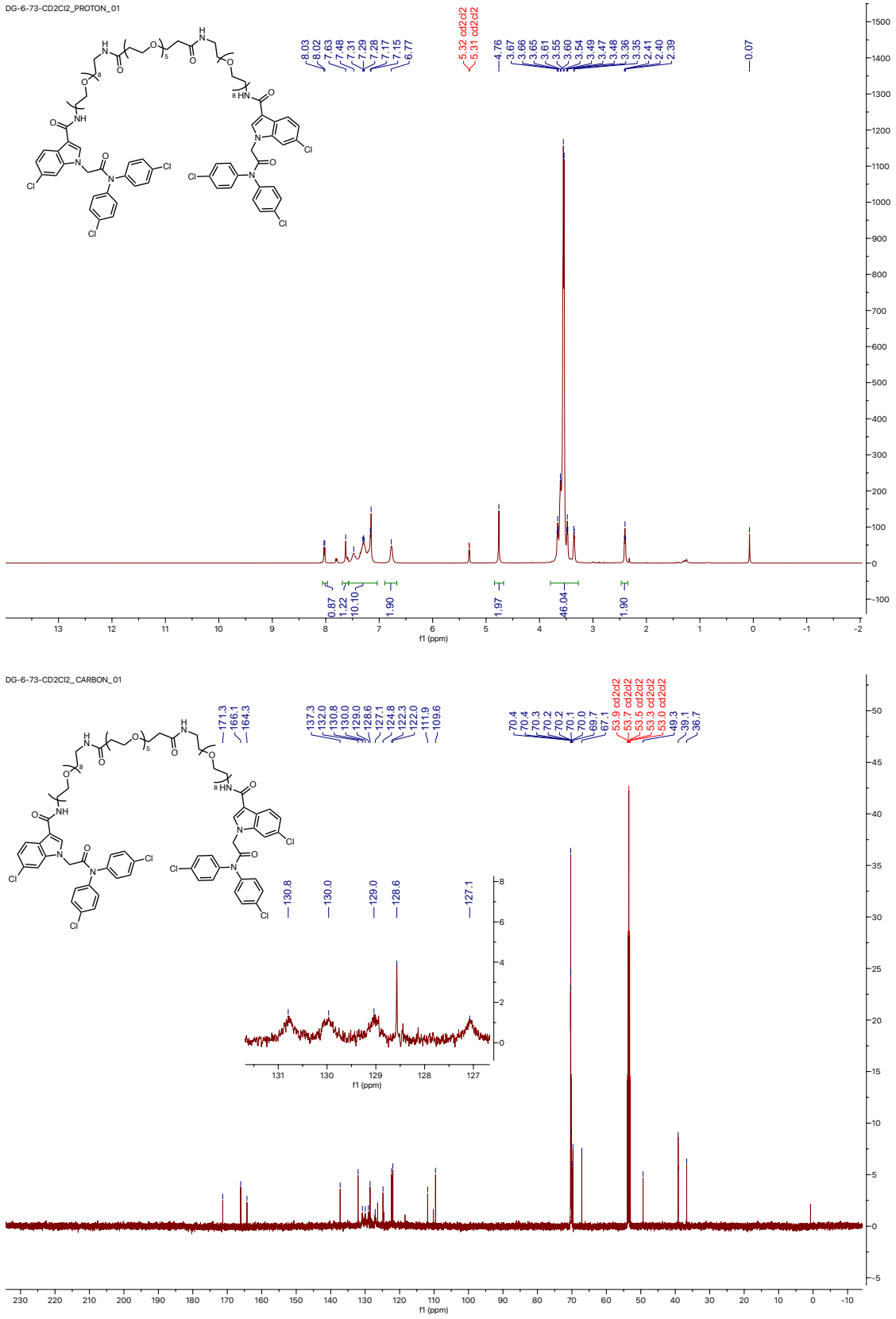

Figure 5.19: ^{1}H and $^{13}C\{1H\}$ NMR spectra of **5-16**

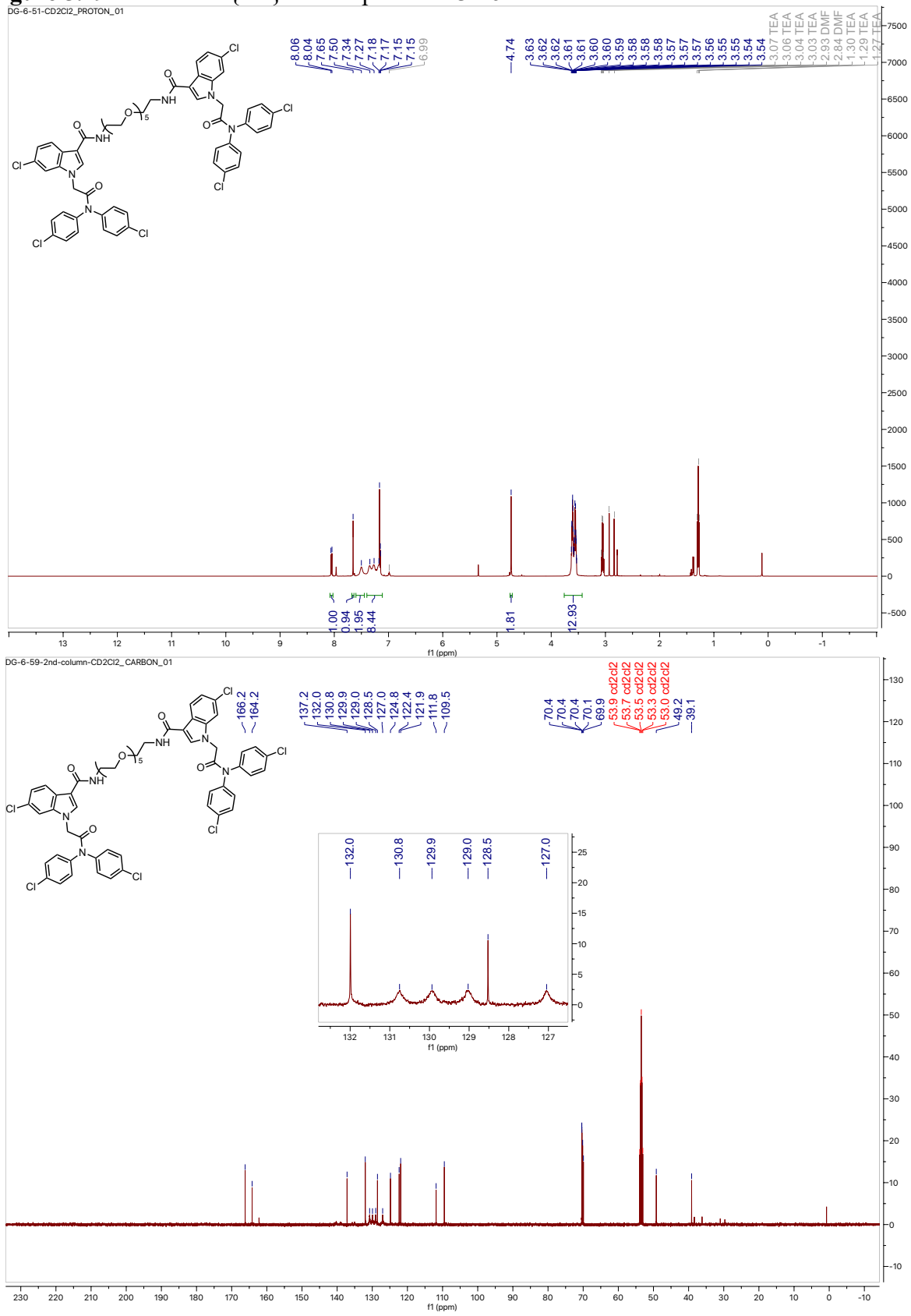

Figure 5.20: ^{1}H and $^{13}C\{1H\}$ NMR spectra of **5-19**

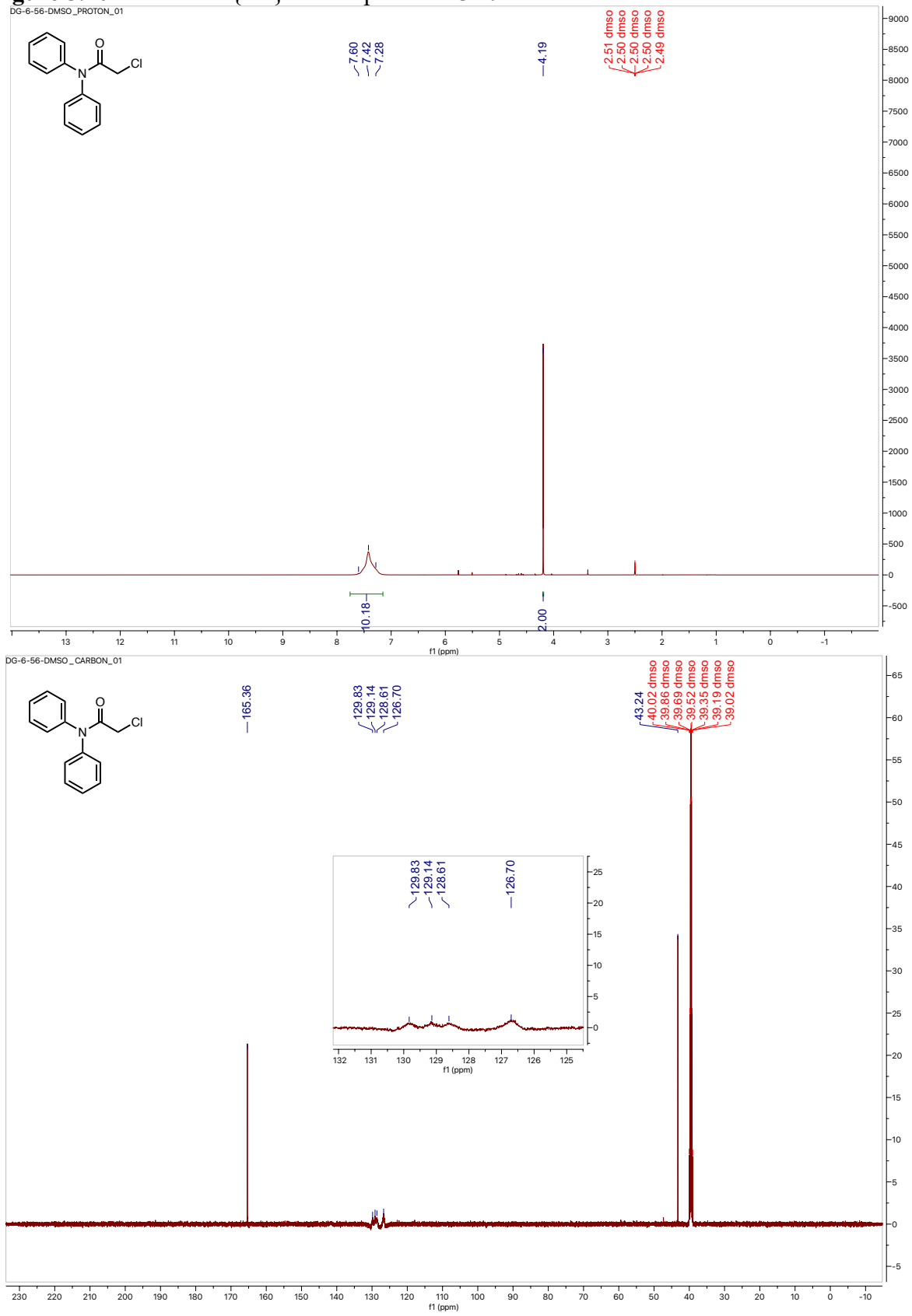

Figure 5.21: ^{1}H and $^{13}C\{1H\}$ NMR spectra of **5-17**

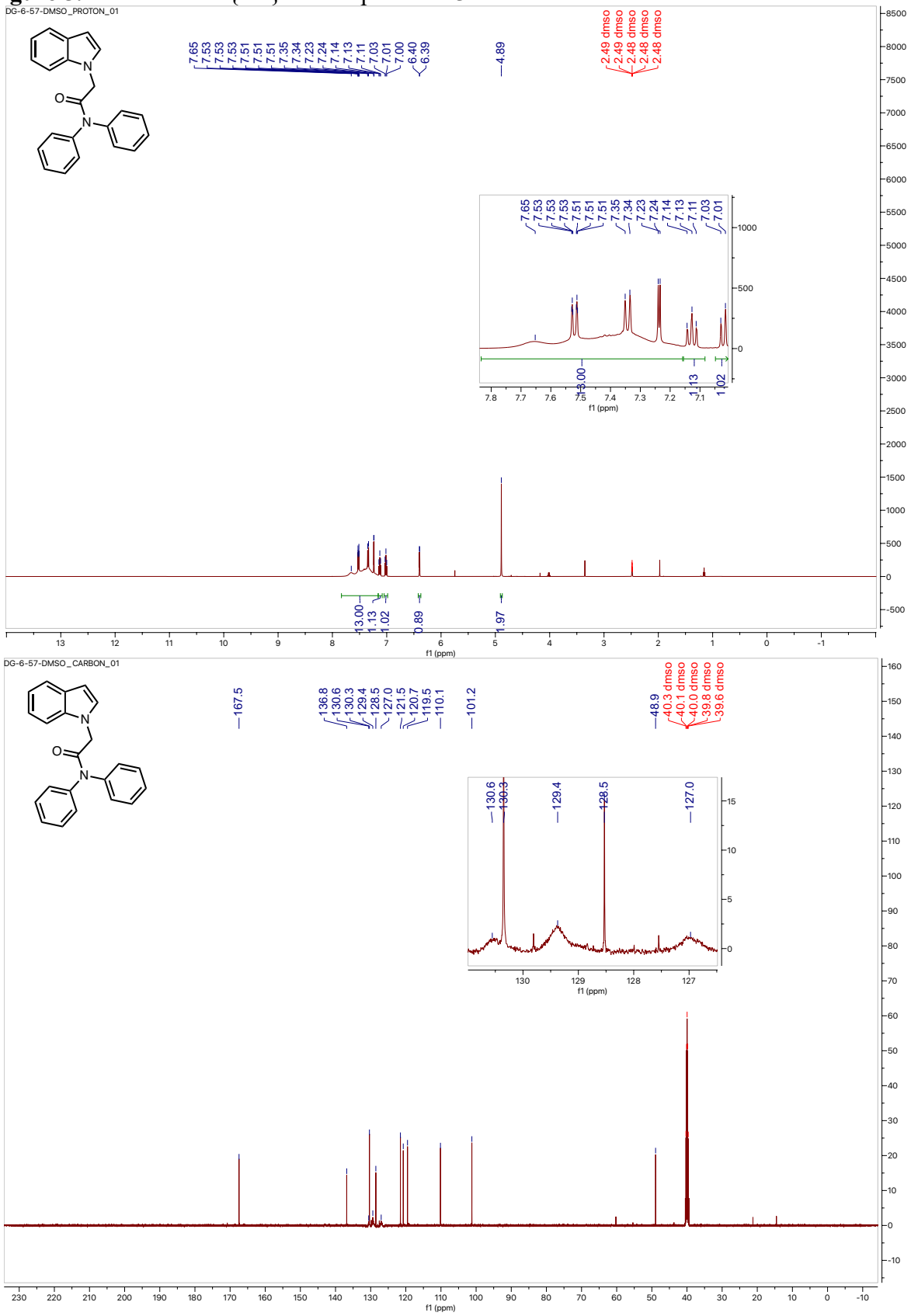

Figure 5.22: ^{1}H and $^{13}C\{1H\}$ NMR spectra of **5-20**

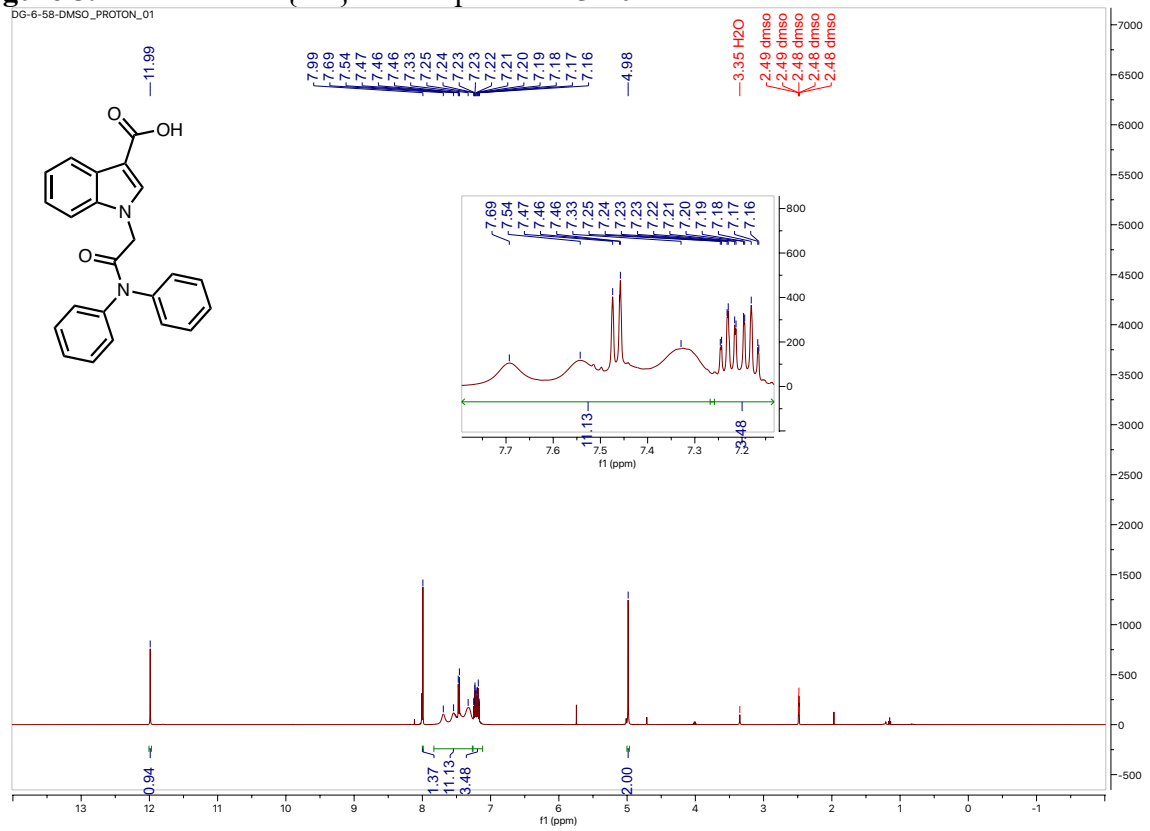

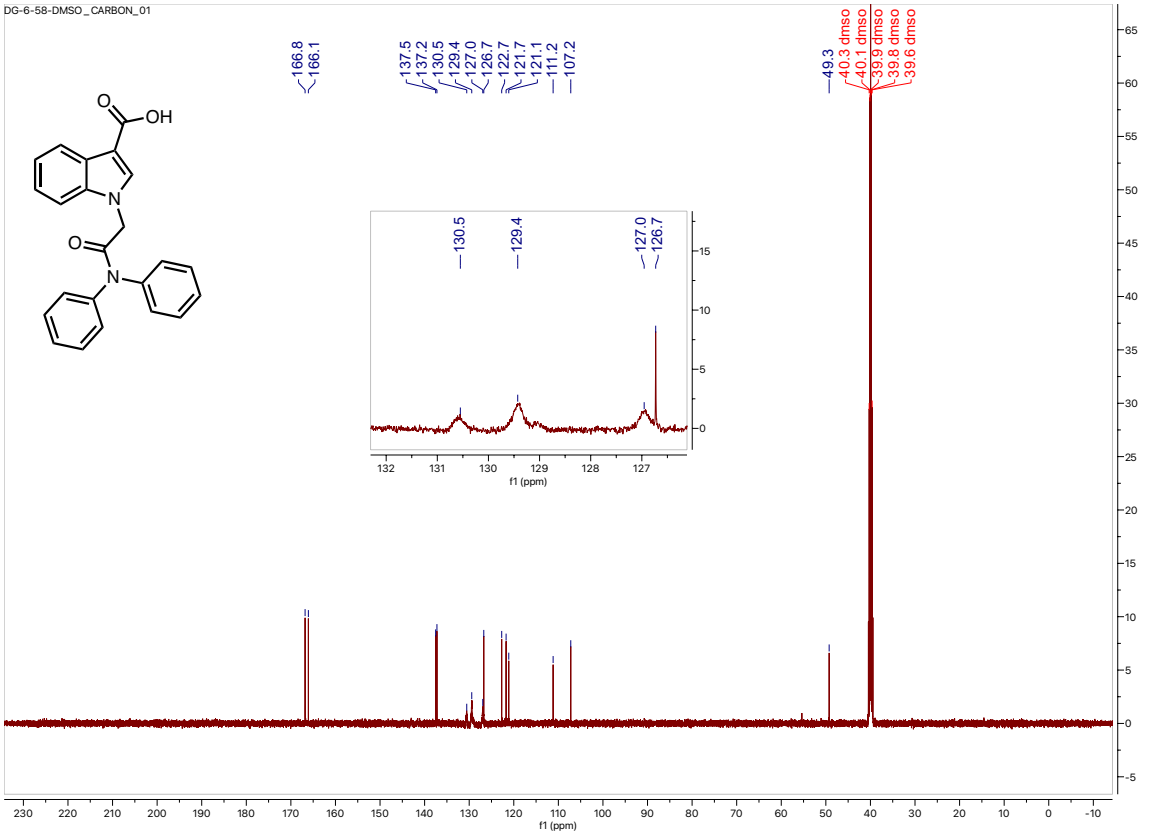

Figure 5.23: ^{1}H and $^{13}C\{1H\}$ NMR spectra of **5-21**

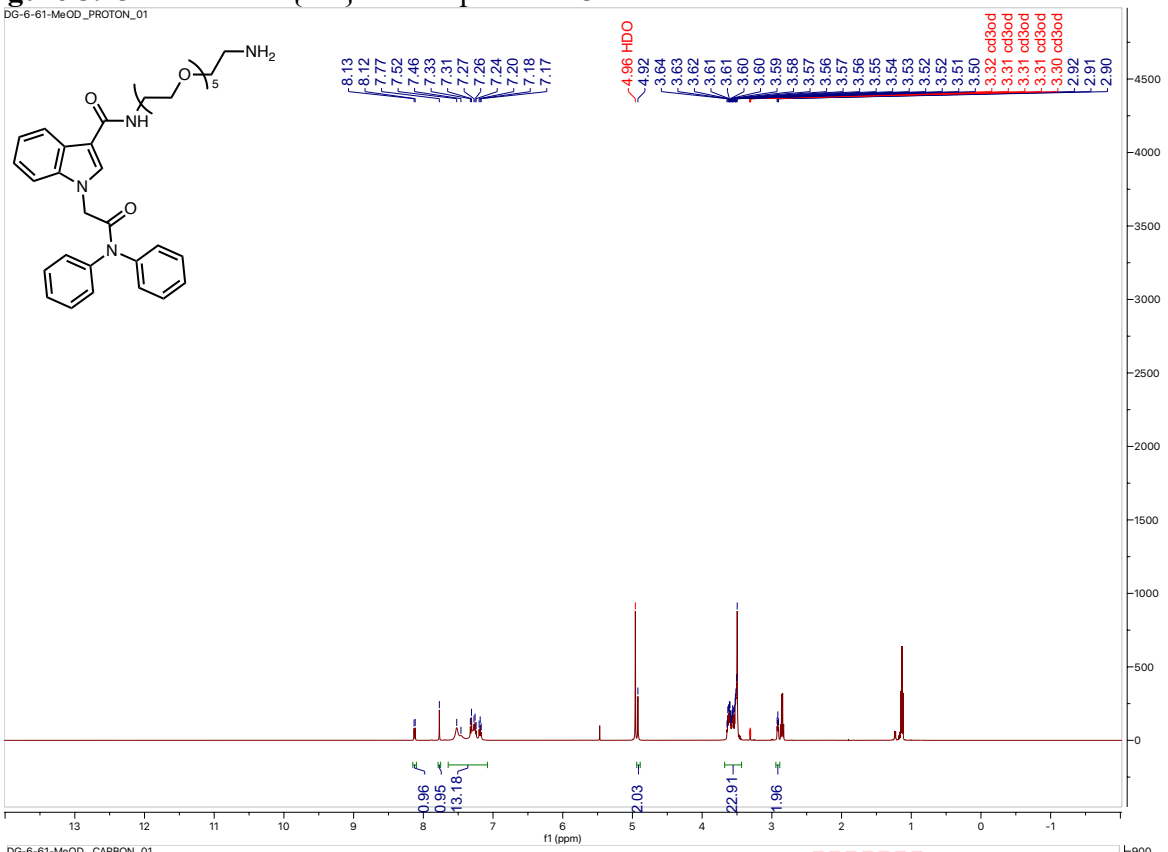

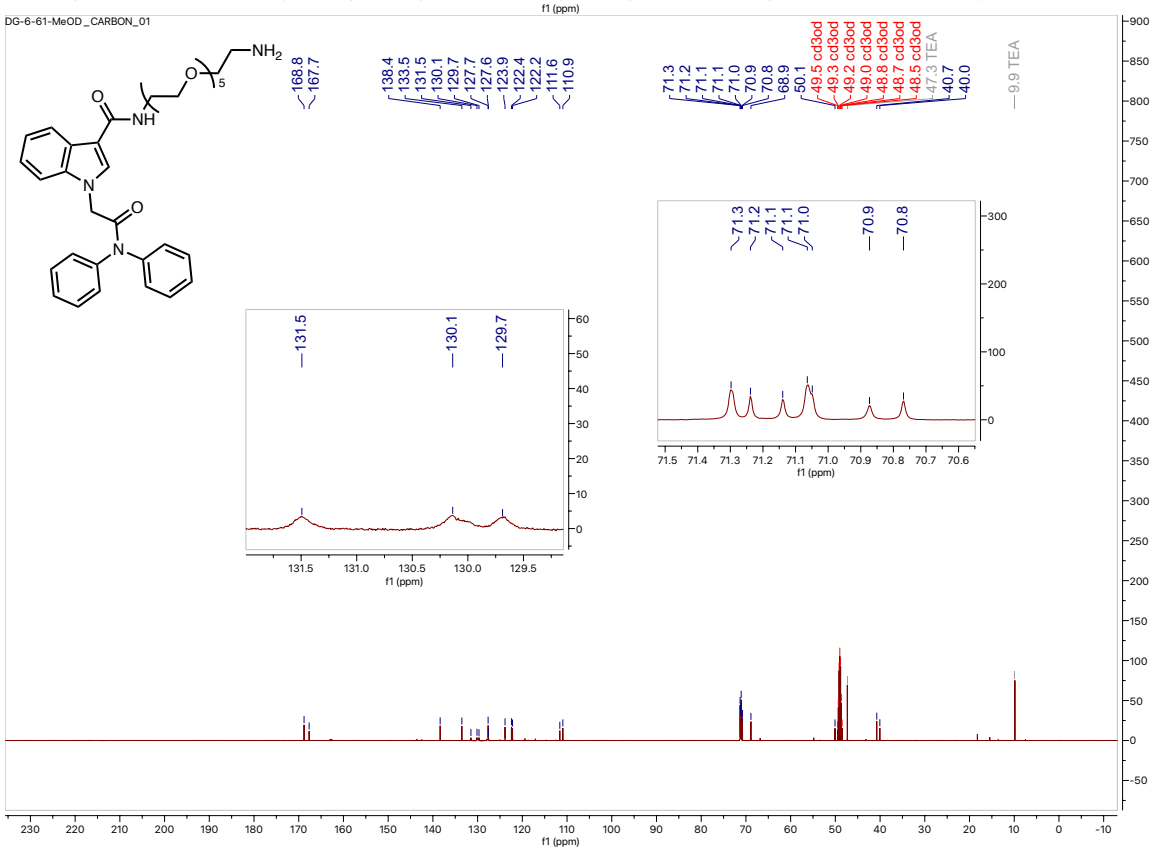

Figure 5.24: ^{1}H and $^{13}C\{1H\}$ NMR spectra of **5-18**

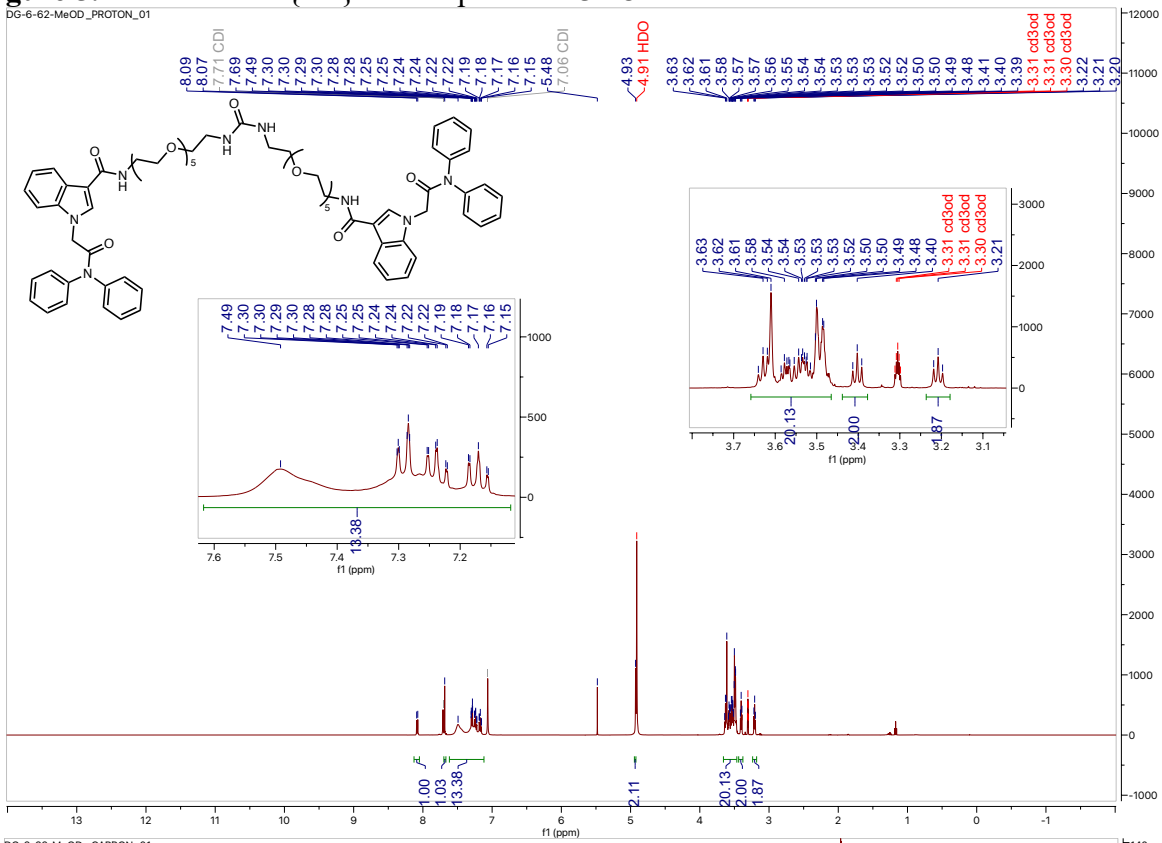

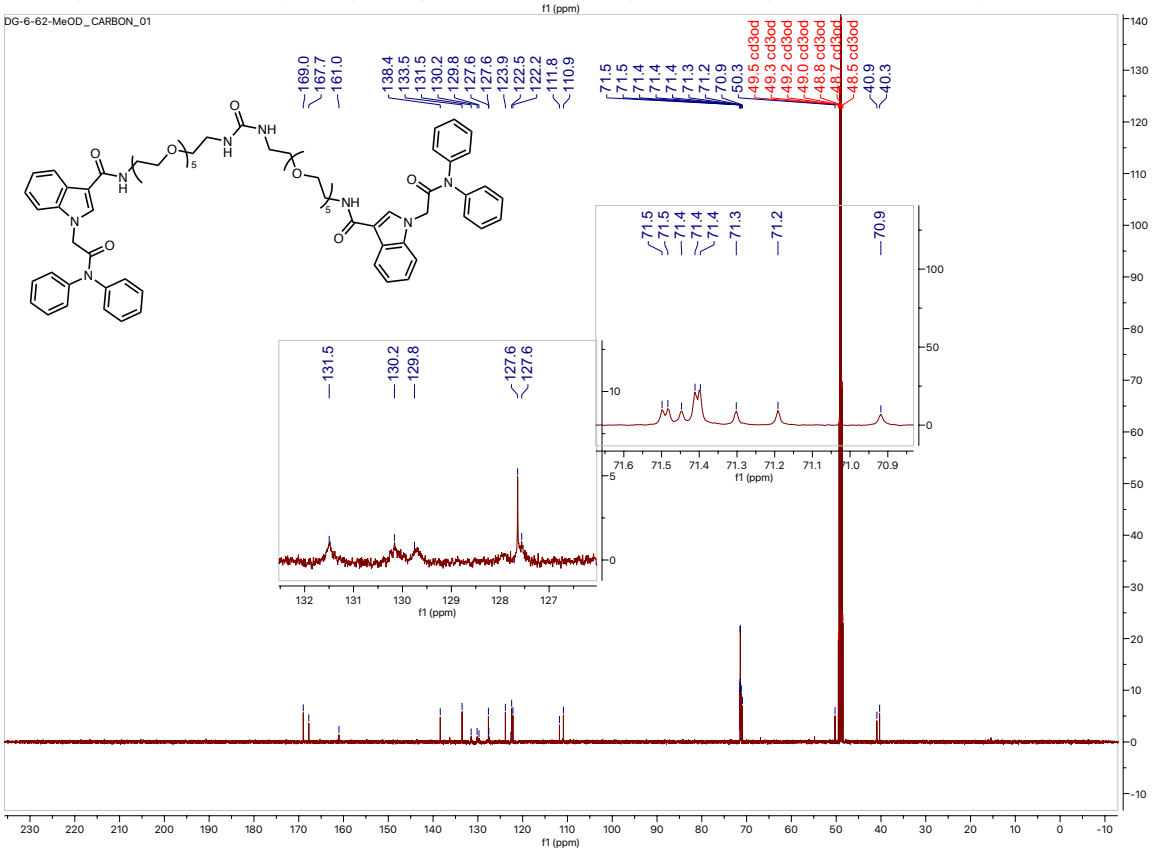

Figure 5.25: ^{1}H and $^{13}C\{1H\}$ NMR spectra of **5-23**

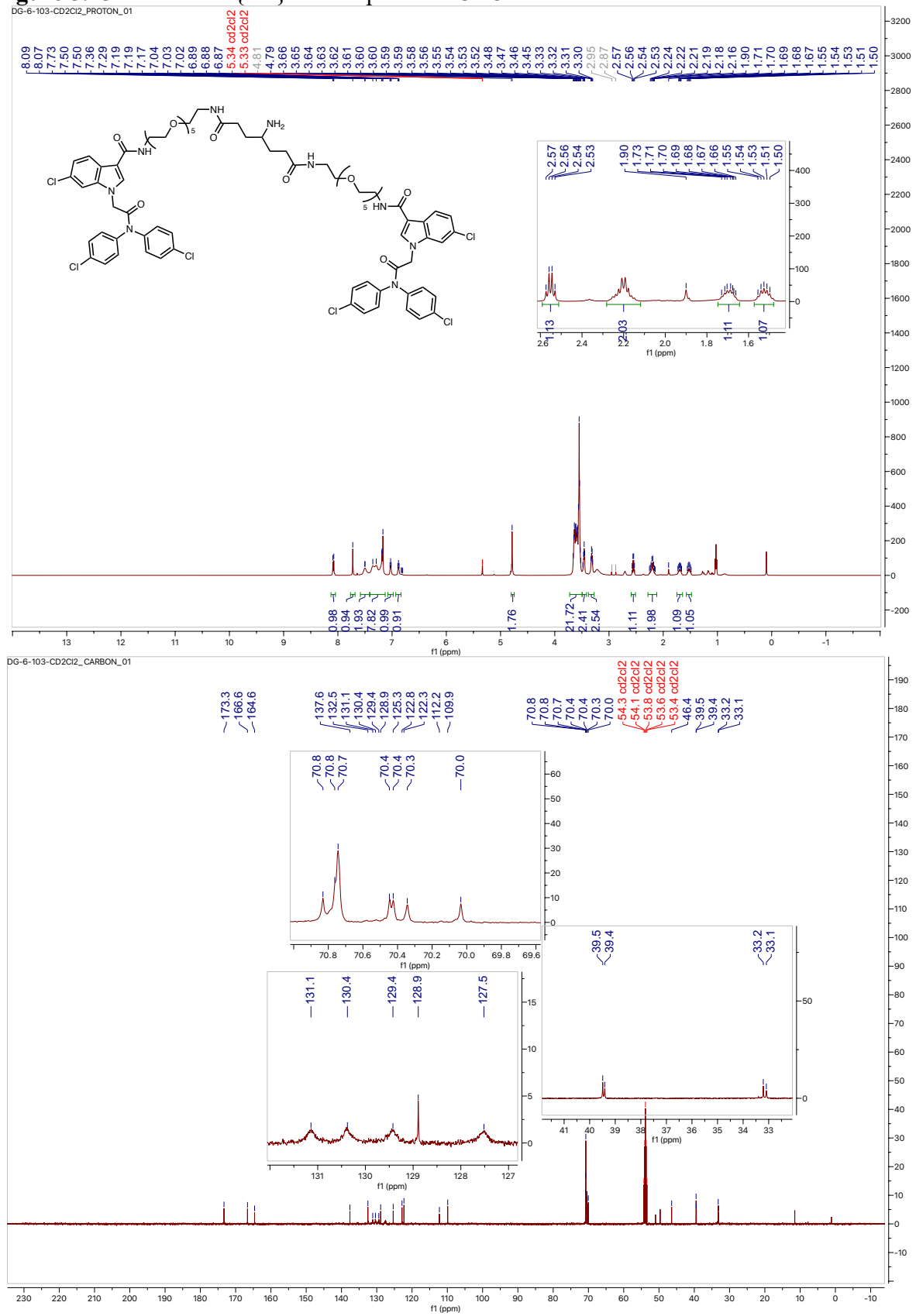

Figure 5.26: ^{1}H and $^{13}C\{1H\}$ NMR spectra of **5-24**

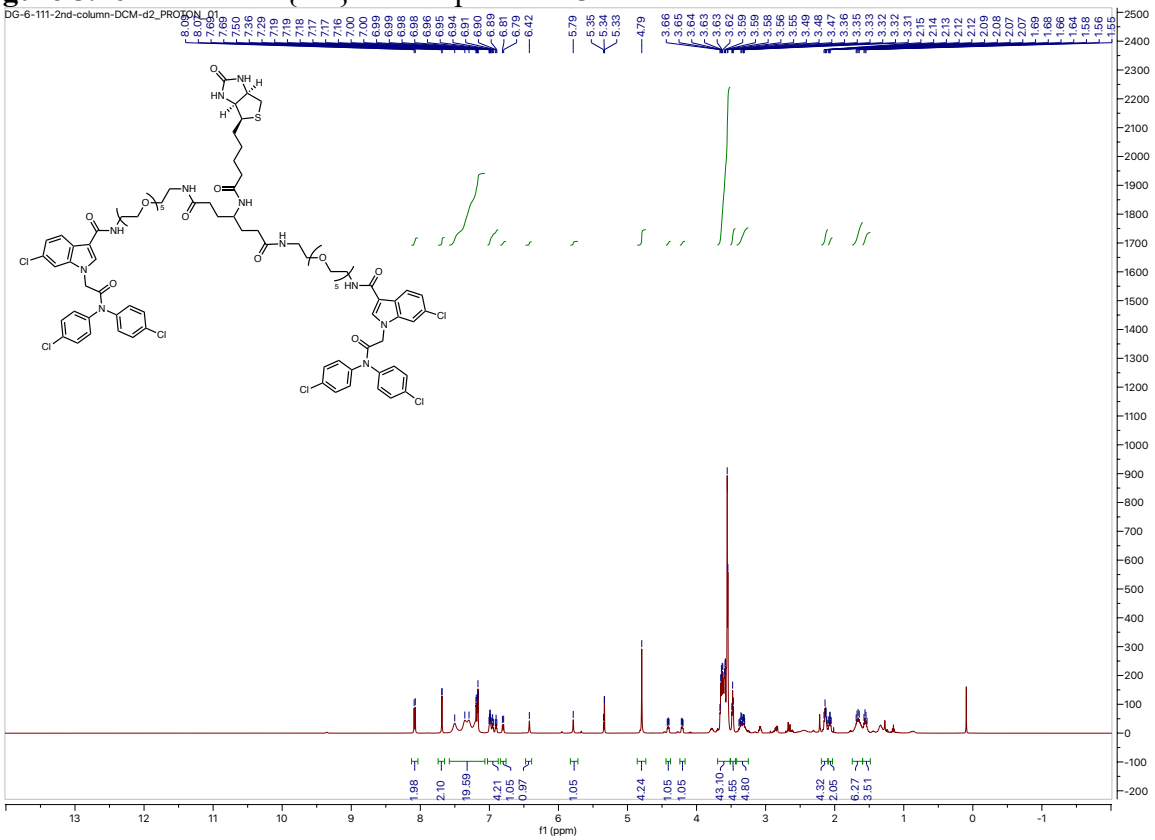

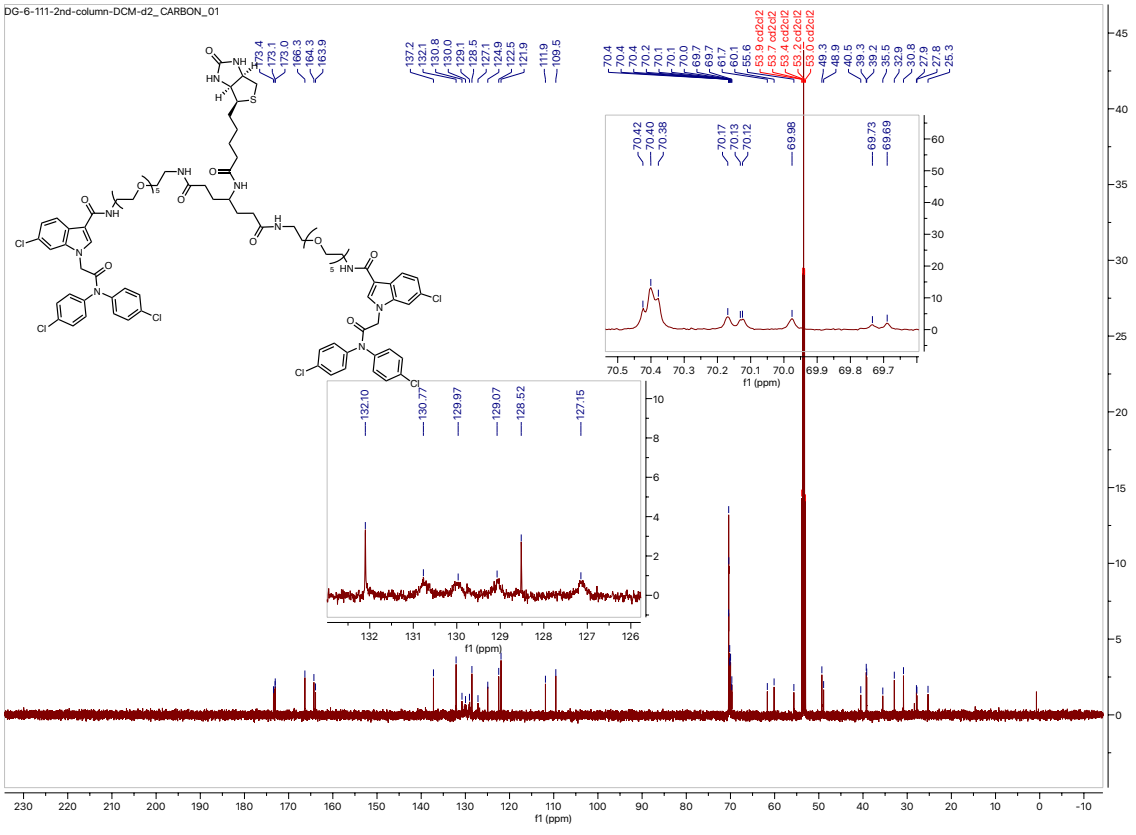

Figure 5.27: ^{1}H and $^{13}C\{1H\}$ NMR spectra of **5-26**

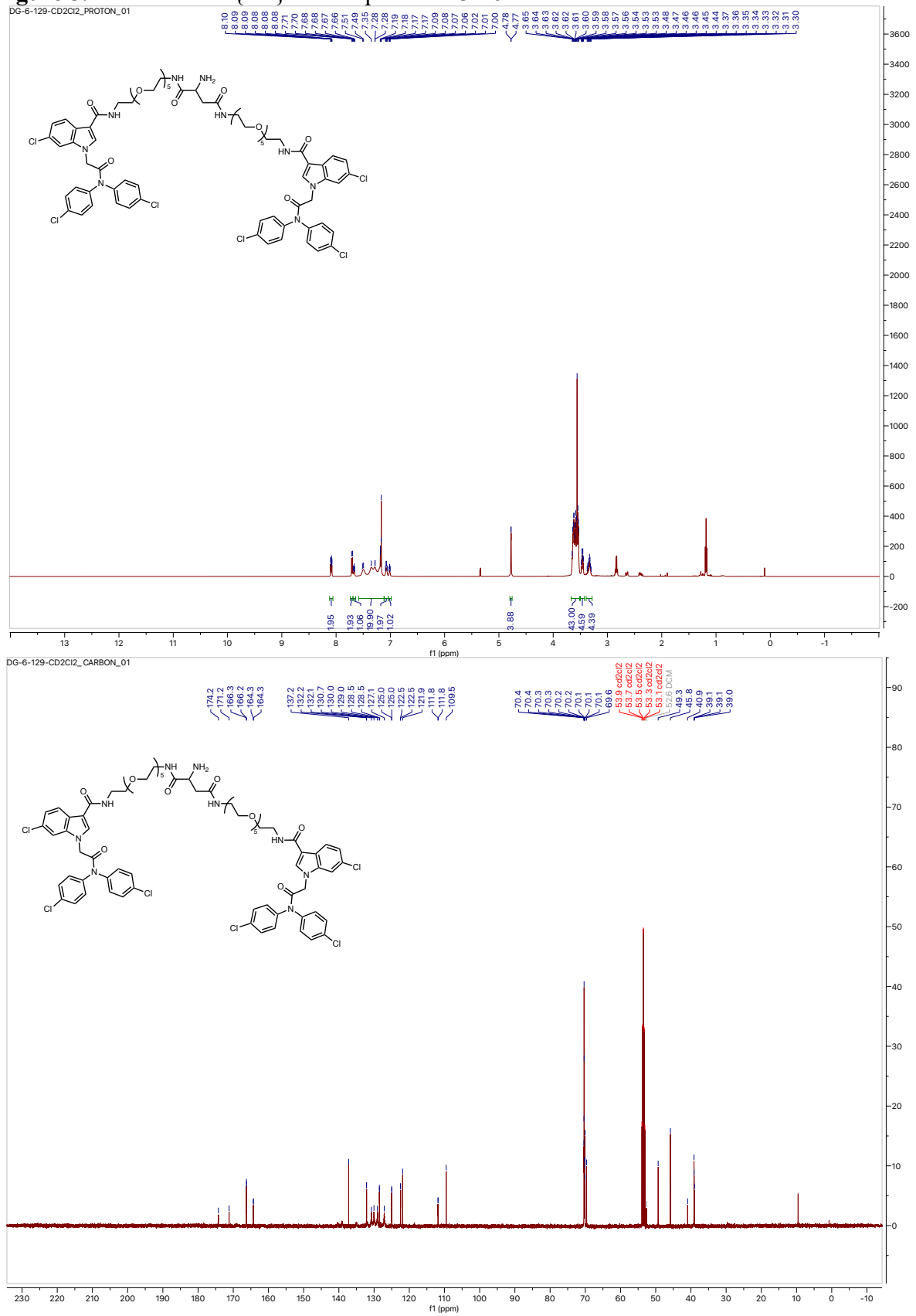

Figure 5.28: ^{1}H and $^{13}C\{1H\}$ NMR spectra of **5-27**

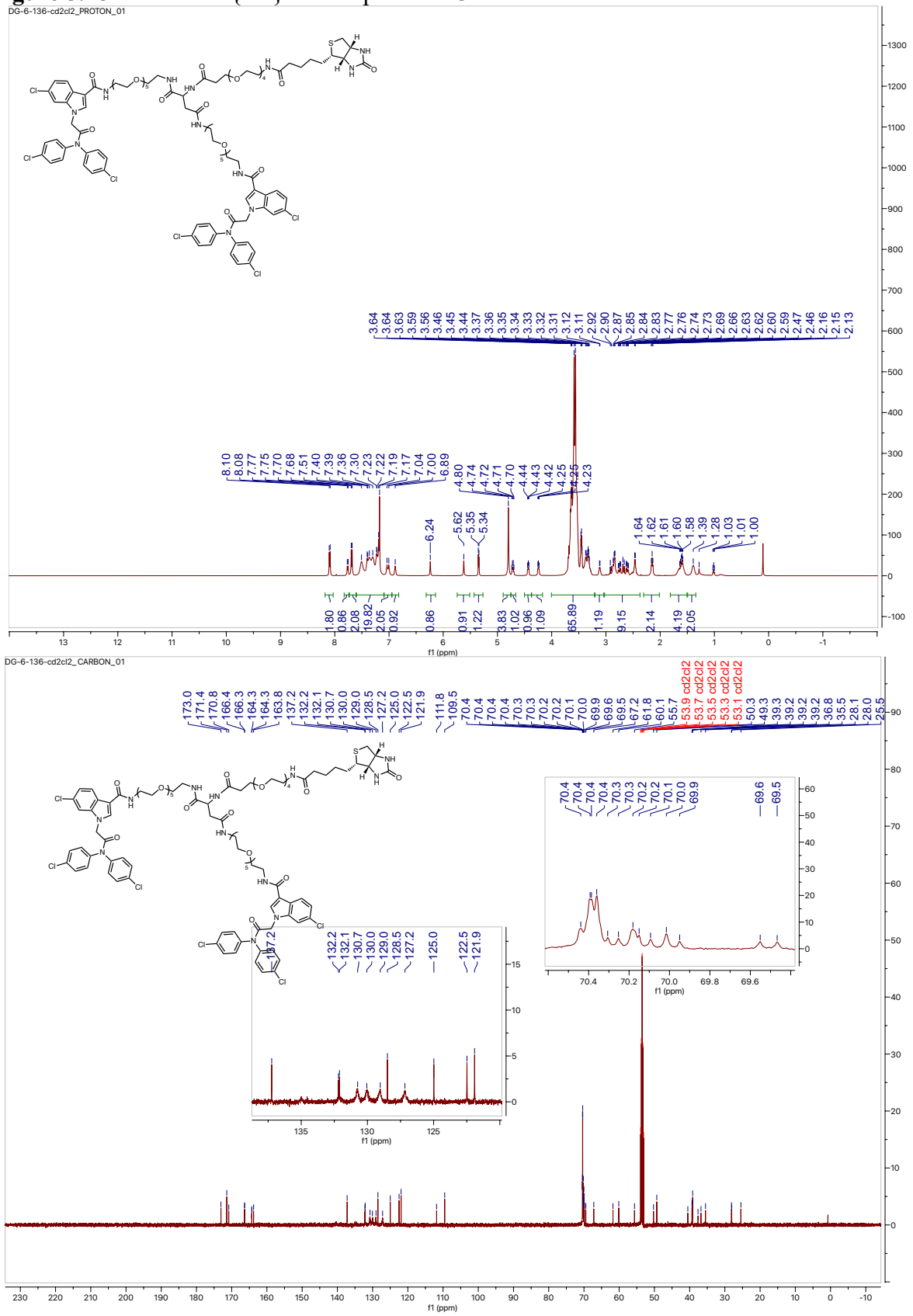

Figure 5.29: ^{1}H and $^{13}C\{1H\}$ NMR spectra of **5-28**

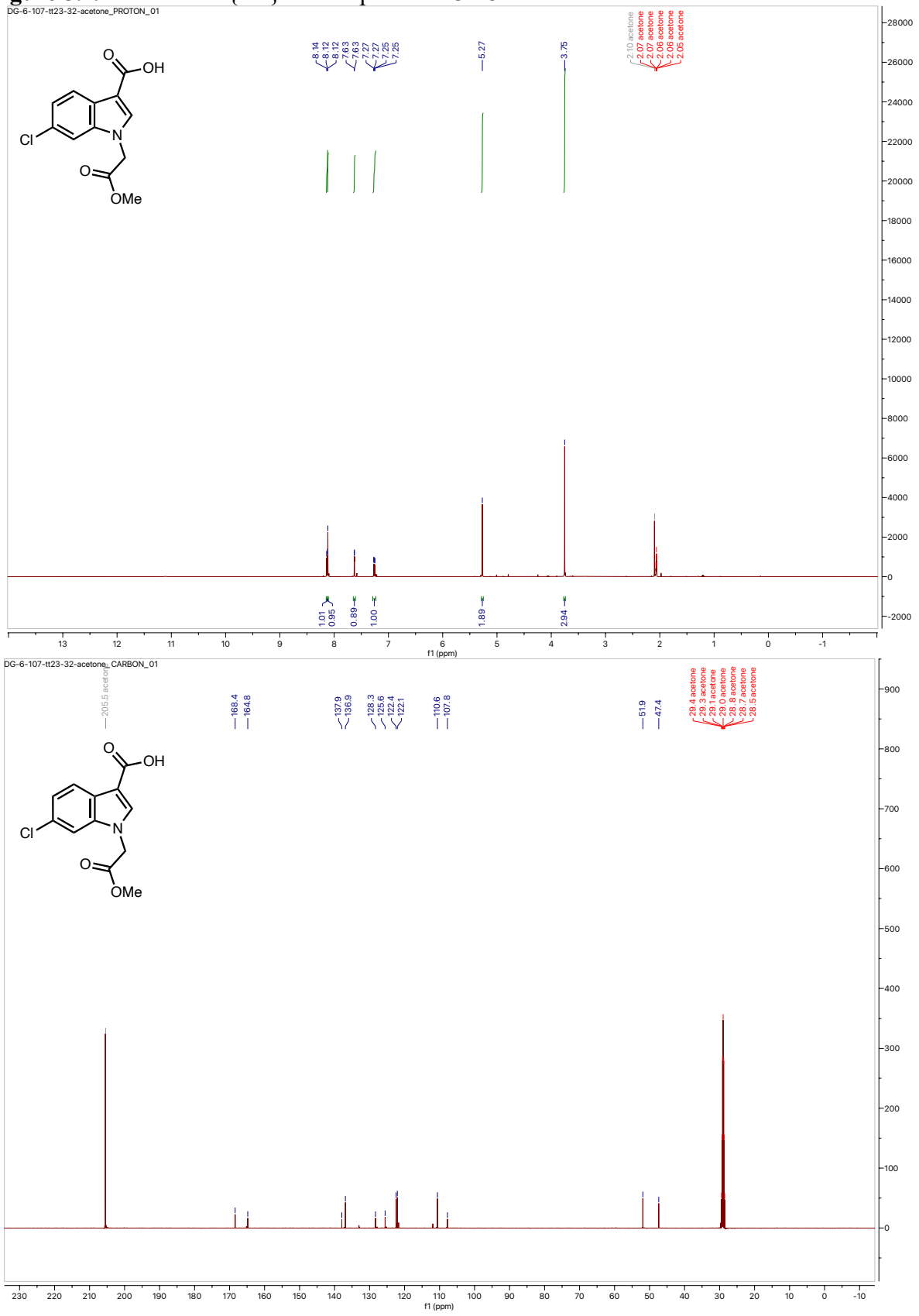

Figure 5.30: ^{1}H and $^{13}C\{1H\}$ NMR spectra of **5-29**

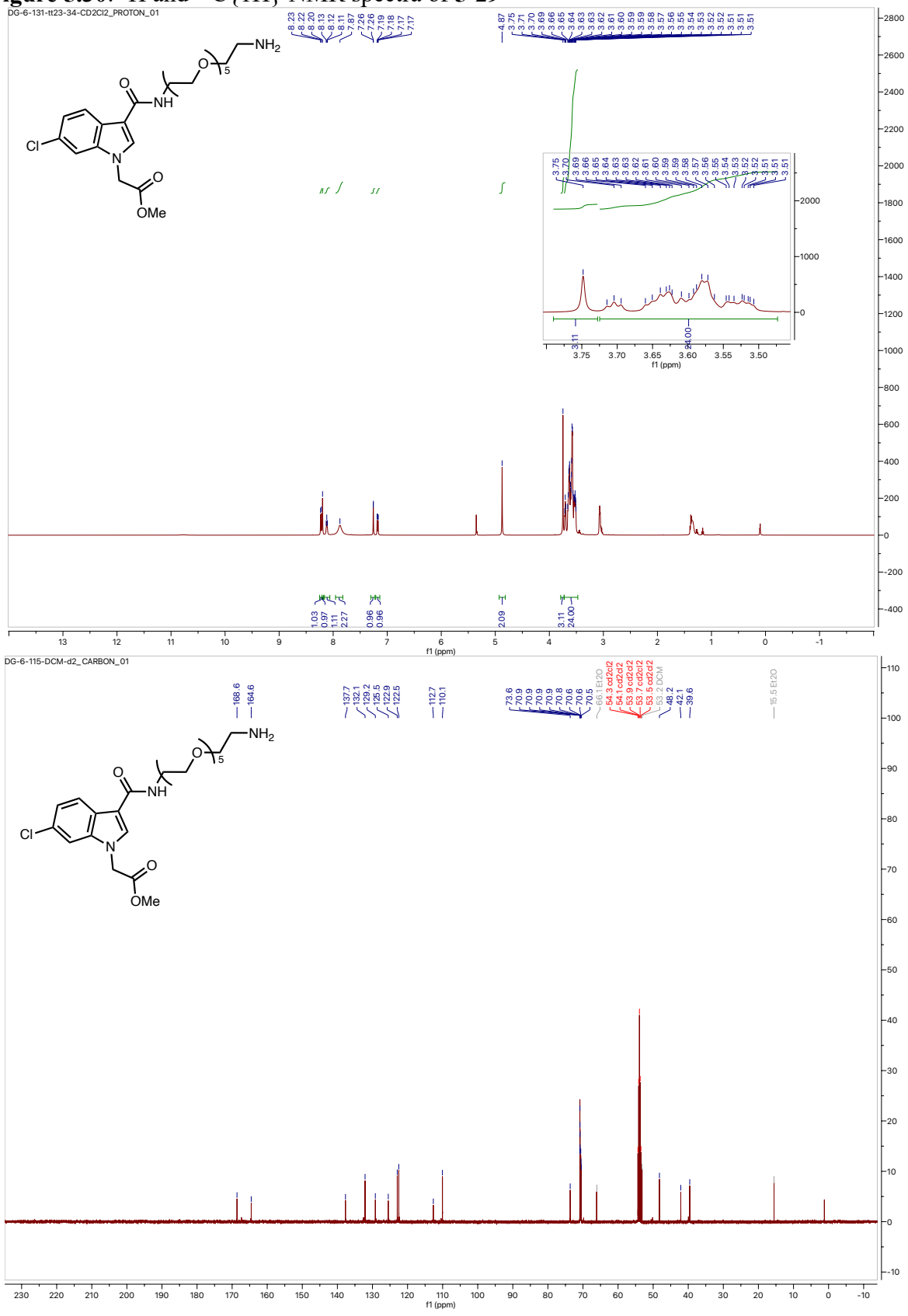

Figure 5.31: ^{1}H and $^{13}C\{1H\}$ NMR spectra of **5-30**

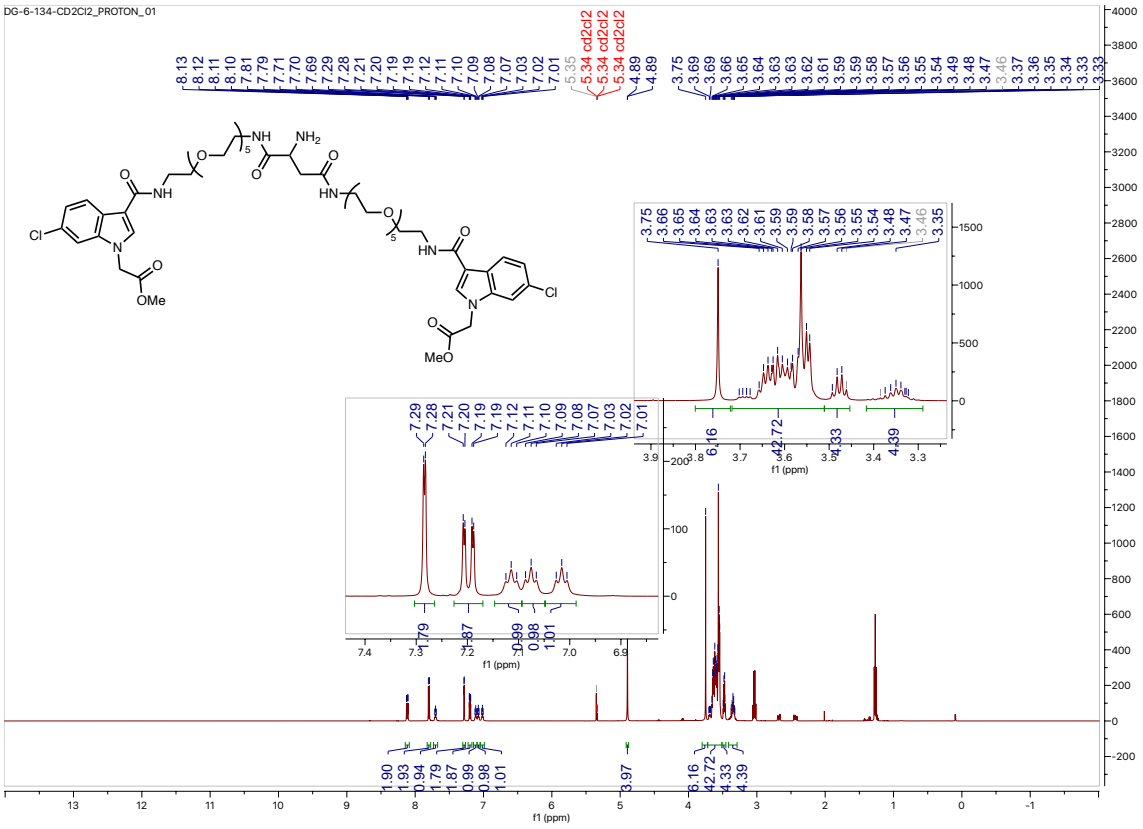

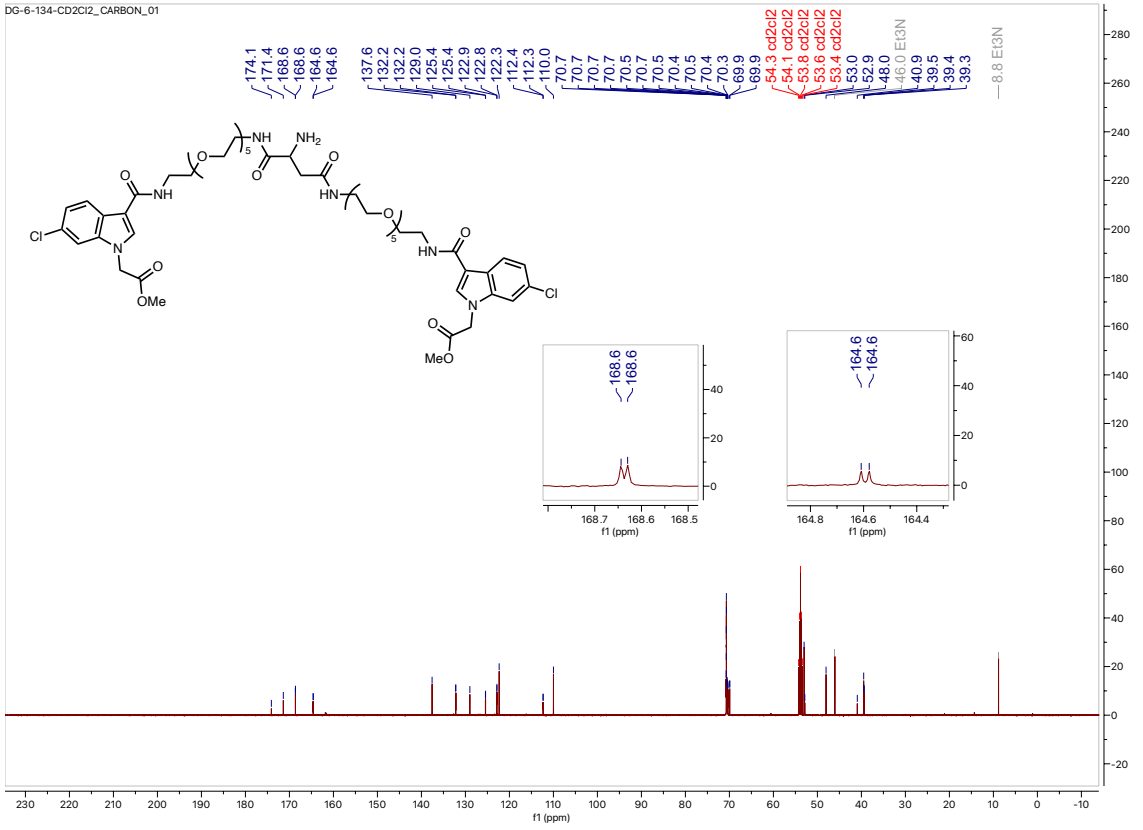

Figure 5.32: ^{1}H and $^{13}C\{1H\}$ NMR spectra of **5-31**

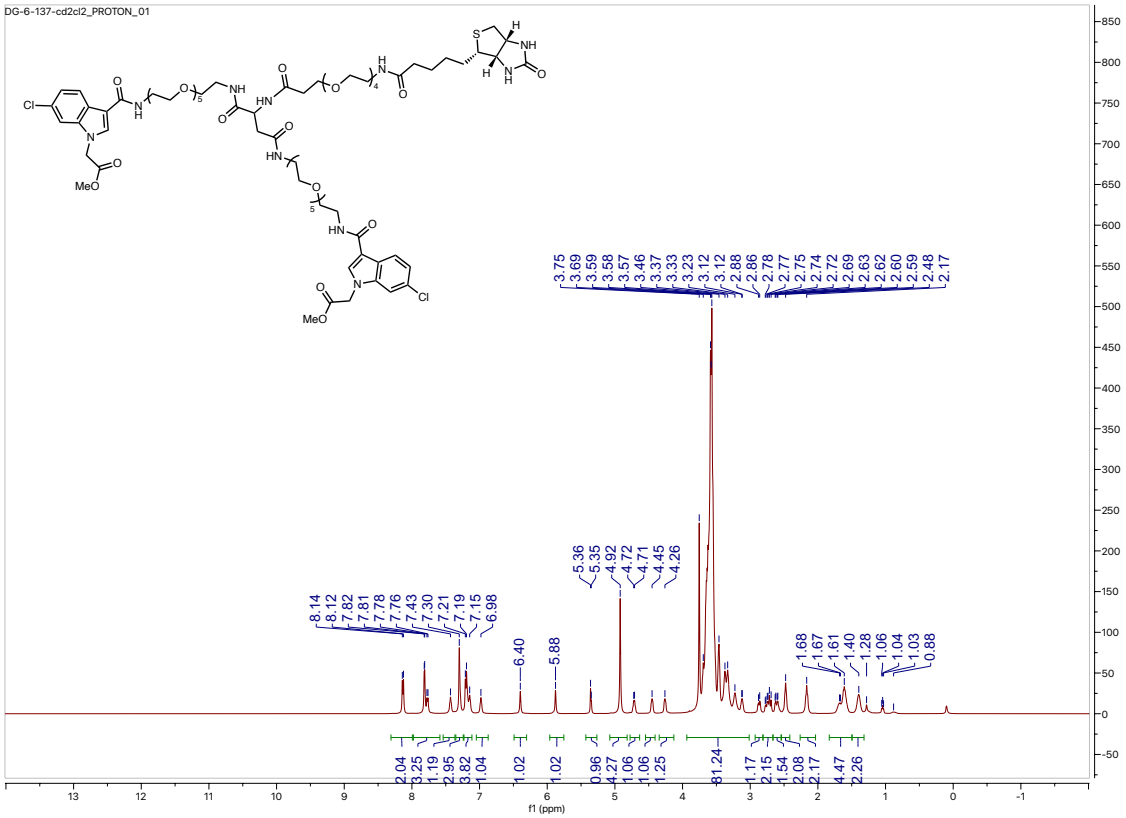

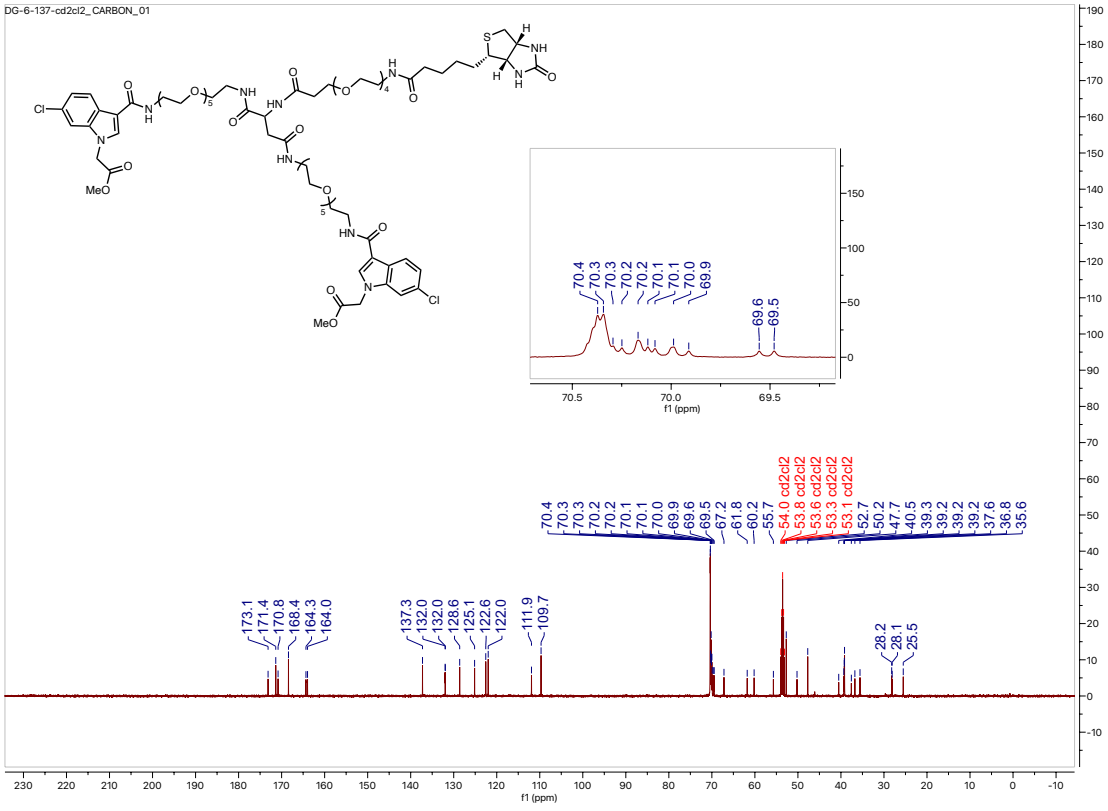

Figure 5.33: ^{1}H and $^{13}C\{1H\}$ NMR spectra of **5-33**